Guadalupes 2008
May 13-22

UT Jackson School of Geosciences
Field Stratigraphy

If found, please return to

____

Phone: ____________________

Field Stratigraphy
Guadalupes Field Trip
May 12-22, 2008

Friday, May 9

Meet at 5:00 beer/field trip planning—Crown and Anchor. If it is really crowded, we can go to Posse East which is right around corner.

Monday, May 12

10:00 am Get field vehicles (I need 3 volunteers to go with me.)

Make sure that each vehicle has an operational spare tire and the equipment to change it.

10:30 am Take vehicles to Wal Mart—buy supplies (anything we don't have), pack coolers and vehicles

Pack these items:

Critical Group Items

1) White Board
2) 6 coolers
3) Jacobs staffs for all
4) Role of large scale plotting paper
5) Duct tape
6) Magic markers
7) Stoves! (how many stoves do we have?)

Critical Personal Items

1. Hand lens
2. grain size card
3. mineral oil
4. 10% hcl
5. rock hammer
6. tent, sleeping bag, sleeping pad
7. suntan lotion, hat, day pack
8. field guide and field book
9. very solid field shoes and sandals
10. appropriate clothing for rain, wind, and sun, rain gear
11. flashlight/headlamp
12. medications, first aid kit, towel, bath supplies
13. camera, batteries, cell phone, charger
14. cup, fork, knife, spoon, water bottles

Field Schedule:
<u>Tuesday, May 13</u>
07:00am —Depart Austin to Salt Flats (~8 hr drive)

16:00 (MTN Time)—Arrive Salt Flats to south of Guads—Overview (PSU arrives El Paso 11:20 am)
Task: Sketch major stratigraphic elements of western escarpment.

May 13, 19:00 (MTN Time)—Arrive Washington Ranch

Camp Washington Ranch

- 18 Rattlesnake Springs Road, Carlsbad, NM 88220
- 22 tent sites reserved, 13th through 20th
- Sites are next to a building where you can store food/equipment, use bathroom/shower
- Group dinner arranged for each night
- $10/tent/night, $7.50/person for dinner
- Contact: Charles – 505-785-2228

<u>Wednesday, May 14</u>

07:00 Depart Washington Ranch to Salt Flat Bench (turb. systems)
Task: Construct Integrated Channel Cross Section
Task: Evaluate connection between channel-filling and overbank deposits

<u>Thursday, May 15</u>

07:00 Depart Wash. Ranch to Guadalupe Canyon (turb. systems)
Task: Slope Channel Systems: Sketch Cross Section
Task: Evaluate models for channel cutting and filling based on preserved stratigraphy.

<u>Friday, May 16</u>

07:00 Depart Wash. Ranch to Williams Ranch (Bone Canyon to Schumard Canyon)
Task: Study Canyon Fill Stratigraphy and Facies
Task: Sketch Large Scale Onlap
Task: Evaluate two stages of erosion (syn- or pre-cutoff)

<u>Saturday, May 17</u>

07:00 Depart Wash. Ranch to McKittrick Canyon – Shelf to Basin
Task: Develop model for carbonate Shelf depositional systems
Task: Measure carbonate Section

Sunday, May 18

07:00 Depart Wash. Ranch to Shattuck Valley Escarpment
Correlation Exercise
Task: Use measured section, cycle stratigraphy and sequence stratigraphy to correlate in mixed carbonate-clastic shelf system

Monday, May 19

AM Group Correlation Project
Task: Complete Correlation Exercise
PM Carlsbad Caverns
Task: Tour Cavern

Tuesday, May 20

All day McKittrick Canyon
Task: Walk reef, look at slope facies, examine geobiology

Wednesday, May 21
All Day Mystery Outcrop

Thursday, May 22
All Day —Return to Austin – 8 hours

Contact Information:
Peter Flemings (512) 750-8411
Rob Skarbek (484) 354-2758
Jon Schueth (814) 933-9118
Matt Reilly (814) 359-6356
Joe Valenti (585) 217-6025
Charles Bohn (814) 404-3424
Melissa Pardi (860) 305-4217
Leah Schneider (814) 280-2854
Dan Jones (651) 245-2775
Mark Patzkowsky (814) 574-3452
Heather Nelson (814) 865-9794 (O)
Heather Nelson (814) 777-1746 (C)
Heather Nelson (814) 867-6058 (H)

Overview

Paleogeography Overview

The Guadalupe Mountains are located on the northern edge of the Permian Basin in southeast New Mexico and northwest Texas. The Permian Basin can be subdivided into smaller basins (Midland Basin, Delaware Basin, and Marfa Basin) and platforms (Central Basin Platform, Diablo Platform). It was formed during the Permian Period in the Late Paleozoic.

Plate tectonics

The Permian period is between 299 and 251 Ma ago. By the Early Permian continents were merged into one huge landmass called "Pangea". The ocean to the west was the Panthalassic Ocean, to the east the Paleo-Tethys Ocean.

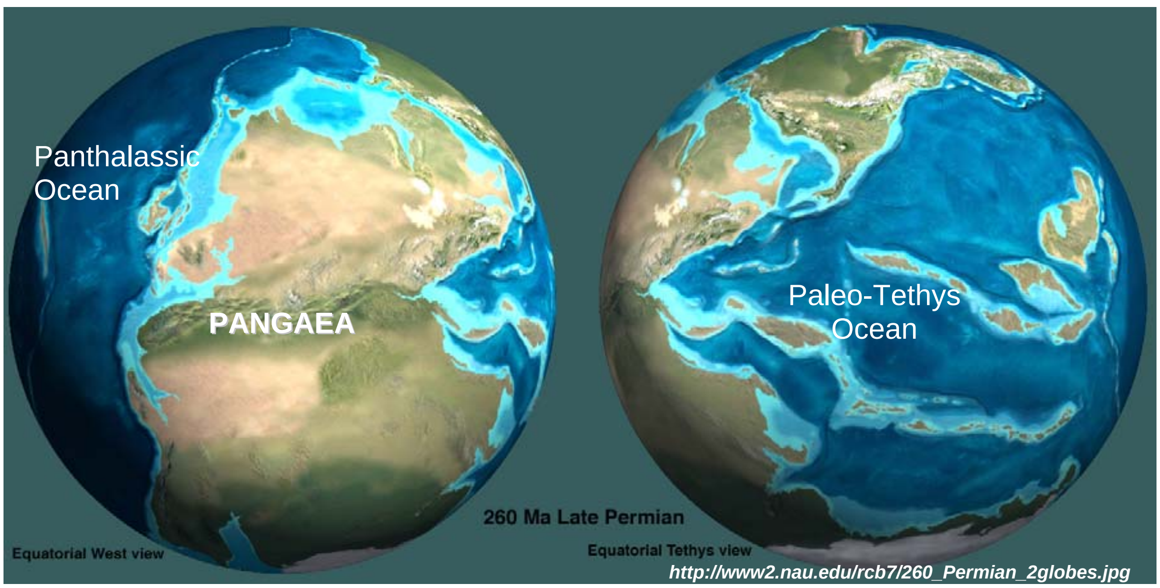

Paleogeography of North America

About 260 Ma ago, North America was located at lower latitude than today. New Mexico and Texas were very close to the continent margin. Aeolian and fluvial redbed sediments were deposited across the western interior of North America during the Late Permian. In the basins, including the Permian Basin, thick carbonates were deposited. Extensive salts were deposited on a craton from

Nebraska to Texas. The Ancestral Rocky Mountains in the northwest of the Permian Basin (New Mexico, Colorado) were a source of siliciclastic sediments.

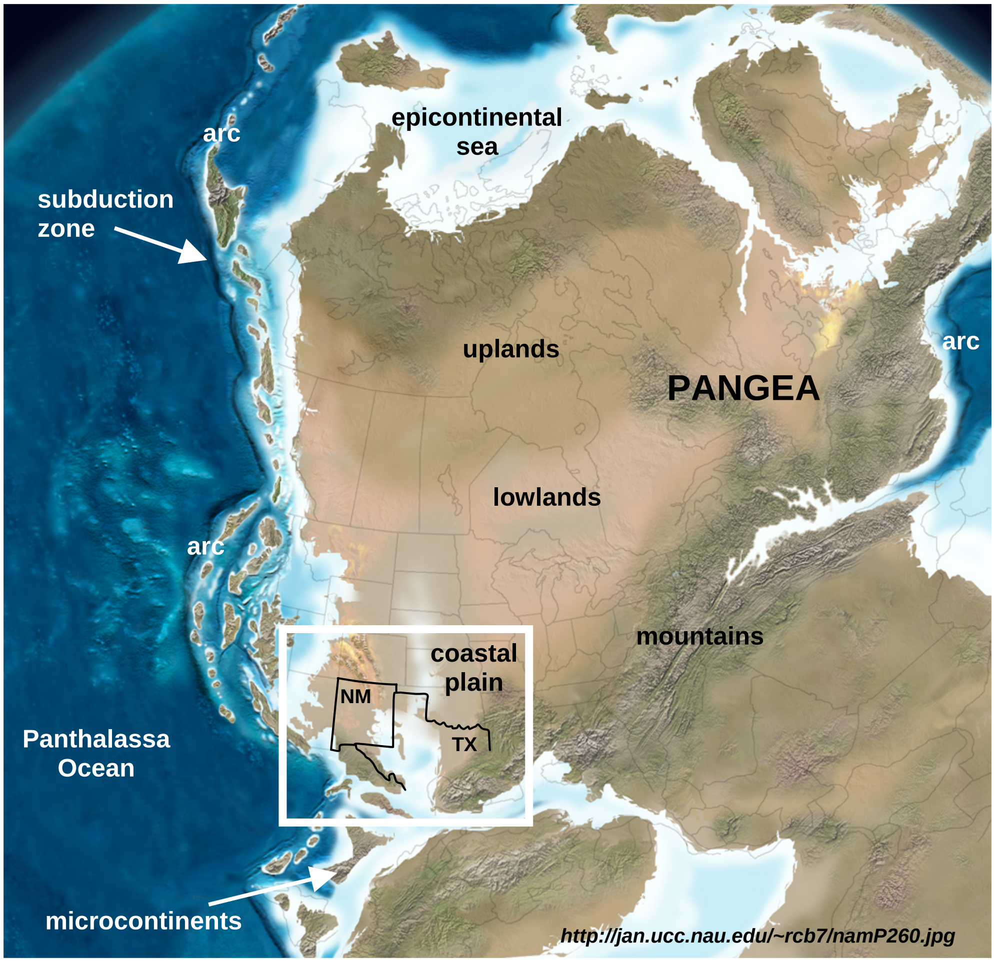

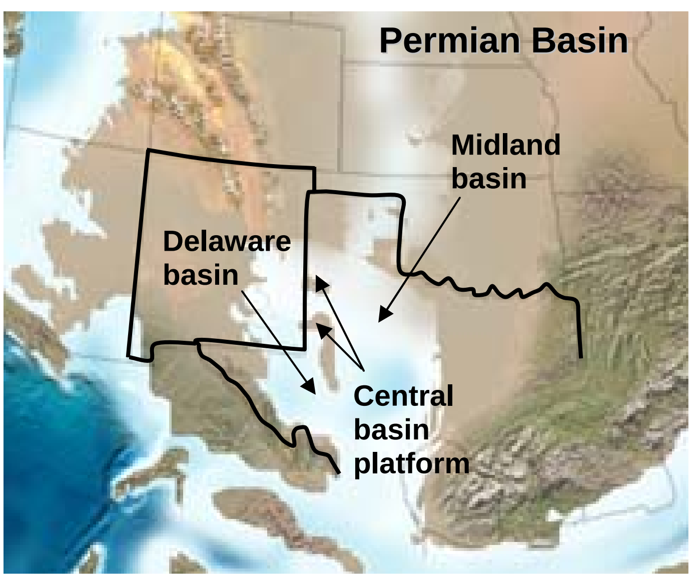

Late Permian (260 Ma ago)

Magnetic polarity changed more often and for longer periods towards the end of the Permian. There were several minor and major Permian – Devonian transgression – regression cycles with an overall regressive trend until the end of the Permian stage when relative sea level was at its lowstand (about 200 meters below present sea level).

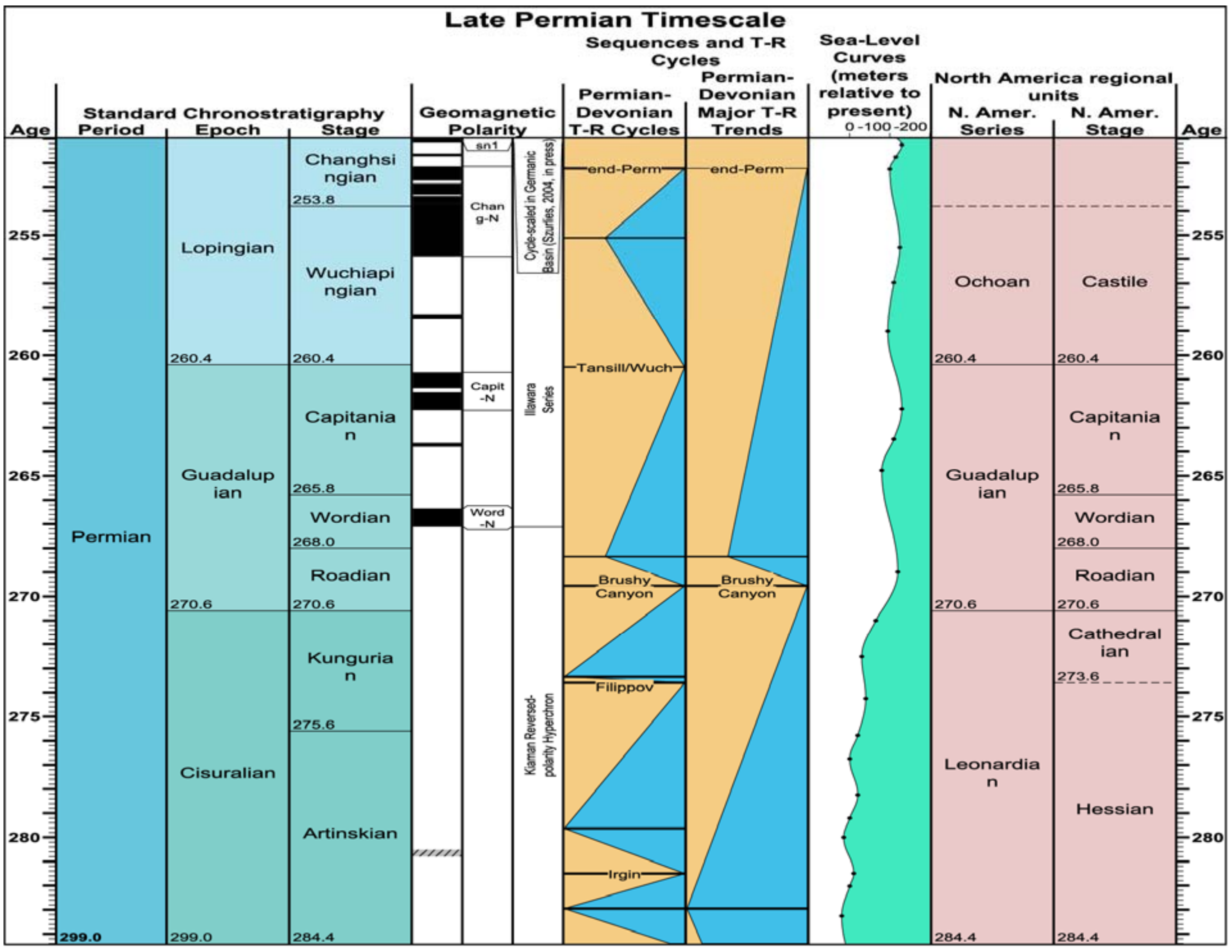

http://www.tscreator.com/download.php

Two-pulse Permian mass extinction

The end of the Permian Period coincides with a severe mass extinction. The mass extinction actually happened in two pulses: at the end of Guadalupian and Tatarian (5 Ma later). About 71% of marine species (e.g. brachiopods, ammonoidea, bryozoans, fusulinacea, gastropods, bivalves) were eliminated during the first brief pulse of extinction at the end of Guadalupian. The second pulse was even worse with 80% extinct marine species. The magnitude of Late

Permian – Early Triassic mass extinction is comparable with extinctions at the ends of Triassic and Cretaceous.

Speculated causes:

There are at least five speculated causes for the mass extinction at the Late Permian:

1) Volcanism:

The Siberian Traps (large igneous province) are evidence for eruption of ash and gases as a result of a mantle plume. The Siberian Traps cover ~2 Mio. km^2 (larger than Europe) and the volume is approximately between 1 – 4 Mio. km^3. SO_2 and CO_2 were erupted into the atmosphere causing a short-term cooling and long-term warming, respectively.

2) Meteorite impact:

A potential meteorite crater might have been found in Australia. An iridium anomaly as well as shocked quartz, both typical evidence for meteorite impacts, have been documented there as well.

3) Climate change:

There is evidence for both, an increasing and decreasing trend in temperature. Due to the dry, hot supercontinent with great seasonal fluctuations and an increase in CO_2 emissions from volcanic activity, the area of coal swamps might have been reduced and the metabolism of creatures might have been slowed down. At the same time, SO_2 emissions from volcanic activity caused cooling, documented by glacial deposits in polar zones and thick dune sands. The presence of carbonate limestones was reduced. Both trends combined might have caused a rapid repeated heating and cooling that did not leave creatures enough time to adapt to one or the other. It might have also caused changes in ocean circulation and salinity.

4) Formation of supercontinent:

Due to one huge landmass (Pangea), the interior was hot and dry and at low elevation. The coastline was reduced, therefore, less habitats were available. Parts of Pangea were located over a pole causing glaciations.

5) Glaciation:

Glacial deposits were found in Australia, Siberia, and the North Sea. Milancovitch cycles can only account for fluctuations in size of ice sheets, but not for actual ice sheet formation. But combined with the fact, that parts of Pangea were located over poles, Milancovitch cycles may have contributed to a global drop in temperature and sea level causing a Late Permian glaciation.

High diversity of Late Permian

From Middle to Late Permian the diversity increased tremendously. Compared to brachiopods, gastropods and bivalves became relatively more abundant, particularly in offshore carbonate environments. Potential causes for the high diversity could be an increase in productivity, fluctuations in environmental stresses, or an onset of anoxia in the deep ocean. Bivalves and gastropods, as opposed to brachiopods, have a better ability to adapt to increased environmental stresses. Therefore, there might have been an increased habitat space for them causing a relative increase in abundance.

References

http://jan.ucc.nau.edu/~rcb7/nam.html
http://www2.nau.edu/rcb7/globehighres.html
http://www.tscreator.com/download.php
http://palaeo.gly.bris.ac.uk/Palaeofiles/Permian/intro.html

Stanley, S.M. & Yang, X. (1994). A Double Mass Extinction at the End of the Paleozoic Era. *Science*, Vol. 266, No. 5189, pp. 1340-1344.

Clapham, M.E. & Bottjer, D.J. (2007). Permian marine paleoecology and its implications for large-scale decoupling of brachiopod and bivalve abundance and diversity during the Lopingian (Late Permian). *Palaeogeography, Palaeoclimatology, Palaeoecology*, Vol. 249, pp. 283-301.

Overview


Gudalupe Peak
Image © 2008 TerraMetrics
Image © 2008 DigitalGlobe
©2007 Google™
Pointer lat 32.016939° lon -104.971912° elev 1249 m
Streaming |||||||||| 100%
Eye alt 25.15 km

Western Escarpment

Stratigraphy

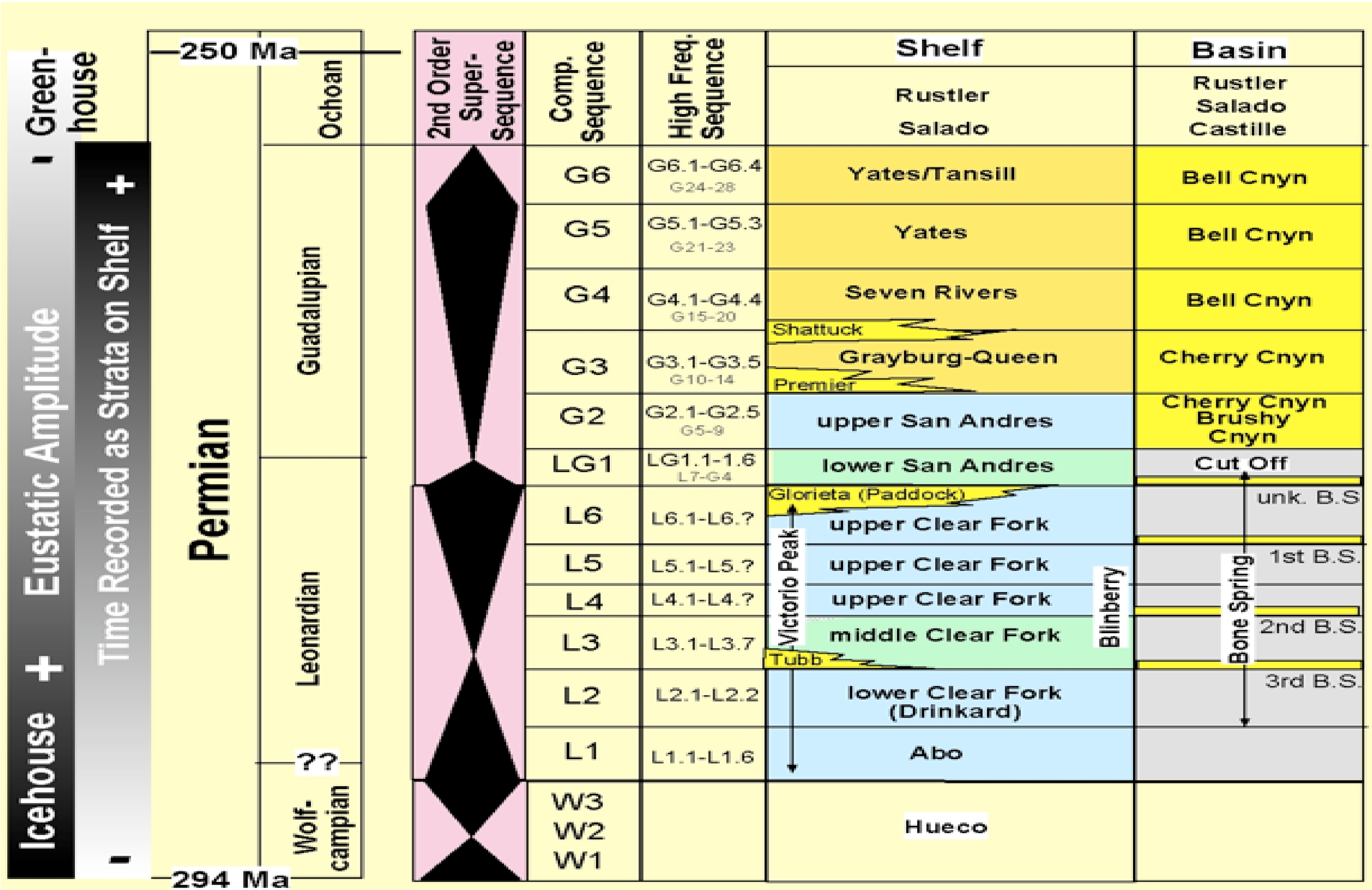

Kerans & Kempter (CD)

Formation distribution in the sequence model

Composite Sequence Framework of the Guadalupe Mountain Region

Composite Sequence	HFS	Northwest Shelf	Shelf Margin	Foreslope	Delaware Basin	
CS-14	Guad. 27-28	Tansill	Upper - CM	Capitan "bedded"	Bell Canyon	Lamar
	Guad. 25-26	Yates	Middle - CM			McCombs
CS-13	Guad. 21-24					Rader
CS-12	Guad. 17-20	Seven Rivers	Lower - CM			Pinery - Hegler
	Guad. 15-16	Shattuck	Capitan "massive" (CM)		Cherry Canyon	Manzanita
CS-11	Guad.13-14	Queen	Goat Seep			South Wells
	Guad. 10-12	Grayburg				
CS-10	Guad. 8-9	upper San Andres				CCT
	Guad. 5-7				Brushy Canyon	
CS-9	Guad. 1-4	lower-middle San Andres			Cutoff	
	Leonardian 7-8					

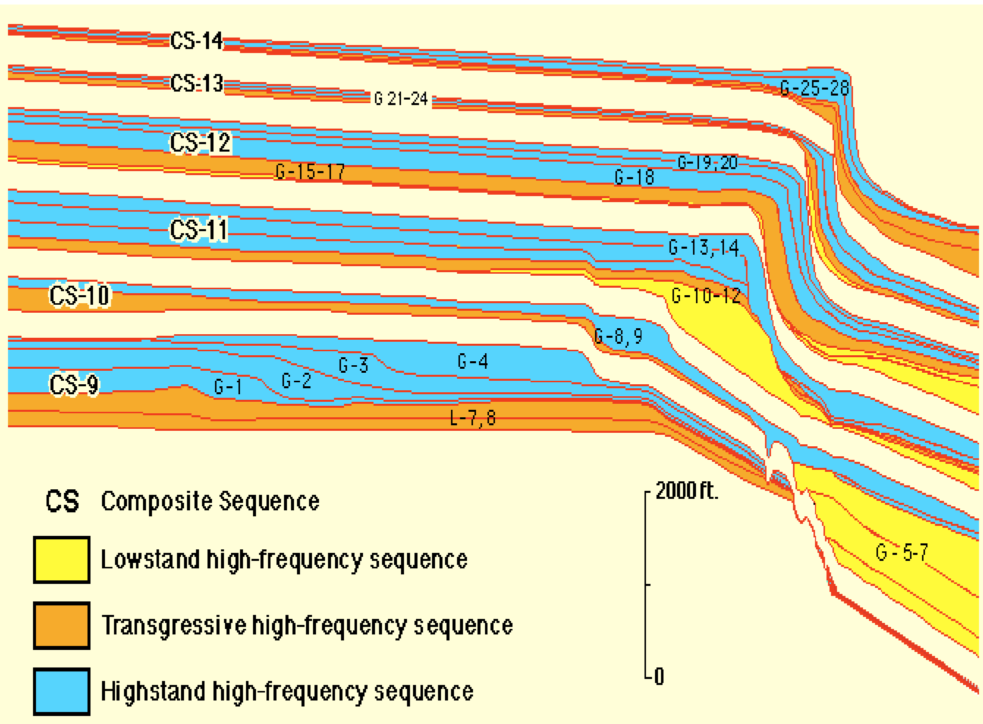

Kerans & Kempter (CD)

Regional Cross-Section of the Guadalupe Mountains, SE New Mexico and West Texas

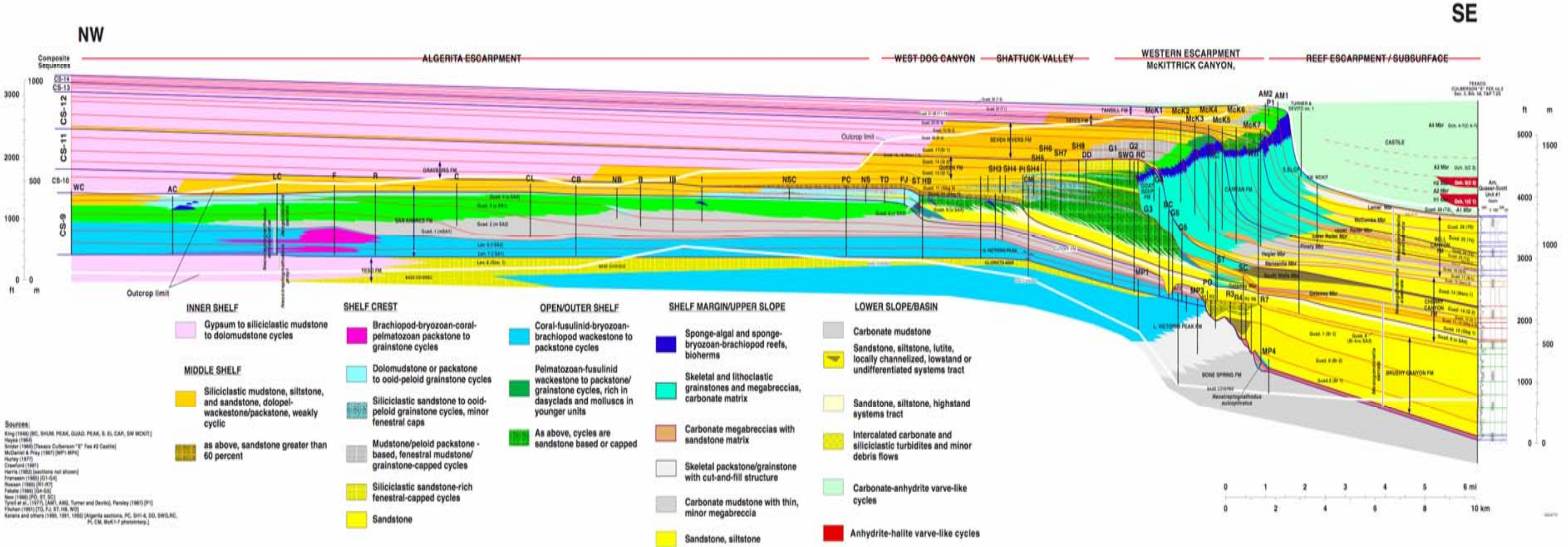

Kerans & Kempter (CD)

Salt Flat Bench

Guadalupe Canyon

Guadalupe Canyon is located in West Texas S-S-W of El Capitan (fig. 1 and 2).

Fig 1. Google Earth aerial view of Guadalupe Canyon and El Capitan

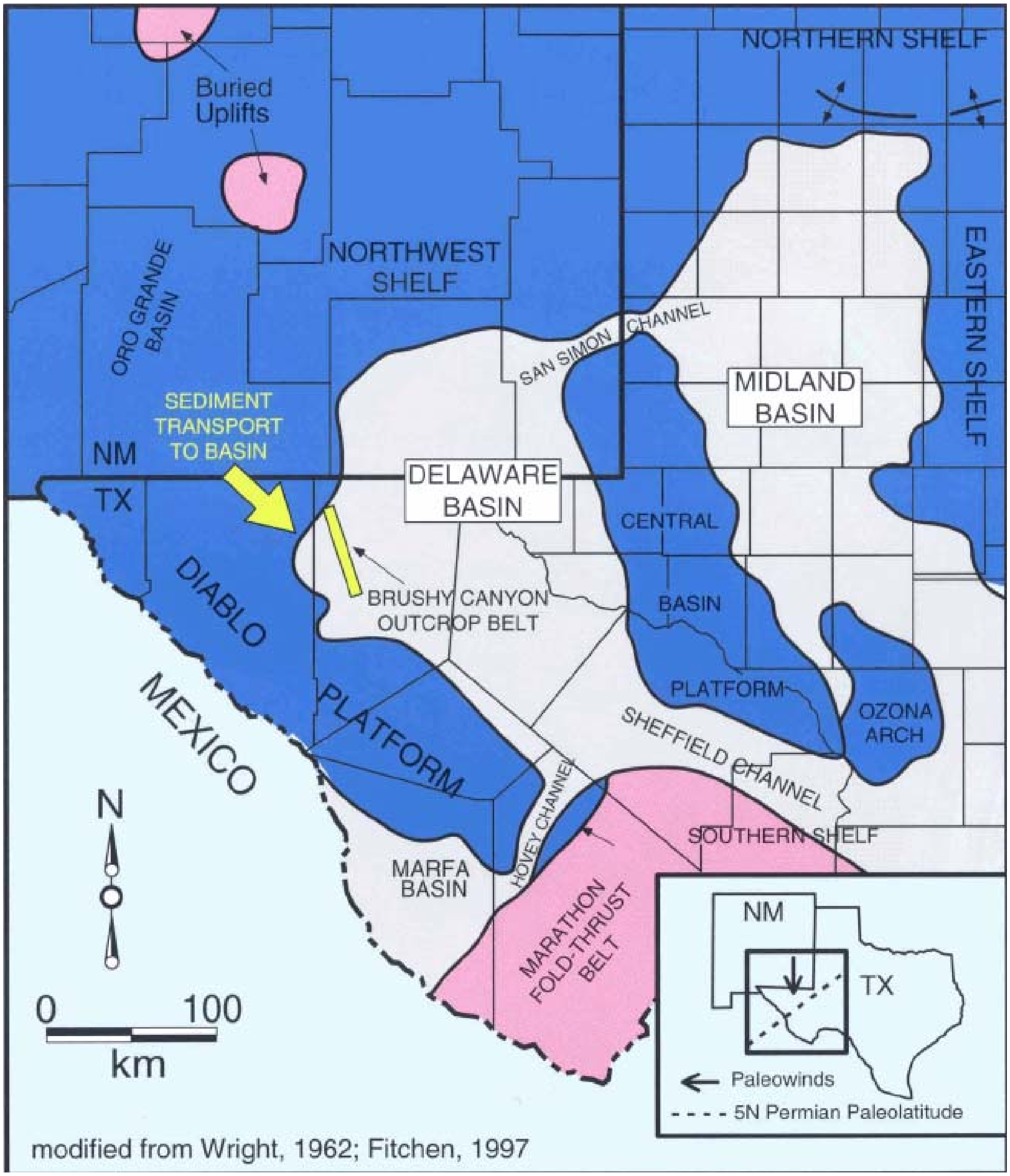

Fig. 2. Regional overview of the location of the Brushy canyon outcrops. Beaubouef et al., 1999.

We will be looking at the Brushy Canyon outcrops in Guadalupe Canyon. The Brushy Canyon outcrops were deposited in the Delaware Basin (fig. 2). The Brushy Canyon Fm. (fig. 3) is comprised of basinally-restricted, deep-water sandstones and siltstones of Guadalupian age up to 360m thick. They were deposited during subaerial exposure of the carbonate shelf as a third order lowstand sequence set. The base of the Brushy Canyon on the slope and basin floor is submarine erosion surface which truncates carbonate rocks of Leonardian and Early Guadalupian age. Laterally persistent siltstone units divide the Brushy Canyon Fm. into three separate, sand prone units (the Upper, Middle, and Lower Brushy Canyon Members).

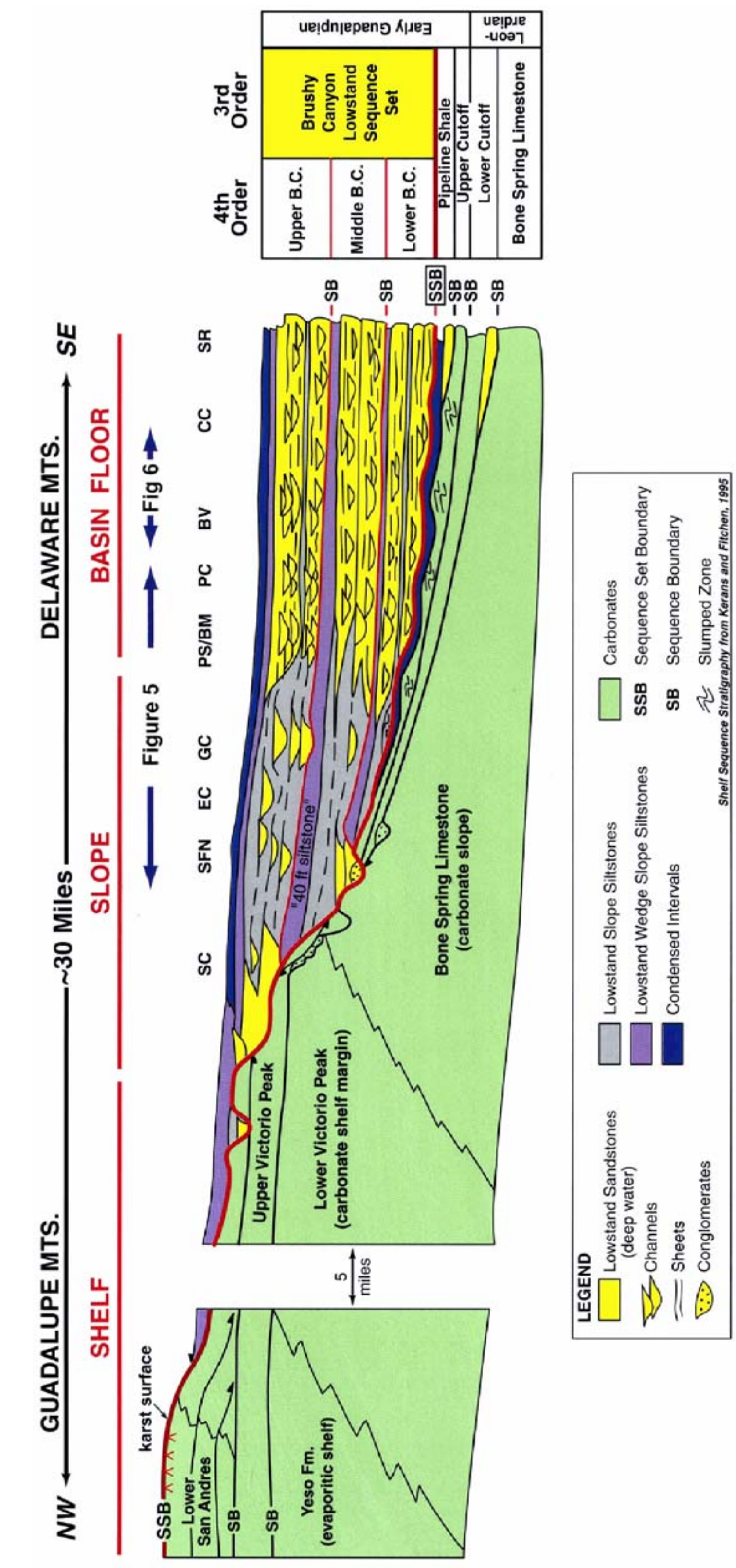

Fig. 3. Schematic diagram of the deposition of the Brushy Canyon Fm. Note the lowstand wedge slope siltstones dividing the Brushy into 3 members. Beaubouef et al., 1999.

The Brushy Canyon Fm. is a lowstand wedge, overlain by the Cherry Canyon Tongue (fig. 4) which is the lowstand wedge for the basal Guadalupian 3rd order sequence. The Brushy Canyon Fm. pinches out on a sequence boundary (the submarine erosion surface described previously). This sequence boundary is correlatable updip to a karsted subaerial exposure surface at the top of the Lower San Andres.

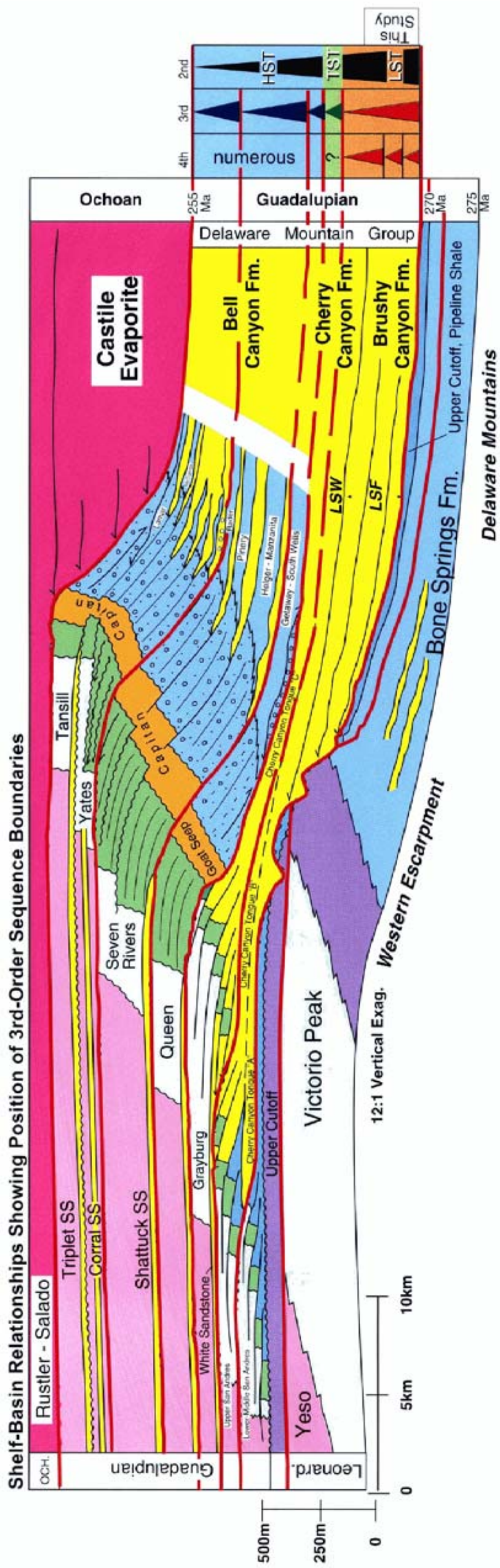

Fig. 4. Diagram showing the larger sequence stratigraphic context of the Brushy Canyon Fm. Beaubouef et al., 1999.

Figures 5 and 6 show the relative location of the outcrops on the slope.

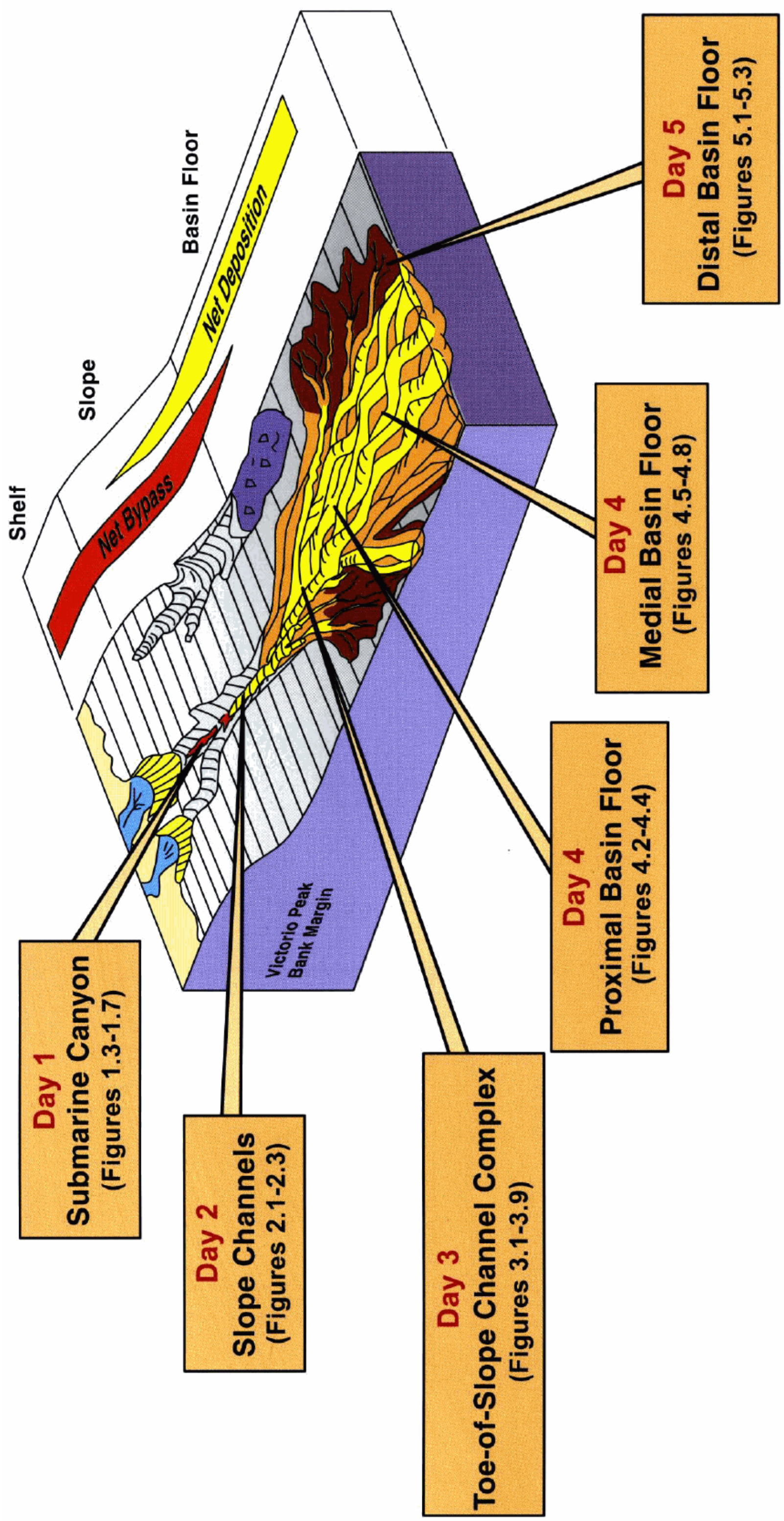

Fig. 5. We will be looking at the mid- to lower-slope channel deposits of the Brushy Canyon, indicated by the Day 2 marker. Beaubouef et al., 1999.

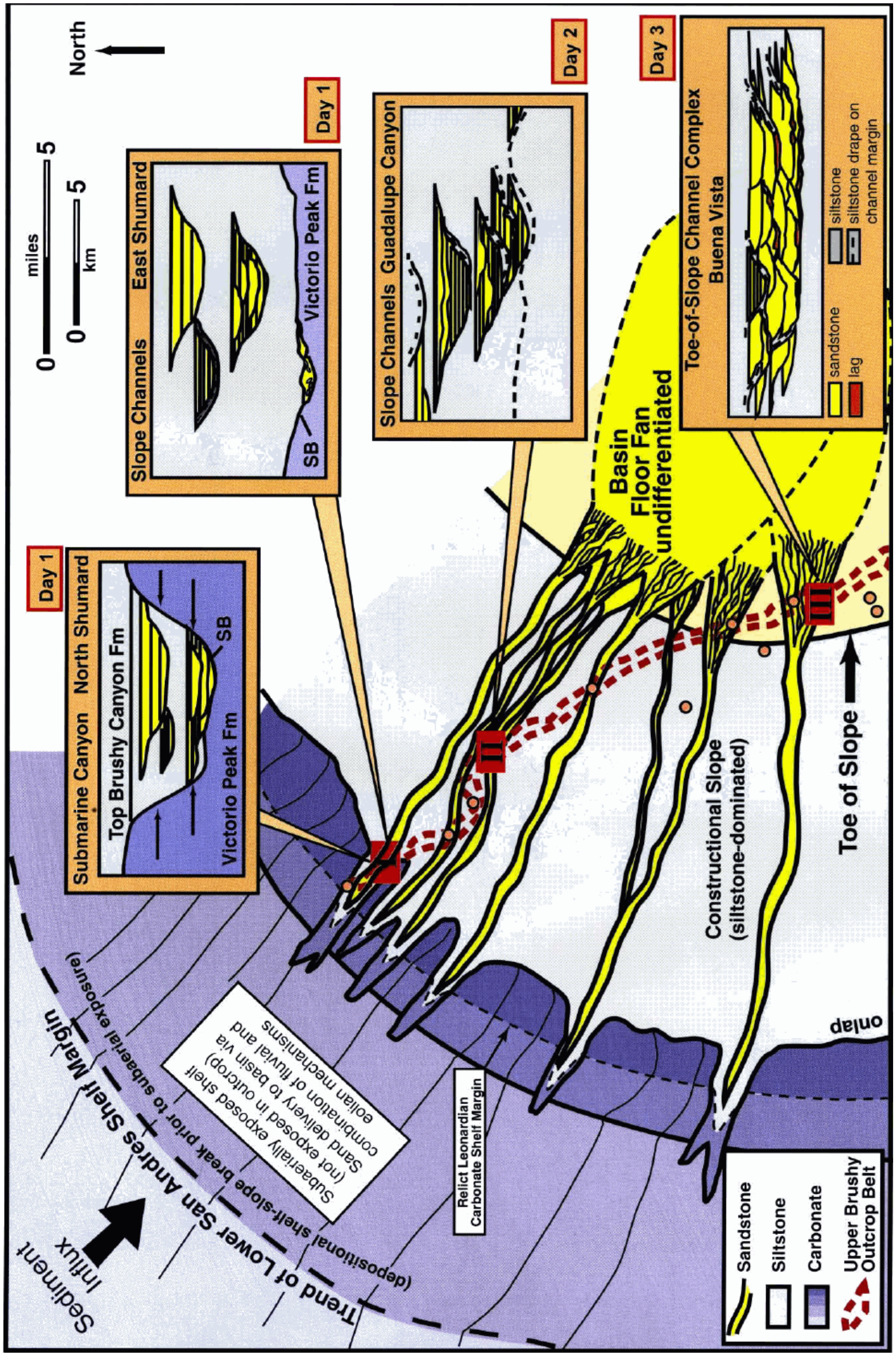

Fig. 6. Map view of the depositional model constructed for the Brushy Canyon Fm. We will be located at approximately II. Beaubouef et al., 1999.

The process by which the channels were created and filled is shown in figure 7. The channels were created by a process of first cutting then filling by turbidites. Turbidites initiate on the upper slope and the head of the turbidite typically erodes the sediment below. The body carries the majority of the sediment and depending on conditions within, the body may either erode, bypass, or deposit. The tail of the turbidite will often deposit thin, fine-grained sediment. The deposits seen in Guadalupe Canyon should generally fall within the red box. Here, rapid fallout from suspension creates structureless beds, which are a common fill within the channels. The cutting and filling of channels depends on the location of the channel relative to the initiation point. Close to the initiation point, the channel will be cut, further out, lag or fine grained tail deposits may build up. Continuing further, the channels will fill with sand. If a channel is abandoned, it may fill with silt. The small diagram at the top indicates where the thickest deposits are relative to the downslope distance.

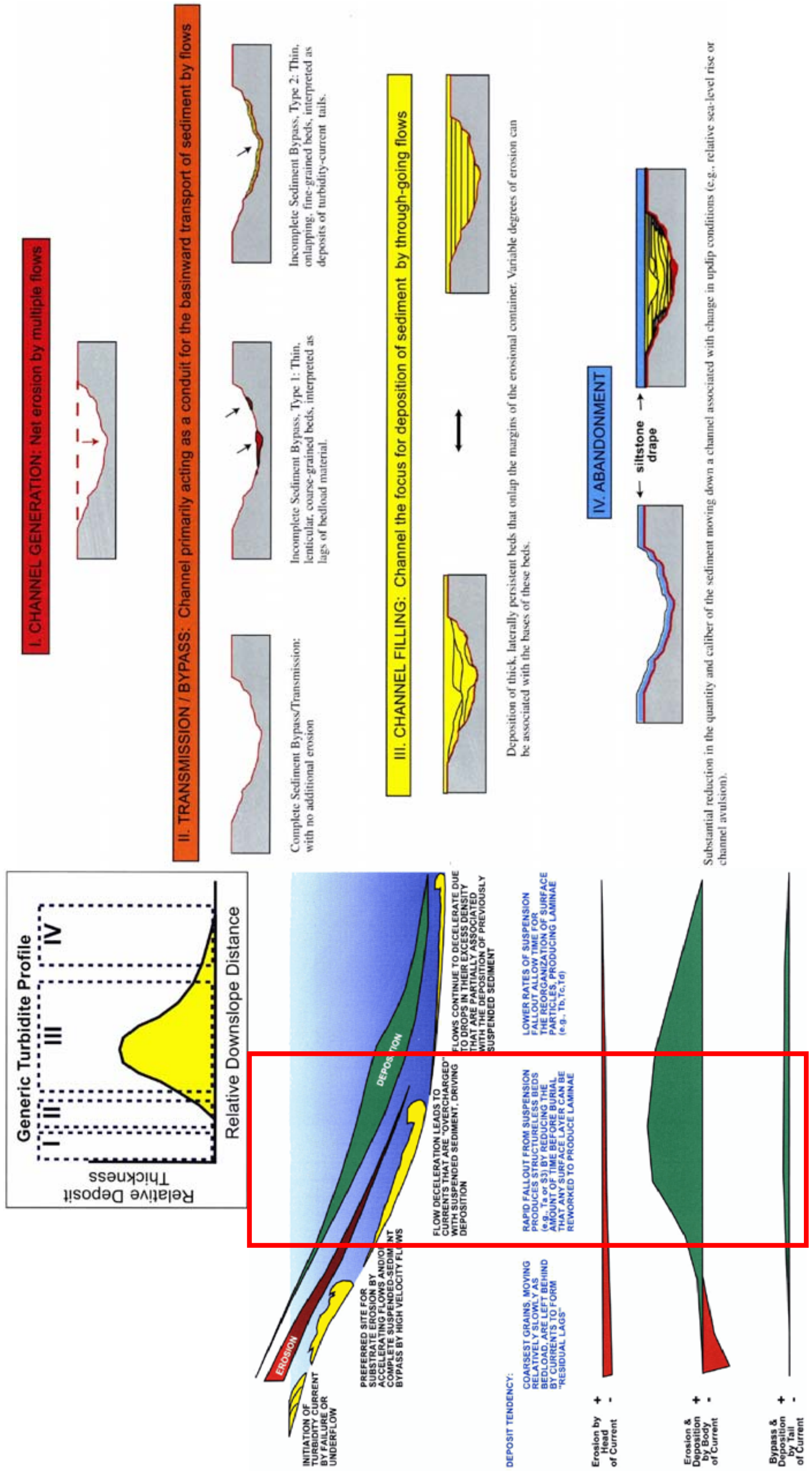

Fig. 7. Illustration of the process by which turbidites create then fill the channels seen in the Upper Brushy Canyon Mbr. Beaubouef et al., 1999.

Figures 8, 9, 10, 11, and 12 show some of what we will see at the outcrop. Figure 7 is a large overview of the canyon wall with several channel cuts and fills mapped.

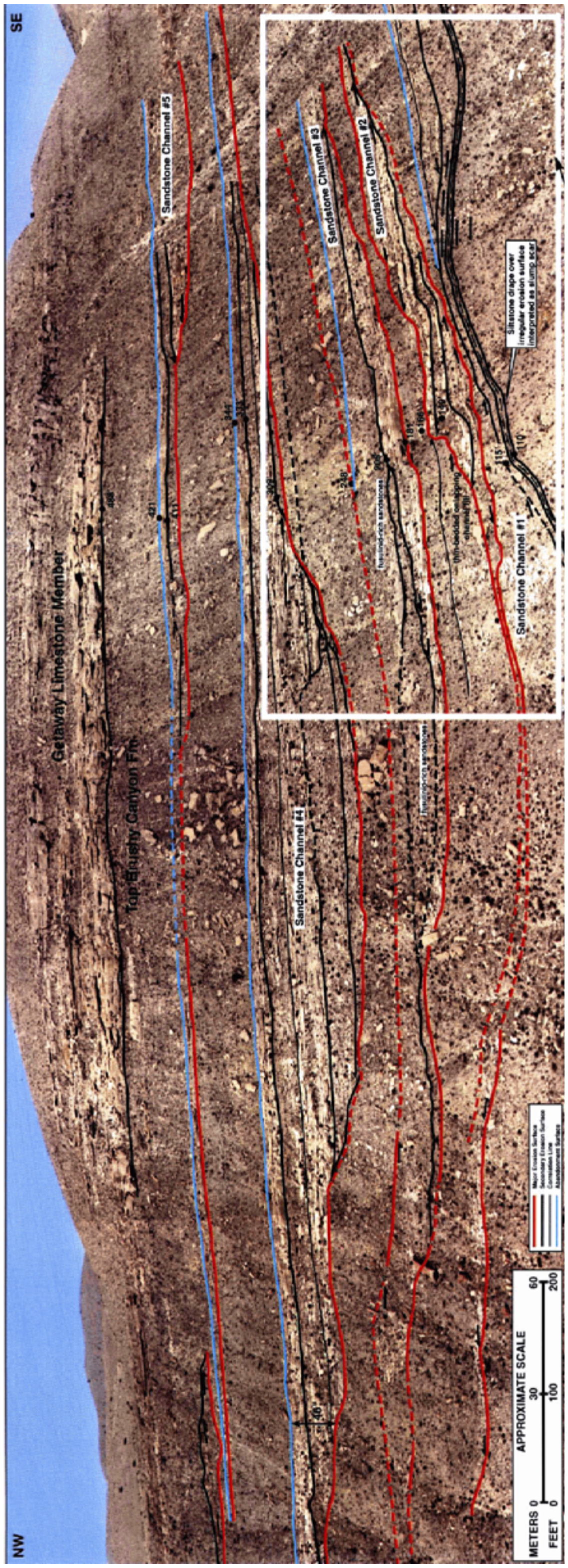

Fig. 8. Mapped channels and fills of the Upper Brushy Canyon Mbr. Red lines are major erosion surfaces, thick black are minor erosion surfaces, thin black lines are correlation surfaces, and blue lines are abandonment surfaces. White box is the blowup for figure 8. Beaubouef et al., 1999.

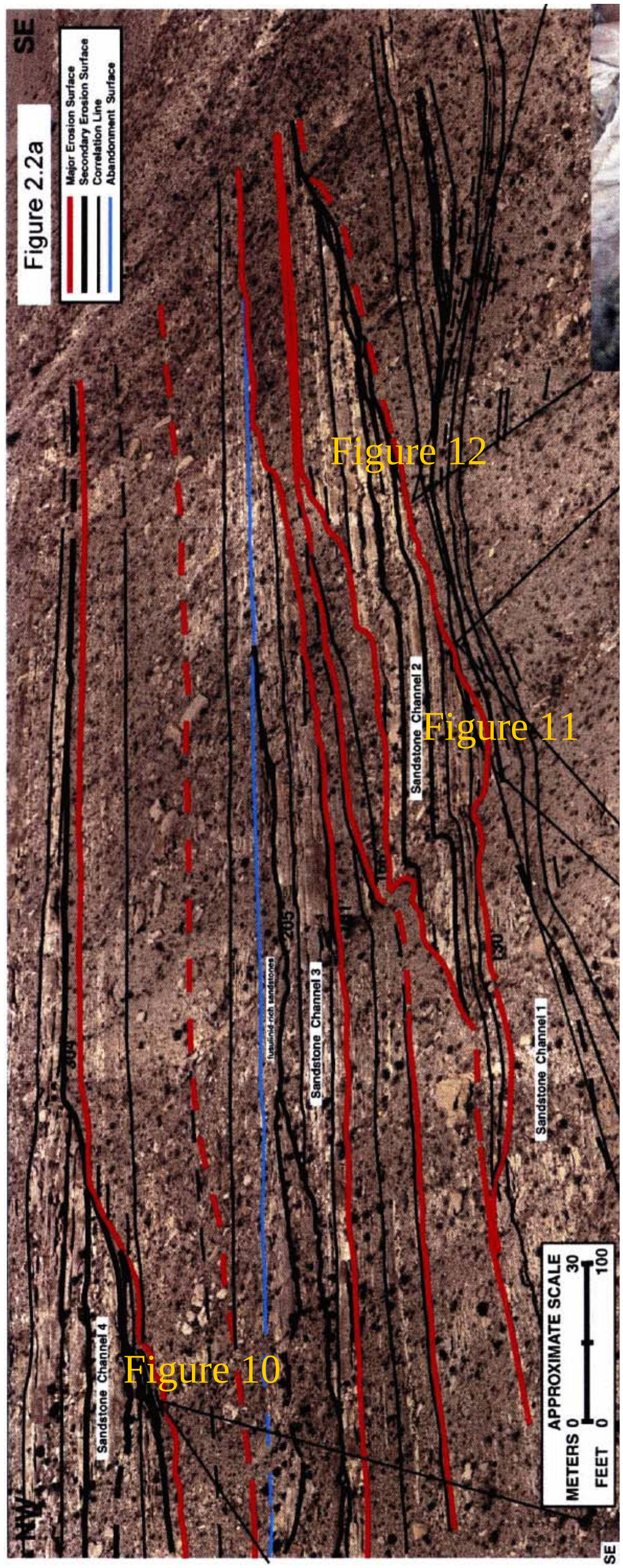

Fig. 9. Blowup of the previous white box. Several areas of interest are pointed out for the next several figures. Beaubouef et al., 1999.

Fig. 10. Stacked erosion surfaces and remnants of small-scale sandstone channel fills. This indicates a complex history of erosion and minor backfilling before later aggradational backfilling by laterally-extensive onlapping sandstones. Beaubouef et al., 1999.

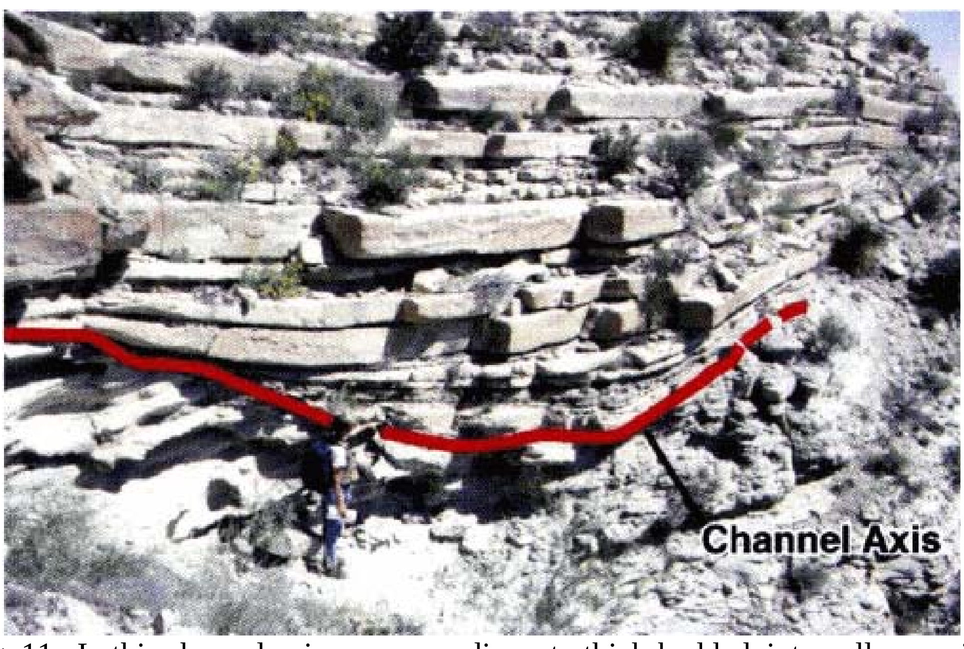

Fig. 11. In this channel axis we see medium- to thick-bedded, internally massive sandstone units which thin towards the channel margin. These are interbedded with siltstones and form composite drapes along the channel margins. Beaubouef et al., 1999.

Fig. 12. This close-up shows the lateral thinning of sandstone beds into zones of inclined sand- and siltstones form the channel margin drape. The master erosion surface is present below the picture. Beaubouef et al., 1999.

Things to look for in outcrop include:

- Channel Geometries:
  - Sand filled
  - Low aspect ratio
  - Up to 45m deep
  - Incised into slope siltstones
  - Confined by master erosion surfaces
- Bypass Indicators:
  - Siltstone draped erosion surfaces and coarse grained lags
  - Thin intervals containing erosion surfaces, very thin lenticular sandstones, and starved ripples at the base of some channel complexes
- Channel Fills:
  - Siltstones
    - Thin-bedded sand- and siltstones overlie ersion surfaces
      - May fill entire channel or form initial fill
  - Sandstones
    - Variable fill styles
      - Dominantly non-amalgamated, medium- to thick-bedded massive sandstones
        - Laterally extensive from channel axis to channel margin, thinning toward margin

- Stacking Patterns
    - Vertical to slightly offset patterns of stacking
        - Indicate focusing of flow by nearby upper slope canyons
        - Slump-related topography may control locations and stacking

Summary

In Guadalupe Canyon, we see several stacking turbidite channels within the Upper Brushy Canyon Member. Lower channels are muddier, but over time, channels are filled with more sand. The channels have been cut into the siltstones that create the slope and become less amalgamated as you move up section into blockier sands. The channels have an overall coarsening upward succession.

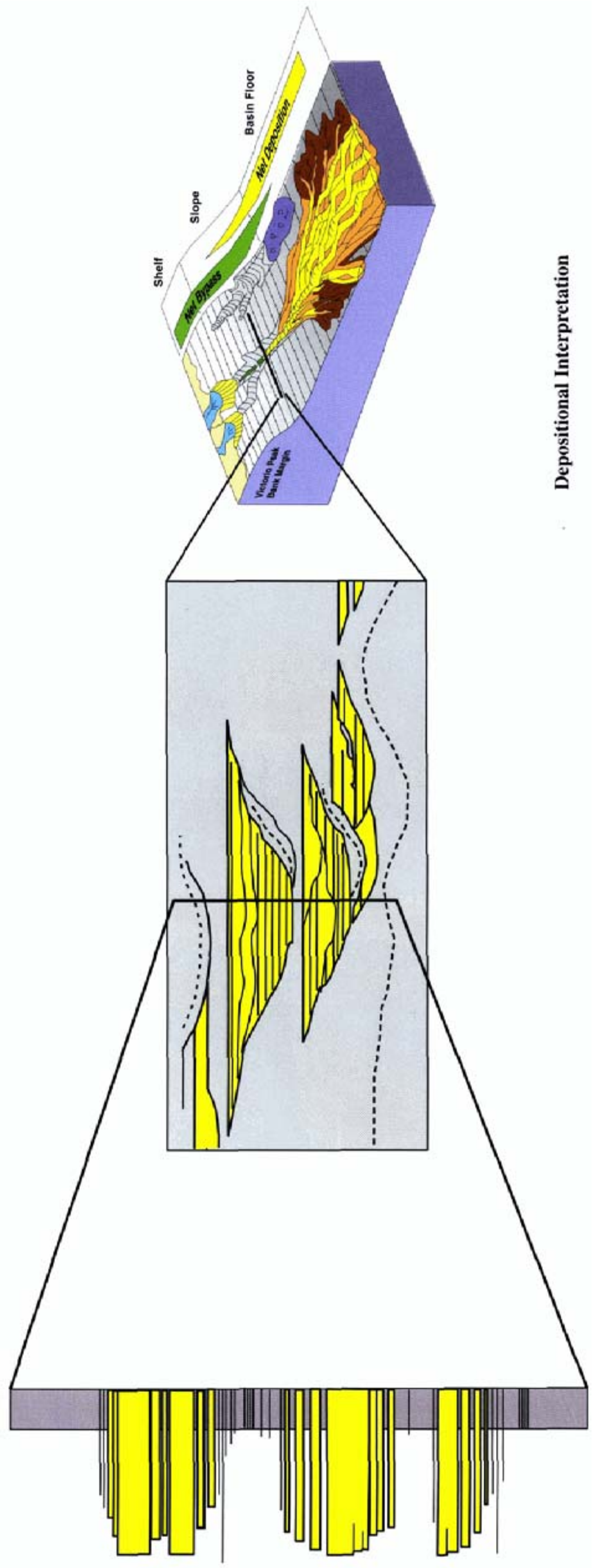

Fig. 13. Summary of the deposition and stacking of the channel fills within the Upper Brushy Canyon Mbr. with a schematic log going upsection. Beaubouef et al., 1999.

Brushy Canyon Formation: Salt Flat Bench

1. Location:

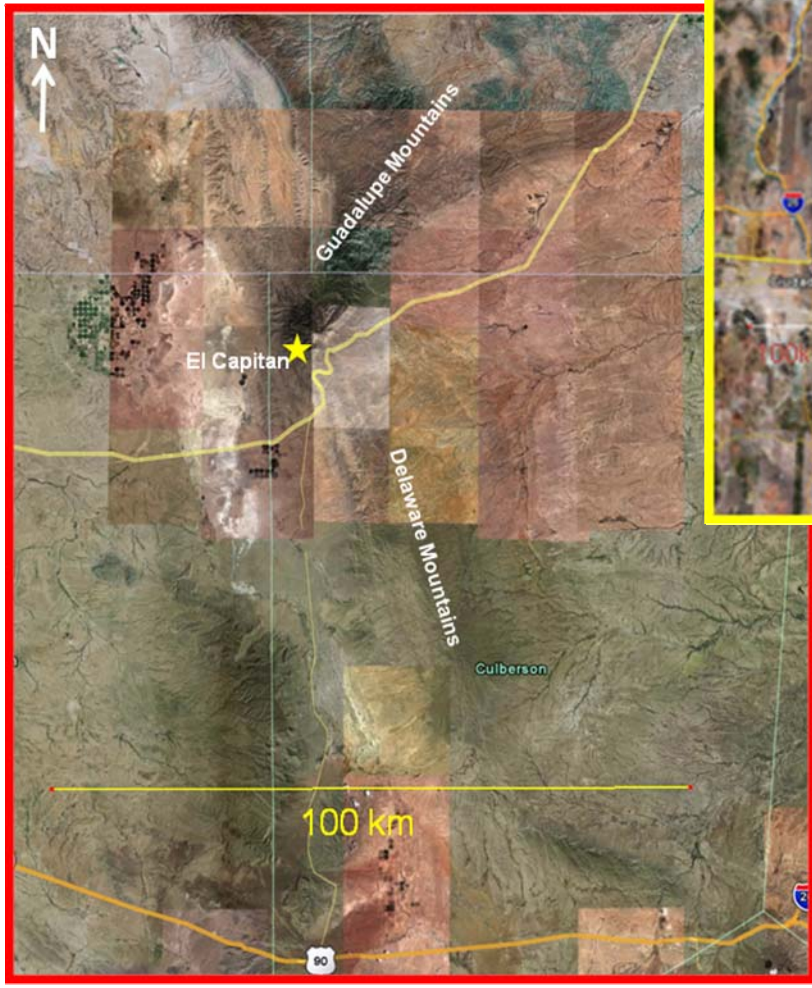

Regional (above) and local (left) google earth maps showing the Guadalupe and Delaware Mountains and the Brushy Canyon outcrop belt (below right).

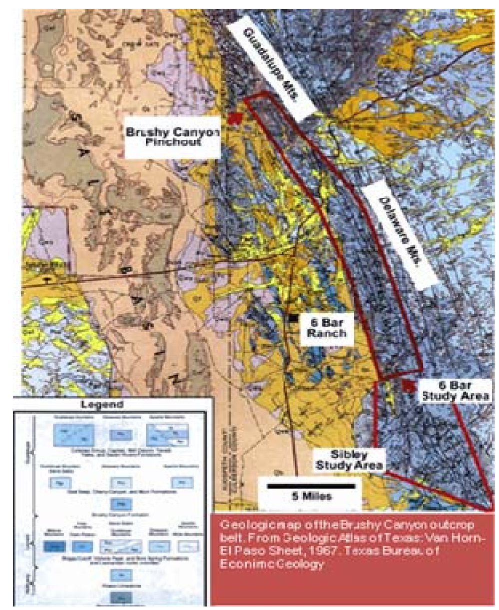

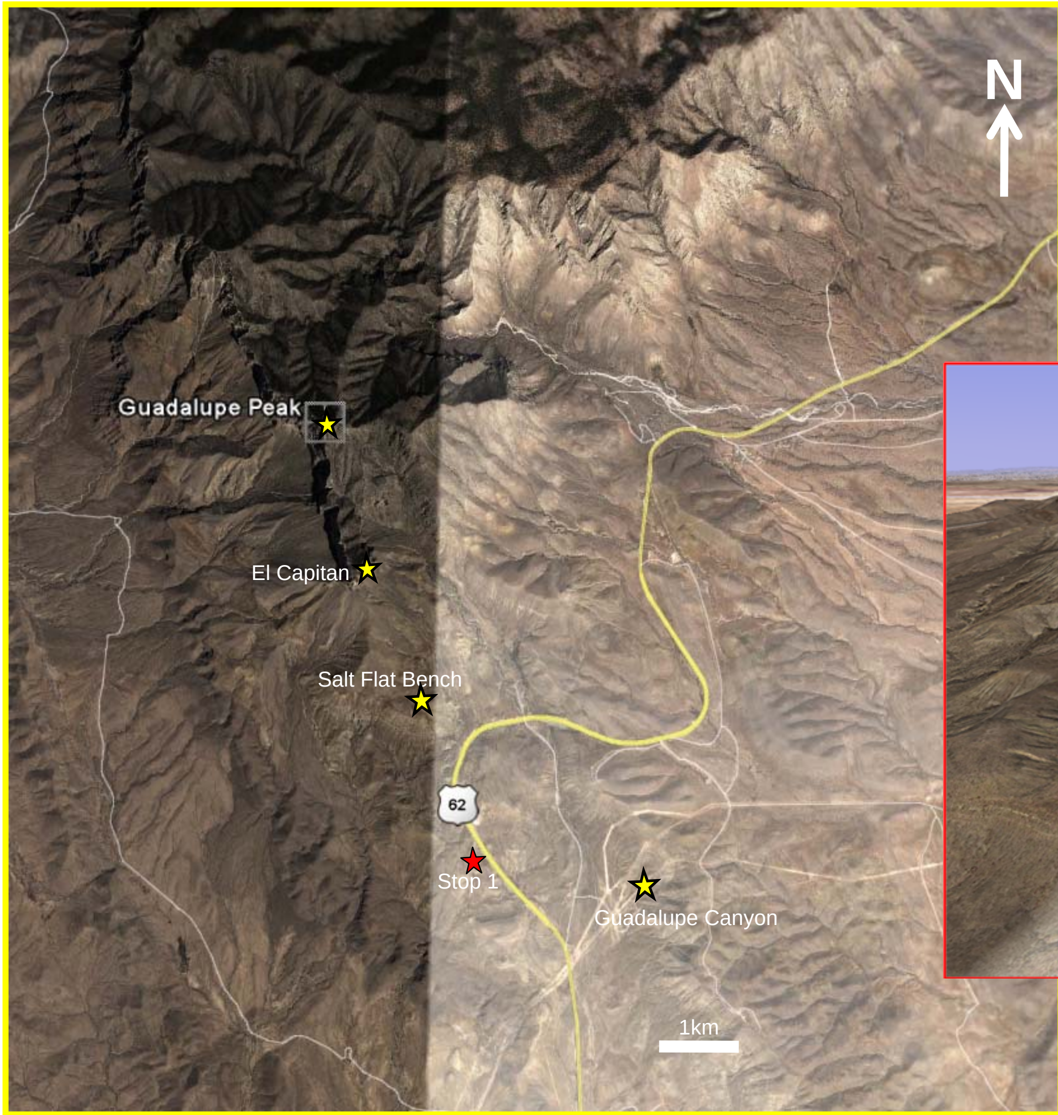

A map (left) showing the location of Salt Flat Bench in relation to El Capitan and Guadalupe Canyon.

A digital google earth aerial view (right) of Salt Flat Bench and El Capitan.

The inset photograph is taken from the location marked with the red star, looking up at El Capitan and Salt Flat Bench.

2. <u>Age and Stratigraphic Context:</u>

The Brushy Canyon Formation is Early Gualalupian in age and is interpreted to be the Low Stand Deposits of a 3rd order cycle. These sandstones and siltstones are believed to have been deposited during relative sea level low stands when the shelf is exposed and lack of shelfal accommodation space drives clastic sedimentation in the basin. Sub aerial exposure on the shelf caused the shut-down of the carbonate factory and allowed the clastic depositional systems to take over.

The Brushy Canyon Formation has been divided into Lower, Middle and Upper Brushy Canyon, based on laterally persistant siltstones believed to represent a 4th order late low stand wedge development concomitant with sand starvation in the Basin. Thinner siltstone deposits have also been interpreted as 5th order abandonment surfaces by Gardner & Borer (2000), on the basis of which the Brushy Canyon Formation was resolved into 7 Fans.

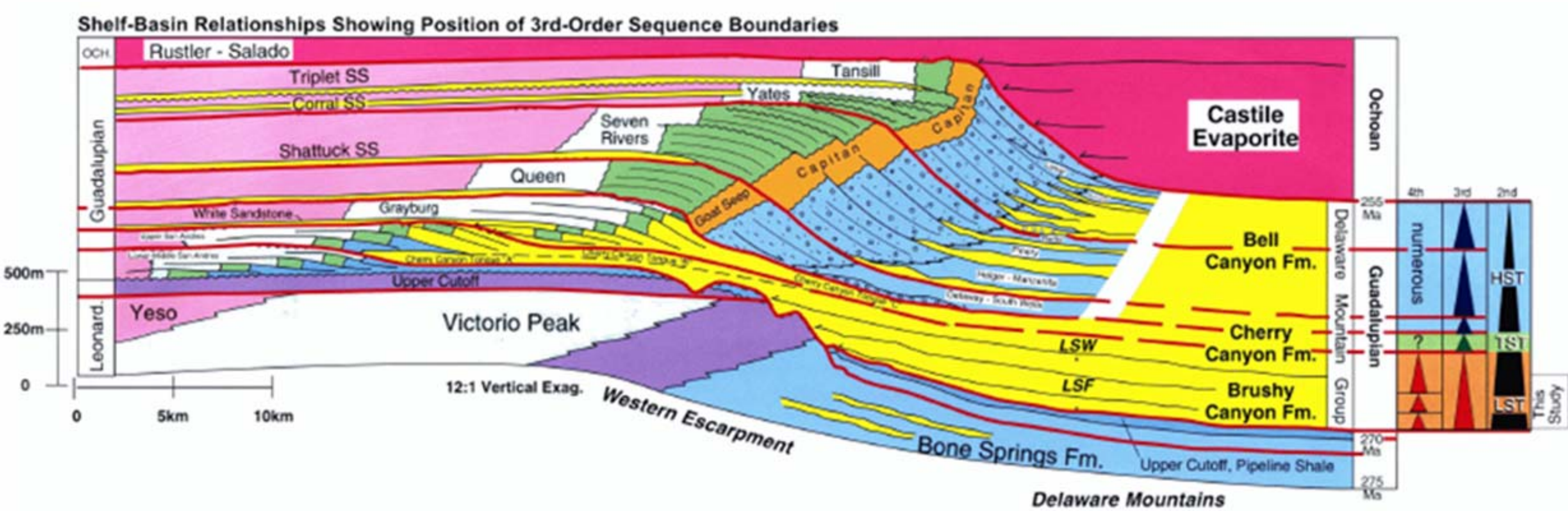

(Kerans & Fitchen. 1995)

These deep water siliciclastic deposits are about 360m/1500ft thick. They onlap against a relict carbonate slope, which consists of eroded shelf and slope carbonate deposits and is laterally correlatable to a karstification/ subaerial exposure surface farther back on the shelf. The steepness of the relict slope suggests that, initially, the slope was mainly a site of sediment bypass.

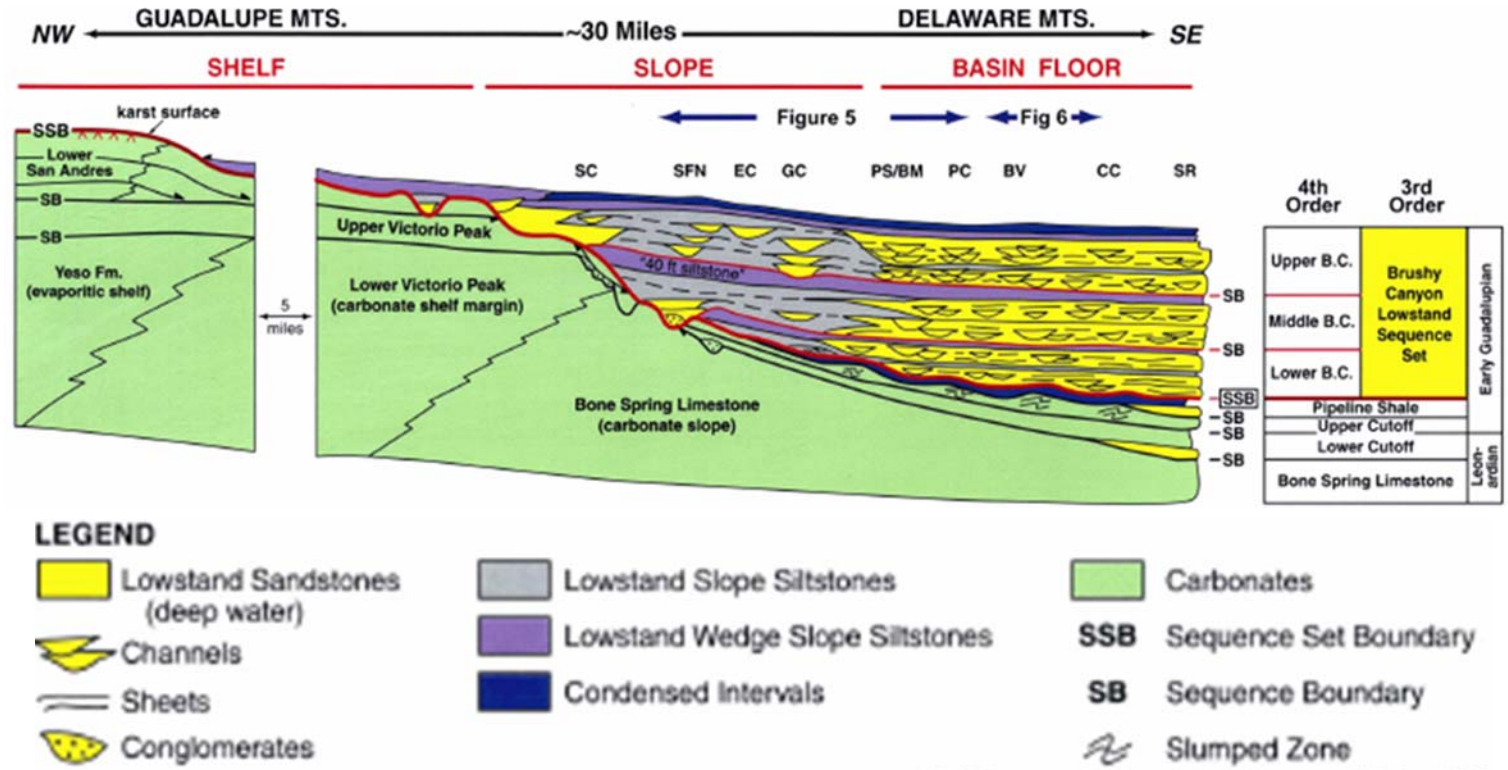

(Kerans & Fitchen, 1995)

1. <u>Siliciclastic Sediment Source</u>

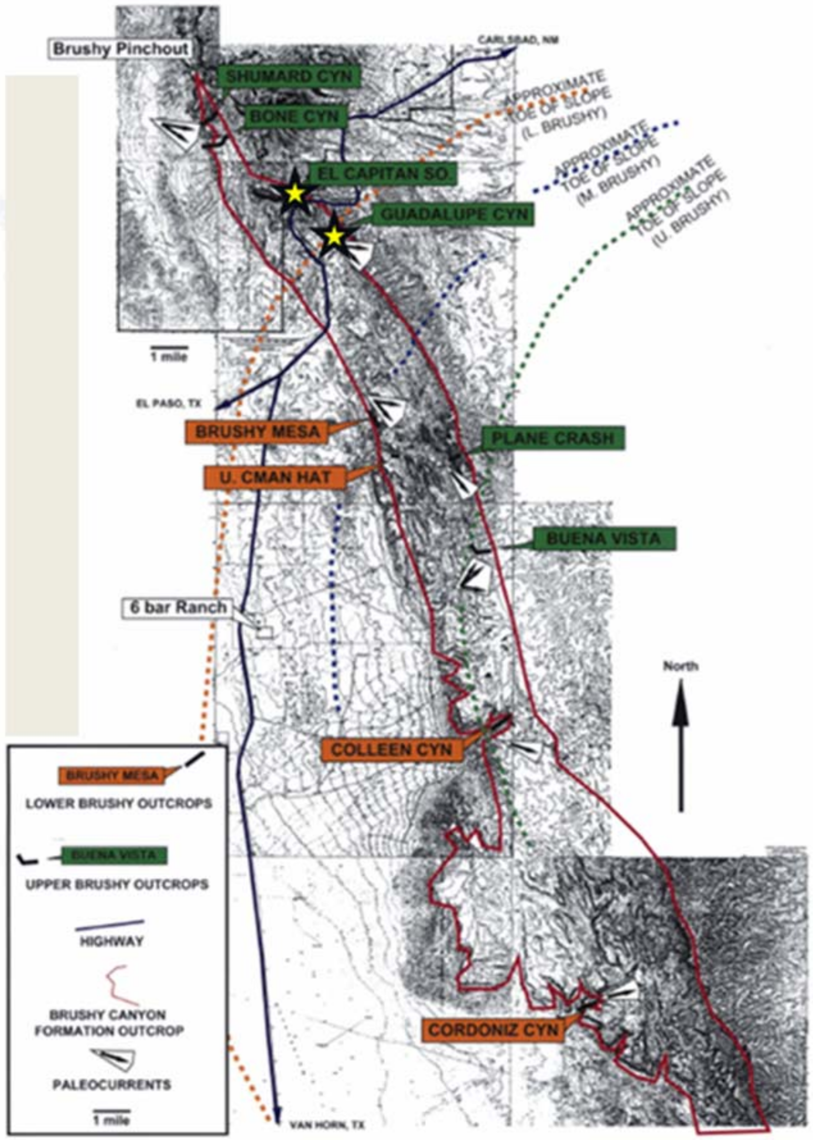

Paleocurrent data shows a variation in sediment transport direction for the Brushy Canyon Formation from North to South along the outcrop belt.

In the North sediment transport is towards the East or South-East

At some locations in the South sediment transport is towards the East and North-East.

Hence it is believed that sediment was supplied from the Northerwestern and Western margins of the basin.

Based on toe-of-slope location, the Brushy canyon deposits were prograding from lower to upper Brushy Canyon time.

The locations of Salt Flat Bench and Guadalupe Canyon are indicated with the yellow stars.

(modified from Beaubouef et al., 1999)

2. <u>Down-dip variation in sand-body architecture</u>

The architecture of siliciclastic deposits from slope to basin floor is a function of flow behavior in terms of net erosion, bypass or deposition. The transition from confined channel complexes on the slope to basin floor sheet sands is illustrated in the associated diagram.

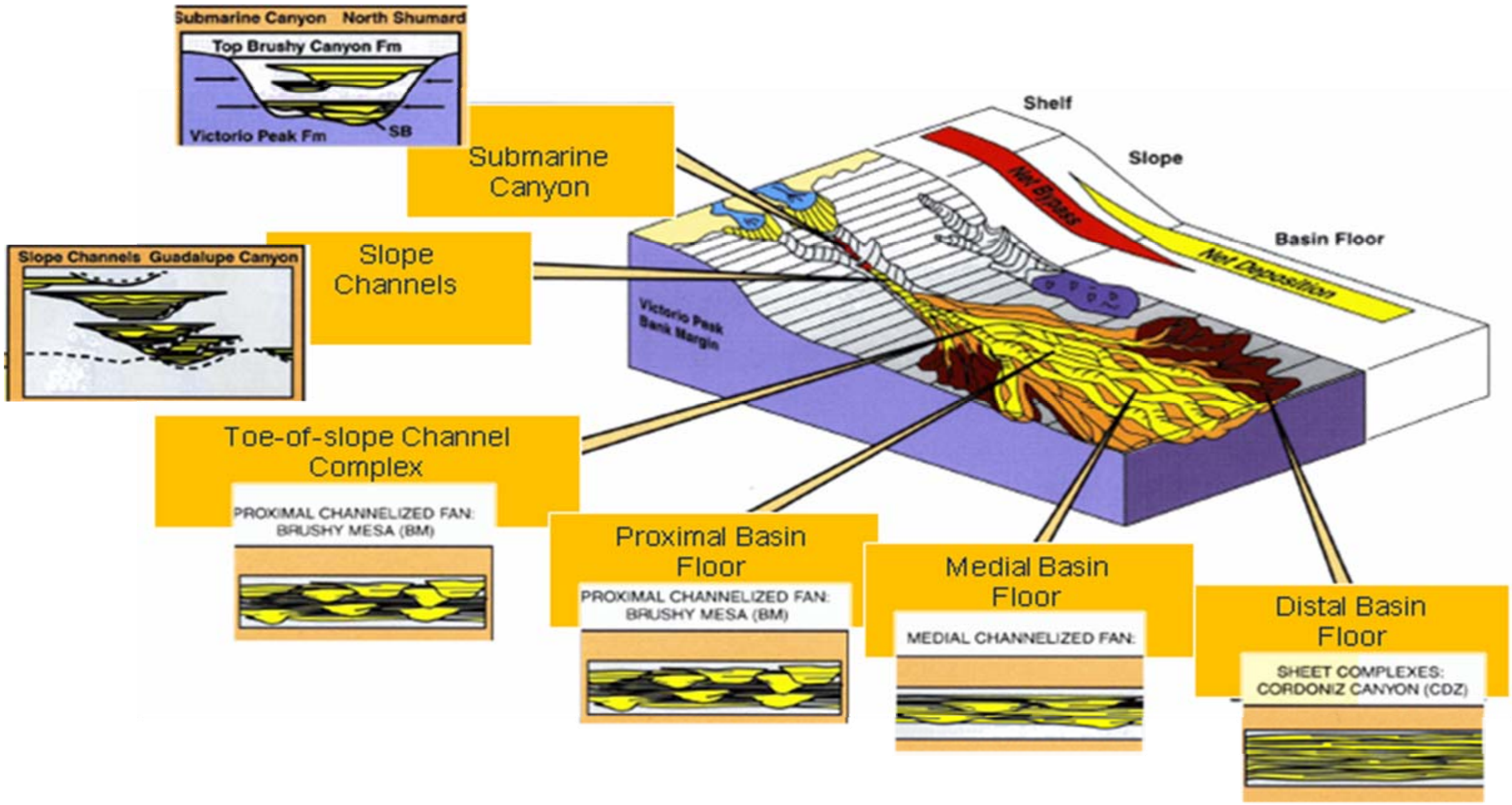

(modified from Beaubouef et al., 1999)

3. Salt Flat Bench

Salt Flat Bench is a 40m thick sand body, which extends laterally for more than a kilometer.

Erosional truncations at the base of the sand body have been interpreted as slump scars. The sand-body is believed to be housed within a 'spoon-shaped' master confinement created by repreated slump scars.

Multiple truncation surfaces within the deposit have been attributed to repeated episodes of cut-and-fill.

The proportion of sand decreases laterally, interpreted as the gradation into overbank deposition.

This deposit is a large isolated sand-body encased in siltstones, interpreted as characteristic channelized deposit found in upper slope settings

A view from Highway 62, looking up at El Capitan and Salt Flat Bench

The abundant siltstones are believed to be the result of deposition away from the main sand fairways. Two siltstone lithofacies have been described by previous workers.

1. Light grey laminated siltstones with milli-meter scale graded laminations are interpreted as deposits of dilute, fine-grained turbidity currents

2. Dark grey organic rich siltstones which contain organic content derived from marine algae. These are believed to represent hemipelagic sedimentation, characteristic of condensed intervals. These are excellent marker horizons.

The siltstone interval above the SFB gets steadily more organically rich and has been interpreted by Gardner & Borer (2000) as the

Chapter 3

DEVELOPMENT OF A TURBIDITE CHANNEL COMPLEX, SALT FLAT BENCH, BRUSHY CANYON FORMATION, GUADALUPE MOUNTAINS, TEXAS, AS AN OUTCROP ANLOGUE FOR SOUTH TIMBALIER 295 TURBIDITE SANDS

Abstract

A turbidite channel complex of the uppermost Brushy Canyon Formation has macro-scale geometry similar to Gulf of Mexico turbidite sands observed through subsurface data. This outcrop analogue provides insight into finer-scale variation not imaged with geophysical data. Channel elements include erosional surfaces, silt drapes, and initial and subsequent fill. Sands thicken and coarsen toward the axis of the channel complex where they are very thickly bedded and medium-grained with large rip-ups. Channel margins preserve silts and medium-to-very fine sands displaying complete Bouma sequences. Topography on a slump scar controlled the distribution of sands and steered channels toward the axis of the depositional low where coarser amalgamated sands accumulated. Flanks of the depositional low preserved less energetic events and were less prone to amalgamation by subsequent turbidite events. Subsurface observations of the K40 turbidite sand (South Timbalier 295, offshore Louisiana) deposited in a salt-withdrawal minibasin reveal

thicker, amalgamated sands downdip and thinner sands with interbedded shales preserved on the flank of the minibasin.

Introduction

To complement our investigation of the K40 turbidite sand of the South Timbalier 295 (ST295) field located offshore Louisiana (Hoover et al., 1997), we studied an outcrop analogue to gain insights into the facies architecture of deep water gravity-flow deposits. An outcrop analogue allows observation at a scale not resolved by subsurface wireline and seismic data. There are many subsurface Gulf of Mexico turbidite studies (for example, Mahaffie, 1994; Holman and Robertson, 1994; and Galloway and McGilvery, 1995) that rely on cores, geophysical logs, and seismic data to characterize reservoir sands. Use of an outcrop analog promotes understanding of lateral variations of the K40 sand and other analogous Gulf of Mexico reservoirs that are poorly resolved by geophysical data.

The Brushy Canyon Formation (middle Permian, lower Guadalupian), exposed in the Guadalupe and Delaware Mountains of west Texas, is a 0 - 1000 ft. thick sequence of deep-water siltstone and sandstone deposited in the Delaware Basin by gravity-driven flows (Harms, 1988; Harms and Williamson, 1988; Rossen and Sarg, 1988; Zelt and Rossen, 1995) (Figures 3.1 and 3.2). This large volume of siliciclastic sediment onlaps the carbonate ramp to the north.

The primary goals of this study are to observe and characterize lateral variability in channelized turbidites and to compare and contrast these observations with those from ST295. This is not intended to be a comprehensive study of Brushy Canyon deposition. Rather, we focus on a single outcrop to characterize deep water sands and infer depositional processes. We then return to our observations from the Gulf of Mexico and draw potential parallels.

Geologic Setting

The study locality, Salt Flat Bench, is located 1.5 km south of El Capitan peak at the western margin of the Delaware basin and the southern limit of the Guadalupe Mountains, (Figure 3.3). The top of this prominent bench, viewed from US route 62/180, marks the upper contact of the Brushy Canyon Formation with the overlying Cherry Canyon Formation.

The development of the Delaware Basin was controlled by faults in the Proterozoic basement of the region (Oriel et al., 1967; Hills, 1984). Bounded to the west by the Diablo platform, to the east by the Central Basin platform, and to the north by the Northwestern shelf, the Delaware basin remained low throughout the Permian (Figure 3.1) (Hills, 1984).

The Delaware Mountain Group, composed of the Brushy Canyon, Cherry Canyon, and Bell Canyon Formations (Figure 3.2), varies from 0 to 3000 feet in thickness in the Delaware Basin and is well-exposed at the southern limit of the Guadalupe Mountains, along the western escarpment, and throughout the Delaware Mountains southeast of the study area. Prominent ledges, largely composed of thickly-bedded massive sandstone, are interpreted by King (1948) to be channels and channel complexes. Recessive intervals are composed of thinly-bedded very fine sands and silts.

Siliciclastic sediments of the Delaware Mountain Group (Permian; Guadalupian) unconformably overlie the Leonardian Bone Spring and Cutoff limestones (Figure 3.2). King (1942, 1948) published the first comprehensive field studies that established relationships between shelf, ramp, and basin sediments. Brushy Canyon sands are interpreted to have been transported to the basin across unconformities within the San Andres Formation (Kerans et al., 1993; Fitchen, 1993; Sonnenfeld, 1993; and Sarg and Lehman, 1986). Wilde (1986) and Kirkby (1988) demonstrate the erosional base of the Brushy Canyon that tops the Cutoff and Victorio Peak Formations basinward of the San Andres Formation.

The geologic setting of the Permian Basin is very different from the Gulf of Mexico, yet in both basins, gravity-driven flows delivered sands to deeper water. The Brushy Canyon Formation is generally accepted as a deep-marine sandstone, though the depositional mechanism has been debated (Harms, 1974; Harms and Williamson, 1988; Rossen and Sarg, 1988, Berg, 1979; Bozanich, 1979). Proponents of a thermohaline density current interpretation note siltstone drapes and a scarcity of classic Bouma sequences (Harms, 1974). Rossen and Sarg (1988) propose point-sourcing of siliciclastics, regional correlation to a paleoshelf disconformity, and normal-marine shallow waters on paleoslopes as evidence against the thermohaline density current interpretation. The distinction between turbidity current and debris flow deposits is also a difficult issue to resolve. Discussion (Hiscott et al., 1997) and reply (Shanmugam et al., 1997), centered on the interpretation of North Sea basin-floor fans, demonstrates the ongoing development of process interpretations of gravity-flow deposits.

Regardless of whether the sandstones of Salt Flat Bench represent turbidity current, thermohaline density flow, or debris flow deposits, they provide a unique perspective on a turbidite channel complex. Numerous channel exposures in the Delaware basin region can be observed in outcrop (photos in Harms and Williamson, 1988), and channels have been inferred from closely-spaced well penetrations of the Brushy Canyon and overlying Cherry Canyon Formations (Harms and Williamson, 1988). The outcrop face described in this study trends perpendicular to flow orientations discussed below and allows us to observe lithofacies variation along an axis-to-margin channel profile.

Field Observations

The sandstones that form Salt Flat Bench are well exposed on its eastern, western, and southern faces. Location A (Figure 3.3) is the western face of Salt Flat Bench with 1600 feet (lateral distance) of exposure that was measured and described in detail at seventeen measured sections (Figures 3.4 and 3.5). From a distance, this outcrop shows sandstones which thin significantly to the north. These cliff-forming sands terminate northward, incising and truncating thinly-bedded very fine sands and silts. To the east, the southern

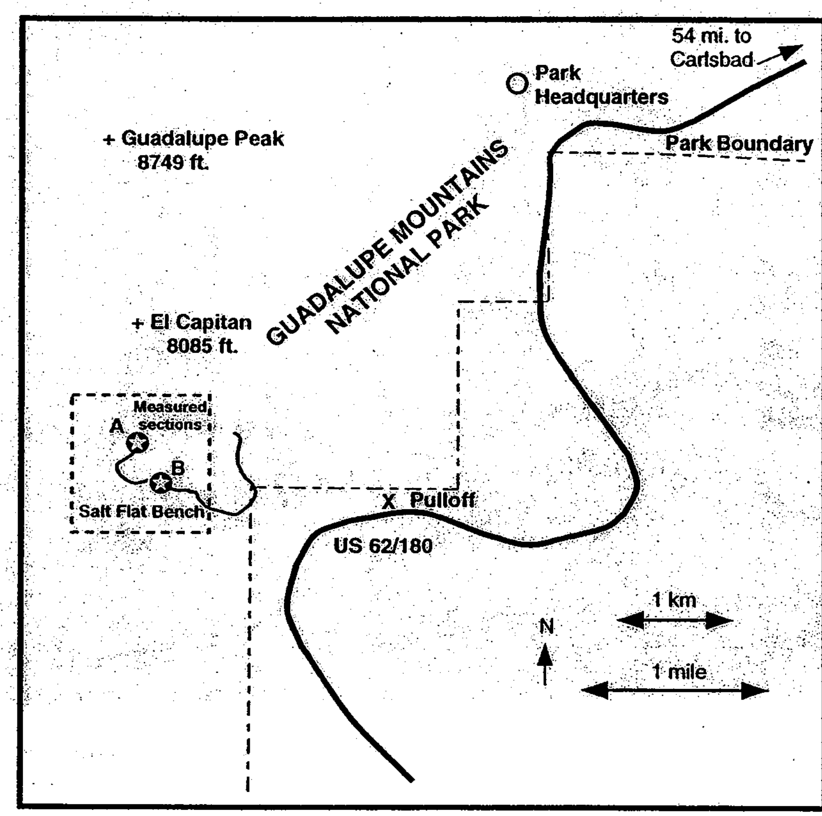

Figure 3.3. Orientation map of Salt Flat Bench study area located at the southern tip of the Guadalupe Mountains within the national park limits. Access to the outcrop is from a pull-off from US62/180 (marked with X on map) that was the old highway.

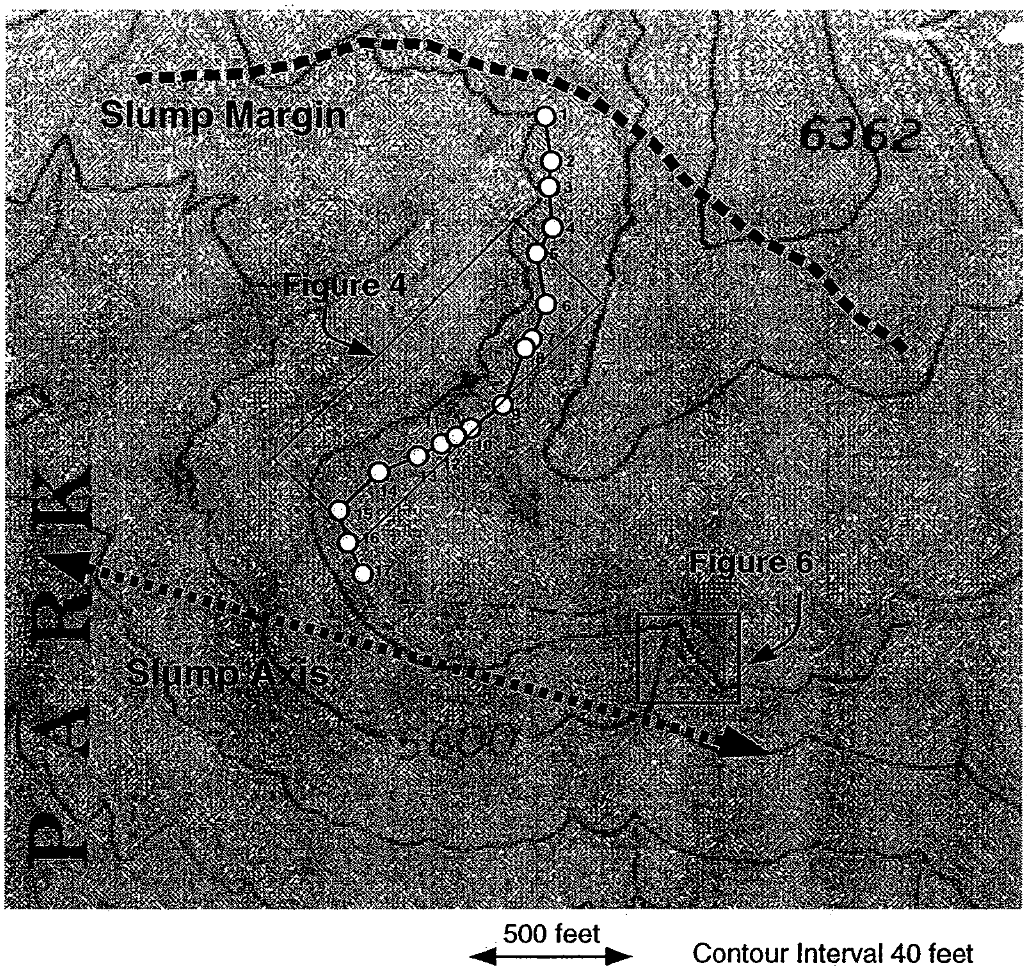

Figure 3.14. Inferred slump orientation in map view, as interpreted from measured sections. Axis of slump is unknown because bench is eroded to south, but orientation is interpreted to parallel dominant flow orientation measured from massive sands in facies D_L. For reference, locations of Figures 3.4 and 3.6 (photos of southward-thickening sandstones are outlined.

The American Association of Petroleum Geologists Bulletin
V. 72, No. 3 (March 1988), P. 299-317, 16 Figs.

Deep-Water Density Current Deposits of Delaware Mountain Group (Permian), Delaware Basin, Texas and New Mexico[1]

JOHN C. HARMS[2] and CHARLES R. WILLIAMSON[3]

ABSTRACT

The Guadalupian Delaware Mountain Group is a 1,000-1,600-m (3,281-5,250-ft) thick section of siltstone and sandstone deposited in a deep-water density-stratified basin surrounded by carbonate banks or reefs and broad shallow evaporite-clastic shelves. The most prevalent style of basinal deposition was suspension settling of silt. Laminated siltstone beds are laterally extensive and cover basin-floor topographic irregularities and flat-floored channels as much as 30 m (99 ft) deep and 1 km or more wide. Channels can be observed in outcrop at the basin margin and can be inferred from closely spaced wells in the basin. The channels are straight to slightly sinuous, trend at high angles to the basin margin, and extend at least 70 km (43 mi) into the basin. Sandstone beds, confined to channels, form numerous stratigraphic traps. Hydrocarbon sealing beds are provided by laminated organic siltstone, which laterally can form the erosional margin where channels are cut into siltstone beds. Thick beds of very fine-grained sandstones fill the channels. These sandstones contain abundant large and small-scale traction-current-produced stratification. These sandy channel deposits generally lack texturally graded sedimentation units and show no regular vertical sequence of stratification types or bed thickness.

Outcrop and subsurface evidence indicates Delaware Mountain Group sediments were deposited by saline density currents. Dense saline water originated on evaporitic shelves and spilled across the carbonate rim, down steep marginal slopes, and into the basin. Basinal waters were density stratified. Denser flows moved along the basin floor cutting channels or depositing sand in existing channels; less-dense flows moved along density interfaces in the water column and carried silt-size material far into the basin where it settled to the floor as thin alternating layers of detrital silt and organic debris. Little proximal to distal change occurred in the size or nature of the channels. Exploration predictions based on submarine fan models formed by turbidity currents would anticipate very different proximal-distal changes in sandstone geometry and facies.

[1]Manuscript received, July 7, 1986; accepted, August 24, 1987.

[2]Harms & Brady, Inc., P. O. Box 406, Littleton, Colorado 80160-0406.
[3]Unocol UK, Ltd., 32 Cadbury Road, Sunbury-on-Thames, Middlesex TW16 7LU, England.

Work on the Delaware Mountain Group was done while J. C. Harms was employed at the Marathon Oil Research Center and C. R. Williamson was a graduate student at the University of Texas, Austin, Texas. Support for C. R. Williamson was provided by grants from the Texas Petroleum Research Committee, Geological Society of America, Phillips Petroleum, and Sigma Xi. Thanks to the Exxon Company USA, Amoco Production Company, and the Geological Information Library of Dallas, Texas, for allowing access to cores, logs, and base maps. Thanks to Unocal for providing drafting assistance for this manuscript, and to M. H. Link, J. Sarg and T. H. Nilsen for their thoughtful suggestions and criticisms in their reviews of this manuscript.

INTRODUCTION

During the middle Permian (Guadalupian) the Delaware basin was a nearly circular basin approximately 160 km (100 mi) in diameter. The deeper water central basin was rimmed by banks and reefs adjacent to broad shallow-water shelves, lagoons, sabkhas, and alluvial plains. Approximately 1,000-1,600 m (3,281-5,250 ft) of terrigenous silt and sand of the Delaware Mountain Group (Guadalupian) (Figure 1) was deposited in the central basin, where water depths are estimated to have been 300-600 m (984-1,969 ft) (King, 1948; Newell et al, 1953; Meissner, 1972; Harms, 1974; Crawford, 1979).

Previous sedimentological studies of the three Delaware Mountain Group formations (Brushy Canyon, Cherry Canyon, and Bell Canyon) (Harms, 1968, 1974; Jacka et al, 1968; Payne, 1976; Williamson, 1978, 1979; Berg, 1979; Bozanich, 1979) have generated much controversy regarding depositional processes. This paper summarizes primarily outcrop and subsurface data from the Brushy Canyon and Bell Canyon Formations (Harms, 1968, 1974; Williamson, 1977, 1978, 1979), and draws on other recent studies of the Delaware Mountain Group and time-equivalent shelf facies to interpret their depositional processes.

We conclude that the basinal sediments of these formations were deposited by saline density currents (Figure 2). Dense shelf water spilled through channels in surrounding carbonate banks, flowed down marginal slopes, and along the basin floor. The denser flows cut channels or deposited sandstone beds confined to channels. At other times, less-dense shelf water spread over more-dense stagnant basin water, as density interflows and rained suspended silt over the basin floor. As a result, the rocks show a distribution of facies, geometry of sandstone units, and vertical arrangement of textures and structures different from rocks common to turbidity currents and submarine fans dominated by episodic sediment-gravity flows. Sandstone mostly is confined to nonbranching linear channels, which form numerous stratigraphic traps. The geometry and trend of channel fills are directly related to the depositional mechanism. One must understand the origin of the channels and the channel fill to better define exploration objectives and aid in develop-

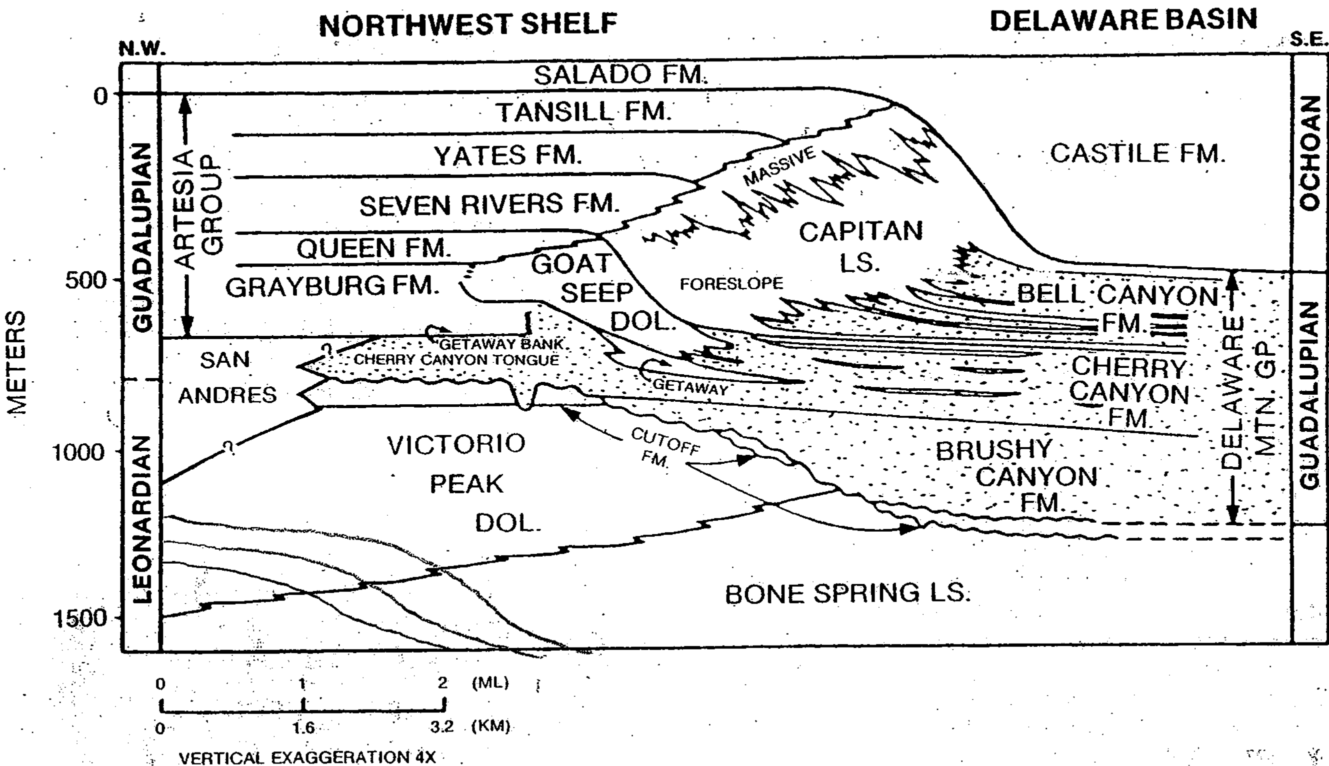

Figure 1—Permian stratigraphic relations, Delaware basin (from Crawford, 1981; originally modified from King, 1948; Tyrrell, 1962; and Hayes, 1964).

ment of the more than 150 oil and gas fields producing from the Delaware Mountain Group in the Delaware basin.

STRATIGRAPHIC AND PALEOGEOGRAPHIC SETTING

Water Paleodepth

The stratigraphic relations among shelf, marginal, and basinal Permian rocks in the Guadalupe Mountains were first comprehensively clarified by King (1942, 1948). Subsequent studies by Newell et al (1953), Boyd (1958), Hayes (1964), King (1965), Oriel et al (1967), and Meissner (1972) provided further refinement of regional facies interpretations and stratigraphic correlations (Figure 1). However, detailed correlations between the basin and shelf for some stratigraphic intervals have remained controversial.

For the upper part of the Delaware Mountain Group (Cherry Canyon and Bell Canyon Formations), the carbonate talus may be seen from the base of the slope updip to shelf margin rocks interpreted to have been deposited at or near sea level. Water paleodepths are estimated to have been 300-600 m (984-1,969 ft) for the upper part of the Bell Canyon Formation (King, 1948; Newell et al, 1953). The shelf-to-basin relief of the Goat Seep–Cherry Canyon transition is approximately 300-400 m (984-1,312 ft) (Crawford, 1979). No direct measurement of the shelf-to-basin relief is possible for the early Guadalupian Brushy Canyon Formation because outcrops unconformably abut against older (Leonardian) rocks (Figure 1). Harms (1974) presented evidence to suggest water paleodepths in excess of 300 m (984 ft) during deposition of the Brushy Canyon Formation.

Stratigraphy

Shelf rocks of the Artesia Group are time equivalent to the upper part of the Delaware Mountain Group (Figure 1) (Meissner, 1972; Smith, 1974). Shelf, as the term is applied here, is not nearly as deep as modern continental shelves. Shelf facies represent a complex of shallow-water peritidal, lagoonal, and emergent flat environments where water depths probably never exceeded several meters. The shelf section generally consists of alternating thick carbonate units and thinner siltstone and sandstone units. The entire shelf section grades landward into red beds and evaporites toward the west and north. Coeval shelf facies of the Brushy Canyon and lower Cherry Canyon Formations are less certain, but at least part of the San Andres Limestone is probably correlative (Figure 1).

Shelf-margin rocks equivalent in age to the upper Delaware Mountain Group consist dominantly of massively bedded limestone and dolomite (Capitan and Goat Seep formations). These carbonate rocks interfinger with siltstone and sandstone of the Cherry Canyon and Bell Canyon Formations in spectacular outcrops along the eastern edge of the Guadalupe Mountains. Interpretations of seismic and outcrop data in the Delaware basin suggest that slightly older siltstone and sandstone of the Brushy Canyon Formation onlap the toe-of-slope facies of the

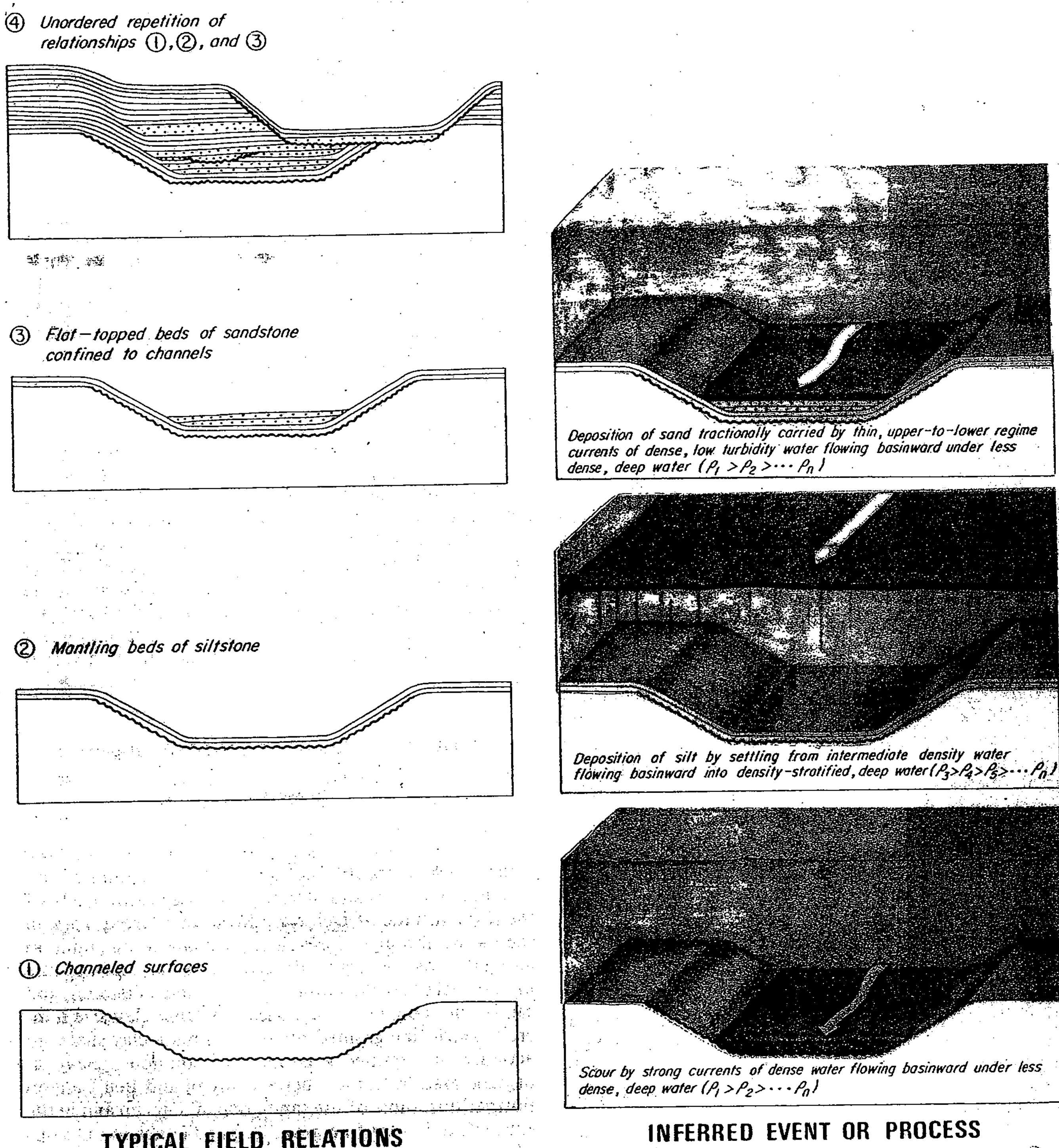

Figure 2—Typical bedding relations in Delaware Mountain Group and their interpretations (from Harms, 1974).

middle San Andres Formation, separated by an erosional sequence boundary (Sarg and Lehmann, 1986). Correlations between basin and shelf are by no means solved for the lower part of the Delaware Mountain Group. The Brushy Canyon Formation must have had shelf equivalents (Wilde, 1986), but they may have been eroded during periods of relatively low sea level.

Tongues of allochthonous carbonate debris derived from the shelf margin are interbedded with siltstone and sandstone in the Delaware Mountain Group. The Lamar Limestone, the uppermost member of the Bell Canyon Formation, is one of many prominent carbonate units that can be traced in outcrop into lower slope carbonate facies of the Capitan Formation (Tyrrell, 1962, 1969; L. Babcock, 1977). Basinward, the Lamar and other limestones in the Delaware Mountain Group become dark organic-rich calcareous siltstones. The Lamar equivalent in the subsurface is referred to as the "Delaware lime."

The Delaware Mountain Group is underlain by the Leonardian Series, a sequence of basinal limestone chert and siltstone. Erosional channels filled with lime mudstone in a style similar to Delaware Mountain Group channel fills suggest that density current processes were important in the Leonardian as well as in the Guadalupian (Harms and Pray, 1974). The Ochoan Series overlying the Delaware Mountain Group reaches a maximum thickness of about 550 m (1,804 ft) and consists mainly of evaporites with increasing amounts of red siltstone in the younger rocks. Evidence indicates that the varved evaporite units of the Castile Formation were abruptly deposited in fairly deep unagitated water in a restricted basin (Anderson et al, 1972; Dean and Anderson, 1982).

Shelf-To-Basin Sediment Supply

One of the most perplexing problems of Delaware basin stratigraphy is the relationship of shelf to basin terrigenous sediments. The thin widespread siltstone and sandstone units of the Artesia Group are believed to represent sediment supply routes for the petrographically similar siltstones and sandstones of the Delaware Mountain Group (Hull, 1957). These shelf units extend nearly to the shelf-margin crest, but few indications exist of how terrigenous sediment was transported through the carbonate shelf margin and down the slope. The origin of the shelf clastics and their relations to basinal sedimentation have generated a great deal of discussion regarding the influence of tectonics and sea level changes on sedimentation. One hypothesis states that the alternations of carbonate and terrigenous rocks on the shelf represent great fluctuations in sea level (10s to 100s of meters). According to this scenario, terrigenous sediments were spread across the shelf and into the basin during lowstands of sea level (Jacka et al, 1968; Meissner, 1969, 1972; Silver and Todd, 1969; Dunham, 1972). More recently, Pray (1977) proposed that the lack of emergence indicators in the Capitan (J. A. Babcock, 1977; Yurewicz, 1977) and the evidence for subaqueous deposition of shelf clastics and evaporites (Sarg, 1977) suggest that small sea level fluctuations (less than 0.5 m or 1.6 ft) satisfactorily explain sedimentation in the Guadalupian. Pray proposed that terrigenous clastics may have been supplied to the basin during maximum sea level by subaqueous currents originating from the spilling of saline lagoon waters.

We believe sufficient evidence exists to demonstrate contemporaneous carbonate and clastic deposition in a subaqueous environment at the outer shelf (Neese and Schwartz, 1977; Wheeler, 1977; Hurley, 1978; Crawford, 1981; McDermott and Scott, 1981). Great variations in sea level (10s to 100s of meters) are unnecessary to explain the observed sedimentation patterns. The mechanism for silt and sand transport and the conduit types that delivered sediment to the basin remain poorly explained, although recent studies have begun to resolve these problems (Crawford, 1981; McDermott and Scott, 1981).

At least three occurrences of terrigenous-filled slope-feeder systems have been recognized in outcrops of the Delaware Mountain Group: (1) a 100-m (328-ft) deep, 175 to 700-m (574 to 2,297-ft) wide channel filled with siltstone, sandstone, and conglomerate that probably is correlative with the Brushy Canyon Formation (Harms, 1974), (2) a "sheet" of Shattuck sandstone (a thin member of the Queen Formation), traceable across the shelf edge and 20-30 m (66-98 ft) down the foreslope separating the Capitan Limestone from the Goat Seep Dolomite (Crawford, 1981), and (3) basinward-trending channels (generally 35-m (115-ft) deep, 400-m (1,312-ft) wide) in the Cherry Canyon Formation sandstone tongue. These channels are transitional with shelf-edge facies of the Grayburg Formation and are filled with sandstone and allochthonous carbonate (McDermott and Scott, 1981).

Two of these occurrences are channel fills and are probably representative of the conduit types that delivered basin sediment. The sandstone sheet described by Crawford (1981) is interpreted to have been deposited where sand and silt spilled over a large area of the shelf margin. Stratigraphic relations at the basinward edge of the Shattuck spillover indicate that the shelf sandstones represent a relatively long time period, enough for at least 50 m (164 ft) of Goat Seep carbonate to prograde beyond the first sandstone that spilled over the shelf edge (Crawford, 1981). The distribution of sandstone in the subsurface (Williamson, 1978; Bozanich, 1979) suggests that both types of sediment delivery were important along various parts of the basin margin at different times.

LITHOLOGY OF DELAWARE MOUNTAIN GROUP

General

Siltstone and sandstone are the major lithologies of the Delaware Mountain Group. Limestone, dolomite, and conglomerate are estimated to comprise less than 5% of the total volume of Delaware Mountain Group rock in the basin, although these rock types are more common along the basin margins. Practically no clay shale occurs in the Delaware Mountain Group and siltstones and sandstones contain no significant detrital clay-size minerals. Dark fine-grained rocks resembling clay shale are actually fine-grained siltstone with abundant clay-size organic matter. In the Cherry Canyon and Bell Canyon Formations, most of the sandstone in outcrop and in the subsurface is very fine grained. Sandstones in outcrops of the Brushy Canyon Formation generally are fine-grained or very fine-grained, with granules or pebbles of older carbonate rock. The mineralogy, stratification types, fossils, and sedimentary structures in the Delaware Mountain Group formations generally are very similar.

Siltstone

Siltstone is the most common rock type in the Delaware Mountain Group. Siltstone comprises approximately 60-70% (estimate from measured sections) of the upper Bell Canyon Formation in the Delaware Mountains and the Brushy Canyon Formation along the western face of the Guadalupe Mountains (Figure 3). A comparable percentage of siltstone is estimated for the upper Bell Canyon Formation in the subsurface of the northern part of the basin. A higher proportion of sandstone and carbonate rocks is present within about a 20-km (13-mi) belt rimming the basin's edge. Bozanich (1979) noted that siltstone accounts for only about 25% of the section in the Cherry Canyon Formation within a 35-km (22-mi) band adjacent to the eastern shelf margin.

The dominant sedimentary structure in outcrops and cores of siltstone is even parallel light and dark laminae ranging from 0.2 to 2 mm (0.01 to 0.08 in.) thick (Figures 4A-C, 5A). Light-gray laminae are coarser grained and contain little organic matter, whereas darker laminae contain abundant organic matter and are composed of slightly finer silt grains. Individual laminae are graded in terms of organic material, with organic content increasing upward. No discernible textural grading of the quartz and feldspar fraction occurs within siltstone laminae or beds. The median diameter of the siltstone ranges from 10 μm to 60 μm. Laminated siltstone commonly contains 5-30% very fine grained sand having a maximum size of 0.1 mm (0.04 in.).

Most siltstone laminae are nearly horizontal and parallel with boundaries of interbedded sandstones. However, in some outcrops and cores, siltstone beds and laminae are locally inclined at angles to the overall bedding (Figures 4D, 6B). Siltstone laminae and beds drape underlying erosional surfaces, marking channel margins. Siltstone beds also cover ripple marks, convex-upward tops of sandstones, and small scours. In all examples, siltstone laminae and beds maintain a nearly constant thickness laterally and mimic the configuration of underlying surfaces. Relations of these siltstones are best observed on outcrops along the western face of the Guadalupe Mountains. The massive, nearly vertical exposures of this area show that siltstone beds drape the erosional outlines of channels and can be traced across channels into interchannel areas with no appreciable change in thickness (Figure 6B). Similar types of mantling relations can be observed on a smaller scale in outcrops in the Delaware Mountains. Laminated siltstone is interpreted from subsurface data to drape large channels and extend into interchannel areas (Williamson, 1978; Berg, 1979) where it can be traced for several kilometers by log correlations.

Features of the laminated siltstone indicate that sediment was deposited from suspension, largely unaffected by bottom currents. Evidence supporting this kind of origin include (1) siltstone drapes underlying surfaces as a uniformly thick blanket, (2) regularity of delicate laminae, lateral continuity of siltstone units, and the general lack of evidence for bottom current activity, (3) abundance of laminated organic material enriched in marine palynomorphs, suggestive of very slow deposition rates, and (4) individual graded silt-organic laminae in siltstone.

plant spores

The siltstone is subarkosic (15-25% feldspar), and similar in composition to the interbedded sandstone. Clay minerals, micas, and microcrystalline carbonate are minor components of most siltstone except for a few dark, clayey, or calcareous siltstones with abundant organic matter. Siltstone is cemented by sparry calcite with lesser amounts of authigenic clay, quartz, and feldspar. Porosity ranges from less than 5% for the finer grained varieties to 22% for some weakly cemented sandy coarse siltstones. Acid-insoluble organic matter from siltstone samples is mostly amorphous and unstructured kerogen. Residues contain abundant marine palynomorphs and pyrite with very little land-derived plant cuticle or woody fragments. Only the more buoyant types of land-derived palynomorphs, such as bladdered conifer pollen, are present.

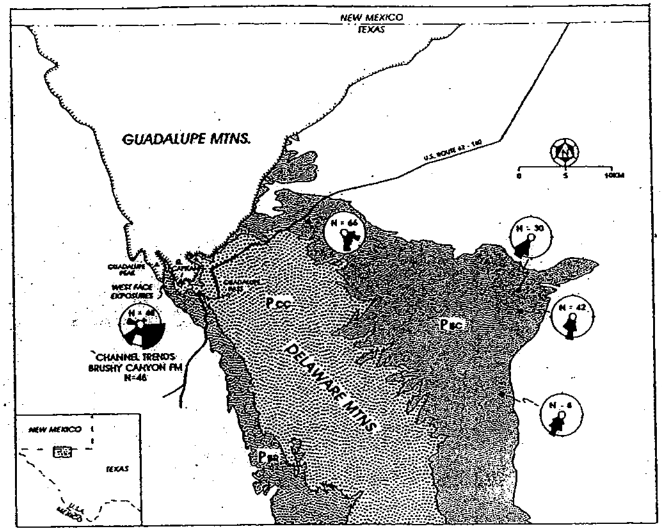

Figure 3—Simplified geologic map of Guadalupe and Delaware Mountains. Outcrop of Delaware Mountain Group is stippled. (PBR = Brushy Canyon, PCC = Cherry Canyon, PBC = Bell Canyon.) Paleocurrent measurements of ripple marks in Bell Canyon Formation in Delaware Mountains and channel trends in Brushy Canyon Formation along west face of Guadalupe Mountains are shown.

Source rock analyses of nine representative siltstone core samples from the upper part of the Bell Canyon Formation in the El Mar and Grice fields show large amounts of unstructured type II kerogen (terminology of Tissot and Welte, 1978). Total organic carbon (TOC) by weight ranges from 0.44 to 5.64% with a mean of 2.58%. Extractable organic matter ranges from 180 ppm (bioturbated, sandy coarse-grained siltstones) to 2,847 ppm (laminated fine-grained siltstone; Figure 5B) with a mean value of 1,513 ppm. The total C^{15+} hydrocarbon fraction ranges from 99 to 1,550 ppm (mean = 789 ppm). The Delaware Mountain Group siltstones seem to be good source rocks and are the most likely source for oils in the interbedded sandstones.

Even parallel laminae are by far the most prevalent structure in siltstones, although bioturbated (Figures 5C, D) siltstones are present at many levels. The degree of bioturbation ranges from slightly disrupted zones less than 1.0 cm (0.39 in.) thick to moderately churned zones several meters thick. Nearly all disruption of laminae is caused by crawling or browsing traces parallel with bedding (*Helminthoida* of the *Nereites* ichnofacies). Rare backfilled vertical burrows identified as *Zoophycus* have been reported from cores of the Cherry Canyon Formation (Bozanich, 1979). Rare occurrences of impressions

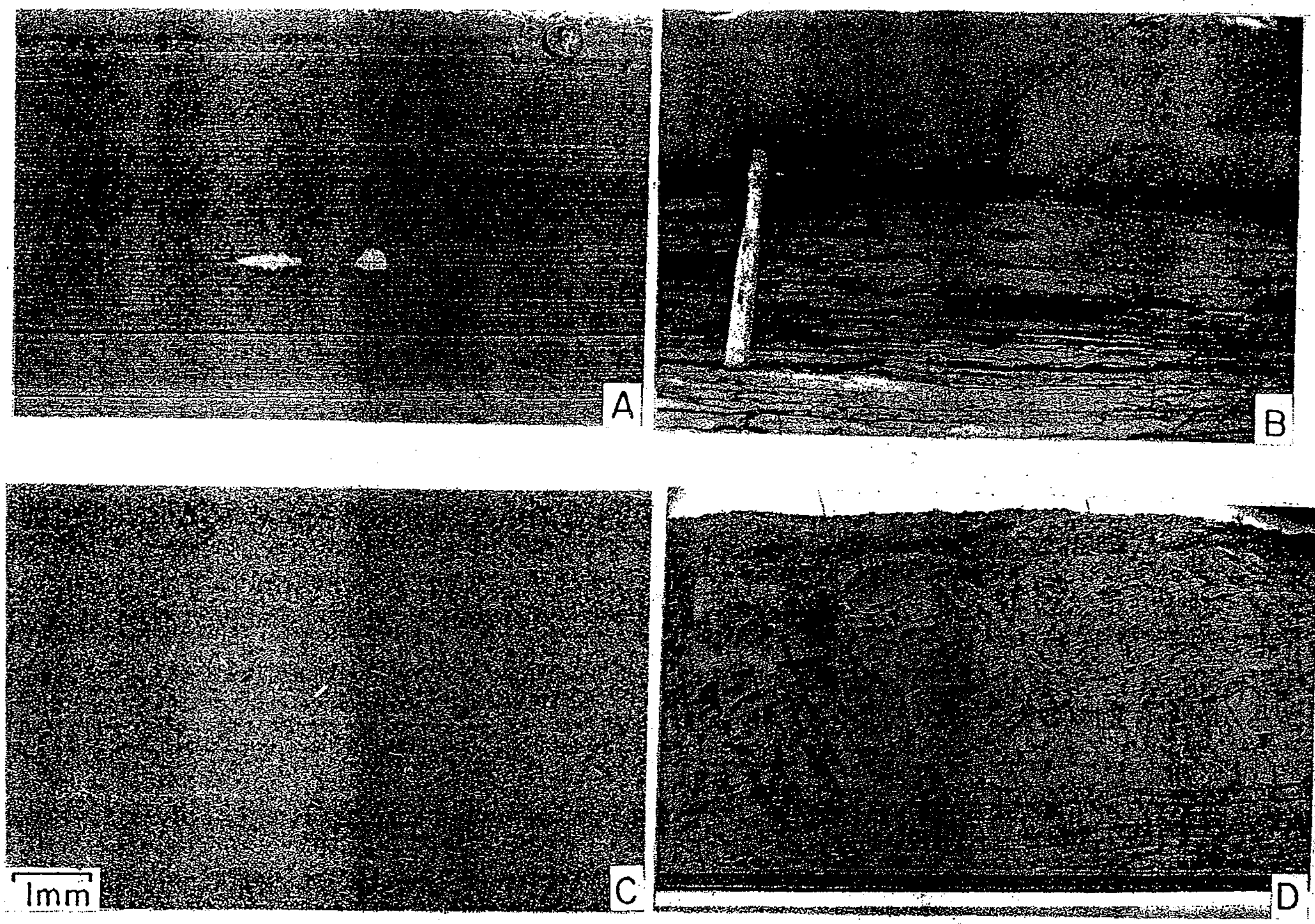

Figure 4—Laminated siltstones: (A) close-up of outcrop of laminated siltstone, Bell Canyon Formation, penny for scale; (B) sandstone-siltstone contact, Bell Canyon Formation; (C) negative print of thin section of laminated siltstone; organic-rich laminae (light colored) separate sandy, coarse silt laminae, Bell Canyon Formation; (D) siltstone-filled channel, Cherry Canyon Formation at Guadalupe Pass. Laminated siltstone is inclined as much as 25° and drapes the erosional margin of the channel.

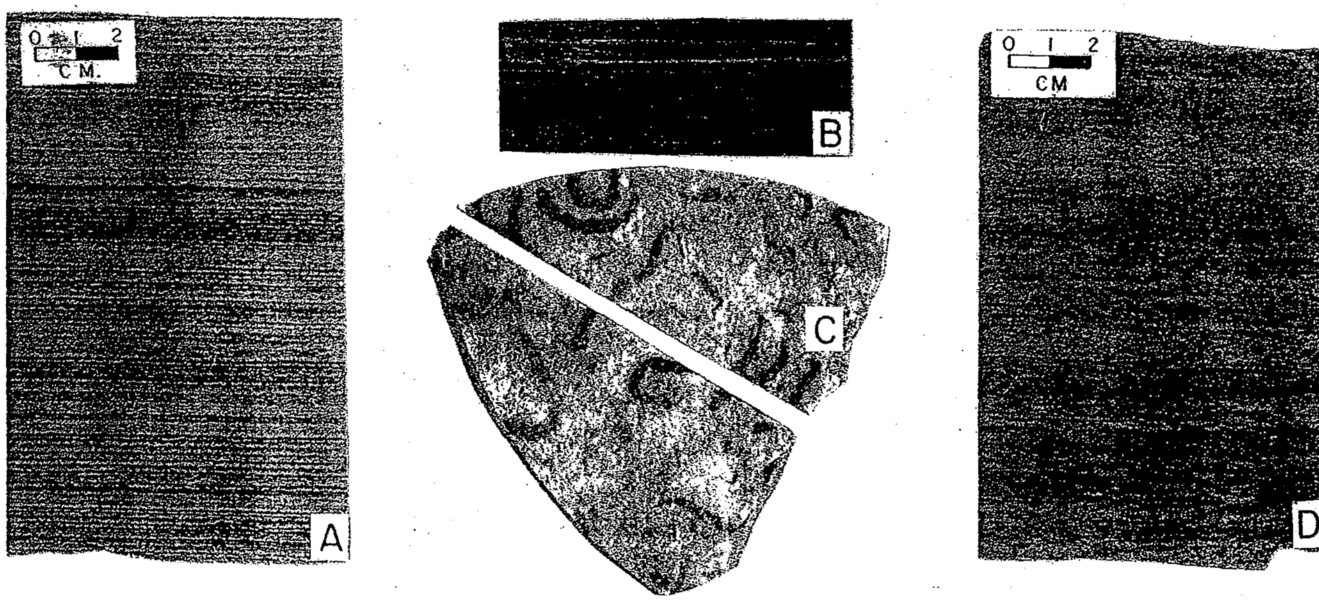

Figure 5—Cores of siltstone, Bell Canyon Formation. (A) Core slab of laminated siltstone typical of subsurface. Note similarity to outcrop (Figure 4A). (B) Organic-rich clayey siltstone. TOC typically is 3.5-5.0% in this lithology. (C) Carbonized crawling or browsing traces (*Helminthoida*) along siltstone bedding plane. (D) Bioturbated siltstone with slightly disrupted texture caused by bedding plane traces similar to Figure 5C.

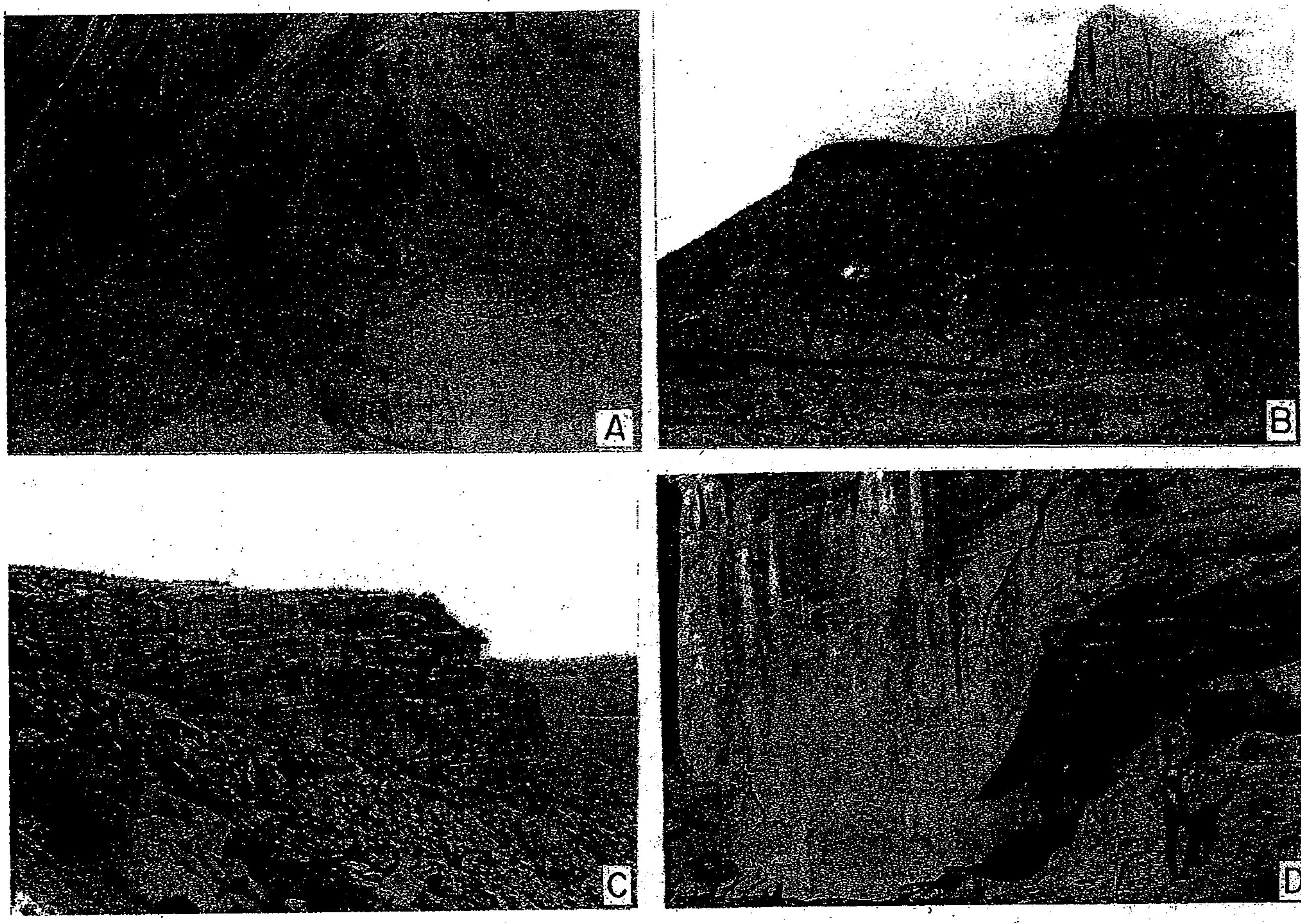

Figure 6—Channels in the Brushy Canyon Formation, Guadalupe Mountains. (A) Oblique aerial view of western face of Guadalupe Mountains showing positions of prominent erosion surfaces. (B) Covering beds of dark-gray siltstone diverge about abutting beds of sandstone. Siltstone beds drape and are parallel with channel erosional surfaces. (C) Flat-topped beds of sandstone abut steep channel wall. (D) Local scour within channel-fill complex.

of plants or soft-bodied organisms, including an excellently preserved worm impression (Williamson, 1978), have been found on outcrop. Bioturbated siltstone most commonly occurs immediately above and below sandstone-filled channels and in association with thin rippled zones in laminated siltstone. These associations suggest temporary aeration of bottom waters may have resulted from the rapid influx of more oxygen-rich surface water by currents transporting sand and silt.

Ripples are a common sedimentary structure in siltstone, but constitute only a few percent of the siltstone beds examined in cores and on outcrops. Most ripples occur within layers only one ripple-set thick and parallel with underlying laminations. Ripples are asymmetric, have rounded profiles, an average spacing of 8-10 cm (3.15-3.94 in.), heights less than 1 cm (0.39 in.), and long straight to slightly sinuous crests. Transport directions measured in outcrops are basinward at high angles to the adjacent shelf margin. The rippled zones are composed of well-sorted quartz silt that resembles the coarser fraction of underlying laminated units. These relations suggest that ripples formed by reworking and winnowing of unconsolidated laminated silt by basinward-flowing currents.

Sandstone

The distribution of sandstone in the Delaware Mountain Group is controlled by the positions of erosional channels. Sandstone-filled channels are well defined on outcrops (Figure 6), and can be mapped from subsurface data. Sandstone percentage depends upon the number and size of channels in any particular location rather than the proximity to the basin margin.

Most sandstones are texturally submature, moderately to well-sorted subarkoses. Cherry Canyon and Bell Canyon sandstones are silty and very fine grained. Maximum quartz or feldspar grain size generally is 0.25 mm (0.01 in.); mean grain size for 53 outcrop and core samples of Bell Canyon sandstones averages 0.09 mm (0.004 in.). Sorting (sigma 1) averages 0.58 phi. Most Bell Canyon sandstones contain 20-50% coarse silt grains. Approximately 40% of the Bell Canyon samples have a weak second mode of anomalously well-rounded medium-size sand grains that compose less than 2% of the sand fraction. These grains are probably reworked eolian or beach sand grains, which have been transported into the basin by bottom currents. Sand grains in the Delaware Mountain Group typically are subangular to subrounded.

Sandstones in the Cherry Canyon and Bell Canyon Formations generally contain 20-50% medium and coarse silt grains. Outcrops of Brushy Canyon sandstones tend to be slightly coarser grained with mean diameters in the very fine to fine sand-size range. Sandstones in the few cores available for the Brushy Canyon are very fine-grained and similar in texture to the Bell Canyon and Cherry Canyon sandstones.

The composition of framework grains for the Delaware Mountain Group sandstones varies little with stratigraphic or geographic position (Hull, 1957; Harms, 1974; Payne, 1976; Williamson, 1978; Berg, 1979; Watson, 1979). Quartz comprises 65-80% of the framework fraction, feldspar 10-25%, and sedimentary and the low-rank metamorphic rock fragments 5-15%. Carbonate rock clasts as large as pebbles or cobbles occur near the basin edge and angular siltstone rip-up clasts are common. Fusulinids and lesser amounts of other transported fossil fragments occur in all formations, but are most abundant in outcrops near the shelf margin.

Delaware Mountain sandstones generally are weakly cemented by calcite or dolomite and small amounts of quartz and authigenic clay. Porosity values are 15-25% in outcrops and in the subsurface. Less porous more tightly calcite-cemented sandstones are in beds with abundant transported skeletal grains and carbonate rock clasts. Horizontal permeability values range from less than 0.1 to 200 md. The amount of authigenic pore-lining chlorite and mixed-layer chlorite/smectite (corrensite) control permeability in Bell Canyon sandstones with porosity greater than 20% (Williamson, 1978). Small amounts of kaolinite and anhydrite cement have also been reported from Delaware Mountain Group reservoirs (Berg, 1979; Jacka, 1979). Petrographic and geochemical data indicate authigenic chlorite and small amounts of quartz and feldspar overgrowths formed during shallow burial (less than 1,000 m or 3,281 ft). Most calcite and dolomite cement precipitated later, and may have formed near present burial depths after the Tertiary tectonic tilting of the basin (Williamson, 1978).

Conglomerate and Limestone

Conglomerate and limestone beds compose a small fraction (less than 5%) of the Delaware Mountain Group, but form prominent outcrops along the southeastern and western faces of the Guadalupe Mountains. Spectacular carbonate megabreccias composed of large boulders (up to 4 m or 13 ft in diameter) of shelf-margin limestone mixed with basinal siltstone and sandstone, and interbedded with carbonate turbidites, form prominent marker beds in the Bell Canyon and Cherry Canyon Formations. The megabreccias occur within about 16 km (10 mi) of the shelf edge and were deposited by debris flows or other types of high-density gravity flows associated with steep basin slopes (Newell et al, 1953; Rigby, 1958; Crawford, 1981).

Massive conglomerate beds from 1-10 m (3.3-33 ft) thick occupy erosional depressions within the lower part of the Brushy Canyon Formation exposed on the western face of the Guadalupe Mountains. Clasts of carbonate rocks derived from the adjacent Permian shelf are up to 30 m (98 ft) in maximum dimension and interbedded with siltstone and sandstone. The conglomerates are poorly sorted, lack internal stratification, terminate laterally by onlapping against sloping boundaries, and may contain large boulders extending above the upper bed's surface. The conglomerates may have been emplaced by debris flows, but they lack basally aligned fabrics and steep marginal slopes. No single transport mechanism adequately explains the observed features. Similar types of conglomerates are not seen in other Delaware Mountain Group outcrops or in the subsurface.

Limestone beds, which thicken updip and are transitional with the Capitan and Goat Seep formations, have been used to stratigraphically subdivide the Bell Canyon and Cherry Canyon Formations into several members. The limestones grade basinward into dark calcareous siltstones and provide good correlation tools in the subsurface. Koss (1977) traced one of these limestone units in outcrop (Pinery Limestone Member of the Bell Canyon Formation) 23 km (14.3 mi) basinward. The sequence thins from 33 m (108 ft) at the basin margin to 6 m (20 ft) at the most basinward outcrop. The limestone beds commonly are texturally normally graded, have erosional bases, and have other structures indicative of turbidity current deposition. Calcareous beds present in cores taken farther basinward generally are organic-rich laminated silty dolomicrite or dolomitic siltstone. Resedimented skeletal debris rarely occurs in the central part of the basin.

CHANNELS AND SANDSTONE GEOMETRY

Sandstone-filled channels in the Delaware Mountain Group are well exposed in outcrop and form important subsurface hydrocarbon reservoirs. Prominent erosion surfaces with as much as 30 m (98 ft) of relief and 1 km (0.62 mi) or more in width occur in the Brushy Canyon and Cherry Canyon Formations along the western face of the Guadalupe Mountains (Figure 6). Smaller channels and partly exposed large channels can be identified throughout the Delaware Mountain Group in the more subdued topography of the Delaware Mountains to the east and southeast of the Guadalupe Mountains. The large channels formed by these prominent erosion surfaces have flat floors and steep walls, which commonly dip 10°-30°. Sandstone beds are restricted to channel floors and abut the steep channel walls, whereas siltstone beds extend across channel floors, slopes, and interchannel areas without appreciable changes in thickness. Not all channels are filled with sandstone. Most are filled in a complex unordered way with siltstone and sandstone. The channels in the Guadalupe Mountains trend southeastward, nearly perpendicular to the shelf margin (Figure 3). Directional features within the channel-filling sandstone also show basinward transport.

Sandstone- and siltstone-filled channels comparable in scale to those described from outcrops are present in the subsurface. The major sandstone-filled channels form stratigraphic traps where they are incised into less perme-

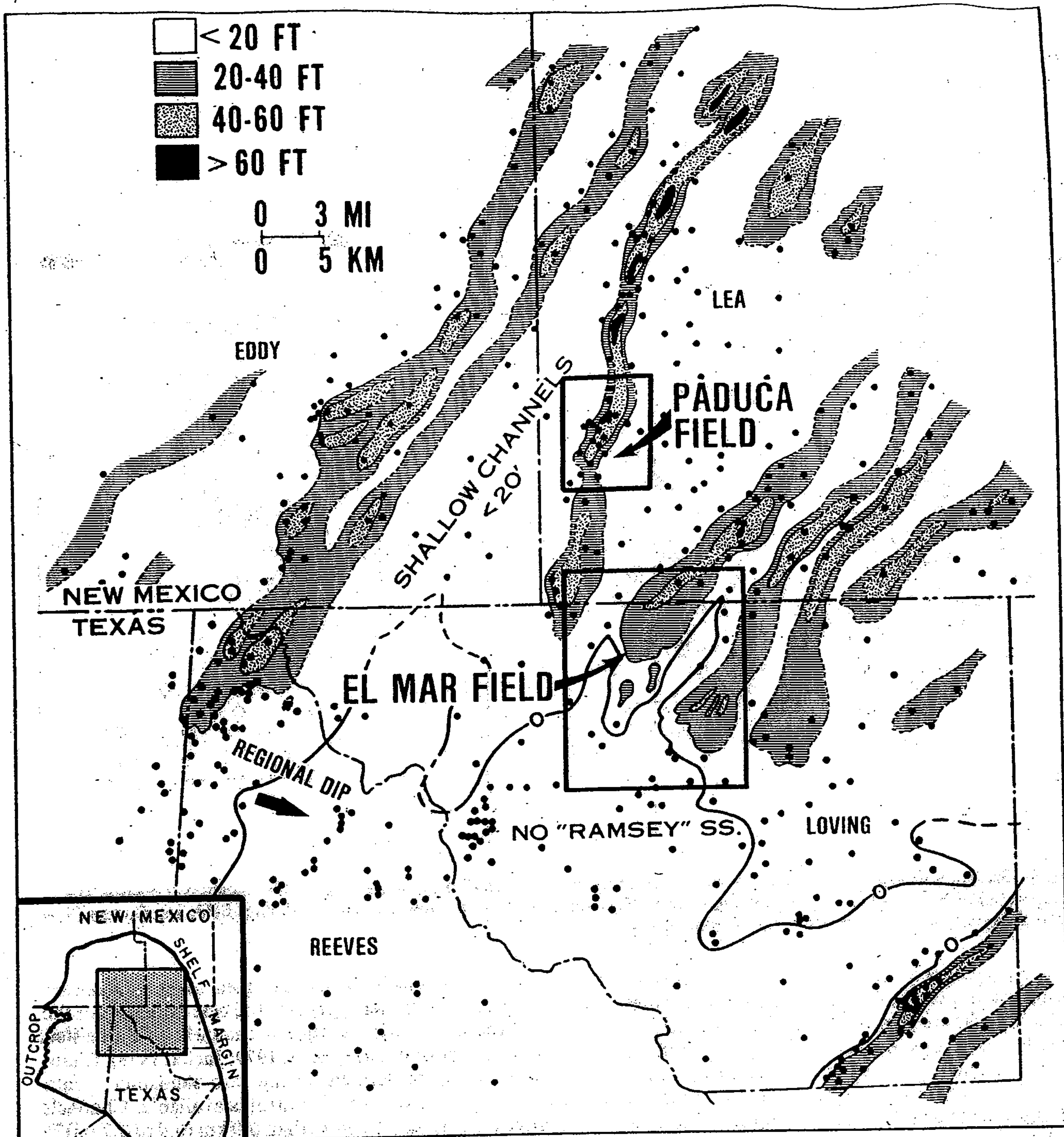

Figure 7—Regional sandstone isolith map of the Ramsey sandstone, upper Bell Canyon Formation. This map is a simplified interpretive version, which emphasizes the maximum northeast-southwest continuity of major channels. Approximately 700 gamma ray–sonic logs and conventional cores from 45 wells provide control.

able laminated siltstone. More than 150 fields have produced 138.8 million barrels of oil from the Delaware Mountain Group (Weinmeister, 1978). Most of the production is from the upper part of the Bell Canyon Formation, the most densely drilled interval in the Delaware Mountain Group. The geometry and style of channel fills on a regional and local scale are best illustrated by the Ramsey sandstone, the informally named uppermost thick sandstone of the Bell Canyon Formation (see Grauten, 1965, for a review of Bell Canyon subsurface stratigraphy). The Ramsey sandstone is the main producing unit in most fields and has the greatest amount of subsurface control.

A regional isolith map of the Ramsey sandstone(Figure 7) shows a prominent S15°W trend of thick sandstones (6-24 m or 20-79 ft) separated by a basinward-thinning "sheet" of interbedded thin sandstone and siltstone. The areas of thickest sandstone mark the axes of

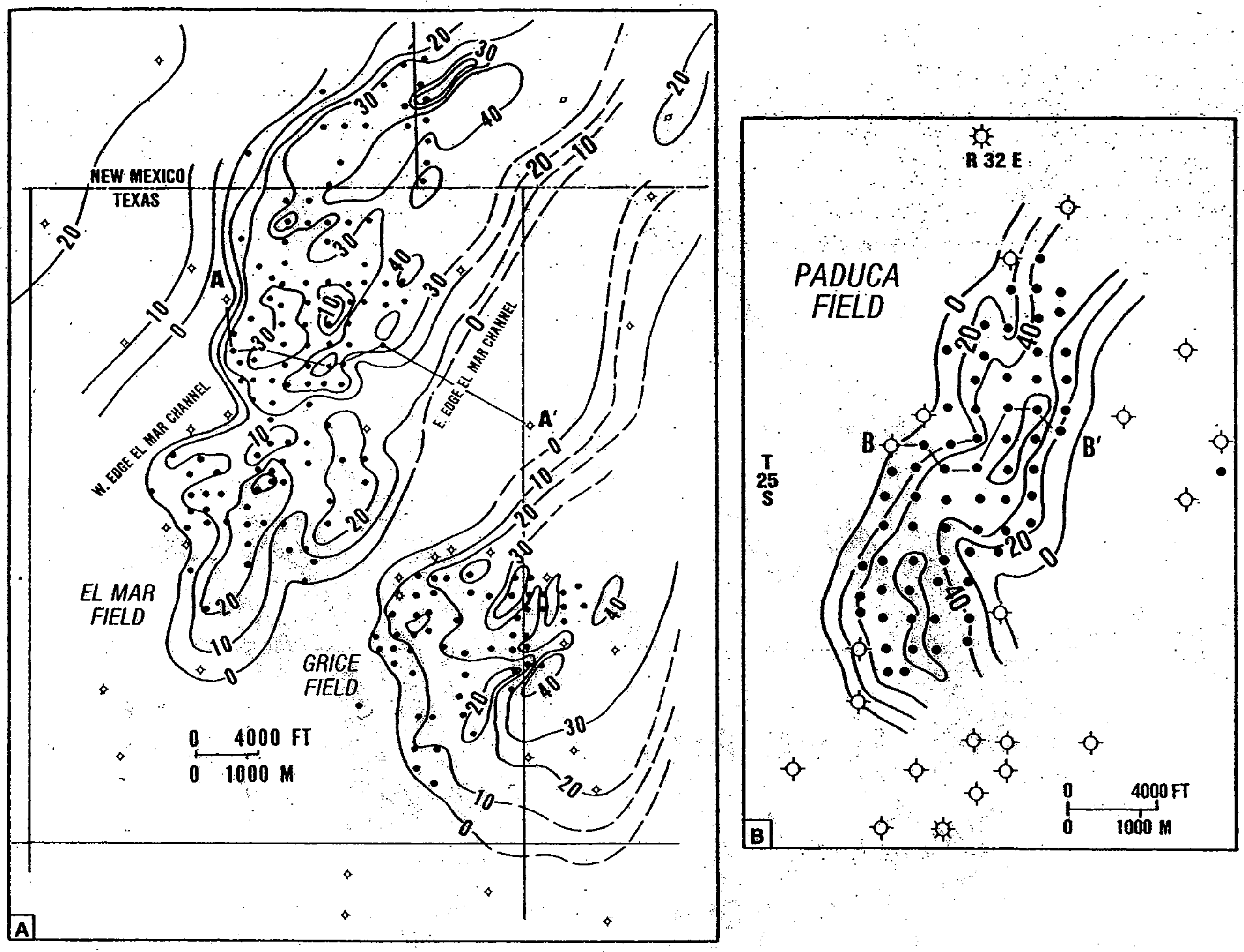

Figure 8—Sandstone isolith maps of Ramsey sandstone, upper Bell Canyon Formation (see Figure 7 for locations); contour values are in feet: (A) El Mar and Grice fields, Loving County, Texas and Lea County, New Mexico; (B) Paduca field, Lea County, New Mexico (Paduca field map modified from Weinmeister, 1978).

deep broad erosional channels filled in a complex way by sandstone and siltstone. The dimensions and geometry of the channel fills are comparable to the large channel fills exposed on outcrops of the Delaware Mountain Group. The deep channels extend far into the basin (at least 70 km or 43 mi from the shelf margin) and are the major stratigraphic controls of oil accumulations in the northern Delaware basin. Oil fields are aligned along these sandstone-filled channels. The accumulations are trapped where channel-fill sandstones abut the updip (to the northwest) erosional margins of the channels. Lateral and top seals for the traps are the relatively impermeable laminated siltstone.

The thin sandstones (less than 6 m or 20 ft) that separate major channels are interpreted to be similar to overlapping sand-filled shallow channels mapped in outcrops of the upper Bell Canyon Formation (Williamson, 1978). Core and log control in these areas is not sufficient to unequivocally demonstrate channeling, but analogy with Bell Canyon outcrops and the discontinuous occurrence of sandstone in the subsurface suggest the presence of thin channel fills interbedded with suspension-deposited blankets of siltstone.

Cores and mechanical logs from several Delaware Mountain Group fields provide the best evidence for the occurrence of major erosional channels (Weinmeister, 1978; Williamson, 1978; Berg, 1979; Jacka, 1979). Channel margins are defined by the zero sandstone isolith where closely spaced well control is available. Channels range from 1.5 km to more than 6.0 km (0.9 to 3.7 mi) in width and generally are 10 to 25 m (33-82 ft) in depth. Depth estimates usually are minimum estimates because of shallow incomplete well penetrations. The channels tend to become shallower and broader basinward. Sandstone isolith maps and cross sections from Paduca field (35 km or 21.7 mi downchannel from the shelf margin) and El Mar field (50 km or 31 mi downchannel from the shelf margin) are given to illustrate the nature of channels and internal complexities of the channel fills (Figures 8, 9).

Cross sections through the subsurface channels are very similar to the channels exposed along the western face of the Guadalupe Mountains. Laminated siltstone covers the erosional margins of the channels and can be correlated into interchannel areas. Like many of the channels in outcrop, the flows that eroded the channels

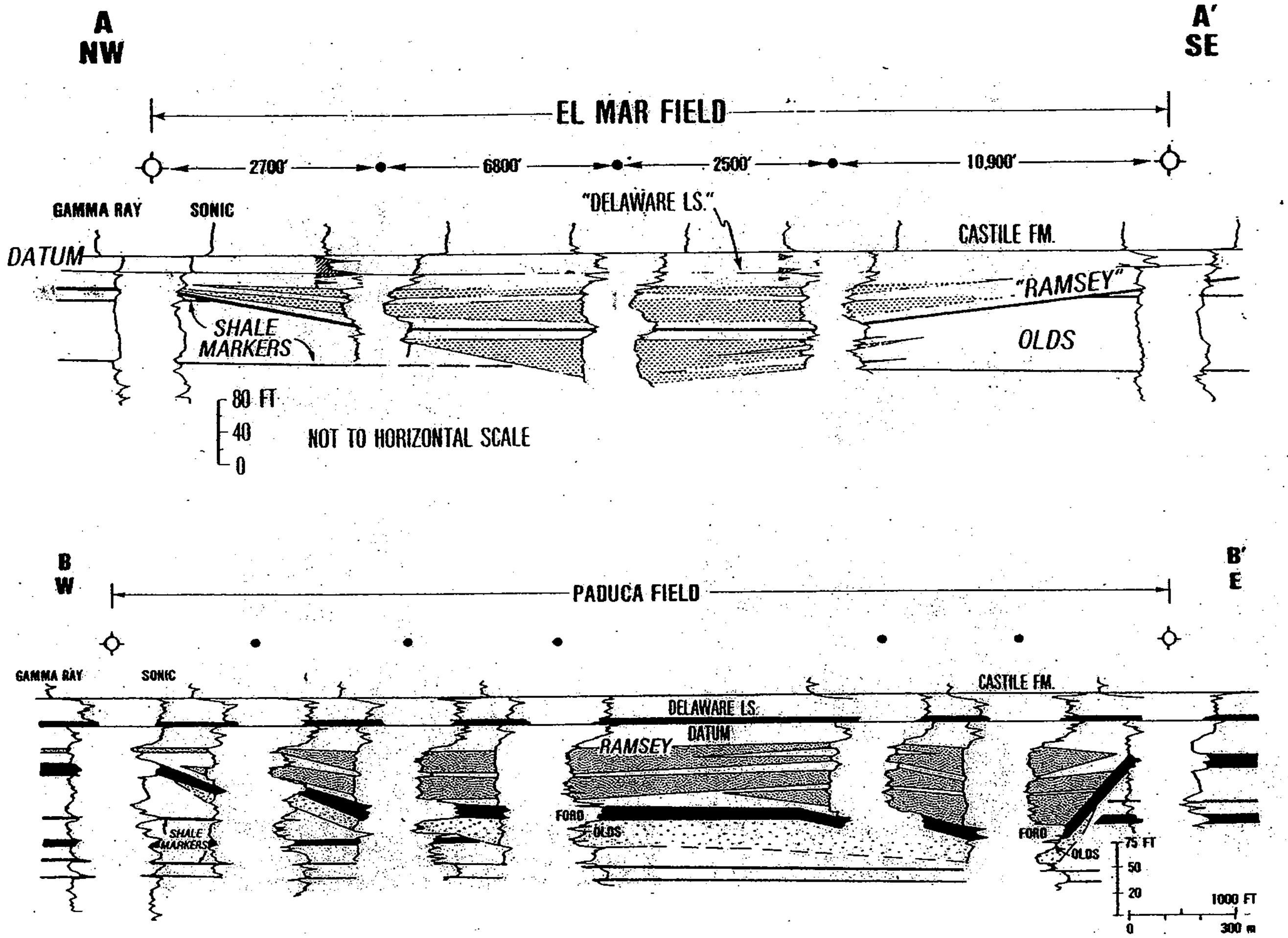

Figure 9—Stratigraphic cross sections showing large erosional channels, upper Bell Canyon Formation (see Figure 8 for location of sections): (A) El Mar field, Texas; (B) Paduca field, New Mexico. Section BB ' modified from Berg (1979).

did not necessarily fill the channel. Impermeable siltstones draping channel margins may provide lateral barriers to oil migration, be updip seals, or vertically segment reservoirs.

The distribution of sandstone and orientation of channels in subsurface indicate that the major source of sediment input was from the northern and eastern shelves in the late Guadalupian (upper Bell Canyon). Older sandstones in the Bell Canyon Formation ("Olds," "Hays") appear to extend slightly farther basinward than the Ramsey sandstone. Often, these sandstones occupy the same erosional channel. These relations suggest that erosional channels are backfilled by progressive upchannel migration of sand deposition. Changes in relative sea level or shifting of depositional loci on the shelf could have caused retreat of the sediment source and led to backfilling of channels.

Channel trends and the sedimentation style are not well known for the older part of the Delaware Mountain Group. Well density in the older formations (Cherry Canyon and Brushy Canyon) rarely is sufficient to define channel trends. At least five small fields produce from the lower Bell Canyon and Cherry Canyon Formations in the northern part of the basin (Cromwell, 1979). One of these fields, the Indian Draw field, produces from a north-south trending channel approximately 1.5 km (0.9 mi) wide. Productive Cherry Canyon sandstones in the Rhoda Walker field along the eastern shelf margin also show indications of overlapping sandstone-filled channels oriented nearly perpendicular to the shelf margin (Bozanich, 1979).

SEDIMENTARY STRUCTURES AND STRATIFICATION IN SANDSTONE

Sedimentary structures and stratification within the Delaware Mountain Group sandstone beds provide useful records of processes and the relative frequencies of processes in the basin. Horizontal lamination (Figures 10A, B) and cross-stratification (Figures 10C, D, 11-13) are common on outcrops and in cores of Delaware Mountain Group sandstones. In the Bell Canyon and Cherry Canyon Formations, the very fine grain size of the sand, lack of clay-size material, and relatively good sorting make stratification difficult to see. The coarser grain size and greater range of grain sizes in sandstone outcrops of the Brushy Canyon make stratification more

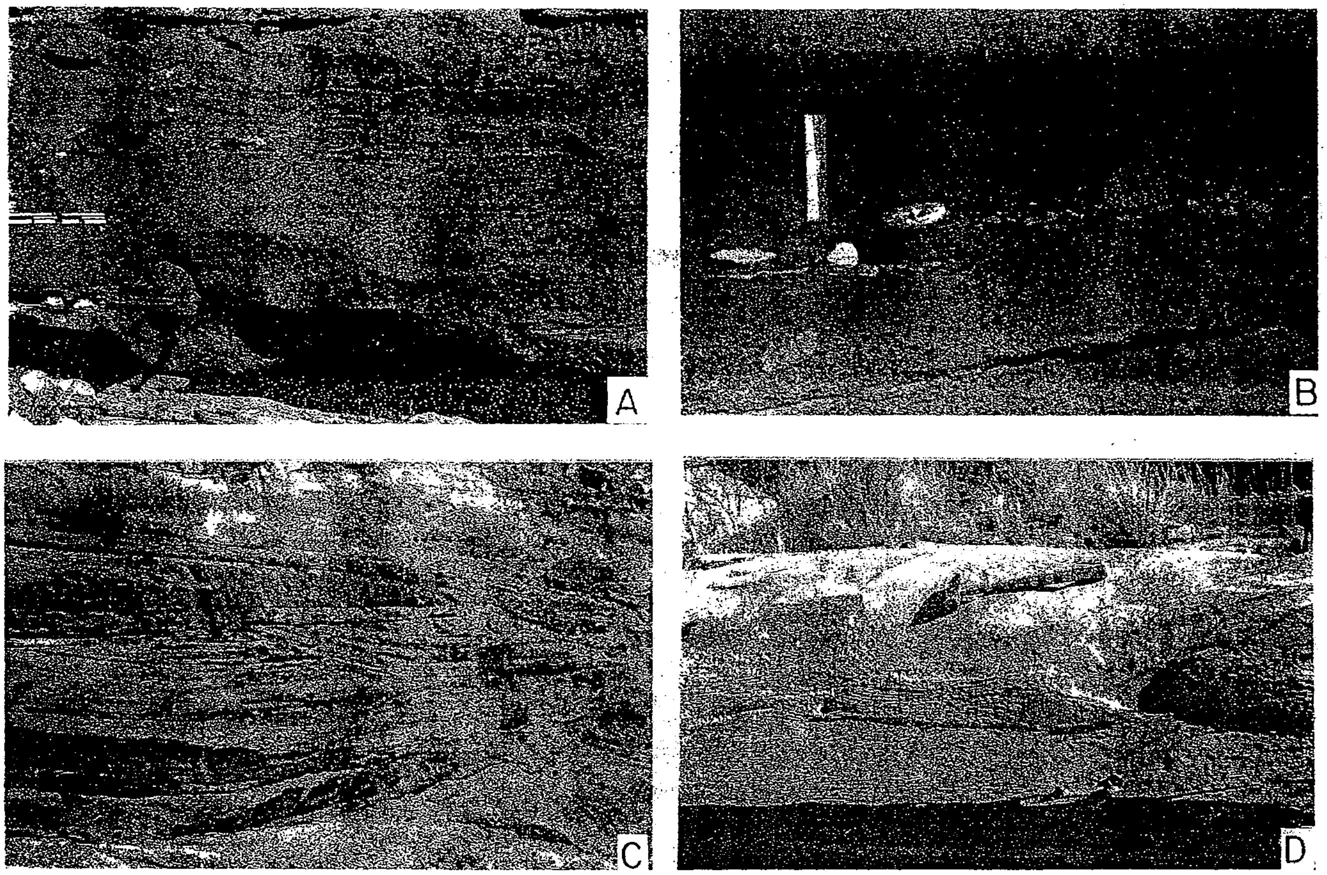

Figure 10—Horizontal lamination of trough cross-stratification in Delaware Mountain Group sandstones: (A) horizontal lamination in very fine-grained Bell Canyon sandstone (scale 20 cm); (B) horizontally stratified fine-grained sandstone with scattered carbonate pebbles and cobbles aligned in bedding, Brushy Canyon Formation (scale 15 cm); (C) broad, shallow-trough cross-strata viewed in upcurrent direction, Brushy Canyon Formation; (D) trough cross-stratification with set boundaries dashed, very fine-grained sandstone, Bell Canyon Formation.

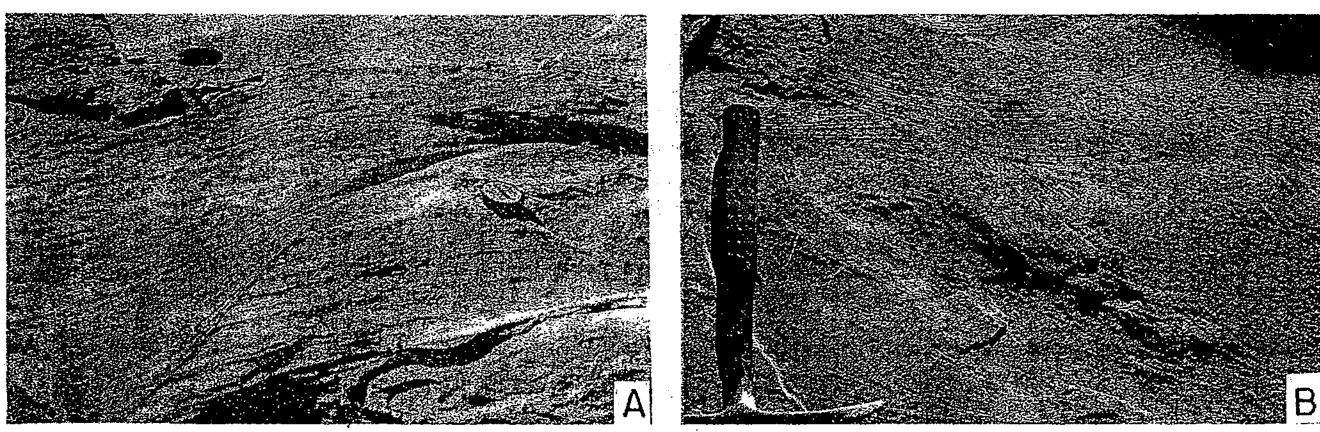

Figure 11—Trough-filled scours and trough cross-stratification: (A) steep-sided trough-filled scour in very fine-grained sandstone, Bell Canyon Formation; view is nearly perpendicular to master bedding. Note steeply dipping onlapping laminae filling scour and nearly horizontal laminae truncated by scour. (B) Close-up of trough cross-lamination showing multiple scours and trough infilling, very fine-grained sandstone, Bell Canyon Formation; view perpendicular to bedding.

clearly visible. In the Brushy Canyon Formation, crude horizontal lamination is the most common structure in sandstone beds (Figure 10B). Trough-shaped cross-stratification is common, but not nearly as abundant as horizontal lamination. Asymmetric ripples and small-scale cross-stratification are less abundant, but do occur in some sandstone beds. These structures suggest that powerful currents forming flat beds were most common,

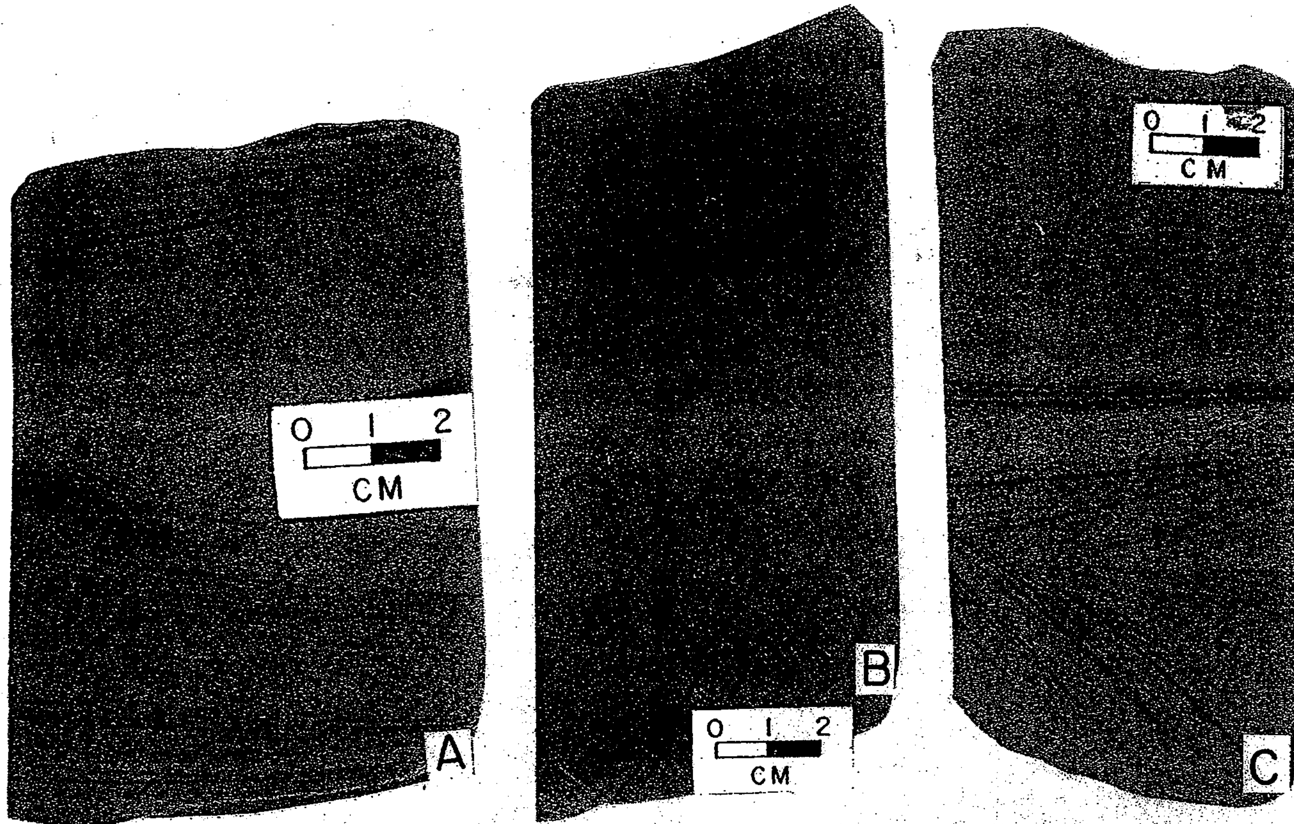

Figure 12—Core slabs of stratified very fine-grained sandstone, upper Bell Canyon Formation. Cores are from several different Bell Canyon reservoirs. Cross-stratification with anomalously steep dips and laminae onlapping set boundaries are similar to trough-filled scours observed on outcrop (Figure 11). Much of the structureless sandstone observed in Delaware Mountain Group sandstone cores shows faint cross-lamination or horizontal lamination similar to that seen in these core slabs.

but flow at lower relative velocities also occurred and produced bed configurations suggesting less energetic transport.

The relative proportions of stratification types in the Bell Canyon and Cherry Canyon Formations are more difficult to assess because of the large percentage of megascopically structureless sections. Approximately 40% of Bell Canyon sandstone beds observed in outcrop (131 beds measured) are megascopically structureless and 70% of upper Bell Canyon sandstone beds observed in cores (163 beds measured) are megascopically structureless. Most of the sandstone is not truly structureless, but is cross-stratified or horizontally laminated. Scattered patches of faint cross-stratification and horizontal lamination are common in otherwise "structureless" sandstone outcrops and cores. X-radiographs of 45 structureless core slabs from 25 wells revealed faint lamination in nearly 70% of the samples. Nearly equal amounts of cross-stratification and horizontal lamination were noted. Therefore, only a few of the massive sandstones are truly structureless. These sandstones may have been deposited by rapid fallout of sand and silt from suspension without time for development of any internal organization within the beds, or any original lamination was destroyed by liquefaction or dewatering during porosity adjustments soon after deposition.

Cross-stratification in Delaware sandstones includes "normal" trough-shaped open-form sets from a few centimeters to 1 m (3.3 ft) thick (Figures 10C, D). These trough sets are common in Brushy Canyon, but are less abundant in the finer grained Cherry Canyon and Bell Canyon Formations. Cross-stratification in these units more commonly takes the form of poorly organized asymmetric trough-filled scours and large-scale ripple-drift cross-lamination (megaripple-drift) (Figures 11-13A-C). These stratification types are largely confined to silty, very fine-grained sandstones. The steep-sided U-shaped (transverse to flow) scours are filled by curving trough laminae that lap onto the sides of the scour surface. Laminae commonly have less steep dips in the upper part of the fill. Bedding plane exposures of the scours show elliptically shaped depressions less than 1 m (3.3 ft) in maximum dimension that have been asymmetrically filled by laminae dipping toward the center of the scour. Orientations of the long dimensions of scours generally are similar to paleocurrent measurements of ripples, but the scour orientation contains a great deal more variation.

The puzzling feature of these scours is their steep sides (some nearly vertical) and the steep dips of sandstone laminae (up to 75°) that fill the scours. Soft-sediment deformation or differential compaction are not preva-

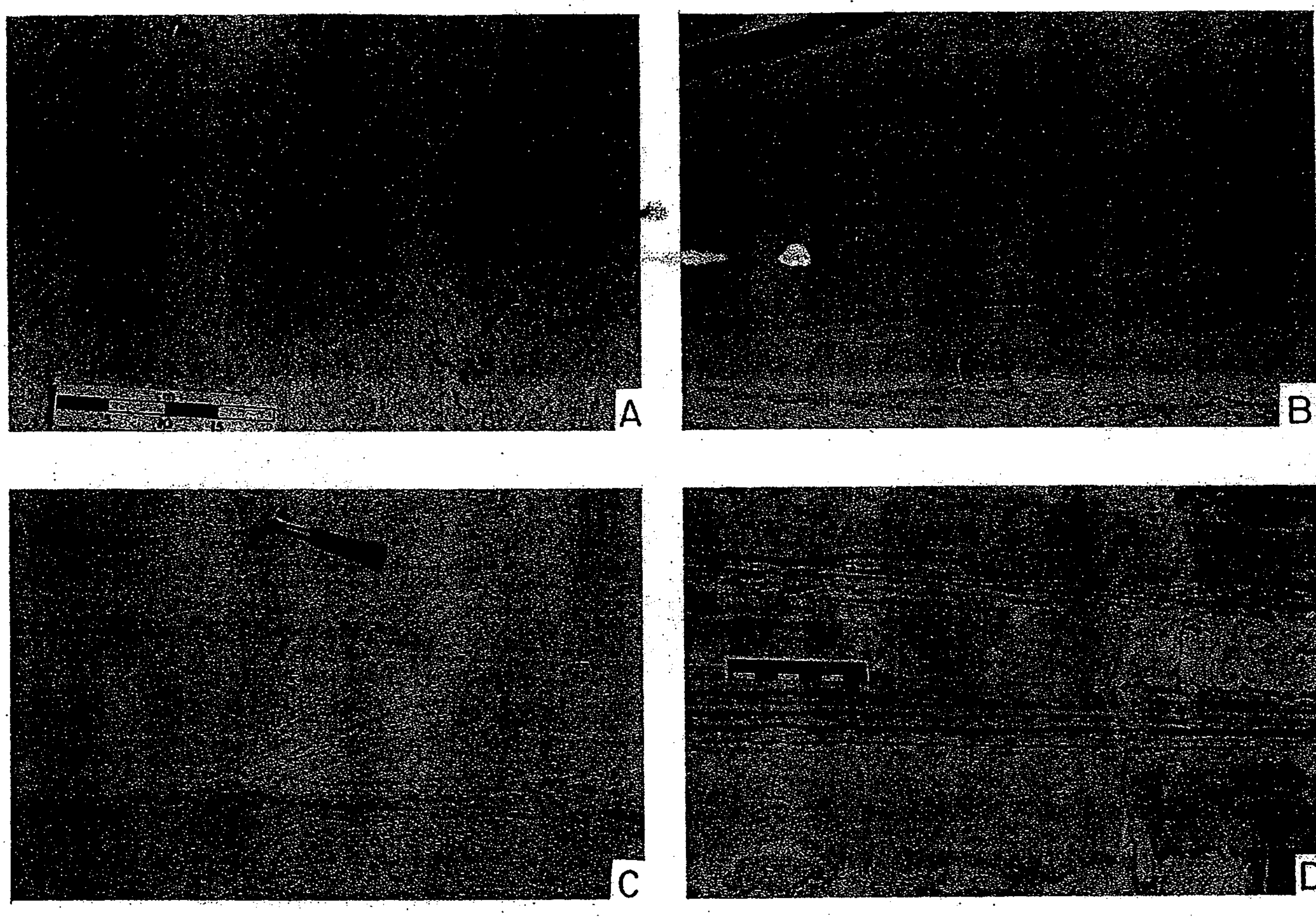

Figure 13—(A) Megaripple-drift cross-lamination (modified Type A) in very fine-grained sandstone, Bell Canyon Formation; flow from left to right. Bedforms were periodically draped by laminae of sand deposited by rapid fallout from suspension. (B) Megaripple-drift cross-lamination in very fine-grained sandstone (transitional between sinusoidal and Type B). View is slightly oblique to bedding plane. Dark horizontal lines are iron stains related to modern ground water. Paleoflow from left to right. (C) Close-up of Figure 13C. Note the preservation of stoss and lee sides and the slight downcurrent migration of megaripple crests. (D) Beds of rippled very fine-grained sandstone alternating with beds of horizontally stratified sandstone, Brushy Canyon Formation.

lent. Erosional bases of scours truncate underlying undeformed horizontal lamination and cross-stratification. Similar types of scours occur less commonly in Brushy Canyon sandstones. Cores from the Bell Canyon and Cherry Canyon Formations show steep-sided trough-shaped scours and an unusual form of cross-stratification with converging inclined lamination that onlaps scour surfaces (Figure 12). These features are interpreted to be trough-filled scours similar to those observed in outcrop.

The trough-filled scours are the most common type of cross-stratification in thick Bell Canyon and Cherry Canyon sandstones. The excavation and initial filling of the scours must have been nearly instantaneous to preserve such steep slopes. Sand and silt laminae were "plastered" against the scour surface as discrete laminae from a highly turbulent flow. In some scours, trough sets assume a more regular open form and lower dips, suggesting that downchannel migration of dune bedforms caused the final filling of the scour holes. More commonly, scours resemble potholes that were eroded and simultaneously filled by steeply dipping sand and silt laminae. These structures suggest that bed configurations developed when transported sediment concentrations were much higher than those leading to the trough cross-strata that appear to be more typical of fluvial processes.

In several exposures, the trough-filled scours were filled with inclined lamination and then overridden by megaripple-drift cross-lamination. The megaripple-drift lamination is a larger scale version of Type-B ripple-drift stratification (Jopling and Walker, 1968). Type-B ripple drift has continuous laminae across the ripple form and an asymmetrical ripple profile with a slight downcurrent migration of the ripple throughout the set. Megaripple-drift cross-lamination in Delaware Mountain Group sandstones (Figures 13B, C) generally has crest spacings of 0.8-1.2 m (2.6-3.9 ft) and shows steeply asymmetric crests. These crests appear to be nonlinear, although their plan views are not well exposed. Megaripple-drift occurs overlying steepsided trough-filled scours and in individual sandstone beds up to 2.5 m (8.2 ft) thick with no discernible breaks in sedimentation. Less commonly, a modified type of megaripple-drift cross-stratification similar to Type-A ripple drift (Jopling and Walker, 1968) also is present in Delaware Mountain Group sandstone

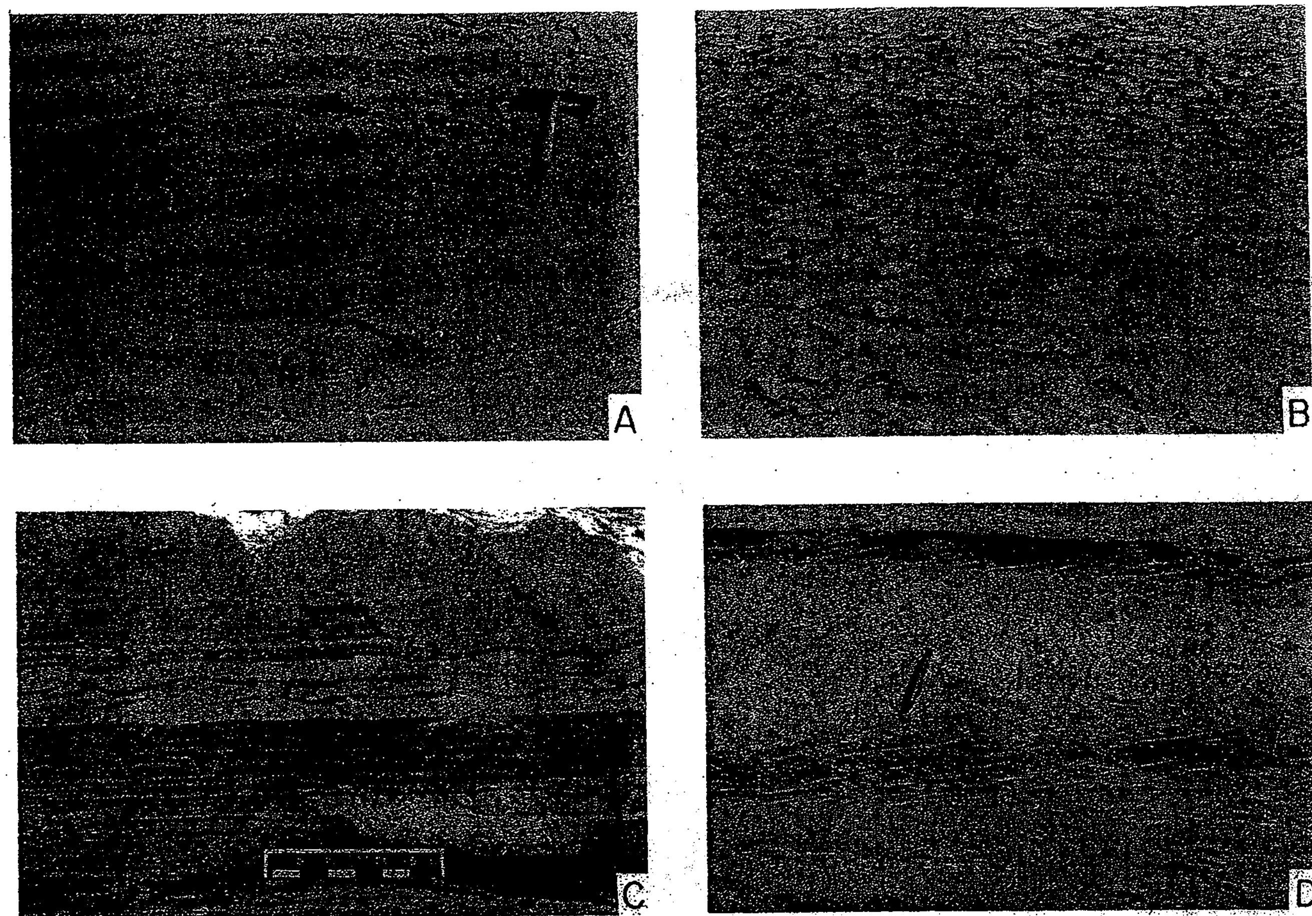

Figure 14—Ripples and ripple-stratification: (A) linear asymmetric current ripples at top of very fine-grained sandstone bed, Bell Canyon Formation; (B) cuspate ripples in very fine-grained sandstone, Bell Canyon Formation; (C) rounded asymmetric ripples of coarse silt with intervening lenses of dark siltstone, transport from right to left, Brushy Canyon Formation; (D) ripple-drift cross-lamination in very fine-grained sandstone, Bell Canyon Formation. Long-crested form of ripples shown on bedding plane parallel with 14 cm pencil.

(Figure 13A). Type A preserves only the leeward sides of ripples. Delaware Mountain Group Type A differs in that ripple forms are larger (30-40 cm or 11.8-15.7 in. ripple length, 8-12 cm or 3.1-4.7 in. height) and sets of cross-laminae are commonly separated by less inclined laminae. Episodes of megaripple migration were separated by rapid fallout of sand and silt from suspension resulting in draped lamination that preserved underlying bedforms (e.g., Gustavson et al, 1975, p. 266).

The occurrence of megaripple-drift cross-stratification indicates exceptionally high rates of sediment supply and aggradation, yet adequate time for development of megaripple bedforms. The association of megaripple-drift stratification and trough-filled scours suggests deposition from highly turbulent flows where rapid fall-out of sand and silt from suspension accompanied tractive bedload deposition. The high concentration of suspended sand and silt in the flow could have increased the viscosity of the flow enough to produce the somewhat unusual types of cross-stratification present. Large-scale bedforms in silty very fine-grained sand are rare in most deposits. The bedform sequence normally expected for this size sediment is ripples to flat bed with increased flow velocity (Harms et al, 1975; Middleton and Southard, 1978). Southard and Grazer (1982) have recently experimentally produced "anomalously large ripples" in silt by increasing the effective viscosity of the flow. High-viscosity density underflows might explain the megaripple-drift cross-lamination common in silty very fine-grained sandstones of the Delaware Mountain Group. The increased viscosity might be attributed to the abundant silt and very fine sand in suspension, the interpreted high salinity of the flows, or both.

Ripples, small-scale cross-stratification, and ripple-drift cross-lamination (Type A) are also common in Delaware Mountain sandstones (Figures 13D; 14; 15D, E). Most ripples are long-crested, asymmetric current ripples (Figure 14A) or strongly curved lunate or lingoid forms (Figure 14B). The ripples are 10-20 cm (3.9-7.9 in.) apart, 1-3 cm (0.4-1.2 in.) high, and indicate unimodal transport downchannel at high angles to the basin margin. The ripples resemble current ripples formed in very fine or fine sand by unidirectional flow, except that the profiles at the crest lines are rounded rather than angular. These forms suggest that the ripples developed under current-dominated processes, but the flow also contained an

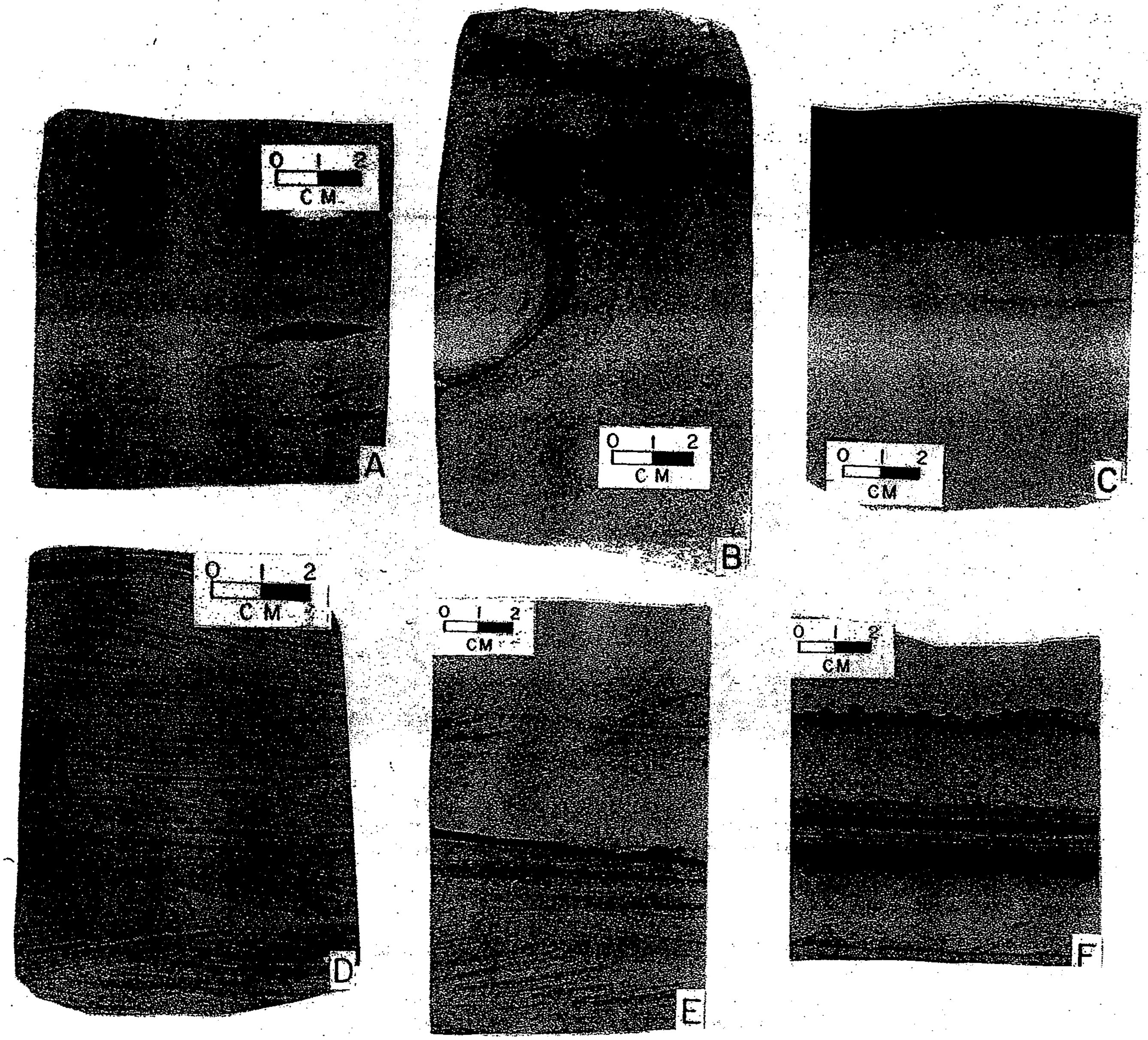

Figure 15—Core slabs of Bell Canyon sandstones. (A) Very fine-grained sandstone with gravel-size siltstone rip-up clasts; (B) sandstone beds separated by laminated siltstones with flame structures; soft-sediment deformation is evident and siltstone rip-up clasts are concentrated at the top of the lowermost sandstone bed; (C) sharp upper contact of sandstone bed with siltstone, with siltstone rip-up clasts concentrated at top of sandstone; (D) ripple-drift cross-laminated siltstone; (E) ripple-drift cross-laminated silty, very fine-grained sandstone with thin dark siltstone drape separating sedimentation units; (F) thinly interbedded siltstone and sandstone with flame structures.

oscillatory component (Harms, 1969). Many of the thin single-ripple-thick zones at the tops of thick-bedded sandstones probably were formed by reworking of sands by weak bottom currents.

Prelithification deformation structures are relatively rare in sandstone beds. The most dramatic examples of deformation occur where conglomerate rests on sandstone in some Brushy Canyon outcrops. Dikes and sills formed by sand injection were observed in a few areas, but little evidence exists for liquefaction in most Delaware Mountain outcrops and cores. Load features and flame structures commonly occur at the bases of thin-bedded sandstones interbedded with siltstones (Figure 15B, F). Sole marks and structures formed by organisms are rare in sandstones. Cylindrical burrows of unknown affinity ranging from 2-5 mm (0.08-0.2 in.) in diameter occur in a few sandstone beds, and s-shaped depressions 10-15 cm (4-6 in.) long on bedding planes were noted. Most sandstones in the study area show no evidence of bioturbation.

The stratification types described above do not occur in well-ordered or cyclic sequences. Many beds show only cross-lamination, horizontal lamination, or massive apparently structureless sandstone (Figure 16). Sedimen-

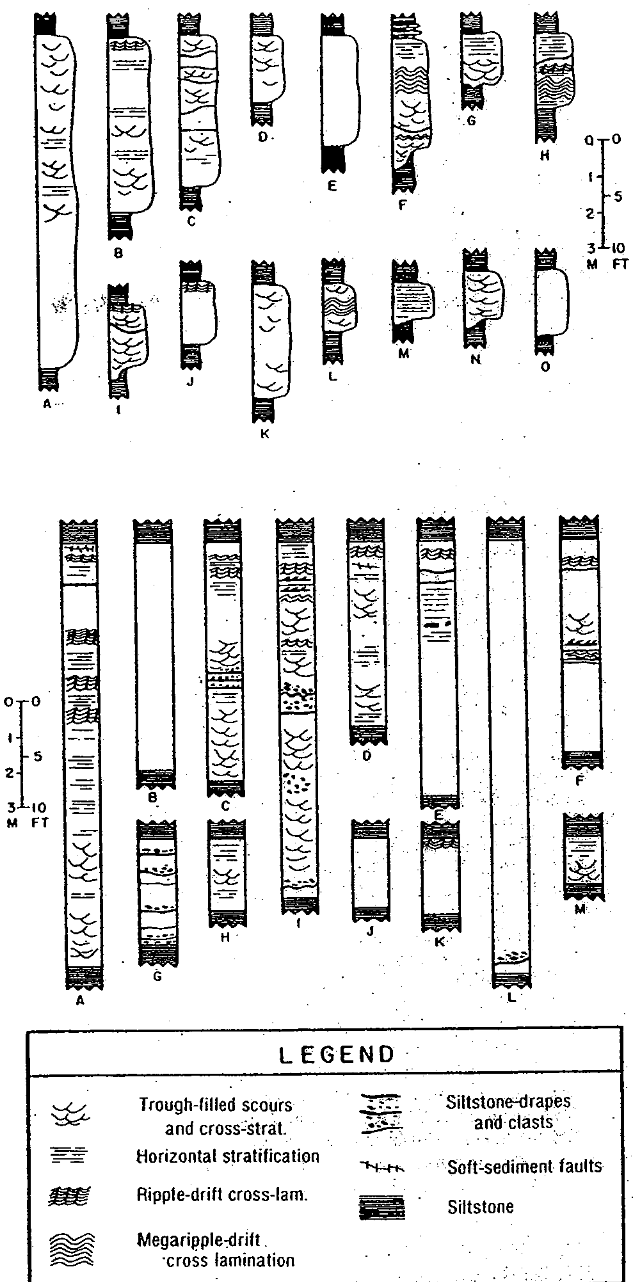

Figure 16—Representative vertical sections of sandstone beds on outcrops (top) and cores (bottom) of the upper Bell Canyon Formation. All are silty, very fine-grained sandstones from channel fills with little vertical variation in grain size. Letters refer to locations given in Williamson (1970).

tation units interpreted to represent one flow event generally are difficult to delineate in sandstone beds. Where sedimentation units can be distinguished by intercalated siltstone drapes, erosive contacts, or basal zones of rip-up clasts, the units range from 0.3 m (1 ft) to several meters thick. In sedimentation units with several types of stratification, and in sandstone beds composed of many sedimentation units, stratification types do not occur in any regular vertical arrangement other than a tendency for ripples to be present near the tops of thick sandstone beds.

Sandstone bed contacts are sharp, either planar or erosional and irregular (Figures 6D; 15B, C); texturally graded beds are rare. Modal analyses of quartz and feldspar maximum grain diameters (100-150 grains per thin section measured in $^1/_4$ phi intervals) of samples taken from the base, middle, and top of 11 sedimentation units show no significant differences in mean grain size or sorting. Grain size ranges from 0.025 to 0.2 mm (0.001 to 0.007 in.). A few sandstones have a minor second mode of medium sand (less than 2%). The medium sand-size grains are not preferentially concentrated near the bases of sedimentation units or at the bases of sandstone beds. Some sedimentation units have a pebble zone of siltstone rip-up clasts concentrated at their bases (Figure 15A); however, no regular upward decrease occurs in the size of the clasts or proportion of matrix, nor are the clasts always concentrated exclusively at the bases of units (Figure 15B, C). Clasts commonly are aligned along horizontal planes throughout the entire thickness of sandstone, and their relative positions are not adequately explained by size and density segregation occurring during deposition from a turbulent suspension.

The assemblage of stratification types and structures is similar for most of the Delaware Mountain Group sandstones. The same stratification types observed on outcrops are present in the subsurface with approximately the same relative frequency of occurrence. Unordered vertical sequences of stratification within thick sedimentation units record irregular fluctuations of flow velocity. Changes from upper to lower and lower to upper flow regimes were common as evidenced by uninterrupted alternations between cross-lamination (trough, trough-filled scours, megaripple-drift, ripples) and horizontal lamination. Most of the sandstones are characterized by structures produced by traction transport and stratification indicative of grain-by-grain bedload deposition from turbulent flows. Cross-stratified beds up to several meters thick attest to the importance of traction transport and flows of long duration.

SUMMARY

The Guadalupian Delaware Mountain Group is a basinal deposit of siltstone and sandstone with unusual characteristics. The unit is 1,000-1,600 m (3,280-5,249 ft) thick and fills a circular basin 160 km (99 mi) in diameter surrounded by carbonate banks or reefs. Basin-margin relations observed on outcrop and in subsurface correlations indicate water depths of several hundred meters within the basin at the time of deposition.

The prevalent style of deposition is laminated siltstone beds, which are laterally extensive and cover basin-floor topographic irregularities and flat-floored channels as much as 30 m (98 ft) deep and 1 km or more wide. The channels commonly are filled with sandstone beds confined to the channel and with mantling siltstone beds, which extend into interchannel areas. These features can be observed in outcrops at the basin margin and inferred from closely spaced wells for oil fields within the basin. The channels trend into the basin at its margins, but extend northeast-southwest far across the basin center for an interval at the very top of the group (Ramsey sandstone), which is best known in the subsurface.

We believe the Delaware Mountain Group sediments are best interpreted as deposits of saline-density currents. The dense water that propelled these currents was spawned in the broad shallow evaporitic shelves adjacent to the carbonate rim that encircled the basin. The saline currents probably flowed mainly through narrow channels cutting across this carbonate rim, carrying terrigenous sediments from land sources into the basin. Basinal waters were density stratified. Denser flows moved along the basin floor cutting channels or depositing sand in existing channels; less-dense flows moved intrastratally and carried silt-size material far into the basin, where it settled to the floor as thin alternating layers of detrital silt and organic debris.

The channels are very long, straight to slightly sinuous, and relatively steep walled. Potential reservoir sandstone beds are confined to channels and terminate abruptly at channel margins. Hydrocarbon sealing beds are provided by laminated organic siltstone, or the lateral seal of potential traps can be formed by the erosional margin where the channel is incised into siltstone beds. Little proximal to distal change occurs in the size or nature of these density-current channels. Exploration predictions based on well-known models of fans formed by turbidity currents would anticipate very different proximal-distal changes in channel style, size, and extent.

From a detailed sedimentologic point of view, the deposits of these saline-density currents form interesting and poorly understood bed configurations and stratification types. The flows were powerful and easily eroded or transported sediment. Much of the sediment was silt or very fine-grained sand with little clay-size detritus, and flows were probably nonturbid but more dense and viscous than fresh surface water. Because of these conditions, we have as yet very little experimental data to guide interpretations of sedimentary structures. Many of the tractional deposits also show clear evidence of rapid local deposition. Disequilibrium transport has been little studied, especially where bedforms are large. Sedimentary structures observed in the Delaware Mountain Group should provide a useful stimulus to the design and scope of future experimental studies aimed at understanding the response of finer sediment in flows of denser and more viscous liquids.

Similar density-current deposits have not as yet been recognized in other basin or geologic systems. However, they may be anticipated wherever a deep basin is surrounded by broad confined evaporitic shelves or lagoons. In such geographic situations, the Delaware basin example may provide a useful model for interpreting stratigraphic relations or for hydrocarbon exploration.

REFERENCES CITED

Anderson, R. Y., W. E. Dean, Jr., D. W. Kirkland, and H. I. Snider, 1972, Permian Castile varved evaporite sequence, west Texas and New Mexico: GSA Bulletin, v. 83, p. 59-86.

Babcock, J. A., 1977, Calcareous algae, organic boundstones, and the genesis of the upper Capitan Limestone (Permian, Guadalupian), Guadalupe Mountains, west Texas and New Mexico, *in* M. E. Hileman and S. J. Mazzullo, eds., Upper Guadalupian facies, Permian reef complex, Guadalupe Mountains, New Mexico and west Texas: Permian Basin Section SEPM Publication 77-16, p. 3-44.

Babcock, L. C., 1977, Life in the Delaware basin: The paleoecology of the Lamar Limestone, *in* M. E. Hileman and S. J. Mazzullo, eds., Upper Guadalupian facies, Permian reef complex, Guadalupe Mountains, New Mexico and west Texas: Permian Basin Section SEPM Publication 77-16, p. 357-389.

Berg, R. R., 1979, Reservoir sandstones of the Delaware Mountain Group, southeast New Mexico, *in* N. M. Sullivan, ed., Guadalupian Delaware Mountain Group of west Texas and southeast New Mexico: Permian Basin Section SEPM Publication 79-18, p. 75-95.

Boyd, D. W., 1958, Permian sedimentary facies, central Guadalupe Mountains: New Mexico Bureau of Mines and Mineral Resources Bulletin 49, 100 p.

Bozanich, R. G., 1979, The Bell Canyon and Cherry Canyon formations, eastern Delaware basin, Texas: Lithology, environments and mechanisms of deposition, *in* N. M. Sullivan, ed., Guadalupian Delaware Mountain Group of west Texas and southeast New Mexico: Permian Basin Section SEPM Publication 79-18, p. 121-141.

Crawford, G. A., 1979, Sedimentology of Goat Seep Dolomite (Guadalupian, Permian), Guadalupe Mountains, west Texas and New Mexico (abs.): AAPG Bulletin, v. 63, p. 437.

——— 1981, Depositional history and diagenesis of the Goat Seep Dolomite (Permian Guadalupian), Guadalupe Mountains, west Texas–New Mexico: PhD thesis, University of Wisconsin, Madison, Wisconsin, 300 p.

Cromwell, D. W., 1979, Indian Draw field: A model for deeper Delaware sand exploration, *in* N. M. Sullivan, ed., Guadalupian Delaware Mountain Group of west Texas and southeast New Mexico: Permian Basin Section SEPM Publication 79-18, p. 142-152.

Dean, W. E., and R. Y. Anderson, 1982, Continuous subaqueous deposition of the Permian Castile evaporites, Delaware basin, Texas and New Mexico, *in* C. R. Handford, R. G. Loucks, and G. R. Davies, eds., Depositional and diagenetic spectra of evaporites: SEPM Core Workshop 3, 395 p.

Dunham, R. J., 1972, Capitan reef, New Mexico and Texas: Facts and questions to aid interpretation and group discussion: Permian Basin Section SEPM Publication 72-14, 270 p.

Grauten, W. F., 1965, Fluid relationships in Delaware Mountain sandstone, *in* A. Young and J. E. Galley, eds., Fluids in subsurface environments: AAPG Memoir 4, p. 294-307.

Gustavson, T. C., G. M. Ashley, and J. C. Boothroyd, 1975, Depositional sequences in glaciolacustrine deltas, *in* A. V. Jopling and B. C. McDonald, eds., Glaciofluvial and glaciolacustrine sedimentation: SEPM Special Publication 23, p. 264-280.

Harms, J. C., 1968, Permian deep-water sedimentation by nonturbid currents, Guadalupe Mountains, Texas: GSA Special Paper 121, p. 127.

——— 1969, Hydraulic significance of some sand ripples: GSA Bulletin, v. 80, p. 363-396.

——— 1974, Brushy Canyon Formation, Texas: A deep-water density current deposit: GSA Bulletin, v. 85, p. 1763-1784.

——— and L. C. Pray, 1974, Erosion and deposition along the Mid-Permian intracratonic basin margin, Guadalupe Mountains, Texas (abs.), *in* W. R. Dickinson, ed., Tectonics and sedimentation: SEPM Special Publication 19, p. 37.

——— J. B. Southard, D. R. Spearing, and R. G. Walker, 1975, Depositional environments as interpreted from primary sedimentary structures and stratification sequences: SEPM Short Course Notes 2, 161 p.

Hayes, P. T., 1964, Geology of the Guadalupe Mountains, New Mexico: USGS Professional Paper 446, 69 p.

Hull, J. P. D., Jr., 1957, Petrogenesis of Permian Delaware Mountain sandstone, Texas and New Mexico: AAPG Bulletin, v. 41, p. 278-307.

Hurley, N. F., 1978, Facies mosaic of the lower Seven Rivers Formation (Permian), North McKittrick Canyon, Guadalupe Mountains, New Mexico: Master's thesis, University of Wisconsin, Madison, Wisconsin, 198 p.

Jacka, A. D., 1979, Deposition and entrapment of hydrocarbons in Bell Canyon and Cherry Canyon deep-sea fans of the Delaware basin, *in* N. M. Sullivan, ed., Guadalupian Delaware Mountain Group of west Texas and southeast New Mexico: Permian Basin Section SEPM Publication 79-18, p. 104-120.

——— R. H. Beck, L. C. St. Germain, and S. C. Harrison, 1968, Permian deep-sea fans of the Delaware Mountain Group (Guadalupian), Delaware basin, *in* B. Silver, ed., Guadalupian facies, Apache Mountains area, west Texas: Permian Basin Section SEPM Publication 68-11, p. 49-90.

Jopling, A. V., and R. G. Walker, 1968, Morphology and origin of ripple-drift cross-lamination with examples from the Pleistocene of Massachusetts: Journal of Sedimentary Petrology, v. 38, p. 971-984.

King, P. B., 1942, Permian of west Texas and southeastern New Mexico: AAPG Bulletin, v. 26, p. 535-763.

——— 1948, Geology of the southern Guadalupe Mountains, Texas: USGS Professional Paper 215, 183 p.

——— 1949, Preliminary regional geologic map of parts of Culberson and Hudspeth Counties, Texas: USGS Oil and Gas Miscellaneous Investigations Map OM-90.

——— 1965, Geology of the Sierra Diablo region, Texas: USGS Professional Paper 480, 185 p.

Koss, G. M., 1977, Carbonate mass flow sequences of the Permian Delaware basin, west Texas, *in* M. E. Hileman and S. J. Mazzullo, eds., Upper Guadalupian facies, Permian reef complex, Guadalupe Mountains, New Mexico and west Texas: Permian Basin Section SEPM Publication 77-16, p. 391-408.

McDermott, R. W., and A. J. Scott, 1981, Sandstone tongue of Cherry Canyon Formation and upper San Andres Formation (Permian), Last Chance Canyon area, southeast New Mexico (abs.): AAPG Bulletin, v. 65, p. 956-957.

Meissner, F. F., 1969, Cyclic sedimentation in Middle Permian strata of the Permian basin, west Texas and New Mexico (abs.), *in* J. G. Elam and S. Chuber, eds., Cyclical sedimentation in the Permian basin: West Texas Geological Society 1967 Symposium, p. 135.

——— 1972, Cyclic sedimentation in middle Permian strata of the Permian basin, *in* J. C. Elam and S. Chuber, eds., Cyclical sedimentation in the Permian basin (2d ed.): West Texas Geological Society Publication 72-60, p. 203-232.

Middleton, G. V., and J. B. Southard, 1978, Mechanics of sediment movement: Eastern Section SEPM Short Course Notes 3, 102 p.

Neese, D. A., and A. H. Schwartz, 1977, Facies mosaic of the upper Yates and lower Tansill Formations, Walnut and Rattlesnake Canyons, Guadalupe Mountains, New Mexico, *in* M. E. Hileman and S. J. Mazzullo, eds., Upper Guadalupian facies, Permian reef complex, Guadalupe Mountains, New Mexico and west Texas: Permian Basin Section SEPM Publication 77-16, p. 437-450.

Newell, N. D., J. K. Rigby, A. G. Fischer, A. J. Whiteman, J. E. Hickox, and J. S. Bradley, 1953, The Permian reef complex of the Guadalupe Mountains region, Texas and New Mexico: San Francisco, W. H. Freeman, 236 p.

Oriel, S. S., D. A. Myers, and E. J. Crosby, 1967, West Texas Permian basin region, *in* Paleotectonic investigations of the Permian System in the United States: USGS Professional Paper 515-C, p. C17-C60

Payne, M. W., 1976, Basinal sandstone facies, Delaware basin, west Texas and southeast New Mexico: AAPG Bulletin, v. 60, p. 517-527.

Pray, L. C., 1977, The all wet constant sea level hypothesis of upper Guadalupian shelf and shelf edge strata, Guadalupe Mountains, New Mexico and Texas, *in* M. E. Hileman and S. J. Mazzullo, eds., Upper Guadalupian facies, Permian reef complex, Guadalupe Mountains, New Mexico and west Texas: Permian Basin Section SEPM Publication 77-16, p. 391-408.

Rigby, J. K., 1958, Mass movements in Permian rocks of trans-Pecos, Texas: Journal of Sedimentary Petrology, v. 28, p. 298-315.

Sarg, J. F., 1977, Sedimentology of the carbonate-evaporite facies transition of the Seven Rivers Formation (Guadalupian Permian) in southeast New Mexico, *in* M. E. Hileman and S. J. Mazzullo, eds., Upper Guadalupian facies, Permian reef complex, Guadalupe Mountains, New Mexico and west Texas: Permian Basin Section SEPM Publication 77-16, p. 451-478.

——— P. J. Lehmann, 1986, Lower-middle Guadalupian facies and stratigraphy, San Andres/Grayburg Formations, Guadalupe Mountains, New Mexico, *in* G. E. Moore and G. L. Wilde, eds., San Andres/Grayburg Formations, Guadalupe Mountains, New Mexico and Texas: Permian Basin SEPM Publication 86-25, p. 1-8.

Silver, B. A., and R. G. Todd, 1969, Permian cyclic strata, northern Midland and Delaware basins, west Texas and southeastern New Mexico: AAPG Bulletin, v. 53, p. 2223-2251.

Smith, D. B., 1974, Sedimentation of upper Artesia (Guadalupian) cyclic deposits of northern Guadalupe Mountains, New Mexico: AAPG Bulletin, v. 58, p. 1699-1730.

Southard, J. B., and R. A. Grazer, 1982, Is there a lower limit of grain size for existence of current ripples? (abs.): International Association of Sedimentologists Abstracts of Papers, p. 3.

Tissot, B. P., and D. H. Welte, 1978, Petroleum formation and occurrence: Berlin, Springer-Verlag, 538 p.

Tyrrell, W. W., Jr., 1962, Petrology and stratigraphy of near reef, Tansill-Lamar strata, Guadalupe Mountains, Texas and New Mexico: Hobbs, Roswell and West Texas Geological Societies Guidebook Publication 62-48, p. 59-75.

——— 1969, Criteria useful in interpreting environments of unlike but time-equivalent carbonate units (Tansill-Capitan-Lamar), Capitan reef complex, west Texas and New Mexico, *in* G. M. Friedman, ed., Depositional environments in carbonate rocks: SEPM Special Publication 14, p. 80-97.

Watson, W. G., 1979, Inhomogeneities of the Ramsey member of the Permian Bell Canyon Formation, Geraldine Ford field, Culberson and Reeves Counties, Texas, *in* N. M. Sullivan ed., Guadalupian Delaware Mountain Group of west Texas and southeast New Mexico: Permian Basin SEPM Publication 79-18, p. 2-38.

Weinmeister, M. P., 1978, Origin of upper Bell Canyon reservoir sandstones (Guadalupian), El Mar and Paduca fields, southeast New Mexico and west Texas: Master's thesis, Texas A&M University, College Station, Texas, 96 p.

Wheeler, C. W., 1977, Goat Seep equivalent proximal shelf facies, Guadalupe Mountains, New Mexico and Texas (abs.): Permian Basin Section SEPM Program with Abstracts, p. 23.

Wilde, G. L., 1986, Stratigraphic relationships of the San Andres and Cutoff Formations, northern Guadalupe Mountains, New Mexico and Texas, *in* G. E. Moore and G. L. Wilds, eds., San Andres/Grayburg Formations, Guadalupe Mountains, New Mexico and Texas: Permian Basin SEPM Publication 86-25, p. 49-64.

Williamson, C. R., 1977, Deep-sea channels of the Bell Canyon Formation (Guadalupian), Delaware basin, Texas-New Mexico, *in* M. E. Hileman and S. J. Mazzullo, eds., Upper Guadalupian facies, Permian reef complex, Guadalupe Mountains, New Mexico and west Texas: Permian Basin Section SEPM Publication 77-16, p. 409-432.

——— 1978, Depositional processes, diagenesis and reservoir properties of Permian deep-sea sandstones, Bell Canyon Formation, Texas-New Mexico: PhD thesis, University of Texas, Austin, Texas, 261 p.

——— 1979, Deep-sea sedimentation and stratigraphic traps, Bell Canyon Formation (Permian), Delaware basin, *in* M. E. Hileman, and S. J. Mazzullo, eds., Guadalupian Delaware Mountain Group of west Texas and southeast New Mexico: Permian Basin Section SEPM Publication 79-18, p. 39-74.

——— 1980, Sedimentology of Guadalupian deep-water clastic facies, Delaware basin, New Mexico and west Texas: New Mexico Geological Society Guidebook, 31st Field Conference, p. 195-204.

Yurewicz, D. A., 1977, The origin of the massive facies of the lower and middle Capitan Limestone (Permian), Guadalupe Mountains, New Mexico and west Texas, *in* M. E. Hileman and S. J. Mazzullo, eds., Upper Guadalupian facies, Permian reef complex, Guadalupe Mountains, New Mexico and west Texas: Permian Basin Section SEPM Publication 77-16, p. 45-92.

CHAPTER TEN

FLYSCH AND TURBIDITES

INTRODUCTION

This chapter attempts to describe flysch sediments and turbidites. These are particularly interesting rocks which have been written about and argued over for many years. The literature of this problem is vast; whole books have been written on it (e.g. Bouma, 1962; Bouma and Brower, 1964; Dzulinsky and Walton, 1965; Lajoie, 1970); accordingly it can only be summarized in this chapter. To begin with, these definitions are important:

Flysch: Thick sequences of interbedded sands and shales. The sandstones generally have erosional bases and are internally graded. The shales contain a marine fauna. First defined in the Alps this word has been applied to similar rocks in geosynclinal belts of all ages and in all parts of the world (for further data see Dzulinsky and Walton, 1965, pp. 1–12; Hsu, 1970).

Turbidity current: 'A current flowing on consequence of the load of sediment it is carrying and which gives it excess density' (Kuenen, 1965, p. 217).

Turbidite: A sediment deposited by a turbidity current.

Greywacke: A poorly sorted sandstone with abundant matrix, feldspar, and/or rock fragments.

For reasons shortly to be described many geologists believe that flysch sandstones are turbidites. Many flysch sandstones, but by no means all, are greywackes. Because of this the terms 'flysch', 'turbidite', and 'greywacke' have been used as synonyms. This is misleading. 'Flysch' describes a facies, 'greywacke' is a petrographic term for a particular kind of rock, and 'turbidite' is a genetic term describing the process which is *thought* to have deposited a sediment. Not only are these three words quite different but they are all extremely loosely defined in the literature.

This chapter begins with an attempt to summarize the characteristics of turbidites. This is followed by a discussion of their origin. The Peira Cava formation, an Alpine flysch sequence, is then described and its environment deduced. The chapter continues with

a summary of flysch and turbidite problems and a discussion of their economic aspects and concludes with a review of their diagnostic criteria in the sub-surface.

DIAGNOSTIC CHARACTERISTICS OF TURBIDITES

Turbidites are identified by no single feature, but by the sum of many criteria. The selection of these is subjective and a function of

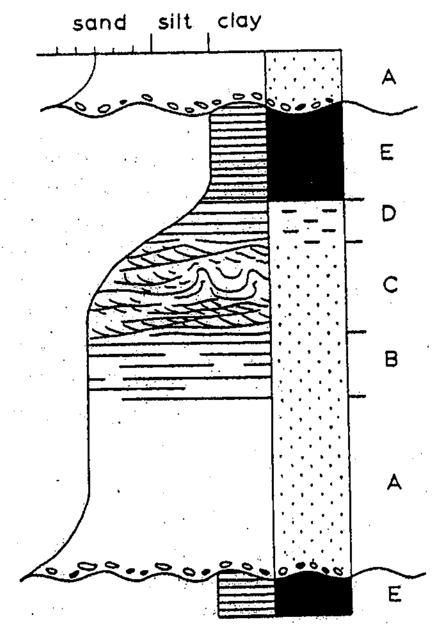

Figure 10. 1. Generalized sequence through a turbidite unit. Alphabetic letters code a vertical sequence of five different units (see text). Modified from Bouma, 1962, Fig. 8, by courtesy of Elsevier Publishing Company.

the prejudices of the individual geologist. An idealized section through a turbidite is shown in Fig. 10.1. Within such a bed it is sometimes possible to detect a wide range of sedimentary structures which are summarized in Table 10.1. This suite of structures has been interpreted in the following way (Walker, 1965; Harms and Fahnestock, 1965; Hubert, 1967). First a current scoured a variety of structures on a mud surface. Sedimentation of the turbidite then took place under waning current conditions. First the massive A unit was deposited, perhaps as antidunes, under an upper flow regime; shooting flow deposited the next laminated B unit and a lower flow regime deposited the micro-crosslaminated C unit. Various explanations have been offered for the upper laminated silt (Walker, 1965). Perhaps it heralds a return to shooting flow, but since the grain size is much finer, the actual current velocity was probably less than that which caused the lower laminated unit. The upper pelitic E unit indicates resumption of the low-energy environment which prevailed before the turbidite was laid down.

TIME	*Process* (*cause*)	*Structure* (*effect*)
↓	Erosion	Current scours, e.g. flute marks, channels, scour and fill. Obstacle scours formed down current of pebbles, shells, etc. Tool marks, i.e. groove marks due to travelling objects
	Deposition	Graded bedding lamination micro-crosslamination.
		Convolute lamination.
	Deformation	Loadcasts, slumps, slides pullaparts, sand dikes, sand volcanoes.

Table 10.1. Summary of sedimentary structures associated with turbidites (see Pettijohn and Potter, 1964, for illustrations and definitions).

It is important to note that the above sequence of structures is seldom completely developed in any one turbidite. The previous interpretation is based on the study of many turbidite sequences. Variations on this motif are discussed by Bouma (1962, pp. 49–54), Walker (1965, p. 3), and Van der Lingen (1969, p. 12). Systematic vertical variations in the frequency of bed forms within sequences of turbidites have been documented by Walker (1967, 1970). There is a tendency for only the upper units to be developed at the base of a turbidite sequence. Moving up the section, progressively lower units

are present within each turbidite until complete A–E sequences appear towards the top of the series. The lower incomplete turbidites, termed 'distal', are believed to have been deposited far from the source. The upper complete units are termed 'proximal' and are believed to have been deposited near the source. A thick sequence of turbidites may thus record a gradual advance of the sediment source into the depositional area.

There has been considerable discussion about the texture of turbidites. Many ancient examples are poorly sorted with clay matrices; petrographically many are greywackes as already mentioned. However, recent deep-sea sands are widely held to be turbidites, but they are often well-sorted and clay-free (Hubert, 1964). Cummings (1962) has suggested that ancient turbidites might often have been deposited as clean, but mineralogically immature, sands in which the matrix developed from the diagenetic break-down of chemically unstable minerals. Turbidites range in grain size from silts to pebbly sandstones. The coarser varieties, often termed fluxoturbidites, are attributed to deposition by a process midway between turbidity flow and gravity slumping. Petrographically many ancient turbidites are greywackes while Recent deep-sea sands are generally protoquartzites. Protoquartzite ancient turbidites have been identified by Sturt (1961). Carbonate turbidites have been described from ancient and Recent sediments (see Table 10.2). This table also shows that turbidites have been described from a very wide range of depositional environments and are not even restricted to sedimentary rocks, but have also been described from layered gabbros (Irvine, 1965). It can be seen therefore that turbidites are characterized by

	Recent	*Ancient*
FIORDS:	Holtedahl (1965)	
LAKES:	Grover and Howard (1938)	Kuenen (1951)
DELTAS:	See Chapter 5	See Chapter 5
REEFS:	?	Carozzi and Frost (1966)
CARBONATE SHELF: MARGINS	Rusnak and Nesteroff (1964)	Thomson and Thomasson (1969) Rech-Frollo (1973)
ANCIENT FLYSCH AND RECENT DEEP-SEA SANDS:	See this chapter.	
LAYERED GABBROS:		Irvine (1965)

Table 10.2. Environments from which turbidites have been recorded.

the sum total of a wide range of sedimentary structures. Texturally turbidites are generally described from poorly sorted sediments, but this is not always the case. Petrographically they are most commonly recorded from greywackes, but also occur in other sandstone types and in limestones. They have been reported from a wide range of environments. With this great diversity of characteristics one might suppose that turbidites were hard to recognize. A review of the literature suggests that, on the contrary, many geologists think that they can identify a turbidite with confidence when they see one.

From what has been said already, it is obviously important to look at modern deep sea sands when trying to understand this facies.

Studies of modern continental margins show that their physiography is analogous to that of desert wadis and alluvial fans (Fig. 10.2).

The continental shelf edge is dissected by submarine channels. The source of these channels lies adjacent to either major river mouths or even coastal beaches. The channels continue down through the continental slope and debouch their sediment load onto a submarine fan, analagous to a subaerial alluvial fan. At the fan apex the submarine channel splits into a radiating complex of small channels, which are often flanked by levees. These channels become more numerous, shallower and wider down the fan. There are also changes down the fan in the sediment facies. The coarsest sand, and sometimes gravel, is deposited in the proximal (near source) part of the fan. Grain size declines distally down fan as the submarine fan sands grade out into pelagic muds of the oceanic basin floor (Shepard, 1971; Dott, 1974; Whitaker, 1976; Kelling and Stanley, 1976).

The deposits of the submarine fans show many of the characteristics of turbidites, which have been previously described and discussed.

The submarine channels are sometimes infilled by turbidites, especially at their distal ends, but they also contain the deposits of other depositional processes. At their proximal ends they may contain heterogenous slumped boulder beds, if they originate in submarine fault scarps.

If, on the other hand, the sediment in the channel is clean sand, brought in by longshore drift or from a river mouth, then a different

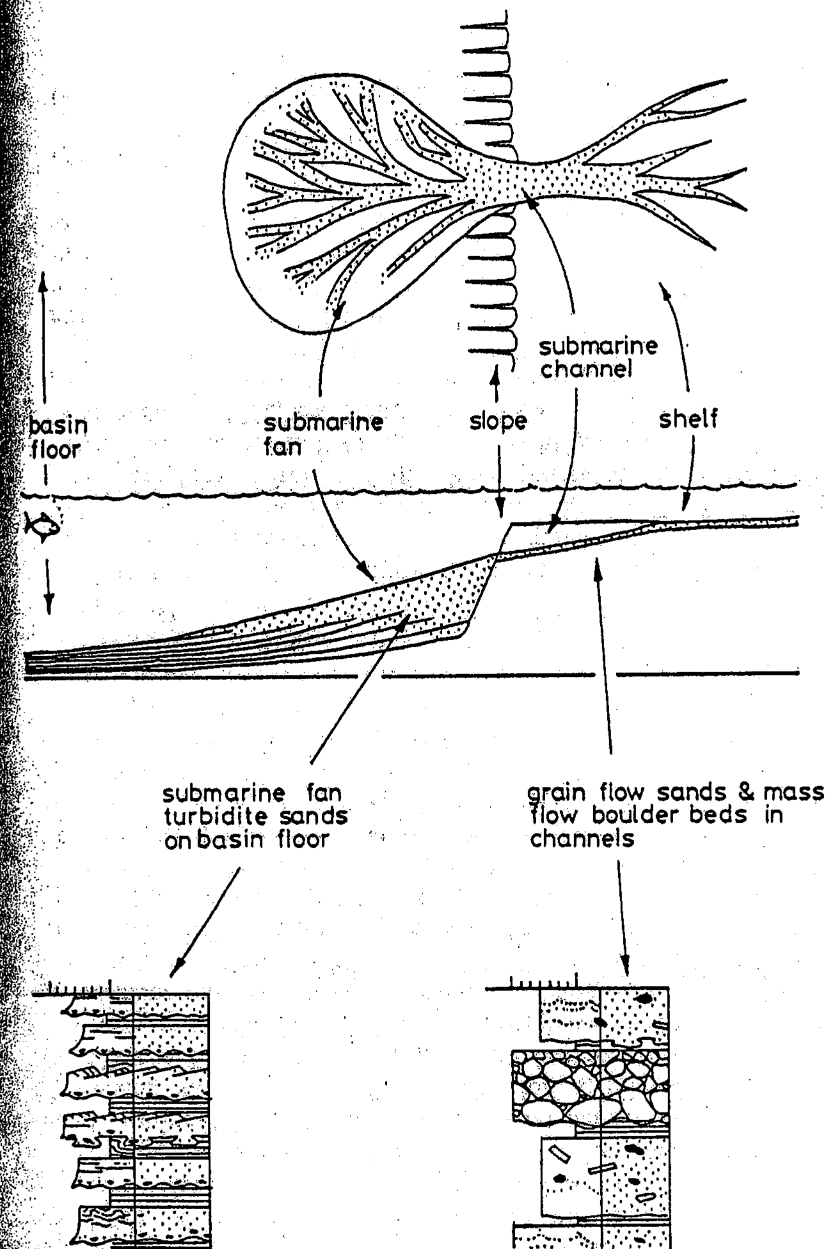

Figure 10.2 Diagrams to illustrate the geomorphology and sedimentology of deep sea sands.

process often prevails. This is known as grainflow and is midway between a mass flow and a turbidite (Bagnold, 1966). The sedimentary features of grain flows have been described by Stauffer (1967) and other geologists. These deposits show neither the graded bedding of turbidites nor the cross-bedding of traction deposits. They are massive sands with abrupt upper and lower contacts. Clasts may occur scattered throughout the bed. Internally this is massive, or may show faint convoluted bedding. Sediments of this type are generally found to have been deposited on the steep slopes of sandy deltas and continental margins. They are often, but not invariably, confined to channels.

Table 10.3 shows the relationship between the geomorphology, processes and facies of submarine channels and fans.

	Geomorphology	*Deposit*
DEEP SEA SANDS	Submarine channels	infilled by either: a) slope muds b) mass flow conglomerates c) grain flow sands d) turbidite sands
	Submarine fans	composed of turbidite sands and pelagic muds

Table 10.3. The geomorphology and deposits of deep sea sedimentary environments.

The slopes with which these are associated may be either accretional or tectonic. Submarine channels and fans are found at the foot of modern deltas, such as the Rhône, and at the foot of such tectonic features as submarine fault scarps and continental margins. Specific accounts of such ancient analogues have been given by Mutti and Lucchi (1972) and Van de Kamp *et al.* (1974) respectively.

DISCUSSION OF THE ORIGIN OF TURBIDITES

It has already been argued (p. 233) that the vertical fining of grain size above a scoured surface suggests that these beds were deposited from waning currents. The suggestion that this current was a turbidity flow was put forward by Kuenen and Migliorini (1950) though the germ of the idea was somewhat older (see Van de Lingen (1969) for a historical review). Subsequently the concept has been greatly elaborated and popularized. The basic idea of the turbidity flow may be summarized thus: In certain regions, such as the edges of continental shelves and deltas, rapid deposition takes place, causing the formation of a steeply sloping pile of waterlogged sediment. Every now and then the slope becomes so unstable that a triggering mechanism, such as an earthquake or storm, starts the sediment moving. Initially it slides and slumps down gullies becoming more and more liquefied until the mixture assumes the characteristics of a turbidity current. That is to say it changes into a muddy liquid whose density is greater than that of the surrounding water. It therefore moves down slope under gravity beneath the clear water. As it gains momentum it becomes erosive, cutting gullies while still on the steep slope and flute marks, etc., on reaching the open-sea floor. On this level surface the velocity starts to diminish. Deposition then takes place, first of the coarsest sediment, and, as the current wanes, of particles of finer and finer grade. When the velocity has returned to zero pelagic mud deposition continues out of suspension as before. All is quiet on the sea floor; a graded bed has been deposited on a scoured surface.

The evidence that turbidity flows deposit the sediments that geologists call turbidites is twofold. It is gathered from experiments and from observations of Recent deep-sea deposits. Graded bedding has been formed from turbidity flows generated artificially in the laboratory (Kuenen, 1948; Kuenen and Migliorini, 1950; Kuenen and Menard, 1952; and Middleton, 1966a, b, and c). Recent deep-sea sands are reported as often showing graded bedding (e.g. Shepard, 1963, p. 406; Horn *et al.*, 1971; and Horn *et al.*, 1972). The suite of internal structures found in ancient turbidites is also sometimes present (e.g. Van Straaten, 1964). The classic oft-quoted reason for believing that Recent deep-sea sands may be turbidites is the case of the 1929 Grand Banks earthquake. This had an epicentre on the edge of the continental shelf off Newfoundland. Telegraphic cables running approximately parallel to the shelf margin were broken in orderly succession downslope. Cores taken subsequently from this area showed a graded bed of silt with shallow water microfossils. This has been interpreted as the product of a turbidity flow which, generated from slumped sediment near the epicentre of the earthquake, ran down the slope ripping up cables and depositing a bed of graded sediment (Heezan and Ewing, 1952; see also Heezan, 1963, p. 743, and Shepard, 1963, p. 339). It has been widely concluded therefore that Recent deep-sea sands are the product of turbidity flows. Ancient sediments which are comparable to deep-sea sands are attributed to the same process and are categorized as turbidites.

This attractive explanation has, none the less, been criticized by a small but articulate group of geologists. Criticism is of two main types, first that deep-sea sands are not turbidites and second that ancient turbidites do not resemble deep-sea sands.

The evidence against a turbidite origin for Recent deep-sea sands has been marshalled by Hubert (1964; 1967), Klein (1967), and Van de Lingen (1969). These authors point out that many deep-sea sands are clean washed, that grading is not always present, and that ripple-marking is common. Traction currents on the ocean floors are strong enough to transport sand, and ripples have been photographed at great depths (e.g. Menard, 1952). It is possible therefore that deep-sea sands are deposited not by catastrophic turbidity flows but by gentle intermittent traction currents. One of the great charms of the turbidite hypothesis was that it could explain the formation of submarine canyons on the edges of the continental shelves. These are now accessible to SCUBA divers and submersibles. Turbidity currents have not been seen in the heads of submarine canyons. Instead sand slowly creeps like a glacier, slumping and cascading over hanging valleys. Attempts to generate turbidity flows in canyon heads have been unsuccessful (Dill, 1964).

Evidence against a turbidite origin for ancient rocks which have been called turbidites hinges therefore on the two arguments that they do not resemble Recent deep-sea sands, and that these may be traction deposits anyway. Of particular interest here are the palaeocurrents of ancient turbidites. It has been noted that slump folds and turbidite bottom structures both tend to indicate movement down the palaeoslope (Walker, 1970). Sometimes however discrepancies have been noted, both between bottom structures and ripple orientations, and palaeoslope, determined from independent criteria (Kelling, 1964, and Klein, 1967). It has been suggested that the reworking of the top of a turbidite by normal oceanic currents may

generate ripples migrating in directions oblique to the (?) down slope oriented bottom structures. This is an attractive compromise. However, Hubert (1967) has discovered an Alpine flysch with plant fragment orientations in the shales which coincide with the sand palaeocurrents. Since the former must be due to the normal oceanic currents perhaps the latter are too. Another curious feature is that not all flysch palaeocurrents are slope-controlled as one would expect to find in gravity-controlled turbidites. Scott (1966) found gravity-controlled slumps which had moved at right angles to associated flysch palaeocurrents. In this context it is interesting to note that Recent oceanic bottom currents are not always slope-controlled and often show a tendency to flow parallel to bathymetric contours (Klein, 1967, p. 376).

The arguments for and against a turbidite origin for ancient 'turbidites' and Recent deep-sea sands are endless. From the necessarily short preceding discussion of this problem the following points should be noted: There is a particularly widespread sedimentological phenomenon found in ancient rocks, especially flysch, which is widely interpreted as due to turbidity current deposition. This conclusion is partly based on experimental work and partly on the analogy with Recent deep-sea sands, which are believed to be turbidites. However, nobody has actually observed a turbidite in nature even in the submarine canyon heads which should be their homes. It has been argued that Recent deep-sea sands could be traction-deposited and that, anyway, they are not as similar to ancient turbidites as some authors have suggested. Ancient turbidites sometimes show features that one would not expect to find in a turbidity deposit, notably that they were laid down by currents which were not slope-controlled.

What is important, however, is the fact that there is a particular type of sedimentary facies which many geologists call 'flysch' and attribute to deposition from turbidity currents. We may not understand the processes which deposit this facies but, once recognized, we may make predictions of its geometry. This is important because this facies often makes excellent hydrocarbon reservoirs.

DESCRIPTION OF THE ANNOT TROUGH FLYSCH, ALPES MARITIMES

The case history chosen to document this chapter is a turbidite-rich flysch series from the type area of flysch facies: the Annot trough curves around the southwestern edge of the Argentera–Mercantour massif in the Maritime Alps of southeastern France (Fig. 10.3). It contains over 650 m of flysch of Upper Eocene to Oligocene age.

Figure 10.3. Geological sketch map of the Annot trough, Alpes Maritimes. Submarine fan flysch facies stippled, coarse marginal submarine channel facies shown by circular ornamentation. Arrows indicate palaeocurrents. Modified from Stanley, 1967, Fig. 1.

The flysch facies conformably overlies Upper Eocene marls in the trough axis. Laterally equivalent thick sandstone bodies in the trough margins cut into the underlying marls. Two distinct sedimentary facies can be recognized. The axial region of the trough contains the flysch. Around the edge of the trough are tongues of coarser sands and conglomerates (Fig. 10.3). The flysch facies of the Peira Cava area have been studied in great detail. These data will now be summarized. The sequence in this area consists of the classic alternation of sandstones and shales. As the formation is traced northwards into the basin sands become less abundant and their grain size decreases. Within any vertical section the sand : shale ratio

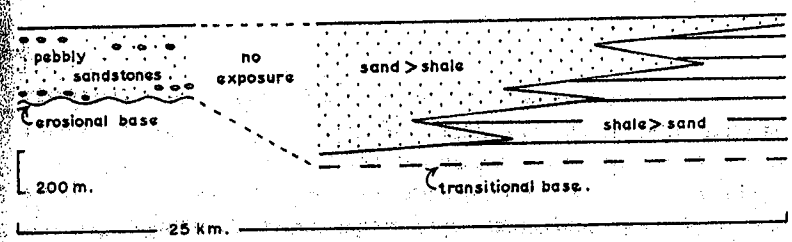

Figure 10.4. Diagrammatic cross-section illustrating the relationship between the submarine channel of the Contes pebbly facies, and the Piera Cava Submarine fan flysch.

increases upward (Fig. 10.4). The sandstones are poorly sorted and range in grain size from coarse to fine. Petrographically they are hard to classify, ranging between arkose and greywacke according to the classification adopted. Sand bed thickness is variable, being generally measurable in decimetres, though beds over 1 m thick are sometimes present. Internally the sands show all the classic features of turbidites. Grading is present in nearly every bed, and the A–E sequence of intrabed units is well developed (Fig. 10.1), being first recognized and defined in this area. The base of the sandstones are erosional with a diverse suite of bottom structures including flute marks, grooves, loadcasts, and scour and fill. Palaeocurrents determined from the sandstones show a generally northerly direction of transport, diverging radially from the southern apex of the present pear-shaped outcrop of the Peira Cava formation.

Trace fossils and body fossils are found in the sequence. Both the sands and the shales are sometimes burrowed, and trail covered sand : shale contacts occur. Some rare gastropods, echinoid spines, and faecal pellets have been found. There is an assemblage of pelagic foraminifera.

A second facies is developed in outliers to the south and west of the flysch in the centre of the Annot trough (Fig. 10.3). These outliers occupy north–south trending synclines. The erosional bases and restricted distribution of these patches strongly suggest that their present geometry broadly corresponds to their original distribution. They are believed to have been deposited, therefore, in huge channels up to 5 km wide and, in some cases, with a relief in excess of several hundred metres. Lithologically the sediment filling the channels contrasts markedly with the flysch to the north. Shale is rare, sandstones are coarse, poorly sorted, and pebbly. Bedding is lenticular due to channelling and there is an abundance of slump bedding. Marine shells are present with foraminifera and plant debris. Graded sand : shale units are rare. The orientations of ripples, scour marks, channel trends, and pebble imbrication indicate northerly flowing palaeocurrents.

DISCUSSION OF THE ANNOT TROUGH SANDSTONES

The flysch sandstones of the Annot trough show all the classic features of turbidites discussed at the beginning of this chapter. The coarse marginal channel facies might, at first glance, be thought to be fluviatile. However, the presence of a marine fauna and slumps suggest that these beds were laid down in northerly sloping submarine channel complexes. The fact that these merge downcurrent with the flysch facies strongly suggests that the latter were deposited on submarine fans which built out northwards into the deper parts of the trough. Particularly striking is the relationship between the pebbly sandstone channel complex at Contes from whose northern end the Peira Cava flysch palaeocurrents radiate (Fig. 10.3).

In conclusion this study provides a classic example of a flysch deposited to a large degree by marine slope-controlled turbidity currents. The similarity with Recent submarine canyon apron fan complexes is most striking.

FLYSCH AND TURBIDITES: CONCLUDING DISCUSSION

This chapter has described the characteristics of a distinctive sedimentological assemblage of sedimentary structures and graded sandstones which are found in many Recent and ancient sedimentary environments. Such sequences have been widely interpreted as turbidites, due to deposition from muddy sediment suspensions of waning velocity. Evidence for ancient turbidites is based partly on experimental work and partly on observed similarities with Recent deep-sea sands interpreted as turbidites.

Flysch facies are popularly thought to be turbidites. Large

volumes of flysch crop out today in mountain chains and are believed to have been deposited in linear troughs termed geosynclines. Many ancient flysch sandstones are poorly sorted with considerable amounts of feldspar and rock fragments. Petrographically such sandstones are greywackes.

There has been considerable discussion of the depth at which turbidites accumulate. As a general rule one might suggest that, though a turbidity flow could occur in shallow water, rapid burial or deposition below wave base would be essential to prevent the turbidite from being re-worked completely by traction currents. As we have seen, however, graded greywackes interpreted as turbidites occur in the Torridonian Series of Scotland interbedded with desiccation-cracked shales (p. 49). Stanley (1968) has reviewed a number of other shallow water turbidites.

The majority of workers, however, have favoured a deep water origin for flysch turbidites. Reasons for this conclusion are largely palaeontological. Many flysch sandstones contain fragments of shallow marine macrofossils, benthonic forams, and plant debris. The interbedded shales however contain pelagic foraminifera which may indicate considerable depths. For example, Natland and Kuenen (1951) described a 19,000-ft turbidite sequence from the Ventura basin, California. At the base foraminifera compare with species living today at depths of 4,000–5,000 ft. Moving up the section foraminifera suggest shallower depths when compared with Recent assemblages. At the top of the sequence the turbidites pass into fluviatile sediments with horse bones. Such studies have been criticized on the grounds that the depth distribution of Recent foraminifera is a function not only of depth but of temperature and other ecological factors (Rech-Frollo, 1962). Two other palaeontological studies bearing on the depth of flysch should be noted. The Jaslo shales (Oligocene) of the Krosno flysch in the Polish Carpathians contain fossil fish with light-bearing organs similar to species living today at oceanic depths (Jerzmanska, 1960). Tertiary flysch from the Pyrenees contains tracks interpreted as bird footprints (Mangin, 1967). Despite this last curious case the weight of the evidence, both faunal and sedimentological, suggests that flysch sands were emplaced at depths below wave base. Deposition was either too deep or too rapid to permit the growth of an abundant benthos. The problem of the depth of deposition of flysch is discussed at greater length by Dzulinski and Walton (1965), Duff, Hallam, and Walton (1967, p. 221), and Van der Lingen (1969).

Criticisms of the turbidite hypothesis put forward to explain flysch have been based on arguments that flysch sands do not resemble deep-sea sands and that, even if they do, the latter may not be turbidites anyway, but due to waning traction currents. Support for this criticism is provided by some palaeocurrent studies which show discrepancies between the palaeoslope and the flysch palaeocurrent indicators. These should coincide if the flysch sandstones were deposited by gravity-controlled turbidity flows.

It is at present difficult to resolve the arguments for and against a turbidite origin of flysch. Despite some three decades of intensive research this fascinating facies provides as challenging a problem to the geologist as it has ever done.

ECONOMIC ASPECTS OF FLYSCH AND TURBIDITES

Deep sea sands of turbidite or flysch facies are obviously not potential hydrocarbon reservoirs when they have been involved in orogenesis within geosynclines. Incipient metamorphism destroys porosity, and breaks down hydrocarbons while structural deformation allows the escape of any pore fluids.

Deep sea sands in non-orogenic situations are often highly productive of oil and gas when they occur at the foot of deltas or in fault-bounded troughs with restricted marine circulation. In these situations the pelagic basin floor muds may act as source beds which generate oil and gas. The hydrocarbons can migrate updip through the turbidite fan sands with which they interfinger. Oil and gas may be trapped both in structural traps, and stratigraphically where submarine channel sands are sealed updip by impermeable slope muds. The turbidite fans generally have lower porosities and permeabilities than the grainflow channel sands, but are laterally more extensive. The Palaeocene fields of the North Sea, including Forties and Montrose, occur in deep sea sands (Parker, 1975).

Another case of prolific oil production in turbidites occurs in western California. Here over 30,000 ft of turbidites were deposited in downfaulted Tertiary basins. Subsequent tectonism has involved only gentle folding. As already mentioned (p. 245) foraminifera in the shales indicate original basin depths of some 5,000 ft. These

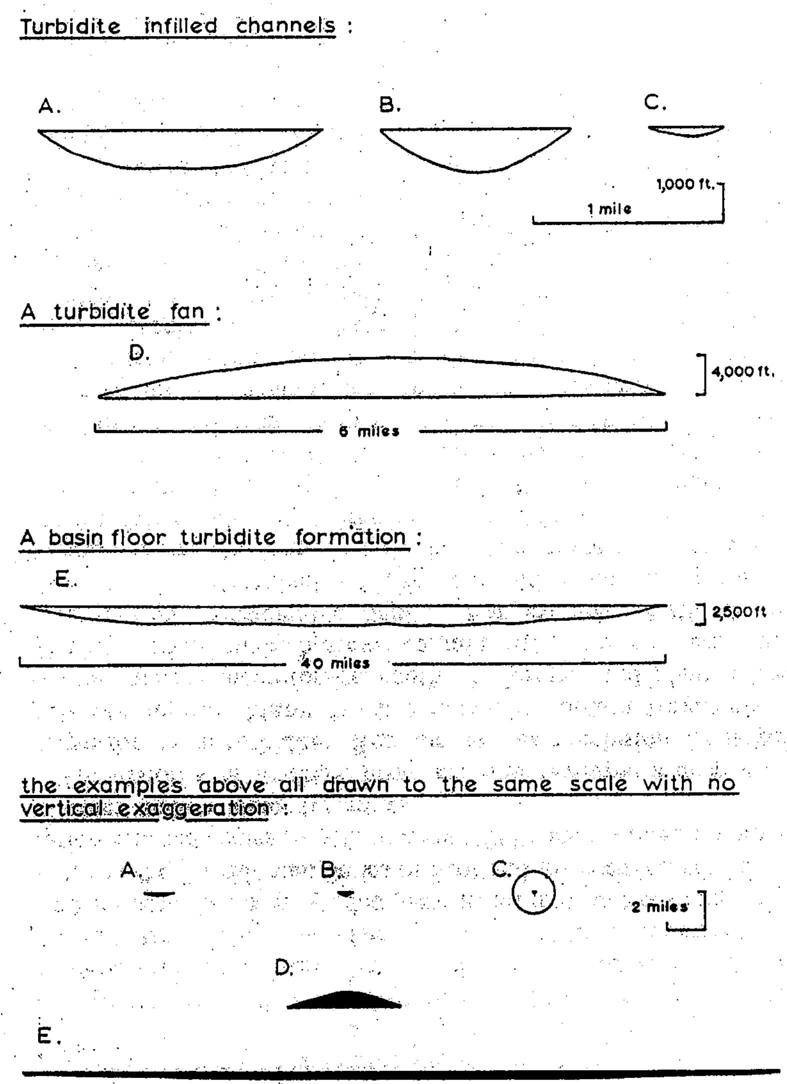

Figure 10.5. Palaeostrike cross-sections of turbidite geometries. Sources of data cited in the text. A. Contes channel, Annot trough, Alpes Maritimes. B. Rosedale channel, San Joaquin basin, California. C. Sansina channel, Los Angeles basin, California. D. Tarzana fan, Los Angeles basin, California. E. Repetto turbidite sheet, Los Angeles basin, California.

shales are presumably the source rocks. Despite poor sorting and relatively low porosity and permeability the turbidite sands are good oil reservoirs. This is because individual beds are of unusually great thickness for turbidites, sometimes in excess of 10 ft. Furthermore, multistorey sand sequences are common, shale between turbidites being absent either due to erosion or to a rapid frequency of turbidity flows.

Three main geometries can be recognized in Tertiary Californian turbidite facies and these can be related to deep-sea sediments now forming off the present-day Californian coast (Hand and Emery, 1964). Shoestring turbidites occupy channels sometimes located along syn-sedimentary synclines (cf. the Contes channel of the Alpes Maritimes). Sullwold (1961) cites an example 150 ft thick and 2,000 ft wide, whose associated foraminifera suggest deposition in 1,000–2,000 ft of water. The Rosedale Channel (Miocene) of the San Joaquin basin was about one mile wide and contains some 1,200 ft of turbidites. It can be traced downslope for about 5 miles and its fauna suggests depths greater than 1,300 ft (Martin, 1963). Other examples are discussed by Webb (1965).

Shoestring turbidite bundles such as these probably formed in submarine channels similar to those of the present-day continental margins.

The second turbidite geometry is fan-shaped in plan and lenticular in cross-section. The Upper Miocene Tarzana fan identified by Sullwold (1961) is about 6 miles wide and 4,000 ft thick. Associated foraminifera indicate a depositional depth of about 3,000 ft. Other examples are lobate and branching (Webb, 1965). Geometries such as these can be directly compared to present-day fans formed by sediment debouching from the mouths of submarine canyons on to abyssal plains.

The third facies geometry found in Californian Tertiary turbidites is a sheet. This is believed to be due to deposition on a basin floor. The Repetto Formation (Lower Pliocene) is an example of this type. It has a maximum thickness of more than 2,500 ft and covers some 800 square miles (Shelton, 1967).

Figure 10.5 illustrates the geometry of those three types of deep sea facies. Sedimentology obviously has a role to play in the exploitation of oil from turbidite facies as, and when, it is found. It is important first to recognize the environment, second to identify the type of geometry, and finally to predict the trend of an individual turbidite bundle.

SUB-SURFACE DIAGNOSIS OF DEEP SEA SANDS

Because of their economic importance great attention has been paid to the recognition of deep sea sands both at outcrop (e.g. Stanley and Unrug, 1972), and in the sub-surface (Selley, 1977).

The geometry of submarine channels and fans may be identified by seismic mapping prior to drilling in marine basins.

Lithologically deep sea sediments are diverse, ranging from boulder beds to the finest silt. Glauconite and carbonaceous detritus are often found mixed together in turbidite sands where the sediment is derived from both deltaic and marine shelf environments. As pointed out earlier, carbonate turbidites occur at the foot of carbonate shelves. An admixture of transported shallow water fauna in the turbidite sands with a pelagic fauna with 'Nereites' ichnofacies in the intervening shales is also typical.

When cores are available the typical Bouma A–E sequences may be found in the submarine fan turbidites, and the diagnostic features of grain flows may be found in the submarine channels.

There are particularly diagnostic gamma and S.P. log motifs but they can be confused with deltaic ones. Turbidite sequences show a very 'nervous' pattern with the curve swinging to and fro with a large amplitude. This reflects the interbedding of sands and shales, but the vertical resolution of both the gamma and S.P. logs is seldom sufficient to actually show individual graded beds. Turbidite fan sequences often show an overall upward-sanding motif which reflects the basinward progradation of the fan over basinal shales.

Submarine channels which are infilled by grainflow sands show steady featureless log profiles with abrupt lower surfaces reflecting the erosional base of the channel floor. These are commonly found above progradational fan motifs. Figure 10.6 shows these log motifs and Figure 10.7 illustrates a real example from the North Sea.

There are also characteristic dipmeter motifs in deep sea sands. Within the submarine channels the heterogenous fabric of boulder beds and grainflow sands may yield a random bag o' nails pattern. Turbidite-infilled channels may show upward-declining red patterns reflecting the gradual infilling of the curved channel floor. Dips will

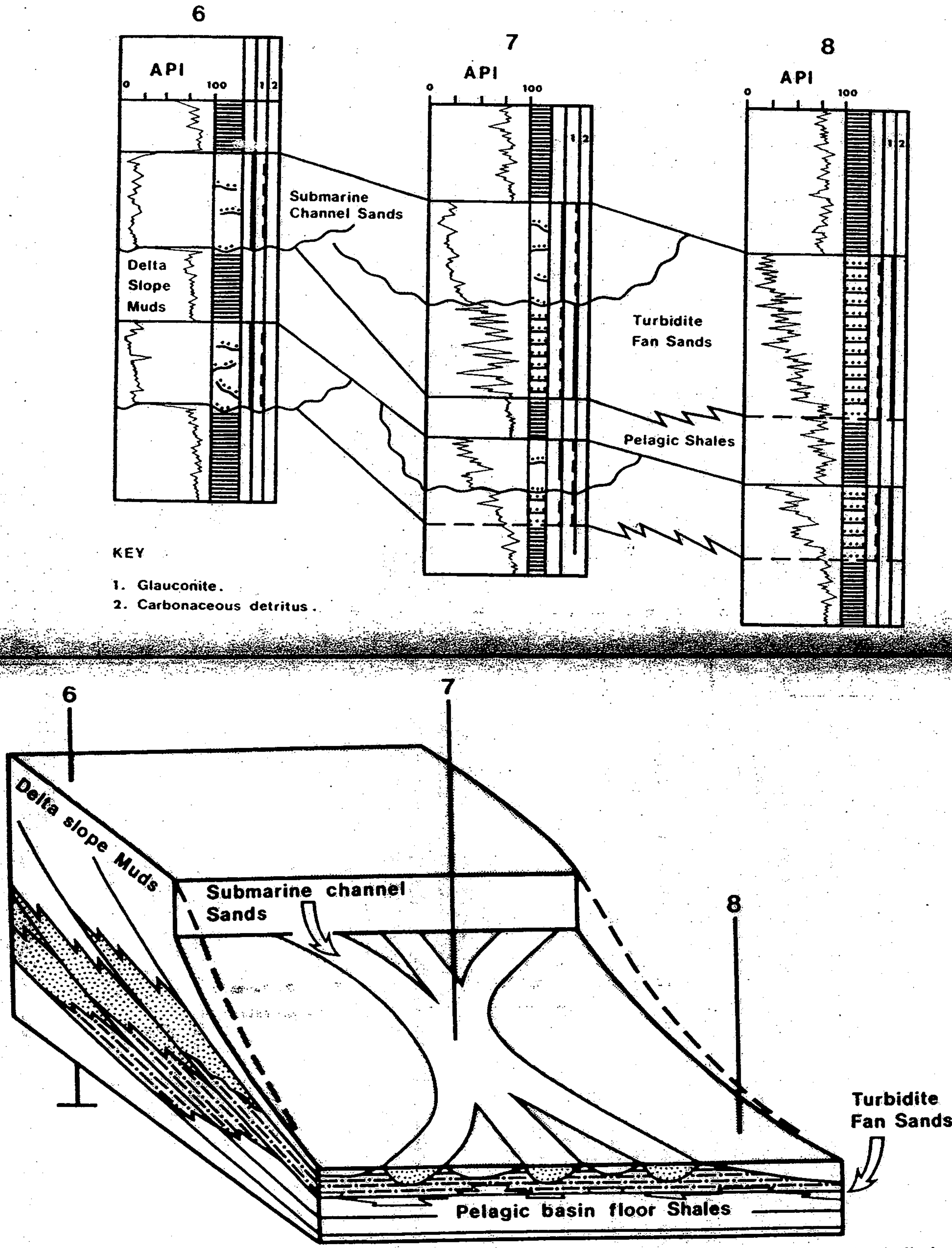

Figure 10.6. Diagrams to illustrate the log motifs (upper) and geometry (lower) of deep sea sands. Note the similarity to the progradational and distributary channel motifs of deltas (Fig. 5.10).

point towards the channel axis, as in shallow water channels (see p. 126), but as cross-bedding is absent there will not be dips pointing down the channel axis. The progradational fan sequences sometimes show upward-increasing blue motifs analogous to those of delta slopes. The dips of those, as in deltas, also point in the direction of sediment progradation (Fig. 10.8).

REFERENCES

The description of the Annot Trough Flysch was based on:

Bouma, A. H., 1959a. Flysch Oligocéne de Peira-Cava (Alpes Maritimes, France). *Eclogae Geol. Helv.*, **51**, pp. 893–900.

——, 1959b. Some data on turbidites from the Alpes Maritimes (France). *Geol. Mijnb.*, **21**, pp. 223–7.

——, 1962. *Sedimentology of Some Flysch Deposits*. Elsevier, Amsterdam. 168 p.

Stanley, D. J., 1962. Etudes sédimentologiques des grès d'Annot et de leurs équivalent latéraux. *Soc. Eds. Technip*. Paris. Ref. 6821, 158 p.

——, 1963. Vertical petrographic variability in Annot sandstones turbidites: some preliminary observations and generalizations. *J. Sediment. Petrol.*, **33**, pp. 783–8.

——, 1965. Heavy minerals and provenance of sands in flysch of central and southern French Alps. *Bull. Amer. Assoc. Petrol. Geol.*, **49**, pp. 22–40.

Stanley, D. J., 1967. Comparing patterns of sedimentation in some ancient and modern submarine canyons. *Preprint Seventh Internat. Sedol. Congress*, 4 p.

——, 1967. Comparing patterns of sedimentation in some modern and ancient submarine canyons. *Earth and Planetry Science Letters*, **3**, pp. 371–80.

——, and Bouma, A. H., 1964. Methodology and palaeogeographic interpretation of flysch formations: a summary of studies in the Maritime Alps. In: *Turbidites*. (Eds. A. H. Bouma and A. Brouwer) Elsevier, Amsterdam. pp. 34–64.

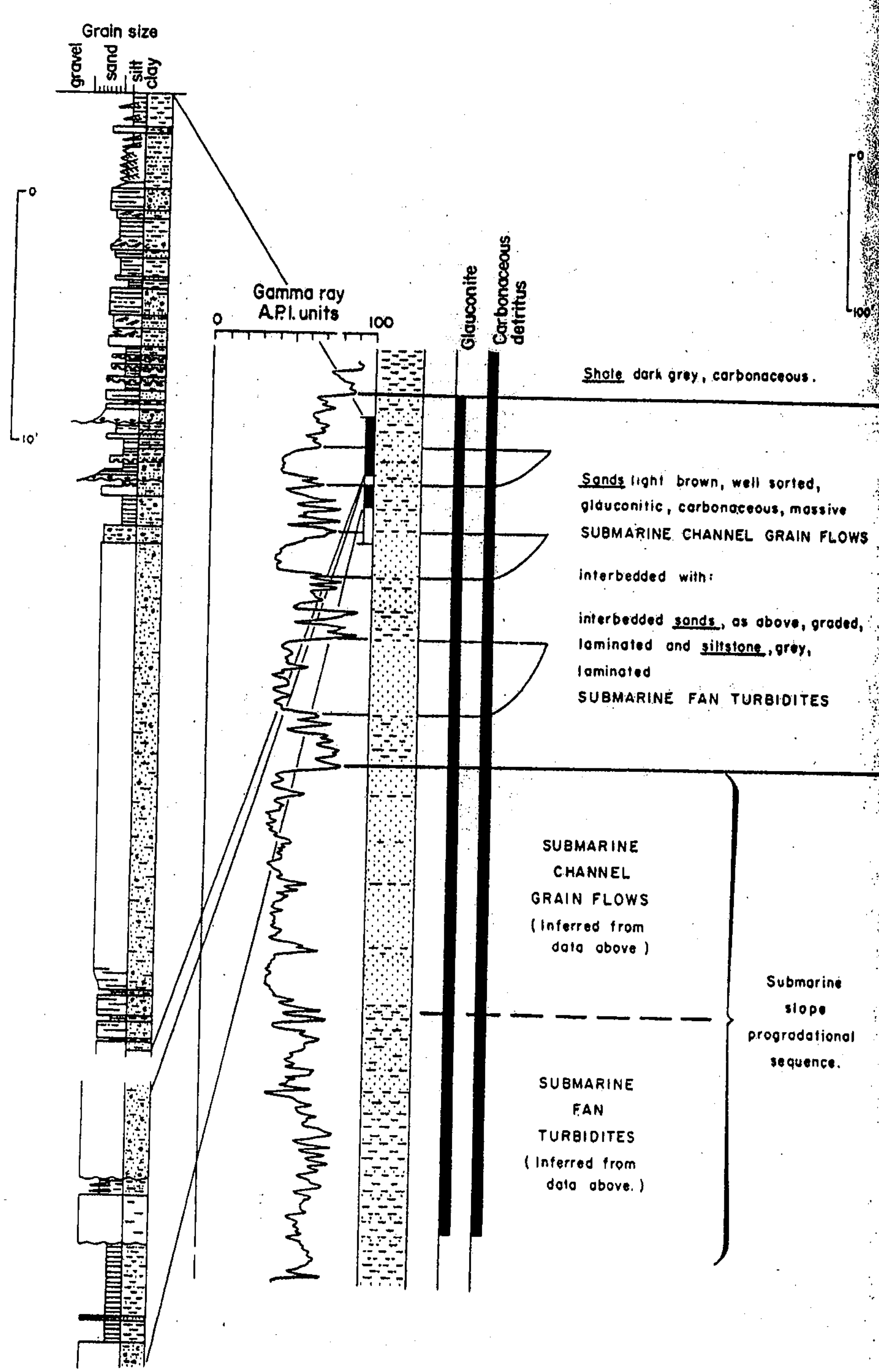

Figure 10.7 Sedimentary core log and gamma log of a deep sea sand from the North Sea. Note how the upper part of the core with turbidite features correlates with an erratic log curve, while the lower part of the core, interpreted as a grainflow, correlates with a steady log curve (from Selley, 1976, Fig. 6, by courtesy of the *American Association of Petroleum Geologists*).

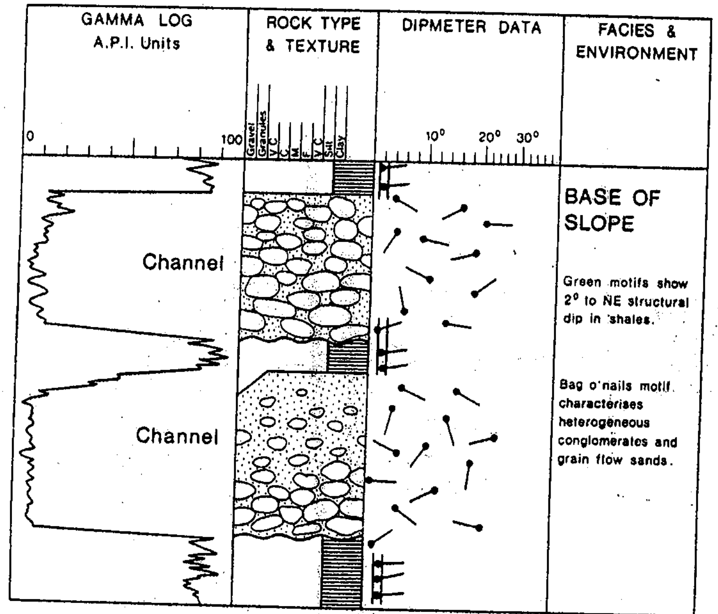

(a)

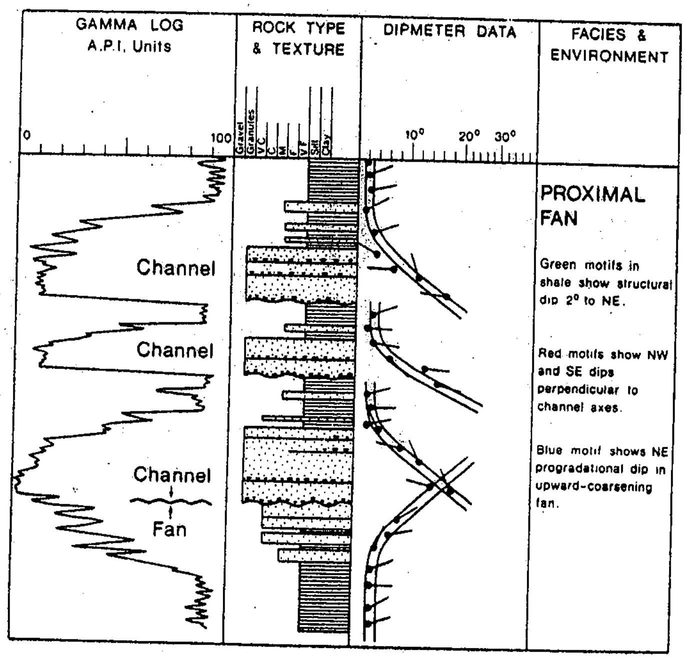

(b)

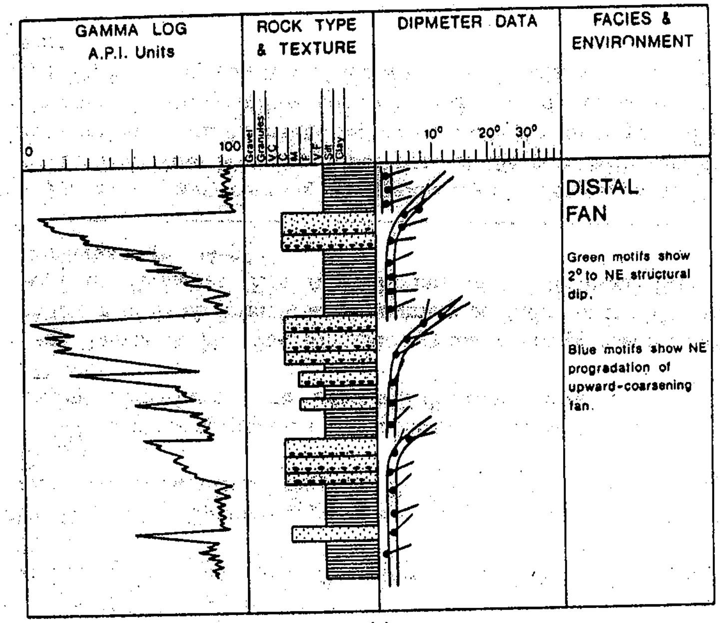

(c)

Figure 10.8. Deep sea sand dip motifs for slope grain flow or conglomerate channels (a), for proximal fan channel confined turbidites (b), and for distal fan turbidites (c). For explanations see text.

Other references cited in this chapter:

Bagnold, R. A., 1966. An approach to the sediment transport problem from general physics. *U.S. Geol. Surv. Prof. Paps.*, 422–I. 37p.

Bouma, A. H., and Brower, A., 1964. *Turbidites.* Elsevier, Amsterdam. 264 p.

Cummings, W. A., 1962. The greywacke problem. *Lpool. Manchr. geol. J.*, 3, pp. 51–72.

Carozzi, A. V., and Frost, S. H., 1966. Turbidites in dolomitized flank beds of Niagaran (Silurian) Reefs, Lapel, Indiana. *J. Sediment. Petrol.*, **36**, pp. 563–75.

Dill, R. F., 1964. Sedimentation and erosion in Scripps submarine canyon head. In: *Marine Geology.* (Ed. R. L. Miller) Macmillan, London. pp. 23–41.

Dott, R. H. (Ed.), 1974. Modern and Ancient geosynclinal sedimentation. *Soc. Econ. Pal. Min.*, Spec. Pub. No. 9.

Duff, P. McL. D., Hallam, A., and Walton, E. K., 1967. *Cyclic Sedimentation.* Elsevier, Amsterdam. 280 p.

Dzulinski, S., and Walton, E. K., 1965. *Sedimentary Features of Flysch and Greywackes.* Elsevier, Amsterdam. 274 p.

Grover, N. C., and Howard, C. S., 1938. The passage of turbid water through Lake Mead. *Trans. Amer. Soc. Civ. Eng.*, **103**, pp. 720–90.

Hand, B. M., and Emery, J. O., 1964. Turbidites and topography of North end of San Diego trough, California. *J. Geol.*, **72**, pp. 526–42.

Harms, J. C., and Fahnestock, R. K., 1965. Stratification, bed forms, and flow phenomena (with an example from the Rio Grande). In: Primary sedimentary structures and their hydrodynamic interpretation. (Ed. G. V. Middleton) *Soc. Econ. Min. Pal.*, Sp. Pub., No. 13, pp. 84–115.

Heezen, B. C., 1963. Turbidity Currents. In: *The Sea*, vol. III. (Ed. M. N. Hill) Interscience, N.Y. pp. 742–75.

——, and Ewing, M., 1952. Turbidity currents and submarine slumps and the Grand Banks earthquake. *Am. J. Sc.*, **250**, pp. 849–73.

Holtedahl, H., 1965. Recent turbidites in the Hardangerfjord, Norway. In: *Submarine Geology and Geophysics.* (Eds. W. F. Whittard and R. Bradshaw) Butterworths, London. pp. 107–42.

Horn, D. R., Ewing, M., Delach, M. N., and Horn, B. M., 1971. Turbidites of the northeast Pacific. *Sedimentology*, **16**, pp. 55–69.

——, Ewing, J. I., and Ewing, M., 1972. Graded-bed sequences emplaced by turbidity currents north of 20° in the Pacific, Atlantic and Mediterranean. *Sedimentology*, **18**, pp. 247–75.

Hsu, K. J., 1970. The meaning of the word Flysch, a short historical search. In: Flysch sedimentology in North America. (Ed. J. Lejoie) *Geol. Soc. Can.*, Sp. Paper 7. pp. 1–11.

Hubert, J. F., 1964. Textural evidence for deposition for many western North Atlantic deep-sea sands by ocean bottom currents rather than turbidity currents. *J. Geol.*, **72**, pp. 757–85.

——, 1967. Sedimentology of pre-alpine flysch sequences, Switzerland. *J. Sediment. Petrol.*, **37**, pp. 885–907.

Irvine, T. N., 1965. Sedimentary structures in Igneous intrusions with particular reference to Duke Island Ultramafic Complex. In: Primary sedimentary structures and their hydrodynamic interpretation. (Ed. G. V. Middleton) *Soc. Econ. Min. Pal.*, Sp. Pub., No. 13, pp. 220–32.

Jerzmanska, A., 1960. Ichthyo-fauna from the Jaslo shales at Sobniow (Poland). *Acta. Palaeontol. Polon.*, **5**, pp. 367–419.

Kelling, G., 1964. The turbidite concept in Britain. In: *Turbidites.* (Eds A. H. Bouma and A. Brouwer) Elsevier, Amsterdam. pp. 75–92.

——, and Stanley, D. J., 1976. Sedimentation in canyon, slope, and base-of-

slope environments. In: *Marine sediment transport and environment management.* (Eds. D. J. Stanley and D. J. P. Swift) J. Wiley, New York. pp. 379–435.

Klein, G. de V., 1967. Paleocurrent analysis in relation to modern sediment dispersal patterns. *Bull. Amer. Assoc. Petrol. Geol.*, **51**, pp. 366–82.

Kuenen, P. H., 1948. Turbidity currents of high density. *Int. Geol. Congr.* 18th Session, pp. 44–52.

——, 1951. Mechanics of varve formation and the action of turbidity currents. *Geol. Fören. Stockholm Förh.*, **73**, pp. 69–84.

——, 1965. Comment. In: Primary sedimentary structures and their hydrodynamic interpretation. (Ed. G. V. Middleton) *Soc. Econ. Min. Pal.*, Sp. Pub., No. 13, pp. 217–18.

——, 1967. Emplacement of flysch-type sand beds. *Sedimentology*, **9**, pp. 203–43.

——, and Migliorini, C. I., 1950. Turbidity currents as a cause of graded bedding. *J. Geol.*, **58**, pp. 91–127.

Lajoie, J., 1970. Flysch sedimentology in North America. *Geol. Soc. Can.*, Sp. Pap. 7. 272p.

Mangin, J. P., 1962. Traces de pattes d'oiseaux et flute-casts associés dansun 'facies flysch' dù Tertiare pyrénéen. *Sedimentology*, **1**, pp. 163–166.

Martin, B. D., 1963. Rosedale Channel: Evidence for Late Miocene submarine erosion in Great Valley of California. *Bull. Amer. Assoc. Petrol. Geol.*, **47**, pp. 441–56.

Menard, H. W., 1952. Deep ripple marks in the sea. *J. Sediment. Petrol.*, **33**, pp. 3–9.

Middleton, G. V., 1966a. Small-scale models of turbidity currents and the criterion for auto-suspension. *J. Sediment. Petrol.*, **36**, pp. 202–8.

——, 1966b. Experiments on density and turbidity currents. I. Motion of the head. *Can. Jnl. Earth Sc.*, **3**, pp. 523–46.

——, 1966c. Experiments on density and turbidity currents. II. Uniform flow of density currents. *Can. Jnl. Earth Sc.*, **3**, pp. 627–37.

——, 1967. Experiments on density and turbidity currents. III. *Can. Jnl. Earth Sc.*, **4**, pp. 475–505.

Mutti, E. and Lucchi, F. R., 1972. Le turbiditii dell'Appennino settentrionale: introduzione all'analisi di facies. *Mem. Soc. Geol. Ital.*, **XI**, pp. 161–99.

Natland, M. L., and Kuenen, P. H., 1951. Sedimentary history of the Ventura Basin, California, and the action of turbidity currents. *Soc. Econ. Min. Pal.*, Sp. Pub., No. 2, pp. 76–107.

Parker, J. R., 1975. Lower Tertiary sand development in the central North Sea. In: *Petroleum and the continental shelf of northwest Europe.*

(Ed. A. W. Woodland) Applied Science Publishers, London. pp. 447–56.

Pettijohn, F. J., and Potter, P. E., 1964. *Atlas and glossary of primary sedimentary structures*. Springer-Verlag, Berlin. 370 p.

Rech-Frollo, M., 1962. Quelques aspects des conditions de dépôt du flysch. *Bull. Geol. Soc. France*, **7**, pp. 41–8.

——, 1973. Flysch carbonates. *Bull. Centre Rech. Pan.*, **7**, pp. 245–63.

Rusnak, G. A., and Nesteroff, W. D., 1964. Modern turbidites: terrigenous abyssal plain versus bioclastic basin. In: *Marine Geology*. (Ed. R. L. Miller) Macmillan, New York. pp. 488–503.

Scott, K. M., 1966. Sedimentology and dispersal pattern of a Cretaceous flysch sequence, Patagonian Andes, southern Chile. *Bull. Amer. Assoc. Petrol. Geol.*, **50**, pp. 72–107.

Selley, R. C., 1976. Sub-surface environmental analysis of North Sea sediments. *Bull. Amer. Assoc. Petrol. Geol.*, **60**, 184–95.

——, 1977. Sub-surface diagnosis of deep sea sands. *Proc. 2nd Northern North Sea Jurassic Symposium*. Norwegian Petroleum Society, Oslo. MNNSS 31p.

Shelton, J. W., 1967. Stratigraphic models and general criteria for recognition of alluvial, barrier bar and turbidity current sand deposits. *Bull. Amer. Assoc. Petrol. Geol.* **51**, pp. 2441–60.

Shepard, F., 1971. *Submarine canyons and other sea valleys*. Wiley, New York. 381p.

Stanley, D. J., 1968. Graded bedding–sole markings–graywacke assemblage and related sedimentary structures in some Carboniferous flood deposits, eastern Massachusetts. *Geol. Soc. Amer. Spec. Pap.* No. 106, pp. 211–39.

——, and Unrug, R., 1972. Submarine channel deposits, fluxoturbidites and other indicators of slope and base of slope environments in modern and ancient marine basins. In: Recognition of Ancient sedimentary environments. (Eds. J. K. Rigby and W. K. Hamblin) *Soc. Econ. Pal. Min.*, Sp. Pub. No. 16. pp. 287–340.

Stauffer, P. H., 1967. Grainflow deposits and their implications, Santa Ynez Mountains, California. *J. Sediment. Petrol.*, **37**, pp. 487–508.

Sturt, B. A., 1961. Discussion in: Some aspects of sedimentation in orogenic belts. *Proc. Geol. Soc. Land.*, No. 1587, p. 78.

Sullwold, H. H., 1961. Turbidites in oil exploration. In *Geometry of Sandstone Bodies*. (Eds. J. A. Peterson and J. C. Osmond) Amer. Assoc. Petrol. Geol. pp. 63–81.

Thomson, A. F., and Thomasson, M. R., 1969. Shallow to deep water facies development in the Dimple limestone (Lower Pennsylvanian), Marathon Region, Texas. In: Depositional environments in carbonate

rocks. (Ed. G. M. Friedman) *Soc. Econ. Min. Pal.*, Sp. Pub., No. 14, pp. 57–78.

Walker, R. G., 1965. The origin and significance of the internal sedimentary structures of turbidites. *Proc. Yorks. Geol. Soc.*, **35**, pp. 1–32.

——, 1967. Turbidite sedimentary structures and their relationship to proximal and distal depositional environments. *J. Sediment. Petrol.*, **37**, pp. 25–43.

——, 1970. Review of the geometry and facies organisation of turbidites and turbidite-bearing basins. In: Flysch sedimentology of North America (Ed. J. Lajoie) *Geol. Soc. Can.*, Sp. Pub. pp. 219–51.

Webb, F. W., 1965. The stratigraphy and sedimentary petrology of Miocene turbidites in San Joaquin Valley (Abs.), *Bull. Amer. Assoc. Petrol. Geol.*, **49**, p. 362.

Whitaker, J. H. McD. (Ed.), 1976. *Submarine canyons and deep-sea fans. Modern and Ancient*. Dowden, Hutchinson & Ross, Stroudsburg, Pa. 426p.

Van de Kamp, P. C., Conniff, J. J., and Morris, D. A., 1974. Facies relations in the Eocene-Oligocene in the Santa Ynez Mountains, California. *J. Geol. Soc. Lond.*, **130**, pp. 54–566.

Van der Lingen, G. J., 1969. The turbidite problem. *N.Z. Jl. Geol. Geophys.*, **12**, pp. 7–50.

Van Straaten, L. M. J. U., 1964. Turbidite sediments in the southeastern Adriatic sea. In: *Turbidites*. (Eds. A. H. Bouma and A. Brouwer) Elsevier, Amsterdam. pp. 142–7.

Bone Canyon

Shumard and Bone Canyon Traverse

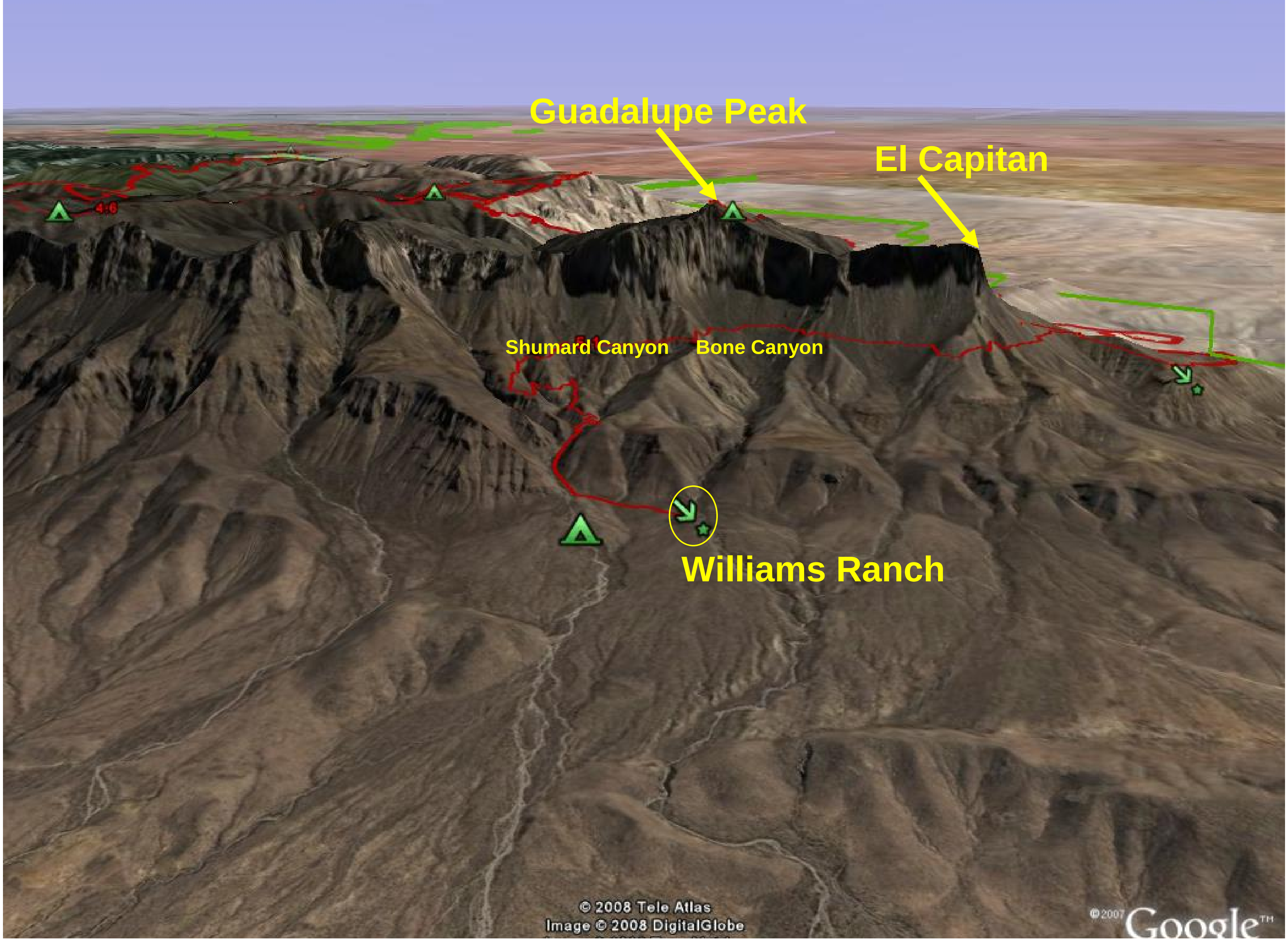

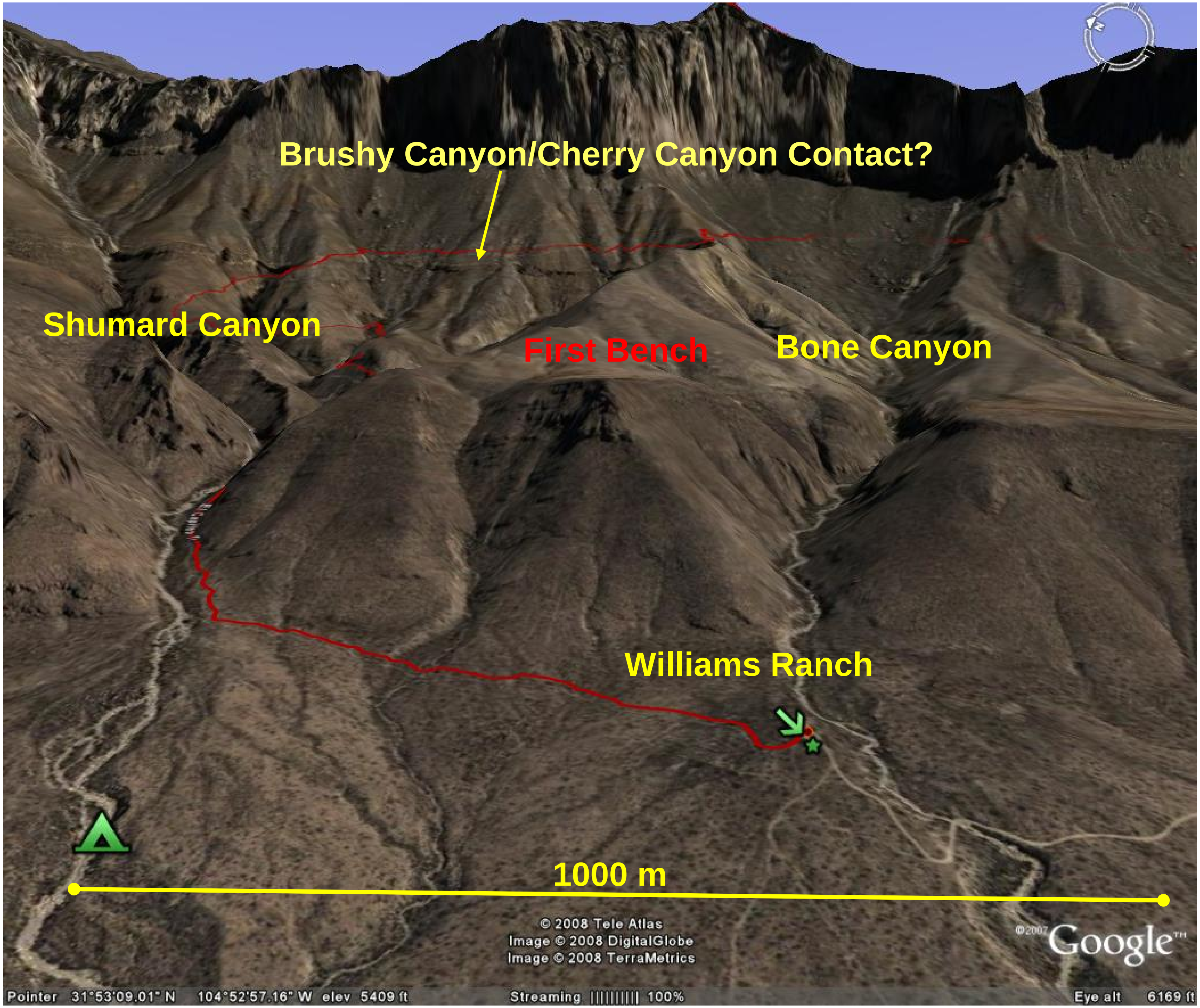
Brushy Canyon/Cherry Canyon Contact?
Shumard Canyon
First Bench
Bone Canyon
Williams Ranch
1000 m
© 2008 Tele Atlas
Image © 2008 DigitalGlobe
Image © 2008 TerraMetrics
©2007 Google™
Pointer 31°53'09.01" N 104°52'57.16" W elev 5409 ft
Streaming |||||||||| 100%
Eye alt 6169 ft

Vertical of Formations (notice how Victorio Peak pinches out between the two canyons). Source: SEPM Field Guide (1988)

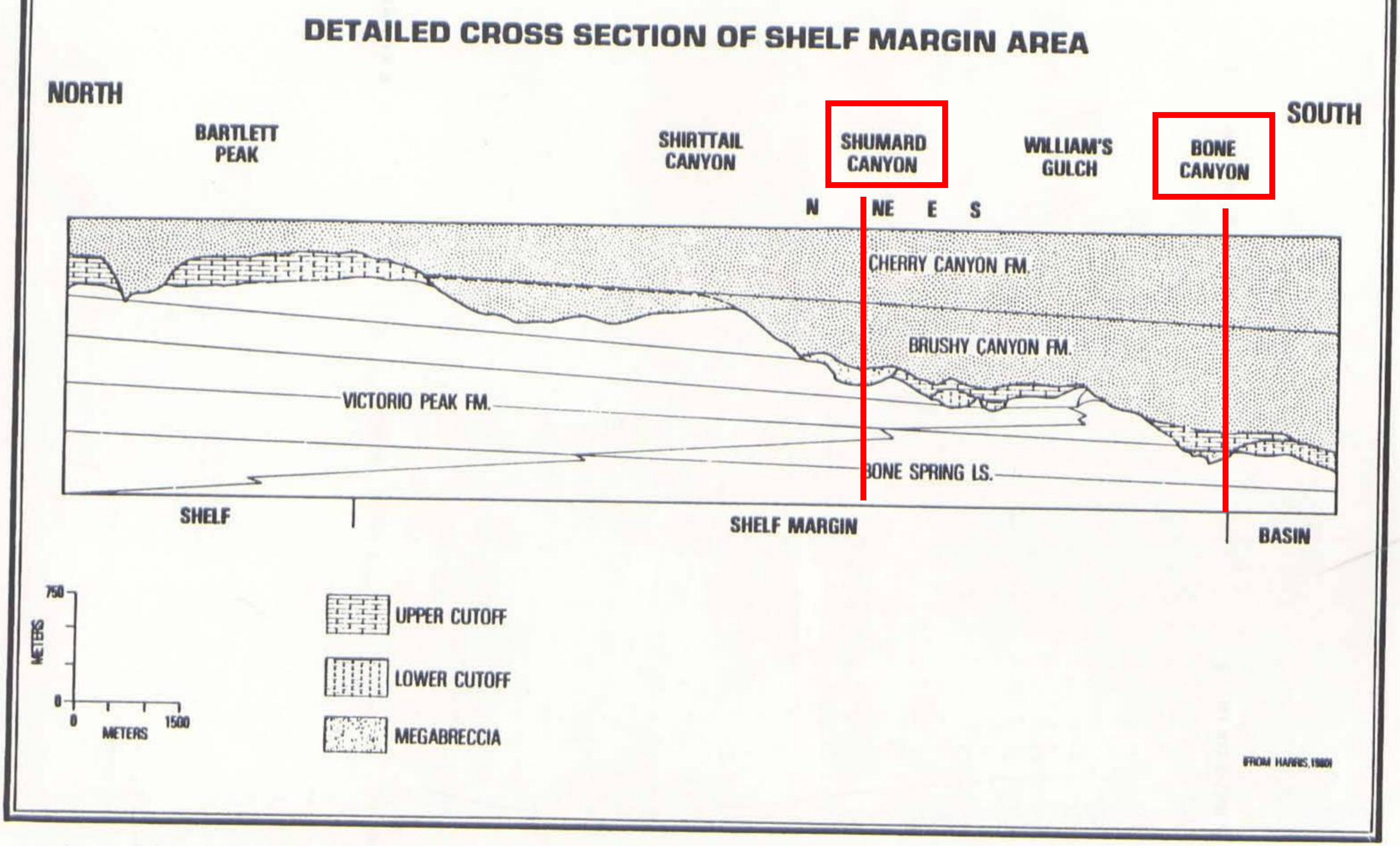

Figure 1-I-6. Cross-section of shelf margin area, Bone Spring, Victorio Peak, Cutoff and Brushy Canyon formations, from Harris (1982).

Map view of formations. Circled are Shumard and Bone Canyons. (AAPG field guide, 1999). Note arrows indicating paleo flow/dip direction.

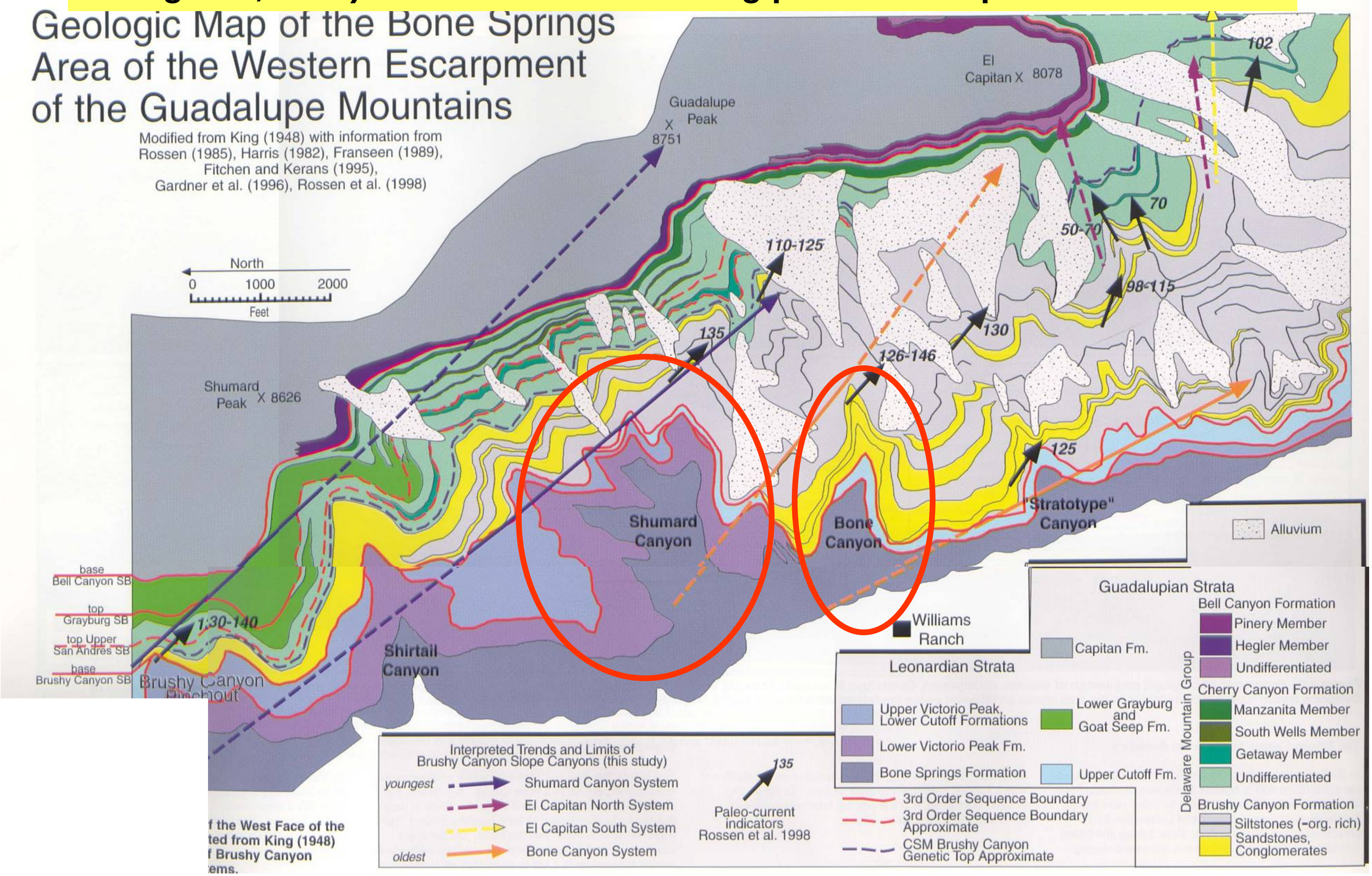

Depositional Model:

Bone Springs Formation deposited in slope-to-basin setting; Victorio Peak Formation deposited in a shelf margin setting (1). Sea level fall, and development of erosional karst surface into Victorio Peak formation (2). Sea level rise, and deposition of Cutoff "wedge": lower Cutoff Formation; (3) and (4).

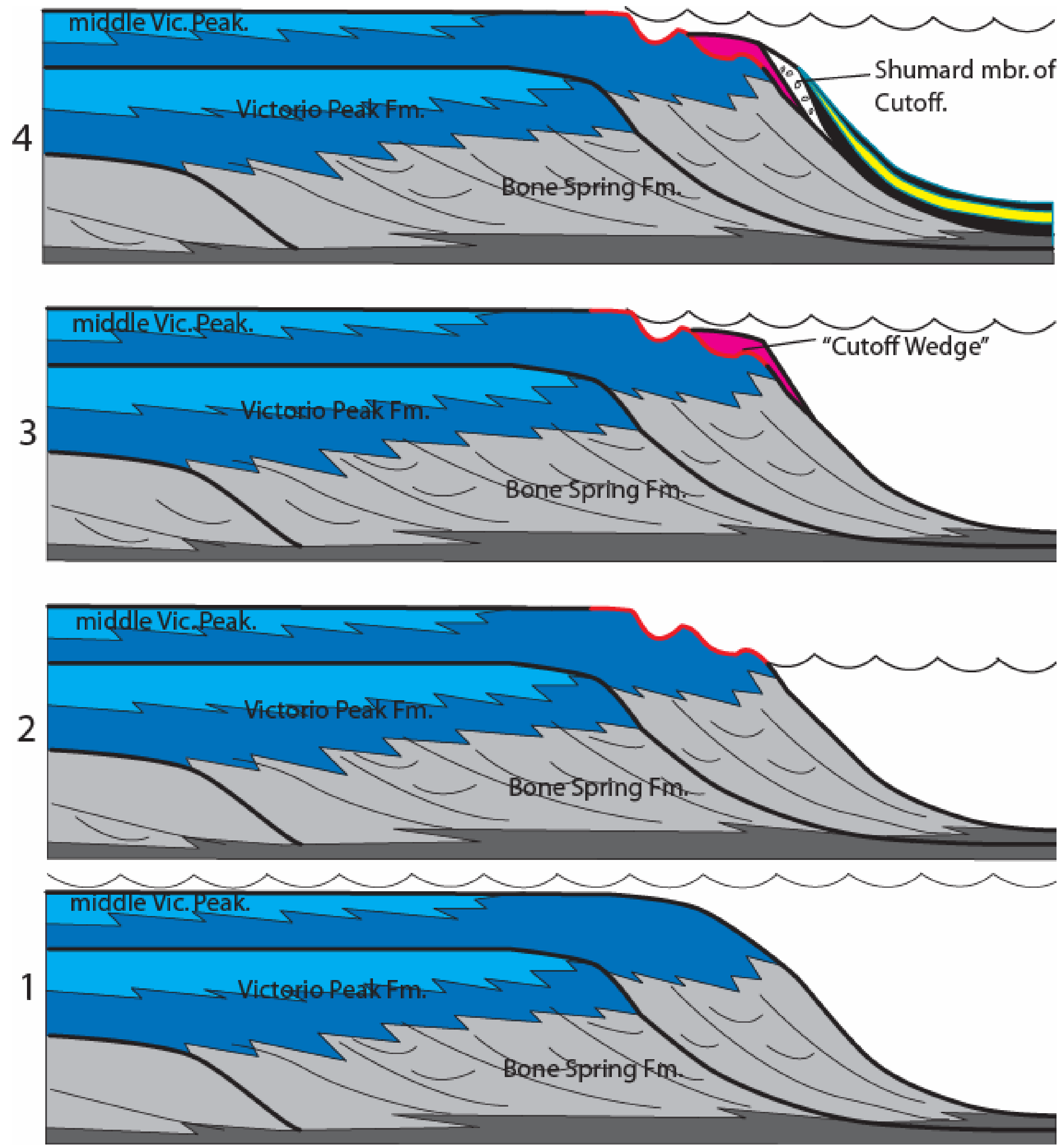

Source: C. Kearns

Depositional Model (continued)

Progradation of San Andreas Formation (land→basin), and synchronous deposition of Cutoff Formation (5). Upper Cutoff Formation caps the units (6), and Brushy Canyon deposition ensues, scouring into underlying Cutoff and Victorio Peak Formations (7)

Source: C. Kearns

7

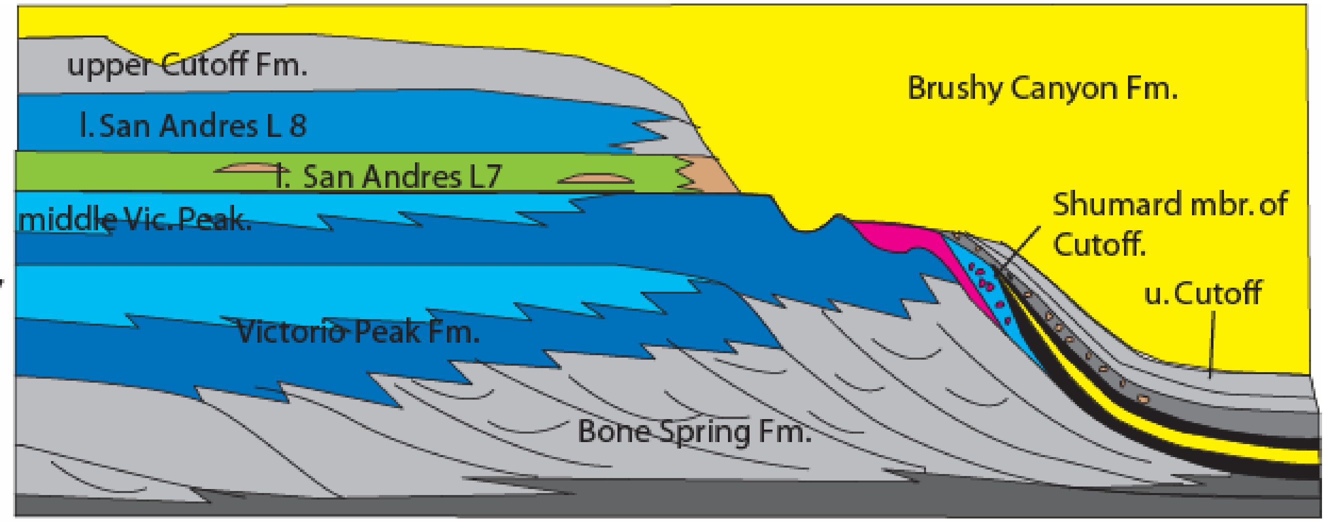

6

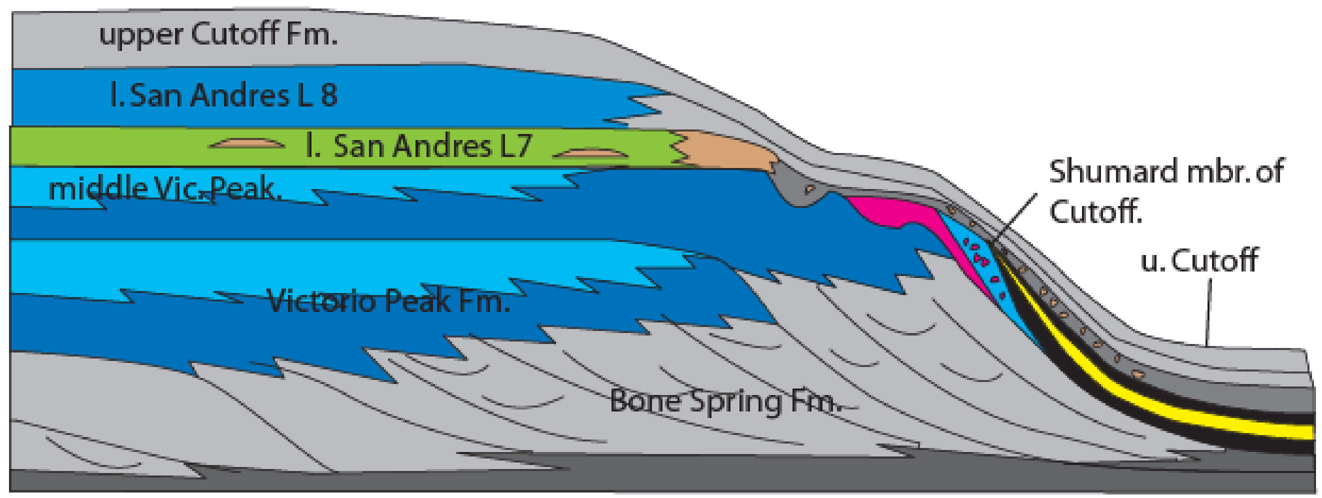

5

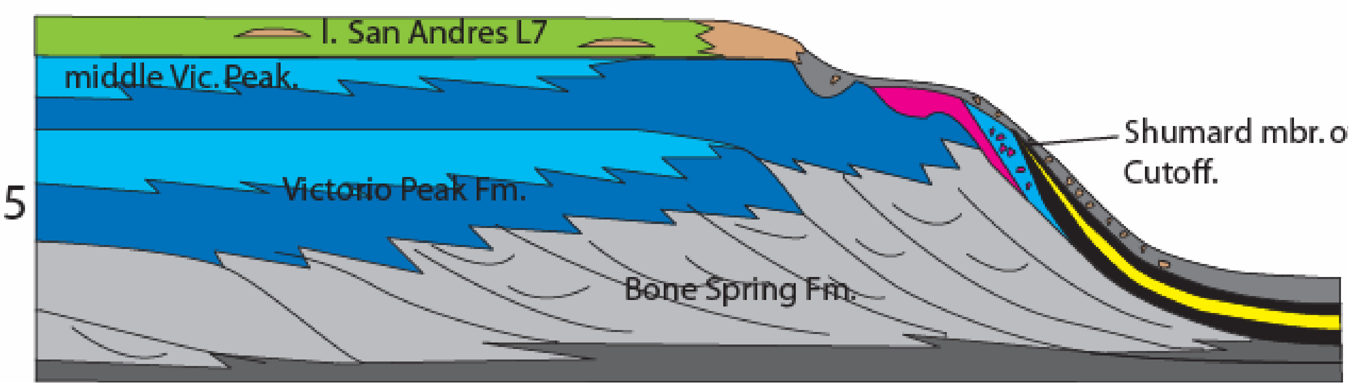

Hierarchy of Stratigraphy

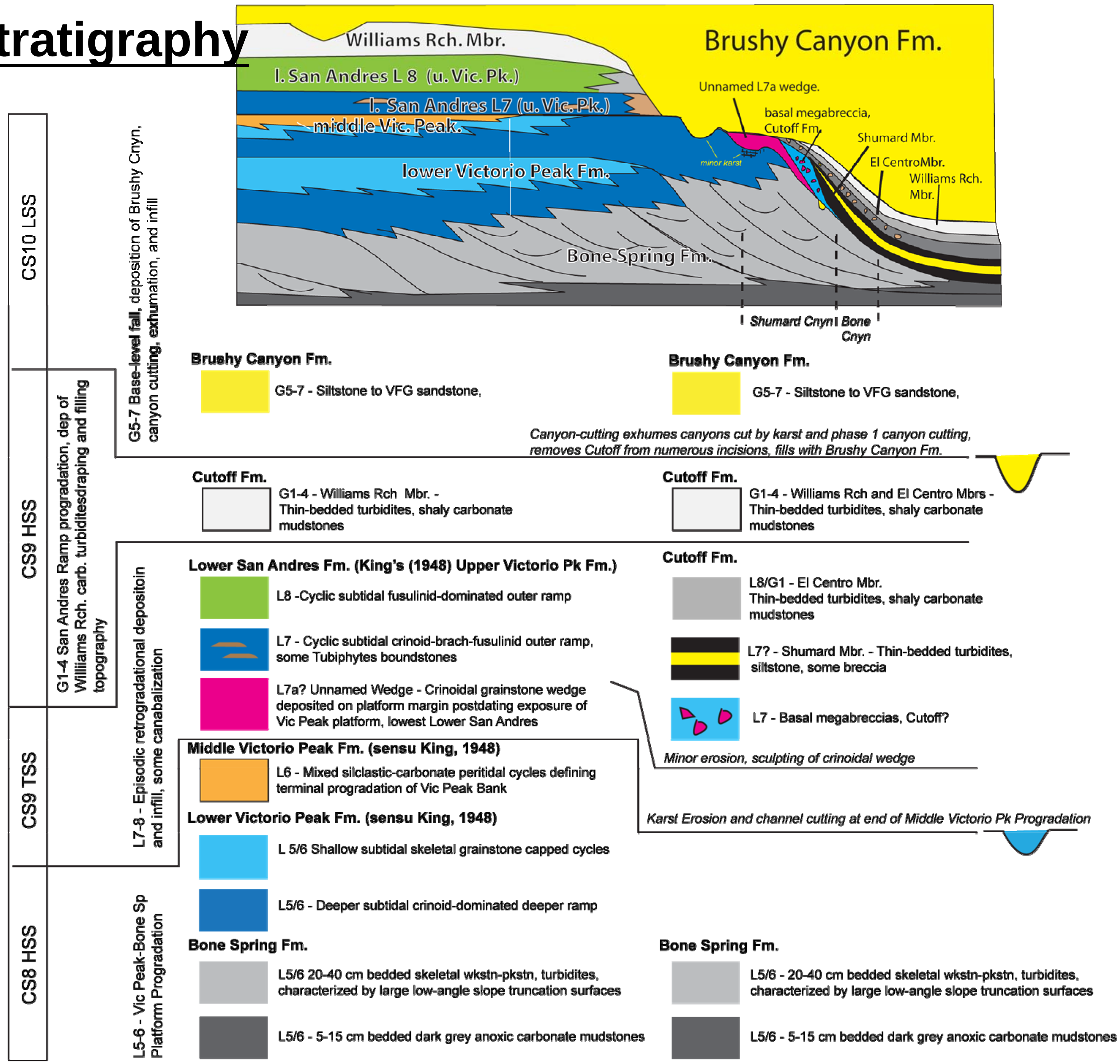

Source: C. Kearns

Larger Depositional Context

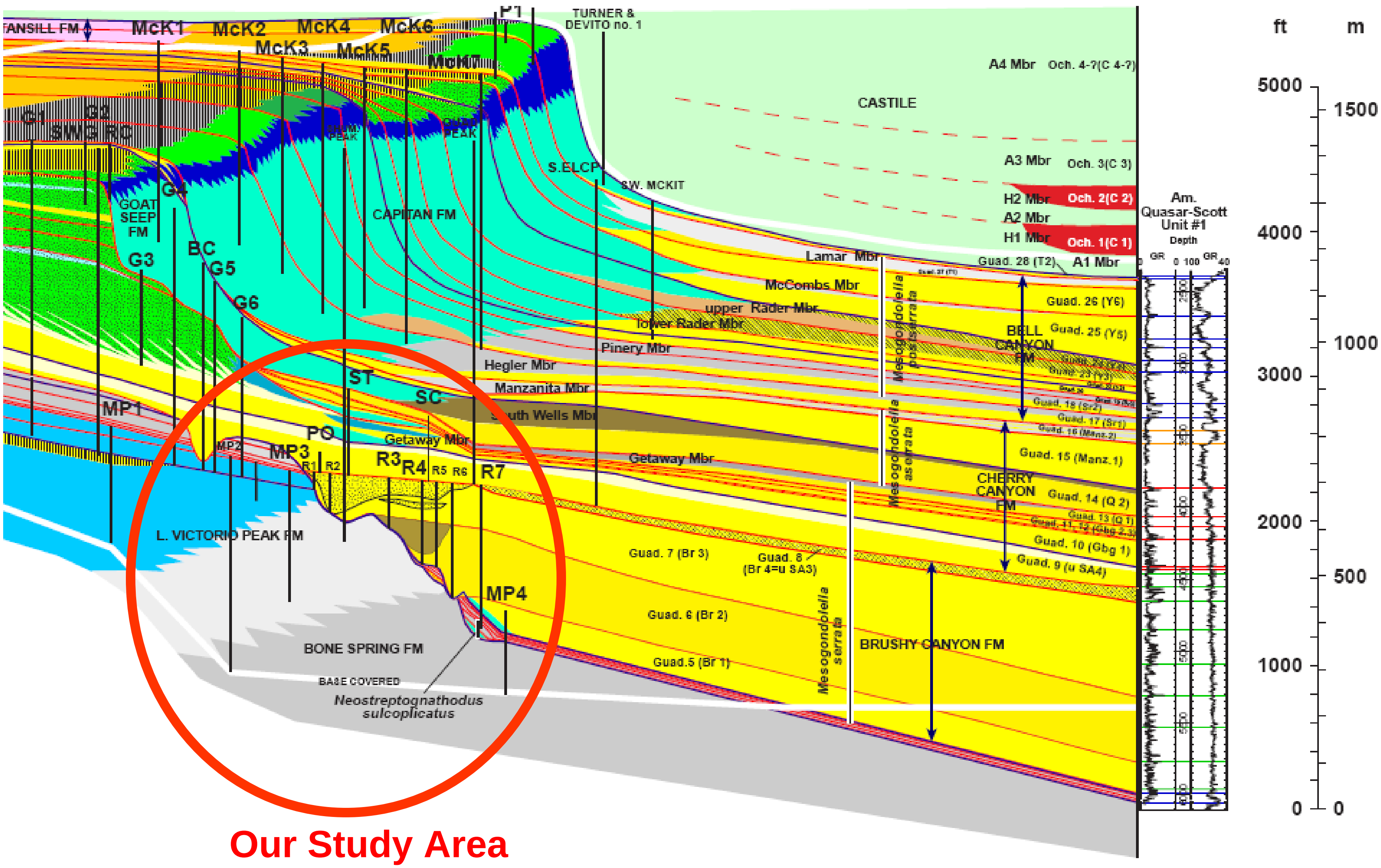

Our Study Area

Source: C. Kearns

Overview: Looking north (circled is Shumard Canyon); note the transition from Victorio Peak Formation to Bone Spring Formation

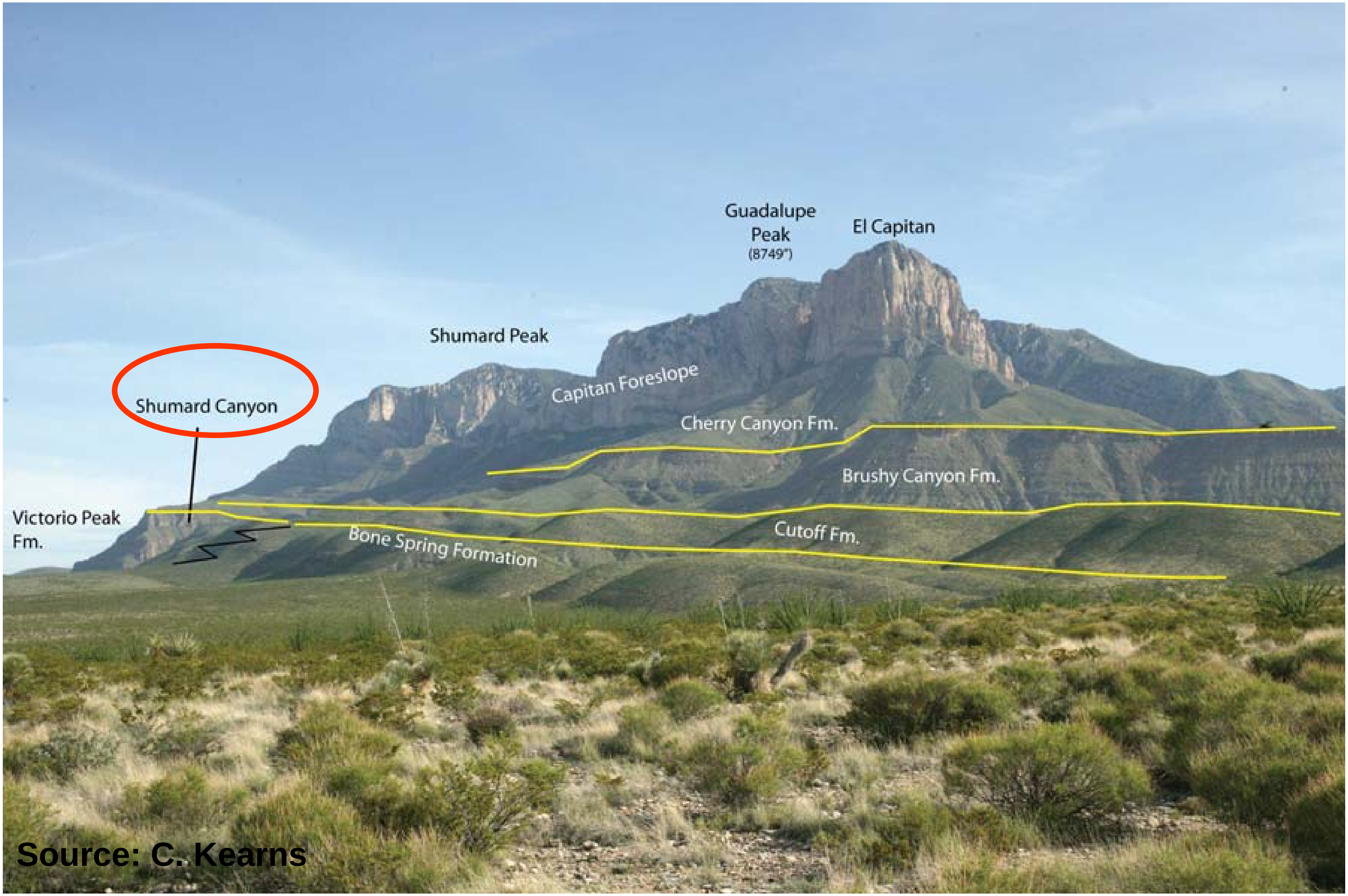

Shumard Canyon *(perspective: looking up canyon toward Guadalupe headwall)*

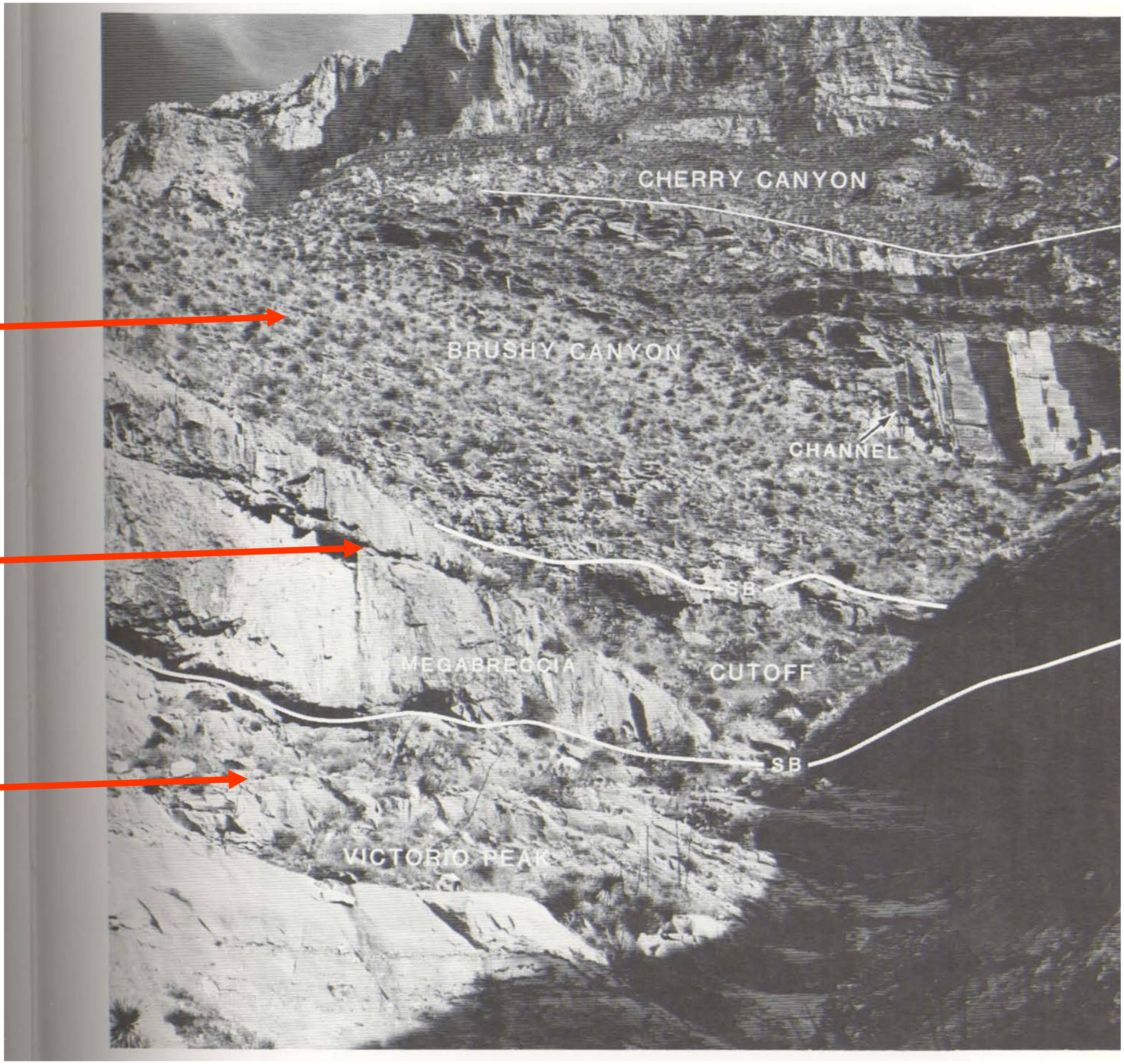

Brushy Canyon

Cutoff Mega Breccia

Victorio Peak

SEPM (1988)

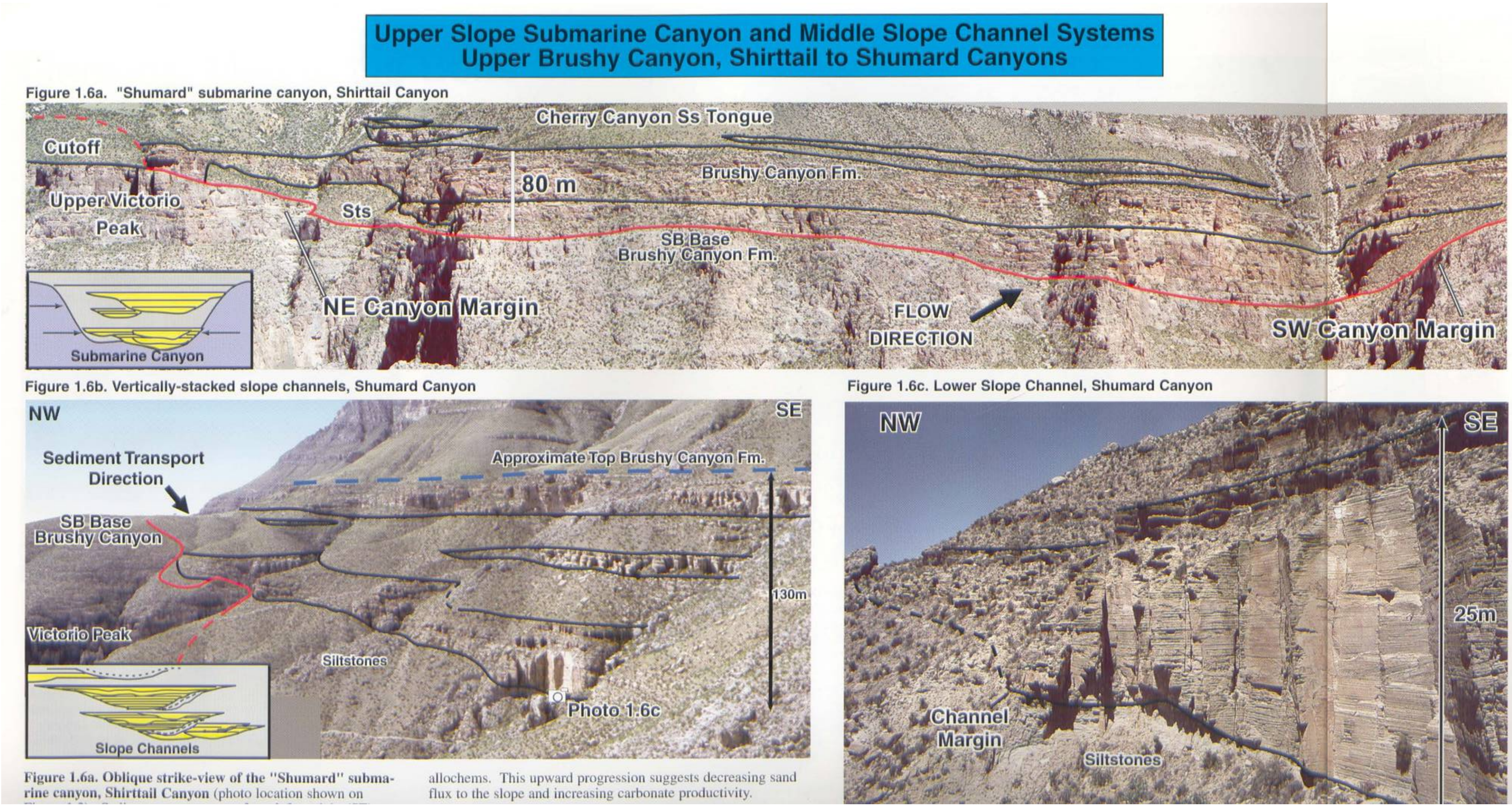

<u>Brushy Canyon Formation (*Shumard Canyon, looking north*):</u> Note sandy (resistant) channel lenses amongst fine grained (recessive) overbank deposits

Source: AAPG/Exxon field guide, 1999

Bone Canyon Overview: Looking at the south face from the north ridge

source: SEPM (1988)

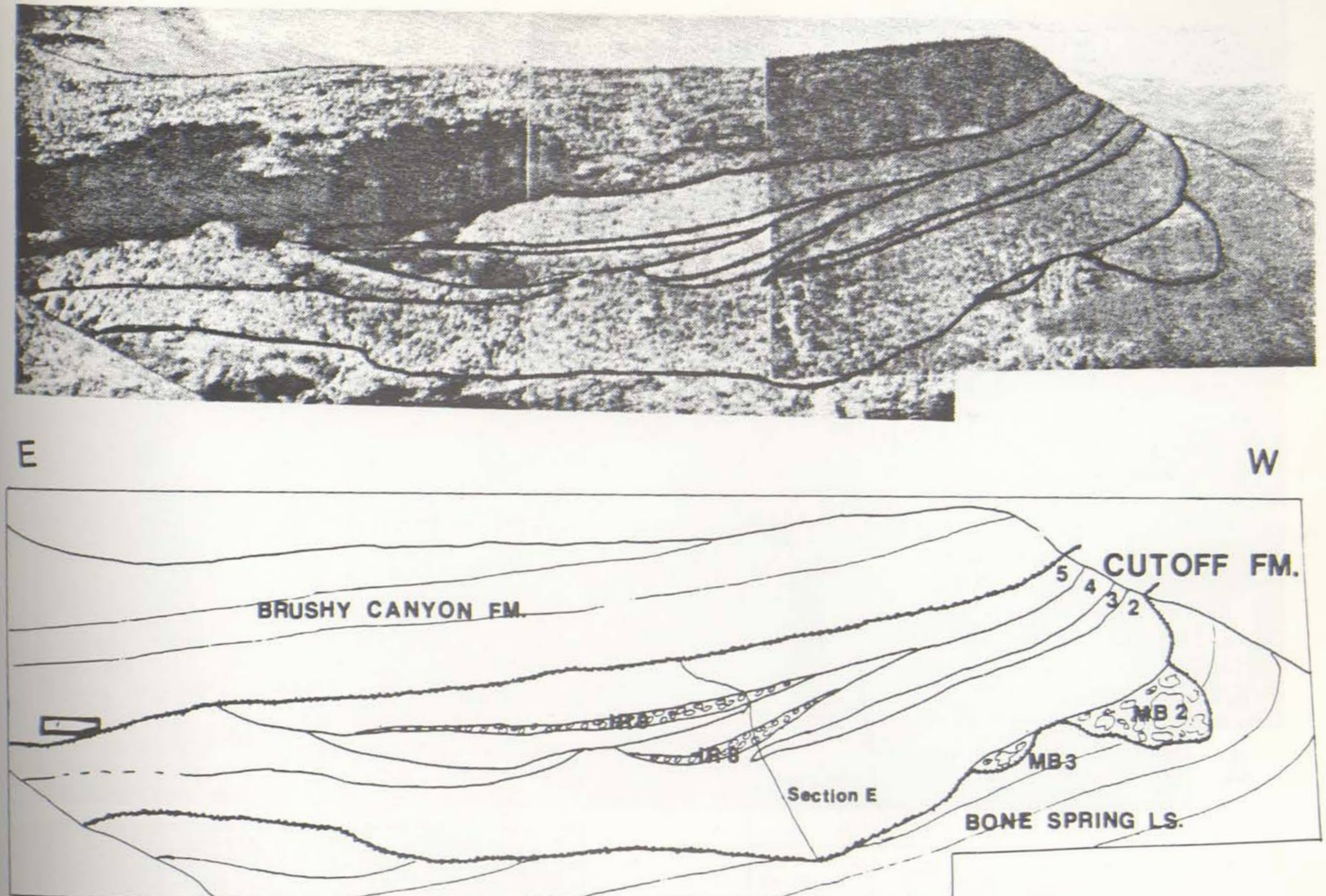

Figure 1-V-2. Sketch of south wall, Bone Canyon, from Harris (1982), showing geometry of basal Cutoff and basal Brushy Canyon sequence boundaries. Note channel-filling carbonate megabreccias at base of Cutoff (MB2 and MB3), and numerous Cutoff intraformational, channelized surfaces filled with intraclast rudstone (IR) or mudstone.

Bone Canyon: Brushy Canyon Formation (clastic turbidite channel outcrop)

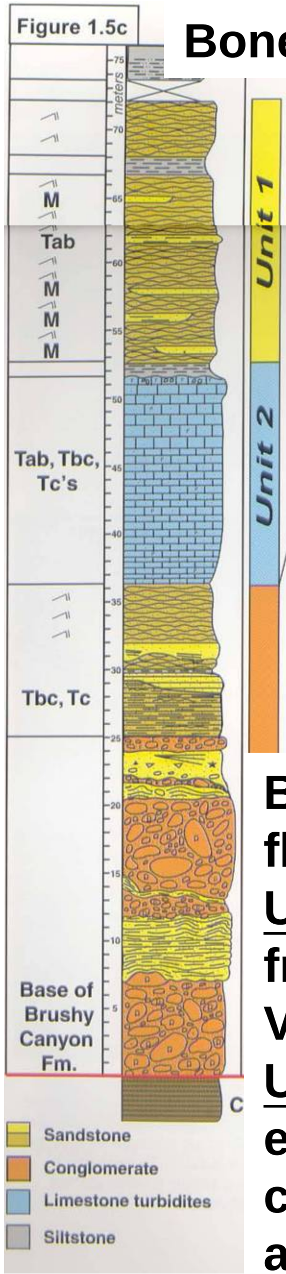

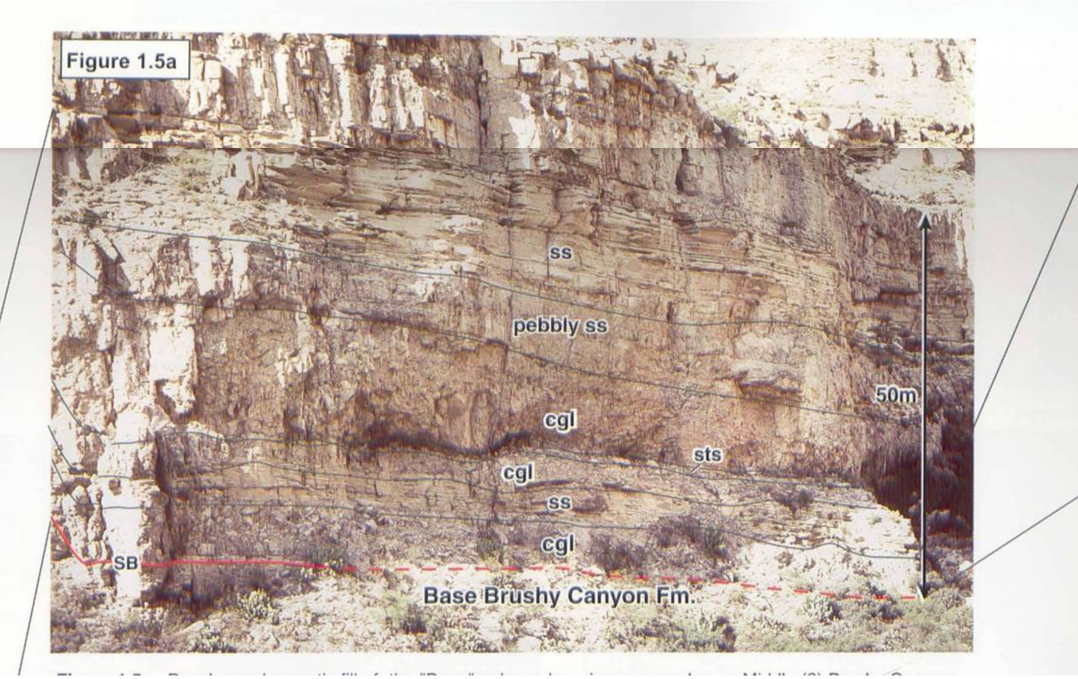

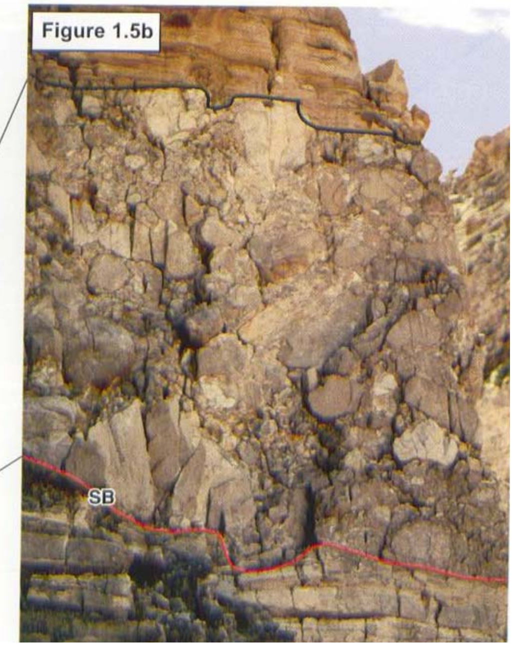

Bone Canyon: Variability of canyon fill is interpreted to reflect variable flow types during late-stage canyon filling

<u>UNIT 1:</u> Carbonate clast conglomerates (1-7.5 m diameter; sourced from underlying strata
Via debris flows)

<u>UNIT 2:</u> Medium to thick beded, sandy peloidal-skeletal grainstones that exhibiting Bouma turbidite subdivisions. Basinward transport of carbonate material derived from shallow marine environments existing at the canyon heads

<u>UNIT 3:</u> Channelized massive sandstones (channel axis facies).

Source: AAPG/Exxon field guide, 1999

Jeffrey Nittrouer May 2008
Guadalupe Field Stratigraphy Course

Bone Canyon and Shumard Canyon Traverse

Introduction:

Directions: HWY 62 west until Williams Ranch Road turnoff (~ 8 miles west from the National Park visitor center turnoff). Right onto Butterfield Trail Road, which begins east, and turns north to Williams Ranch (distance: ~8 miles from HWY 62 turnoff). We will begin at Williams Ranch (elev. 5000 ft), along the western escarpment of the Guadulupe Mountains. The ranch is situated between the outlet of Shumard Canyon (north) and Bone Canyon (south). As mentioned in class, our hike will likely begin up Bone Canyon in order to take advantage of the well-packed trail present in Shumard Canyon for our descent (National Park trail). Our hike will ascend upsection, starting with the Bone Spring Limestone, and work through the Victorio Peak Formation, Upper Cutoff Formation, and the Brushy Canyon Formation. The top of the first bench (situated on the ridge between the two canyons) is the contact between the Cutoff Formation and the Brushy Canyon Formation (elev. 5700 ft). In general, our north-to-south perspective of the western escarpment provides a near-dip view of the platform-to-basin depositional setting (paleo current indicators suggest a south to south-east transport trend). The base formations (Bone Springs and Victorio Peak) are limestone; the Cutoff Formation follows as a transitional unit, and the Brushy Canyon Formation consists of a mixture of clastic and carbonate sediments, derived from turbidites and debris flows.

The information acquired for this write up derive from two field guides. The first was published in 1988 by SEPM ("Geologic guide to the Western Escarpment, Guadalupe Mountains, Texas"), and the second is an AAPG/Exxon guide published in 1999 ("Deep-water Sanstones, Brushy Canyon Formation, West Texas"). Charlie Kearns provided additional figures. I have no personal experience working in this area, so my comments originate only from interpretation of the field guides and notes.

Please review the attached figures and pictures for further clarification of the formation outcrops found in Bone and Shumard Canyons.

Rock Units and Depositional Setting:

Bone Springs Limestone: The base formation from which we will begin. This unit is characterized by dark gray color, cherty and thin bedded internally laminated lime mudstone. It is organic rich, and perhaps sparsely to non-fossiliferous (from the SEPM guide; Charlie disputes the idea of a lack of fossils). Depositional setting is considered transitional, from the slope to the basin.

Victoria Peak Formation: This rock unit is a carbonate bank margin facies, having been deposited near the break between the platform top and the deeper slope setting. The formation is only present in Shumard Canyon, as it pinches out before Bone Canyon. The rock is characterized by medium/light gray color, thick bedding, massive dolomites, and an abundance of fossils (lime grainstones).

Cutoff Formation: This complex formation is heterogeneous in both composition and spatial exposure. The two predominant lithologies found in Shumard and Bone Canyons are lime mudstones and massive carbonate breccia, which are expressed as recessive and resistant units, respectively. Interpretation of the depositional environment is varied; sea level lowering post Victorio Peak deposition is believed to have exposed the carbonate platform and bank subaerially, promoting karst development. Ensuing sea level rise flooded the margin, and the topographically variable karst surface is speculated to have provided conduits for sediment transport (gravity-driven) to the slope and basin. Continued sea level rise eventually flooded the entire platform surface, leading to the time-synchronous development of the San Andres formation on the platform. The upper Cutoff Formation caps both the landward San Andres Formation and the matching lower Cutoff formation at the shelf break and slope.

Brushy Canyon Formation: Clastic turbidite packages consisting of sandy, amalgamated channel fills amongst fine-grained, recessive siltstone (likely drape deposits). There are erosional surfaces cut into the underlying carbonate formations (Cutoff and Victorio Peak). The AAPG/Exxon field guide describes a Brushy Canyon submarine channel fill deposits from Bone Canyon as consisting of three distinct units: (1): Carbonate clast conglomerates (1-7 m diameter, and sourced from the eroded underlying strata; debris flow?); (2): Medium to thick bedded, sandy peloidal-skeletal grainstones exhibiting Bouma turbidite subdivisions. Basinward transport of carbonate material derived from shallow marine environments existing at the canyon heads; (3): Channelized massive sandstones (channel axis facies).

TRAIL GUIDE FOR DAY 1: SHUMARD TO BONE CANYON TRAVERSE

C. ROSSEN
P. J. LEHMANN
J. F. SARG
Exxon Production Research Co.

INTRODUCTION TO THE FIELD TRAVERSE

Geologic Setting

The locale of this field traverse is the western escarpment of the Guadalupe Mountains where the autochthonous and allochthonous facies of the shelf-edge and basin margin are exposed along the major western boundary-fault escarpment. Details of the regional setting for this trip to selected localities on the Late Leonard-Early Guadalupian basin margin are well known. The major pertinent reference is that of King (1948).

The stratigraphic units of concern on this day trip are the Bone Spring, Victorio Peak, Cutoff, and Brushy Canyon formations (see Fig. 3 of introduction to guidebook). The geologic setting of these formations is that of the rim of a broad carbonate shelf province to the north and northwest (Northwest Shelf) and a deeper intracratonic basin (Delaware Basin) on the southeast and east. The strata of principal concern for today are marine carbonates of the basin margin and siliciclastic wedges of the toe-of-slope and basin. The structural history during late Leonard-early Guadalupian deposition was that of regional subsidence at rates that (1) permitted the shelf to remain shallow, and (2) permitted the development of low angle (5 degrees or less) shelf-to-basin bank margins.

Purpose and Scope

This field traverse and the accompanying locality guide do not attempt comprehensive coverage of the Permian strata such as that of King. Nor do we here attempt an overall topical coverage. Our purpose is to concentrate on two major interpretive problems of the Late Leonard-Early Guadalupian shelf and basin margin: (1) the genesis of the depositional geometries and accompanying facies of the Bone Spring to Brushy Canyon strata; and (2) the correlation of the basin margin strata further to the north. Examination of the shelf strata is recommended as subsequent Days 2 and 3 to this Day 1. Road logs and locality guides for these days are found in Sarg and Lehmann, 1986 (Permian Basin Section-SEPM pub. 86-25). Application of depositional sequence concepts has, we think, provided new interpretational leverage in understanding the genesis of the late Permian rocks of the Delaware Basin. Application of sequence stratigraphy includes both correlation of major physical surfaces (i.e., sequence boundaries, downlap surfaces) and biostratigraphic time markers. The fusulinid biostratigraphy has been provided by Garner L. Wilde (see articles in PBS-SEPM pub. 86-25). Details of the depositional environments and their paleobathymetry, and of the degree to which sea-level fluctuation exposed the shelf and basin-margin strata and controlled deposition are the subjects of intense continuing discussion. Some of these are dealt with on this field trip.

Acknowledgments

We gratefully acknowledge the support of Exxon Production Research Company for the past and continuing program in the Guadalupe Mountains. We also thank Exxon Production Research Company for permission to publish this work. We thank the staff of the Guadalupe Mountain National Park for their support and cooperation in making the field work for this report a success.

STRATIGRAPHIC FRAMEWORK OF THE BONE SPRING TO BRUSHY CANYON STRATA

To provide a stratigraphic framework for the interpretations presented on this field trip, it is helpful to recognize several specific depositional systems tracts (Brown and Fisher, 1977) (i.e., a linkage of contemporaneous depositional facies—such as shelf, slope, and basin) bounded by sequence boundaries[1] and/or downlap surfaces[2]. The chronostratigraphic significance of an unconformity or sequence boundary is that all the rocks below the unconformity are older than the rocks above it. The ages of strata immediately above and below the unconformity differ geographically according to the areal extent of erosion or nondeposition. The duration of the hiatus associated with an unconformity differs correspondingly, but the unconformity itself is a chronostratigraphic boundary because it separates rocks of different ages, and no chronostratigraphic surfaces cross it.

Although several chronostratigraphic surfaces may merge along an unconformity, none actually cross the unconformity. For these reasons, unconformities are not diachronous but are time boundaries that may be assigned a specific geologic age dated in those areas where the hiatus is least and/or where the rocks above and below become conformable. By careful identification of unconformities and their correlative conformities, a sedimentary section can be divided into genetic depositional sequences bounded by these unconformities (Vail et al., 1984).

The Permian strata of the Delaware and Midland basins comprise a number of depositional sequences. Each sequence is composed of three parts or systems tracts: (1) a wedge restricted to the basin and slope areas that is interpeted to have been deposited during a relative fall and lowstand of sea level; and (2) a transgressive depositional systems tract deposited during a regional landward shift in the shoreline intepreted to have been deposited during a relative sea level rise; and (3) a capping progradational or regressive depositional systems tract interpreted to have been deposited during a relative highstand in sea level.

[1]Sequence boundary: Unconformity and its correlative conformity. Unconformity is defined as a surface representing a significant time gap with erosional truncation (subaerial or subaqueous) and/or subaerial exposure. Erosional truncation is commonly evident at the basin margin. The sequence boundary surface commonly becomes conformable over much of both the shelf and basin areas. Marine surfaces with significant hiatuses, but without evidence of erosion, are not unconformities according to this usage (Vail et al., 1984).

[2]Downlap surface: Submarine surface that is characterized seismically by a downlap over a concordant pattern and is commonly associated with a marine hiatus. Downlap surfaces associated with marine condensed sections mark the change from the end of transgression to the start of regression (Vail et al., 1984).

The western escarpment of the Guadalupe Mountians exposes the slope to basin transition of six Permian sequence boundaries which range in age from Late Leonardian to Late Guadalupian. These sequence boundaries subdivide the strata into five genetic depositional sequences (see summary sequence diagram in front of guidebook). The portions of the two sequence boundaries that we will observe today in a slope and toe-of-slope position are highly erosional and appear to be submarine in origin. These boundaries are: (1) top of the Victorio Peak/Bone Spring formations, and (2) the top of the Cutoff Formation/base of the Brushy Canyon Formation. High above our traverse in the rocks exposed along the escarpment are the sequence boundaries, or correlative basinward conformities that correspond to (3) the top of the San Andres Formation, (4) the top of the Grayburg Formation, (5) the top of the Goat Seep Formation/base Manzanita Member, and (6) the top of the Hegler Member of the Capitan Reef Complex. Days 2 and 3 of this trip will examine the shelfward expression of the two sequence boundaries we will examine today and the sequence boundary at the top of the San Andres Formation, and their enclosed strata. The first sequence boundary we will encounter today, the top of the Victorio Peak/Bone Spring, correlates shelfward to the base of the Glorieta Member of the Yeso Formation of the northern Guadalupe Mountains and forms the base of the sequence which includes the lower and middle parts of the San Andres Formation of Hayes (1964). The second major sequence boundary we will examine, the base of the Brushy Canyon, correlates shelfward to the top of the middle San Andres of Sarg and Lehmann (1986) and forms the basal boundary of a sequence which includes the upper San Andres. The upper San Andres carbonate bank is capped by the sequence boundary that forms the base of the Grayburg Formation. In the basin margin position, this boundary is overlain by Grayburg Formation quartz sandstones and dolomites interpreted to be of shallow-water to tidal origin (Sarg and Lehamnn, 1986). In addition to the sequence boundaries, we want to emphasize three major features we will see today: (1) debris flow breccias deposited on top of the sequence boundaries in slope to toe-of-slope positions which are intepreted, by us, to be the result of erosion of the bank margins during falls and lowstands in sea level; (2) two basinally restricted wedges consisting of (a) limestone strata of the lower Cutoff Formation intepreted to have been deposited during rising sea level, and (b) siliciclastics of the Brushy Canyon Formation interpreted to be the result of shelf bypass during a lowstand in sea level; and (3) the slope to basin transition of two carbonate banks deposited during highstands in sea level, the upper Victorio Peak/Bone Spring formations and the upper Cutoff Formation.

STOP 1—BASIN/SLOPE TO BANK TRANSITION, BONE SPRING LIMESTONE AND VICTORIO PEAK FORMATIONS

Starting from William's Ranch, we will follow the Guadalupe Mountain National Park trail up into Shumard Canyon (Fig. 1-I-1). In Shumard Canyon, we will observe the lithofacies, sedimentary structures, and geometries associated with a classic vertical facies transition from a lower slope to basin environment to a carbonate bank environment. This transition encompasses the Leonardian-age, coeval, Bone Spring Limestone (slope/basin) and Victorio Peak Formation (bank). These formations have been mapped and studied by King (1948), Newell and others (1953), McDaniel and Pray (1967), and Kirkby (Upper Victorio Peak, 1982, 1984).

The Bone Spring Limestone is interpreted as a euxinic, slope to basin deposit (King, 1948, Newell and others, 1953, and McDaniel and Pray, 1967). It consists of dark gray, cherty, thin-bedded, internally laminated lime mudstones that are organic-rich and sparsely- to non-fossiliferous. In contrast, the Victorio Peak Formation consists of medium to light gray, fossiliferous, thick-bedded, predominantly massive dolomites and minor limestones that are interpreted as carbonate bank deposits. The Victorio Peak can be further subdivided into a bank facies (lime grainstones and dolopackstones) and a bank margin facies (dolowackestones and mudstones)(see Fig. 1-I-3 and enclosed abstract of McDaniel and Pray, 1967). In a shelfward direction (approximately 15-20 miles northwest of Shumard Canyon), normal-marine, fossiliferous carbonates of the Victorio Peak Formation change facies into sparsely fossiliferous, interbedded dolomites, siltstones and gypsum of the Yeso Formation (Boyd, 1958).

In the Guadalupe Mountains, an incomplete Bone Spring-Victorio Peak section (maximum thickness 520 m, 1700 ft) is exposed (King, 1948). Distribution of the Bone Spring and Victorio Peak formations in the area of today's traverse is shown on King's (1948) map of the Bone Canyon area (Figure 1-I-2, in pocket). Figures 1-I-4 and 1-I-5 from McDaniel and Pray (1967) show the distribution of lithologies and facies within the Victorio Peak and Bone Spring formations. The Victorio Peak-Bone Spring bank complex prograded 3-5 km (2-3 miles) during the accumulation of 460 m (1500 ft) of Leonardian carbonates (McDaniel and Pray, 1967).

As we will see on our traverse today through Shumard and Bone Canyons, the Bone Spring-Victorio Peak section thins dramatically in a southeast (basinward) direction. Basinward thinning of the Victorio Peak-Bone Spring section results in part from depositional downlap, but is primarily due to post-depositional erosion associated with the sequence boundary that forms the base of the overlying Cutoff Formation (Fig. 1-I-6). This sequence boundary truncates 250 m (780 ft) of strata over a distance of 3 km (1.8 miles) (Pray et al., 1980).

Stop 1a — Bone Spring Lithofacies

Examples of characteristic Bone Spring (slope to basin environment) lithofacies (Fig. 1-I-7) can be seen in outcrops on the south side of the trail at the mouth of Shumard Canyon (Stop 1a, Fig.1-I-1). The Bone Spring typically consists of thin-bedded, dark gray, organic-rich, lime mudstones (actually fine silt-sized packstones, Pray, pers. comm. and Fig. 1-I-8). Chert is abundant and commonly forms lenses parallel to bedding. Beds are internally laminated, and display both planar and irregular laminations. The irregularity of some laminations is due to soft sediment deformation and the formation of small-scale ripples. According to Pray irregular laminations are more common in proximity to the basin margin. Evidence of autochthonous organic activity in the Bone Spring Limestone is sparse and consists of silicious sponge spicules and uncommon trace fossils on bedding planes.

Stop 1b — Intraformational Bone Spring Erosion Surfaces

Proceeding up the canyon from Stop 1a, numerous intraformational erosion surfaces, marked by discordances in bedding orientation, are evident within the Bone Spring Limestone. These surfaces are spectacularly exposed on the north wall of Shumard Canyon and are diagrammed on cross section B-B' of King's map (Fig. 1-I-2, in pocket). The erosion surfaces have up to 30 m (100 ft) or more of relief and are dipping, planar to curved,

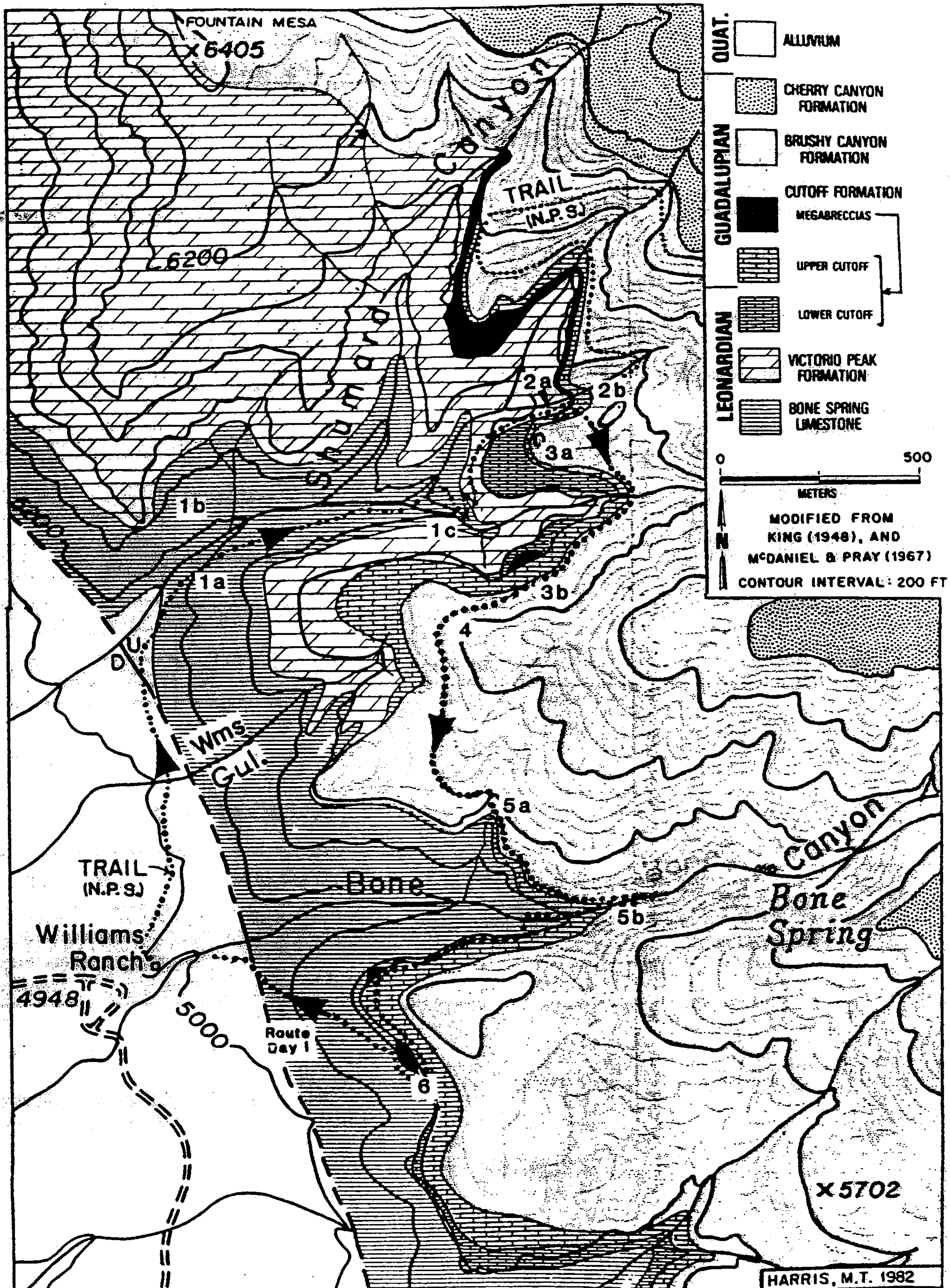

Figure 1-I-1. Geologic map of Shumard Canyon/Bone Canyon area showing traverse and stop locations for Fieldtrip Day 1: "Western Escarpment of the Guadalupe Mountains."

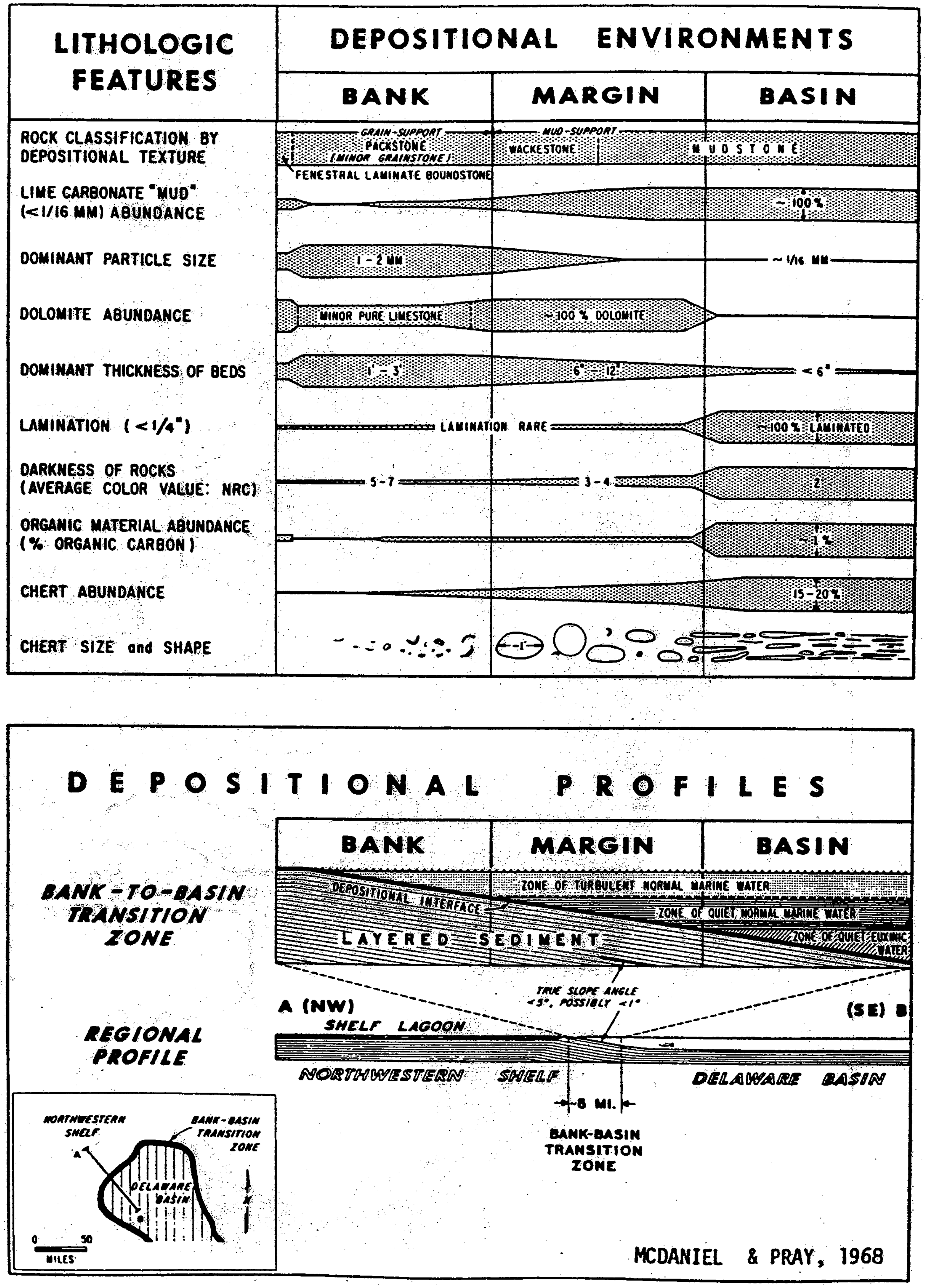

Figure 1-1-3. Lithologic features of bank, bank margin and basin facies, Victorio Peak and Bone Spring Limestone formations.

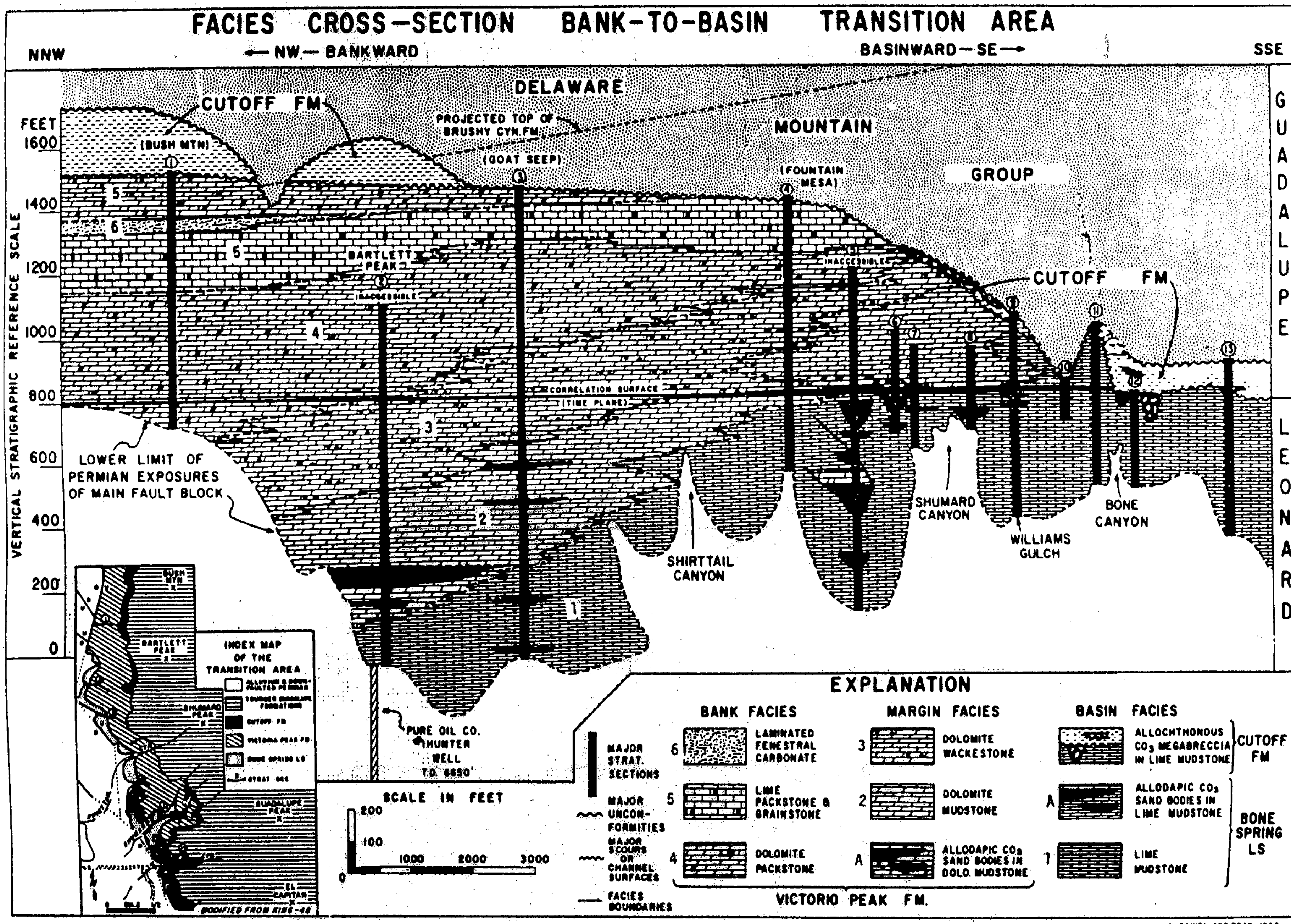

Figure 1-1-4. Facies cross-section of bank to basin transition area, Victorio Peak and Bone Spring Limestone formations, from McDaniel and Pray (1967).

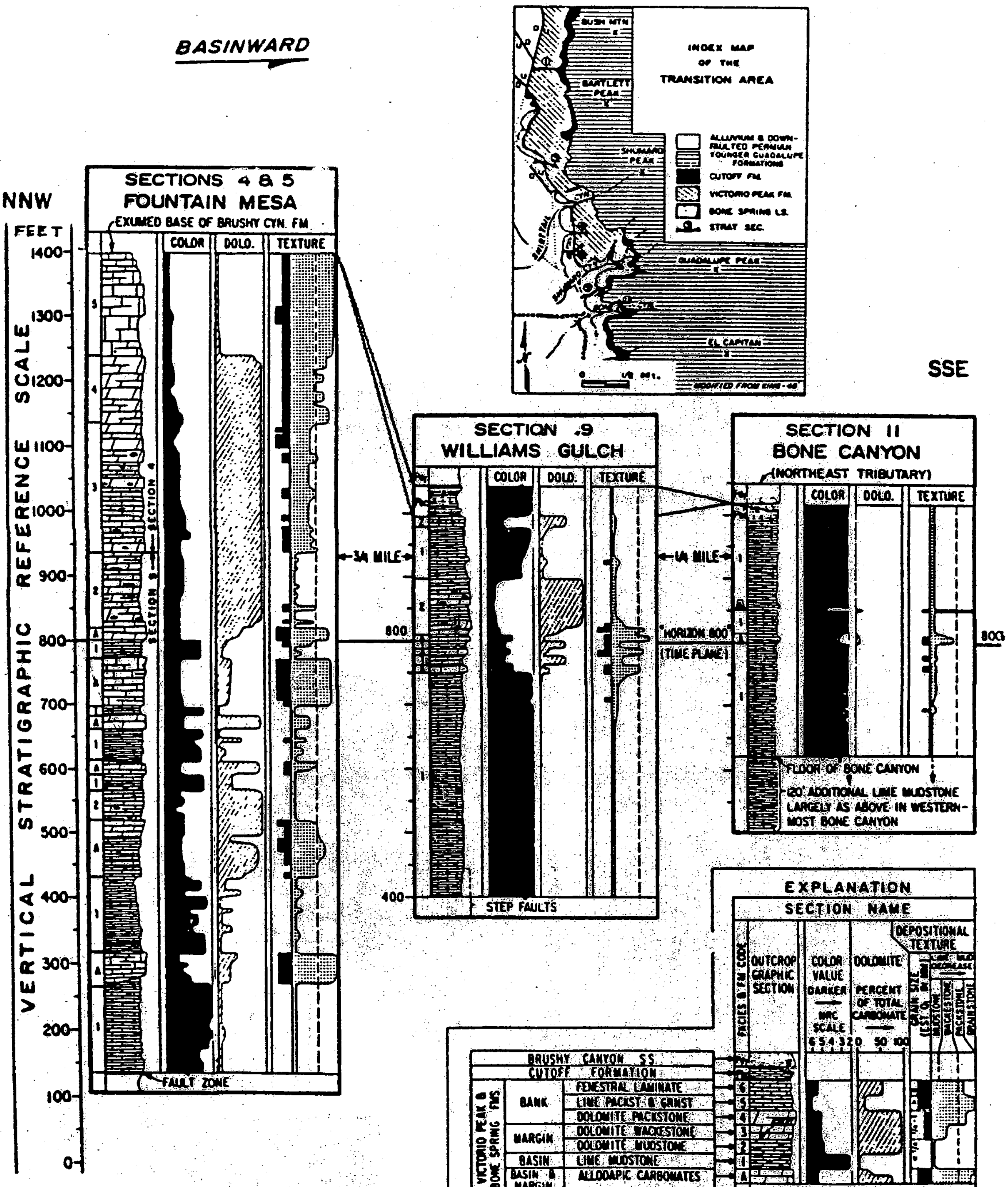

Figure 1-I-5. Stratigraphic sections of the bank to basin transition area, Victorio Peak and Bone Spring Limestone formations, from McDaniel and Pray (1968).

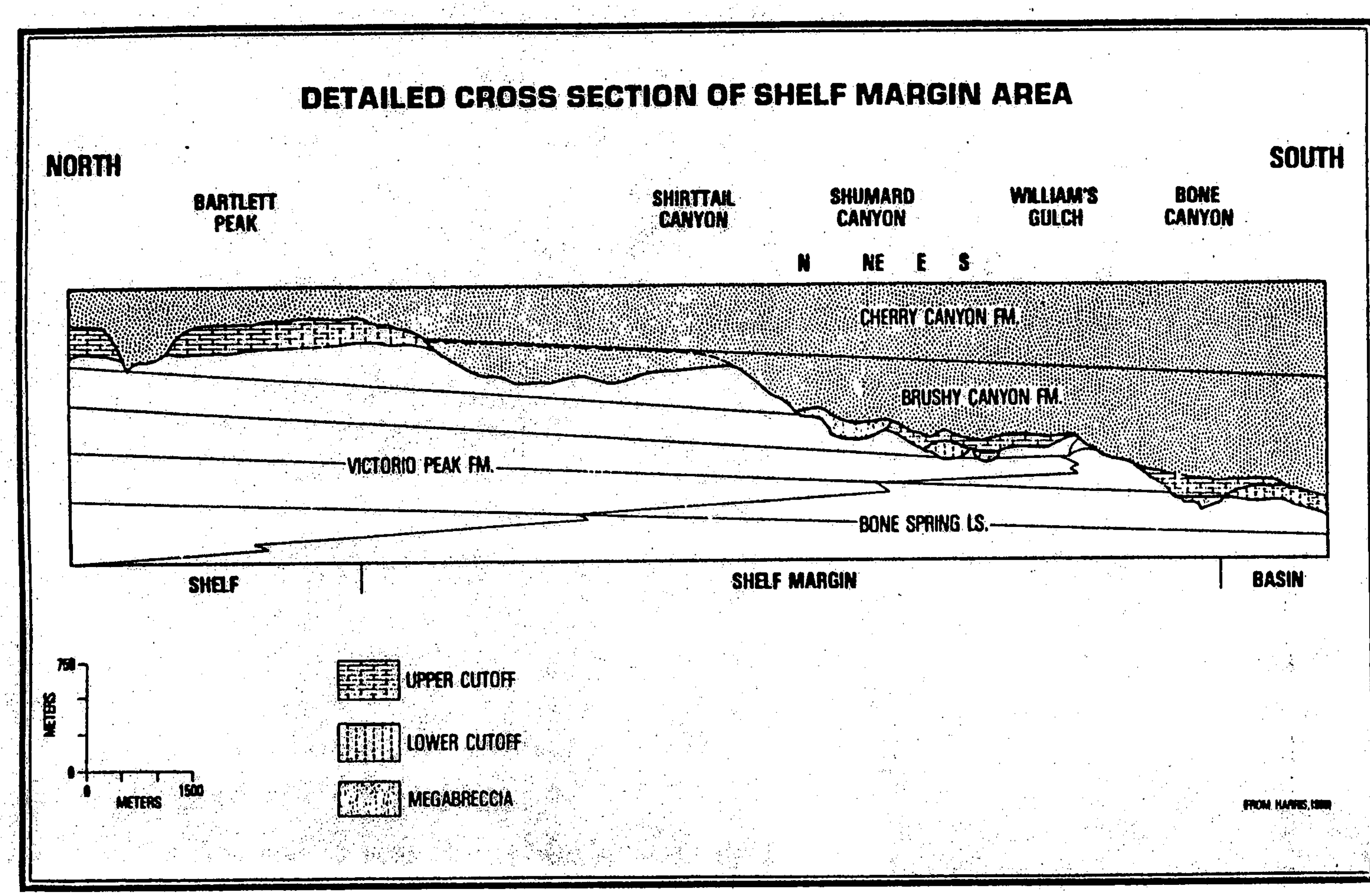

Figure 1-1-6. Cross-section of shelf margin area, Bone Spring, Victorio Peak, Cutoff and Brushy Canyon formations, from Harris (1982).

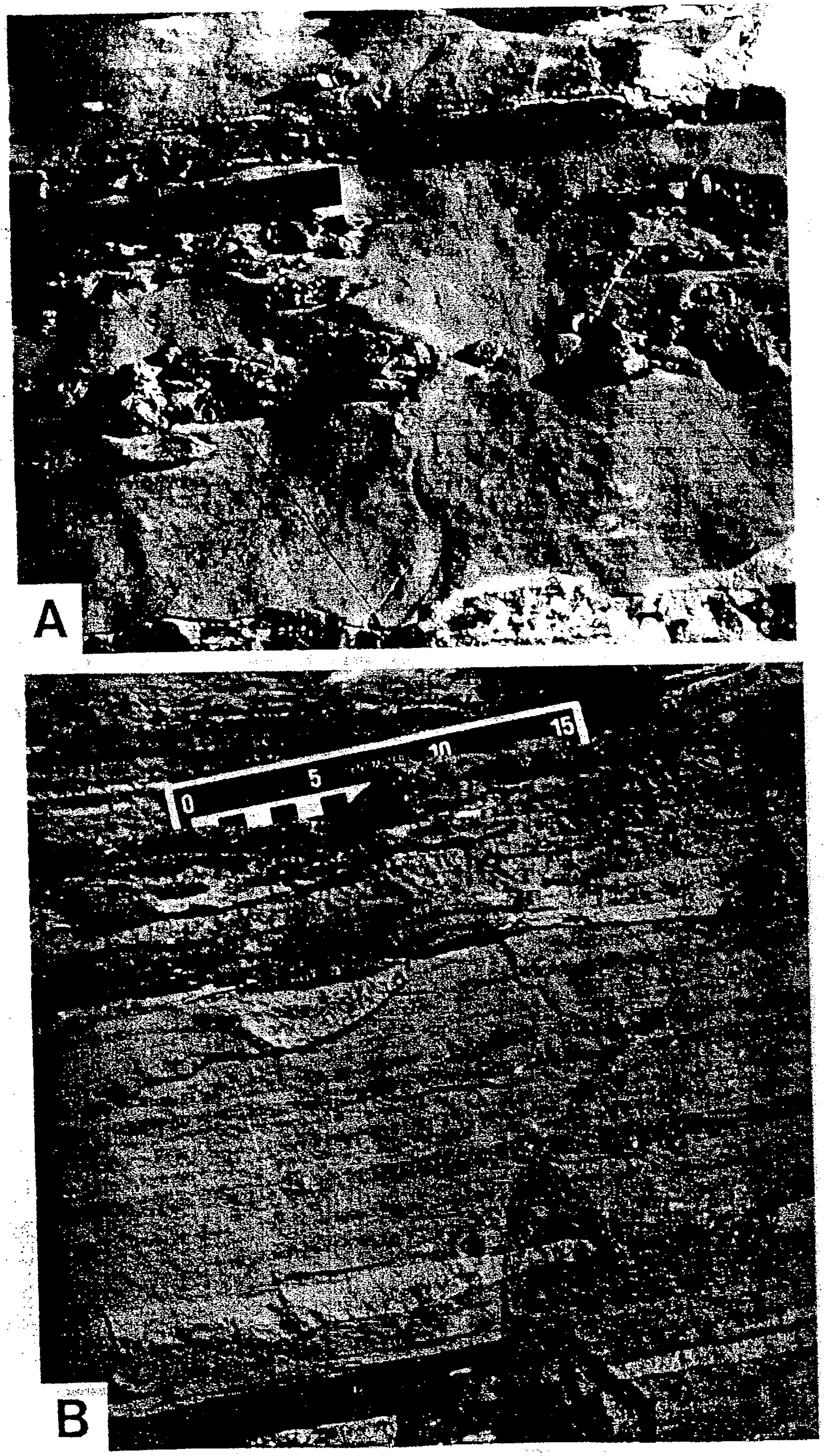

Figure I-I-7. Characteristic lithofacies of Bone Spring Limestone (slope/basin facies). Stop Ia. Shumard Canyon. **A.** *Example of* **planar laminated** *lithofacies with resistent chert lenses. B. Example of irregularly laminated lithofacies.* **Irregular laminae show evidence of small-scale** *current ripples and soft sediment deformation.*

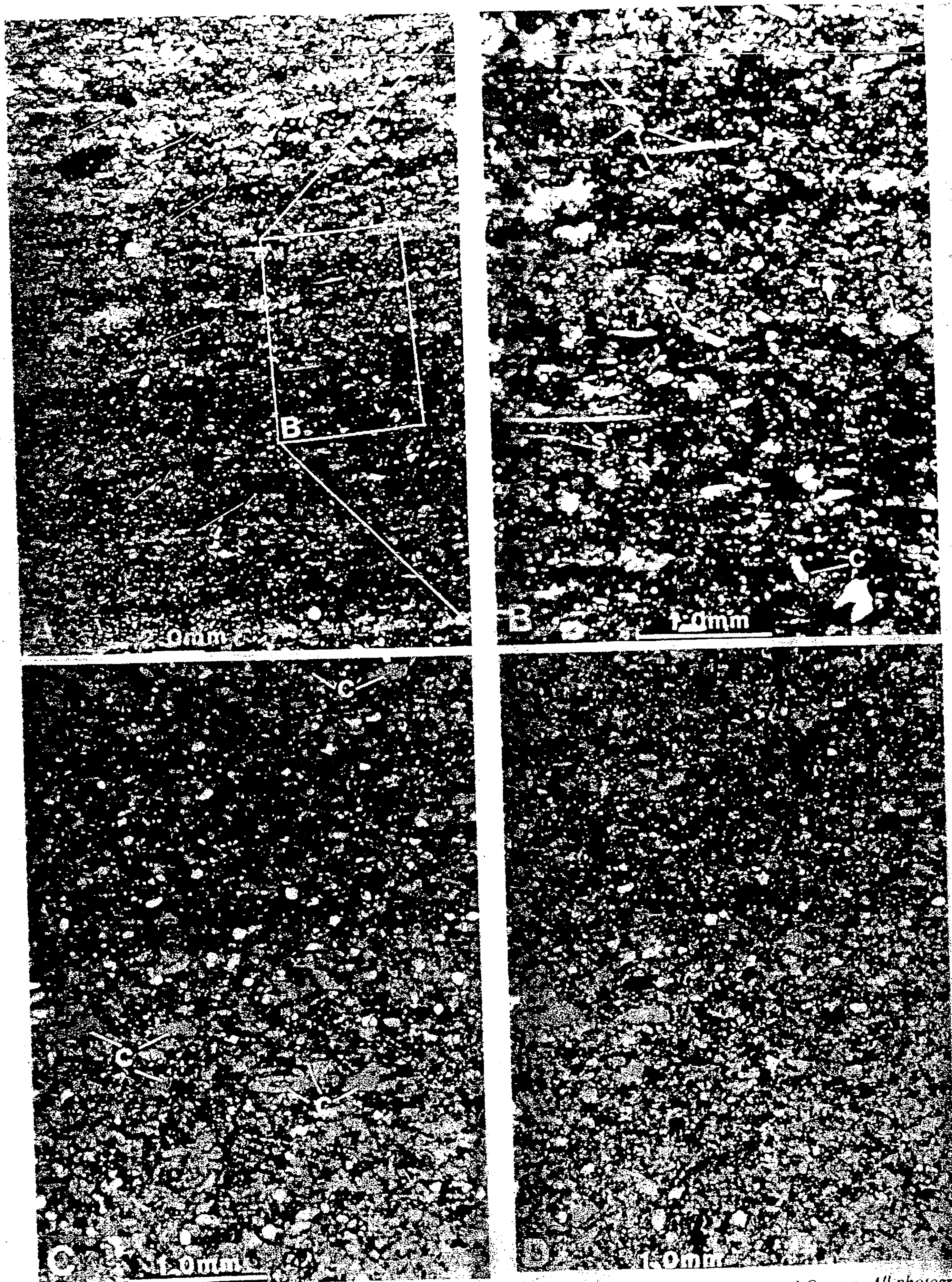

Figure 1-1-8. Thin section photomicrographs of the Bone Spring Limestone lithofacies. Stop 1a. Shumard Canyon. All photographs are oriented with present stratigraphic up at the top of photograph. A&B. Thin section photomicrographs, plane polarized light of the sample shown in outcrop in Fig. 1-1-7. Spicules (S), echinoderm (crinoid) debris (C) and quartz silt are conspicuous in this fine grained skeletal packstone/wackestone. Note the inclined laminations interpreted as current ripples (arrows). C&D. Thin section photomicrographs. C-plane polarized light and D-cross polarized light. Quartz silt and echinoderm fragments (C) are common in this fine grained packstone/wackestone. This sample shows alternation of coarser (lower half of photo) and finer grained laminations.

concave-up in geometry. At the mouth of the canyon, eastward-dipping surfaces are prominent. Farther up canyon, erosion surfaces dipping to the west can be observed. As was first described by King (1948), beds below the erosion surfaces are cleanly truncated and show no evidence of deformation or brecciation. Beds above the erosion surface typically parallel or drape the underlying erosional surface and are similar in lithofacies to beds below the erosion surfaces.

Origin of the intraformational erosion surfaces has been attributed to: 1) development of basinward-trending channels on the slope, 2) detachment surfaces related to slumping, and 3) faulting. The intraformational erosion surfaces are limited in distribution to an area extending from Shumard Canyon to a point about 1 mile south of Bone Canyon (King, 1948). This distribution suggests that the erosion surfaces were formed by processes active in a slope environment. Many of the large-scale erosional features in Shumard Canyon do not show onlap fill by material coarser than the underlying lime mud, but show drape by lime mud onto lime mud. Further south, in the Delaware Mountains, large-scale sediment deformation features (King, 1948, p. 15-16 and Plate 11B) are abundant in the upper Bone Spring limestones. The lack of coarse fill material and the downdip slump features suggests that these surfaces originated as detachment surfaces. Some of the erosional surfaces are, however, overlain by coarser-grained deposits favoring an erosional channel origin for these surfaces. Erosion surfaces, interpreted as channel structures (King, 1948, and Kirkby, 1982) do occur in Shumard Canyon in the lower part (basin margin facies) of the overlying Victorio Peak Formation.

Stop 1c — Allocthonous Carbonate Sand Sheet (Allodapic Sand)

Thick allochthonous channel-fill and sheet deposits composed of skeletal grainstones, packstones, and wackestones are common to basin margin facies of the lower Victorio Peak Formation and slope to basin facies of the Bone Spring Limestone (McDaniel and Pray, 1967). These allochthonous deposits were shed from the bank and bank margin areas of the Victorio Peak bank complex and are allodapic carbonate sands and sandy muds.

A thick allodapic skeletal grainstone unit is well exposed on the south wall of Shumard Canyon where the National Park trail crosses a gully (Figs. 1-I-1, 1-I-9). The base of this 10 m (33 ft) thick unit is poorly exposed below the park trail in the gully. Generally, however, these units exhibit sharp erosional bases. The lower half of the unit consists of medium to thick beds, with thick to very thick beds in the upper half. Internal channelling and trough cross-bedding are present (Fig. 1-I-10). Flow directions obtained from these features are roughly east-southeast in a basinward direction. The top of the unit is clearly marked by a change in bedding style from thick-bedded grainstones with trough cross-bedding to thin to medium-bedded mudstones and wackestones with lenticular chert lenses that are characteristic of the Bone Spring Limestone. Skeletal grains in these grainstones include: brachiopods, crinoids and echinoderm spines, fusulinids and other benthonic foraminifers, bryozoans, gastropods, calcareous algae and other finer skeletal debris (Fig. 1-I-10). The brachiopod fauna is diverse. Skeletal grains with micrite envelopes are common suggesting a shoal water source for these allochthonous deposits.

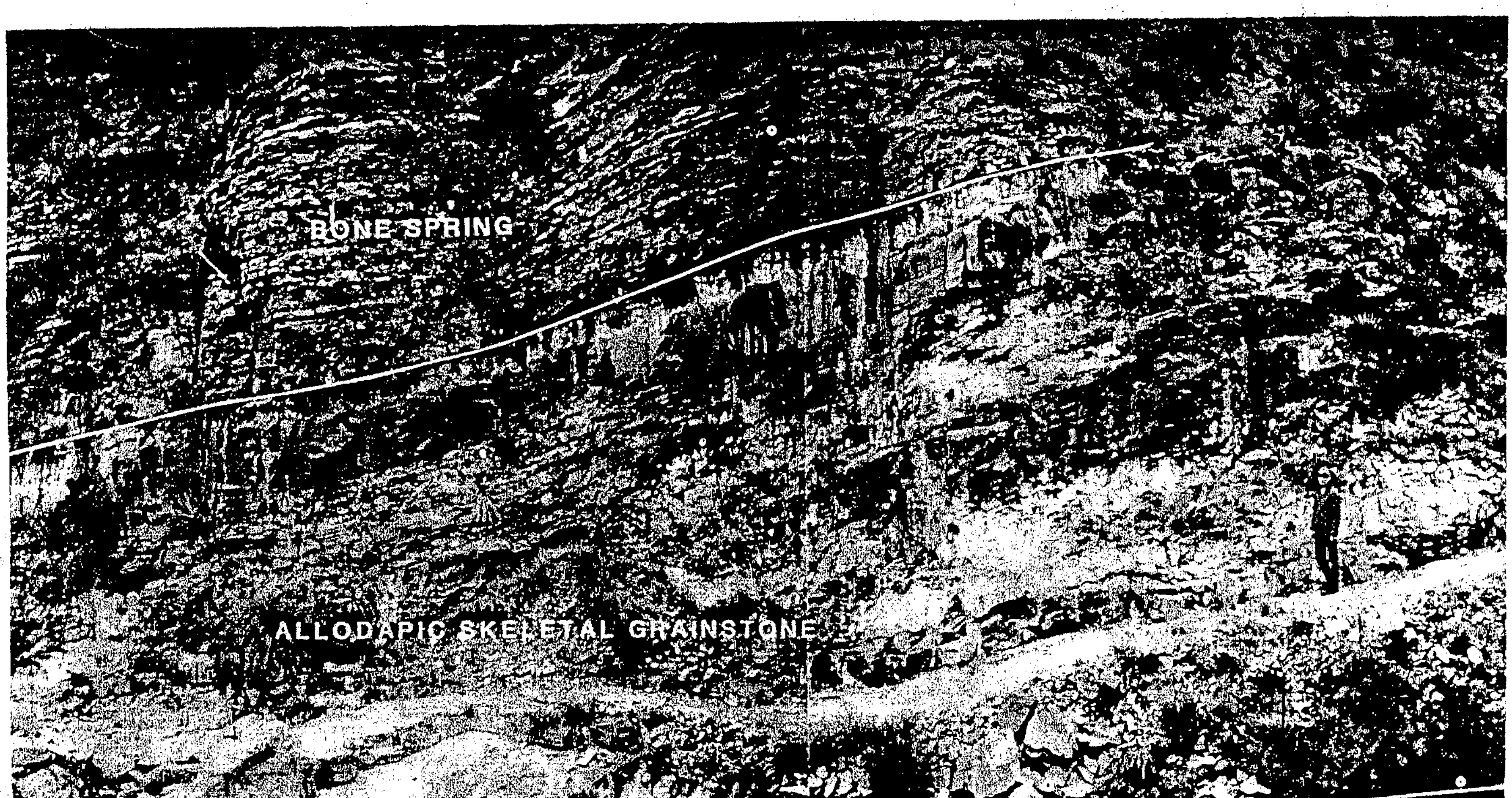

Figure 1-I-9. Unit of allochthonous skeletal grainstone to packstone within Bone Spring Limestone Formation along National Park trail, Stop 1c, Shumard Canyon.

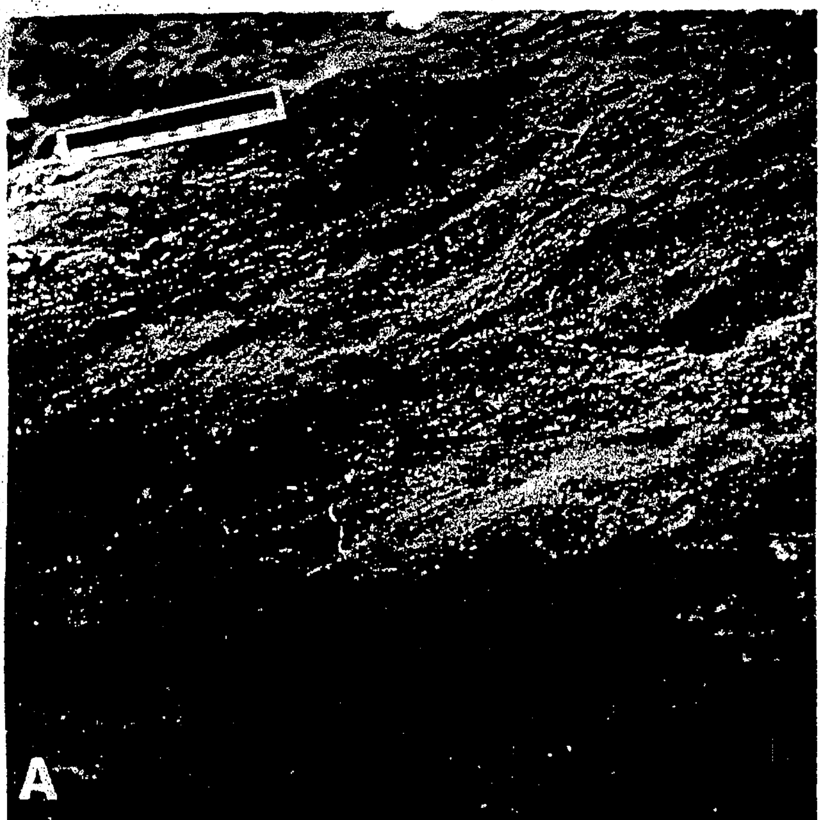

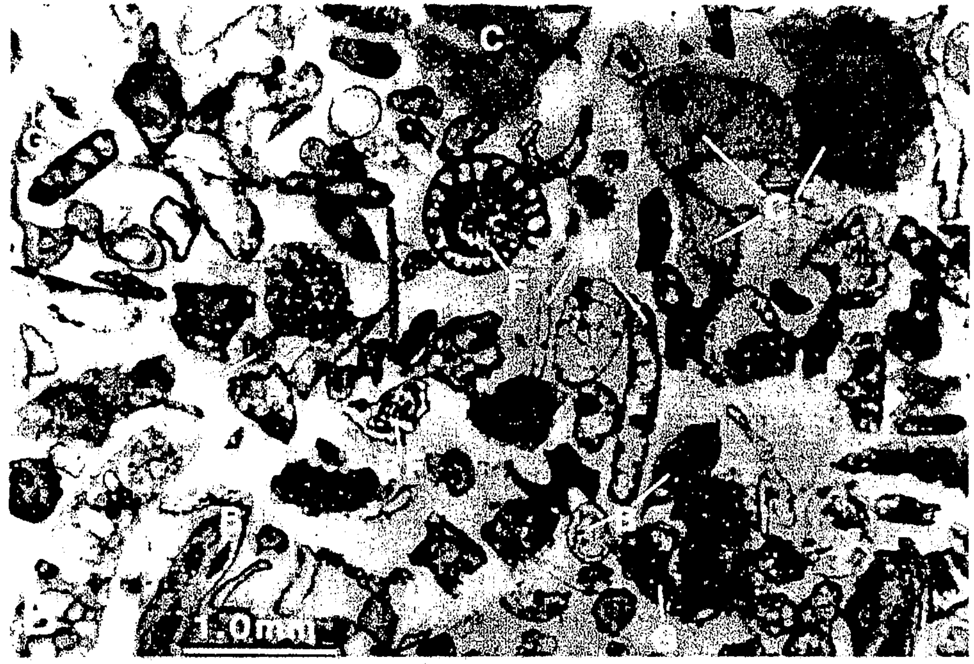

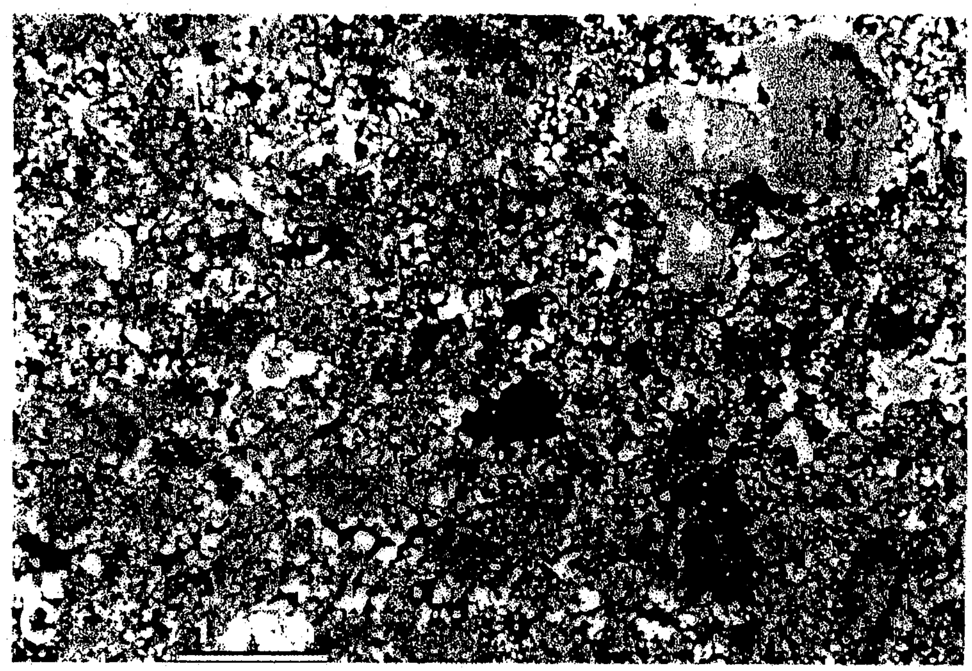

Figure 1-1-10. Outcrop and thin section photographs of the allodapic skeletal grainstone pictured in Fig. 1-1-9, Stop 1c, from Shumard Canyon. All photographs are oriented with present stratigraphic up at the top of the photograph. A. Outcrop photograph of trough cross-bedded grainstone located just above the geologist's head in Fig. 1-1-9. Scale is 15cm. B. Thin section photomicrograph, plane polarized light of the allodapic, skeletal dolomite grainstone shown in A. Grains consist largely of skeletal fragments including: echinoderm (crinoid) fragments (C), bryozoans (B), molluscan fragments preserved as micrite envelopes, (M), fusulinids (F), other benthonic foraminifers (BF), gastropods (G), and other unidentifiable skeletal debris. C. Thin section photomicrograph, cross polarized light of sample shown in B. Porosity in this grainstone has been completely occluded by megaquartz and chert.

STOP 5 — BONE CANYON

Stop 5a — Overview of south wall, Bone Canyon

Bone Canyon is situated at the "toe of slope" of the basinward-sloping sequence boundaries that mark the base of the Cutoff and of the Brushy Canyon formations (Fig. 1-I-6). The sequence boundaries and the lithofacies deposited on them are well exposed on the south wall of Bone Canyon (Fig. 1-V-1 and Fig. 1-V-2). The Bone Spring Limestone comprises the resistant, thin-bedded, dark-colored strata that form the lower visible part of the canyon wall. The recessive, grayish, vegetated slopes make up the Cutoff Formation, and the overlying resistant, tannish cliff consists of basal strata of the Brushy Canyon.

Fig. 1-V-2 shows the detailed geometry of the basal Cutoff and Brushy Canyon sequence boundaries along this wall, and lithofacies and intraformational erosion surfaces of the Cutoff Formation. Key features exposed here are listed below.

1) *The sequence boundary at the base of the Cutoff Formation.* Along much of the canyon wall, the basal Cutoff sequence boundary truncates underlying Bone Spring strata at a low angle. The boundary is overlain by lime mudstones and silicious shales of the upper Cutoff (Harris, 1982). At the west end of the canyon wall, two steep-sided, channel-shaped erosional surfaces filled with resistant, gray, massive-weathering megabreccia carbonates are developed on the sequence boundary (Fig. 1-V-2, 1-V-3A). These masses were first interpreted as patch reefs by King (1948), and Newell and others (1953) largely due to their internal massive character and abundance of fossils. They were subsequently reinterpreted as allochthonous megabreccias by Pray and Stehli (1962, see enclosed abstract) and Harris (1982), based on the following characteristics: 1) common erosional basal contacts, 2) presence within the masses of clasts of basinal to shallow-marine origin, and 3) chaotic orientation of geopetal fabrics from clast to clast. We will examine the contacts and internal fabric of a similar megabreccia located 0.25 km (0.15 mi) south of Bone Canyon during the final stop of the day (Stop 6).

2) *Intraformational erosion surfaces within the Cutoff.* These surfaces are broad, shallow, channel-like features up to 10 m (32 ft) deep, and 100-200 m (330-650 ft) wide (Harris, 1982). The scours are filled with coarse-grained material (intraclast rudstone) or with fine-grained material (lime mudstone and siliceous shale).

3) *Sequence boundary at the base of the Brushy Canyon Formation.* On the south wall of Bone Canyon, this boundary is a predominantly planar, eastward-dipping surface (strike N10E, dip 13° E). Brushy Canyon strata deposited on this surface comprise a coarse-grained package (unit BC of Fig. I-II-5), up to 75 m (240 ft) thick, which consists of megaconglomerate, planar-stratified sandstone, and allochthonous, fossiliferous lime grainstone (the gray, blocky weathering unit at the top, west end of the canyon wall). On both the south and north walls of the canyon, basal Brushy Canyon strata thin and pinchout to the west by onlap onto the eastward-sloping sequence boundary (Fig. 1-V-3B). These basal Brushy Canyon strata also pinch out by onlap to the north such that the 75 m thick package of sandstone, megaconglomerate and limestone is absent in Shumard Canyon, 1 km to the north.

Stop 5b — Traverse from north wall to floor of Bone Canyon

The traverse from the rim of the north wall of Bone Canyon to the canyon floor provides an opportunity to examine: 1) the sequence boundary separating the Cutoff and Brushy Canyon formations, and 2) the lithofacies and sedimentary structures present at the base of the Brushy Canyon in this "toe of slope" position.

Fig. 1-V-4 is a section of the basal 75 m of the Brushy Canyon Formation in Bone Canyon. Representative lithofacies of this coarse-grained section are well exposed in the prominent draw located at the center of the north wall of Bone Canyon (Fig. 1-I-1). These units are, from top to bottom:

1) *Gray-weathering, allochthonous carbonates*, 32 m (66 ft) thick, consisting of sandy, dolomitic, skeletal-peloidal grainstones. Beds are internally massive, or exhibit Tabc, Tab, and Tbc Bouma sequences (Fig. 1-V-5A). Skeletal grains consist of fusulinids, crinoids, brachiopods, and rugose corals; nonskeletal grains consist of peloids, ooids and sand-sized intraclasts (1-V-8C, D). These grains are believed to have been derived from a contemporaneous shallow, normal-marine environment.

2) *Fine-grained sandstones*, 10 m (33 ft) thick, are parallel-laminated, current-rippled or display broad, shallow, trough cross-stratification. Lenses of pebble to cobble-sized carbonate clasts indicate high-energy flow conditions.

3) *Carbonate-clast megaconglomerate*, 2.5 m (8.2 ft) thick, forms the base of the Brushy Canyon at this locality (Fig. 1-V-6). This megaconglomerate is similar to other megaconglomerates that occur with interbedded parallel-stratified sandstones in the basal 25 m (78 ft) of the Brushy Canyon in Bone Canyon. Common characteristics of the megaconglomerates (Fig. 1-V-5B, 1-V-7A) are: 1) clast-support texture, 2) matrix of very fine sandstone, 3) clast sizes ranging from pebbles to boulders up to 5 m (16 ft) in longest dimension, and 4) internally massive, ungraded character. In a few megaconglomerates, large clasts protrude above the tops of beds as if they had been rafted (1-V-7B). The megaconglomerates are interpreted as debris flow deposits (Harms, 1974, Rossen, 1985). Megaconglomerate clast types include: (1) dark gray lime mudstones, (2) light gray skeletal wackestones, packstones and grainstones of limestone and dolomite composition, (3) lesser amounts of fenestral limestone and dolomite (Fig. 1-V-7A and Fig. 1-V-8 A, B), and (4) very fine-grained quartz sandstone. With the exception of the fenestral dolomite and limestone, these clast types are similar to lithologies found in the Cutoff, Victorio Peak and Bone Spring formations beneath the basal Brushy Canyon sequence boundary. Fenestral dolomite clasts may have been eroded from bank top Victorio Peak strata that are now preserved to the north at Cutoff Mountain in the lower part of the Upper Victorio Peak, or from uppermost Victorio Peak strata that were completely eroded during formation of the basal Brushy Canyon sequence boundary.

Strata of the Cutoff Formation, consisting of gently eastward-dipping, thin-bedded, dark gray, lime mudstones, crop out directly beneath the Brushy Canyon megaconglomerate on the east side of the draw (Fig. 1-V-6). The subhorizontal lime mudstone beds truncated below the Cutoff beds are strata of the Bone Spring Limestone. The Cutoff Formation thins to the west by truncation beneath the basal Brushy Canyon sequence boundary, and pinches out completely some 10 m (30 ft) west of the draw (Harris, 1982). This truncation marks the shelfward pinchout of the basin segment of the Cutoff (Fig. 1-I-6). The Cutoff reappears beneath the basal Brushy Canyon sequence boundary approximately 0.25 km (0.15 mi) north of Bone Canyon.

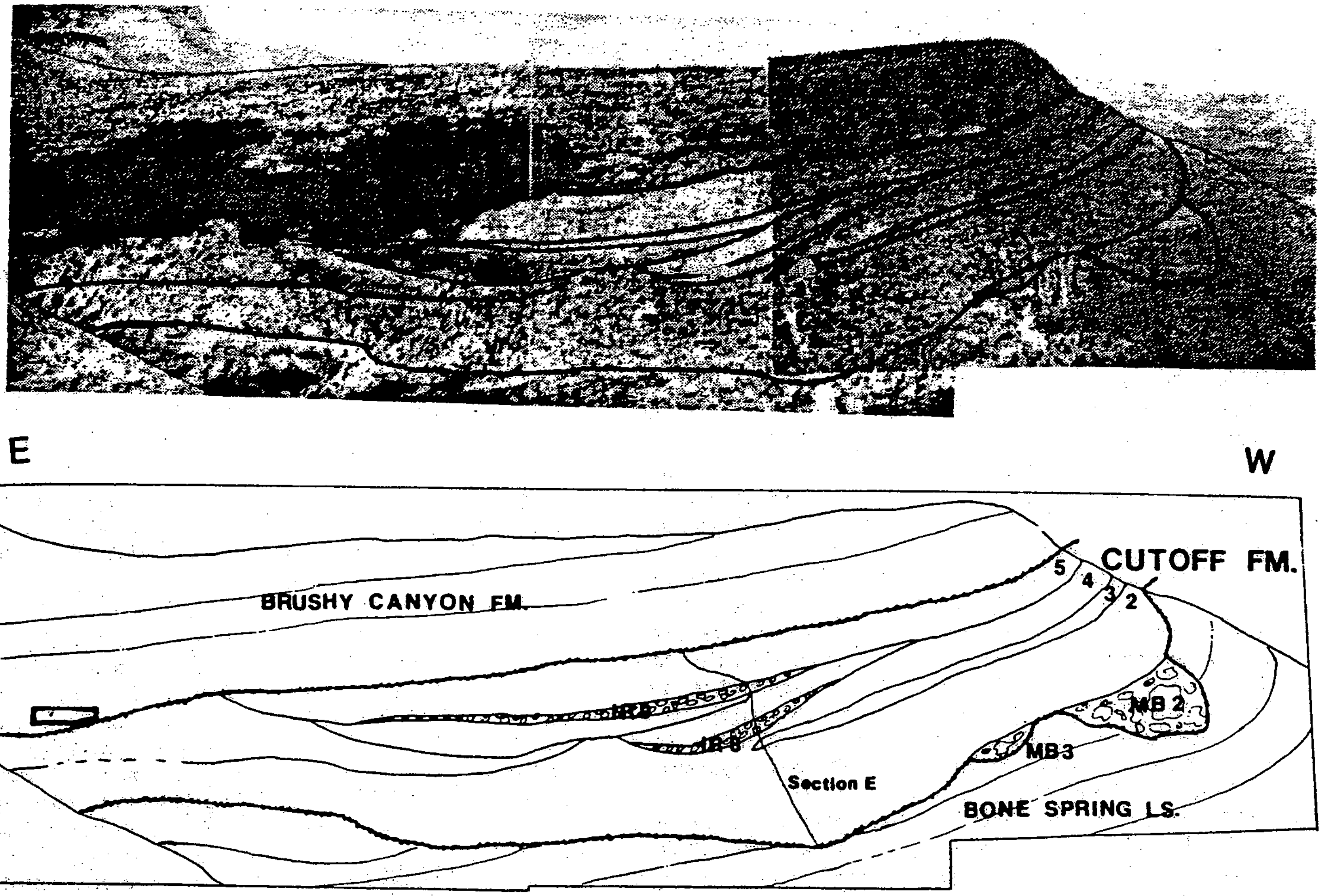

Figure 1-V-2. Sketch of south wall, Bone Canyon, from Harris (1982), showing geometry of basal Cutoff and basal Brushy Canyon sequence boundaries. Note channel-filling carbonate megabreccias at base of Cutoff (MB2 and MB3), and numerous Cutoff intraformational, channelized surfaces filled with intraclast rudstone (IR) or mudstone.

Stop 5c — Floor of Bone Canyon at the Juniper Tree

At this locality, the interbedded megaconglomerates and sandstones which form the basal 10 m (33 ft) of the Brushy Canyon Formation (Fig. 1-V-7B) can be examined.

Traverse along south wall of Bone Canyon to Cutoff megabreccia of Stop 6.

As you walk along the south wall of Bone Canyon, the following features can be noted on the north wall of Bone Canyon:

1) East end of canyon wall; westward thinning and pinchout of basal Brushy Canyon megaconglomerates and sandstones by onlap onto the smooth, eastward-dipping, basal Brushy Canyon sequence boundary (Fig. 1-V-3B).

2) West and central parts of canyon wall; irregular, undulating morphology of basal Brushy Canyon sequence boundary on underlying thin-bedded strata of the Bone Spring Limestone.

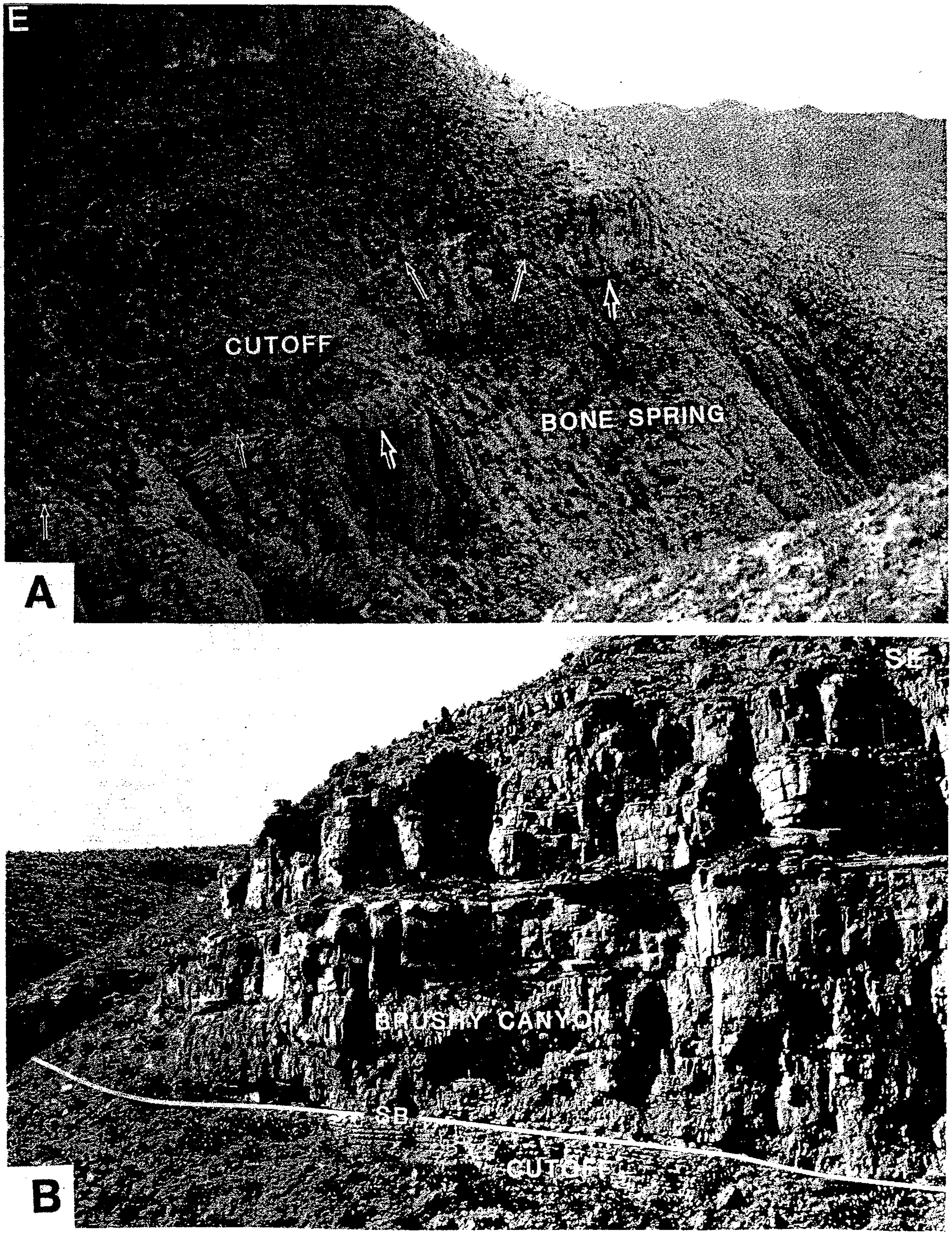

Figure 1-V-3. A. Close-up of Cutoff carbonate megabreccias (large arrows), MB2 and MB3 of Fig. 1-V-2, at base of Cutoff Formation, west end of south wall, Bone Canyon. Megabreccias fill spoon-shaped scours developed on basal Cutoff sequence boundary (small arrows) that are incised into underlying strata of the Bone Spring Limestone. B. View of Cutoff Formation and interbedded sandstones and conglomerates of basal 25 m (80 ft) of Brushy Canyon Formation, north wall Bone Canyon. Basal Brushy Canyon strata thin to the west (left) by onlap onto the eastward-dipping basal Brushy Canyon sequence boundary (SB).

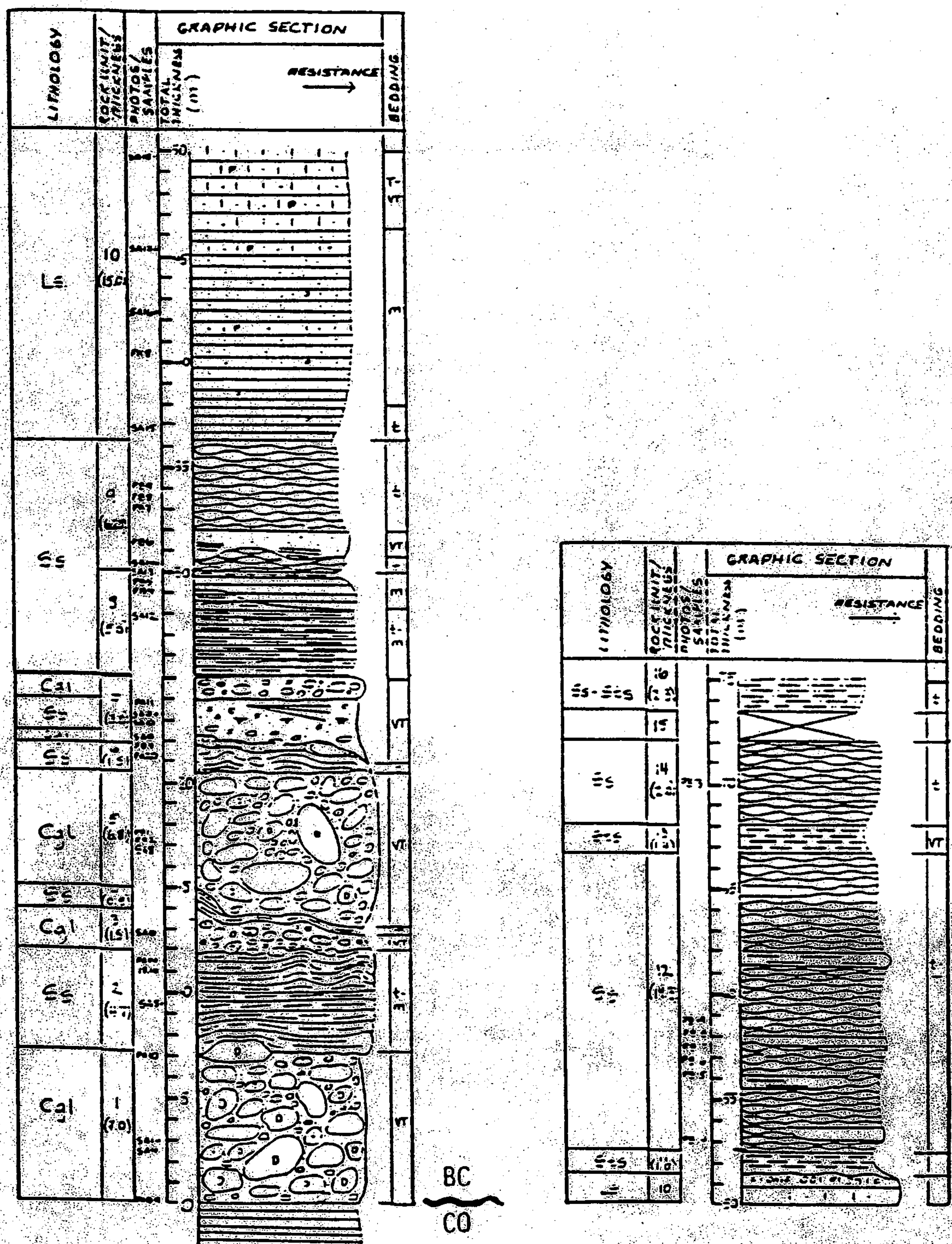

Figure 1-V-4. Stratigraphic section of basal 75 m (250 ft) of Brushy Canyon Formation in Bone Canyon, as measured along canyon floor, from Rossen (1985). BC = Brushy Canyon Fm., CO = Cutoff Fm.

LEGEND FOR GRAPHIC SECTIONS

MAJOR LITHOLOGIES:

Siltstone

- light-colored, coarse silt
- organic-rich(dk gray) medium-coarse silt
- organic-rich (gray) medium-coarse silt

Sandstone

- medium
- very fine-fine

MINOR LITHOLOGIES:

Conglomerate

- clast support
- matrix support

Clast types:

- sandstone
- limestone
- dolomite
- chert
- unidentified

Limestone

- • sandy
- M mudstone
- W wackestone
- P packstone
- G grainstone

SEDIMENTARY STRUCTURES:

- thin laminations
- thick laminations
- ripples
- cross-bedding
- massive
- contorted layer

For example:

- interbedded ripples and thin laminations

FOSSILS:

- F fusulinid
- forams (undifferentiated)
- brachiopod
- crinoid
- mollusc
- Q gastropod
- T trace fossil
- unidentified

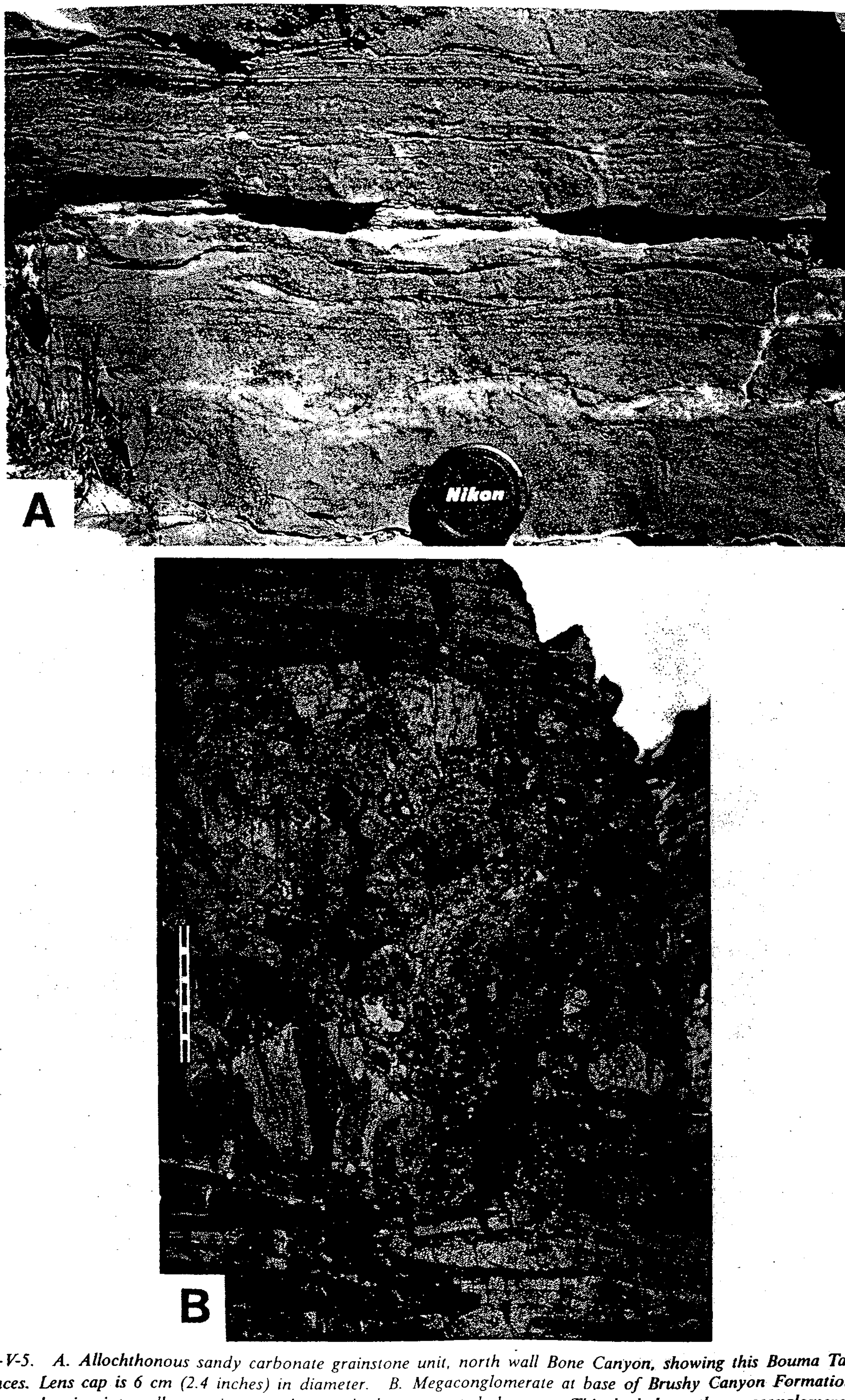

Figure 1-V-5. A. Allochthonous sandy carbonate grainstone unit, north wall Bone Canyon, showing this Bouma Tab, Tabc, and Tbc sequences. Lens cap is 6 cm (2.4 inches) in diameter. B. Megaconglomerate at base of Brushy Canyon Formation, north wall Bone Canyon, showing internally massive, poorly-sorted, clast-supported character. Thin beds beneath megaconglomerate are Cutoff strata. Scale bar =0.5 m (1.6 ft).

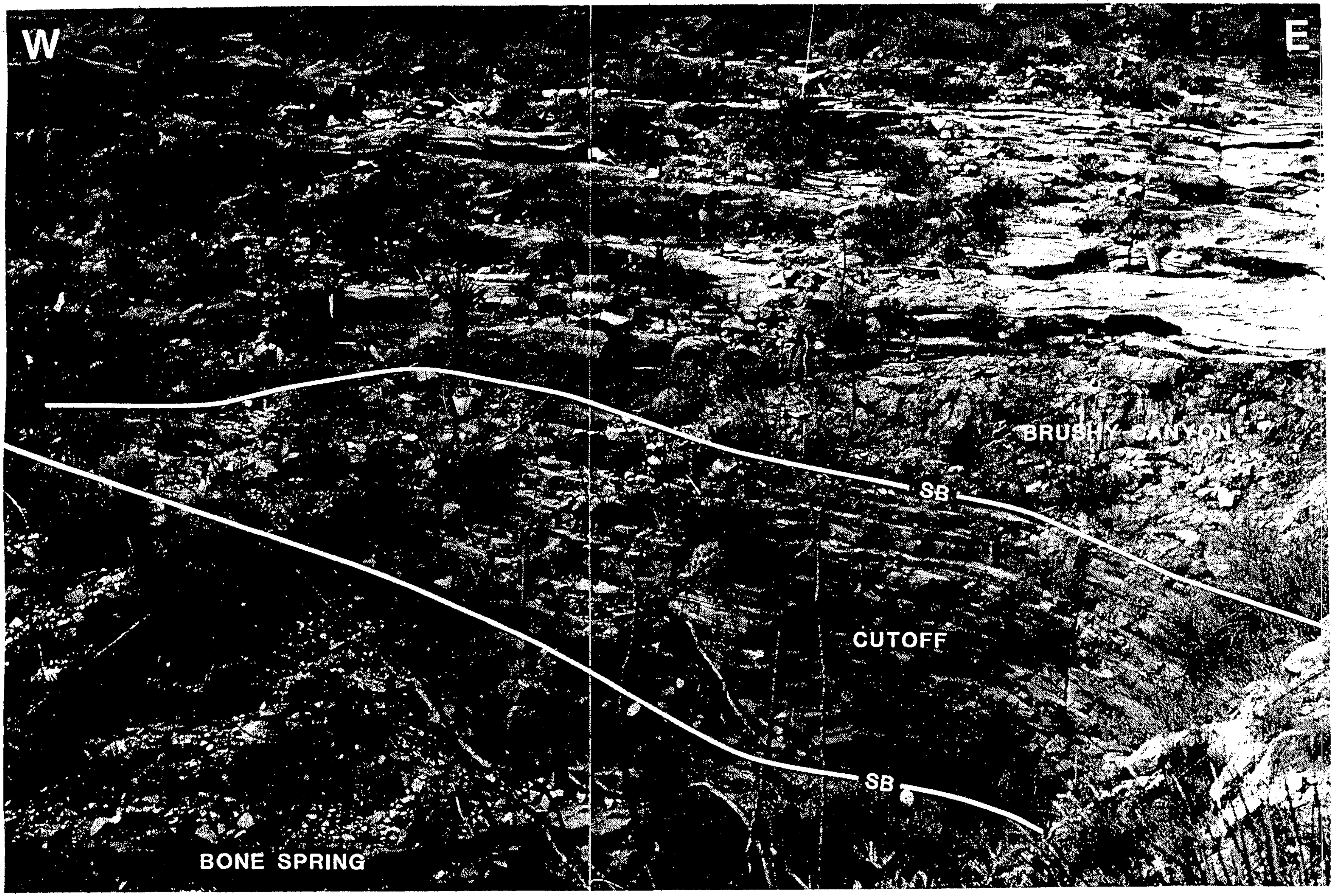

Figure 1-V-6. Basal Cutoff and basal Brushy Canyon sequence boundaries (SB) exposed in prominent draw located at center of north wall, Bone Canyon. Gently eastward-dipping strata of Cutoff Formation overlie truncated, subhorizontal beds of Bone Spring Limestone. The Cutoff Formation thins to pinchout towards the west as the result of truncation by the overlying basal Brushy Canyon sequence boundary. Megaconglomerate at base of Brushy Canyon Formation thins to west by onlap onto eastward-dipping basal Brushy Canyon sequence boundary.

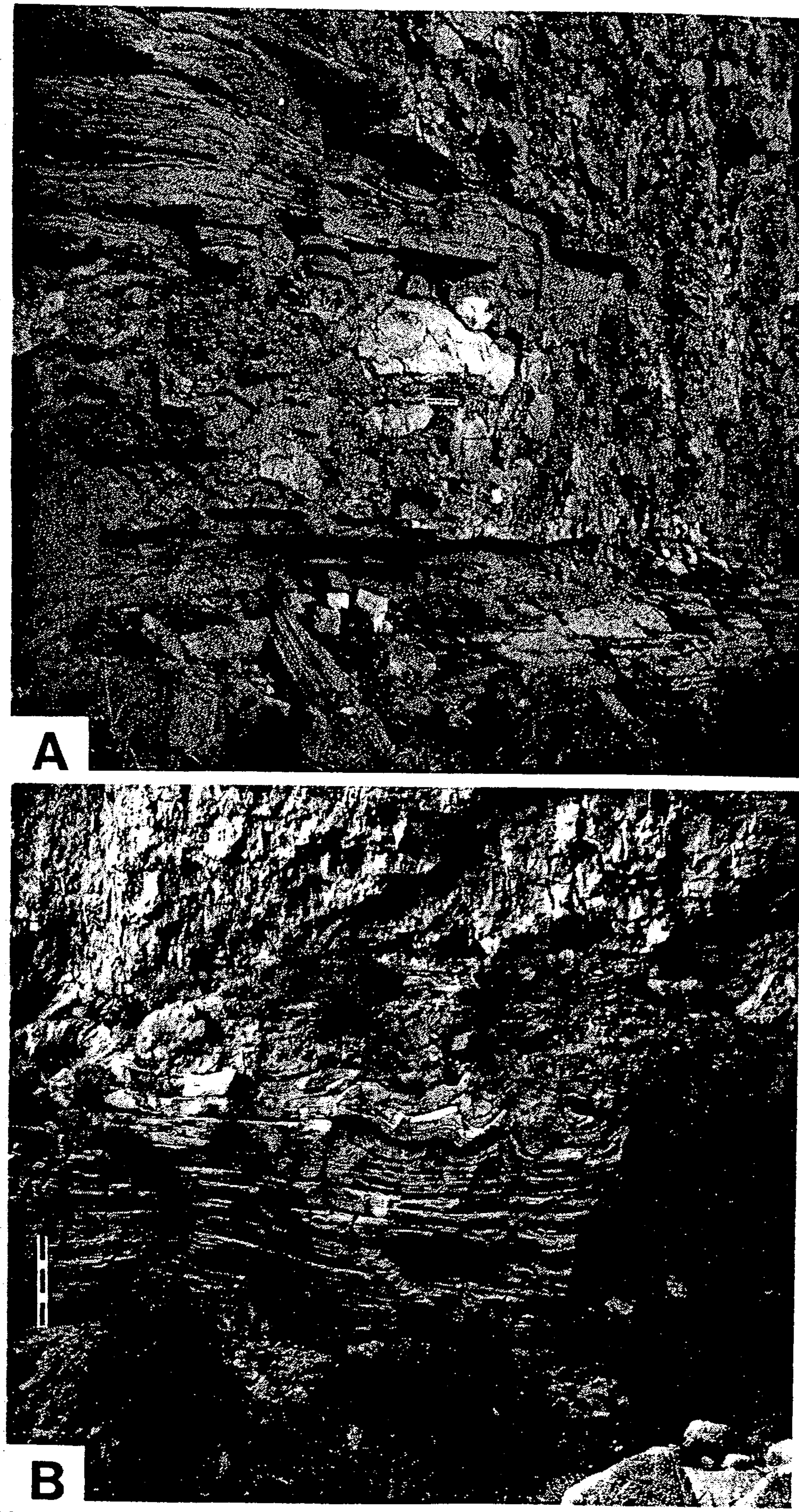

Figure 1-V-7. A. Megaconglomerates and interbedded parallel-laminated sandstone of basal Brushy Canyon Formation, north wall Bone Canyon. Cutoff Formation comprises thin beds below recessive in lower 1/3 of photo. Scale is 15 cm. Prominent white clast above scale consists of fenestral lime grainstone (see Fig. 1-V-8A,B). B. Parallel-laminated sandstone unit interbedded with megaconglomerates in basal 15 m of Brushy Canyon Formation, canyon floor near Juniper tree, Bone Canyon. At base of sandstone unit, note drape of sandstone laminae over boulder (0.5 m relief) protruding from top of underlying megaconglomerate. Sandstone is deformed into fold and flame structures beneath overlying megaconglomerate. Scale bar = 1.0 m (3.28 ft).

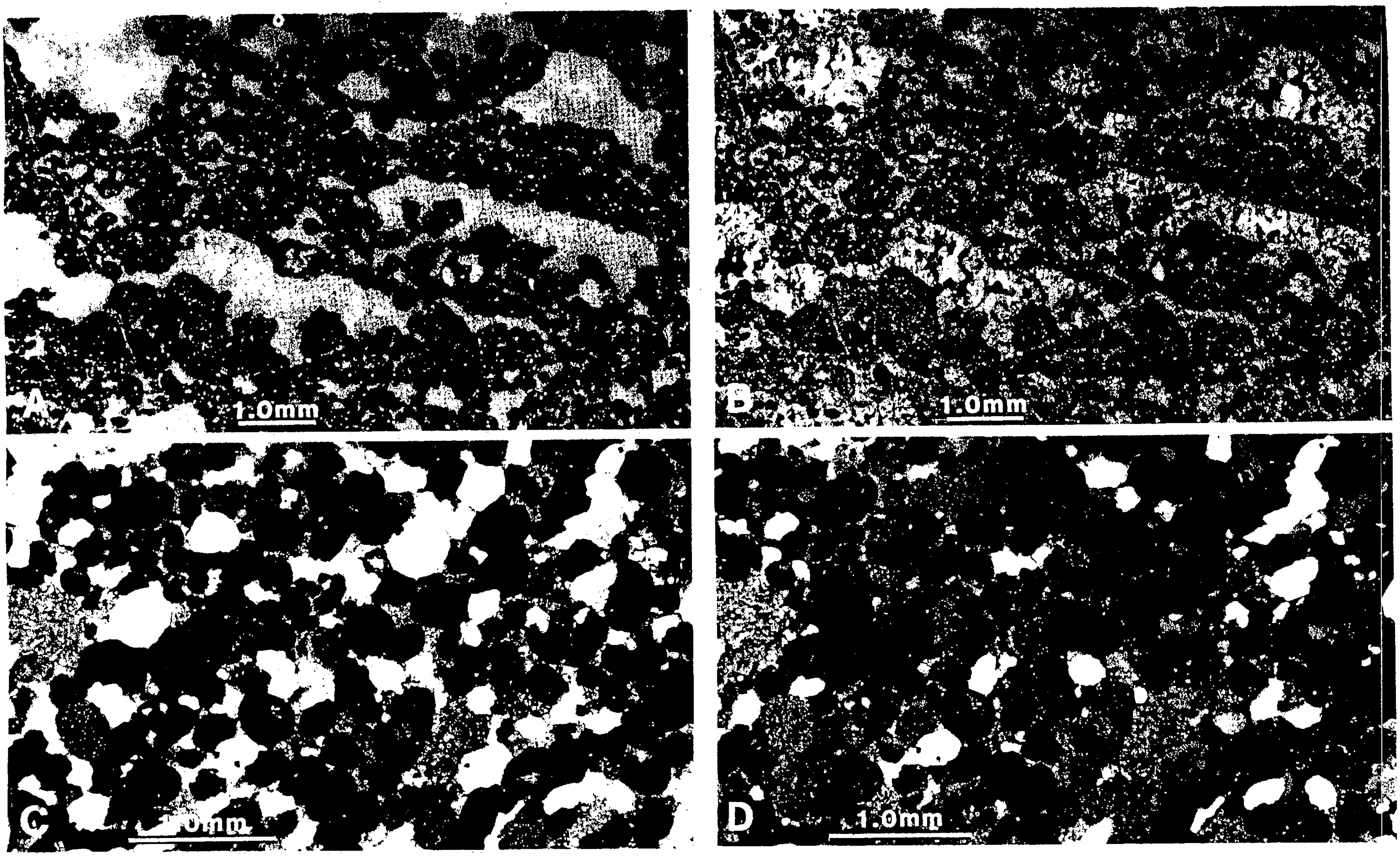

Figure 1-V-8. Thin section photomicrographs from the lower Brushy Canyon Formation, north wall Bone Canyon. All photographs are oriented with present stratigraphic up to the top of photograph. A&B. Thin section photomicrographs, A-plane polarized light and B-cross polarized light of a sample taken from the light colored boulder in the center of the photo in Fig. 1-V-7. The fenestrae are overturned as collected in the field. This meter-sized boulder is composed of a peloid, intraclast, lime grainstone. Two generations of cement fill the large fenestrae: 1) a fibrous to bladed isopachous cement of probable marine origin and 2) a coarse equant calcite spar of probable meteoric origin. These cements are interpreted to have been precipitated in a shelf setting before being redeposited in the slope setting where they are preserved today. C&D. Thin section photomicrographs, C-plane polarized light and D-cross polarized light, from a parallel-laminated dolomite sample taken from the allochthonous carbonate unit of lower Brushy Canyon. This grainstone is composed of rounded dolomite and siliciclastic grains. The dolomite grains include: intraclasts (including ooid grainstones), peloids (some of which are likely former ooids or skeletal grains), and ooids. The siliciclastic grains include: quartz, chert, and K-feldspar.

McKittrick Canyon

Katherine Goepfert
April 30, 2008

McKittrick Canyon (Permian Reef Trail)

Overview/ Introduction:
McKittrick Canyon is located on the eastern side of the Guadalupe Mountains near El Capitan. The mouth of McKittrick Canyon shows great exposures of the shelf crest, outer shelf, reef, slope, and toe of slope leading out onto the Delaware basin.

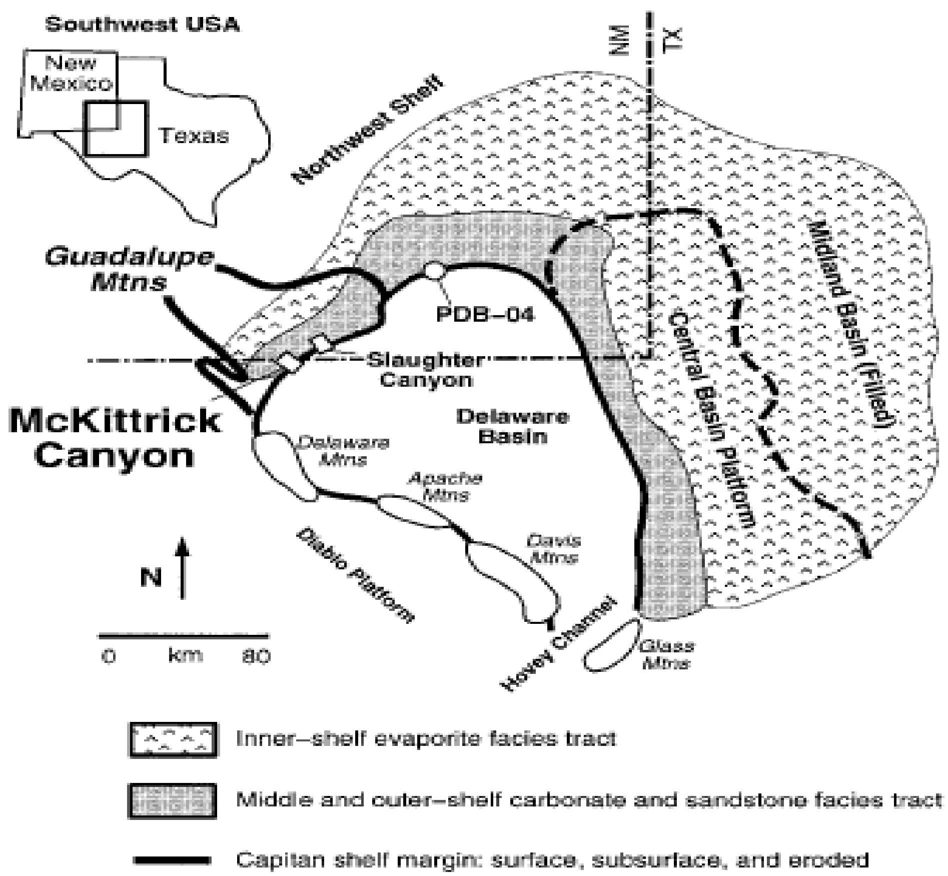

Figure 1: Regional location of McKittrick Canyon during the Permian. (Tinker, 1998)

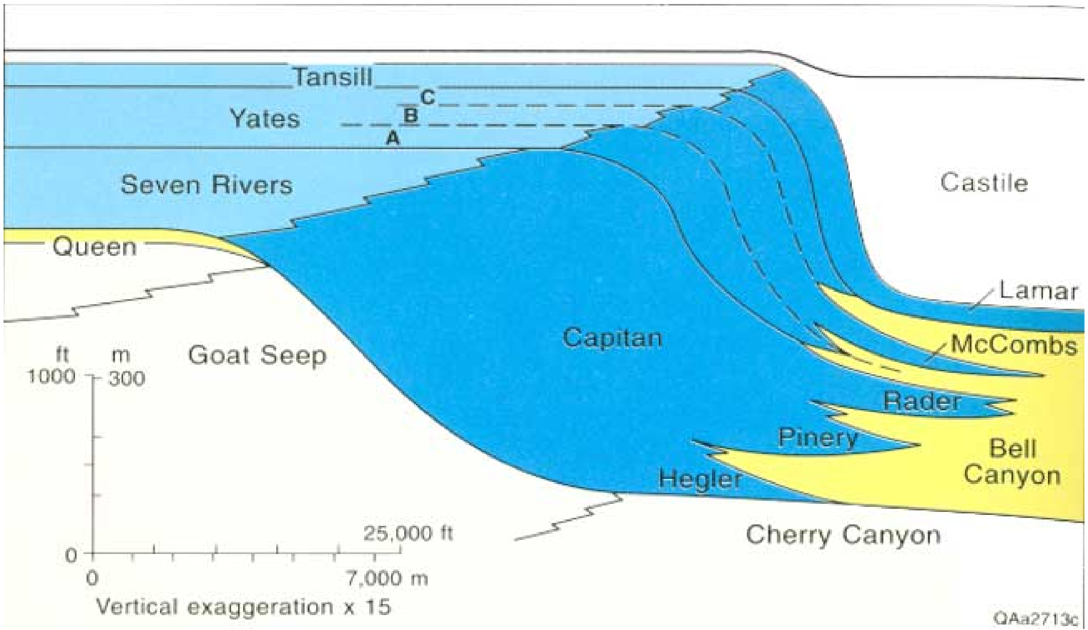

Figure 2: Cross section showing shelf-to-basin correlations of the Capitan Formation and equivalents. Modified from Garber and others (1989).

Only the younger units, the Lamar Member of the Bell Canyon Formation, the Yates Formation, and the Tansil Formation can be seen along the trail. This is a great example of a reef-rimmed platform which occurred during the Guadalupian 16-28 High Frequency Sequences.

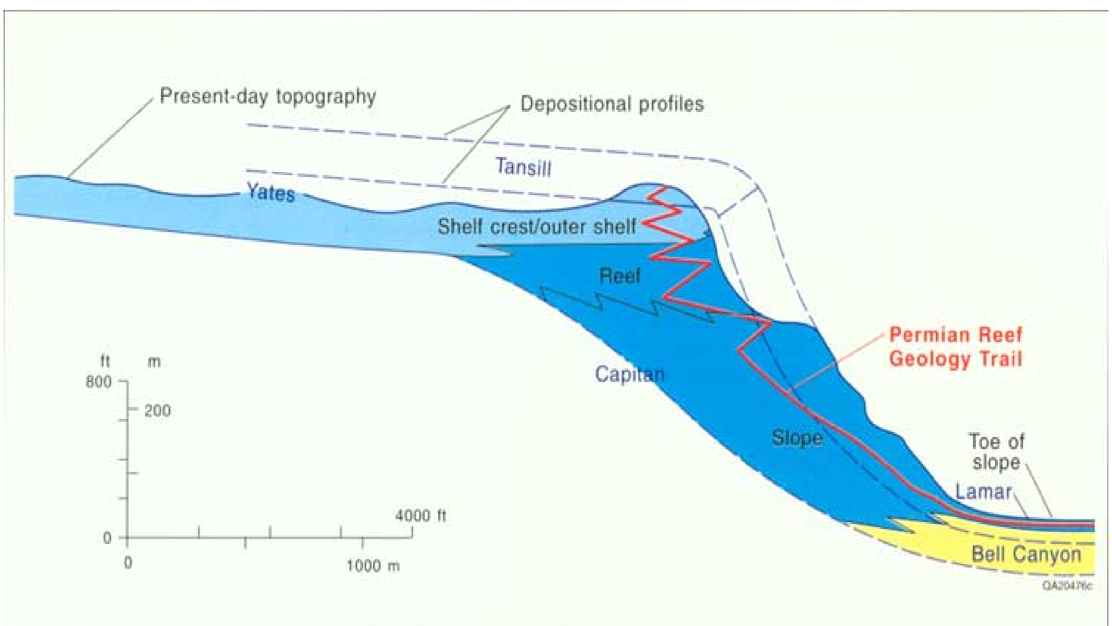

Figure 3: Shows location of Permian Reef Trail on the erosional cross-section of the North Wall of McKittrick Canyon. (Bebout et al., 1993)

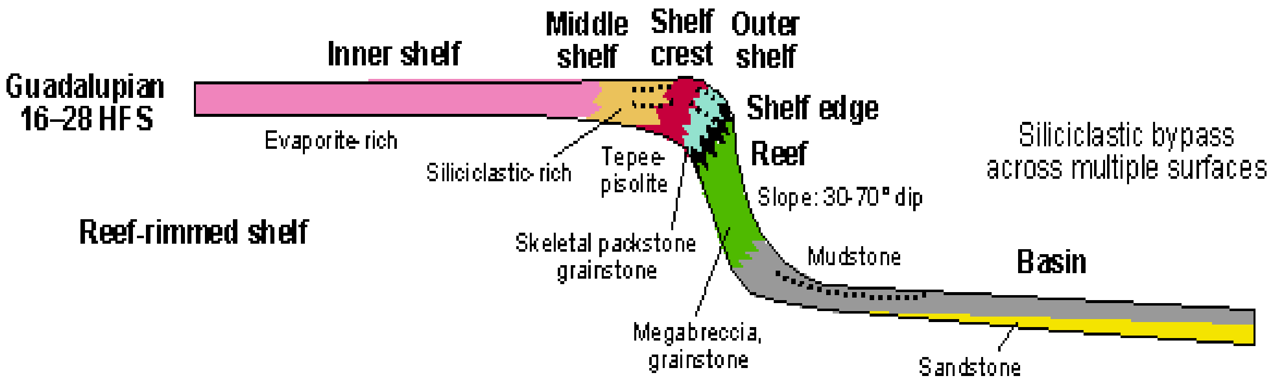

Figure 4: Simplified Facies of the Reef-Rimmed Shelf from the Guadaulupian 16-28 High Frequency Sequences. (Kerans and Kempter, 2000)

Toe of Slope:
The toe of slope lies in the Lamar Member which is the upper unit of the Bell Canyon Formation. It is dominantly laminated to thinly bedded skeletal wackestone with less prevalent thin layers of skeletal packstone. The amount of skeletal packstone increases with increasing dip and unit layer thickness (closer to the slope). These units were mostly created by turbidity currents and debris flows from the slope and shelf margin. Common fossils in these units are foraminifera, sponge spicules, ostracodes, brachiopods, and bryozoans. Most of these fossils are not in-situ, but carried by the gravity flows or sediment settling out of suspension to the toe of slope.

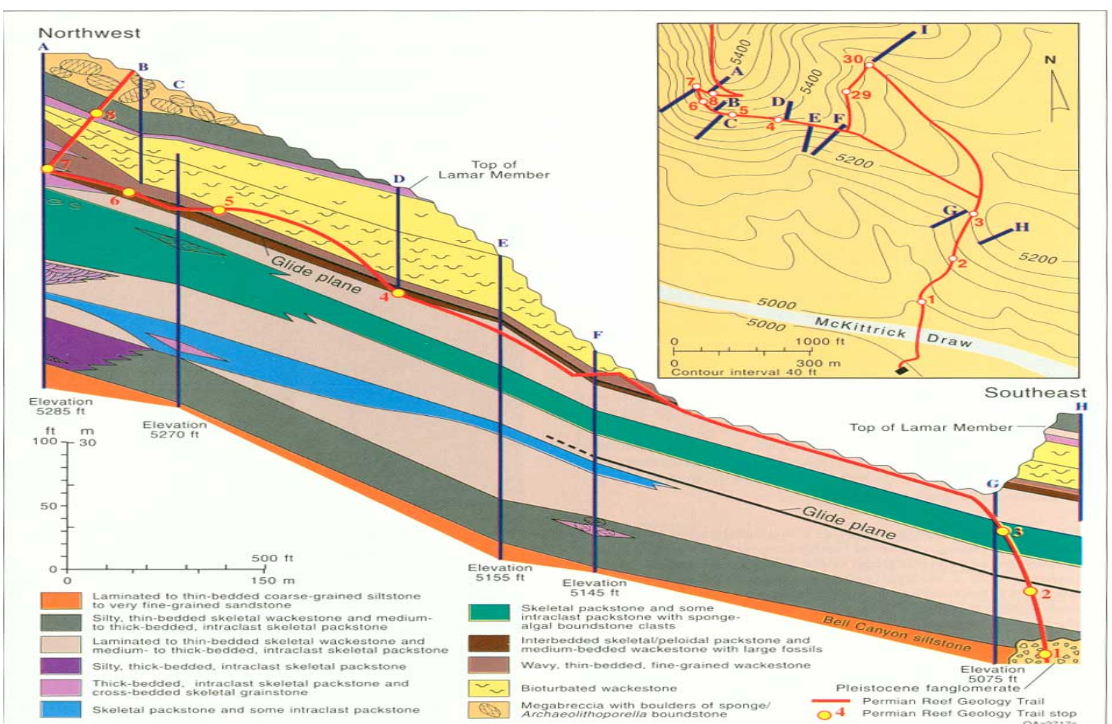

Figure 5: Diagram showing the facies present in the toe of slope and the path the Permian Reef Trail takes through it. (Bebout et al., 1993)

Slope:

The slope is part of the Capitan Formation and the Yates-equivalent and Tansil-equivalent sections are exposed in McKittrick Canyon. As you walk up the lower and middle slope, you will be in the Tansil-equivalent part of the formation. This unit has facies ranging from skeletal wackestones to grainstones, as well as megabreccias. The upper slope will be Yates-equivalent and has skeletal wackestones to grainstones, siliclastics, and reef talus. The siliclastics are believed to have been deposited during a lowstand. The reef talus near the top of the slope has large blocks of sponge-algal boundstones from the overlying reef. The slope has beds that were mostly deposited from gravity flows and have dips ranging from 10-70^{o}. The closer to the reef, the steeper the beds dip. The fossils found are sponges, bryozoans, brachiopods, crinoids, fusulinids, gastropods, and encrusting Archaeolithporella (algae). Most of these fossils can be found in the reef itself. The fusulinid grainstone at the top of the slope might be evidence for a channel going through the reef because these fusulinids are very common behind the reef in the outer shelf.

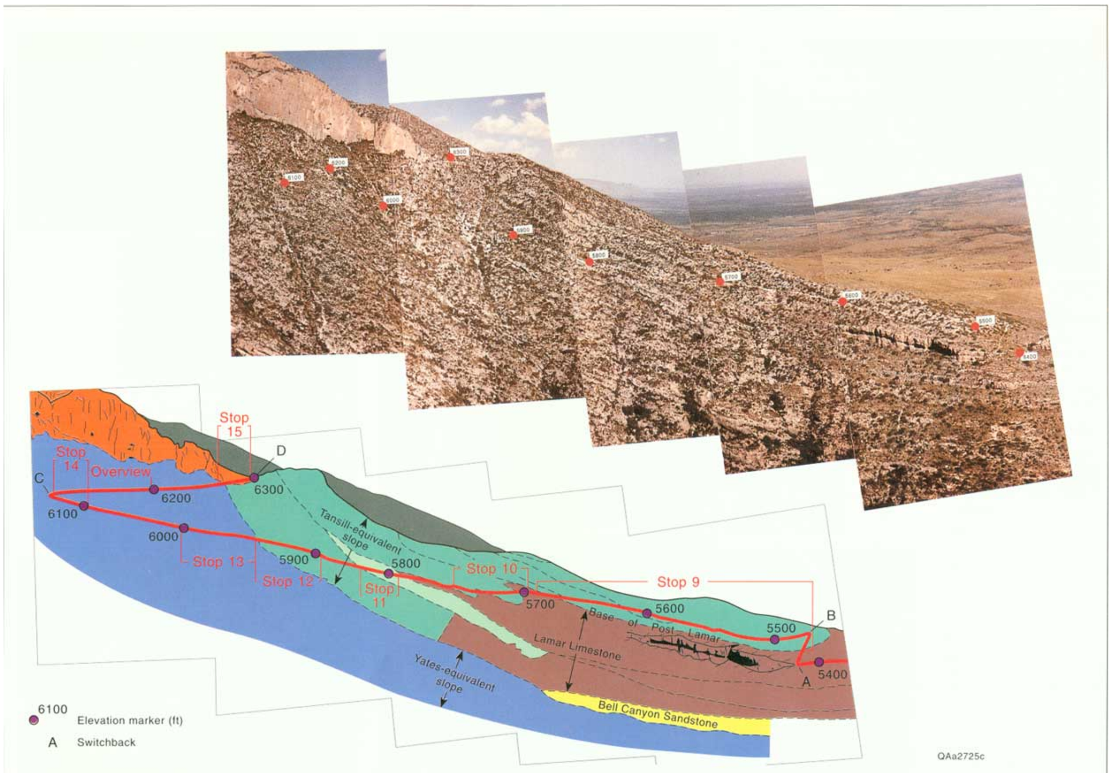

Figure 6: Diagram and Photomosaic of slope on north wall of McKittrick Canyon. Shows path of the Permian Reef Trail and the formations is crosses. (Bebout et al., 1993)

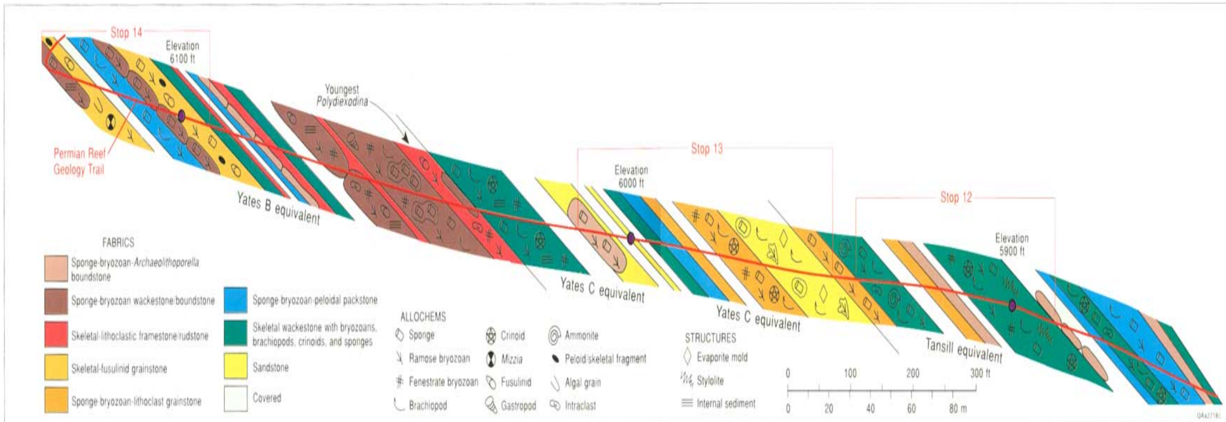

Figure 7: Diagram showing facies and dominant fossils for the transition between the Tansil-equivalent part of the slope and the Yates-equivalent portion. (Bebout et al., 1993)

Reef:
The reef is a steeply dipping (near vertical) part of the Capitan Formation. Tansil-equivalent portion of the reef has been eroded in the McKittrick Canyon locality so you are only seeing the Yates-equivalent part of the reef. For this reef-rimmed platform, the reef is not the topographic high. It is down-dip form the higher shelf crest in estimated water depths of 30-43 meters. The reef would prograde outwards, become unstable and create the gravity flows which are deposited on the slope and toe of slope. The dominant reef-builders are a variety of sponges, bryozoans, Tubiphytes, and *Archaeolithoporella*, with minor crinoids, fusulinids, and *Collenella* (a type of algae). The presence of the *Collenella* at the top of the reef might indicate that the reef was in shallower waters at the termination of the Yates Formation. There are several types of cement present in the reef. There is the botryoidal cement, the isopachous fibrous cement, the inclusion-rich prismatic cement, dolomite, and three types of calcite spar. The botryoidal cement is found around botryoidal fans and fills in framework voids. The isopachous fibrous cement tends to line framework voids while the inclusion-rich prismatic cement tends to fill the rest of the void in.

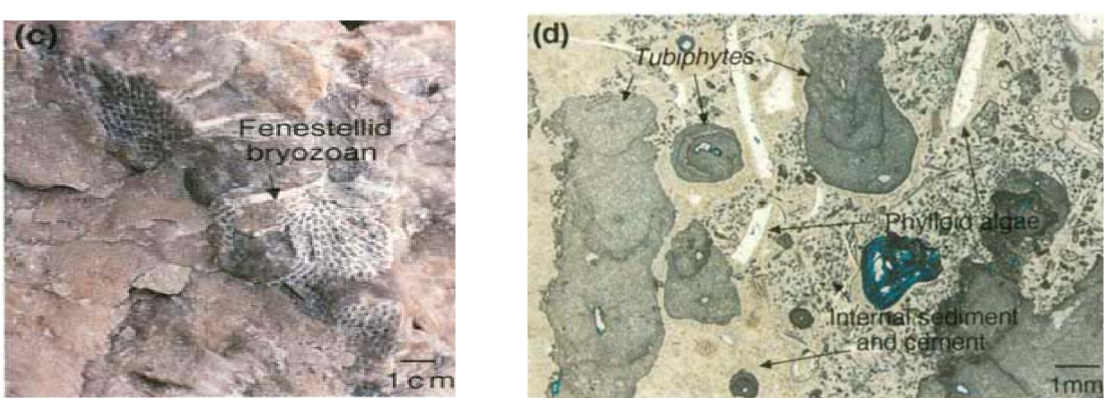

Figure 8: Pictures of fenestellid bryozoans, Tubiphytes, and phylloid algae in outcrop and thin section taken from Permian Reef Trail in McKittrick Canyon. (Bebout et al., 1993)

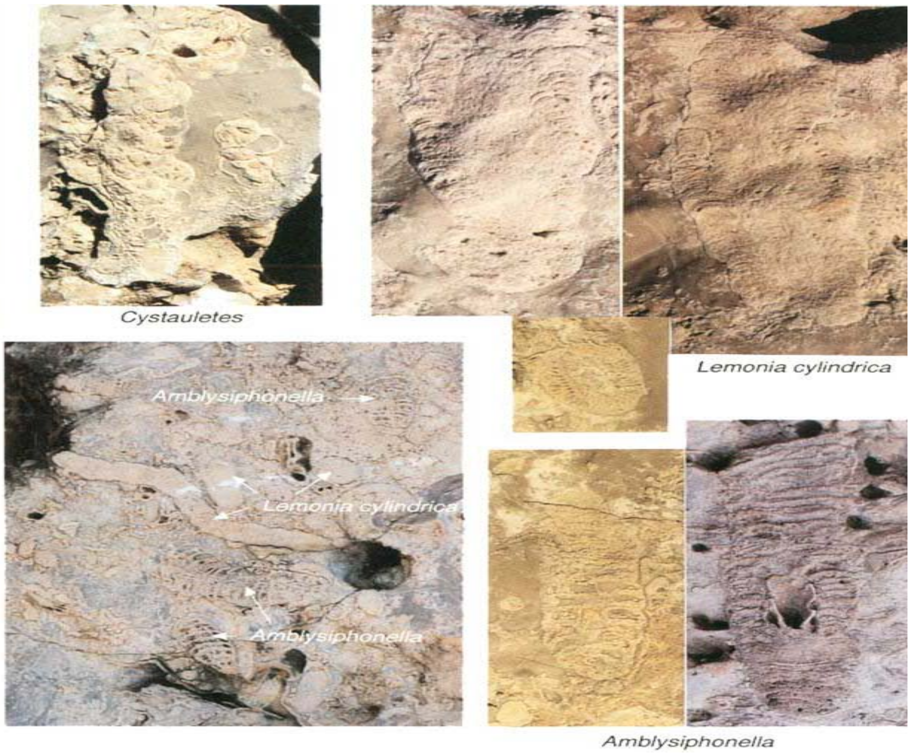

Figure 9: Pictures of a variety of sponges in outcrop along the Permian Reef Trail. (Bebout et al., 1993)

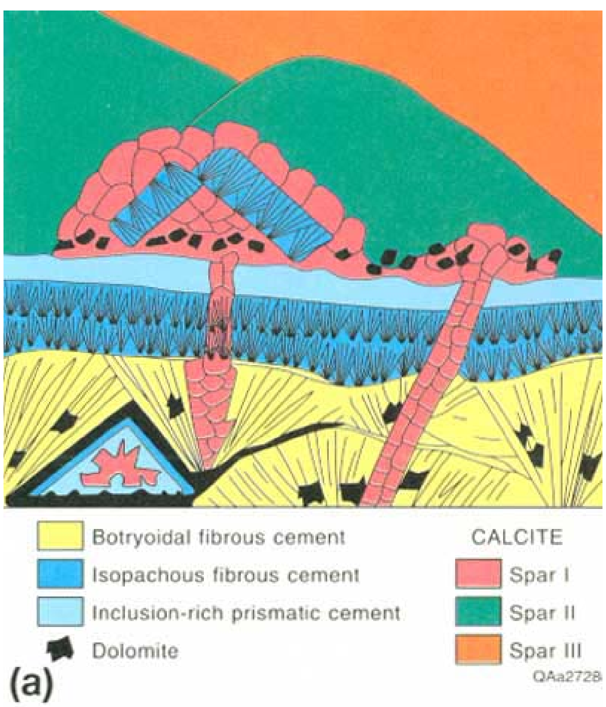

Figure 10: Diagram of the different cements found in the reef and in other parts of the margin in McKittrick Canyon. (Bebout et al., 1993)

Outer Shelf/ Shelf Crest:

The beds dip down in the outer shelf going from the shelf crest to the reef. The fossils that make up these units are fusulinids, crinoids, bivalves, gastropods, pisolites, ooids, and algae. The algae are seen in the forms of Stromatolites and fenestral laminites.

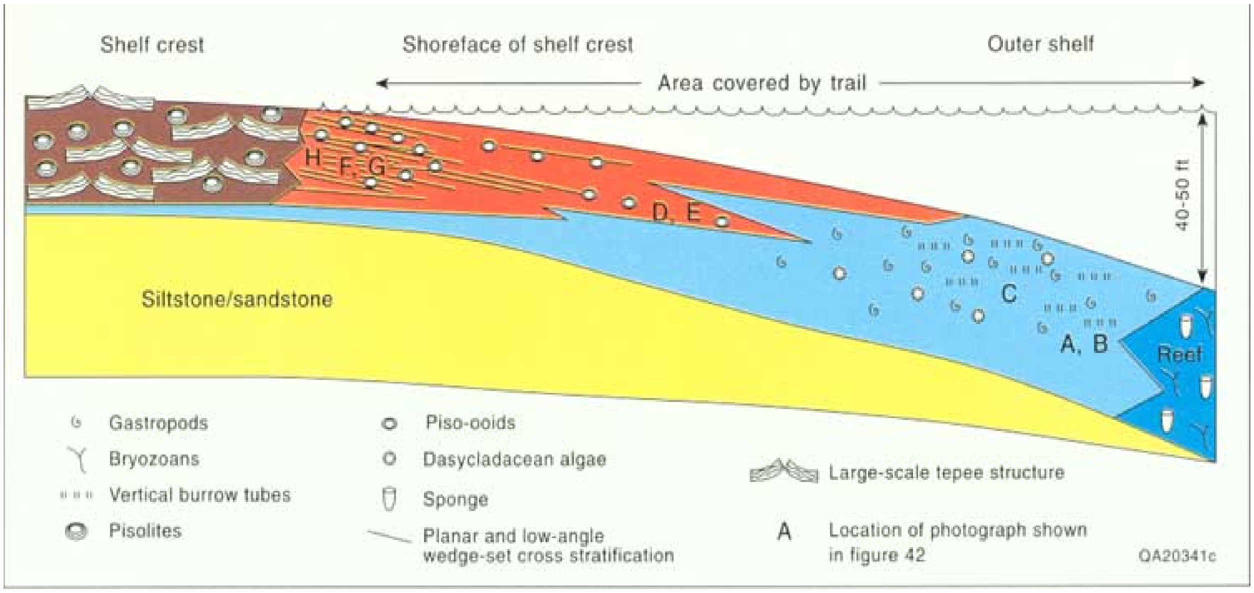

Figure 11: Diagram showing the transition from reef to shelf crest. (Bebout et al., 1993)

The outer shelf of the Yates Formation shows a transition from open-marine facies (fusulinid skeletal packstone) to subaerial exposure (evidence in algal laminites) to middle shelf facies (siliclastics).

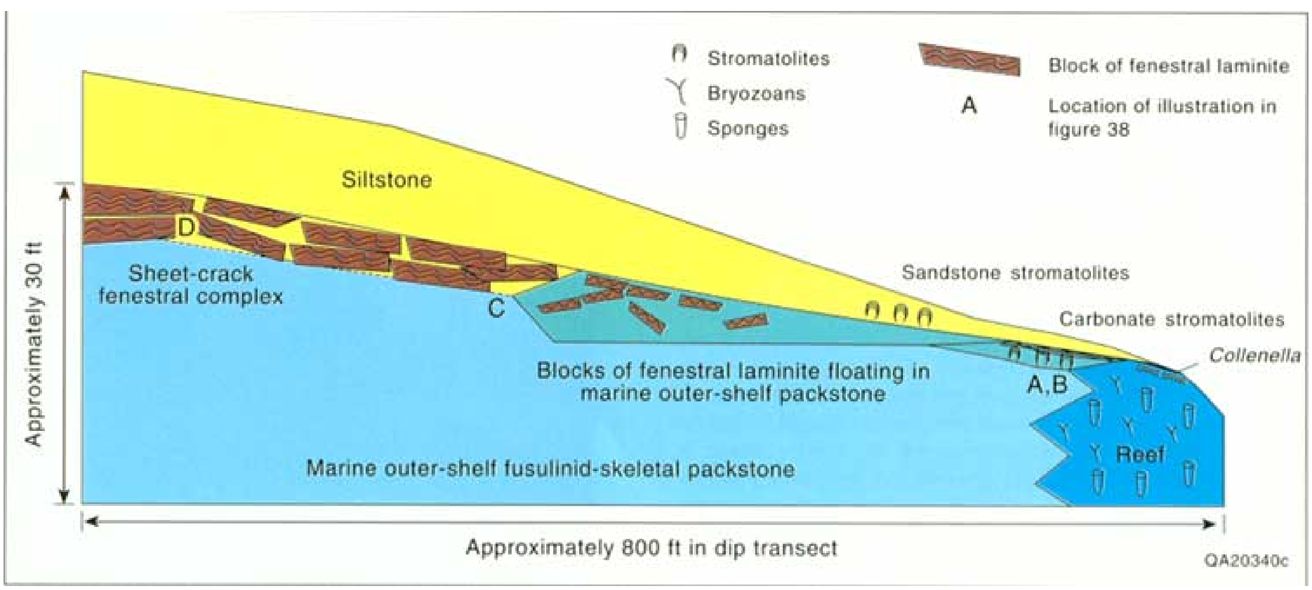

Figure 12: Diagram showing changes in facies as you move up section in the outer shelf of the Yates Formation. (Bebout et al., 1993)

In the outer shelf Tansil Formation there are strong upward-coarsening cycles. These cycles go from a subtidal wackestone/packstone up to tidal flats. There are also tepee structures found near the top of the Tansil. This indicates that increasing subaerial exposure as the relative sea-level drops throughout the deposition of the Tansil in this area.

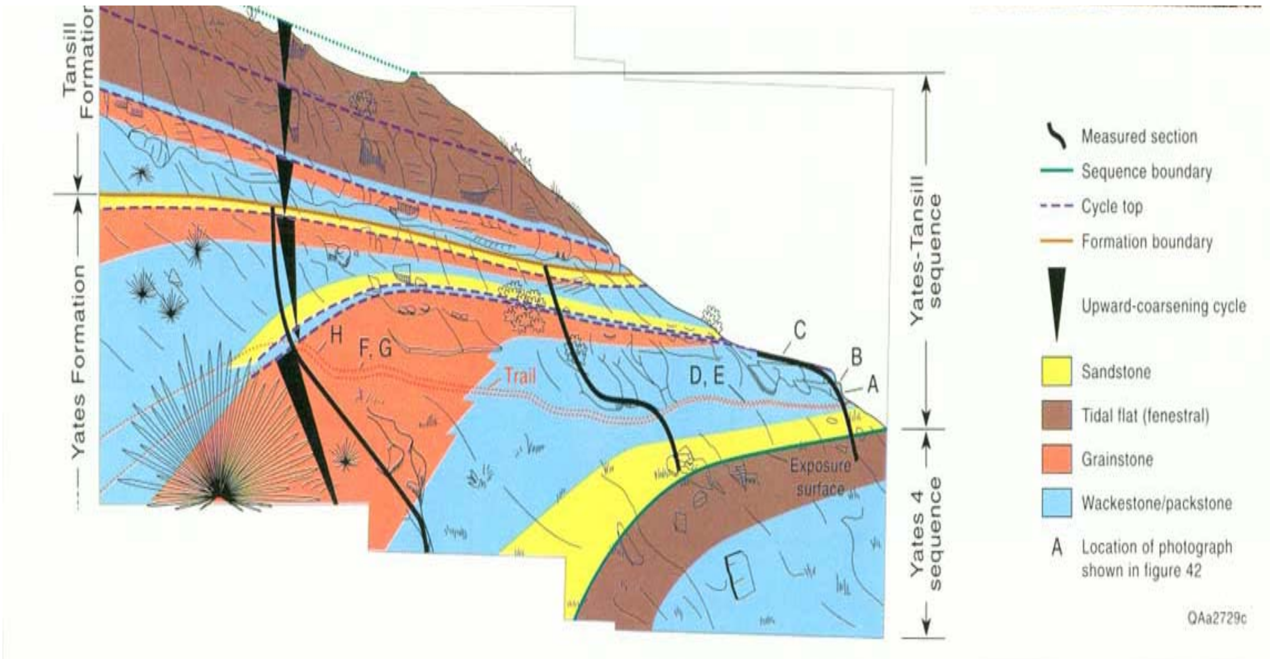

. Figure 13: Diagram showing changing facies as you go from the Yates Formation to the Tansil Formation of the outer shelf along the Permian Reef Trail. (Bebout et al., 1993)

WEST TEXAS GEOLOGICAL SOCIETY 1988 FIELD SEMINAR TO GUADALUPE MOUNTAINS

ROAD LOG: SECOND DAY McKITTRICK CANYON

Compiled by the Road Log Committee
with contributions by Alton Brown and Bob Loucks

ROADLOG STARTS FROM INTERSECTION OF HIGHWAY 62/182 WITH THE McKITTRICK CANYON ROAD

MILES

Cum	Int.
0.0	**0.0** Intersection of U.S. 62/180 with McKittrick Canyon Road.
0.3	**0.3** Lamar Limestone capping hills on right at 2 o'clock. Upper Bell Canyon Sandstone forms the slopes below and small knob at 3 o'clock.
0.5	**0.2** Water well and tank on left at 9 o'clock. Well is 400 ft deep.
0.8	**0.3** Bell Canyon Sandstone in hill at 9 o'clock.
1.1	**0.3** Bell Canyon Sandstone to right, Bear Creek on left. One of Mr. Pratt's water wells in Bear Canyon encountered more than 100 ft of Quaternary alluvium before reaching bedrock. Thick alluvial sediments are typical of the side canyons originating on the high escarpments of this region.
1.7	**0.6** Wooden guard rails.
1.9	**0.2** Stock pens at right.
2.0	**0.1 JUNCTION (OPTIONAL STOP).** Detour to the left on a private road (locked gate) leading to "The Ship in the Desert", Mr. Pratt's former home. Continuing on McKittrick Canyon paved road, Capitan reef ahead. Note the steep dip of the reef talus beds on the lower slope at 10 o'clock. Road crosses outcrop which has been correlated with the McCombs member of the Bell Canyon Group, but is about 150 ft out of place to be so designated. This limestone is a "stray" and is unnamed. It pinches out a short distance from this outcrop. This point is very close to the divide separating Black River and Delaware Draw drainage.
2.2	**0.2** Water reservoir to right.
3.3	**1.1** Road curves left. Lamar limestone in scarp ahead and across McKittrick Draw. To the right of the massive cliff is an anticline which is subparallel to the reef front. The Lamar at the crest of the anticline, forming the low hill at 2 o'clock, has been eroded but is present in the creek bank at 3 o'clock. Note how much more massive and thicker this unit is than in the scarp along the highway. Note also how rapidly the dip of the Lamar increases toward the mountain front where it forms a dip slope and merges with the cliff near the crest of the ridge.
3.7	**0.4** Windmill. Now crossing the axis of a northwest-southeast syncline.
3.8	**0.1** Cliff on the left is Lamar limestone containing mound-shaped structures. These structures were called bioherms by earlier workers, but they fail to fulfill the requirements for any variety of true organic reef deposits. Newell et al., 1953, estimated that the depth of water in the Delaware basin two miles from the rim was 1700 ft during Lamar time. This would make any reef interpretation of these structures questionable. The structures here are quite different from the primary slump structures, seen later in McKittrick Canyon, which are obviously the result of reef and reef talus debris sliding down the front, picking up more material as it moves, and contorting semiconsolidated beds before it. As would be expected such slump bodies are composed of broken skeletal material (of all sorts of organisms) in a lime mud matrix, and seldom display any sort of symmetry. The structures here, are very symmetrical with no contortion of sediment either beneath or on either side. The lateral slopes of the mounds are filled in with thin-bedded material to where flat beds again can be seen covering the structures. This gives the appearance of bioherms, but the textural fabric of the mounds precludes such a possibility. They are composed of micro-crystalline lime mud with no discernable skeletal remains. Chert, in the form of small nodules is present but extremely rare. It has been suggested that these structures are lime mud "banks" or "ridges" and that these outcrops are cross sections of linear deposits that parallel the reef front.
4.2	**0.4** Cattleguard.
4.3	**0.1 STOP 2-3, PHOTOS A, B.** National Park Service Information Station and McKittrick Draw. The park information station stands approximately at the same stratigraphic horizon as the Rader limestone, 400 ft below the top of the Bell Canyon, while equivalent parts of the reef section in the north wall of the canyon rise some 2000 ft due to greater thicknesses as it goes from basinal to reef facies. McKittrick Canyon has incised a cross sectional cut of the Capitan reef complex

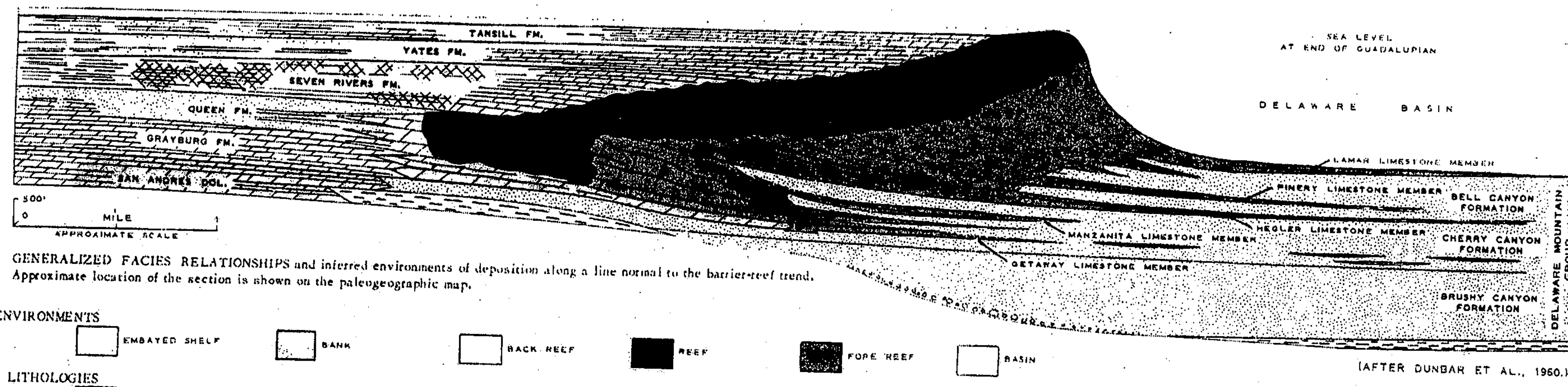

GENERALIZED FACIES RELATIONSHIPS and inferred environments of deposition along a line normal to the barrier-reef trend. Approximate location of the section is shown on the paleogeographic map.

ENVIRONMENTS

EMBAYED SHELF · BANK · BACK REEF · REEF · FORE REEF · BASIN

LITHOLOGIES

BEDDED DOLOMITE AND DOLOMITIZED LIMESTONE · UNBEDDED LIMESTONE · MASSIVELY BEDDED LIMESTONE BRECCIA · BEDDED LIMESTONE · SANDSTONE AND SILTSTONE · SHALE · EVAPORITE · CONGLOMERATE

Courtesy of Exxon Production Research Co.

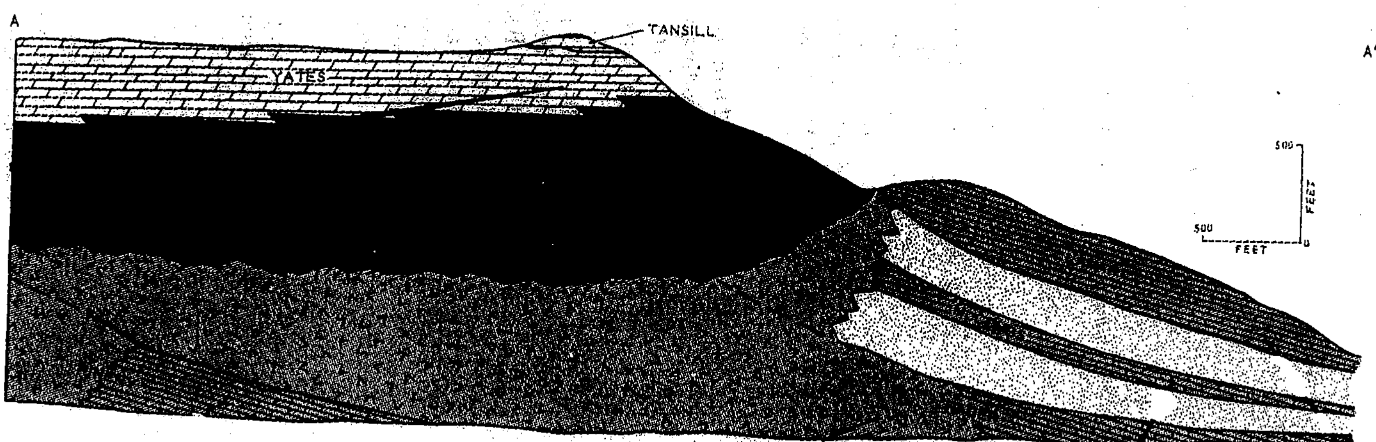

FACIES RELATIONSHIPS and inferred environments of deposition of the reef complex and basin forming the north wall of McKittrick Canyon. Location of cross section is shown on index map. Arrows point to the approximate interpreted positions of the illustrated textures.

ENVIRONMENTS

BACK REEF · REEF · FORE REEF · BASIN

LITHOLOGIES

DOLOMITIZED LIMESTONE · UNBEDDED LIMESTONE · MASSIVELY BEDDED LIMESTONE BRECCIA · BEDDED LIMESTONE · SANDSTONE AND SILTSTONE

Courtesy of Exxon Production Research Co.

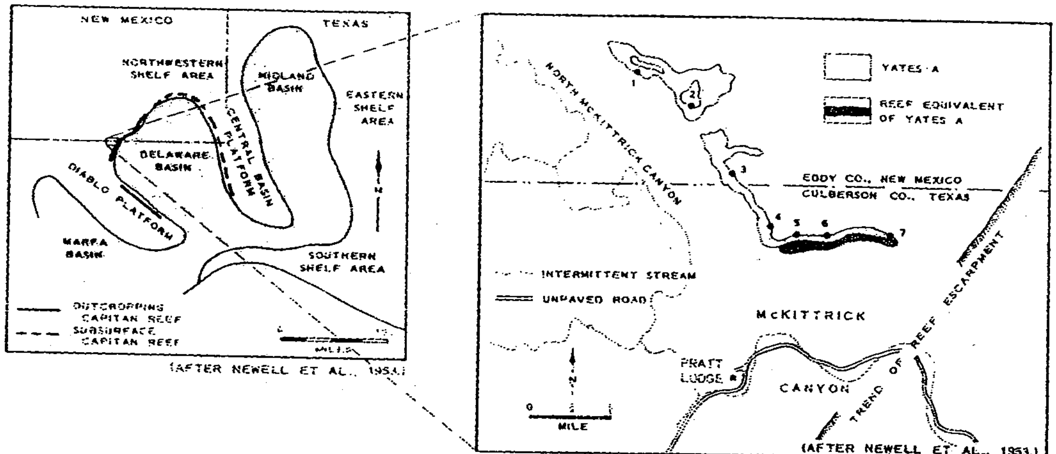

LOCATION OF THE MEASURED SECTIONS below and surface distribution of Yates A and of reef portion equivalent to Yates A.

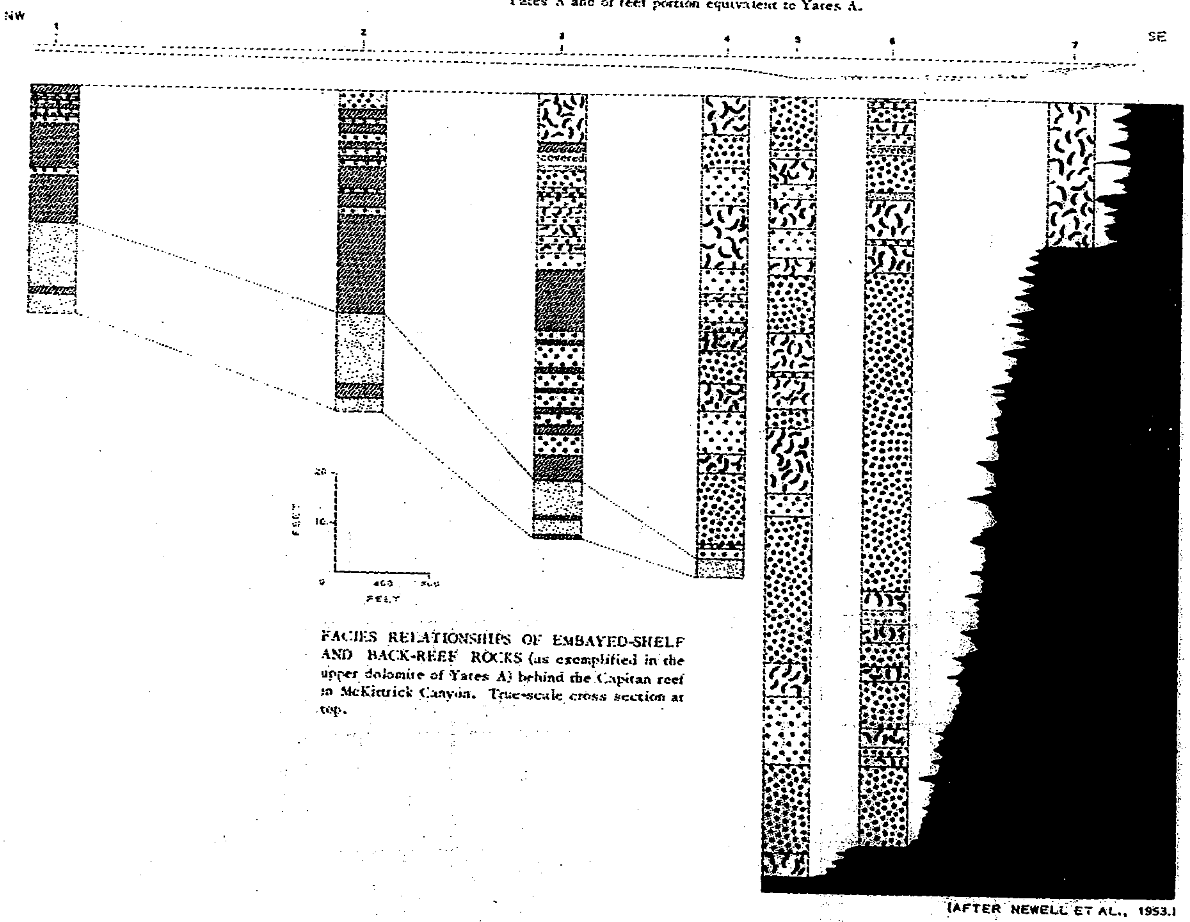

FACIES RELATIONSHIPS OF EMBAYED-SHELF AND BACK-REEF ROCKS (as exemplified in the upper dolomite of Yates A) behind the Capitan reef in McKittrick Canyon. True-scale cross section at top.

Courtesy of Exxon Production Research Co.

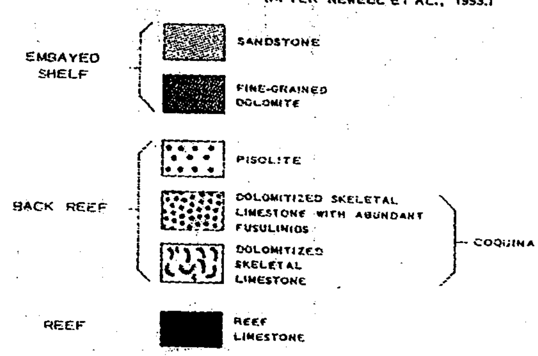

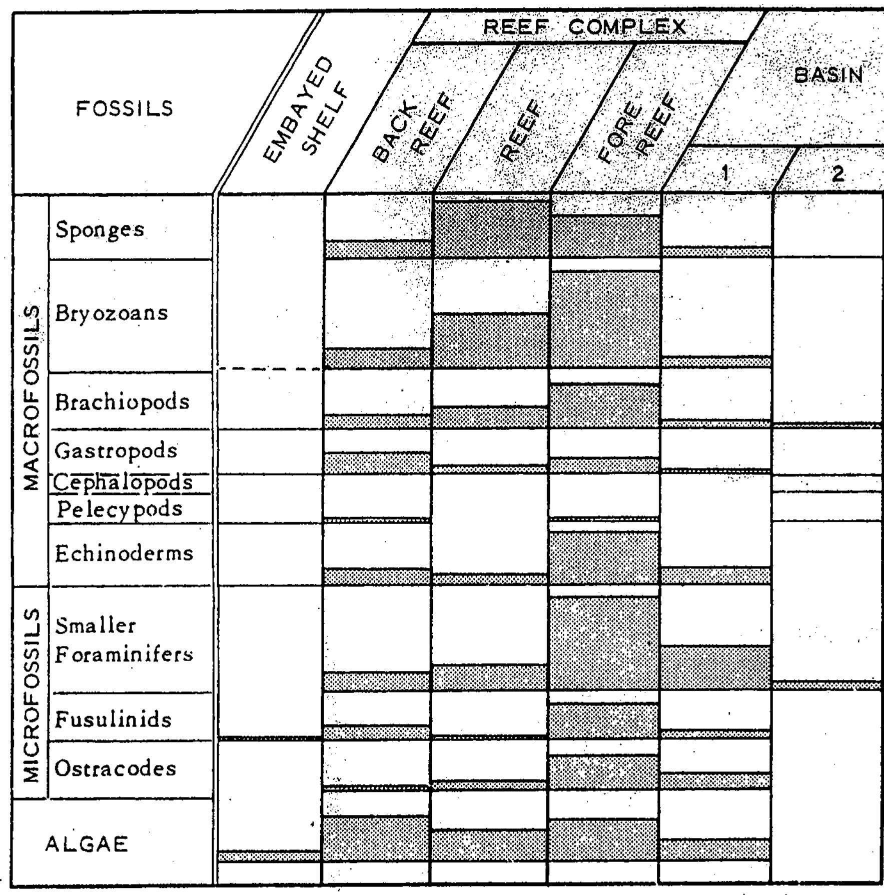

1 *Dark-colored limestones made up of submarine-slide material and other limestones containing abundant transported debris.*

2 *Dark-colored, thin-bedded, laminated limestone, massive sandstone, and thin-bedded, laminated, fine-grained sandstone and siltstone.*

RELATIVE ABUNDANCES of major fossil groups of the embayed-shelf, reef-complex, and basin rocks as determined from examination of polished surfaces, peels, thin sections, and the literature.

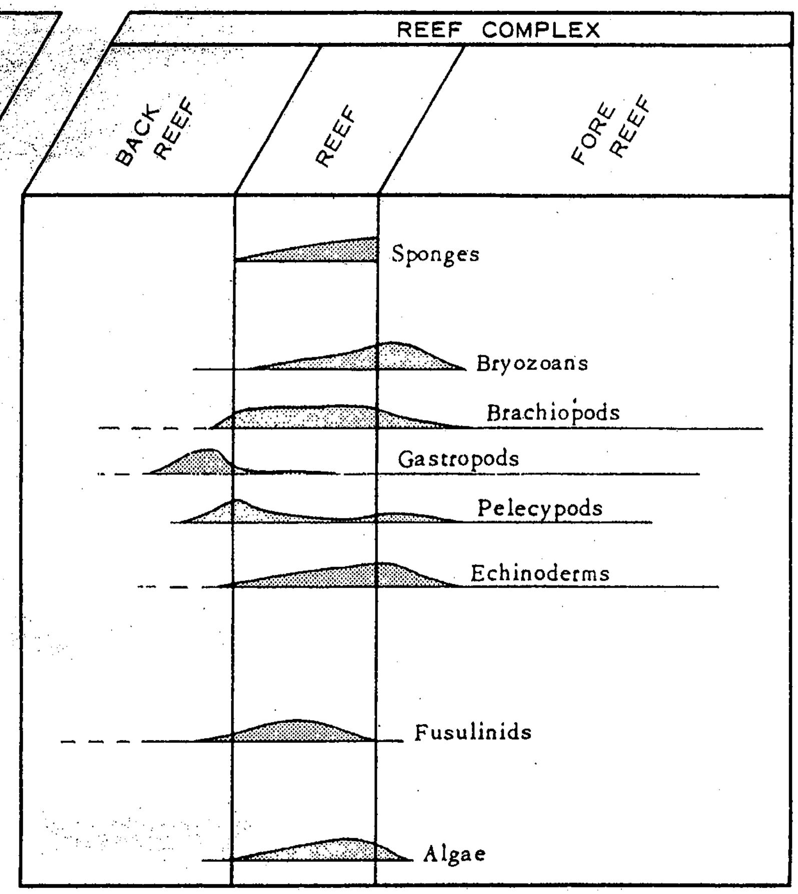

PROBABLE LIFE DISTRIBUTION of major fossil groups in the Capitan reef and associated environments as reported by Newell et al., 1953.

Courtesy of Exxon Production Research Co.

Photo A. McKittrick Canyon Visitor Center (Stop 2-3).

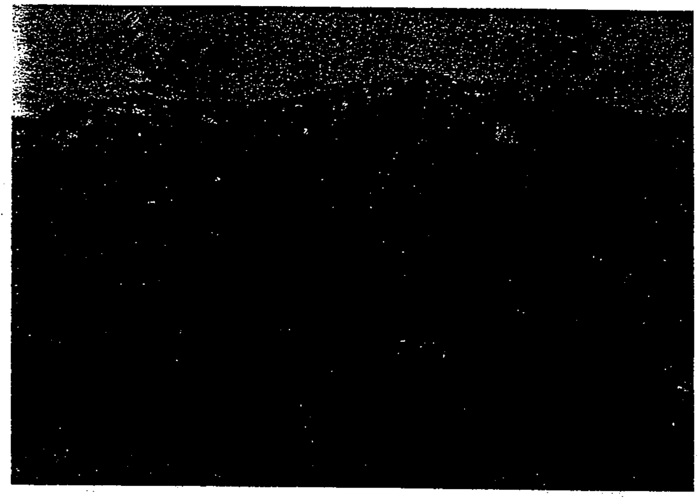

Photo B. North wall of McKittrick Canyon (Stop 2-3).

that includes fore-reef, reef wall and backreef facies. For about the last mile coming up the stream bed, the road traversed the fore-reef facies, with its large amount of debris shed off the reef into the Delaware basin.

Most of the rock in the walls of the canyon at this point is bedded fore-reef material, but on the north wall, the cliff forming Capitan reef wall stands out prominently. It is age equivalent to the Lamar. The reef grew laterally in a basinal direction, with the older fore-reef talus forming the substrate for continued reef growth. The Lamar member can be traced along the north side of the canyon from its basin-floor position, through its fore-reef equivalent and then merging into the reef-wall facies. The back-reef facies immediately overlies the reef-wall facies and represents a more basinal extension of the reef that is no longer present due to erosion.

Northwestward up the canyon, the base of the back-reef facies drops lower in the section with less and less of the reef and fore-reef facies present. After several miles, the canyon walls, nearly 2000 ft high, are composed of backreef facies only.

The volume of true reef wall seen in the Capitan reef complex is much smaller than the volume of either fore-reef or back-reef material preserved in the section. A living reef is a complex balance between the processes of construction and destruction. It is never a static feature. The process of reef destruction carries the once living reef material elsewhere for preservation. Only a small portion of the reef itself survives the processes of destruction to be preserved in the geologic column.

King's map of the southern Guadalupes shows a northeasterly plunging syncline marking the edge of the Delaware basin here, roughly parallel and in front of the fore-reef facies. Basinward of this syncline is a roughly parallel anticline. The limb common to both of these structural features has northerly dips, and shallow waterwells in the Bell Canyon on this feature have unusual shows of oil in them.

Newell et al., 1953, studied the Rader limestones and concluded they were slides of reef debris (some of this debris is very large) into the basin. Before his efforts these occurrences of reef material, four miles out in the basin in waters some 1500 ft deep, were considered to be patch reefs, even though their position in the basin posed distinct problems.

Fore-reef, Reef and Back-reef Facies

The Bell Canyon Fm is interbedded fore-reef limestones and basinal sandstones. The limestones are light gray proximal to the reef and become dark basinward. They are comprised primarily of reef derived material including bryozoans, sponges, brachiopods, foraminifera, crinoids and algae, and grade completely from coarse, unsorted talus near the reef to finer grained, sorted and laminated calcarenite basinward. Primary dips near the reef are 20 to 35 degrees. Diagenesis has resulted in permeability reduction due to recrystallization and secondary cementation, and there is patchy dolomitization. Basinal sandstone between the limestone units is light gray to buff and ranges from massive to laminated and, toward the reef, wedge out into the reef talus.

The Capitan Limestone, the reef unit, is an unstratified, fine-grained, light-colored limestone with a varied fossil fauna. The calcareous framework was provided by calcareous sponges, calcareous algae, bryozoans and hydrocorallines(?). Other members of the reef community include solitary corals, fusulinids and brachiopods. This facies is vuggy, with the vugs commonly infilled with sediment generated within the reef itself.

The back-reef Yates Fm. is a dolomitized limestone with abundant pisolites and a highly varied and abundant fauna of dasycladacean algae, foraminifera, brachiopods, gastropods, sponges, and bryozoans. Fossil material from the reef itself is carried into the back-reef and preserved there. Near the reef, the back-reef beds are thick to massive limestones with indistinct and erratic bedding, but landward the time-equivalent units become interbedded sandstones and fine-grained dolomites.

McKITTRICK CANYON

by Alton Brown and Bob Loucks

McKittrick Canyon is a world-famous location illustrating the translation from shallow-to deep-water carbonate sedimentation across a platform margin. We will examine the lower-slope limestones and sandstones exposed here and observe stratigraphic relationships exposed on the south canyon wall.

Upon leaving the visitor center, proceed down the trail marked "Pratt's Lodge." The trail crosses unlithified alluvium from the Lamar and Capitan Formations for about the first 250 yards. The first bedrock outcrop begins as the trail drops into the creek crossing. From here, we will leave the trail and follow the creek bed up the canyon. The units exposed in the first long outcrop are the McComb Limestone and underlying Bell Canyon Sandstones. Scattered exposures along the creek from here to the next trailcrossing of the creek are more exposures of Bell Canyon sandstones and the upper part of the Rader Limestone. After examining these units, continue up the creek past the second trail crossing. Most of the cemented, round-boulder conglomerates with porous matrix are Quaternary stream deposits. The best Radar Limestone exposure lies about 200 yards upstream from where the second trail crosses the creek.

The McComb Limestone consists of silty, medium to-thin-bedded, lime grainstone. Several beds of relatively pure, fine to very-fine grained sandstones are intercalcated into the unit along with coarse-grained carbonate turbidites. This member of the Bell Canyon Fm is not traceable far into the basin.

The underlying Bell Canyon Sandstone is a fine to very-fine grained, well sorted sandstone. This outcrop consists of broad channeling and laminated bedding with scattered low-relief hydrodynamic sedimentary structures typical of Bell Canyon sandstones. The long exposure also contains boulders of dolomitized Capitan in the Bell Canyon Sandstone. At this stratigraphic level, boulders become more abundant up depositional slope, until the sandstone interfingers with carbonate debris flows and breccias.

The uppermost Rader Limestone Mbr of the Bell Canyon Fm is exposed in scattered outcrops southeast of the second trail crossing. The upper part of the Rader Limestone generally consists of carbonate turbidite grainstones. Debris flows and transported boulders occur lower in the formation, as exposed in the low cliff on the north side of the creek beyond the trail crossing. The largest boulder, over 8 ft high and 20 ft wide, shows well-developed sponge-algal fabric characteristic of the upper part of the Capitan Fm. Finer-grained units below the boulder are silty, platey limestones.

The Lamar Limestone and Capitan Fm can be examined on the Geology trail, if time permits. This trail also provides an overview of slope facies relationships. Most of the lower part of the trail follows a dip slope in the middle part of the Lamar Mbr. Typical lithologies are thin-bedded, platey mudstones to wackestones. A thin, burrowed wackestone occurs near the top of the cliff section. Silicified fossils are common along some beds. These fossils are characteristic of the upper slope facies and contain few species found in the lower deposits of the Capitan Fm. Lamar debris flow beds are exposed in small isolated outcrops about 20 to 40 ft below the trail level near the cliff.

The cliff area has a good, shaded overview of the stratigraphic relationships exposed on the south wall of the canyon. Dipping units of the McComb Limestone, Bell Canyon Sandstone and Rader Limestone can be traced from the creek outcrops up the canyon wall. The sandstone units thin up slope and carbonate units thicken. Most sand-rich units have an intermediate facies with abundant carbonate boulders just downdip of merging with the Capitan Fm. The percentage of boulder beds in the carbonates generally increases up slope. Individual beds are difficult to trace. The more massive, thick-bedded limestones are characteristic of the Capitan Fm.

After the second switchback farther up the trail, good sponge-algal fabrics in the upper part of the Capitan facies are exposed on weathered surfaces and the low blasted cuts along the trail. The trail leads on to other exposures of Capitan Fm. Even farther up the trail, the Tansill Fm is exposed. these outcrops are too far up the trail to visit today.

SHELF-TO-BASIN FACIES DISTRIBUTIONS AND SEQUENCE STRATIGRAPHY OF A STEEP-RIMMED CARBONATE MARGIN: CAPITAN DEPOSITIONAL SYSTEM, MCKITTRICK CANYON, NEW MEXICO AND TEXAS

SCOTT W. TINKER

Marathon Oil Company, Petroleum Technology Center, Littleton, Colorado, U.S.A. and Department of Geological Sciences, University of Colorado, Boulder, Colorado, U.S.A.; Mailing Address, 5895 East Kettle Place, Englewood, Colorado 80112, U.S.A.

ABSTRACT: **Shelf-to-basin outcrop studies in steep-rimmed, shelf-margin settings are uncommon because continuous shelf-to-basin transects are rarely exposed in a single outcrop. Discontinuous or absent stratigraphic marker beds across the shelf margin further complicate outcrop studies in the shelf-margin setting. This paper discusses the results of a high-resolution investigation of the shelf-to-basin profile along the north wall of North McKittrick Canyon, New Mexico and Texas. In McKittrick Canyon, carbonate-dominated sedimentary rocks associated with the steep-rimmed, Upper Permian Capitan depositional system are exposed along a continuous 5-km outcrop face. Measured sections, lateral transects, scintillometer readings, and geochemical data were synthesized into a digital database and interpreted in conjunction with a digital photomosaic of the entire canyon wall.**

Results of this work include a shelf-to-basin facies map and sedimentologic interpretation of the north wall of North McKittrick Canyon, and indicate that the dominant bathymetric profile during Capitan deposition was a marginal mound. In this model, the Capitan reef facies was deposited at the shelf–slope break in water depths ranging from 15 to 75 m, but always downdip from the topographically higher shelf crest. This model is supported by the following observations and interpretations: (1) a facies progression from the shelf crest to the shelf margin interpreted to represent a shallow-to-deeper-water succession; (2) proportional expansion of beds in a downdip direction; (3) presence of oriented (transported) fusulinid grainstones downdip from *in situ* fusulinid wackestones and packstones updip; (4) siltstones that thin and pinch out towards the shelf margin; (5) a decrease in dolomite from the shelf crest to the shelf margin; and (6) the absence of true toplap stratal geometries.

In reality, a static paleobathymetric model cannot characterize the depositional system, because the facies distributions, facies proportions, stratal geometries, and quantified depositional parameters vary systematically from the Seven Rivers through the Tansill. In order to understand the observed variations, emphasis was placed on *quantifying* key depositional parameters such as progradation, aggradation, offlap angle, outer-shelf dip, water depth, distance to the shelf margin and toe of slope, and facies-tract width. The systematic variations in these parameters, in conjunction with the facies distribution map and stratal geometries, helped to define the sequence-stratigraphic framework, and allowed for comparative evaluation of such things as sediment accumulation rates and sites, and stratigraphic evolution.

The Capitan depositional system is represented by three composite sequences, each containing four high-frequency sequences. Two and one half of these composite sequences are exposed in McKittrick Canyon. The overall depositional system is interpreted to have evolved predictably from a deeper-water margin in the Seven Rivers composite sequence, to a shallow-water margin in the Tansill composite sequence. The subtidal outer-shelf and shelf-margin facies tracts were sites of major sediment production. Accumulation rates across the shelf margin indicate a relatively continuous growth history, with periods of nondeposition or erosion limited to the terminal phase of each composite sequence. As a result, the preserved sedimentary record of high-frequency and composite sequences in the outer-shelf to upper-slope position is equally proportioned between transgressive and highstand systems tracts. This symmetric outer-shelf to upper-slope record of carbonate accumulation is significantly different from the asymmetric, highstand-dominated middle-shelf accumulation record reported previously for this and many other carbonate shelves.

INTRODUCTION AND OBJECTIVE

Carbonate shelf strata have been studied in detail in recent years (e.g., Read 1989; Koerschner and Read 1989; Goldhammer et al. 1990; Borer and Harris 1991; Crevello 1991; Osleger and Read 1991; Drummond and Wilkinson 1993; Goldhammer et al. 1993; Montañez and Osleger 1993). Less attention has been given to the more complex, shelf-to-basin stratigraphic setting because continuous shelf-to-basin transects are not commonly exposed in a single outcrop (e.g., Playford et al. 1989; Legarreta 1991; García-Mondéjar and Fernández-Mendiola 1993; Pomar 1993; Sonnenfeld and Cross 1993; Fitchen et al. 1995). Even when exposures are continuous, physical correlation across steeply dipping shelf margins is difficult, because lateral facies changes occur in short distances, and lithostratigraphic markers in shelf-margin and slope facies are rare (Wilson 1975). Because correlation across a steep-rimmed margin is difficult, data regarding stratal geometry, progradation, aggradation, and stratigraphic cyclicity are rarely synthesized.

The objective of this study is to map the stratal geometries and facies distributions along the continuous, shelf-to-basin outcrop exposures of the steep-rimmed carbonate margin associated with the upper Permian Capitan Formation. The following goals were implicit within the overall objective: (1) a more complete, high-frequency sequence-stratigraphic interpretation; (2) an updated shelf-to-basin stratigraphic correlation for the Capitan depositional system; (3) a critical evaluation of the long-standing controversy regarding the nature of the Capitan paleobathymetric profile and depositional model; and (4) collection of data regarding spatial and temporal variability in cyclicity, facies distribution, stratal geometry, and sediment accumulation rates and sites in a steep-rimmed setting.

GEOLOGIC BACKGROUND

The Permian reef complex, located on the northwest margin of the Delaware Basin, is partially exhumed in the Guadalupe Mountains. By the late Guadalupian, the Midland basin east of the Central Basin Platform was filled, and the Capitan reef and age-equivalent strata were deposited around the rim of the Delaware basin (Fig. 1). The Guadalupe Mountains, which dip gently as a block to the northeast, are bounded on the west by ''basin-and-range'' normal faults (King 1948). The present-day topography along the east side of the Guadalupe Mountains is an erosional profile along the Capitan reef margin (Fig. 2).

The Guadalupe Mountains provide spectacular, shelf-to-basin outcrop exposures of carbonate–siliciclastic sequences. The north wall of North McKittrick Canyon, located in New Mexico and Texas, represents a complete shelf-to-basin exposure across the upper Permian (upper Guadalupian) Capitan shelf margin (Figs. 2, 3). North McKittrick Canyon trends WNW, nearly perpendicular to the Capitan reef margin, is approximately five kilometers long, and has from 350 to 550 m of relief from the valley floor to the rim. The Permian Reef Geology Trail, one of the world's classic

JOURNAL OF SEDIMENTARY RESEARCH, VOL. 68, NO. 6, NOVEMBER, 1998, P. 1146–1174

1073-130X/98/068-1146/$03.00

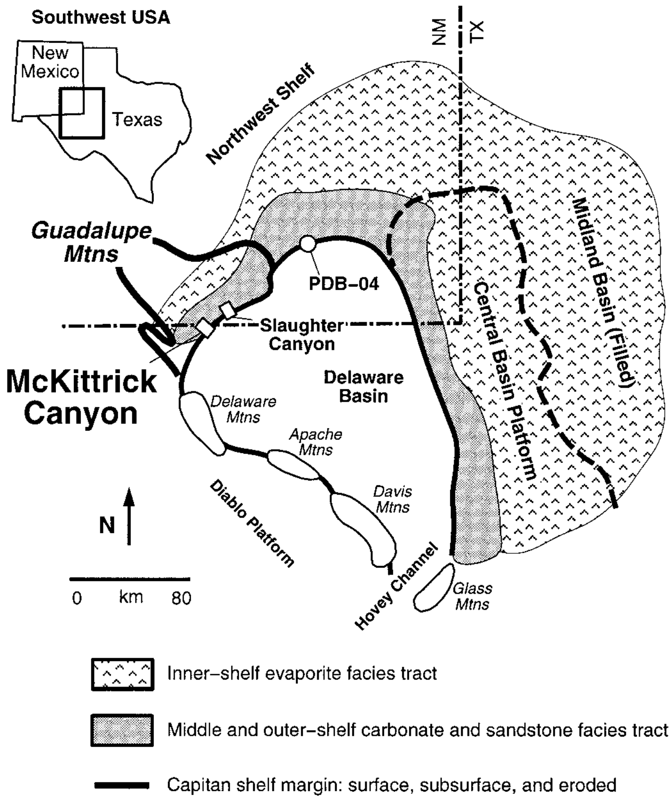

FIG. 1.—Simplified map of late Guadalupian facies in the Permian basin, west Texas and southeast New Mexico (modified from Ward et al. 1986). Note location of McKittrick Canyon, Slaughter Canyon, and the Gulf PDB-04 well.

carbonate field-trip locations (Bebout and Kerans 1993), is situated at the mouth of McKittrick Canyon.

The Guadalupe Mountains have received as much attention in the geologic literature as any ancient carbonate province in the world. Correlative strata in the Delaware and Midland basins are some of the most prolific hydrocarbon-producing reservoirs in the United States (Ward et al. 1986). King (1948), Newell et al. (1953), Hayes (1964), and Dunham (1972) did important regional studies of the general geology of the Guadalupe Mountains. Models for shelf deposition and cyclicity of late Guadalupian rocks in the Permian basin include publications by Silver and Todd (1969), Meissner (1972), Dunham (1972), Hurley (1978), Garber et al. (1989), and Borer and Harris (1991). Detailed studies of the Capitan Reef complex include those by Adams and Frenzel (1950), Achauer (1969), Babcock (1977), Yurewicz (1976, 1977), and Melim (1991). Recent studies have helped to put the Permian of the Guadalupe Mountains and Delaware Basin into a sequence-stratigraphic context (Sarg and Lehmann 1986; Kerans and Nance 1991; Kerans et al. 1992; Kerans et al. 1994; Sonnenfeld and Cross 1993; Kerans and Fitchen 1995; Gardner and Sonnenfeld 1996).

TERMINOLOGY

High-frequency cycles (referred herein as cycles; Fig. 4) are the fundamental stratigraphic building blocks in this study, and refer to the smallest set of genetically related lithofacies (facies) deposited during a single base-level cycle (James 1979; Grotzinger 1986; Koerschner and Read 1989; Goldhammer et al. 1990; Borer and Harris 1991; Crevello 1991). Cycles are analogous to the siliciclastic parasequence (Van Wagoner et al. 1988) but can contain a deepening and shallowing component. Allogenic cycles (vs. autogenic) are composed of vertical facies successions that can be mapped across multiple facies tracts. In McKittrick Canyon, cycles are easily recognizable in the intertidal to supratidal setting of the middle shelf and shelf crest, but are more difficult to document in the subtidal setting of the outer shelf, where thick vertical successions of similar facies dominate. Cycles are analogous in scale to fifth-order cycles (Goldhammer et al. 1990).

Several cycles make up a cycle set (Fig. 4), defined as a set of cycles bounded by marine flooding surfaces (Harris et al. 1993; Kerans et al. 1994) whose component cycles typically show a consistent progradational, aggradational, or retrogradational trend (Kerans and Tinker 1997). The lateral distribution, proportions, and geometry of facies within a cycle set commonly vary predictably as a function of position within the overall sequence-stratigraphic hierarchy.

Cycles and cycle sets make up high-frequency sequences (HFSs; Fig. 4).

FIG. 2.—Oblique air photograph of the southern end of the Guadalupe Mountains (photo courtesy of C. Kerans). The erosional Capitan reef margin trends from southwest (lower left) to northeast (upper right). Regional structural dip is to the ENE. Basin-and-range-related normal faults define the western limit of the Guadalupe Mountains as seen along the Algerita Escarpment and Shattuck Valley wall (upper left).

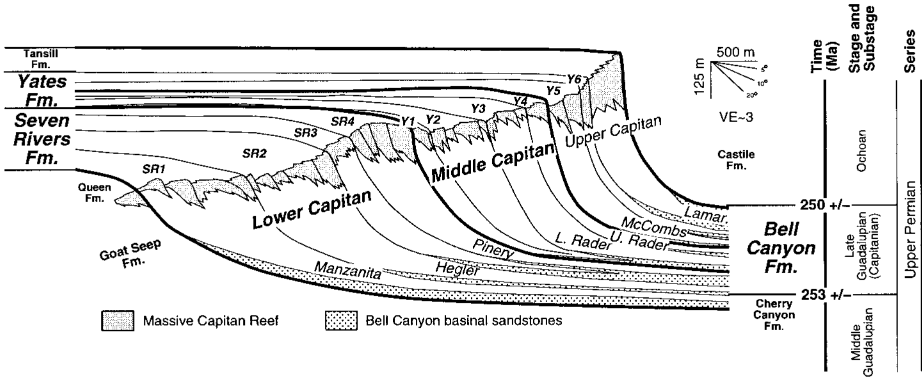

FIG. 3.—Simplified cross section of McKittrick Canyon. Heavy lines are CS boundaries. SR1 through SR4 make up the Seven Rivers CS. Y1 through Y4 make up the Yates CS. Y5 and Y6 are part of the genetic CS following the Yates CS. Thin lines are high-frequency sequence (HFS) boundaries. Formations included in this study are the Seven Rivers and Yates on the shelf, the lower and middle Capitan at the shelf margin, and the Bell Canyon in the basin. Time estimates are from Ross and Ross (1987).

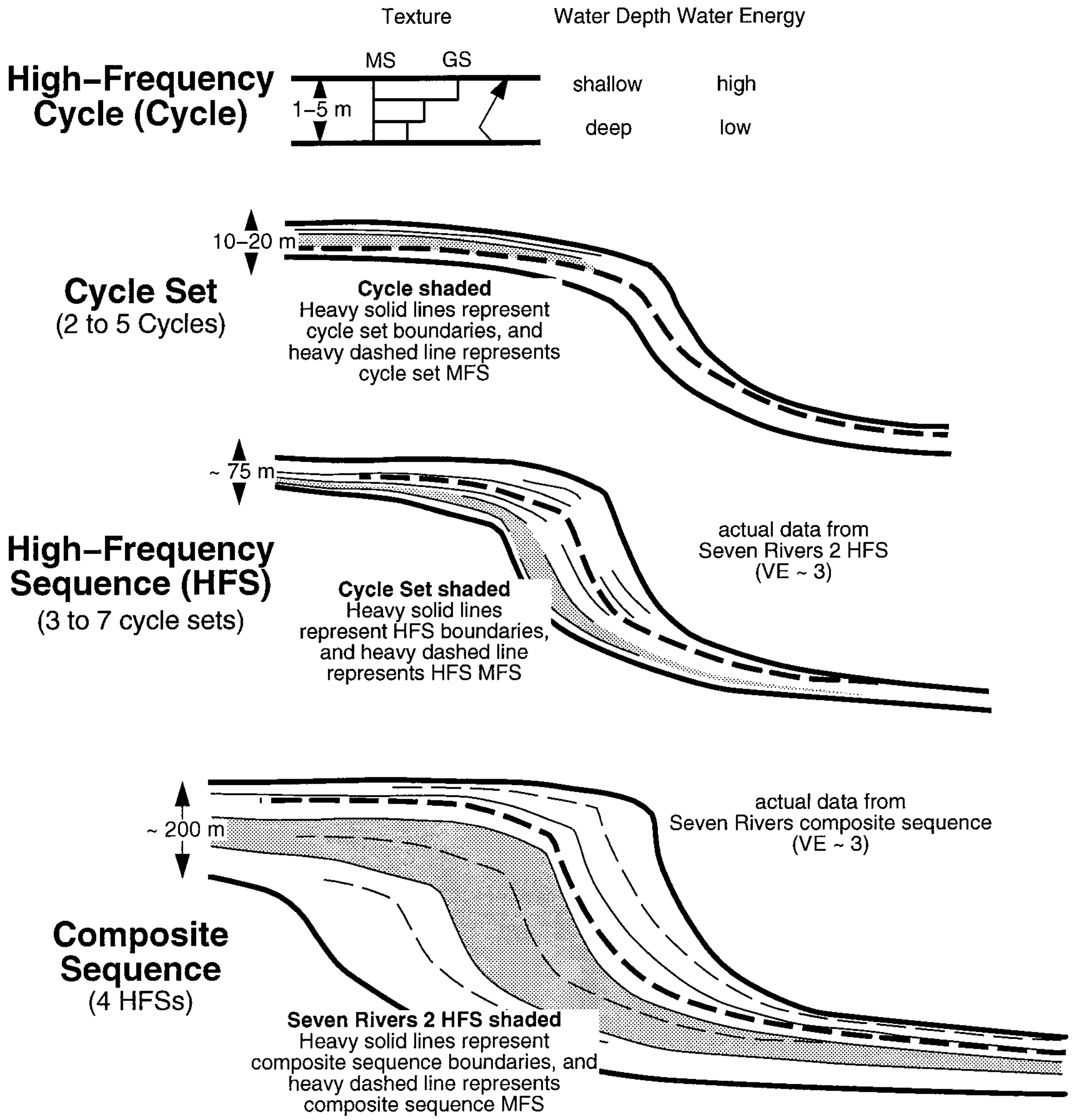

FIG. 4.—Hierarchy of cyclicity. Each stratigraphic element is a component of the subsequent lower-order element. Specific interpretations from McKittrick Canyon were used to construct the figures, as noted.

HFSs are intermediate-order cycles bounded locally by unconformities (Mitchum and Van Wagoner 1991), and are composed of lowstand, transgressive, and highstand systems tracts (LST, TST, and HST). The TST is separated from the HST by a maximum flooding surface (MFS). In McKittrick Canyon, the MFSs are commonly represented by the maximum landward position of outer-shelf facies, a more highly aggrading shelf margin, and a condensed zone overlain by progradational downlap geometry in the basin. HFSs are estimated to represent time periods of 100–400 ky, and are analogous in scale to fourth-order cycles (Goldhammer et al. 1990).

Composite sequences (CSs; Fig. 4; Mitchum and Van Wagoner 1991) are the lowest order of cyclicity discussed in this study, and are analogous in scale to depositional sequences (Mitchum et al. 1977; Vail et al. 1977; Vail 1987; Van Wagoner et al. 1988) and third-order cycles (Goldhammer et al. 1990). Composite sequences, estimated to represent average time periods of 1–3 my, are composed of multiple, unconformity-bounded HFSs, and therefore differ subtly from depositional sequences, which are defined as a single unconformity-bounded rock succession.

In McKittrick Canyon, two complete CSs were recognized, and named ''Seven Rivers'' and ''Yates'' to remain consistent with the formation names on the shelf established by Hayes (1964). However, each CS incorporates part of the Capitan Formation across the shelf margin and Bell Canyon Formation in the basin. Four HFSs in the Seven Rivers CS (SR1 to SR4; Fig. 3), and four HFSs in the Yates CS (Y1 to Y4; Fig. 3) were identified. These HFSs are equivalent to Guadalupian 20 through 26 of Kerans et al. (1992). In addition, two HFSs were recognized in the CS deposited after the Yates CS, but were named Y5 and Y6 to remain consistent with the shelf formation names of Hayes (1964).

METHODS

Data in the study come from 36 vertical measured sections (1900 m), six published sections (330 m; Hurley 1978; Kerans and Harris 1993), several miles of lateral transects (Fig. 5), approximately 500 thin sections, scintillometer measurements (780 m), a digital photomosaic, and wireline logs from the Pratt #1 well drilled at the mouth of McKittrick canyon, the Guadalupe Ridge #1 well drilled on Wilderness Ridge, and the PDB-04 well (Fig. 1). Many of the data used in the interpretation were collected from shelf deposits, because slope deposits are commonly covered in talus and vegetation, and have crude to chaotic bedding with disorganized spatial textural variations. The slope and basin interpretations in this study are based on one vertical measured section, two basin-to-margin transects, correlation with the Pratt #1 well, data from exposures along the geology trail at the mouth of the canyon, bed tracing from helicopter and low-angle photographs taken from the south wall of the canyon, and use of data from other studies of the slope (Garber et al. 1989; Brown and Loucks 1993; Mruk and Bebout 1993; Melim and Scholle 1995).

Eighteen color photographs taken during a helicopter flight down the axis of the canyon were used to create a 2-D digital photomosaic. Reference points were marked on the photographs in the field every 5–20 m, and tied to vertical measured sections. Beds were traced laterally in the field, and marked on the photographs to document stratal geometries and facies variations. Graphical facies data were scaled vertically to fit between each photo-reference point marked in the field, and the resulting combination of measured sections, lateral transects, and the digital photomosaic were used to construct a stratigraphic and structural line interpretation on ''photo thickness'' (Fig. 6).

The photomosaic distorts the 3-D topography of the north McKittrick Canyon wall onto a 2-D projection. For example, 50 vertical meters at the base of the canyon wall, which was closer to the helicopter, appears much thicker than 50 vertical meters at the top of the canyon wall, which was farther from the helicopter. This is a common problem when interpreting photographic data in most field studies. Because the photomosaic line interpretation is on ''photo thickness'', it had to be converted to true vertical thickness (TVT) in order to quantify the depositional parameters determined from the sequence-stratigraphic interpretation (Fig. 7).

Texture, lithology, porosity, grain components, sedimentary structures, and cycles were described in the field for all measured sections on a per-foot basis. A hand-held scintillometer was used to measure the natural radioactivity of 780 m of section for comparison to subsurface gamma-ray logs. All of the quantified measured section data were entered into a digital SAS™ (Statistical Analysis Systems) dataset (1.52 million cells) on a SGI™ (Silicon Graphics) workstation for analysis and output.

Nearly 500 hand samples were slabbed and polished. A vacuum-impregnated thin section and/or acetate peel was made from each hand sample, and 50% of each section was stained with Alizarin red S. Petrography included systematic visual estimates of lithology (%), calcite cement (%), and present-day porosity (%), as well as description of grain types, texture, and dolomite crystal size. The descriptions and estimates of lithology, porosity, and texture made in the field were checked by petrographic analysis, and field estimates vary less than 10% from petrographic data (Tinker 1996b).

In addition to petrographic work, stable isotopes ($\delta^{18}O$ and $\delta^{13}C$) were examined from two densely sampled reef to back-reef vertical transects. Acetate peels of each sample were made to determine the best locations to sample for isotopic analysis. Eighty samples were analyzed by the University of Michigan Stable Isotope Laboratory with a reported precision (standard deviation) of $< 0.05‰$.

APPROACH

The data collection and interpretation phase of this study proceeded as follows: description of vertical sections; identification of cycles; walking of stratigraphic contacts; documentation of stratal geometries; interpretation of photomosaics; mapping of lateral facies distributions; description of thin sections; construction of depositional models; and interpretation of the sequence-stratigraphic framework (cycle sets, HFSs, and CSs). Many of the collection and interpretation steps overlapped, and several iterations were made over a period of five years and four field seasons.

The remaining sections of this paper are presented in the general order of interpretation, with descriptions of facies and facies tracts first, followed by an interpretation of the static depositional models based on facies and sedimentologic data, and then a sequence-stratigraphic interpretation made with the initial depositional models in mind. The interpretations are followed by discussions regarding the dynamic stratigraphic and sedimentologic variations, the paleobathymetric model, and the sites and rates of sediment accumulation.

FACIES AND FACIES TRACTS

Eighteen distinct facies were recognized and described in McKittrick Canyon, defined using a combination of lithology, texture, grain composition, and sedimentary structures. Most of these facies have been described previously by other workers examining upper Guadalupian strata in the Guadalupe Mountains (e.g., Dunham 1972; Babcock 1977; Yurewicz 1976; Hurley 1978). Detailed facies descriptions for rocks in McKittrick Canyon can be found in Tinker (1996b). Therefore, the detailed measured section data, petrographic data, scintillometer data, well data, and lateral transect data for each facies are presented here in summary form only (Table 1). The tabular summary of the facies data is not intended to diminish their significance. To the contrary, the sedimentologic understanding that resulted from the descriptive work was critical to the interpretation of the initial depositional models and the subsequent sequence-stratigraphic interpretation; it is impossible to separate sedimentology and sequence stratigraphy.

A ''map'' of true vertical thickness (TVT) facies distribution and stratal geometry was constructed for the entire north wall of McKittrick Canyon

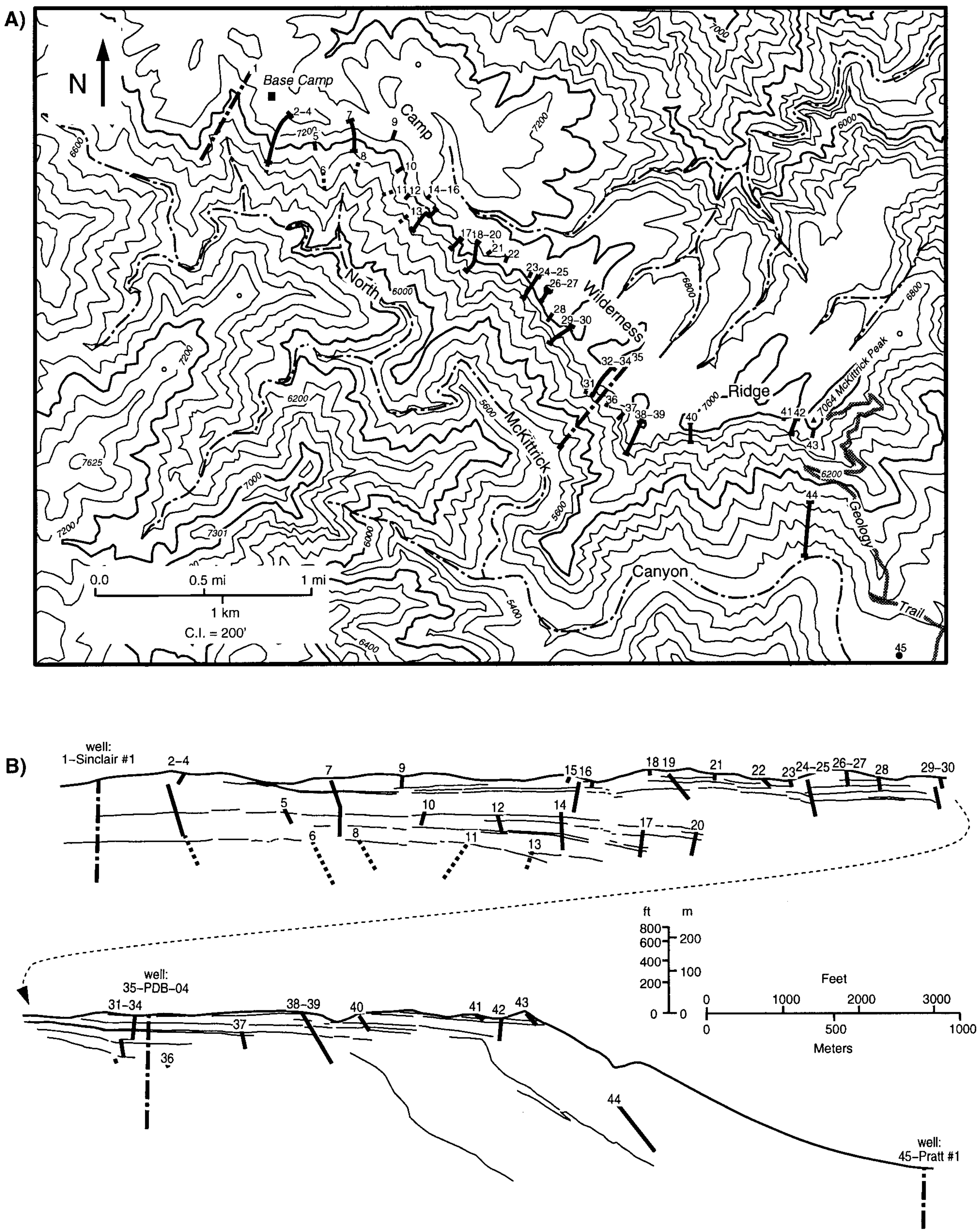

FIG. 5.—Topographic base map of McKittrick Canyon showing the location of measured sections (A, B) and lateral transects (thin horizontal lines) made in the field (B). Short-dashed lines (4, 6, 8, 11, 13) represent sections measured by Hurley (1978). Variable dashed lines are wells. See text for explanation of the variable vertical scale.

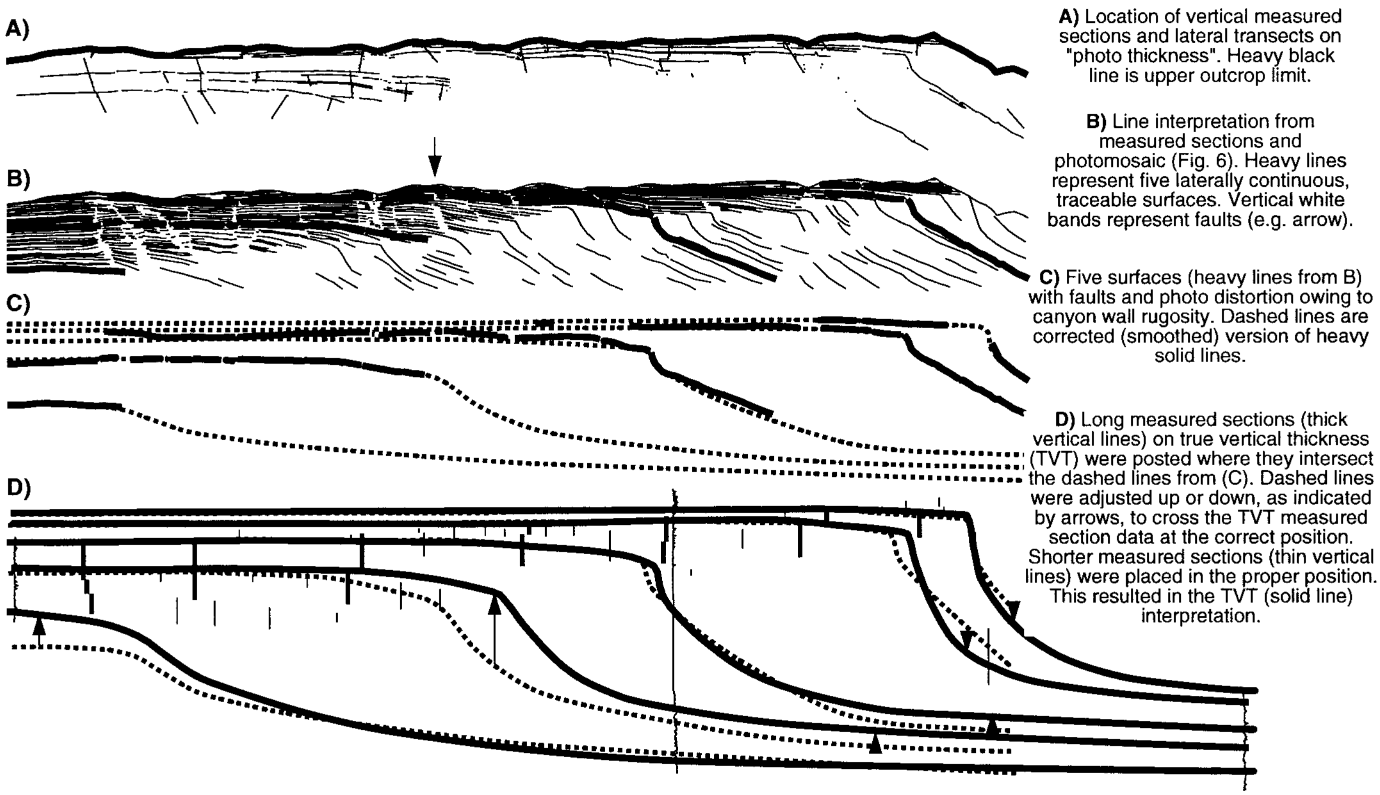

FIG. 7.—Steps to convert the photomosaic from ''photo thickness'' to true vertical thickness (TVT).

(Fig. 8) using the measured section data, lateral transect data, and the photomosaic. The TVT map represents the spatial distribution of all eighteen facies described in each measured section; no vertical averaging was done.

Owing to autocyclic processes, depositional topography, and position in the long-term eustatic hierarchy, individual facies are not always laterally continuous. Therefore, it is useful to group facies into facies tracts. A facies tract is a genetically linked association of facies and facies successions that records a discrete energy–water depth–sediment supply setting (*sensu* Kerans and Fitchen 1995, and analogous to a facies belt of Wilson 1975). Eight facies tracts were defined in McKittrick Canyon (Fig. 9), ranging along a depositional dip profile from the shelf-crest supratidal to the basinal. A generalized map of the facies tracts for the entire north wall of North McKittrick Canyon (Fig. 10) illustrates the complex yet systematic variation in proportion, width, thickness, and geometry of facies tracts.

Most carbonate depositional systems have key ''indicator'' facies or facies tracts, defined on the basis of lithology, grain components, and sedimentary structures. These indicator facies represent interpreted depth/energy positions such as shoreline, fair-weather wave base, and storm wave base (Kerans and Tinker 1997), and are therefore very useful for sequence-stratigraphic interpretation. In McKittrick Canyon the shelf-crest supratidal, outer-shelf subtidal, and shelf-margin facies tracts are such ''indicators''.

The *shelf-crest supratidal facies tract* is composed of cryptalgal laminite boundstone, composite-grain rudstone, and pisoid rudstone, with rare to common small (a few centimeters tall) to large (several meters tall) teepee complexes (see also Esteban and Pray 1983). This facies tract is a shoreline indicator. The *outer-shelf subtidal facies tract* has a low- to moderate-energy component composed principally of silty, peloid, bioclast, foram dolowackestones and dolopackstones, and a moderate- to high-energy component composed principally of foram, *Mizzia*, bioclast, peloid, fusulinid packstones and grainstones. The low- to moderate-energy component is interpreted to indicate a position from well below fair-weather wave base to below storm wave base, and represents the flooding events on the shelf. The moderate- to high-energy component is interpreted to indicate a position just below fair-weather wave base. The *shelf-margin facies tract*, commonly called the Capitan reef, is composed of marine-cemented, sponge, algal, bryozoan, *Archaeolithoporella* (ALP), *Tubiphytes* framestones and boundstones (see also Kirkland et al. 1993; Wood et al. 1994). This facies represents a similar fair-weather to sub-storm-wave-base position as the low- to moderate-energy component of the outer-shelf subtidal facies tract.

In addition, there is a siltstone and very-fine grained sandstone facies (referred to collectively as siltstones) that cuts across most facies tracts (S1, OS1, SC1 in Figure 8; Table 1). The siltstones are composed of quartz, potassium feldspar, kaolinite, and illite, have dolomite and calcite cements, are remarkably devoid of diagnostic sedimentary structures (see also Candelaria 1982), and are more naturally radioactive than the associated carbonates. The siltstones are a very useful indicator of stratal geometry, because their position can be followed in outcrop with a high degree of confidence.

DEPOSITIONAL MODELS

By definition, a depositional model is a generalization, because the depositional setting and associated facies arrangements are not static, but are instead strongly related to the position in the overall composite sea-level curve. For example, the depositional model for a TST in the SR1 HFS is quite different from the depositional model for the HST in the SR1 HFS. The same variation is observed at the CS scale.

Stratigraphic and sedimentologic data in McKittrick Canyon uphold the model of reciprocal sedimentation. The concept of ''reciprocal sedimentation'' (Wilson 1967) was first applied to Permian strata in the Delaware basin by Silver and Todd (1969), Jacka et al. (1972), and Meissner (1972). The model involves clastic progradation and bypass across the shelf into the basin during relative sea-level lowstand, and carbonate growth on the

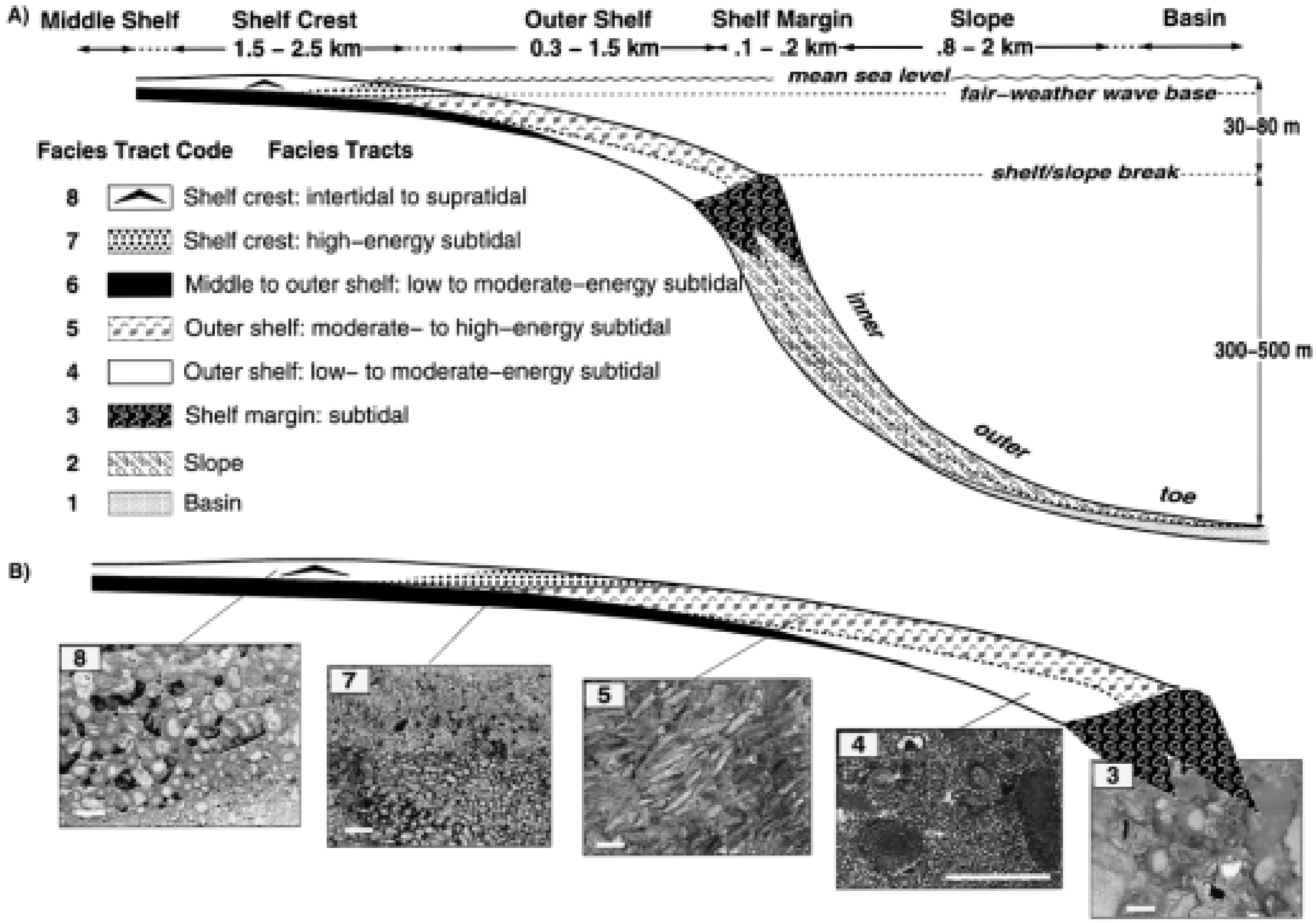

FIG. 9.—**A)** Generalized 2-D cycle showing vertical and lateral position and width ranges of major facies tracts related to paleobathymetric profile. **B)** Expanded shelf part of the cycle with photographs of key facies showing a general decrease in interpreted depositional energy downdip. Scale bar is 1 cm for all photographs. Numbers correspond to facies-tract legend.

shelf during relative sea-level rise and highstand. Detailed petrography and facies mapping on the shelf in McKittrick Canyon documents a higher-frequency timing of siliciclastic sediment delivery, similar to that proposed by Borer and Harris (1989, 1991) for the Yates Formation, Gardner (1992) for the Bell Canyon Formation, Brown and Loucks (1993) for the Tansill-equivalent toe-of-slope, and Melim and Scholle (1995) for the Capitan slope.

In the continuous outcrops of McKittrick Canyon, sedimentology, petrography, stratal geometry, and vertical and lateral facies associations were all used to develop the initial depositional models. Closely spaced vertical measured sections and lateral transects within the Y3 HFS were used to construct a detailed 2-D cross section (Fig. 11) and a series of 3-D block diagrams (LST, TST, HST; Fig. 12) that represent the depositional history of a typical HFS. Unless otherwise cited, the interpretations that follow are based on this work (see also Tinker 1996b).

Lowstand Systems Tract

Siltstones were transported tens to hundreds of kilometers across the shelf into the basin by eolian (Mazzullo et al. 1985) and shallow-water marine-coastal processes (Candelaria 1982; Figure 12), where they were deposited by suspension in deep water. At maximum relative sea-level lowstand, the entire *shelf crest* and much of the *middle shelf* were subaerially exposed, and underwent either erosion or silt deposition by eolian and sabkha processes. Individual siltstone deposits thin towards the shelf margin owing to increased depositional slope in the outer shelf and slope, and silt transport across the margin by storm-related, marine processes. *The outer shelf* and *shelf margin* remained submerged, the outer-shelf facies tract was narrow (500 m), the shelf margin was narrow (20 m) and relatively shallow (~ 15 m), and a minimal volume of carbonate sediment was transported into the *basin.*

Transgressive Systems Tract

During marine transgression the shoreline receded, and shelf siltstones were partially to completely reworked and buried by low-energy carbonate deposits. *Shelf-crest* deposits backstepped and aggraded (Figs. 11, 12).

Outer-shelf rates of carbonate-sediment production were at a maximum, which is common for the TST in most HFSs in McKittrick Canyon (see outer-shelf thickness in Figures 8, 10, 11). There was a systematic, landward increase in current reworking, resulting in higher-energy, grainier facies updip from lower-energy, muddier facies (Figs. 9, 11, 12). Fusulinid grainstones are an exception, and can be found downdip from the lower-energy facies in close proximity to the shelf margin. Fusulinid tests in these grainstones are commonly oriented parallel to depositional dip, indicating mobilization and downslope transport of fusulinids.

Fusulinids are important indicators of paleoenvironment. The large (1–3 cm) Guadalupian fusulinids found in outer-shelf facies of the Seven Riv-

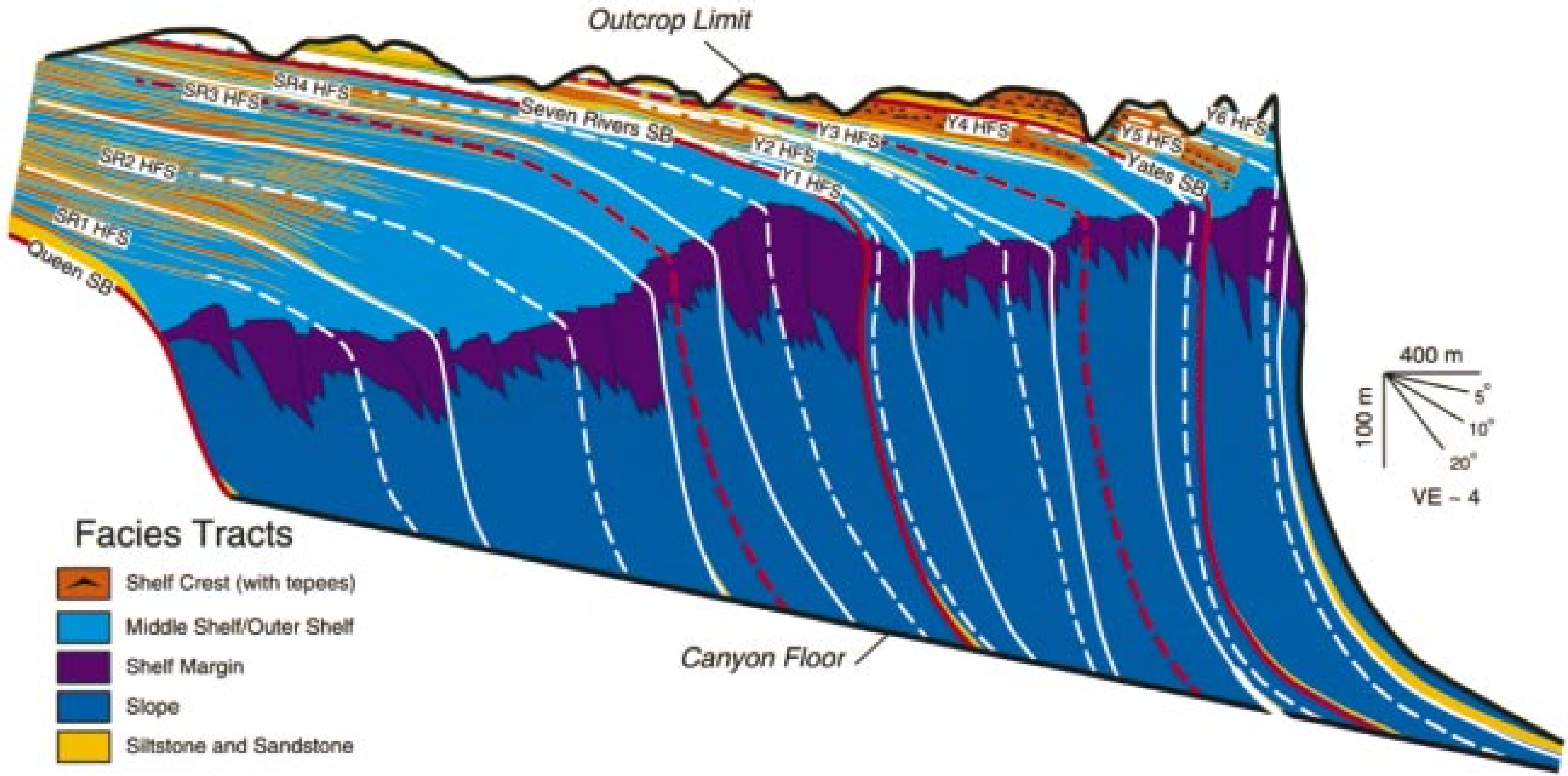

FIG. 10.—Facies-tract distribution, simplified from Figure 8, illustrating the organization in McKittrick Canyon. Figure is shown with present-day, tectonically enhanced basinward dip (to the right) to illustrate the potential pitfall of misinterpreting the amalgamated shelf-crest facies (Y2 to Y5) as a single lithostratigraphic unit (similar to the Yates Formation definition by Hayes 1964). Solid red lines are CS boundaries, dashed red lines are CS MFSs, solid white lines are HFS boundaries, and dashed white lines are HFS MFSs.

TABLE 1.—*Lithofacies data*

Facies: Code	Facies: Major Grain(s)	Facies: Texture[1]	Facies: Minor grain(s)	Facies Tract: Energy Modifier	Depositional Environment (water–depth range in parentheses)
SC8	Pisoid	RS	Composite grain, eploid	Shelf crest: intertidal to supratidal	Intertidal to supratidal; subaerial island
SC7	Composite grain	RS	Pisolite, peolid, ooid, mollusc	Shelf crest: intertidal to supratidal	Intertidal to supratidal; rare subaerial exposure
SC5	Cryptalgal, peloid	WS/BS	Foram, ostracod	Shelf crest: intertidal to supratidal	Intertidal to supratidal tidal flat
SC6	Ooid, coated grain	GDPS/GS	Foram, peloid, pisoid	Shelf crest: high-energy subtidal	Lower foreshore and shoreface (3–10 m)
SC4	Peloid, bioclast, intraclast	PS/GS	Foram, mollusc	Middle shelf: low to moderate-energy subtidal	Shallow subtidal shoals (5–10 m)
SC3	Peloid, bioclast	MS/WS	Foram, mollusc	Middle shelf: low to moderate-energy subtidal	Subtidal (10–25 m)
SC2	Silty dolomite	MS/WS	Peloid, bioclast	Middle shelf: low to moderate-energy subtidal	Erg transport, transgressive reworking and subtidal preservation
SC1	Siltstone (dolomitic)		Peliod	Middle shelf: low to moderate-energy subtidal	Erg transport, transgressive reworking and subtidal preservation
OS9	Ooid, coated-grain, foram	GS	Foram, peliod, pisoid	Outer shelf: moderate to high-energy subtidal	Shoals (5–10 m)
OS8	Oncolite	RS	Ooid, peloid, composite grain, foram	Outer shelf: moderate to high-energy subtidal	Shoal and intershoal; transported deposits (5–30 m)
OS7A	Fusulinid, ooid	GS	Peloid	Outer shelf: moderate to high-energy subtidal	Shoal and intershoal; transported deposits (5–40 m)
OS7	Peloid, bioclast, fusulinid	GDPS/GS	Foram, mollusc	Outer shelf: moderate to high-energy subtidal	Shoal and intershoal (5–50 m)
OS6	Peloid, bioclast, fusulinid	WS/PS	Foram, mollusc	Outer shelf: moderate to high-energy subtidal	Intershoal (10–80 m)
OS5	Foram, mizzia, bioclast	PS/GS	Peloid	Outer shelf: moderate to high-energy subtidal	Moderately protected back reef (5–50 m)
OS4	Crinoid, foram, peloid	WS/PS	Mizzia, Bioclast	Outer shelf: low- to moderate-energy subtidal	Immediate back reef (20–80 m)
OS3	Peloid, bioclast	MS/WS	Foram, mollusc	Outer shelf: low- to moderate-energy subtidal	Quiet-water outer shelf (10–80 m)
OS2	Silty dolomite	MS/WS	Peloid, bioclast	Outer shelf: lowstand transport, transagressive reworking	Erg transport, transgressive reworking and subtidal preservation
OS1	Siltstone (dolomitic)		Peloid	Outer shelf: lowstand transport, transagressive reworking	Erg transport, transgressive reworking and subtidal preservation
OS0	Sponge, ALP, cement	FS/BS	Sediment, bryozoan, cephalopod, tubiphytes, foram	Shelf margin reef	Organic, cement reef, dominantly quiet water (10–80 m)
S5	Bioclast, lithoclast	RS/GS/BR/CG	Spectrum of shelf and shelf margin derived grains	Slope (inner)	Upper and middle slope, rock fall, grain flow, debris flow
S4	Bioclast, lithoclast	RS/WS/PS/CG	Spectrum of shelf and shelf margin derived grains	Slope (inner to outer)	Lower slope, debris flow, high-density turbidite
S3	Peloid, foram	MS/WS	Spectrum of shelf and shelf margin derived grains	Slope (outer) and basin	Toe of slope, low-density turbidity current
S2	Silty dolomite	MS/WS	Peloid, bioclast	Slope (outer) and basin	Distal slope and basin, low-density turbidity current
S1	Siltstone (dolomitic)		Peloid	Basin	Distal slope and basin, low-density turbidity current
S0	Vf–md sand			Basin	Distal slope and basin, low-density turbidity current

[1] After Embry and Klovan's (1971) modification of Dunham's (1962) classification. GDPS is grain-dominated packstone after Lucia (1995).

TABLE 1.—*Continued.*

Code	Sedimentary Structures	Lithology (Average %)[2]						Pore Type(s)[3]	Radioactivity (cps)/# Measurements[4]	Measured Feet (#)/Thin Sections (#)[5]
		ST/SD	DM	LM	Calcite	Oth	⌀			
SC8	Tepee, sheet crack, breccia	0	64	14	15	1	6	BP, WP, BR, SH	63/359	886/29
SC7	Tepee, sheet crack, breccia	1	68	15	10	0	6	BP, WP, BR, SH	67/94	252/51
SC5	Fenestral to wavy laminated, stromatolite	1	73	11	9	0	6	FE, BC, FR, MO	68/168	322/39
SC6	Planar and cross stratified	1	55	30	8	0	6	BP, BC, MO	62/123	211/24
SC4	Planar laminated	1	59	27	8	1	4	BP, BC, MO	70/356	822/89
SC3	Laminated to massive, vertical burrow	2	79	13	4	0	2	mBC, BC, BP	65/23	289/16
SC2	Planar laminated, graded beds	24	71	0	1	1	3	mBC	101/55	160/15
SC1	Planar laminated, graded beds	67	22	0	2	0	9		134/47	371/8
OS9	Planar and cross stratified	0	64	16	10	0	10	BP, BC, MO, WP	63/61	180/21
OS8	Planar laminated	0	53	28	13	0	6	BP, WP	58/10	344/6
OS7A	Planar and minor cross stratified	0	62	15	13	0	10	BP, BC, MO	66/82	258/6
OS7	Planar laminated	2	53	29	8	0	8	BP, BC, MO	63/510	1074/30
OS6	Planar laminated	0	60	23	11	0	6	BP, BC, MO	68/241	781/33
OS5	Planar laminated	0	59	24	12	0	5	BP, BC, MO	64/19	138/9
OS4	Planar laminated	0	43	41	12	0	4	BP, BC, MO	58/13	73/8
OS3	Laminated to massive, vertical burrow	2	92	0	2	0	4	mBC, BC, BP	83/15	24/5
OS2	Planar laminated, graded beds	29	59	0	7	0	5	mBC	89/16	59/5
OS1	Planar laminated, graded beds	53	15	0	20	2	10		112/22	55/3
OS0	Massive	0	30	50	18	0	2	VG, FR, MO, BP	53/21	187/50
S5	Steep dipping, medium to chaotic bedded	0	51	26	18	0	5	BP, MO, VG, FR	48/77	138/7
S4	Planar and cross stratified, inverse graded	0	50	40	7	0	3	BP, MO, VG, FR	48/202	383/7
S3	Fine laminated to thick bedded, graded beds							BP, WP FR		
S2	Planar laminated, bioturbated, graded beds							mBC		1/1
S1	Planar laminated, bioturbated, graded beds									1/1
S0	Laminated to thin bedded	70	10	0	5	5	10		63/2	2/1

[2] Average of all samples based on visual estimates in the field, calibrated by thin section petrography: ST/SD = siltstone/sandstone; DM = dolomite; LM = limestone; Oth = other, ⌀ = porosity.
[3] After Choquette and Pray (1970).
[4] From hand-held Scintillometer.
[5] Includes samples from lateral transects.

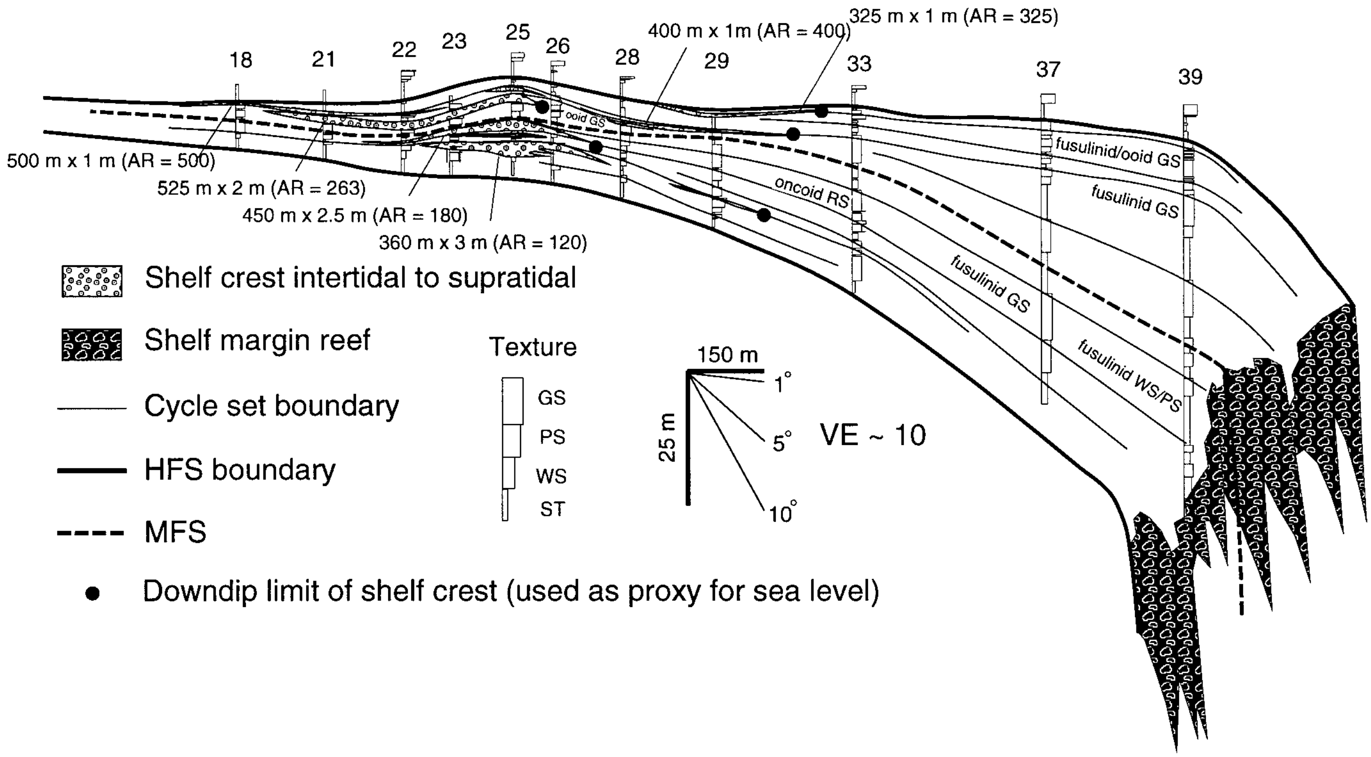

FIG. 11.—Detailed cross section of the Y3 HFS. Note: (1) the proportional expansion in thickness of cycle sets, and the systematic progression from high-energy shelf-crest facies (PS/GS) to lower-energy, outer-shelf facies (WS/PS) from the shelf crest downdip to the shelf margin; (2) the downdip limit of the shelf-crest facies tract (black circles) backsteps to just above the maximum flooding surface (MFS), and progrades above the MFS; (3) the aspect ratios (AR) of the shelf crest bodies increase upwards toward the MFS and decrease away from the MFS. MS, Mudstone; WS, Wackestone; PS, Packstone; GS, Grainstone; ST, Siltstone. Measured section numbers correspond to Figures 5, 6, and 8.

ers through the middle Yates are *Polydiexodina.* Considerably smaller fusulinids, *Yabeina* and *Codonofusiella,* first occur in the lower Tansill Formation, and the still smaller *Reichelina* first occurs in the middle Tansill (Tyrrell 1969; Wilde 1975). Although these Paleozoic fusulinids are extinct, *Alveolinella quoyi* is considered a modern counterpart (Severin and Lipps 1988). Fusulinids and alveolines (Miliolida) belong to different suborders because of variations in test structure, yet their similar morphology, taphonomy, associated rock types, and latitudinal ranges argue that the development of individuals, and the community in which they lived, must have been comparable (Haynes 1981). On Papua New Guinea, *A. quoyi* is most abundant ($750/m^{2)}$ on stable sand and coral rubble slopes in water depths from 12 to 30 m. Alveolinids are most abundant between 25 and 35 m in the Gulf of Aqaba and in the Maldives. In addition, the deeper-water modern alveolinids have greater length-to-thickness ratios than the shallower forms (Haynes 1981).

The *shelf-margin* facies tract was dominantly aggradational (Fig. 12). This aggradational mode was common for the shelf-margin facies tract during the marine transgressive phase of most HFSs in McKittrick Canyon, and is also observed at the CS scale (Figs. 8, 10).

Whereas shelf-derived *slope* deposits were a mix of siltstones and carbonates during the early TST, they were dominantly carbonate during the late TST, and were probably deposited as downlapping strata onto toe-of-slope and basinal carbonates and siltstones (documented for the Tansill-equivalent Lamar member by Brown and Loucks 1993).

Highstand Systems Tract

With progressive infill of shelf accommodation, the *shelf-crest* and *outer-shelf* facies tract deposits were forced to prograde basinward (Fig. 11, 12). The decrease in accommodation is documented by the changing aspect ratio of the shelf-crest supratidal facies tract, which increased from 100 to 200 (350 to 450 m width and 2 to 3 m thickness) in the TST, to 200 to 500 (300 to 500 m width and 1 to 2 m thickness) in the HST (Fig. 11). Kerans and Fitchen (1995) have documented a similar relationship for the shelf-crest facies in San Andres and Grayburg ramp deposits.

Facies diversity and the net volume of grain-dominated sediments increased in the higher-energy, *outer-shelf* facies tract of the HST relative to the lower-energy, outer-shelf facies tract of the TST (Fig. 12). The *shelf-margin* reef was progradational, and shelf-derived *slope* deposits were grain-dominated (documented for the Tansill-equivalent Lamar member by Brown and Loucks 1993).

SEQUENCE STRATIGRAPHIC INTERPRETATION

Carbonate strata commonly show an ordered stratigraphic hierarchy that repeats at many scales (Cross et al. 1993; Goldhammer et al. 1993; Montañez and Osleger 1993). Many workers in the Permian of West Texas and New Mexico have recognized this type of ordered stratigraphic hierarchy (Borer and Harris 1991; Sonnenfeld 1991; Kerans et al. 1992; Kerans et al. 1994; Kerans and Fitchen 1995). It is possible to challenge the statistical significance, or even the existence, of an ordered stratigraphic hierarchy, by isolating only 1-D data (Wilkinson et al. 1997). However, the challenge weakens considerably when 2-D data are considered, because facies proportions, cycle thickness, and stratal geometries commonly vary along depositional dip in most carbonate settings (see Figures 8, 9, 10). Therefore, even in ordered stratigraphic systems the 1-D succession of facies will vary as certain facies substitute laterally for other facies. In McKittrick Canyon, analysis of the 2-D facies distribution data indicates a remarkably well organized stratigraphic hierarchy, emphasizing the need to examine all of the data using as many analytical ''tools'' as possible.

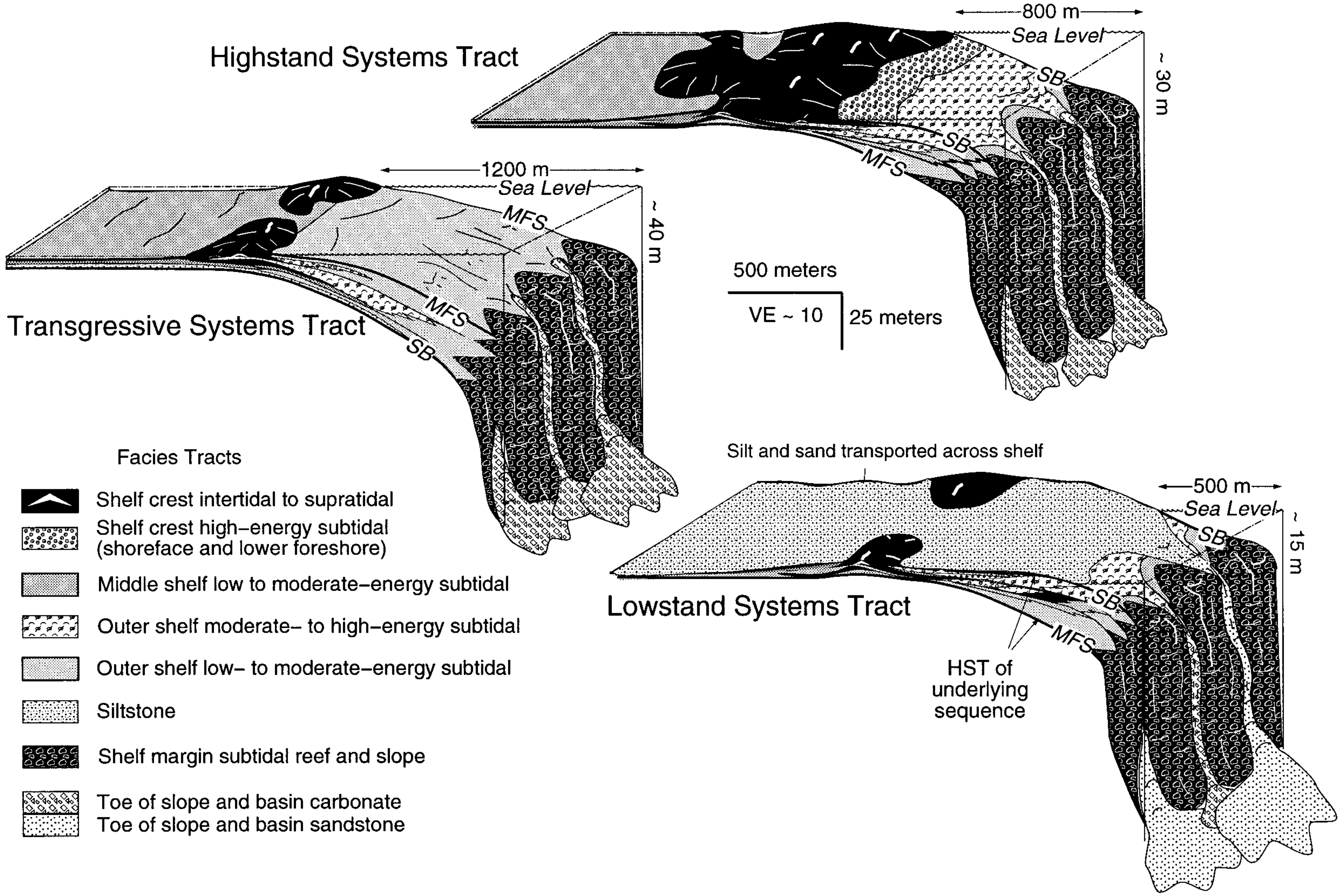

FIG. 12.—Three-dimensional facies distribution based on the Y3 HFS depositional model in Figure 11. Note: (1) increasing interpreted depth to the top of the shelf-margin reef from the LST to the TST; (2) greater distance from the shelf-crest shoreline to the shelf margin in the TST versus HST; and (3) greater shelf-crest width and outer-shelf facies diversity in the HST versus the TST. SB, sequence boundary. MFS, maximum flooding surface. This systematic variation in facies is observed in most of the Seven Rivers and Yates HFSs and CSs (Figs. 8, 10).

TABLE 2.—*Sequential Facies Data*

Lithofacies Below		Lithofacies Above: SC8	SC7	SC5	SC6	SC4	SC3	SC2	SC1	OS9	OS8	OS7a	OS7	OS6	OS5	OS4	OS3	OS2	OS1	OS0
	SC8		*20%*	*22%*	*17%*	*25%*	*16%*	***30%***	***42%***	*3%*	*6%*	*2%*	*1%*	*6%*			*9%*		*8%*	
	SC7	**25%**		9%	5%	6%	14%	8%	4%	8%	12%	4%	1%	2%						
	SC5	29%	**29%**		24%	15%	9%	8%	13%		5%		2%	2%	5%					
	SC6	11%	11%	**14%**		8%	3%	11%	7%		4%									
	SC4	9%	13%	34%	**44%**		16%	9%	11%		18%		2%							
	SC3	4%	10%	4%	1%	**19%**			3%		14%									
	SC2	6%	3%	8%	4%	**12%**	8%		**17%**	2%			1%							
	SC1	8%		2%	1%	5%	7%	**32%**			1%				16%					
	OS9	*3%*	*3%*	*1%*		*1%*	*3%*	*1%*			*11%*	*13%*	*13%*	*3%*	*5%*			***16%***	***17%***	
	OS8	3%	8%	2%	2%	7%	**22%**		1%	**15%**		5%	8%	2%	11%			3%	8%	
	OS7a	0%	1%			1%				**18%**	5%		11%	11%				22%	8%	
	OS7	2%	2%	2%	2%	2%			3%	36%	16%	**66%**		38%	11%	14%	27%	31%	33%	
	OS6									8%	4%	5%	**49%**		16%		18%	19%	8%	
	OS5			2%				1%		2%	1%	4%		**11%**		14%				
	OS4													4%	**32%**					
	OS3									2%			1%	9%						
	OS2			1%						6%	4%	2%	7%	9%			**36%**		17%	
	OS1	1%		1%						2%			4%	2%			9%	**9%**		
	OS0					1%	3%								5%	71%				
	Total Count	216	126	178	96	183	76	76	72	66	83	56	150	95	19	7	11	32	12	0

Notes: The table is read as follows: 49% of the time facies OS7 is preceded by facies OS6 (light gray boxes). Although there is a broad range in the vertical succession, the bold numbers represent the largest percentage, and dictate the sequential placement. Percentages calculated for lithofacies with a Total Count <30 (OS0-OS5) are less reliable. When a facies is followed by itself, it is dropped from the calculation (vertical striped shading). Two ''ideal'' cycles are represented by the vertical successions of lithofacies, the Outer Shelf (OS0-OS9) and the Shelf Crest (SC1-SC8). Facies OS9 (italics) represents the uppermost facies in the OS cycle, and is most commonly followed by OS1 and OS2 to begin a new cycle. Facie SC8 (italics) represents the uppermost facies in the SC cycle, and is most commonly followed by SC1 and SC2 to begin a new cycle.

Several analytical tools or techniques were used to examine the 2-D stacking patterns in McKittrick Canyon. *Lithologic analysis* and *facies proportion analysis* examine the changing percentage of a given lithology or facies preserved in each cycle, respectively. It can also be useful to examine the preservation of facies in transgressive (base-level rise) and regressive (base-level fall) hemicycles (Gardner 1993; Tinker 1996b, Kerans and Tinker 1997). *Facies offset analysis* examines changes in facies that interrupt the anticipated vertical (''Waltherian'') facies succession (e.g., a fusulinid packstone lying sharply above a pisolite rudstone represents a significant, non-Waltherian increase in depositional water depth). *Scintillometer* measurements provide data regarding the spatial variation in natural radioactivity. *Geochemical stratigraphy* looks at changes in a chemical signature (e.g., carbon isotopes) that can be indicative of stratigraphic and/or diagenetic processes. *Cycle thickness analysis* examines the spatial variation in thickness of each cycle. *Stratal geometry* provides information about depositional topography along dip, and when combined with other information, is an indicator of varying accommodation conditions through time.

A subsurface interpretation would proceed in much the same fashion as on the outcrop, using 1-D sedimentologic and facies data from logs and cores, and 2-D and 3-D data from seismic, interwell production tests, and predictive Walther's Law models. Multivariate (e.g., lithology, facies proportions, facies offsets, cycle thickness) stacking-pattern analysis performed on several wells provides a powerful tool for prediction of stratal geometry and facies distributions in 2-D and 3-D (Tinker 1996a; Kerans and Tinker 1997). Because the resolution of the 2-D and 3-D data in the subsurface is significantly lower than from continuous outcrops, the confidence in the subsurface interpretation is also lower. Tinker (1996a) provides examples of stratigraphic interpretation problems in the subsurface, and the subsequent impact on 3-D reservoir characterization.

The interpretation criteria, analytical ''tools'' used, and specific observations are discussed below for each of the stratigraphic elements in McKittrick Canyon.

Cycles

Field observations of facies (texture, grain composition and sedimentary structures), lithology, porosity, radioactivity, and the nature of the bounding contacts indicate crudely ordered (nonrandom) vertical successions. For example, OS8 commonly follows OS7; OS7 commonly follows OS6, and so on. These ordered successions were described as cycles in the field.

Statistical analysis of the facies database supports the field observations of facies successions (Table 2). Because facies were described every foot, successive feet commonly have repeating facies. For example, one foot of OS7 is most commonly preceded by another foot of OS7. However, when OS7 is not preceded by OS7, 49% of the time it is preceded by OS6. Using this kind of analysis, all of the facies were arranged in their most commonly observed vertical succession (Table 2, Fig. 13). When average lithology, porosity, radioactivity and texture are compared in the most common vertical facies succession, two stacking patterns are apparent (Tables 1, 2; Fig. 13), one for the shelf crest (SC) and one for the outer shelf (OS).

From the base up, the stacking pattern in the shelf crest (SC) setting consists of: (1) a sharp basal contact overlain by siltstones (9% porosity; SC1); (2) decreased siltstones and increased, thick-bedded, low-energy subtidal dolomudstones and dolowackestones (2–3% porosity; SC2, SC3); (3) planar-laminated to cross-laminated, moderate to high energy, subtidal lime to dolopackstones (4–6% porosity; SC4, SC6); (4) fenestral-laminated, peritidal dolowackestones (6% porosity; SC5); and (5) sheet-cracked, teepee, peritidal to supratidal dolorudstones (6% porosity; SC8). This pattern describes an initial increase and then dominant decrease in accommodation upward (Fig. 13).

In contrast to the shelf crest, the outer shelf (OS) has a greater proportion of subtidal facies. From the base up, the stacking pattern in the outer shelf (OS) setting consists of: (1) low- to moderate-energy dolomudstones to dolopackstones (4% porosity; OS3, OS4); (2) moderate- to high-energy subtidal dolopackstones and dolograinstones (5–10% porosity; OS5 through OS9); and (3) rare peritidal to supratidal dolowackestones capping

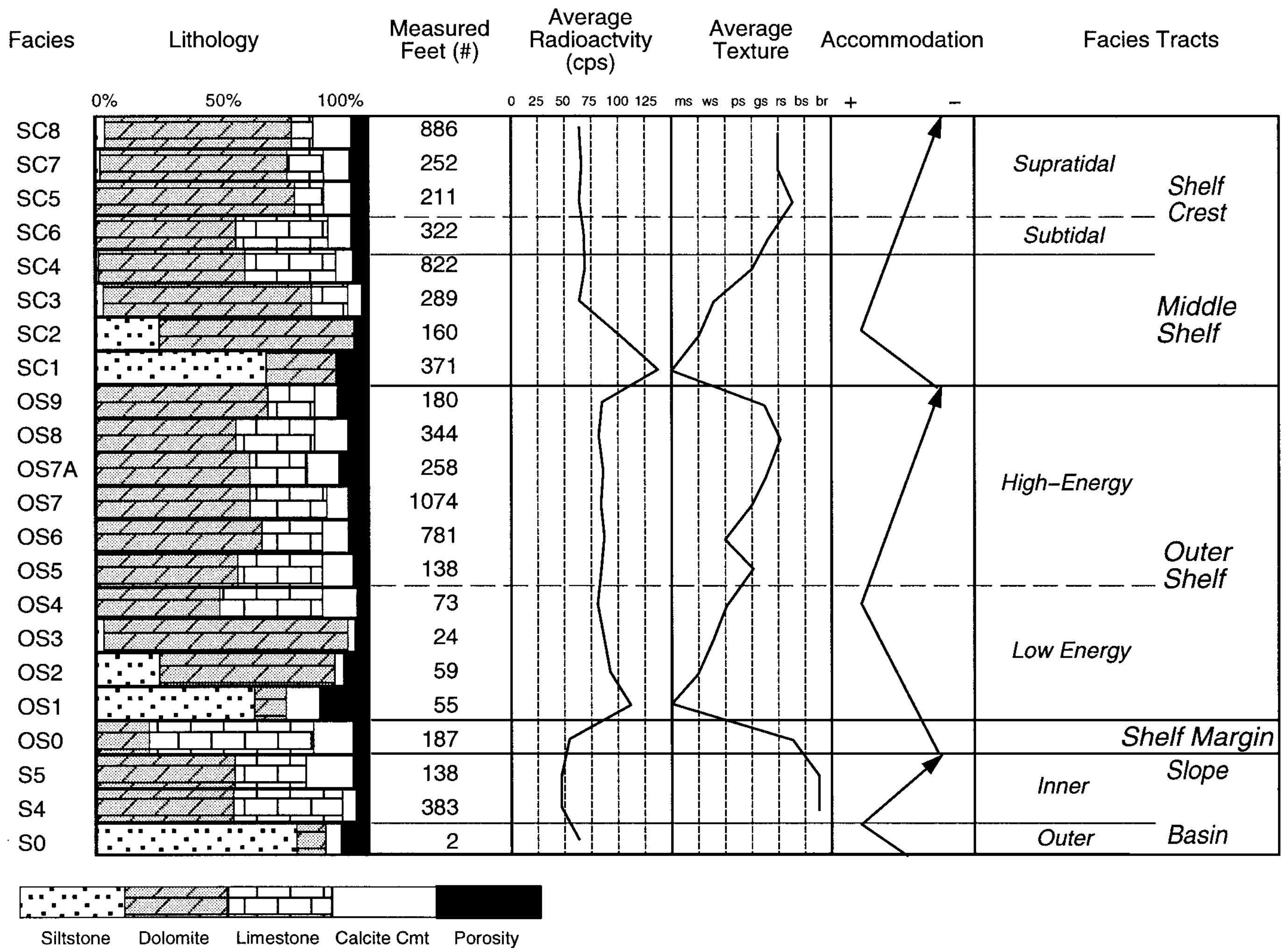

FIG. 13.—Stacking patterns as determined from lithology, porosity, radioactivity, and texture averages of the complete measured section database. Facies are arranged in terms of the most common vertical succession of facies (Table 2). Solid and dashed horizontal lines separate the facies into facies tracts. Lithology, porosity, radioactivity, and texture trends were used to help derive the accommodation interpretation.

the succession (Fig. 13). Like the shelf crest, the stacking pattern in the outer-shelf setting indicates an initial increase and then decrease in accommodation upward (Fig. 13). However, the increase in the proportion of subtidal facies in the outer shelf relative to the middle shelf supports a deeper-water interpretation for the outer shelf.

Cycle Sets

Cycle sets are defined by variations in facies, lithology, porosity, and thickness of component cycles. Whereas individual cycles may not be laterally continuous, cycle sets commonly can be traced across the dip width of the entire canyon wall. An initial deepening and then overall shallowing-upward succession of component facies, and a crude thinning-upward succession of component cycles characterize cycle sets. Cycle sets thicken towards the outer shelf, and have a thicker proportion of subtidal facies in their lower portions (Figs 8, 10, 11). Cycle sets can be defined using 1-D data alone, but 2-D data are valuable in order to document the basinward expansion and changing facies proportions.

Cycle sets in the Seven Rivers CS (Fig. 14) typically begin with a cycle dominated by siltstone or lime mudstone at the base, followed by a relatively thick succession of subtidal carbonate wackestone or packstone cycles, capped by thin shelf-crest supratidal rudstone and fenestral laminated cycles. The upper contact is commonly sharp, and is frequently overlain by a cycle dominated by siltstone or lime mudstone at the base of the subsequent cycle set.

Cycle sets in the Yates CS (Fig. 15) are considerably more amalgamated, and are either dominated by stacked subtidal cycles (Y2, Y3) or stacked intertidal to supratidal cycles (Y4, Y5). Cycle set boundaries in the amalgamated supratidal setting are interpreted where very thin mudstone or siltstone overlies erosionally truncated tepees.

HFSs and CSs

HFSs were defined using a combination of vertical variation in component cycle sets, facies, lithology, porosity, thickness, geochemical signature, and stratal geometry interpreted from the photomosaic and from lateral tracing of contacts in the field. CSs were defined using the same criteria, as well as variations in component HFSs.

1-D Data

HFS stacking patterns are defined on the shelf by an overall thickening and deepening (subtidal-dominated) succession of component cycle sets upward, interpreted to represent the TST, followed by an overall thinning

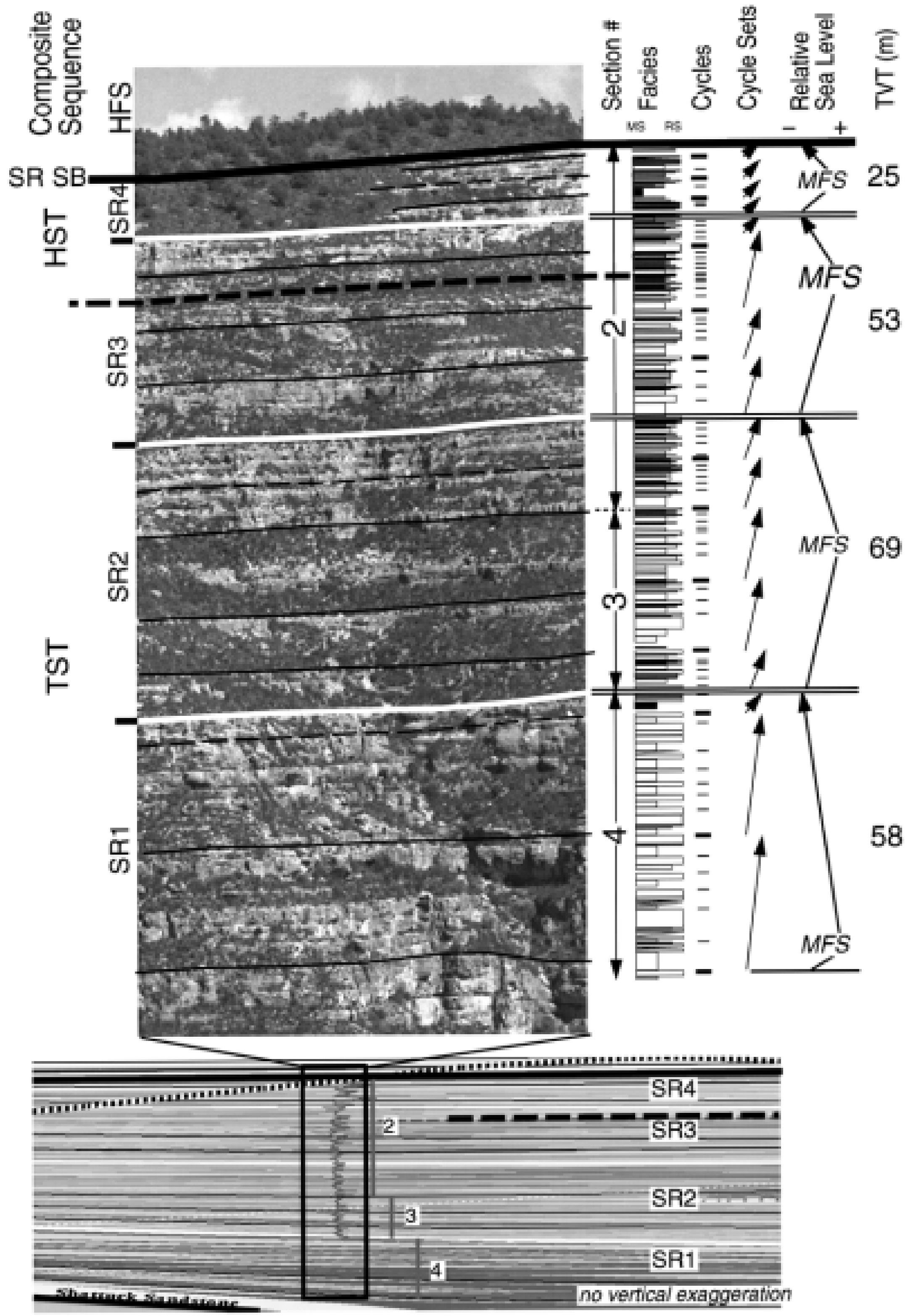

FIG. 14.—Stacking patterns illustrated using outcrop photograph and measured sections in the Seven Rivers CS. Location of measured sections 2, 3, and 4 on the sequence-stratigraphic interpretation (Fig. 8) is shown in the window at the bottom of figure, which represents 600 m from left to right. True vertical thickness (TVT, in meters) illustrates the outcrop distortion from bottom to top.

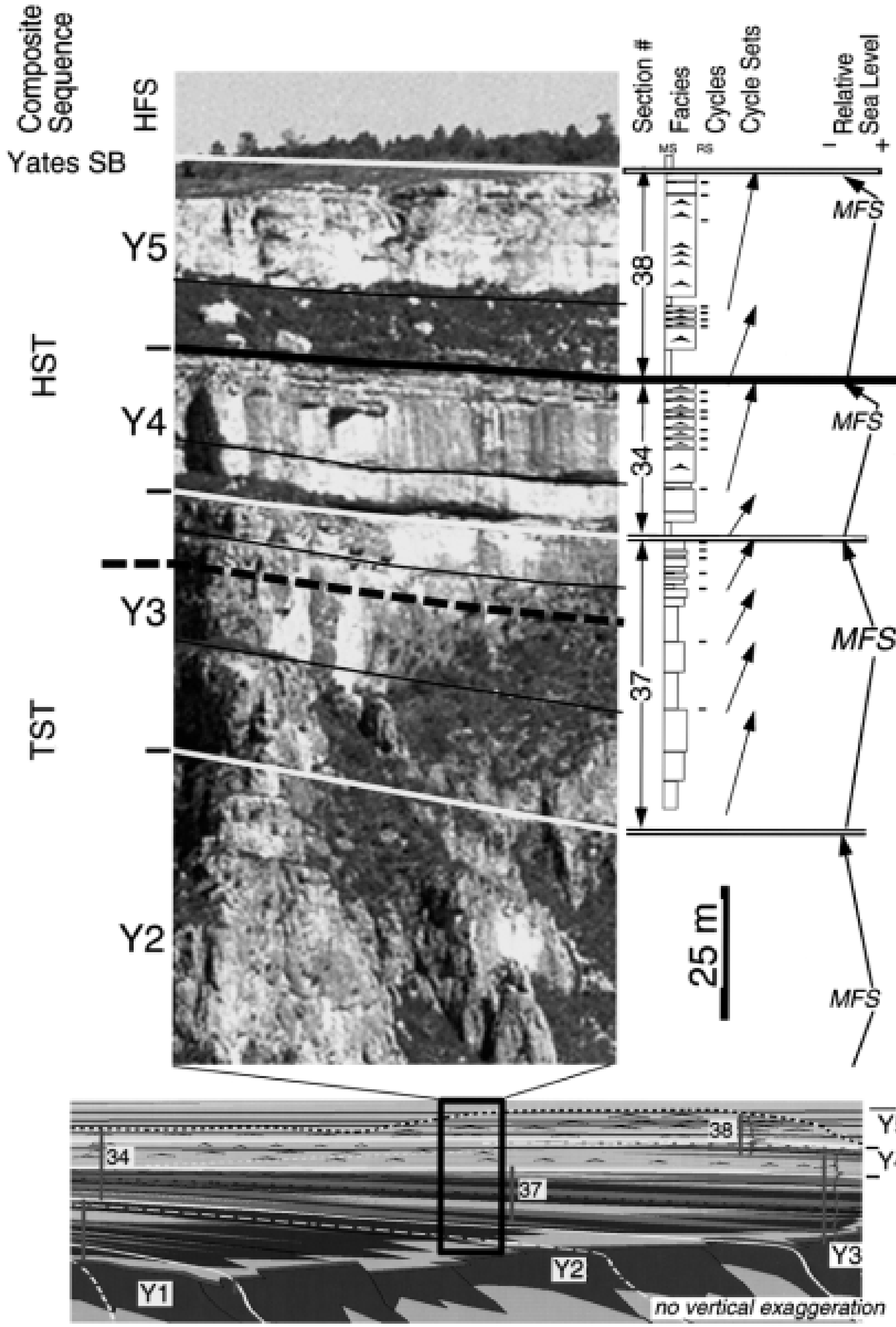

FIG. 15.—Stacking patterns in the Yates CS. Window at the bottom of figure represents 650 m from left to right. Measured sections 34, 37, and 38 are projected onto a single vertical section.

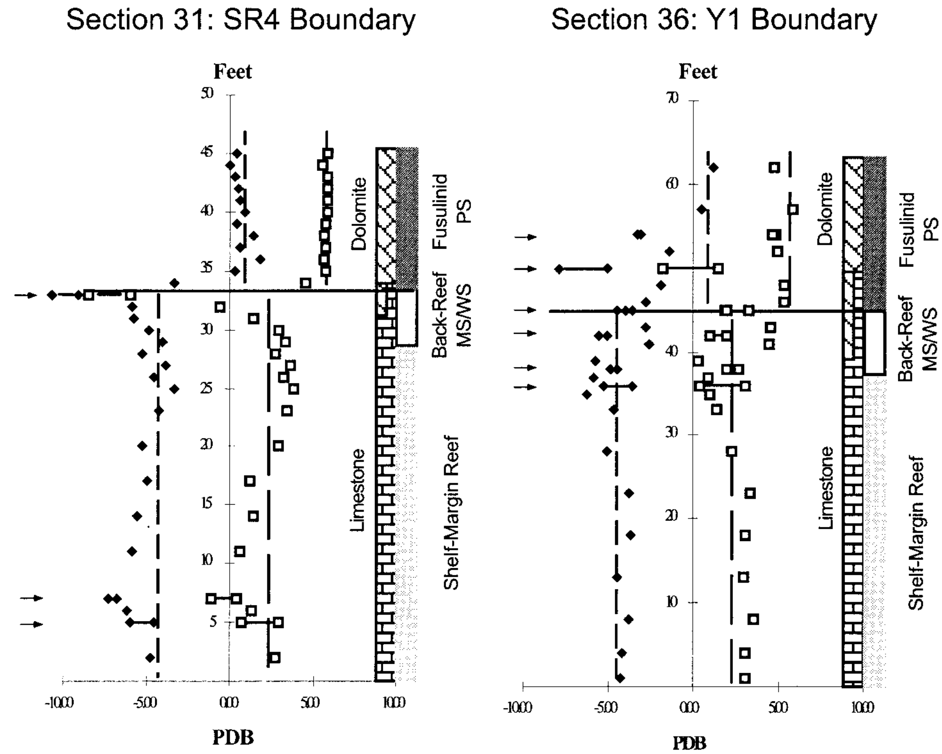

FIG. 16.—Geochemical stratigraphy. Vertical distribution of $\delta^{18}O$ (diamonds) and $\delta^{13}C$ (squares) in two reef transects, with dominant lithology and facies illustrated for each. Some hand samples were analyzed twice (indicated by arrows to left of each plot), using powder from two different areas of the sample. Vertical short-dashed lines indicate the approximate mean oxygen values (base line), and vertical long-dashed lines indicate the approximate mean carbon values (base line) for limestone and dolomite. Note the sharp boundary near the top of the limestone reef (33 feet; 10.1 m) in SR4 as compared to a more gradual transition (32 to 50 feet; 9.8–15.2 m) in Y1.

and shallowing (shelf-crest-dominated) succession of component cycle sets upward, interpreted to represent the HST (Figs. 14, 15). Comparison of 1-D sections shows that the proportion of TST versus HST tends to increase downdip within a HFS (Figs. 8, 10).

CS stacking patterns are characterized on the shelf by an overall thickening- and deepening-upward (subtidal dominated) succession of component HFSs (SR1 to SR2; Y1 to Y3; Figs. 8, 10, 14), followed by an overall thinning- and shallowing-upward (shelf-crest dominated) succession of component HFSs (SR2 to SR4; Y3 to Y4; Figs. 8, 10, 15). Using the 1-D data shown in Figure 14 alone, the CS MFS could be picked erroneously within SR2 instead of SR3, emphasizing the importance of analyzing multiple 1-D sections, and the added value of 2-D data.

Stable isotopes provide another important kind of 1-D data for identifying HFS and CS boundaries. Two vertical sample transects were made, one across the interpreted SR4 HFS boundary (Section 31; Figs. 6, 8), and one across the Y1 HFS boundary (Section 36; Figs. 6, 8). Microsamples (~ 3 mm diameter sample area) of the Capitan massive limestone and immediate back-reef dolostones were collected for stable-isotope analysis from the ''micritic'' part of each sample on the assumption that they were the most likely to preserve depositional and early diagenetic signatures (Given and Lohmann 1986).

The results for SR4 indicate a sharp, negative isotopic shift in $\delta^{18}O$ relative to an average base line near the top of the limestone reef, followed by an abrupt positive shift (~ 10‰) associated with passage into the dolomitized back-reef facies (Fig. 16). These $\delta^{18}O$ shifts relative to a base line exceed those reasonably expected from simple limestone-to-dolomite lithologic change (3–6‰; Land 1992). The pronounced negative shift at the top of the back reef, overlain by a positive shift across the SR4 (Seven Rivers CS) boundary, supports the possibility of subaerial exposure and depletion of the reef limestone by meteoric water prior to deposition and dolomitization of the overlying back reef sediment (*sensu* Allen and Matthews 1982). The results for Y1 show lower positive shifts in $\delta^{18}O$ (~ 7‰), and more gradual transitions (ranging over an 18-foot (5.5 m) interval), indicating little, if any, subaerial exposure at the shelf margin across this boundary.

The $\delta^{13}C$ response in SR4 shows a similar negative isotopic shift relative to an average base line near the top of the limestone reef, followed by an abrupt positive shift (~12‰) associated with passage into the dolomitized back reef facies (Fig. 16). This depleted response at the top of the reef could reflect the influence of a non-rock carbon source such as a biogenic soil zone, supporting the possibility of a subaerial exposure surface across the SR4 boundary. Additional work testing this hypothesis across other HFS boundaries is needed before definitive conclusions are drawn.

2-D Data

The 2-D distribution of four ''indicator'' facies, introduced in the Facies and Facies Tracts Section and described in the Depositional Model section, is critical for defining HFS and CS boundaries, maximum flooding surfaces (MFSs), and internal sequence architecture.

Siltstones.—Silts were delivered across the shelf during times of relative sea-level lowstand. Therefore, the 2-D position and spatial thickness variation of siltstones provide important criteria for sequence-stratigraphic interpretation. Thick siltstones with the greatest basinward extent help to define HFS and CS boundaries, because greater exposure time likely allowed for silt delivery farther across the shelf. Thin or absent siltstone helps to define HFS and CS maximum flooding, because the shoreline was pushed landward.

The base of the Seven Rivers CS boundary is marked by a thick (up to 10 m) siltstone, present across the complete outer shelf (Fig. 17). A thin (up to 3 m) siltstone that persists nearly to the shelf margin helps to define the upper SR1 HFS boundary (Fig. 17).

Two-dimensional stacking-pattern analysis of siltstones was used to help define the TST, MFS, and TST within each CS. Within the TST of the Seven Rivers CS, individual siltstones thin upward, the vertical distance between siltstones generally increases upward, and the downdip limit of siltstone preservation steps landward. Within the HST of the Seven Rivers

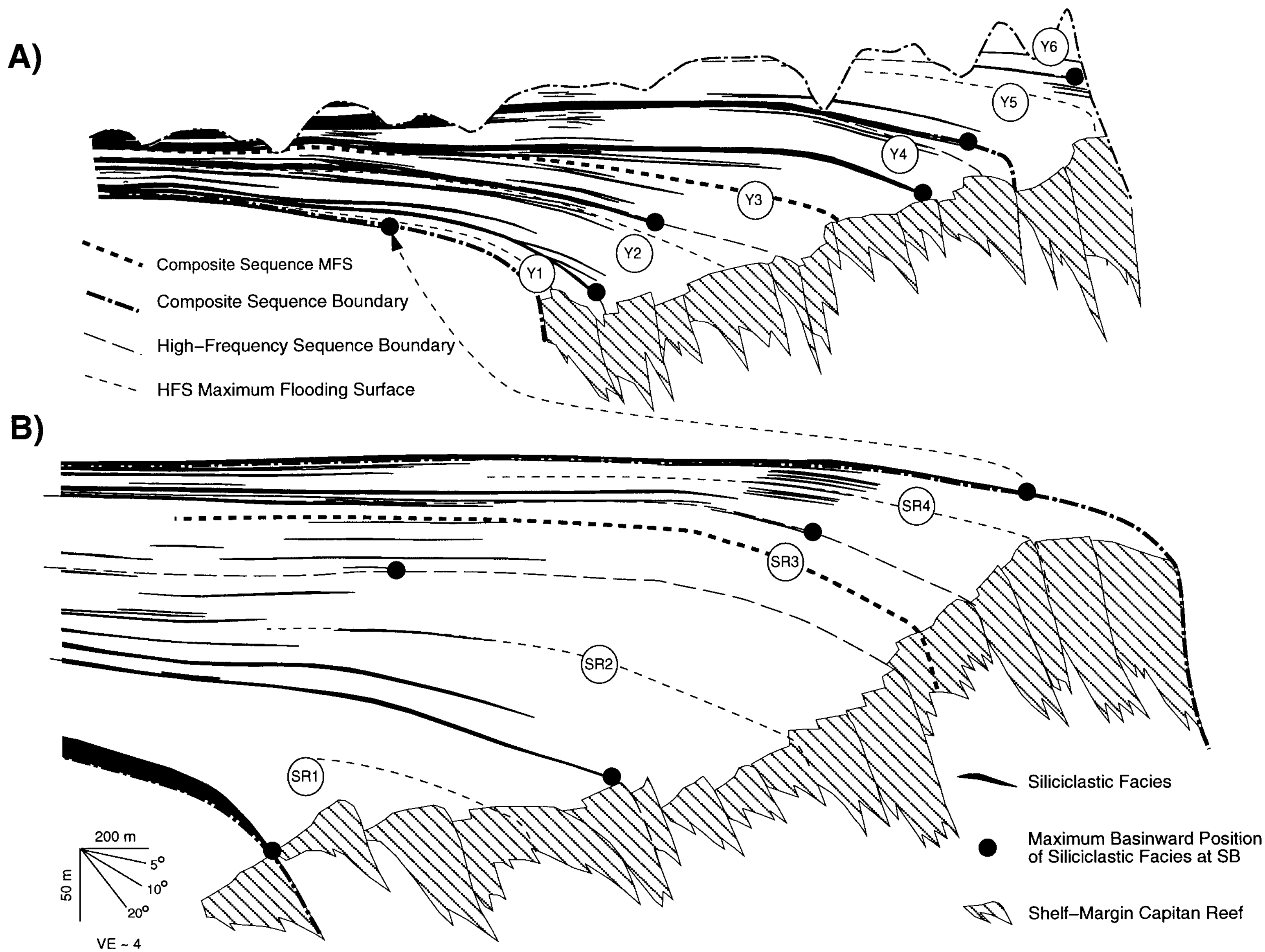

FIG. 17.—Distribution of siltstone and very fine sandstone in McKittrick Canyon. **A)** Y1–Y5 HFSs. **B)** Seven Rivers CS. Note the thickness increase of siltstones at HFS and CS boundaries, and the backstepping and thinning toward the MFS.

CS, individual siltstones thicken, the vertical distance between siltstones decreases, and the downdip limit of siltstone preservation steps basinward (Fig. 17). There is a 500-m basinward shift in siltstone position across the upper SR3 HFS boundary. Above the Seven Rivers CS boundary, a thick (up to 5 m) siltstone reaches to within 400 m of the shelf margin (Fig. 17).

Relative to the Seven Rivers, the Yates CS shows an overall increase in percentage of siltstone, thickness of individual siltstone bodies, and maximum basinward position of siltstone deposits (Fig. 17). In the Yates CS, siltstones are strongly aggradational in the HST (Y1, Y2, Y3) and strongly progradational in the HST (Y4).

The same general stacking pattern observed at the CS scale is repeated at the HFS scale in both the Seven Rivers and Yates CSs, whereby siltstones aggrade or step slightly landward toward the MFS, and step strongly seaward at HFS boundaries (Fig. 17). Two-dimensional stacking-pattern analysis is less reliable when applied to higher-frequency stratigraphic elements, because the effects of inherited topography and autocyclic processes can have a greater influence on deposition over the shorter time duration.

Shelf Crest.—Shelf-crest supratidal facies-tract deposits tended to fill the available accommodation. Therefore, the basinward edge of the shelf-crest facies tract can be used as a shoreline proxy to track movements of sea level (*sensu* Pomar 1993), and steps landward overall in the TST and seaward in the HST, at both the CS and HFS scales. The proportion of shelf-crest facies, the abundance and size of tepees, and the thickness of individual shelf-crest bodies are used as interpretation criteria as follows: abundance should decrease in the TST and increase in the HST at the CS scale; thick, amalgamated, aggradational shelf-crest deposits should represent HFS-scale TSTs deposited during early CS-scale transgression or late highstand; and the aspect ratio of shelf-crest sediment bodies should be lower (narrower and thicker deposits) in the TST compared to the HST of a HFS or CS.

At the CS scale, shelf-crest facies tracts aggrade during relative sea-level rise (TST) and prograde strongly during relative sea-level fall (HST). For example, in the Yates TST, the downdip position of the shelf-crest facies tract below the MFS (Y1 and Y2) is virtually the same (Fig. 18). Above the MFS, as accommodation decreased (Y3 and Y4), the shelf crest prograded significantly. By contrast, Y5 is shifted only 500 m basinward of Y4, has an aggradational stacking pattern of component cycles, and thus records the first HFS of the subsequent CS. This pattern is repeated at the HFS scale, whereby shelf-crest deposits aggrade or step slightly landward systematically in each TST (circles to squares in Figure 18), whereas they are strongly seaward stepping in each HST (squares to circles in Figure 18).

Outer Shelf.—Because the deepest-water shelf deposits are found in the outer shelf, the maximum landward position of this facies tract is used as an important criterion for defining CS and HFS-scale MFSs.

An interesting phenomenon occurs at the HFS and CS scale, whereby in the TST the shelf crest retrogrades at the same time the shelf margin progrades, causing the dip width of the intervening outer-shelf facies tract to expand bidirectionally (squares in Figure 18). In addition, there is a general decrease in outer-shelf width upward through the Seven Rivers, and again through the Yates CS, to a point where the shelf-crest facies tract is nearly coincident with the shelf margin by SR4 and Y5 time (Fig. 18).

Paleoecology provides additional data for sequence-stratigraphic interpretation. Using the analogy between the Permian fusulinids and the modern alveolines, it is reasonable to infer that the peloid–fusulinid WS/PS in the outer-shelf facies tract represents water depths in the range of 12 to 35 m. The water-depth interpretation indicates that the stratal geometries observed in the outer shelf are dominantly depositional in origin.

In addition, by analogy with the modern alveolinid morphology, the stratigraphic change from the large *Polydiexodina* (greater length-to-thickness ratios) in the Seven Rivers and Yates Formations to the smaller *Yabeina, Codonofusiella,* and *Reichelina* (lower length-to-thickness ratios) in the lower Tansill Formation indicates a progressive shallowing of water in the outer-shelf high-energy facies tract through time. The overall upward increase in abundance of *Mizzia,* a dasycladacean alga common in higher-energy, back-reef deposits (Kirkland and Moore 1990), from the Seven Rivers through the Yates CS also supports a shallowing profile through time.

Shelf Margin.—The paleoecology of the shelf-margin reef facies has been studied by several workers (Adams and Frenzel 1950; Achauer 1969; Babcock 1977; Yurewicz 1976, 1977; Kirkland and Moore 1990; Melim 1991; Kirkland et al. 1993; Wood et al. 1994; Kirkland 1995). Although the sedimentology and paleoecology cannot be used to determine specific water depths for the reef, documented faunal changes from the lower to the upper Capitan are interpreted to represent a shallowing of the reef through time (Babcock and Yurewicz 1989). The paleoecologic data are consistent with the water-depth interpretations from on the sequence-stratigraphic framework (see also Kerans and Tinker 1998).

The shelf-margin facies tract was used in conjunction with other shelf data to help define the TST, HST, and MFS at both the HFS and CS scales. The shelf margin prograded when accommodation was limited, and when there was an underlying slope foundation over which to prograde. Such conditions existed in the TST and late HST of the CS (Fig. 18). The shelf margin aggraded during times of maximum transgression, when the margin was trying to keep up with the accommodation being created during relative sea-level rise. Such conditions existed in the late TST and early HST of the CS (Fig. 18). These progradation/aggradation data, and several other stratigraphic parameters that emphasize the dynamic, yet systematic nature of the Capitan system, are quantified and discussed below.

DISCUSSION

Dynamic Stratigraphic and Sedimentologic Variations

The stratigraphic evolution of the Capitan depositional system can be examined by quantifying (Table 3) and visualizing (Figs. 19–21) several key depositional parameters. The shelf-crest (sea level), shelf-margin (shelf/slope break), and outer-slope facies tracts were used as bathymetric ''tie points'' (*sensu* Pomar 1993; Franseen et al. 1993) to calculate the following key depositional parameters: progradation and aggradation (and associated offlap angle) of the shelf-crest and shelf-margin facies tract; distance from the shelf crest to reef; reef depth; outer-shelf dip angle; and lateral distance and depth from the shelf crest to the toe of slope. Definitions for each of these parameters are contained in the footnotes of Table 3.

The more important variations in these depositional parameters are summarized for the shelf crest and shelf margin in Figures 19–21. These variations emphasize the dynamic nature of the Capitan system, and indicate that depositional styles were not random but varied systematically in time and space as a function of the HFS position within the longer-term CS (Table 3; Figs. 8, 10, 17–21). This type of dynamic system has been observed by other workers in a variety of carbonate and siliciclastic sediment environments (e.g., Wilkinson 1975; Galloway 1986; Grotzinger 1986; Cross et al. 1993; Gardner 1993; Sonnenfeld and Cross 1993; Kerans et al. 1994; Kerans and Fitchen 1995).

In a general sense, during marine transgression at the CS scale, shelf-crest deposits were thinner and retrogradational, outer-shelf deposits expanded in width, and shelf-margin deposits aggraded and prograded to ''keep up'' with a rising sea level. Commonly there was simultaneous retrogradation of the shelf crest and progradation of the shelf margin (Fig. 19). During highstand at the CS scale, shelf-crest deposits amalgamated and prograded as they filled available space, outer-shelf deposits narrowed in width, and shelf-margin deposits prograded. This same general pattern is observed at the HFS scale but varies as a function of position within the CS.

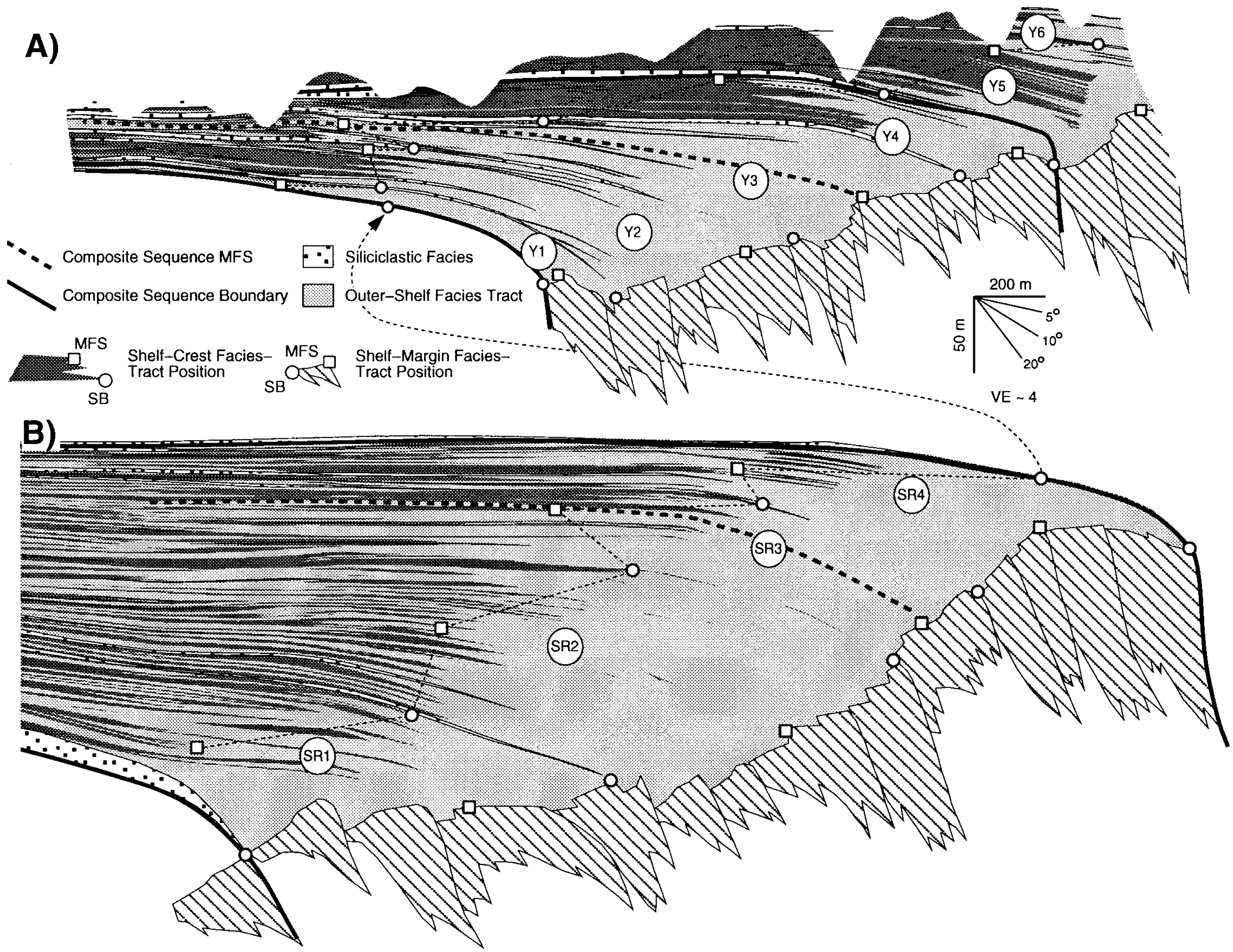

FIG. 18.—Generalized facies-tract distribution on the shelf in McKittrick Canyon. **A)** Y1–Y5 HFSs. **B)** Seven Rivers CS. The maximum basinward position of the shelf-crest facies and maximum landward position of the shelf-margin facies are marked for each HFS boundary (circles) and MFS (squares). Note the systematic backstepping of the shelf crest, broadening of the outer shelf, and aggradation of the shelf margin in the TST of each HFS (from circles to squares) and CS. The pattern is reversed in the HSTs (squares to circles). Note also the overall aggradational nature of the CS TST, and prodradational nature of the CS HST.

TABLE 3.—*Quantified Stratigraphic Data*

	Shelf Crest[1]							Shelf Margin[2]							Shelf Crest	Depth	Outer Shelf	Shelf Crest	Depth to	Composite
	Prograd.	Aggrad.	Pro/Agg	Offlap Angle[3]		Accum. Rate[4]		Prograd.	Aggrad.	Pro/Agg	Offlap Angle		Accum. Rate[5]		to Reef	of Reef	Dip[6]	to Basin[7]	Basin[8]	Sequence
	(meters)	(meters)		(degrees)	(vector)	HFS	(Bubnoffs)	(meters)	(meters)		(degrees)	(vector)	HFS	(Bubnoffs)	(meters)	(meters)	(degrees)	(meters)	(meters)	
Y5-HST	285	4	71	0.8		Y4	80	80	30	3	20.6		Y4	806	195	14	4.1	1387	618	
Y5-TST	288	28	10	5.6				235	38	6	9.2				405	41	5.8			SB
Y4-HST	432	-10	-43	-1.3		Y3	45	100	-9	-11	-5.1		Y3	650	446	44	5.6	1551	596	
Y4-TST	480	28	17	3.3				160	16	10	5.7				820	51	3.6			
Y3-HST	555	4	139	0.4		Y2	50	255	14	18	3.1		Y2	1142	1140	39	2.0	2280	593	MFS
Y3-TST	-255	16	-16	-3.6				200	28	7	8.0				1430	50	2.0			
Y2-HST	195	1	195	0.3		Y1	65	120	18	7	8.5		Y1	1206	1035	60	3.3	2139	601	
Y2-TST	-35	25	-1	-35.6				360	31	12	4.9				1045	70	3.8			
Y1-HST	275	-1	-275	-0.2		Y0	35	155	-15	-10	-5.5		Y0	476	645	76	6.7	1998	576	
Y1-TST	-285	15	-19	-3.0				35	6	6	9.7				765	63	4.7			SB
SR4-HST	855	-6	-143	-0.4		SR4	48	420	-15	-28	-2.0		SR4	1439	420	49	6.7	1889	576	
SR4-TST	-75	25	-3	-18.4				155	45	3	16.2				855	41	2.7			
SR3-HST	585	4	146	0.4		SR3	118	160	23	7	8.2		SR3	637	605	63	5.9	2350	568	MFS
SR3-TST	-220	43	-5	-11.1				90	26	3	16.1				1035	81	4.5			
SR2-HST	590	40	15	3.9		SR2	253	300	50	6	9.5		SR2	1999	730	64	5.0	2374	534	
SR2-TST	85	61	1	35.7				495	34	15	3.9				975	73	4.3			
SR1-HST	605	23	26	2.2		SR1-HFS	58	395	19	21	2.8		SR1-HFS	2566	560	45	4.6	2350	459	
SR1-TST								630	34	19	3.1				765	43	3.2			

(1) **Shelf Crest** (sea level proxy) is defined as the downdip limit of the shelf crest facies tract.
(2) **Shelf Margin** is defined as the updip limit of the shelf margin facies tract.
(3) **Offlap Angle** is illustrated in Figure 19, and is positive during times of prograding stratigraphic rise, and negative during times of prograding stratigraphic fall or retrograding stratigraphic rise.
(4) **Accumulation Rate** is the rate of sediment accumulation (Bubnoffs; meters/1000 years) calculated assuming a 400 k.y. HFS duration. Shelf Crest accumulation assumes horizontal time lines and vertical growth (sum of the aggradation component; Fig. 23).
(5) **Accumulation Rate** calculation for the shelf margin assumes dipping time lines and lateral growth (accounts for both the aggradation and progradation component; Fig. 23).
(6) **Outer Shelf Dip** is the primary stratigraphic dip angle of the outer shelf, measured along a vector from the shelf crest to the shelf margin (see Fig. 21).
(7) **Shelf Crest to Basin** is the horizontal distance from the shelf crest to the toe of slope (a point where where the basinward dip is less than ~5°).
(8) **Depth to Basin** is the vertical distance from the shelf crest to the toe of slope.

Summary by Composite Sequence

	Shelf Crest					Shelf Margin				
	Pro (m)	Agg (m)	Pro/Agg	Pro (%)	Agg (%)	Pro (m)	Agg (m)	Pro/Agg	Pro (%)	Agg (%)
Yates HST	1467	22	66.7	108%	28%	515	21	24.5	37%	24%
Yates TST	-105	56	-1.9	-8%	72%	870	68	12.8	63%	76%
7R HST	1365	23	59.3	56%	12%	735	53	13.9	28%	25%
7R TST	1060	167	6.3	44%	88%	1910	163	11.7	72%	75%

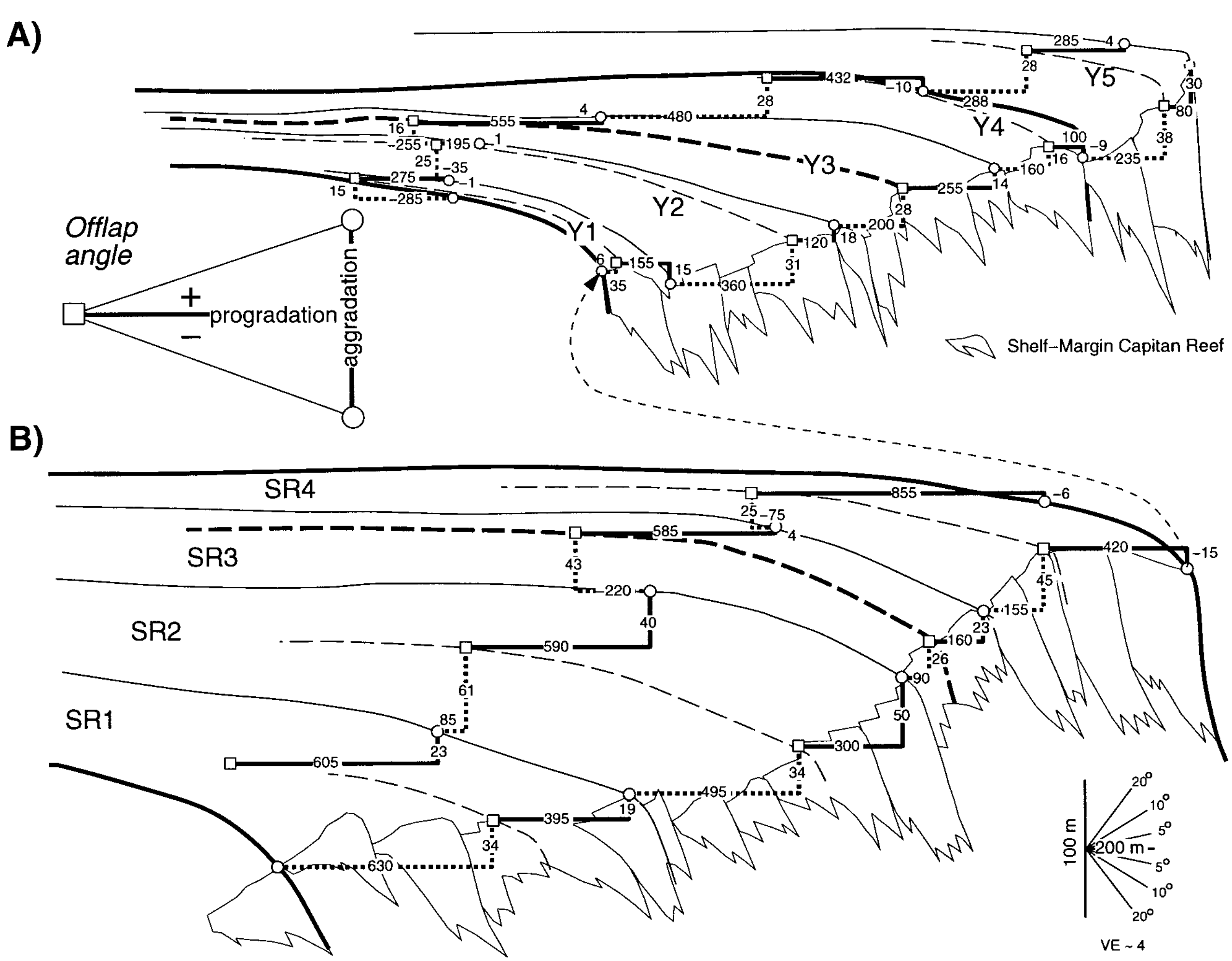

Shelf Crest

For each HFS, offlap angle and aggradation are greater in the TST than the HST.

In the TSTs of SR3, SR4, Y1, Y2, and Y3, the dip width of the outer shelf expands bidirectionally.

Shelf Margin

For every HFS except SR2, offlap angle and aggradation are greater in the TST than in the HST.

The P/A ratio of each HFS decreases toward the composite–sequence MFS, and then increases toward the upper composite–sequence boundary; concurrently the offlap angle increases and then decreases.

Fig. 19.—Method for determining progradation and aggradation distances of the shelf crest and shelf margin. Circles and squares are from Figure 18. Positive numbers represent basinward shifts or positive aggradation; negative numbers represent landward shifts or negative aggradation. Offlap angle is the angle between a horizontal line and the vector connecting a circle and square (see Table 3). Systematic changes are noted to the right of figure.

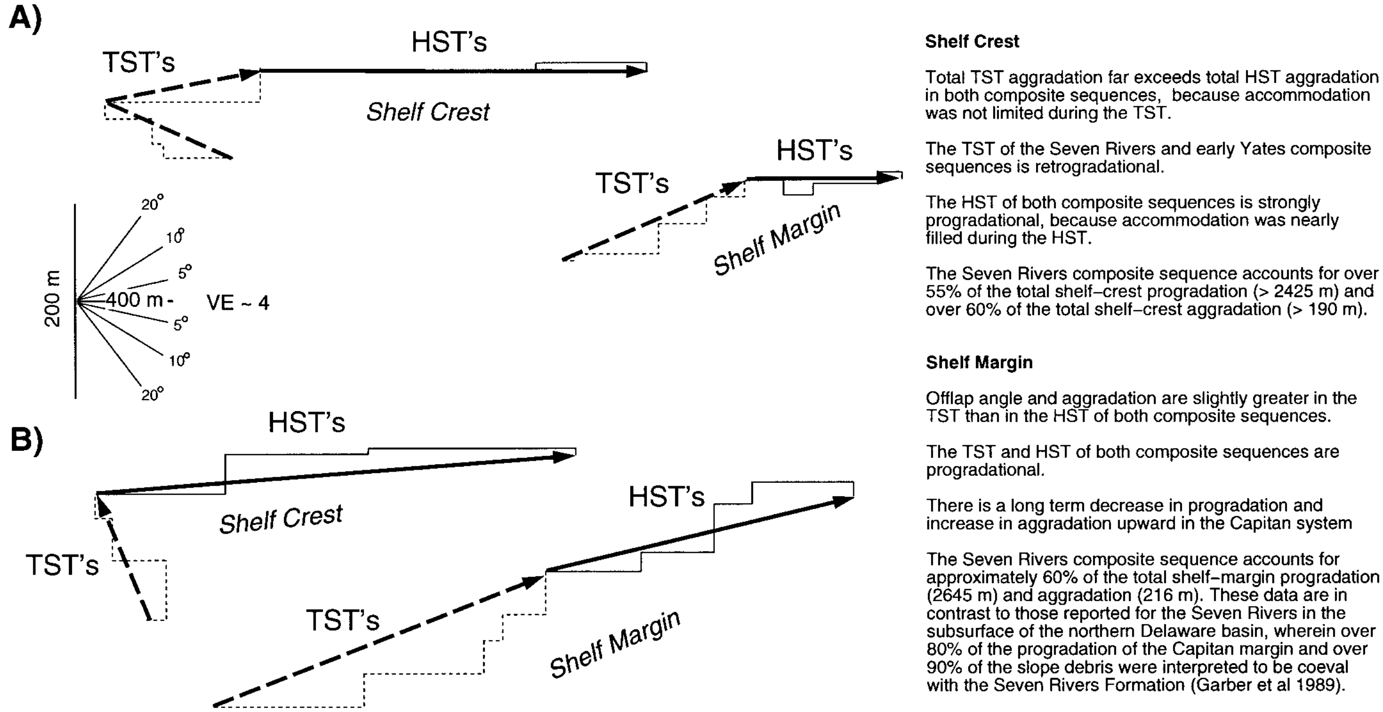

FIG. 20.—The dashed (TST) and solid (HST) lines from Figure 19 have been consecutively stacked to illustrate the cumulative TST and HST components for each CS. Note the simultaneous retrogradation/aggradation of the shelf crest and progradation/aggradation of the shelf margin during marine transgression (TST). Systematic changes are noted to the right of figure.

In addition to the variations highlighted by the depositional parameters (Figs. 19–21), several other systematic variations warrant mention.

(1) Low-energy facies dominate the HFS TST, whereas higher-energy facies dominate the HFS HST. This is interpreted to be the result of higher-energy wave and tidal currents in the shallow-water deposits of the HST.

(2) Individual cycles are easier to define in the Seven Rivers CS (Fig. 14) because accommodation conditions favored high-frequency subtidal–supratidal facies alternations. By contrast, in the Yates CS (Fig. 15) accommodation conditions favored amalgamation of fusulinid facies in the subtidal setting (Y2, Y3), and of pisolite facies in the supratidal setting (Y4, Y5).

(3) Shelf-crest facies-tract deposits amalgamated and aggraded (up to 30 m) when the TST of a HFS was in phase with the HST of a CS (TST of SR4, Y4) because HFS-scale transgression created the necessary accommodation for aggradation (Fig. 18; see also Kerans and Harris 1992). By contrast, when the HST of a HFS was in phase with the HST of a CS (HST of SR4, Y4), accommodation was limited, and shelf-crest deposits were thinner and prograded basinward. Regardless of position within the HFS, shelf-crest facies-tract deposits are commonly thin and discrete, and often backstep in the TST of a CS (SR1, SR2, SR3, Y1, Y2, and Y3), owing to conditions of high accommodation. The exception is Y5, which contains a significant thickness of aggradational shelf-crest facies deposited in the first HFS of the Tansill composite sequence.

(4) When the HSTs of a HFS and composite sequence were in phase (SR4 and Y5), the dip width of the outer-shelf facies tract was compressed, outer-shelf facies diversity was great, much of the outer shelf accommodation was filled, and the likelihood of protracted subaerial exposure of the shelf crest was maximized (Figs. 8, 10).

(5) During HFS transgression, facies in the outermost shelf were dominantly aggradational or backstepping, and shelf-margin facies were aggradational, as sediment production tried to keep pace with increasing accommodation created by rising relative sea level. During HFS highstand, sediment production rates exceeded available accommodation, and facies in the outer-shelf and shelf margin were dominantly progradational, as indicated by the progradation:aggradation ratios (Table 3; Figs. 8, 19).

(6) The negative progradation:aggradation ratios recorded in the HST of SR4 represent a time of downstepping or stratigraphic fall (Table 3; Fig. 19). This stratigraphic signature can be indicative of extremely limited accommodation caused by relative sea-level fall (see also Sonnenfeld and Cross 1993). When combined with other stratigraphic and facies data, this geometry supports the interpretation of the upper Seven Rivers composite-sequence boundary.

(7) The Y1 HFS can be interpreted either as the last HFS of the Seven Rivers CS, deposited as a shelf-margin systems tract (*sensu* Van Wagoner et al. 1988) during relative sea-level fall, or as the first HFS of the Yates CS, deposited during the initial Yates transgression, which was not of sufficient magnitude to completely flood the shelf (Fig. 8). Although the depositional environment would be similar in either interpretation, the major Yates CS boundary would be above Y1 in the first interpretation and below Y1 in the second interpretation. Geochemical stratigraphy (Fig. 16) supports the second interpretation.

(8) Although mud- and silt-dominated rocks (OS1-OS3) represent only a minimal volume of the outer-shelf facies tract (Fig. 13), they are significant because 60–80% of the time they are preserved within the TST of a HFS (Fig. 8).

(9) The Seven Rivers CS contains a greater volume of subtidal deposits than does the Yates CS, because outer-shelf accommodation was greater (Fig. 8).

These variations illustrate that care must be taken when applying interpretations from a limited geographic window to a basin-wide scale. Similarly, using the detailed facies architecture interpretations as an analog for interpretation of older or younger stratigraphic units must be done with care.

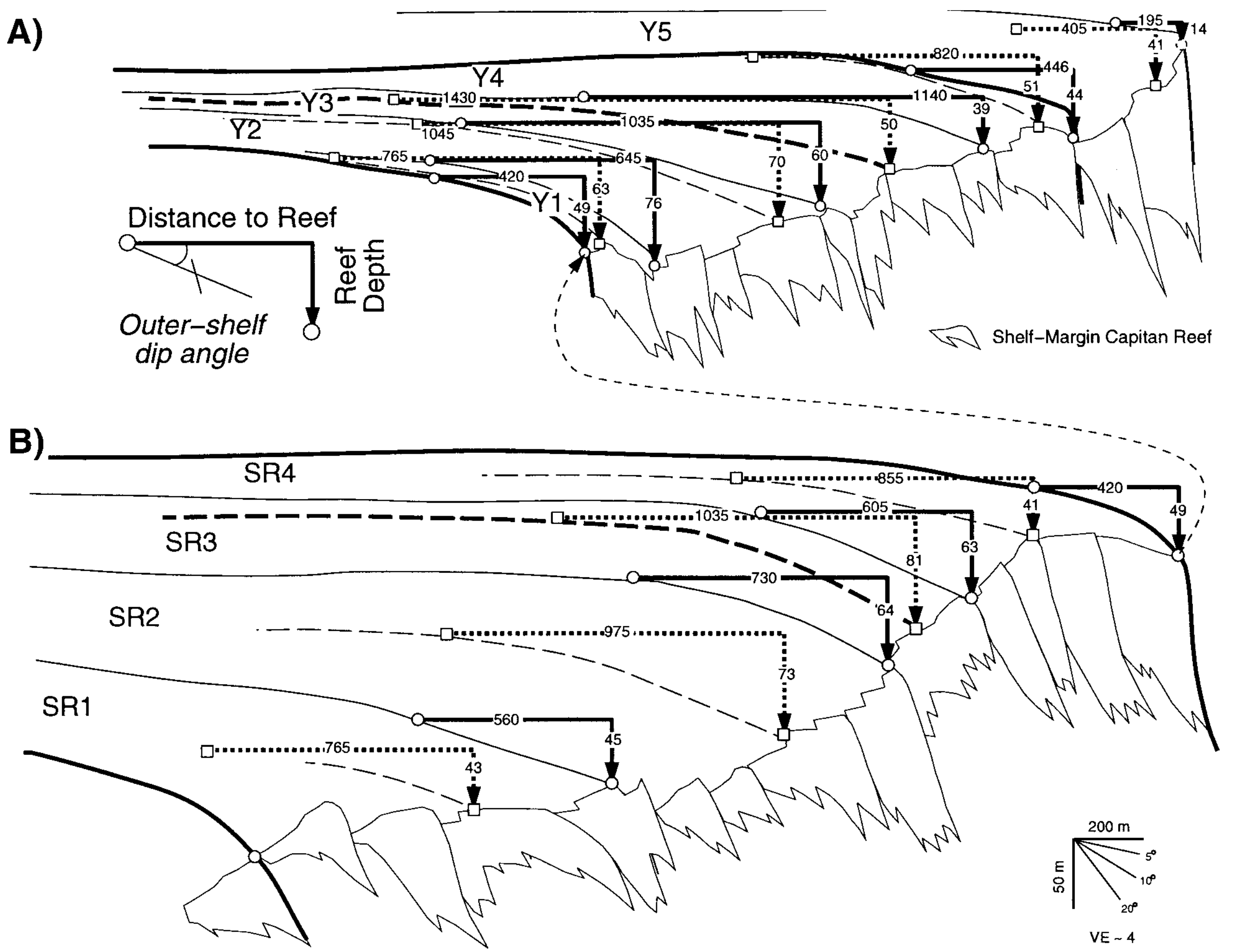

The distance from shelf crest to reef is greater at the MFS than the sequence boundary of every HFS.

The depth to reef increases in the TST and decreases in the HST of the Seven Rivers and Yates composite sequences.

The outer–shelf dip angle ranges from 2 to 7 degrees, and tends to decrease at the MFS and increase at the sequence boundary of a composite sequence.

There is an overall decrease in reef depth, distance to outer shelf from SR1 through Y4, and outer shelf dip angle.

Fig. 21.—Method for determining distances from the shelf crest to the shelf margin, and reef depths. Circles and squares are from Figure 18. These numbers are represented in Table 3. Systematic changes are noted to the right of figure.

Paleobathymetric Models

Although the Capitan depositional system has been studied extensively, the interpretation of its paleobathymetric profile remains somewhat controversial. There are two viable end-member models, the marginal mound and the barrier reef. Early investigators converged on a barrier-reef hypothesis (Crandall 1929; Lloyd 1929), and later studies supported this model (Newell et al. 1953; Hayes 1957, 1964; Boyd 1958). Dunham (1972) argued for a marginal-mound hypothesis, for which he gave credit to Lang (1937). In this model, shallow-subtidal carbonate grainstones were deposited downdip from topographically high, intertidal to supratidal, shelf-crest deposits. Subsequent workers in the 1970s and 1980s tended to support the marginal-mound hypothesis (Babcock 1977; Pray 1977; Yurewicz 1977; Hurley 1978, 1979, 1989). However, Kirkland and Moore (1990) and Kirkland (1995) resurrected a modified version of the barrier-reef model on the basis of studies of the upper Yates and Tansill-equivalent reef and outer shelf. Saller (1996) argued in support of this revision. Hunt et al. (1995) proposed a flat-topped platform created prior to ''differential compaction-induced subsidence'', resulting in toplap geometries.

The critical issue regarding paleobathymetry is whether the present-day outer-shelf dip is primary or secondary. If the paleobathymetric profile was a marginal mound and the outer-shelf basinward dips are primary, then the facies and stratigraphic architecture of the outer shelf should indicate a progressive deepening towards the margin. If the paleobathymetric profile was a barrier reef (flat-topped platform), and the outer-shelf dip was caused by syndepositional or postdepositional tilting of once flat-lying outer-shelf beds (Smith 1973) or early differential compaction of the underlying slope (Hunt et al. 1995, Saller 1996), then the opposite relationships should be found.

Data from McKittrick Canyon indicate that the Capitan paleobathymetric profile was a marginal mound. However, the depth to the top of the shelf margin and associated outer-shelf dips increased and then decreased substantially within each CS, and decreased overall from the Seven Rivers through the Tansill, such that by Tansill time the shelf-margin reef was deposited in relatively shallow water. Key observations and interpretations include: (1) the progression from high-energy, supratidal-capped cycles in the shelf crest to lower-energy, subtidal-capped, fusulinid-rich cycles in the outer shelf (Figs. 8, 9), which would not exist in a flat-topped model; (2) an expansion of cycle-set thickness downdip across the outer shelf (Figs. 9, 11, 12), which could not exist in a flat-topped model; (3) *systematic* changes in progradation and aggradation, offlap angles, shelf crest to reef distance, reef depth, and outer-shelf dip angle at both the HFS and CS scale that can be correlated around the basin (Osleger 1998; Osleger and Tinker in press), resulting in a stratigraphic organization that would be very difficult to produce with postdepositional tilting or differential compaction; (4) outer-shelf water depths in the range of 12 to 35 m on the basis of analogy with the modern alveolinids, and reef water depths ranging from 14 to 81 m; (5) oriented fusulinid grainstones near the shelf margin, indicating mobilization and probable sediment-gravity-flow transport of fusulinids into water depths greater than 12–35 m; (6) the abundance of the shallow reef indicator *Mizzia* in the upper Yates and Tansill CSs relative to the Seven Rivers CS, indicating progressive shallowing of the Capitan system; (7) the decrease in percent dolomite from the shelf crest to the shelf margin (also see Melim 1991); and (8) the absence of true toplap stratal geometries. Differential compaction or postdepositional tilting of an original flat-topped shelf-margin barrier reef system cannot explain this combination of facies and stratigraphic data.

Testing An Alternative Model.—If the differential compaction model were viable, then the late Yates HFSs, which were deposited above slope clinoforms with nearly 400 m of total relief, should have compacted more than the early Seven Rivers HFSs, which were deposited above clinoforms with less than 150 m of relief, resulting in greater outer-shelf dips in the upper Yates. The opposite is observed (Table 3; Fig. 21).

To test the postdepositional compaction hypothesis, the mechanics of differential compaction were examined graphically with data from a 50–100-m thick interval in the SR2 HFS. This type of analysis requires translation of photo thickness to true vertical thickness. Present-day stratal geometries illustrate the outer-shelf dip and proportional bed-thickness expansion from the shelf crest to the shelf margin (Fig. 22A, B). The same cycle thickness is illustrated for a ''barrier reef'' model (Fig. 22C). The vertical compaction vectors necessary to change the lower, pre-compaction boundary in the barrier-reef model (L2) to the observed geometry (L1) are illustrated in Figure 22D. The same compaction history, even if it was very early, must also have acted on the upper surface (U2) of the barrier-reef model. However, when the vertical differential compaction vectors determined for the lower barrier-reef boundary are applied to its upper surface (U2), the result (U?, Fig. 22E) looks nothing like the observed bedding clinoforms (U1, Fig. 22B). This simple data-driven graphic illustrates the untenable nature of the compaction hypothesis when applied to the Seven Rivers and Yates CSs in McKittrick Canyon.

Sediment Accumulation Rates, Sites, and Variation

Sediment accumulation volumes are controlled by the ratio of accommodation to sediment supply (e.g., Swift and Thorne 1991; Cross et al. 1993). In a simple system, as the ratio of accommodation to sediment supply decreases, the volume of sediment that can be accumulated at a given geographic/bathymetric location decreases, because more sediment is available than space. This commonly results in progradation. By contrast, when the accommodation:sediment supply ratio increases, the volume of sediments that can accumulated at a given geographic/bathymetric location increases. This can result in aggradation or backstepping.

In terms of direct comparative value, sedimentation-rate calculations are limited, because they require an estimate of the depositional duration for each stratigraphic interval of interest. Assuming that the late Guadalupian represents approximately 2 to 3 my (Ross and Ross 1987), each of the eight Seven Rivers and Yates HFSs represent from 250 to 375 ky. Accumulation rates, uncorrected for compaction or missing rock, were calculated in McKittrick Canyon along a vector perpendicular to growth direction in all locations (Fig. 23). To be conservative, values were calculated using a 400 ky duration for each HFS.

Results indicate that Seven Rivers accumulation rates are generally greater than Yates accumulation rates (Fig. 23). This can be explained, in part, by the fact that Yates HFSs contain significantly more accommodation-limited shelf-crest supratidal facies than do the Seven Rivers HFSs, resulting in considerably greater periods of slow deposition, nondeposition, or erosion. Particularly noteworthy is that the shelf-margin accumulation rates are at least one order of magnitude greater than those calculated for the outer shelf (Fig. 23).

The sediment accumulation data from McKittrick Canyon are significant for two reasons. First, the high accumulation rates in the outer shelf and especially the shelf margin (20–80 m water depth), relative to the middle shelf and shelf crest ($<$ 10 m water depth), are significantly different from commonly accepted models that report the greatest sedimentation rates in the warm, shallow waters of the inner to middle shelf (e.g., Tucker and Wright 1990; Enos 1991). It is important to emphasize that most of the sediment accumulated in the outer shelf was locally sourced, and not transported to the outer shelf from the middle or inner shelf. Second, sediment accumulation rates in dominantly subtidal settings, such as the outer shelf in McKittrick Canyon, were high in both the TST and the HST, which contrasts with many reports of HST-dominated production for other carbonate shelf models (e.g., Coogan 1969; Wilson 1975; James 1979, 1984; Wilkinson 1982; Sarg 1995).

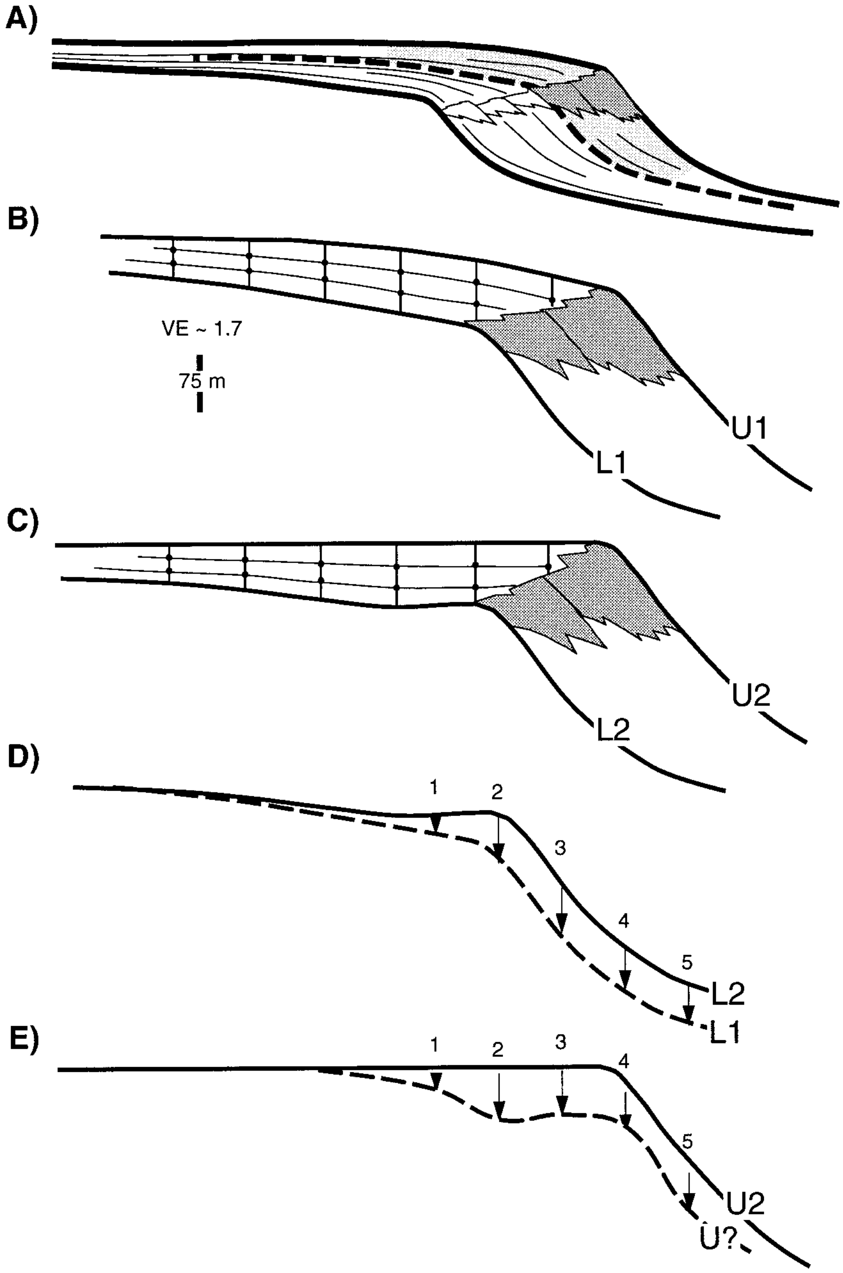

FIG. 22.—Illustration of the inability of differential compaction to explain outer-shelf dip geometries. **A)** SR2 HFS with HST detail area shown in (B) shaded light gray and shelf margin shaded dark gray. **B)** Detail area from (A) showing observed stratal geometries and bed thickness relationships. L1 is lower bounding surface and U1 is upper bounding surface. Three cycle sets are illustrated. **C)** Reinterpretation of (B) using same thickness but with a pre-compaction, ''barrier-reef'' geometry. L2 and U2 are the pre-compaction lower and upper bounding surfaces for this model. **D)** Vertical differential compaction vectors necessary to change L2 pre-compaction geometry to L1 observed geometry. **E)** Vertical differential compaction vectors from (D) applied to U2 result in U?, which does not resemble the U1 observed geometry at all, but should if the compaction model were valid.

CONCLUSIONS

The sequence-stratigraphic interpretation presented in this work documents a high degree of stratigraphic order in the Capitan depositional system, reflected by systematic changes in facies distributions, facies proportions, stratal geometries, and progradation:aggradation ratios. These parameters were quantified using a 2-D facies distribution and stratal geometry ''map'' of the 5-km continuous outcrop wall in North McKittrick Canyon, and would be difficult to work out from a more limited stratigraphic or geographic window. The sequence-stratigraphic interpretation resulted in a revised outer shelf and shelf-to-basin correlation (see Tinker 1996b for a detailed description of shelf-to-basin stratigraphic correlations; compare Figure 3 to the frequently referenced cross sections of King 1948 and Garber et. al. 1989).

The systematic evolution documented in McKittrick Canyon is hierarchical (repeated at several scales). Within a high-frequency sequence (HFS), the dip width of the shelf-crest facies tract decreases upward to the maximum flooding surface (MFS) and increases upward to the HFS boundary, whereas the dip width of the outer-shelf facies tract and the angle of outer-shelf basinward dip increase upward to the MFS and decrease upward to the upper sequence boundary. This pattern is repeated at the CS scale. The aspect ratios of shelf-crest sediment bodies tend to be lower (narrower and thicker deposits) in the transgressive systems tract (TST) than in the highstand systems tract (HST) of HFSs and CSs. The progradation/aggradation ratio decreases toward the MFS and then increases toward the upper sequence boundary at both the HFS and CS scales. The distance from shelf crest to reef and the interpreted water depth to the reef is greater in the TST than the HST of HFSs and CSs.

The sequence-stratigraphic interpretation in McKittrick Canyon provides several important results. First, all of the data, including facies associations, cyclicity, stratal geometry, and paleoecology, support a marginal-mound

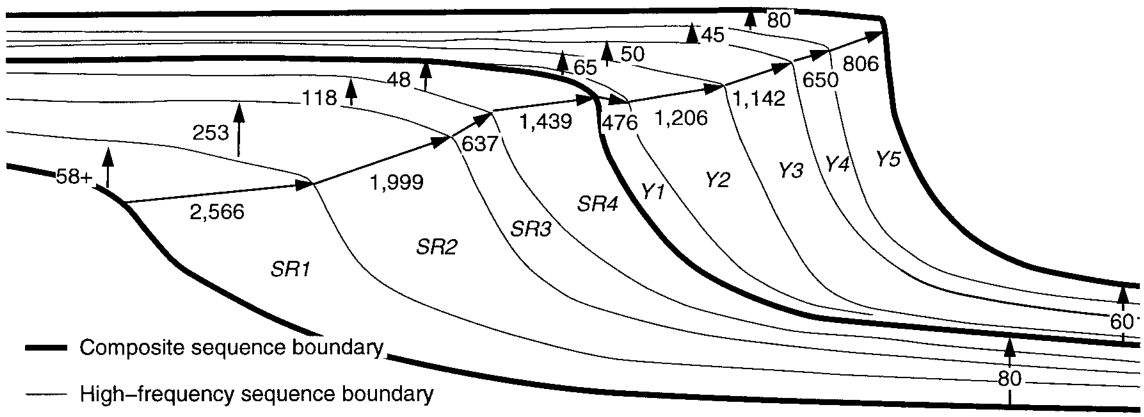

FIG. 23.—Accumulation rates, uncorrected for compaction or missing rock, calculated along a vector perpendicular to interpreted growth direction. Values are based on an estimated 400 ky HFS duration, and reported in Bubnoffs (μm/yr; mm/1000 yr).

depositional model in which the shelf-margin reef is located downdip from the shelf-crest facies tract. However, there was an initial increase and then decrease in water depth at the shelf margin within each composite sequence, and an overall decrease in water depth from Seven Rivers through Tansill time. Second, predictable variations in the quantified depositional parameters such as progradation, aggradation, offlap angle, outer-shelf dip, water depth, and distance between facies tracts emphasize the dynamic yet systematic nature of the Capitan system. A stratigraphic hierarchy similar to that from McKittrick Canyon has been documented along strike (Osleger and Tinker in press), which strengthens the overall interpretation and helps document the basinwide evolution of the Capitan system. Third, the most active sediment production and accumulation sites were located in the subtidal, outermost-shelf and shelf-margin facies tracts of both the TST and HST. This is significantly different from commonly accepted models that report the greatest sedimentation rates in the warm, shallow ($<$ 10 m) waters of the inner and middle shelf (e.g., Tucker and Wright 1990; Enos 1991). Fourth, the high accumulation rates support the possibility of a relatively complete shelf-margin sedimentation and accumulation record, which results in a comparatively equal (''symmetrical'') TST and HST sediment-preservation record on the shelf and across the shelf margin. This record is different from many asymmetric, HST-dominated shoaling-upward carbonate sedimentation models (e.g., Coogan 1969; Wilson 1975; James 1979, 1984; Wilkinson 1982; Sarg 1995). Finally, the 2-D cycle hierarchy, facies distributions, and general timing of siliciclastic sediment bypass into the basin can be worked out from vertical 1-D data. However, in contrast to flat or low-angle ramps and shelves, the 2-D prediction of facies and stratal geometries in a shelf-margin setting requires a depositional model that includes information regarding the paleobathymetric profile.

ACKNOWLEDGMENTS

I would like to thank Marathon Oil Company for permission to publish this work, and for financial support for the color figures, fieldwork, and laboratory work. Sincere thanks to the following: the staff at Guadalupe National Park, especially Fred Anderson, and the staff at the Lincoln National Forest, for permission to conduct field work in McKittrick Canyon; David Budd, Charlie Kerans, Mark Sonnenfeld, Neil Hurley, Emily Stoudt, Julie Kupecz, Laura Zahm, and John Southard for thoughtful reviews and excellent suggestions for improvement of the manuscript; Jerry Lucia and Charlie Kerans at the Texas Bureau of Economic Geology for providing the original helicopter photographs; D. Henry at Digital Video Productions for the final mosaic created in PHOTOSHOP™; Charlie Kerans and Lisë Brinton for lively discussions in the field; field assistants Mark Tinker, Chris Stephenson, Allyson Tinker, and Clint Cowan; David Budd and Scott Raymond for support during crunch time; and Allyson, Nathan, Derek, and Tyler, too.

REFERENCES

ACHAUER, C.W., 1969, Origin of Capitan Formation, Guadalupe Mountains, New Mexico and Texas: American Association of Petroleum Geologists, Bulletin, v. 53, p. 2314–2323.

ADAMS, J.E., AND FRENZEL, H.N., 1950, Capitan barrier reef, Texas and New Mexico: Journal of Geology, v. 58, p. 289–312.

ALLEN, J.R., AND MATTHEWS, R.K., 1982, Isotope signatures associated with early meteoric diagenesis: Sedimentology, v. 29, p. 797–817.

BABCOCK, J.A., 1977, Calcareous algae, organic boundstones, and the genesis of the Upper Capitan Limestone (Permian, Guadalupian), Guadalupe Mountains, West Texas and New Mexico, *in* Hileman, M.E., and Mazzullo, S.J., eds., Upper Guadalupian Facies, Permian Reef Complex, Guadalupe Mountains, New Mexico and West Texas: 1977 Field Conference Guidebook, v. 1, Permian Basin Section SEPM, Publication 77–16, p. 3–44.

BABCOCK, J.A., AND YUREWICZ, D.A., 1989, The massive facies of the Capitan Limestone, Guadalupe Mountains, Texas and New Mexico, *in* Harris, P.M., and Grover, G.A., eds., Subsurface and Outcrop Examination of the Capitan Shelf Margin, Northern Delaware Basin: SEPM, Core Workshop 13, p. 365–372.

BEBOUT, D.G., AND KERANS, C., eds., 1993, Guide to the Permian Reef Geology Trail, McKittrick Canyon, Guadalupe Mountains National Park, West Texas: Texas Bureau of Economic Geology, Guidebook 26, 48 p.

BORER, J.M., AND HARRIS, P.M., 1989, Depositional facies and cycles in Yates Formation outcrops, Guadalupe Mountains, New Mexico, *in* Harris, P.M., and Grover, G.A., eds., Subsurface and Outcrop Examination of the Capitan Shelf Margin, Northern Delaware Basin: SEPM, Core Workshop 13, p. 305–317.

BORER, J.M., AND HARRIS, P.M., 1991, Facies and cyclicity of the Yates Formation, Permian Basin: Implications for reservoir heterogeneity: American Association of Petroleum Geologists, Bulletin, v. 75, p. 726–779.

BOYD, D.W., 1958, Permian sedimentary facies, central Guadalupe Mountains, New Mexico: New Mexico Bureau of Mines and Mineral Resources, Bulletin 49, 100 p.

BROWN, A.A., AND LOUCKS, R.G., 1993, Influence of sediment type and depositional processes on stratal patterns in the Permian basin-margin Lamar limestone, McKittrick Canyon, Texas, *in* Loucks, R.G., and Sarg, J.F., eds., Carbonate Sequence Stratigraphy: Recent Developments and Applications: American Association of Petroleum Geologists, Memoir 57, p. 435–474.

CANDELARIA, M.P., 1982, Sedimentology and depositional environment of Upper Yates Formation siliciclastics (Permian, Guadalupian), Guadalupe Mountains, southeast New Mexico [unpublished M.S. thesis]: University of Wisconsin, Madison, Wisconsin, 267 p.

CHOQUETTE, P.W., AND PRAY, L.C., 1970, Geologic nomenclature and classification of porosity in sedimentary carbonates: American Association of Petroleum Geologists, Bulletin, v. 54, p. 207–250.

COOGAN, A.H., 1969, Recent and ancient carbonate cyclic sequences, *in* Cyclic Sedimentation in the Permian Basin, 1st Edition: Midland, Texas, West Texas Geological Society, p. 5–27.

CRANDALL, K.H., 1929, Permian stratigraphy of southeastern New Mexico and adjacent parts of western Texas: American Association of Petroleum Geologists, Bulletin, v. 13, p. 927–944.

CREVELLO, P.D., 1991, High-frequency carbonate cycles and stacking patterns: interplay of orbital forcing and subsidence on Lower Jurassic rift platforms, High Atlas, Morocco, *in* Franseen, E.K., Watney, W.L., Kendall, C.G.St.C., and Ross, W., eds., Sedimentary Modeling: Computer Simulations and Methods for Improved Parameter Definition: Kansas Geological Survey, Bulletin 233, p. 207–230.

CROSS, T.A., BAKER, M.R., CHAPIN, M.A., CLARK, M.S., GARDNER, M.H., HANSON, M.S., LESSENGER, M.A., LITTLE, L.D., MCDONOUGH, K.J., SONNENFELD, M.D., VALASEK, D.W., WILLIAMS, M.R., AND WITTER, D.N., 1993, Applications of high-resolution sequence stratigraphy to reservoir analysis, *in* Eschard, R., and Doligez, B., eds., Subsurface Reservoir Characterization from Outcrop Observations: 7th Institute of French Petroleum Exploration and Production Conference, Proceedings, p. 11–33.

DRUMMOND, C.N., AND WILKINSON, B.H, 1993; Carbonate cycle stacking patterns and hierarchies of orbitally forced eustatic sea level change: Journal of Sedimentary Petrology, v. 63, p. 369–377.

DUNHAM, R.J., 1962, A classification of carbonate rock types according to depositional texture, *in* Ham, W.E., ed., Classification of Carbonate Rocks: American Association of Petroleum Geologists, Memoir 1, p. 108–122.

DUNHAM, R.J., 1972, Capitan Reef, New Mexico and Texas: facts and questions to aid interpretation and group discussion: Society of Economic Paleontologists and Mineralogists, Permian Basin Section, Publication 72–14, 291 p.

EMBRY, A.F., AND KLOVAN, J.E., 1971, A late Devonian reef tract on northeastern Banks Island, N.W.T.: Bulletin of Canadian Petroleum Geology, v. 19, p. 730–781.

ENOS, P., 1991, Sedimentary parameters for computer modeling, *in* Franseen, E.K., Watney, W.L., Kendall, C.G.St.C., and Ross, W., eds., Sedimentary Modeling: Computer Simulations and Methods for Improved Parameter Definition: Kansas Geological Survey, Bulletin 233, p. 63–99.

ESTEBAN, M., AND PRAY, L.C., 1983, Pisoids and pisolite facies (Permian), Guadalupe Mountains, New Mexico and West Texas, *in* Peryt, T.M., ed., Coated Grains: New York, Springer-Verlag, p. 503–537.

FITCHEN, W.M., STARCHER, M.A., BUFFLER, R.T., AND WILDE, G.L., 1995, Sequence stratigraphic framework of lower Permian carbonate platform margins, Sierra Diablo, west Texas, *in* Garber, R.A., and Lindsay, R.F., eds., Wolfcampian–Leonardian Shelf Margin Facies of the Sierra Diablo—Seismic Scale Models for Subsurface Exploration: West Texas Geological Society, Publication 95–97, p. 23–66.

FRANSEEN, E.K., GOLDSTEIN, R.H., AND WHITESELL, T.E., 1993, Sequence stratigraphy of Miocene carbonate complexes, Las Negras area, southeastern Spain: implications for quantification of changes in relative sea level, *in* Loucks, R.G., and Sarg, J.F., eds., Carbonate Sequence Stratigraphy: Recent Developments and Applications: American Association of Petroleum Geologists, Memoir 57, p. 409–434.

GALLOWAY, W.E., 1986, Reservoir facies architecture of microtidal barrier systems: American Association of Petroleum Geologists, Bulletin, v. 70, p. 787–808.

GARBER, R.A., GROVER, G.A., AND HARRIS, P.M., 1989, Geology of the Capitan shelf margin—subsurface data from the northern Delaware basin, *in* Harris, P.M., and Grover, G.A., eds., Subsurface and Outcrop Examination of the Capitan Shelf Margin, Northern Delaware Basin: SEPM, Core Workshop 13, p. 3.

GARCÍA-MONDÉJAR, J., AND FERNÁNDEZ-MENDIOLA, A., 1993, Sequence stratigraphy and systems tracts of a mixed carbonate and siliciclastic platform-basin setting: the Albian of Lunada and Soba, northern Spain: American Association of Petroleum Geologists Bulletin, v. 77, p. 245–275.

GARDNER, M.H., 1992, Sequence stratigraphy of eolian-derived turbidites: deep water sedimentation patterns along an arid carbonate platform and their impact on hydrocarbon recovery in Delaware Mountain Group reservoirs, West Texas, *in* Mruk, D.H., and Curran, B.C., eds., Permian Basin Exploration and Production Strategies: Applications of Sequence Stratigraphic and Reservoir Characterization Concepts: West Texas Geological Society, Symposium 92–91, p. 7–11.

GARDNER, M.H., 1993, Sequence stratigraphy of upper Ferron sandstone member of the Mancos shale, east central Utah [unpublished Ph.D. thesis]: Colorado School of Mines, Golden Colorado, 528 p.

GARDNER, M.H., AND SONNENFELD, M.D., 1996, Stratigraphic changes in facies architecture of the Permian Brushy Canyon Formation in Guadalupe Mountains National Park, west Texas *in* DeMis, W.D., and Cole, A.G., eds., The Brushy Canyon Play in Outcrop and Subsurface: Concepts and Examples: SEPM Permian Basin Section, Publication 96-38, p. 17–40.

GIVEN, R.K., AND LOHMANN, K.C, 1986, Isotopic evidence for the early meteoric diagenesis of the reef facies, Permian Reef Complex of West Texas and New Mexico: Journal of Sedimentary Petrology, v. 56, p. 183–193.

GOLDHAMMER, R.K., DUNN, P.A., AND HARDIE, L.A., 1990, Depositional cycles, composite sea-level changes, cycle stacking patterns, and the hierarchy of stratigraphic forcing: Examples from Alpine Triassic platform carbonates: Geological Society America, Bulletin, v. 102, p. 535–562.

GOLDHAMMER, R.K., LEHMANN, P.J., AND DUNN, P.A., 1993, The origin of high-frequency platform carbonate cycles and third-order sequences (Lower Ordovician El Paso Gp, west Texas): constraints from outcrop data and stratigraphic modeling: Journal of Sedimentary Petrology, v. 63, p. 318–359.

GROTZINGER, J.P., 1986, Cyclicity and paleoenvironmental dynamics, Rocknest platform, northwest Canada: Geological Society of America, Bulletin, v. 97, p. 1208–1231.

HARRIS, P.M., KERANS, C., AND BEBOUT, D.G., 1993, Ancient outcrop and modern examples of platform carbonate cycles—implications for subsurface correlation and understanding reservoir heterogeneity, *in* Loucks, R.G., and Sarg, J.F., eds., Carbonate Sequence Stratigraphy: Recent Developments and Applications: American Association of Petroleum Geologists, Memoir 57, p. 475–492.

HAYES, P.T., 1957, Geology of the Carlsbad Caverns east quadrangle, New Mexico: U.S. Geological Survey, Geologic Quadrangle Map GQ-98.

HAYES, P.T., 1964, Geology of the Guadalupe Mountains, New Mexico: U.S. Geological Survey, Professional Paper 446, 69 p.

HAYNES, J., 1981, Foraminifera: New York, Wiley, 433 p.

HUNT, D., ALLSOP, T., AND SWARBRICK, R., 1995, Compaction as a primary control on the architecture and development of depositional sequences: conceptual framework, applications and implications, *in* Howell, J., and Aitken, J.F., eds., High Resolution Sequence Stratigraphy: Innovations and Applications: Geological Society of London, Special Publication 104, p. 321–345.

HURLEY, N.F., 1978, Facies mosaic of the Lower Seven Rivers Formation (Permian), North McKittrick Canyon, Guadalupe Mountains, New Mexico [unpublished M.S. thesis]: University of Wisconsin, Madison, Wisconsin, 198 p.

HURLEY, N.F., 1979, Seaward primary dip of fall-in beds, lower Seven Rivers Formation, Permian, Guadalupe Mountains, New Mexico (abstract): American Association of Petroleum Geologists, Bulletin, v. 63, p. 471.

HURLEY, N.F., 1989, Facies Mosaic of the Lower Seven Rivers Formation, McKittrick Canyon, New Mexico, *in* Harris, P.M., and Grover, G.A., eds., Subsurface and Outcrop Examination of the Capitan Shelf Margin, Northern Delaware Basin: SEPM, Core Workshop 13, p. 325–346.

JACKA, A.D., THOMAS, C.M., BECK, R.H., WILLIAMS, K.W., AND HARRISON, S.C., 1972, Guadalupian depositional cycles of the Delaware Basin and Northwest Shelf, *in* Elam, J.G., and Chuber, S., eds., Cyclic Sedimentation in the Permian Basin, 2nd Edition: West Texas Geological Society, Publication 69-56, p. 152–196.

JAMES, N.P., 1979, Shallowing-upward sequences in carbonates, *in* Walker, R.G., ed., Facies Models: Geoscience Canada, Reprint Series 1, p. 109–119.

JAMES, N.P., 1984, Shallowing-upward sequences in carbonates, *in* Walker, R.G., ed., Facies Models, 2nd Edition: Geoscience Canada, Reprint Series 1, p. 213–228.

KERANS, C., AND FITCHEN, W.M., 1995, Sequence hierarchy and facies architecture of a carbonate-ramp system: San Andres Formation of the Algerita escarpment and western Guadalupe mountains, West Texas and New Mexico: Texas Bureau of Economic Geology, Report of Investigations 235, 86 p.

KERANS, C., AND HARRIS, P.M., 1992, Relative sea level record of Yates and Tansill Formation shelf facies, Permian reef geology trail: implications for platform development (abstract): American Association of Petroleum Geologists, Annual Convention, Book of Abstracts, v. 1, p. 65.

KERANS, C., AND HARRIS, P.M., 1993, Outer shelf and shelf crest, *in* Bebout, D.G., and Kerans, C., eds., Guide to the Permian Reef Geology Trail, McKittrick Canyon, Guadalupe Mountains National Park, West Texas: Texas Bureau of Economic Geology, Guidebook 26, p. 32–42.

KERANS, C., AND NANCE, H.S., 1991, High frequency cyclicity and regional depositional patterns of the Grayburg Formation, Guadalupe Mountains, New Mexico, *in* Meader-Roberts, S., Candelaria, M.P., and Moore, G.E., eds., Sequence Stratigraphy, Facies, and Reservoir Geometries of the San Andres, Grayburg, and Queen Formations, Guadalupe Mountains, New Mexico and Texas: SEPM, Permian Basin Section, Publication 91–32, p. 53–69.

KERANS, C., AND TINKER, S.W., 1997, Sequence Stratigraphy and Characterization of Carbonate Reservoirs: SEPM, Short Course Notes 40, 130 p.

KERANS, C., AND TINKER, S.W., in press, Extrinsic stratigraphic controls on development of the Capitan reef complex, *in* Saller, A.H., Harris, P.M., Kirkland-George, B., and Mazzullo, S.J., eds., Geologic Framework of the Capitan Reef: SEPM, Concepts in Sedimentology and Paleontology.

KERANS, C., FITCHEN, W.M., GARDNER, M.H., SONNENFELD, M.D., TINKER, S.W., AND WARDLAW, B.R., 1992, Styles of sequence development within uppermost Leonardian through Guadalupian strata of the Guadalupe Mountains, Texas and New Mexico, *in* Mruk, D.H., and Curran, B.C., eds., Permian Basin Exploration and Production Strategies: Applications of Sequence Stratigraphic and Reservoir Characterization Concepts: West Texas Geological Society, Symposium 92–91, p. 1–7.

KERANS, C., LUCIA, F.J., AND SENGER, R.K., 1994, Integrated characterization of carbonate ramp reservoirs using Permian San Andres Formation outcrop analogs: American Association of Petroleum Geologists, Bulletin, v. 78, p. 181–216.

KING, P.B., 1948, Geology of the southern Guadalupe Mountains, Texas: U.S. Geological Survey, Professional Paper 215, 183 p.

KIRKLAND, B.L., 1995, More evidence for a barrier reef: microfacies analysis of the Tansill outer shelf, Permian Capitan reef complex (abstract): American Association of Petroleum Geologists, Annual Convention, Book of Abstracts, v. 4, p. 50A.

KIRKLAND, B.L., AND MOORE, C.H., JR., 1990, New evidence for the barrier reef model, Permian Capitan Reef Complex, New Mexico (abstract): American Association of Petroleum Geologists, Bulletin, v. 74, p. 696.

KIRKLAND, B.L., LONGACRE, S.A., AND STOUDT, E.L., 1993, Reef, *in* Bebout, D.G., and Kerans, C., eds., Guide to the Permian Reef Geology Trail, McKittrick Canyon, Guadalupe Mountains National Park, West Texas: Texas Bureau of Economic Geology, Guidebook 26, p. 23–31.

KOERSCHNER, W.F., AND READ, J.F., 1989, Field and modeling studies of Cambrian carbonate cycles, Virginia Appalachians: Journal of Sedimentary Petrology, v. 59, p. 654–687.

LAND, L.S., 1992, The dolomite problem: stable and radiogenic isotope clues, *in* Clauer, N. and Chaudhuri, S., eds., Isotopic Signatures and Sedimentary Records: Berlin, Springer-Verlag, Lecture Notes in Earth Science 43, p. 49–68.

LANG, W.B., 1937, The Permian formations of the Pecos Valley of New Mexico and Texas: American Association of Petroleum Geologists, Bulletin, v. 21, p. 833–898.

LEGARRETA, L., 1991, Evolution of a Callovian–Oxfordian carbonate margin in the Neuquen basin of west-central Argentina: facies, architecture, depositional sequences and global sea level changes: Sedimentary Geology, v. 70, p. 209–240.

LLOYD, E.R., 1929, Capitan Limestone and associated formations of New Mexico and Texas: American Association of Petroleum Geologists, Bulletin, v. 13, p. 645–658.

LUCIA, F.J., 1995, Rock-fabric/petrophysical classification of carbonate pore space for reservoir characterization: American Association of Petroleum Geologists, Bulletin, v. 79, p. 1275–1300.

MAZZULLO, S.J., MAZZULLO, J., AND HARRIS, P.M., 1985, Eolian origin of quartzose sheet sands in Permian shelf facies, Guadalupe Mountains (abstract), *in* Cunningham, B.K., and Hedrick, C.L., eds., Permian Carbonate/Clastic Sedimentology, Guadalupe Mountains: Analogs for Shelf and Basin Reservoirs: SEPM, Permian Basin Section, Publication 85-24, p. 71.

MEISSNER, F.F., 1972, Cyclic sedimentation in Middle Permian strata of the Permian Basin, *in*

Elam, J.G., and Chuber, S., eds., Cyclic Sedimentation in the Permian Basin, 2nd Edition: West Texas Geological Society, Publication 72-60, p. 203–232.

Melim, L.A., 1991, The origin of dolomite in the Permian (Guadalupian) Capitan Formation, Delaware Basin, west Texas and New Mexico: Implications for dolomitization models [unpublished Ph.D. thesis]: Southern Methodist University, Dallas, Texas, 200 p.

Melim, L.A., and Scholle, P.A., 1995, The forereef facies of the Permian Capitan Formation: the role of sediment supply versus sea-level changes: Journal of Sedimentary Research, v. B65, p. 107–118.

Mitchum, R.M., and Van Wagoner, J.C., 1991, High-frequency sequences and their stacking patterns: sequence stratigraphic correlation evidence of high-frequency eustatic cycles: Sedimentary Geology, v. 70, p. 131–160.

Mitchum, R.M., Vail, P.R., and Thompson, S., III, 1977, Seismic stratigraphy and global changes in sea level, Part 2: The depositional sequence as a basic unit for stratigraphic analysis, *in* Payton, C.E., ed., Seismic Stratigraphy—Applications to Hydrocarbon Exploration: American Association of Petroleum Geologists, Memoir 26, p. 63–81.

Montañez, I.P., and Osleger, D.A., 1993, Parasequence stacking patterns, third-order accommodation events, and sequence stratigraphy of middle to upper Cambrian platform carbonates, Bonanza King Formation, southern Great Basin, *in* Loucks, R.G., and Sarg, J.F., eds., Carbonate Sequence Stratigraphy: Recent Developments and Applications: American Association of Petroleum Geologists, Memoir 57, p. 305–326.

Mruk, D.H., and Bebout, D.G., 1993, Slope, *in* Bebout, D.G., and Kerans, C., eds., Guide to the Permian Reef Geology Trail, McKittrick Canyon, Guadalupe Mountains National Park, West Texas: Texas Bureau of Economic Geology, Guidebook 26, p. 14–22.

Newell, N.D., Rigby, J.K., Fischer, A.G., Whiteman, A.J., Hickox, J.E., and Bradley, J.S., 1953, The Permian Reef Complex of the Guadalupe Mountains region, Texas and New Mexico: San Francisco, W.H. Freeman, 236 p.

Osleger, D.A., 1998, Sequence architecture and sea level dynamics of late Permian shelfal facies, Guadalupe Mountains, southern New Mexico: Journal of Sedimentary Research, v. 68, p. 327–346.

Osleger, D.A., and Read, J.F., 1991, Relation of eustacy to stacking patterns of meter-scale carbonate cycles, Late Cambrian, U.S.A.: Journal of Sedimentary Petrology, v. 61, p. 1225–1252.

Osleger, D.A., and Tinker, S.W., in press, Three-dimensional architecture of upper Permian high-frequency sequences, Yates–Capitan shelf margin, Permian basin, USA, *in* Harris, P.M., Saller, A.H., Simo, T., and Handford, R., eds., Advances in Carbonate Sequence Stratigraphy—Application to Reservoirs, Outcrops, and Models: SEPM, Special Publication.

Playford, P.E., Hurley, N.H., Kerans, C., and Middleton, M.F., 1989, Reefal development, Devonian of the Canning Basin, western Australia, *in* Crevello, P., Wilson, J.L., Sarg, J.F., and Read, J.F., eds., Controls on Carbonate Platform and Basin Development: SEPM, Special Publication 44, p. 187–202.

Pomar, L., 1993, High-resolution sequence stratigraphy in prograding Miocene carbonates: application to seismic interpretation, *in* Loucks, R.G., and Sarg, J.F., eds., Carbonate Sequence Stratigraphy: Recent Developments and Applications: American Association of Petroleum Geologists, Memoir 57, p. 389–408.

Pray, L.C., 1977, The shelf-edge Capitan-massive and the outer-shelf facies, *in* Pray, L.C., and Esteban, M., eds., Upper Guadalupian Facies, Permian Reef Complex, Guadalupe Mountains, New Mexico and West Texas, Vol. 2, Road Logs and Locality Guides: SEPM, Permian Basin Section, Publication 77-16, p. G-5 to G-16 and G-79 to G-81.

Read, J.F., 1989, Controls on evolution of Cambrian–Ordovician passive margin, U.S. Appalachians, *in* Crevello, P., Wilson, J.L., Sarg, J.F., and Read, J.F., eds., Controls on Carbonate Platform and Basin Development: SEPM, Special Publication 44, p. 147–165.

Ross, C.A., and Ross, J.R.P., 1987, Late Paleozoic sea levels and depositional sequences, *in* Ross, C.A., and Haman, D., eds., Timing and Depositional History of Eustatic Sequences, Constraints on Seismic Stratigraphy: Cushman Foundation for Foraminiferal Research, Special Publication 24, p. 137–149.

Saller, A., 1996, Differential compaction and basinward tilting of the prograding Capitan reef complex, Permian, west Texas and southeast New Mexico, USA: Sedimentary Geology, v. 101, p. 21–30.

Sarg, J.F., 1995, Carbonate sequence architecture and sea-level records (abstract), *in* First SEPM Congress on Sedimentary Geology, Program and Abstracts Volume 1.

Sarg, J.F., and Lehmann, P.J., 1986, Lower–middle Guadalupian facies and stratigraphy, San Andres/Grayburg formations, Permian Basin, Guadalupe Mountains, New Mexico, *in* Moore, G.E., and Wilde, G.L., eds., Lower and Middle Guadalupian Facies, Stratigraphy, and Reservoir Geometries, San Andres/Grayburg Formations, Guadalupe Mountains, New Mexico and Texas: SEPM, Permian Basin Section, Publication 86-25, p. 1–8.

Severin, K.P., and Lipps, J.H., 1988, Comparative taphonomy of large fusiform foraminifera: test destruction by biotic agents during deposition (abstract): Geological Society of America, Annual Meeting, Abstracts with Programs, p. A370.

Silver, B.A., and Todd, R.G., 1969, Permian cyclic strata, northern Midland and Delaware basins, West Texas and southeastern New Mexico: American Association of Petroleum Geologists, Bulletin, v. 53, p. 2223–2251.

Smith, D.B., 1973, Geometry and correlation along Permian Capitan escarp ment, New Mexico and Texas: discussion: American Association of Petroleum Geologists, Bulletin, v. 57, p. 940–945.

Sonnenfeld, M.D., 1991, High-frequency cyclicity within shelf-margin and slope strata of the upper San Andres sequence, Last Chance Canyon, *in* Meader-Roberts, S., Candelaria, M.P., and Moore, G.E., eds., Sequence Stratigraphy, Facies, and Reservoir Geometries of the San Andres, Grayburg, and Queen Formations, Guadalupe Mountains, New Mexico and Texas: SEPM, Permian Basin Section, Publication 91-32, p. 11–51.

Sonnenfeld, M.D., and Cross, T.A., 1993, Volumetric partitioning and facies differentiation within the Permian Upper San Andres Formation of Last Chance Canyon, Guadalupe Mountains, New Mexico, *in* Loucks, R.G., and Sarg, J.F., eds., Carbonate Sequence Stratigraphy: Recent Developments and Applications: American Association of Petroleum Geologists, Memoir 57, p. 435–474.

Swift, D.J.P., and Thorne, J.A., 1991, Sedimentation on continental margins, I: A general model for shelf sedimentation, *in* Swift, D.J.P., Oertel, G.F., Tillman, R.W., and Thorne, J.A., eds., Shelf and Sandstone Bodies—Geometry, Facies, and Sequence Stratigraphy: International Association of Sedimentologists, Special Publication 14, p. 3–31.

Tinker, S.W., 1996a, Building the 3-D jigsaw puzzle: applications of sequence stratigraphy to 3-D reservoir characterization, Permian basin: American Association of Petroleum Geologists, Bulletin, v. 80, p. 460–485.

Tinker, S.W., 1996b, Reservoir-scale sequence stratigraphy: McKittrick Canyon and three-dimensional subsurface examples, west Texas and New Mexico [unpublished Ph.D. thesis]: Boulder, Colorado, The University of Colorado, 245 p.

Tucker, M.E., and Wright, V.P., 1990, Carbonate Sedimentology: London, Blackwell, 482 p.

Tyrrell, W.W., Jr., 1969, Criteria useful in interpreting environments of unlike but time-equivalent carbonate units (Tansill–Capitan–Lamar), Capitan Reef Complex, West Texas and New Mexico, *in* Friedman, G.M., ed., Depositional Environments in Carbonate Rocks: Society of Economic Paleontologists and Mineralogists, Special Publication 14, p. 80–97.

Vail, P.R., 1987, Seismic stratigraphy interpretation procedure, *in* Bally, A.W., ed., Atlas of Seismic Stratigraphy: American Association of Petroleum Geologists, Studies in Geology, v. 1, p. 1–10.

Vail, P.R., Mitchum, R.M., Jr., and Thompson, S., III, 1977, Seismic stratigraphy and global changes of sea level, Part 4: global cycles of relative changes of sea level, *in* Payton, C.E., ed., Seismic Stratigraphy—Applications to Hydrocarbon Exploration: American Association of Petroleum Geologists, Memoir 26, p. 83–97.

Van Wagoner, J.C., Posamentier, H.W., Mitchum, R.M., Vail, P.R., Sarg, J.F., Loutit, T.S., and Hardenbol, J., 1988, An overview of the fundamentals of sequence stratigraphy and key definitions, *in* Wilgus, C.K., Hastings, B.S., Kendall, C.G.St.C., Posamentier, H.W., Ross, C.A., and Van Wagoner, J.C., eds., Sea-Level Changes: An Integrated Approach: SEPM, Special Publication 42, p. 39–45.

Ward, R.F., Kendall, C.G.St.C., and Harris, P.M., 1986, Upper Permian (Guadalupian) facies and their association with hydrocarbons—Permian Basin, West Texas and New Mexico: American Association of Petroleum Geologists, Bulletin, v. 70, p. 239–262.

Wilde, G.L., 1975, Fusulinid-defined Permian stages, *in* Cys, J.M., and Toomey, D.F., eds., Permian Exploration, Boundaries, and Stratigraphy: West Texas Geological Society, Publication 75-65, p. 67–83.

Wilkinson, B.H., 1975, Matagorda Island, Texas: the evolution of a Gulf Coast barrier complex: Geological Society of America, Bulletin, v. 86, p. 959–967.

Wilkinson, B.H., 1982, Cyclic cratonic carbonates and Phanerozoic calcite seas: Journal of Geological Education, v. 30, p. 189–203.

Wilkinson, B.H., Drummond, C.N., Rothman, E.D., and Diedrich, N.W., 1997, Stratal order in peritidal carbonate sequences: Journal of Sedimentary Petrology, v. 67, p. 1068–1082.

Wilson, J.L., 1967, Cyclic and reciprocal sedimentation in Virgilian strata of southern New Mexico: Geological Society of America, Bulletin, v. 78, p. 805–818.

Wilson, J.L., 1975, Carbonate Facies in Geologic History: New York, Springer-Verlag, 471 p.

Wood, R., Dickson, J.A.D., and Kirkland-George, B., 1994, Turning the Capitan reef upside down: a new appraisal of the ecology of the Permian Capitan reef, Guadalupe Mountains, Texas and New Mexico: PALAIOS, v. 9. p. 422–427.

Yurewicz, D.A., 1976, Sedimentology, paleoecology, and diagenesis of the massive facies of the Lower and Middle Capitan Limestone (Permian), Guadalupe Mountains, New Mexico and West Texas [unpublished Ph.D. thesis]: University of Wisconsin, Madison, Wisconsin, 278 p.

Yurewicz, D.A., 1977, The origin of the massive facies of the Lower and Middle Capitan Limestone (Permian), Guadalupe Mountains, New Mexico and West Texas, *in* Hileman, M.E., and Mazzullo, S.J., eds., Upper Guadalupian Facies, Permian Reef Complex, Guadalupe Mountains, New Mexico and West Texas: 1977 Field Conference Guidebook, Vol. 1: SEPM, Permian Basin Section, Publication 77-16, p. 45–92.

Received 25 August 1997; accepted 16 June 1998.

Slaughter Canyon

SEQUENCE ARCHITECTURE AND SEA-LEVEL DYNAMICS OF UPPER PERMIAN SHELFAL FACIES, GUADALUPE MOUNTAINS, SOUTHERN NEW MEXICO

DAVID A. OSLEGER
Department of Geology, University of California, Davis, California 95616, U.S.A.

ABSTRACT: A 3.2 km profile of mixed carbonates and clastics is superbly exposed in Slaughter Canyon in the Guadalupe Mountains of southern New Mexico and provides a seismic-scale panorama of stratal architecture and cyclic facies relationships across the Upper Permian shelf margin of the Delaware basin. The upper Seven Rivers and Yates Formations exposed in the mapped profile behind the Capitan reef margin are characterized by extreme seaward thickening and strongly progradational architecture. Meter-scale cycles exhibit systematic lithofacies changes in a seaward direction, spanning pisolitic shelf-crest to skeletal outer-shelf facies tracts. Retrogradational, aggradational, and progradational stacking patterns of meter-scale cycles in the Yates define four complete high-frequency sequences (Y1–Y4) and the lower half of a fifth (Y5) that continues into the overlying Tansill Formation. Individual Yates high-frequency sequences are fundamentally macroscale versions of Yates meter-scale cycles, on the basis of comparable internal arrangements of lithofacies and their seaward-thickening geometry.

The evolution of the Yates–Capitan shelf margin from Y1 through Y4 is expressed by systematic trends in downdip thickness changes, lateral extent of facies tracts relative to the Capitan reef margin, aspect ratios of facies tracts, progradation:aggradation ratios and derived offlap angles, and progradation rates. These trends reflect the position of individual high-frequency sequences in the larger scale Yates–Tansill composite sequence. Long-term changes in aspect ratios record the progressive seaward migration and lateral expansion of the shelf-crest facies tract from Y1 through Y4 and the reciprocal seaward-stepping architecture and lateral contraction of the outer-shelf facies tract. The four Yates high-frequency sequences in Slaughter Canyon are characterized by an average offlap angle of 3.6°, whereas the corresponding average growth angle for the time-equivalent Capitan reef is 5.2°. The higher reef growth angle reflects the greater amount of accommodation available near the outer shelf-to-reef transition as well as limitations to seaward growth imposed by the steepness of the reef front. The Yates shelf prograded at an average rate of 2.1 m/k.y., whereas the time-equivalent Capitan reef prograded at a rate of 1.7 m/k.y. The strongly progradational architecture of the Yates shelf resulted in a progressive decrease in the depth of the Capitan reef through time from a maximum of $\sim$ 65 m during early Yates time to near sea level during the latest stages of the Yates platform.

The abrupt seaward expansion within each Yates high-frequency sequence occurs directly above the terminal reef margin of the preceding high-frequency sequence. The underlying reef likely acted as a foundation to localize the basinward shift in deposition associated with sea-level fall along high-frequency sequence boundaries, contributing to the seaward thickening and progradational ''step-out'' of the outer shelf. Architectural changes controlled by the interaction between relative sea level and antecedent depositional topography may be a fundamental characteristic of many progradational shelf margins.

INTRODUCTION

Several recent studies of ancient carbonate platforms have based their sequence stratigraphic interpretations on the detailed ''mapping'' of well-exposed, two-dimensional profiles (e.g., Sonnenfeld and Cross 1993; Franseen et al. 1993; Pomar 1993; Kerans and Fitchen 1995; Tinker 1996). These high-resolution studies provide critical field documentation, at the sub-seismic scale, of published conceptual models of how carbonate platforms are geometrically constructed. They also reveal a level of detail beyond other outcrop-based sequence stratigraphic studies that are forced to rely solely on the subjective correlation of vertical stacking patterns of cyclic successions between isolated sections. The current emphasis on the detailed mapping of seismic-scale profiles to determine stratal architecture is a natural outgrowth of older stratigraphic field studies that recognized the insight provided by two- and three-dimensional models of deposition (e.g., McKee 1945; Hickox *in* Newell et al. 1953).

This study documents the stratal architecture, cyclic facies relationships, and sea-level dynamics of seismic-scale, laterally continuous exposures of Upper Permian mixed carbonates and clastics superbly exposed in Slaughter Canyon in the Guadalupe Mountains of southern New Mexico (Fig. 1A). These strata (upper Seven Rivers and Yates Formations) were deposited during middle to late Guadalupian time on the Northwest Shelf behind the coeval Capitan reef complex that rimmed the Delaware basin (Fig. 1B). The primary goals of this paper are to (1) document the detailed stratal architecture of high-frequency sequences, (2) improve the genetic, and thus chronostratigraphic, resolution, and (3) quantify depositional variables such as aspect ratios, progradation:aggradation ratios, offlap angles, and platform progradation rates which reflect the sea-level dynamics controlling sequence deposition. This study contributes toward improved visualization of the two-dimensional architecture of mixed carbonate–siliciclastic deposits on highly progradational rimmed shelf margins, and provides an outcrop analog for lateral and vertical facies heterogeneity within subsurface reservoirs.

Previous Work

Previous sedimentologic work on the Seven Rivers–Yates interval in the Guadalupe Mountains has documented the overall facies distribution and has identified multiple forms of stratigraphic cyclicity (e.g., Hayes and Koogle 1958; Hayes 1964; Silver and Todd 1969; Kendall 1969; Dunham 1972; Meissner 1972; Smith 1974; Esteban and Pray 1977; Neese and Schwartz 1977; Sarg 1981; Hurley 1989; Candelaria 1989; Borer and Harris 1991; Mutti and Simo 1993). Recent sequence stratigraphic approaches to the Seven Rivers–Yates succession, primarily based on the spectacular exposures in McKittrick Canyon, have been taken by Kerans et al. (1992), Kerans and Harris (1993), and Tinker (1996).

In Slaughter Canyon, Achauer (1969) constructed a generalized dip section of shelfal facies relations behind the Capitan reef, providing significantly greater detail than the Slaughter Canyon cross section constructed by Newell et al. (1953). Other work in Slaughter Canyon consists of Babcock (1977) and Yurewicz (1977), who investigated the Capitan reef massif, and Melim and Scholle (1995), who focused on the Capitan foreslope. Rankey and Lehrmann (1996) interpreted toplap geometries in the ''upper Seven Rivers'' in a 100 m $\times$ 700 m window in Slaughter Canyon. The architectural and genetic relations described in this paper provide critical detail about the shelf crest and outer shelf of the Yates platform, complementing the work of Borer and Harris (1991), who used isolated outcrops from the Guadalupe Mountains and borehole data from the Northwest Shelf and Central Basin Platform to construct cross-platform profiles of the Yates Formation.

Study Area and Methods

Slaughter Canyon trends south-to-southeast, normal to the Capitan Escarpment of the Guadalupe Mountains, providing a seismic-scale dip sec-

JOURNAL OF SEDIMENTARY RESEARCH, VOL. 68, NO. 2, MARCH, 1998, P. 327–346
 1073-130X/98/068-327/$03.00

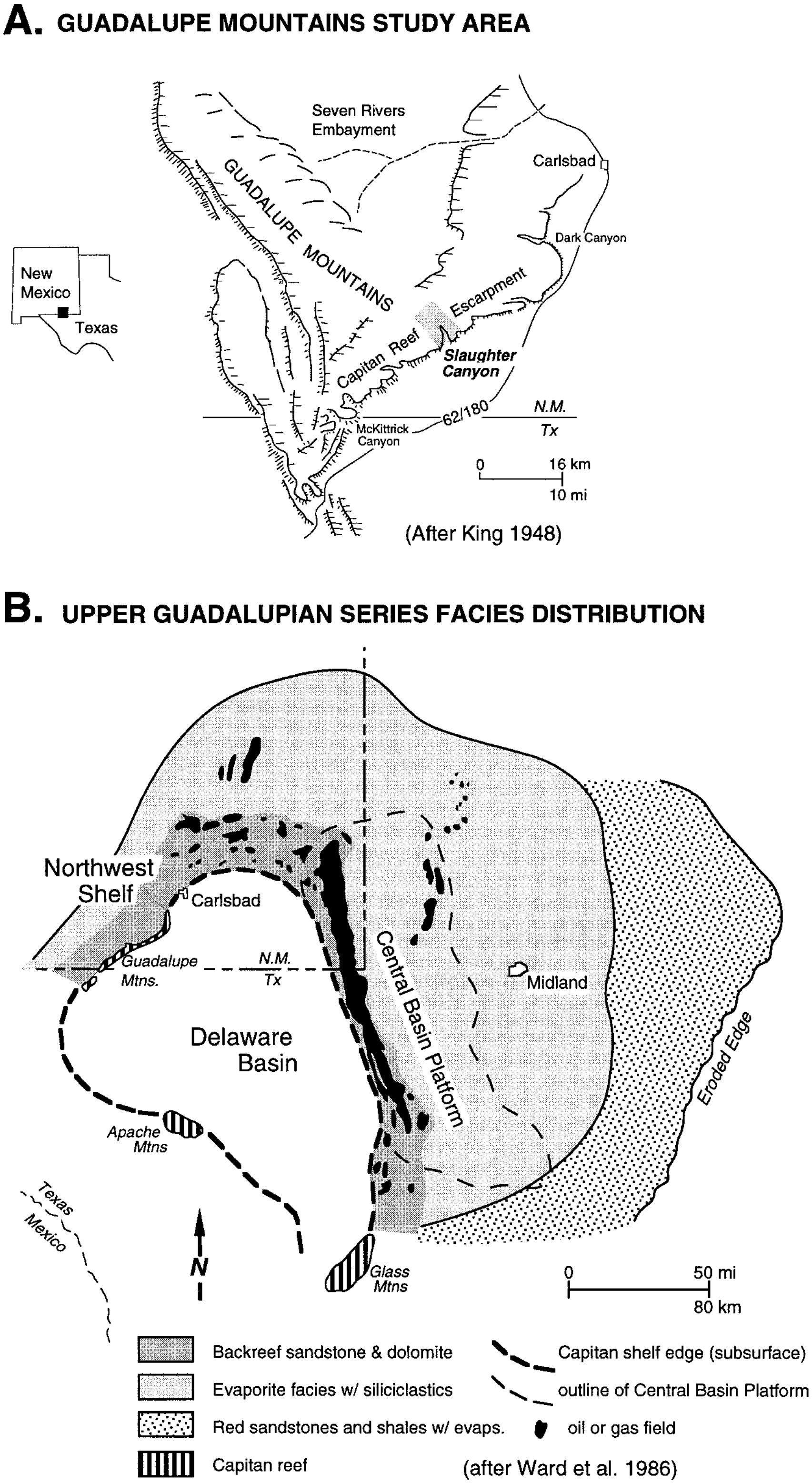

FIG. 1.—**A)** Location map of the study area (shaded) in Slaughter Canyon, Guadalupe Mountains, southern New Mexico. **B)** Facies distribution of the Queen, Seven Rivers, and Yates Formations around the perimeter of the deep-water Delaware basin (after Ward et al. 1986). Oil and gas fields producing from these formations are shown in black.

tion of the upper Seven Rivers and Yates bedded shelf strata behind the massive Capitan reef and foreslope (Fig. 2). Formation boundaries were mapped in the canyon by Hayes and Koogle (1958) and Hayes (1964) (Fig. 3). For this study, eleven sections, spaced 100–400 m apart, were measured and logged in detail along a 3.2 km transect on the northeast wall (Fig. 4). On the outcrop, measured section data were transcribed to color copies of panoramic photographs. Several critical surfaces and most siliciclastic beds were physically traced between adjacent sections, essentially correlating on the outcrop with the aid of the panoramic photographs and tying loops between sections. Selected individual cycles were traced updip and down-

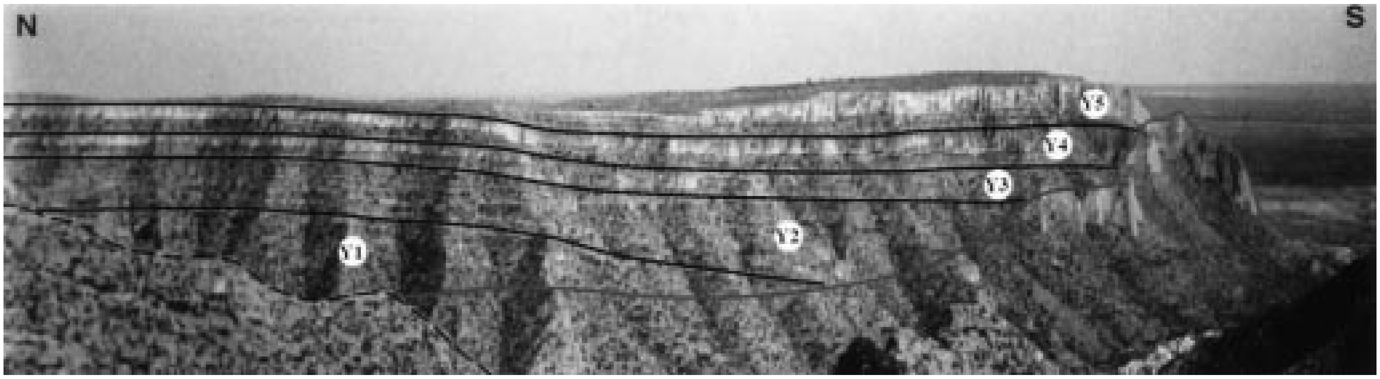

FIG. 2.—Panoramic photo of northeast wall of Slaughter Canyon illustrating the seismic scale of the outcrop. Photo spans ~ 2.5 km extending from the mouth of the canyon (right) back toward the northwest (left). Superimposed form lines show the transition between shelfal strata and the Capitan reef and foreslope, and boundaries of high-frequency sequences through the Yates study interval. The majority of the lower walls in both canyons are composed of Capitan reef and foreslope facies, with the upper part composed of backreef shelfal strata of the Seven Rivers and Yates Formations. Y1–Y5 are high-frequency sequences.

dip to document lateral facies transitions from the seaward contact with the Capitan reef to the most landward settings in the lee of the shelf crest. Three sets of photographs were used that provided differing perspectives and levels of resolution: (1) wide-angle pans taken from several vantage points on the opposite canyon wall, (2) blow-ups of Hasselblad pans, and (3) low-angle oblique photos taken from a helicopter. Petrographic analysis of > 150 thin sections of shelfal lithologies enhanced field descriptions of lithofacies and permitted the recognition of rock fabrics, porosity types, and cementation history.

STRATIGRAPHIC AND TECTONIC SETTING

During the Late Permian, the Guadalupe Mountains of southeastern New Mexico and west Texas were located approximately 10° north of the equator and were part of the extensive western collisional margin of Pangea that faced the Panthalassan ocean (Scotese 1994; Golonka et al. 1994). The regional climate was one of extreme aridity, indicated by the development of broad coastal siliciclastic sabkhas and associated evaporative environments (Ward et al. 1986; Andreason 1992). Global climate models of Pangean continental configurations indirectly support widespread aridity across Pangea but also suggest strong seasonality with significant winter cooling (Crowley et al. 1989) and monsoonal circulation (Kutzbach and Gallimore 1989). The Late Permian in general was a transitional phase between peak icehouse conditions during the Pennsylvanian through early Permian and peak greenhouse conditions during the Jurassic and Cretaceous.

Upper Permian facies of the study interval in the Guadalupe Mountains were deposited on the Northwest shelf of the Delaware basin during the late Guadalupian (Fig. 1B). The Capitan reef formed a marginal rim around the basin, creating semi-restricted conditions in the deep-water interior. The upper Seven Rivers and Yates Formations shelfal strata are equivalent to massive reefal and forereef carbonates of the Capitan Formation and to basinal siliciclastics of the middle Bell Canyon Formation (Fig. 5). The

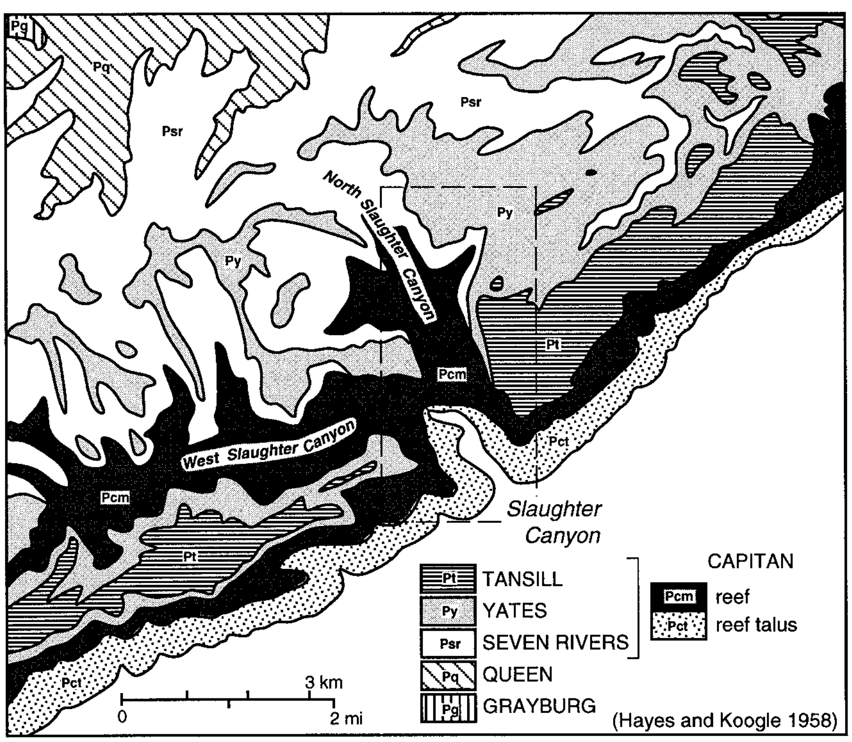

FIG. 3.—Geologic map of the Guadalupe Mountains near Slaughter Canyon (after Hayes and Koogle 1958).

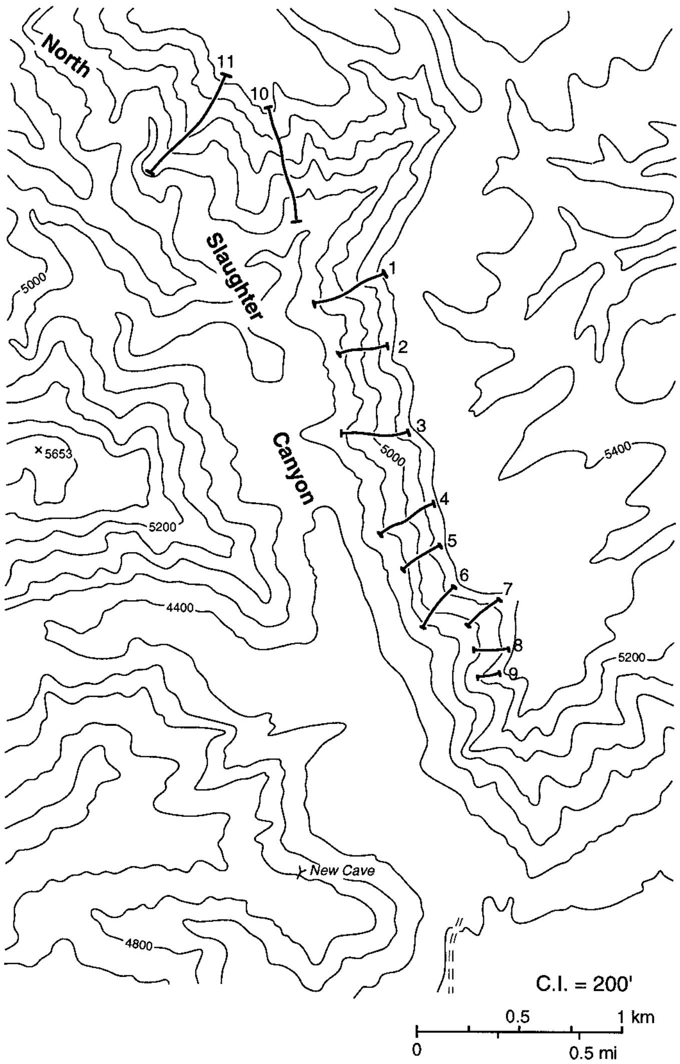

FIG. 4.—Topographic base map of Slaughter Canyon showing locations of measured sections along the east-northeast wall. Adapted from the Serpentine Bends and Grapevine Draw U.S.G.S. quadrangles.

sole index fossil for establishing shelf-to-basin correlations in the late Guadalupian is the fusulinid *Polydiexodina.* The study interval comprises part of the Capitanian substage of the Guadalupian stage, a time interval estimated to span about 2.5 m.y. (Ross and Ross 1987; Harland et al. 1989). Using maximum thicknesses for the study interval proportioned to these time spans, the upper Seven Rivers and Yates Formations are estimated to collectively range from 0.7 to 1 m.y. in duration. Of course, the time scale for these estimates is based on stratigraphic inference; the nearest radiometric dates that can be tied to biostratigraphic zonation are at the Pennsylvanian–Permian boundary (295 ± 6 Ma) and the Permo-Triassic boundary (251 ± 3 Ma) (Ross et al. 1994).

FACIES DISTRIBUTION

Physical tracing of shelf-to-reef time slices in this study corroborates the marginal mound model of Dunham (1972). This paleobathymetric model defines a lateral succession of depositional environments extending seaward from an interior evaporitic lagoon, across a shelf-crest pisolite shoal complex, then down a dipping outer shelf that grades into the submergent Capitan reef (Fig. 6). The mapped profile in Slaughter Canyon is dominated by lithofacies comprising the shelf-crest and outer-shelf facies tracts. (''Facies tract'' is used in this paper as a genetically linked association of facies that records a discrete energy/water depth/sediment supply setting, *sensu* Kerans and Fitchen 1995). Carbonate lithofacies of the shelf-crest and outer-shelf facies tracts have been exhaustively reviewed in the literature; observations from Slaughter Canyon are compiled in Figure 6.

Fine quartzose sandstones to coarse siltstones are commonly interbedded with carbonates of the Yates Formation and are important reservoir facies in the Permian basin (Borer and Harris 1991; Andreason 1992). In Slaughter Canyon, siliciclastic facies are composed of very well-sorted, subangular to subrounded quartz grains cemented by dolomite or anhydrite. Individual beds typically are featureless and massive but have sharp bases that gradationally become more dolomitic upward, eventually dissipating into pure carbonate facies. Laterally, siliciclastic beds tend to be amalgamated into a single bed updip, but commonly bifurcate into two to three distinct beds downdip before feathering out near the immediate backreef. Depositional interpretations of these siliciclastics range from shallow subaqueous to eolian (e.g., Silver and Todd 1969; Kendall 1969; Smith 1974; Fischer and Sarnthein 1988; Candelaria 1989).

Capitan-age shelfal strata tend to increase in dip and thicken considerably as they approach the Capitan reef, a geometry that is readily apparent on canyon walls throughout the Guadalupes (Fig. 2). King (1948) and Newell et al. (1953) recognized this ''basinward tilting of backreef deposits'', and Pray has informally designated these inclined outer-shelf units ''fall-in'' beds (Pray and Esteban 1977). Hurley (1989) demonstrated that the tilt is

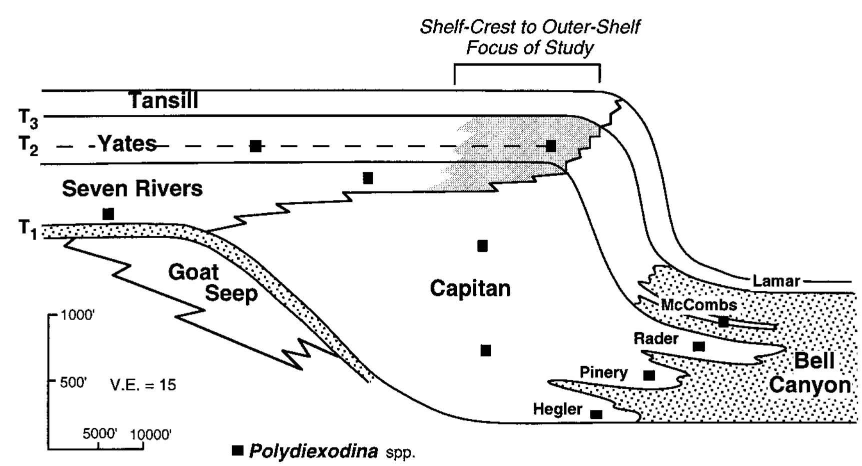

FIG. 5.—Shelf-to-basin correlations for the Upper Permian of the Northwest shelf, modified from Garber et al. (1989). T1, T2, and T3 represent time lines. Shaded area denotes the backreef facies of the uppermost Seven Rivers and Yates Formations, which are the focus of this study.

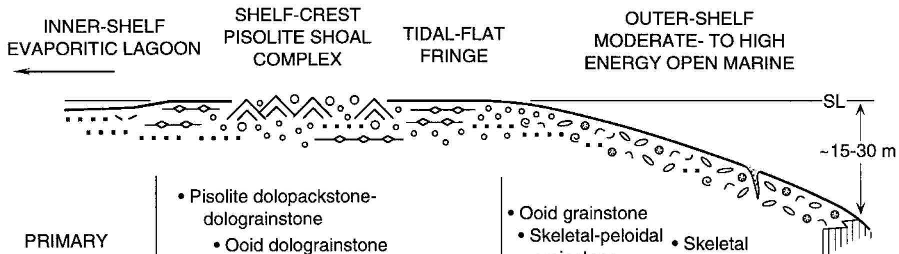

PRIMARY ROCK TYPES	• Pisolite dolopackstone-dolograinstone • Ooid dolograinstone • Fenestral peloidal dolo-wackestone-dolopackstone	• Ooid grainstone • Skeletal-peloidal grainstone • Skeletal packstone-grainstone
OUTCROP CHARACTERISTICS	• ledge- & cliff-forming, thin to massive beds • interbedded lithofacies commonly lensoid and laterally discontinuous • common teepees, vadose caliche crusts, horizontal sheet cracks, & intraclast lenses • common reverse grading from ooids upward into increasingly larger pisolites • primarily laminar fenestrae within white peloidal dolowackestone-dolopackstone • sandstone-filled neptunian dikes • uncommon cryptalgal laminites	• variable from resistant cliff-formers to stairstep topography • massive to thick bedding that increases in thickness downdip • typically structureless with less common low- to high-angle planar crossbedding • dolomitic limestones and limy dolostones • sandstone-filled neptunian dikes • degree of sorting increases updip • medium- to very coarse-grained textures • common fusulinid coquinas
INTERNAL COMPOSITION	• complex, polygenetic pisolites exhibiting multiple episodes of growth, leaching, & fracturing • abundant internal sediment and multiple generations of cement within fitted polygonal fabric • fenestral facies composed of dolomitized peloids and lime mud • common subrounded to subangular, micritic intraclasts • rare to common evaporite molds in laminar fenestral facies • rare to abundant subangular quartz silt	• abundant whole fusulinids and fragmental dascyclad algae • common bivalve, bryozoa, & echinoderm fragments and miliolid forams • large gastropod molds and steinkerns • common intraclasts and peloids • common superficially coated grains & micrite envelopes • common well-sorted, medium- to fine-grained ooid grainstones updip • widely disseminated subangular quartz silt
DIAGENETIC & PETROPHYSICAL CHARACTERISTICS	Pisolite Grainstones -- • cements: dolomicrite of pisolite laminae, isopachous bladed-to-fibrous dolomite after calcite, minor calcite spar, anhydrite • pore types: intraparticle and interparticle • pisolite grainstone avg. porosity = 6.6% avg. permeability = 0.36 md Fenestral Dolomites -- • cements: isopachous bladed, fibrous botryoidal, minor calcite spar, anhydrite • pore types: fenestral, moldic, & vuggy • fenestral dolomite avg. porosity = 6.6% avg. permeability = 1.43 md	• cements: isopachous bladed-to-fibrous calcite, blocky calcite spar, kaolinite • dolomite: partial to complete fabric-retentive replacement and void-lining cements • pore types: intraparticle, interparticle, moldic, shelter, and vuggy • common peloidal geopetal fill within gastropod shells • outer-shelf facies avg. porosity = 5.7% avg. permeability = 10.8 md

FIG. 6.—Outcrop and petrographic characteristics of carbonate lithofacies exposed along the shelf-crest to outer-shelf profile in Slaughter Canyon.

mainly depositional in origin, with only a minor component of tectonic or compactional overprint. In contrast, Saller (1996) recognized up to 10° of postdepositional tilt, which he attributed to differential compaction of slope and basinal carbonate muds. In Slaughter Canyon, measured depositional dips of the outer shelf vary from ~ 1–2° updip to ~ 6–10° downdip (corrected for the 5–6° structural tilt imparted by the underlying flexure of the Huapache Monocline).

SEQUENCE STRATIGRAPHY

The sequence stratigraphic terminology of Mitchum and Van Wagoner (1991) is followed in this paper: large-scale ''composite sequences'' are internally composed of ''high-frequency sequences'' (HFSs), which in turn are composed of meter-scale cycles. This paper does not use the terminology of ''orders'' (i.e., third, fourth, fifth) because of the arbitrary time boundaries separating the various scales of cyclicity and the relatively poor time control in the studied rocks.

A generalized cross section of the upper Seven Rivers and Yates exposed along the outer 3.2 km of the northeastern wall of Slaughter Canyon (Fig. 7) provides an overall stratigraphic framework for the following documentation of sequence stratigraphy. The Yates Formation consists of four complete high-frequency sequences (Y1–Y4) and the lower half of a fifth (Y5) that continues into the overlying Tansill Formation. The contact between the Yates and Seven Rivers is interpreted to be a major composite sequence boundary (Kerans et al. 1992; Tinker 1996). Only the outer-shelf parts of the uppermost high-frequency sequences in the Seven Rivers are exposed in the studied profile and are not discussed in detail in this paper. The vertical and lateral stacking patterns of meter-scale cycles are key criteria for defining high-frequency sequences in the upper Seven River and Yates and thus are discussed first.

Meter-Scale Cycle Architecture and Stacking Patterns

Cross-Platform Characteristics.—Meter-scale cycles are the fundamental chronostratigraphic unit in the upper Seven Rivers and Yates Formations and have been described by several previous workers, usually in the context of vertical measured sections. In the two-dimensional profile exposed in Slaughter Canyon, cycles vary systematically across the platform and also with position within high-frequency sequences (Fig. 8). The architecture of individual cycles in Figure 8 is generalized to reflect the fundamental depositional profile across the platform, regardless of position within the larger-scale accommodation signal.

Lithofacies within cycles are typically arranged as asymmetric regressive hemicycles, with minor skewed symmetric patterns also evident in downdip positions. Siliciclastics commonly form the basal component to individual cycles, but may or may not always be present, depending on shelfal location and position within high-frequency sequences. For instance, basal siliciclastic facies are uncommon toward outer shelf locations and also within

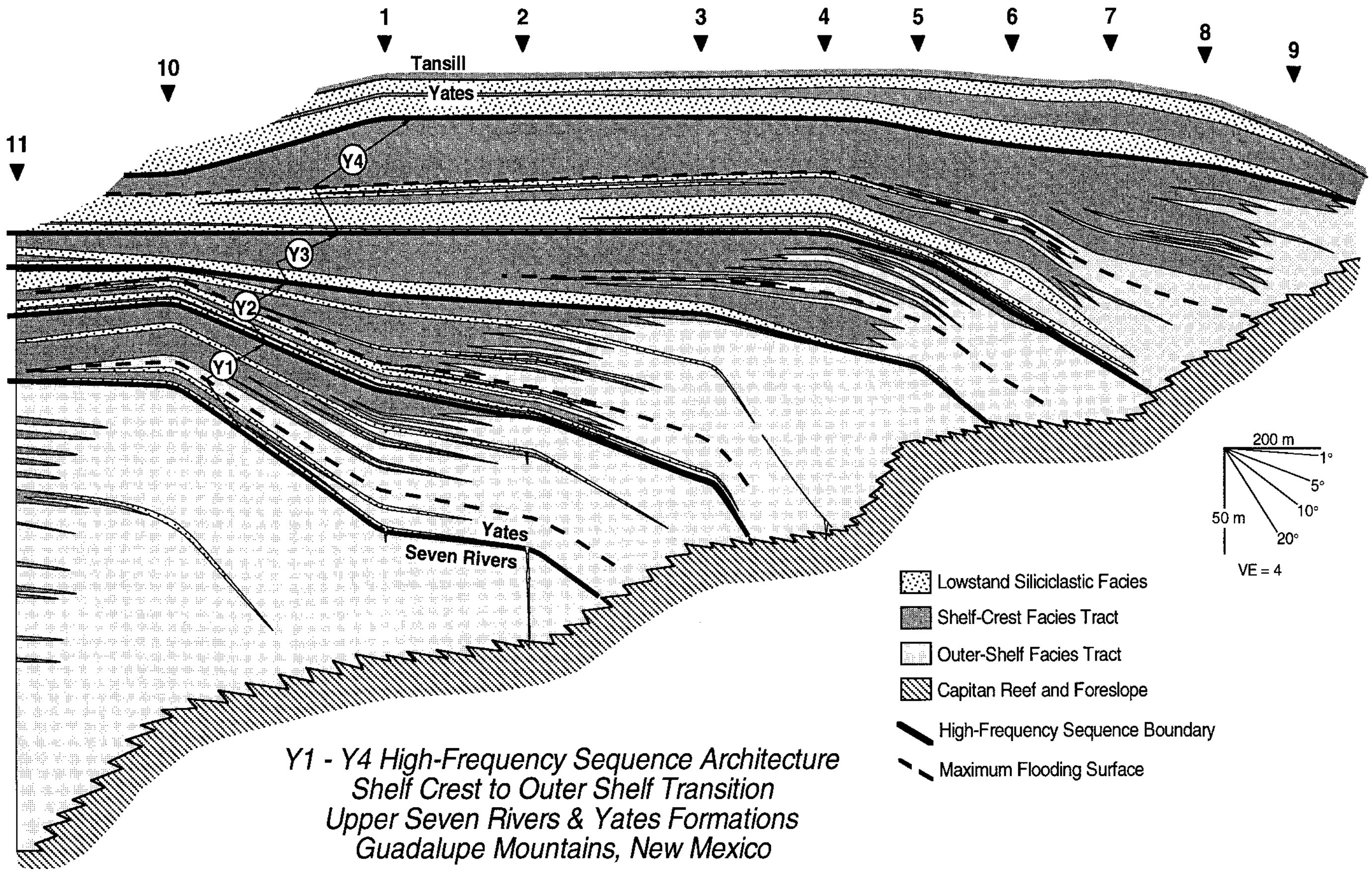

FIG. 7.—Facies tracts and high-frequency sequence architecture across 3.2 km of the transition from shelf crest to outer shelf of the upper Seven Rivers and Yates Formations exposed in Slaughter Canyon. Two datums were used in the cross section: from Sections 11 to 4, the Y3–Y4 HFS boundary was used; from Sections 4 to 9, an approximation of the actual dip along the Y4–Y5 HFS boundary was used. The contact between shelfal facies and the Capitan reef tends to be transitional over 10 m or so and is characterized in vertical sections by alternating thick beds of fusulinid–skeletal grainstone-to-wackestone and massive, muddy reefal facies showing evidence of framework such as sponges, *Archaeolithoporella,* and botryoidal marine cements. The actual contact is seldom sharp, but rather an intertonguing, gradational transition. The vertical, downward-tapering objects are five sandstone-filled dikes, approximately to vertical scale, that have been documented on outcrop.

the upper highstand parts of high-frequency sequences. Basal siliciclastics are common, however, across the entire shelf crest to outer shelf within the transgressive and lower highstand parts of high-frequency sequences. If siliciclastic lithofacies are present, they typically exhibit an abrupt, erosional contact with carbonates of the underlying cycle and a gradational upper contact with overlying dolomitic lithofacies. Evidence for erosional lower contacts is equivocal in outer-shelf locations where siliciclastics are interbedded with coarse, skeletal–peloidal grainstones and packstones.

In updip positions 2.5–3 km from the Capitan reef (Fig. 8), cycles consist of a lower siltstone overlain by peloidal, fenestral laminites or mudstones.

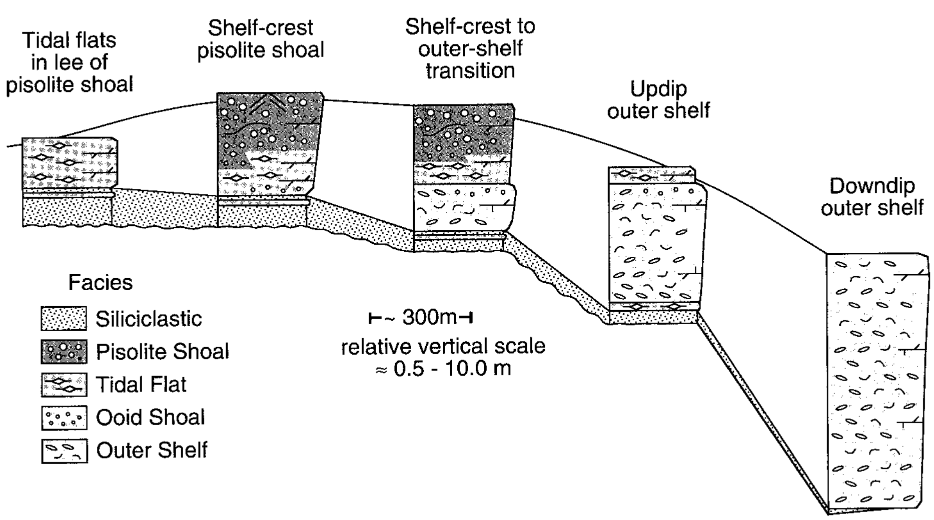

FIG. 8.—Schematic diagram of cycle architecture across the upper Seven Rivers and Yates shelf. Vertical scale for each cycle is strictly relative (0.5 to ~ 10 m). Major facies tracts are composed of several distinct subfacies, which have been generalized for the figure. A similar schematic is presented in Smith (1974, his fig. 22).

These cycles are best expressed in Sections 10 and 11 in Slaughter Canyon (Fig. 7), which are located along the seaward margin of the ''middle shelf'', the site of the most productive reservoir facies in the Yates Formation (Ward et al. 1986; Borer and Harris 1991; Andreason 1992). Siliciclastics within individual cycles in this updip platform position tend to be the thickest across the platform and are commonly amalgamated composites of two or three distinct siliciclastic units of seaward equivalents (Fig. 7).

Near the shelf crest, meter-scale cycles may exhibit either siliciclastics or fenestral laminites as the basal lithofacies (Fig. 8), depending upon position within high-frequency sequences. These lithofacies grade upward into oolitic, peloidal, and pisolitic packstones that coarsen upward into pisolite grainstones exhibiting erosionally truncated teepees, intraclast breccias, and micritic crusts. Shelf-crest, pisolitic cycles in Slaughter Canyon are inconsistently organized, exhibit considerable vertical and lateral variability, and are difficult to physically trace along the outcrop.

Near the transition from shelf crest to outer shelf (Fig. 8), basal siliciclastics grade upward into thin, dolomitic tidal-flat facies before giving way vertically to outer-shelf packstones or grainstones composed of ooids, coated grains, fusulinids, dascyclad algae, bioclastic debris, peloids, and intraclasts. Cycles developed within this zone may be capped by either pisolitic shoal facies or, slightly more downdip, oolitic or tidal-flat facies.

In outer-shelf and immediate backreef environments, massively bedded packstones and grainstones of the ''fall-in'' beds may exhibit a cryptic cyclicity where subtle coarsening-upward patterns can be discerned in some downdip sections. Outer-shelf cycles within the upper Yates have been documented by Kerans and Harris (1993) in McKittrick Canyon, where distinct weathering differences make the alternating lithofacies relatively easy to recognize. In Slaughter Canyon, coarsening-upward outer-shelf cycles are difficult to define in the lower parts of high-frequency sequences, where these facies typically form massive resistant cliffs. Outer-shelf cyclicity is more evident in upper parts of high-frequency sequences, where they typically weather as a stairstep topography of ledges (grainstones) and slopes (packstones).

Interpretation of Cycle Development.—Meter-scale cycles developed across the platform within individual chronostratigraphic increments (Fig. 8) are interpreted to record a single high-frequency (10^5 yr scale) change in relative sea level. This model is hardly new; it has been promulgated for Upper Permian strata of the Northwest Shelf for several decades, perhaps most emphatically by authors in the forward-thinking book ''Cyclic Sedimentation in the Permian Basin'' (Elam and Chuber 1967). During lowstands, siliciclastics were transported across the subaerially exposed shelf by eolian and perhaps fluvial processes, and were deposited in the adjoining deep-water basin. Siliciclastics that remained on the platform during the subsequent transgression were reworked in shallow marine environments and preserved in the stratigraphic record. Cycles without basal siliciclastics may reflect either complete bypass or lack of siliciclastic transport to outer-shelf localities; both options are likely a function of position within high-frequency sequences. Complete bypass is suggested for cycles that dominate the upper highstand parts of high-frequency sequences. Capping carbonate lithofacies within these upper highstand cycles exhibit disseminated quartz sand and silt, perhaps reflecting migration of siliciclastic environments across the exposed surface until sediment supply was exhausted. The second option, insufficient distance of transport to outer-shelf localities, is suggested for cycles developed within the transgressive and lower highstand parts of high-frequency sequences when siliciclastic sources were forced back to their most landward position.

Complete flooding and the ''catch-up'' phase of sedimentation is recorded in each cycle by skeletal–peloidal packstones and grainstones of the outer-shelf facies tract. The steepness of the depositional slope on the outer shelf (up to 8–10°) likely precluded extensive encroachment of outer-shelf lithofacies onto the platform. Consequently, cycles that developed on top and in the lee of the shelf-crest barrier shoal typically lack outer-shelf components (Fig. 8).

Progradation and the ''keep-up'' phase of sedimentation is recorded within outer-shelf facies by subtle upward-coarsening trends that suggest migration of high-energy, shallow subtidal environments over slightly deeper-water, open-shelf environments. Repetitive development of this trend upward within individual high-frequency sequences resulted in a progressive decrease in depositional slope of the outer shelf. Tidal-flat laminites and oolites capping outer-shelf grainstones reflect the seaward migration of the tidal zone fronting the pisolitic shelf crest, complete infilling of available accommodation at that platform locality, and thus the position of sea level at the end of a single depositional cycle. Pisolite grainstone caps of cycles record the seaward progradation of the shelf-crest barrier shoal, which ultimately culminated in subaerial exposure of the shelf and the renewed influx of siliciclastics.

Vertical Cycle Stacking Patterns.—Measured section #1 illustrates the vertical arrangement of cycles and component lithofacies within high-frequency sequences in a relatively updip setting (Fig. 9). It also is located at a position on the platform comparable to the Gulf PDB-04 well drilled 65 km to the north (Garber et al. 1989), enabling an evaluation of the degree of lateral correlatability of siliciclastics along strike. Well-defined repetition of lithofacies marks the Y1 and Y2 HFSs in section #1, primarily due to shelfal position near intertonguing outer-shelf and shelf-crest facies tracts. Similar cyclic patterns are difficult to define in the massive pisolite shoal facies that dominate Y3 and Y4 near Section #1, primarily because of a lack of intertonguing outer-shelf facies, but also partially related to cycle amalgamation. (As a side note, pisolite shoal facies are tightly cemented, forming steep and generally inaccessible cliffs along the Slaughter Canyon walls, making physical tracing of cycle boundaries within this facies logistically difficult.) More complete cycle development can be recognized in Y3 and Y4 in downdip positions near the transition from shelf crest to outer shelf.

Vertical cycle stacking patterns have limited utility for defining HFSs overall because of pervasive cycle amalgamation and the extreme lateral variability of cycle development. In general, in any one HFS cycles tend to be highly amalgamated and poorly defined updip in massive pisolite shoal facies, well-defined in the transition zone between shelf-crest and outer-shelf facies tracts, and highly amalgamated and poorly defined downdip in massive, outer-shelf skeletal packstones and grainstones. Vertical stacking patterns do have some predictive value, however, when used in conjunction with a knowledge of relative position on the platform and a depositional model that evolves with position in the overall high-frequency sequence (Kerans and Tinker 1997; Osleger and Tinker, in press).

High-Frequency Sequence Architecture

The spatial distribution of facies tracts and high-frequency sequences in the upper Seven Rivers and Yates is illustrated in the sets of interpreted low-angle oblique photo pans shown in Figure 10A–H. Several figures integrated into the discussion below were generated from these mapped panoramic photos. The generalized cross section shown in Figure 7 and the three cross sections showing the spatial distribution of facies tracts within HFSs (Fig. 11) are intended to convey the overall seaward-stepping, progradational architecture of the Yates shelf margin. The cross section of selected time lines (Fig. 12) and the reconstructed HFSs (Fig. 13) illustrate stratal geometries and platform architecture for individual HFSs near the time of deposition. The following section describes general characteristics of Yates HFSs and criteria that define them as discrete chronostratigraphic units, providing a broad introduction to the detailed descriptions of HFS Y1 through Y4 below.

General Characteristics.—The five sequence boundaries separating the four complete Yates high-frequency sequences were identified as significant exposure surfaces that mark relatively abrupt basinward shifts in facies as well as large-scale changes in lateral stacking patterns. Below individual HFS boundaries, cycle stacking patterns exhibit their greatest extent of

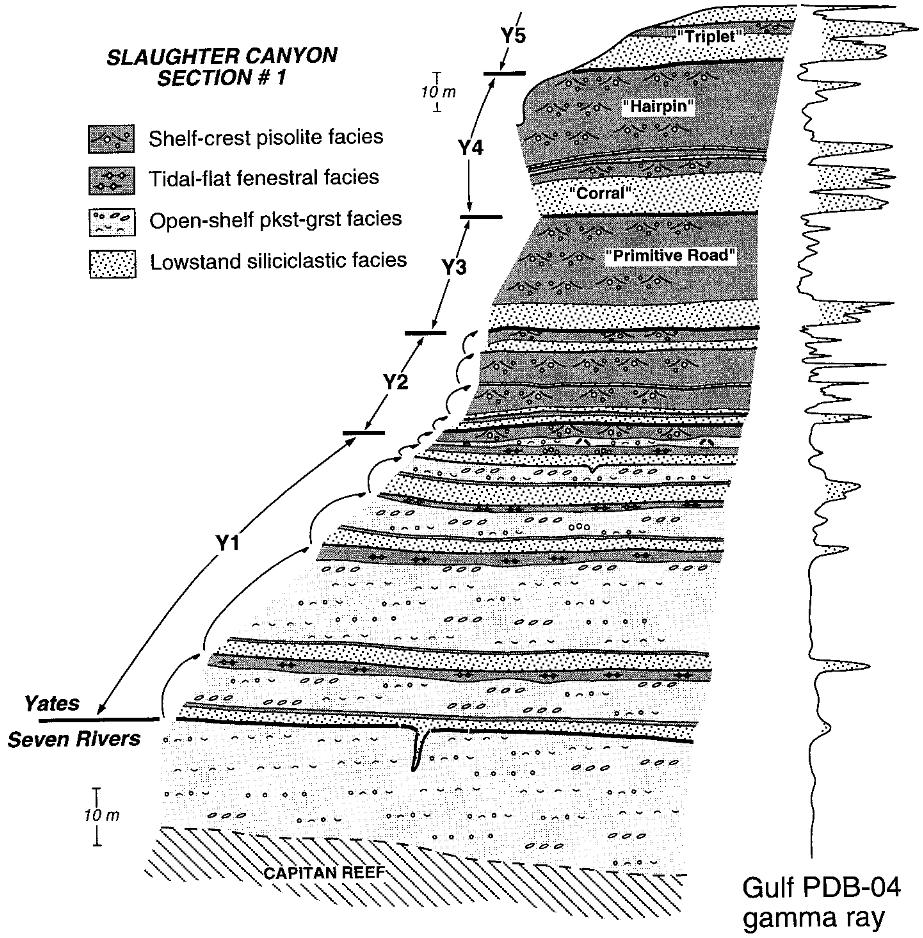

FIG. 9.—Photointerpretation of Hasselblad pan spanning measured Section #1 paired with gamma ray log of Gulf PDB-04, located 65 km to the northeast, for comparison. Section #1 and PDB-04 occupy comparable positions 2+ km behind the terminal Yates reef margin. Thicknesses of carbonate units on the gamma ray log have been rescaled slightly to conform to thicknesses on the measured section; the actual Yates thickness in PDB-04 is 190 m whereas the measured thickness at Section #1 is ~ 200 m. Siliciclastic units recorded in the gamma ray log are stippled. Arched arrows illustrate meter-scale cycles in the Y1 and Y2 HFSs. Several distinctive subfacies are grouped into four major lithofacies assemblages for simplicity of illustration. ''Triplet'', ''Hairpin'', ''Corral'', and ''Primitive Road'' are useful informal lithostratigraphic names defined by Pray et al. (1977). Vertical scale changes upward in the photointerpretation. Lateral distance along outcrop about 50 m.

seaward progradation, with the shelf-crest facies tract reaching to within half a kilometer or less of the Capitan reef margin. Stratal geometries below HFS boundaries suggest toplapping arrangements (Fig. 12), although direct evidence on the outcrop is commonly equivocal or cryptic. Thick siliciclastic units overlie all five HFS boundaries, reflecting the seaward shift of continental environments across the exposed carbonate platform. These lowstand siliciclastics are typically succeeded by mildly landward-stepping or aggradational cycles.

Individual high-frequency sequences within the Yates are fundamentally macroscale versions of meter-scale cycles, on the basis of comparable internal arrangements of lithofacies and their seaward-thickening geometry (Fig. 13). Similarly to meter-scale cycles, the lower parts of HFSs are characterized by higher volumes of siliciclastics whereas upper parts tend to be more carbonate-dominated. In a lateral sense, and also similarly to meter-scale cycles, updip parts of HFSs contain thick siliciclastic units whereas downdip parts exhibit dominantly carbonate lithofacies.

Systems tracts are identified within each HFS on the basis of retrogradational, aggradational, and progradational cycle stacking patterns. Maximum flooding surfaces are defined within each HFS on the basis of the most landward-reaching tongue of outer-shelf lithofacies onto the platform, commonly lying within the lower part of each HFS and imparting a distinct asymmetry between transgressive and highstand systems tracts (Figs. 7, 13). The transgressive systems tract (TST) in each HFS includes basal ''lowstand'' siliciclastics and overlying, landward-migrating outer-shelf carbonates. These siliciclastics are termed ''lowstand'' on the basis of their derivation during the initial phase of negative accommodation above sequence-bounding unconformities, but they are included within the TST because of their reworking and preservation during initial flooding that trapped unbypassed siliciclastic sediment on the platform top. The highstand systems tract (HST) in each HFS is dominated by mildly to strongly seaward-stepping cycle sets characterized by progressively increasing volumes of pisolitic shelf-crest lithofacies. It is inferred, but not directly observed in most cases, that prograding clinoforms in individual HFSs evolve from sigmoidal to shingled, low-angle oblique geometries, on the basis of the distribution of time lines through each HFS (Fig. 12) and the extreme seaward increases in thickness.

High-Frequency Sequence Y1.—The basal Y1 sequence boundary likely coincides with the Seven Rivers–Yates contact on the basis of Hayes'

→

FIG. 10.—Paired photographs of uninterpreted pans of the west-facing wall of Slaughter Canyon with their mapped interpretations. See section locations on the topographic base (Fig. 4) to relate photo pan to position within canyon. Relief along the mapped part of the canyon wall is approximately 250 m, providing an estimate of vertical scale. Inverted triangles note positions of overlap between photos. Key to facies tracts is shown in Figure 10G. Updip sections 10 and 11 are not shown. It should be noted that these photointerpretations incorporate the topography of the canyon wall and thus some geometries are apparent, especially in the reef-to-backreef transition zone. **A, B)** Mapped area spans Sections 1 and 2. **C, D)** Sections 3 through 5. **E, F)** Sections 6 through 8. **G, H)** Sections 8 and 9, with the massive Capitan reef and foreslope facies dominating the mouth of the canyon.

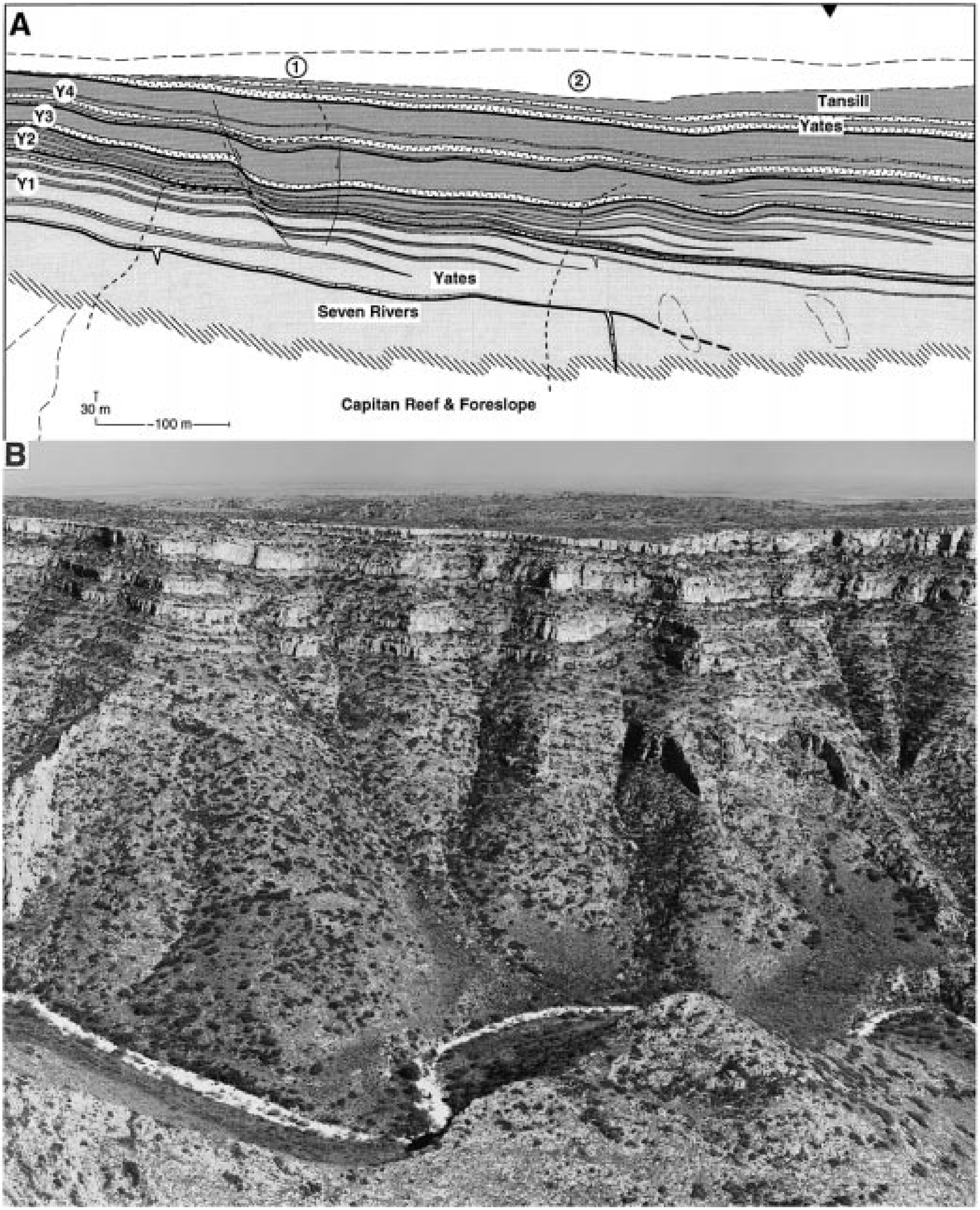
A
1
2
Y4
Y3
Y2
Y1
Tansill
Yates
Yates
Seven Rivers
30 m
100 m
Capitan Reef & Foreslope
B

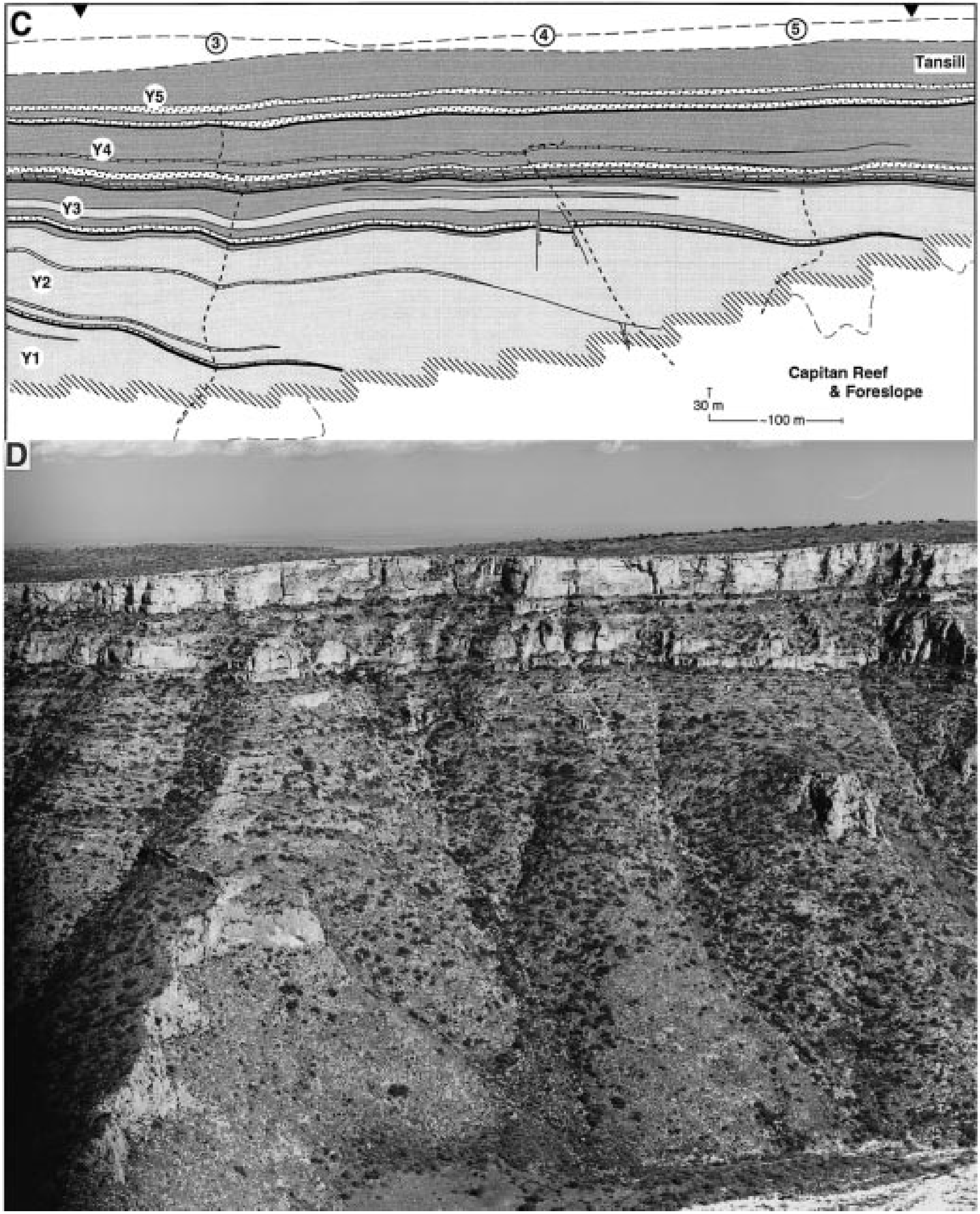

FIG. 10.—Continued.

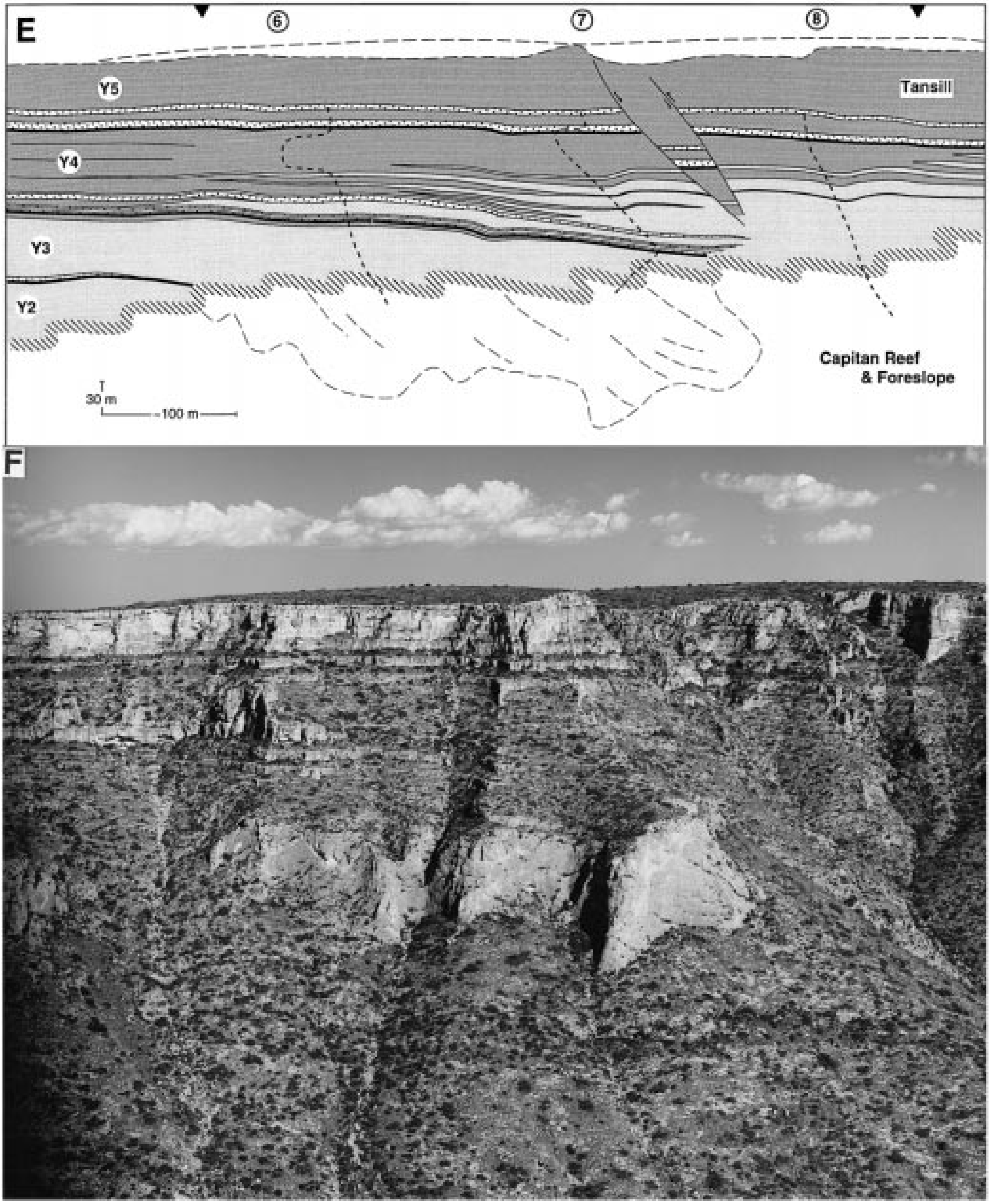

FIG. 10.—Continued.

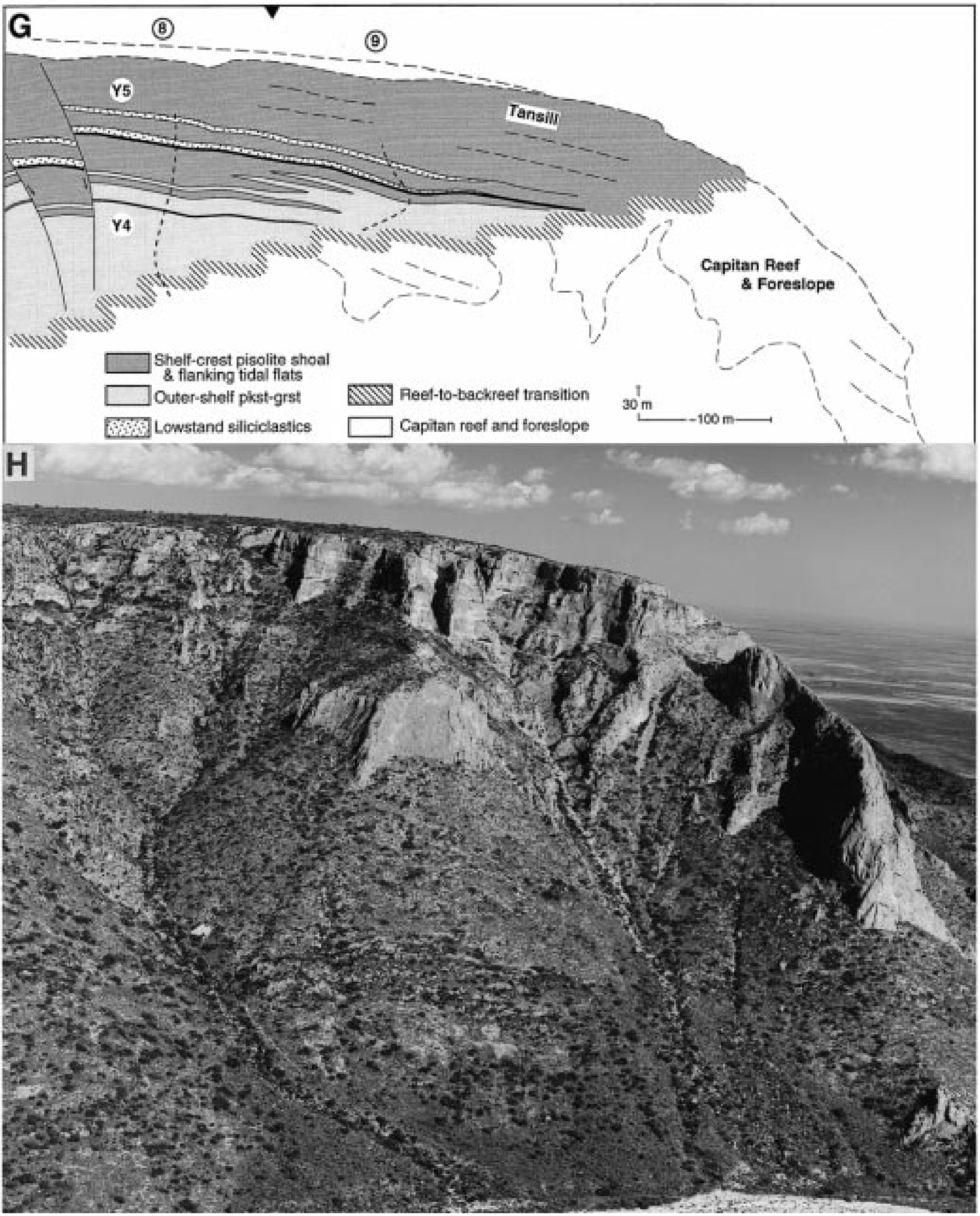

FIG. 10.—Continued.

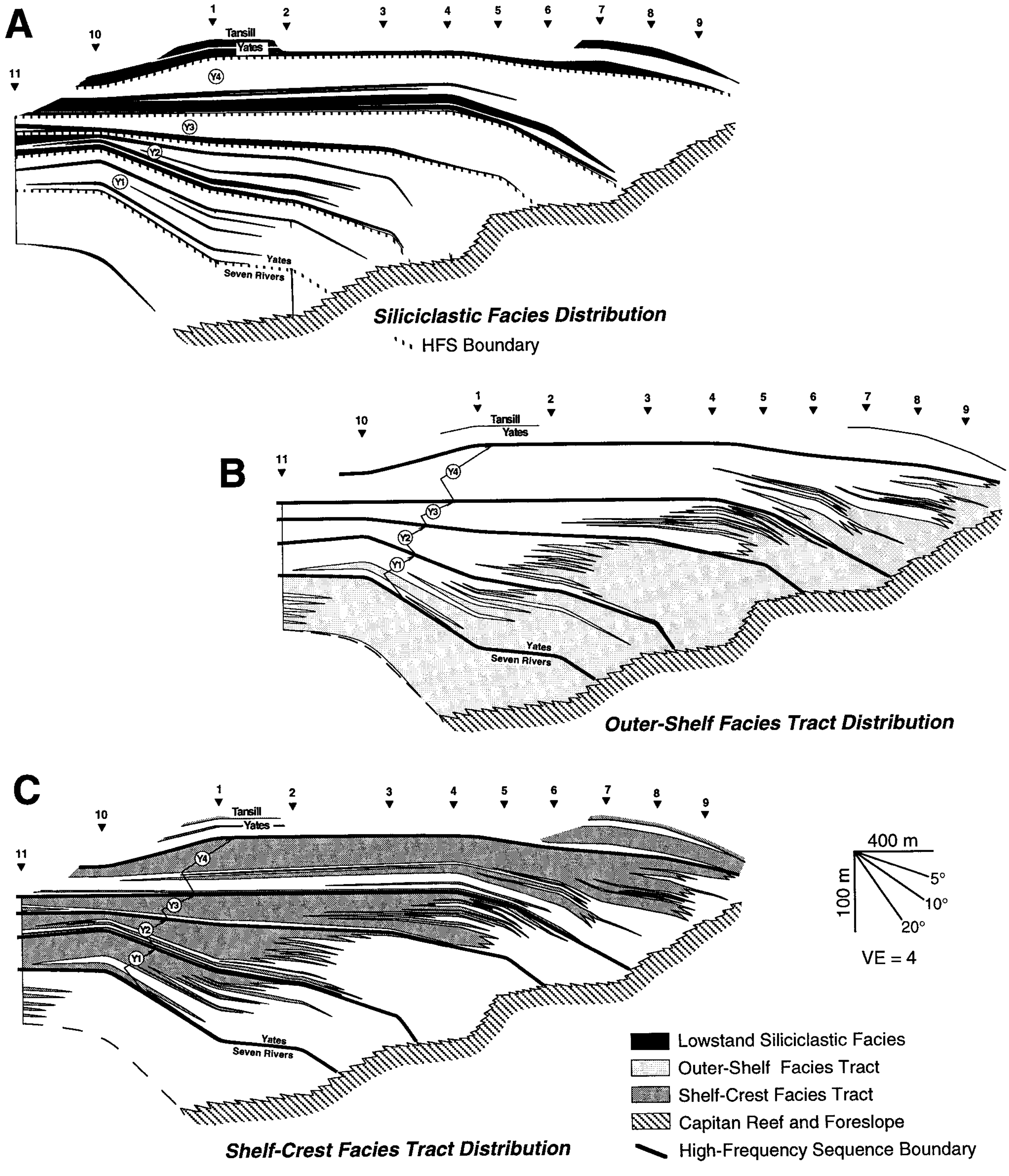

FIG. 11.—Spatial distribution of three primary facies tracts across the shelf margin exposed in Slaughter Canyon, relative to position within HFSs. **A)** Siliciclastics tend to dominate the lower parts and the updip positions of high-frequency sequences Y2–Y4. **B)** Outer-shelf facies exhibit progressively less landward extent onto the platform top with each successive HFS. **C)** Pisolite shelf-crest facies tend to dominate the upper parts of individual HFSs and step progressively seaward with each successive HFS.

(1964) definition of the contact in Slaughter Canyon as lying at the first significant siliciclastic bed above the dominantly carbonate outer-shelf facies of the underlying Seven Rivers. The sandstone overlying this disconformable surface marks an abrupt basinward offset of facies above fusulinid-rich outer-shelf facies of the underlying Seven Rivers. This sandstone can be traced downdip to a surface that is cut by a sandstone-filled dike (near Section #2) that extends downward approximately 40 m into underlying Seven Rivers outer-shelf facies and continues for about 10 m into

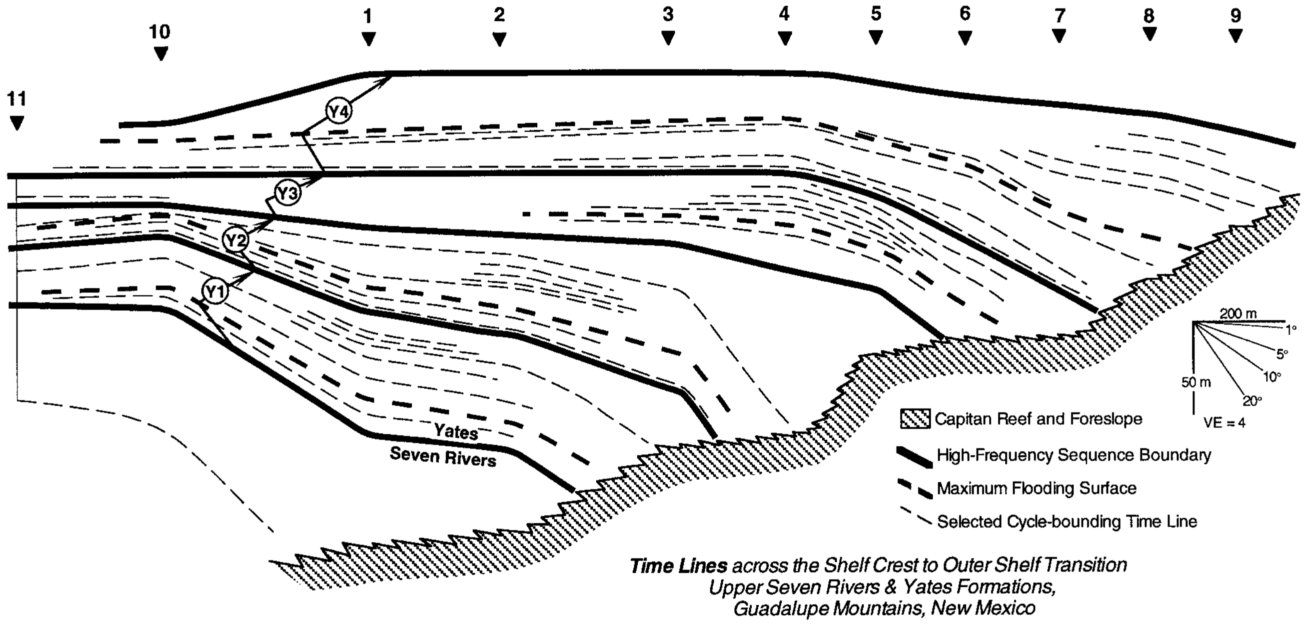

FIG. 12.—Selected time lines across individual HFSs within the Yates. Time lines shown on the plot are those that are the most obvious cycle boundaries that are relatively easy to physically trace across the outcrop. Obscure or equivocal cycle breaks are not plotted, specifically those comprising the massive pisolite shoal facies complex and massive outer-shelf facies in the immediate backreef. Time lines often correspond with the bases of fine sandstone or siltstone beds because they commonly define cycle breaks. In zones without siliciclastics, time lines are commonly defined by significant transgressive tongues of outer-shelf facies. The measured lower part of the Seven Rivers in Sections 10 and 11 are not well constrained and have been excluded from this figure. Likewise, the uppermost ''Triplet'' in the Yates and the lower Tansill have also been left off the plot.

the underlying Capitan reef (Figs. 7, 10A). A similar sandstone-filled dike is recognized along the basal Y1 sequence boundary updip near Section #1 but extends only ~ 2–4 m into underlying outer shelf grainstones of the upper Seven Rivers.

The TST in Y1 is characterized by a set of sigmoidal, backstepping cycles overlain by a tongue of outer-shelf facies that extends 1.4 km landward from the time-equivalent reef margin (Figs. 7, 13). This tongue is interpreted to represent maximum flooding of the Y1 HFS. The HST of Y1 is marked by a seaward-stepping cycle set that culminates with the seaward edge of the shelf crest positioned approximately half a kilometer from the reef margin. The shelf crest is a narrow belt (~ 0.9 km) in Y1 and is characterized by small, irregular pisolites and incipient teepees of low relief.

A fundamental difference in interpretation exists for stratal geometries in the interval spanning the Seven Rivers–Yates contact. Rankey and Lehrmann (1996) interpreted a toplap geometry within the ''upper Seven Rivers'' whereas this study documents sigmoidal clinoforms that show landward-thinning, and even backstepping, relationships within the same outcrop window (lower Yates of this study). Individual sandstone beds can be matched one-for-one between the two studies, but the basic difference is the lateral continuity and geometric relationships of these units. Rankey and Lehrmann interpreted four of the sandstones to ''amalgamate'' against a master sandstone bed that marks an interpreted sequence boundary. Physical walking out of each of these sandstone beds in this study reveals that each can be traced out updip as discrete beds with no evidence for termination against a single master surface. Each sandstone bed maintains its integrity for over a kilometer, but dramatic landward thinning occurs in the carbonate beds between sandstones. It is acknowledged, however, that the relatively low quality of exposure in this interval may result in equivocal interpretations that require further study to reconcile.

High-Frequency Sequence Y2.—The basal sequence boundary of Y2 is placed at a facies offset where continentally derived siltstones extend over outer-shelf grainstones to within 100 m of the reef margin (Figs. 10C, 11A). Overlying cycles with basal siliciclastics backstep up to a maximum flooding surface defined by an outer-shelf tongue that extends approximately 900 m landward from the reef margin. The TST of Y2 thickens seaward from ~ 10 m updip to ~ 20 m downdip, and four individual sandstone-based cycles can be traced for 1.4–1.8 km. The lack of direct evidence of onlap, the broad lateral extent of component cycles, and the minimal thickening suggests that the TST of Y2 was deposited as a series of draping blankets above the Y1 HFS rather than as an onlapping wedge.

Aggradational cycle stacking patterns overlying the maximum flooding surface define the lower HST in Y2 (Figs. 10C, 12, 13). A laterally extensive sandstone in the upper Y2 can be traced updip beyond the shelf crest (Section #11), where it thickens to 9 m, and downdip to a surface within outer-shelf facies just behind the reef margin (Section #4). This sandstone records a paleoslope on the outer shelf of approximately 10° over a 300 m distance.

Above this steeply dipping surface, the locus of sediment accumulation lies in an outer-shelf wedge bounded above by the top Y2 sequence boundary (Fig. 13). The exact mode of infilling of the outer shelf is difficult to see along the canyon wall (Fig. 10C, D), but the extreme thickening within the wedge dictates that accumulation took place without much accommodation available updip on the platform. Evidence for toplapping relations in this uppermost wedge can be seen updip between Sections #1 and #10 (upcanyon in Goat Cave Wash), where bedded shelf-crest facies wedge out at a low angle beneath the overlying HFS boundary. The pisolitic shelf crest within the upper HST of Y2 spans ~ 1 km in width (versus 0.5 km for the Y1 shelf crest) and extends to within 0.5 km of the time-equivalent reef margin.

High-Frequency Sequence Y3.—The basal Y3 HFS boundary is overlain by a seaward-thinning wedge of fine sandstone that extends to within 100 m of the reef, accompanied by an overlying wedge of pisolite shoal facies (Figs. 10C, 11A, 13). Physical tracing of this sandstone between Sections #3 and #4 reveals a narrow (~ 2 m) channel incised 1.5 m into underlying Y2 tidal-flat facies. The significant basinward shift of the pi-

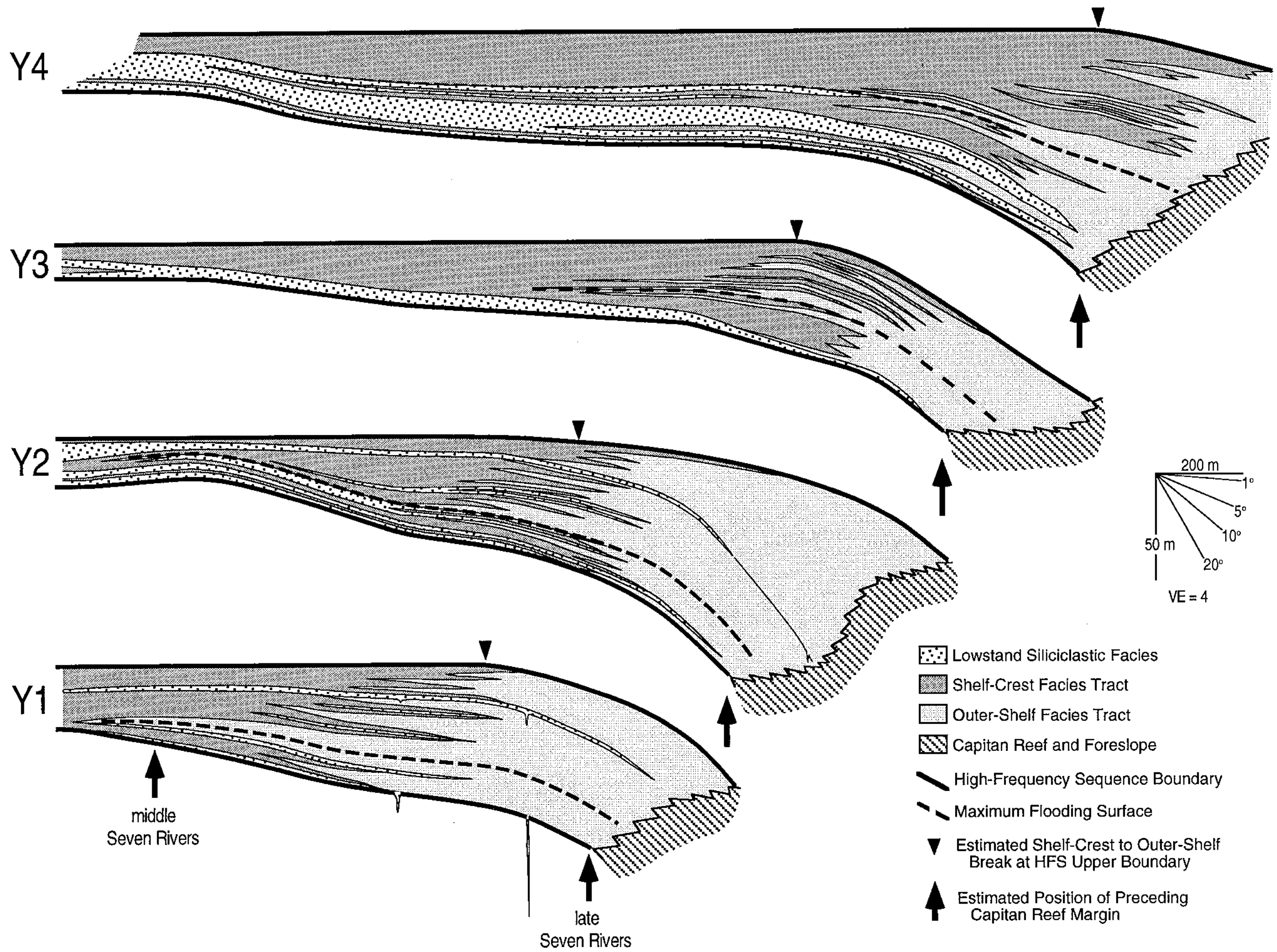

FIG. 13.—Individual Yates HFSs qualitatively reconstructed to (1) estimate original depositional topography near the time of upper sequence boundary formation and (2) remove the rotational effects of syndepositional and postdepositional compaction and Cenozoic structural tilting. Depositional slope break (upper triangles) is arbitrarily estimated from position of underlying tongues of outer-shelf facies.

solitic shelf crest above the basal sandstone is also recognized in McKittrick Canyon (Osleger and Tinker, in press), and is interpreted to reflect reduced accommodation and a subdued topographic profile of the platform. Flooding onto this flattened shelf resulted in tongues of outer-shelf facies extending ~ 1 km landward from the time-equivalent reef edge in Slaughter Canyon.

The Y3 HST is characterized by extreme progradation, exhibited on the canyon wall by the Y3 pisolitic shelf crest extending 0.7–1 km beyond the seaward edge of the underlying Y2 shelf crest. Time lines within the HST of Y3 (Fig. 12) illustrate the seaward progradation of the shelf-crest facies tract above the maximum flooding surface. Toward the end of Y3 deposition, the most seaward tongue of pisolite shoal facies reaches to within 200 m of the reef edge, reducing the outer shelf to a narrow belt. Chronostratigraphically significant surfaces recognized near the transition from shelf crest to outer shelf cannot be traced landward through the steep, massively bedded pisolitic facies that dominate the Y3 platform top, precluding direct identification of updip stratal geometries. The overall Y3 HFS thickens by 230% over 2.4 km, however, and when combined with the geometry of available time lines, suggests that toplapping geometries may exist updip.

High-Frequency Sequence Y4.—The thick succession of reworked terrigenous siliciclastics overlying the basal Y4 HFS boundary marks a significant base-level fall and consequent basinward shift in facies tracts above the underlying Y3 shelf crest (Fig. 11A, 13). These siliciclastics consist of five discrete sandstone tongues that amalgamate into two thick units approximately 2.5 km updip. The basal three sandstones extend very nearly to the reef margin (Fig. 10E), but the remaining two sandstones extend only to within ~ 1 km. Interbedded shelf-crest facies also pinch out progressively farther landward, indicative of overall retrogradation within the TST of Y4. The uppermost sandstone is overlain by a tongue of outer-shelf facies (near Section #5) that extends 0.9 km from the reef margin and marks maximum flooding during Y4 time.

The HST of Y4 exhibits strong progradational geometries overall in a stepwise fashion, with thick seaward-directed tongues of shelf-crest facies alternating with thick landward-directed tongues of outer-shelf facies (Fig. 13). The most seaward tongues of pisolite shoal facies immediately below the upper HFS boundary extend to within 100 m of the reef edge, but the steepness of exposures in this area preclude a detailed examination (Fig. 10G, H). This same stratigraphic location was investigated in McKittrick Canyon by Kerans and Harris (1993), who documented 9–12 m of relief from the terminal shelf crest to the reef top. They also recognized an abrupt facies offset near the top Y4 surface that juxtaposed peritidal facies and exposure breccias above outer shelf and reefal facies, suggesting a sea-level fall of ~ 12 m and near-sea-level conditions at this phase of late Capitan reef development. Mutti and Simo (1993) also evaluated this upper Y4 HFS boundary in Walnut Canyon and interpreted brecciation, fractur-

TABLE 1.—*Depositional variables per Yates HFS*

HFS	Downdip Thickness Increase (%)	Shelf-Crest Aspect Ratio	Outer-Shelf Aspect Ratio	Distance from Shelf-Crest to Reef (m)	Landward Extent of Maximum Flooding (m)
Y4	380	0.017	0.065	~100	900
Y3	330	0.017	0.051	250	1200
Y2	430	0.031	0.078	500	900
Y1	240	0.041	0.045	550	1400
Avg.	345	0.027	0.06	350	1100

HFS	Shelf P : A Ratio	Shelf Offlap Angle	Shelf Crest Progradation Rate (m/ky)	Reef P : A Ratio	Reef Offlap Angle	Depth to Reef (m)
Y4	11	5.1°	2.7	7	8.2°	~10
Y3	170	0.3	2.1	23	2.5	25
Y2	15	3.9	2.2	10	5.5	35
Y1	11	5.2	1.3	13	4.5	65
Avg.	52	3.6°	2.1	13	5.2°	34

ing, moldic porosity formation, and dolomitization at this contact as a result of subaerial exposure and subsequent marine reworking. The thick overlying sandstones of the uppermost Yates (''Triplet'') represent the seaward shift in facies tracts that accompanied the base-level fall along the top Y4 HFS boundary.

SEA-LEVEL DYNAMICS AND SHELF-MARGIN EVOLUTION

The long-term dynamics of sea-level change and the overall evolution of the Yates–Capitan shelf margin from Y1 through Y4 can be quantified by systematic trends in downdip thickness changes, lateral extent of facies tracts relative to the Capitan reef margin, aspect ratios of facies tracts, progradation:aggradation ratios and derived offlap angles, and progradation rates (Table 1; Figs. 14, 15). These long-term trends in select depositional variables through the Y1–Y4 HFSs reveal the larger-scale evolution of the Yates–Tansill composite sequence, defined by Kerans et al. (1992) from exposures in McKittrick Canyon. The basal Y1 sequence boundary is likely the lower sequence boundary of the Yates–Tansill composite sequence, making Y1 the basal HFS in the composite sequence.

All of the following calculations assume that the dominantly east-southeast depositional dips measured on the southwest-facing wall of Slaughter Canyon represent the dominant progradation direction. Outcrops on the opposite northeast-facing wall in Slaughter and to the southwest in Middle Slaughter Canyon (Fig. 3) appear to have a northeast-dipping component, which raises the probability of changing primary depositional dip orientations through time on the Yates outer shelf. Along-strike variations in sediment supply and progradation direction have been proposed for the Vercors (Everts et al. 1995) and Maiella (Mutti et al. 1996) platform margins, which are skeletal-sand-rich margins with characteristics comparable to the Yates platform.

Seaward Thickening and Progradation Distance

Two of the most fundamental characteristics of Yates HFSs are their extreme seaward thickening and progradational architecture. These two attributes are expressed in the mapped profile by the episodic but progressive seaward ''step-out'' of the shelf margin between adjacent HFSs (Figs. 7, 13). These architectural characteristics can also be illustrated in plots of downdip thickness increases per HFS and lateral extent of facies tracts relative to the reef margin (Figs. 15A, B). Downdip increases in thickness vary with position in the overall Yates–Tansill composite sequence. The mildly retrogradational Y1 HFS represents the transgressive phase of the composite sequence and shows the least amount of seaward thickening, a characteristic interpreted to reflect initial flooding of the underlying Seven Rivers platform and moderate accommodation potential. The dramatic seaward thickening of HFS Y2 and its generally aggradational architecture records the early highstand phase of the composite sequence and the highest overall accommodation potential. HFS Y3 and Y4 exhibit substantially less seaward thickening than Y2 and strongly progradational geometries, characteristic of low accommodation during the middle to late highstand.

The overall seaward progradation from Y1 to Y4 is also reflected in the general decrease in distance from the most downdip extent of shelf-crest facies immediately underlying the HFS boundary to the reef (Fig. 15B). The terminal extent of the Y1 and Y2 shelf crests reach to within a half kilometer of the reef, but by the end of Y4 time, the shelf crest reaches to within ~ 100 m of the reef. The lateral extent of outer-shelf tongues onto the platform reach their greatest distance during Y1 time, extending 1.4 km landward relative to the reef edge (Fig. 15B). This tongue is interpreted to represent maximum flooding, not only of the Y1 HFS but also of the entire Yates–Tansill composite sequence. The interpreted position of the maximum flooding event within Y1 imparts a highly asymmetric, strongly progradational pattern to the composite sequence, an architecture well expressed in the mapped profile (Figs. 7, 11).

Aspect Ratios

The progressive seaward migration and lateral expansion of the shelf-crest facies tract from Y1 through Y4 is matched by a reciprocal seaward-stepping architecture and lateral contraction of the outer-shelf facies tract through Yates time (Fig. 11). These apparent changes in volume and spatial distribution can be directly compared using aspect ratios, a measure of the maximum thickness of a facies tract versus its dip width within individual HFSs (Kerans and Fitchen 1995). Consistent points of reference must be

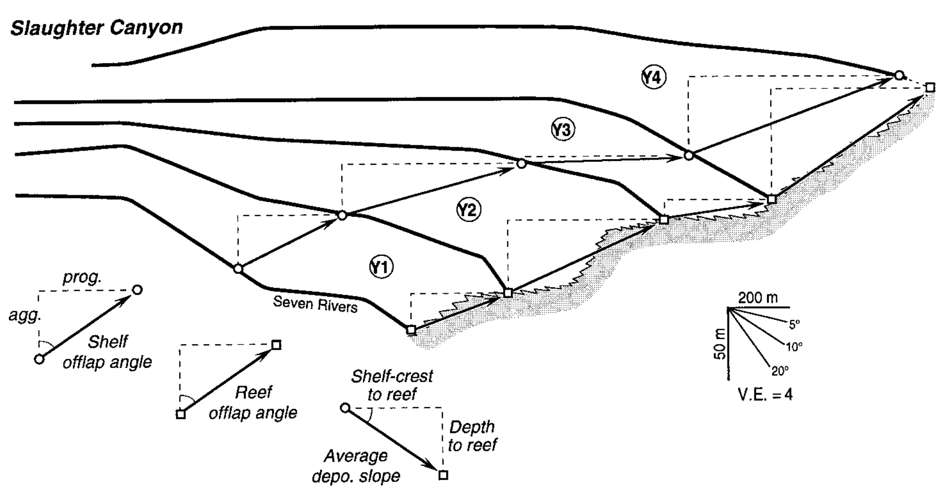

FIG. 14.—Skeleton plot of Yates profile from Slaughter Canyon illustrating the tie points for determining several of the depositional variables within each HFS (plotted in Figure 15). Circles mark the seaward edge of the shelf-crest facies tract just prior to exposure and formation of HFS boundary (assumed to represent a paleoshoreline and thus sea level). Squares mark the position of the reef margin at HFS boundaries. The distance from the shelf crest to reef, the maximum extent of flooding, and the depth of the reef along upper HFS boundaries were determined from simple measurements made relative to the time-equivalent reef margin.

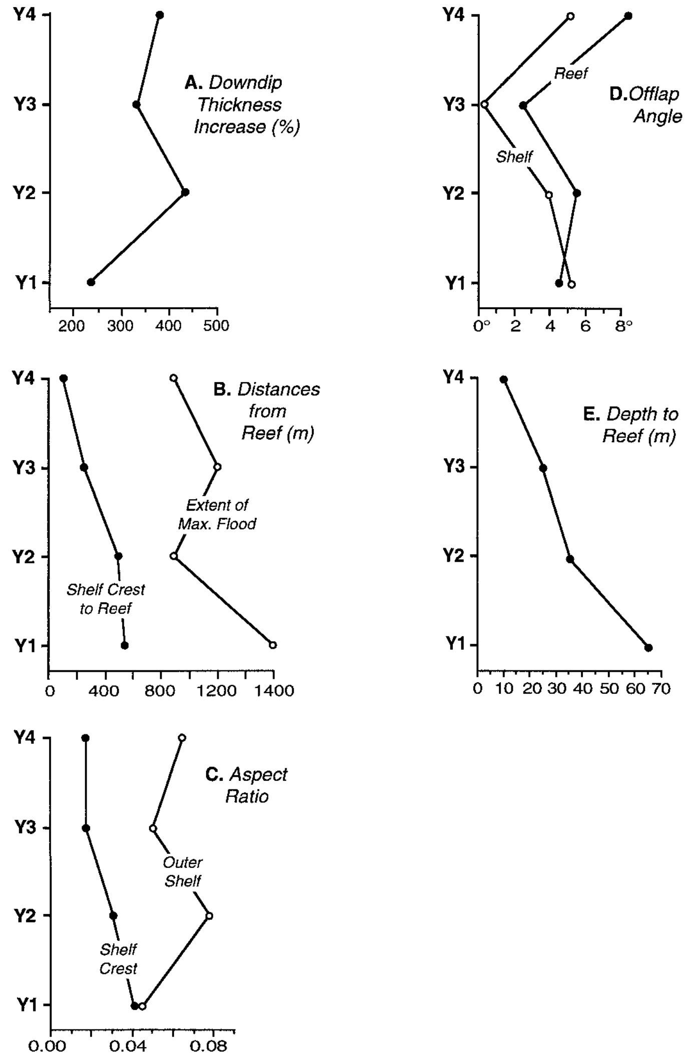

FIG. 15.—Trends in selected depositional variables through Yates time, plotted stratigraphically. Data are compiled in Table 1. Actual measurements were determined from an expanded-scale cross section calibrated against photointerpretations. **A)** Downdip thickness increases determined from most updip section versus maximum thickness of each HFS. **B)** Aspect ratios can be visualized qualitatively in Figure 11. **C)** Distances measured from expanded version of Figure 7 and panoramic photographs. **D)** Offlap angle equals the arctangent of the aggradation:progradation ratio. **E)** Reef depth at the end of deposition for each HFS estimated from the vertical distance between the terminus of the shelf crest below the HFS boundary and the equivalent reef edge. Error in the depth estimates is ~ 10 m.

used to make this depositional variable useful. The width of the shelf crest is defined on the updip side by the presence of dominantly fenestral tidal-flat facies flanking the pisolite shoal and on the downdip side by the most seaward extent of shelf-crest facies near the top of each HFS. The width of the outer shelf is determined by the distance from the most landward extent of maximum flooding facies to the terminal reef edge near the top of each HFS.

Aspect ratios of the shelf-crest facies tract decrease from Y1 to Y4 (Table 1; Fig. 15C), primarily because of progressive lateral expansion through time rather than an increase in maximum thickness. The width of the shelf crest grows from ~ 0.9 km in Y1 to 2.9 km in Y4, whereas the maximum thickness for all four shelf crests varies only between 36–50 m. There is noticeable expansion in shelf-crest width between aggradational Y2 (1.4 km) and progradational Y3 (2.1 km), reflecting reduced accommodation during the transition from early to middle highstand. Concomitant with progressive expansion of the shelf crest, the outer shelf exhibits a reciprocal decrease in width from 1.5 km in Y1 to 0.9 km in Y4. Outer-shelf aspect ratios are higher than those for the shelf crest because outer-shelf successions show overall greater thicknesses and relatively more equidimensional geometry per HFS (Fig. 15C). Maximum thicknesses of outer-shelf facies tracts reflect their position within the overall composite sequence and thus their accommodation potential, ranging from 68 m within transgressive Y1, to 94 m within aggradational Y2, to ~ 55 m in progradational Y3 and Y4.

The thick accumulations of outer-shelf facies accentuate the seaward step-out that occurs between adjacent HFSs (Fig. 13). This basinward shift in the locus of sedimentation is interpreted to be a response to base-level fall along HFS boundaries (cf. Borer and Harris 1995). Steep antecedent topography along the front of the underlying outer shelf and reef may enhance the space available for accumulation of thick piles of poorly sorted, massively bedded outer-shelf packstones and grainstones. The abrupt expansion within each Yates HFS appears to occur directly above the terminal reef margin of the preceding HFS (Fig. 13). The underlying reef margin likely acts as a foundation to localize the basinward shift, contributing to the seaward expansion and step-out of the outer shelf. Syndepositional differential compaction has been proposed as an accommodation-generating process on actively prograding shelf margins (cf. Hunt et al 1995; Saller 1996), and may have contributed an indeterminate amount to the seaward step-out of each Yates HFS. Differential compaction is not a viable mechanism for all seaward thickening in Yates HFSs, however, because of the documented retrogradational to aggradational to progradational geometries in each HFS. These stacking patterns would require systematic, high-frequency changes in the rate of differential compaction, a tenuous proposition.

Offlap Angles and Progradation Rates

Calculation of progradation:aggradation (P:A) ratios, offlap angles, and progradation rates per HFS requires a unique bathymetric tie point within each HFS. Along any one time line on the Yates platform, the contact between the downdip limit of shelf-crest flanking facies (fenestral tidal-flat facies) and the updip, littoral limit of outer-shelf facies (oolites, coated grains, or skeletal grainstones) provides a reasonable approximation of the location of sea level. The position of this tie point systematically varies within each HFS, however, and thus should be measured at a consistent phase of HFS development. Therefore, thicknesses and widths involved in the calculation of P:A ratios and progradation rates were determined from the terminal seaward edge of the shelf crest in each Yates HFS (Fig. 14). The time control necessary to estimate progradation rates per Yates HFS is also a significant problem (cf. Borer and Harris 1991). In this study, each Yates HFS is estimated to span ~ 250 k.y. (± 50%), assuming a 1 m.y. total duration for Yates time (based on Ross and Ross 1987 and Harland et al. 1989). Results are shown in Table 1 and Figure 15D along with P:A ratios and offlap angles for time-equivalent portions of the Capitan reef.

Offlap angles for each HFS and equivalent phases in Capitan reef development tend to track each other, with higher angles of the reef likely reflecting the steep reef front that inhibited seaward growth (Fig. 15D). Y1 and the time-equivalent Capitan reef exhibit comparable offlap angles of 5.2° and 4.5°, respectively, interpreted to record moderate accommodation conditions associated with the initial flooding of the Yates platform subsequent to exposure along the underlying composite sequence boundary. The relatively slow progradation rate of 1.3 m/k.y. during Y1 time also reflects the dominance of retrogradation and aggradation over progradation at this early transgressive phase of the Yates–Tansill composite sequence. During Y2 time, shelfal offlap angles decreased while reef angles increased, a trend that may reflect an aggradational flattening of the Yates shelf coincident with aggradational upbuilding of the Capitan reef in response to high accommodation conditions. The increase in Y2 shelf-crest progradation rate beyond the Y1 rate also may record more rapid migration across a flattened shelf profile.

P:A ratios increase dramatically for strongly progradational Y3, with the corresponding low offlap angle of 0.3° matched by a generally low reef growth angle of 2.5°. Progradation rates during Y3 time kept pace with those of Y2 during this phase of greatly reduced shelfal accommodation, which forced the locus of sedimentation seaward. Offlap angles of both the shelf and time-equivalent reef steepen considerably during Y4 (Fig. 15D), reflected in the dominantly aggradational stratal patterns of the Y4 shelf. This is a phase of extreme upbuilding by the Capitan reef, with growth angles approaching 8.2°. These high offlap angles may partly record a renewed increase in accommodation during the late highstand of the Yates–Tansill composite sequence, but more likely they are a product of the steep front of the Capitan reef, which limited the foundation for greater seaward progradation of both the shelf and reef. The resultant flattened depositional topography permitted shelf-crest progradation to very near the reef edge by the end of Y4 time (cf. Kerans and Harris 1993). Thick siliciclastics (''Triplet'') accumulated on top of the flat Y4 shelf prior to strong seaward migration of shelf-crest facies of the Tansill Formation.

Overall, the Y1–Y4 HFSs in Slaughter Canyon are characterized by an average P:A ratio of 52 and an average offlap angle of 3.6°, values corroborating the dominantly progradational architecture evident in outcrop. Corresponding averages for the time-equivalent Capitan reef are a P:A ratio of 13 and a 5.2° angle of growth, values that reflect the high amount of accommodation available near the transition from outer shelf to reef, as well as limitations to seaward growth imposed by the steepness of the reef front. The Yates shelf prograded at an average rate of 2.1 m/k.y. This shelfal progradation rate is similar to rates calculated from seismic sequences of comparable temporal and spatial scale comprising the Bahamas platform (~ 2.8 m/k.y.; Eberli and Ginsburg 1989). The Yates-equivalent Capitan reef prograded ~ 1.7 km in ~ 1 m.y. (1.7 m/k.y.), a rate within the range estimated by Garber et al. (1989) for the entire Yates–Tansill phase of reef growth (1.1–2.6 m/k.y.).

Depth of Capitan Reef

The strongly progradational character of the Yates shelf resulted in a progressive decrease in the depth of the Capitan reef from a maximum of ~ 65 m during early Yates time to near sea level during the latest stages of the Yates platform (Fig. 15E). The actual depth of the reef likely varied episodically through Yates time, though, because of shorter-term depth changes superimposed in response to cycle-scale and HFS-scale relative sea-level changes. Within any one HFS, the greatest depths were attained during maximum flooding and the shallowest during subaerial exposure along HFS boundaries. The estimates of reef depth were measured from the same reference point in each HFS (Fig. 14) but are hardly absolute owing to the limited knowledge of original depositional topography and postdepositional tilting, but the overall trend of decreasing depth through time is clear. This long-term pattern emphasizes the point that previous published estimates of the depth of the Capitan reef represent single episodes in time within the overall progressive decrease in reef depth.

MAGNITUDES OF RELATIVE SEA-LEVEL CHANGE

The magnitudes of sea-level oscillations that produced meter-scale cycles within the upper Seven Rivers and Yates interval have been estimated by several workers to have been in the range of 2–20 m (Smith 1974; Borer and Harris 1991, 1995; Kerans and Harris 1993; Rankey and Lehrmann 1996). In Slaughter Canyon, certain cycles were traced along paleoslope to determine the vertical distances between the updip position of tidal-flat facies, the downdip extent of unequivocal subaerial exposure features along the same cycle top, and the updip position of immediately overlying transgressive facies. These vertical distances provide minimum values of relative sea-level changes associated with exposure along cycle and sequence boundaries (''pinning point method'' of Franseen et al. 1993). Estimates of cycle-scale sea-level changes from the mapped transect in Slaughter Canyon are highly variable, ranging from 4 to 27 m in the Y1 HFS, 5 to 20 m in Y2, 4 to 15 m in Y3, and ~ 10 to 30 m in Y4. A general trend that can be discerned is an overall decrease in estimated magnitudes upward within individual HFSs; several exceptions to this trend are recognized, however, suggesting that the magnitudes of high-frequency sea-level pulses evolved erratically rather than systematically through Yates time.

Estimates of the magnitude of both relative and eustatic sea-level fluctuations governing larger-scale HFSs and composite sequences are invariably based upon assumptions about compaction history, isostatic and tectonic subsidence history, flexural rigidity of underlying lithosphere, and original depositional topography. Beyond the inherent ambiguity of estimating these variables, the actual composite sea-level history is likely a complex set of interfering waves comprising a spectrum of frequencies and amplitudes, complicating the task of deconvolving the higher-frequency, cycle-scale fluctuations from the lower-frequency, HFS-scale fluctuations. Yates HFSs do not merely reflect the cumulative effects of the higher-frequency fluctuations, however, because the mildly retrogradational, to aggradational, to strongly progradational stacking patterns intrinsic to each Yates HFS dictate that a longer-term driver must have been present.

Perhaps the least equivocal estimates of Yates HFS-scale sea-level magnitudes result from forward modeling experiments. Borer and Harris (1995) performed sensitivity tests to determine a ''best-fit'' simulation to Yates stacking patterns and arrived at magnitudes on the order of 30–40 m per Yates HFS. In another approach, Ye et al. (1996) used extensive outcrop observations in the Guadalupe and Delaware Mountains to document multiple shoreline positions through 38 HFSs spanning 30 m.y. of Permian deposition. The history of relative sea level derived from topographic changes in paleoshoreline position was subjected to two-dimensional backstripping techniques that separated the steadily changing subsidence rate from the highly oscillatory eustatic signal. The HFS-scale eustatic magnitudes during Yates time determined by Ye et al. ranged from ~ 40 m to ~ 50 m, a total that reflects the combined high- and low-frequency oscillations.

Glacio-eustasy is commonly identified as the primary control on relative sea-level fluctuations during deposition of Capitan-age cyclic strata (e.g., Silver and Todd 1969; Meissner 1972; Borer and Harris 1991; Rankey and Lehrmann 1996). The chronology of continental glaciation through the late Paleozoic compiled by Veevers and Powell (1987), however, indicates that major continental glaciers were gone from Gondwana by the late Leonardian. Thus the Guadalupian was a transitional phase between earlier icehouse climates and subsequent Mesozoic greenhouse climates. Considering the low- to moderate-amplitude sea-level fluctuations inferred from the stratigraphic cyclicity, this transitional timing suggests that reservoirs for storage and release of global water other than continental glaciers must have existed during the Guadalupian. Thus the assumption that glacio-eustasy was the primary control may need to be reassessed until other mechanisms that affect the volume of seawater in the oceans can be identified.

CONCLUSIONS

(1) Individual Yates high-frequency sequences are fundamentally macroscale versions of Yates meter-scale cycles, on the basis of comparable internal arrangements of lithofacies and their seaward-thickening geometry. This scale-independent architecture of chronostratigraphic units has been recognized by many workers and may reflect the scale-independent nature of the controlling process, interpreted to be composite eustasy in this Late Permian example.

(2) Stratigraphic trends in quantified depositional variables such as aspect ratios, progradation:aggradation ratios, offlap angles, and platform pro-

gradation rates reflect the long-term accommodation history that controlled the evolution of the Yates–Capitan shelf margin. Stratal geometries and cycle stacking patterns represented by the quantified variables change in a complex, yet systematic, manner upward through HFSs constituting a composite sequence. Similar long-term trends in quantified depositional variables may enable the recognition of larger-scale evolutionary patterns in other shelf-margin settings.

(3) Architectural changes evident in successive Yates HFSs reveal the interaction between changes in relative sea level and depositional topography, which drives seaward progradation. Sea-level fall along exposed HFS boundaries forces the locus of sedimentation onto the steep antecedent topography of the outer shelf and reef of the underlying HFS. With consequent sea-level rise, this steep gradient provides a foundation for the accumulation of a thick pile of open-shelf skeletal carbonate, which eventually flattens the depositional topography of the shelf, enhancing the seaward migration of peritidal environments. In the case of the Yates–Capitan shelf margin, the steepness of the reef front and foreslope ultimately limits the extent of progradation and thus controls the large-scale architecture of Yates HFSs.

(4) Seismic-scale, two-dimensional profiles such as this Upper Permian example provide visual analogs for subsurface reservoirs, potentially improving fluid-flow simulations and reservoir engineering (e.g., Kerans et al. 1994). Field-documented stratal geometries and density estimates can also be used to generate synthetic seismic models to evaluate reflection contact relationships on actual seismic sections (e.g., Stafleu and Sonnenfeld 1994). Moreover, mapped profiles serve as the ''ground truth'' for computer simulations that attempt to quantify potential accommodation histories and the likely controlling variables of deposition.

ACKNOWLEDGMENTS

Hasselblad pans were provided by Exxon Production Research, and low-angle oblique photos were supplied by Charlie Kerans of The University of Texas Bureau of Economic Geology. Permission to work in the study area was granted by the Carlsbad Caverns National Park Service. The manuscript benefited from discussions with Scott Tinker, Charlie Kerans, and Steve Ruppel, as well as from comprehensive reviews by Gregor Eberli, Maria Mutti, Toni Simo, and John Southard. Funding for this project was provided by the Petroleum Research Fund, administered by the American Chemical Society, and Exxon Production Research Company.

REFERENCES

Achauer, C.W., 1969, Origin of Capitan Formation, Guadalupe Mountains, New Mexico and Texas: American Association of Petroleum Geologists, Bulletin, v. 53, p. 2314–2323.

Andreason, M.W., 1992, Coastal siliciclastic sabkhas and related evaporative environments of the Permian Yates Formation, North Ward–Estes Field, Ward County, Texas: American Association of Petroleum Geologists, Bulletin, v. 76, p. 1735–1759.

Babcock, J.A., 1977, Calcareous algae, organic boundstones, and the genesis of the Upper Capitan Limestone (Permian, Guadalupian), Guadalupe Mountains, West Texas and New Mexico, *in* Hileman, M.E., and Mazzullo, S.J., eds., Upper Guadalupian Facies, Permian reef Complex, Guadalupe Mountains, New Mexico and West Texas: SEPM, Permian Section, Publication 77-16, 1977 Field Conference Guidebook, vol. 1, p. 3–44.

Borer, J.M., and Harris, P.M., 1991, Lithofacies and cyclicity of the Yates Formation, Permian Basin: Implications for reservoir heterogeneity: American Association of Petroleum Geologists, Bulletin, v. 75, p. 726–779.

Borer, J.M., and Harris, P.M., 1995, Computer simulation of the Yates Formation (Permian, Delaware Basin)—Sequence stratigraphy and shelf-to-basin correlation implications, *in* Martin, R.L., ed., In Search of New Permian Basin Oil and Gas Fields: Using Today's Technologies and Tomorrow's Ideas for Exploration, Development, and 3D Seismic in a Mature Basin: West Texas Geological Society, Publication 95-98, p. 111–132.

Candelaria, M.P., 1989, Shallow marine sheet sandstones, upper Yates Formation, Northwest shelf, Delaware Basin, New Mexico, *in* Harris, P.M., and Grover, G.A., eds., Subsurface and Outcrop Examination of the Capitan Shelf Margin, Northern Delaware Basin: SEPM, Core Workshop 13, p. 319–324.

Crowley, T.J., Hyde, W.T., and Short, D.A., 1989, Seasonal cycle variations on the supercontinent of Pangaea: Geology, v. 17, p. 457–460.

Dunham, R.J., 1972, Capitan reef, New Mexico and Texas: facts and questions to aid interpretation and group discussion: SEPM, Permian Basin Section, Publication 72-14, 297 p.

Eberli, G.P., and Ginsburg, R.N., 1989, Cenozoic progradation of northwestern Great Bahama Bank, a record of lateral platform growth and sea-level fluctuations, *in* Crevello, P.D., Wilson, J.L., Sarg, J.F., and Read, J.F., eds., Controls on Carbonate Platform and Basin Development: SEPM, Special Publication 44, p. 339–351.

Elam, J.G., and Chuber, S., 1967, Cyclic Sedimentation in the Permian Basin: West Texas Geological Society, Midland, Texas, 232 p.

Esteban, M., and Pray, L.C., 1977, Origin of the pisolite facies of the shelf crest, *in* Hileman, M.E., and Mazzullo, S.J., eds., Upper Guadalupian Facies, Permian Reef Complex, Guadalupe Mountains, New Mexico and West Texas: SEPM, Permian Section, Publication 77-16, 1977 Field Conference Guidebook, vol. 1, p. 479–486.

Everts, A.J.W., Stafleu, J., Schlager, W., Fouke, B.W., and Zwart, E.W., 1995, Stratal patterns, sediment composition, and sequence stratigraphy at the margin of the Vercors carbonate platform (Lower Cretaceous, SE France): Journal of Sedimentary Research, v. B65, p. 119–131.

Fischer, A.G., and Sarnthein, M., 1988, Airborne silts and dune-derived sands from the Permian of the Delaware basin: Journal of Sedimentary Petrology, v. 58, p. 637–643.

Franseen, E.K., Goldstein, R.H., and Whitesell, T.E., 1993, Sequence stratigraphy of Miocene carbonate complexes, Las Negras area, southeastern Spain: Implications for quantification of changes in relative sea level, *in* Loucks, R.G., and Sarg, J.F., eds., Carbonate Sequence Stratigraphy: Recent Developments and Applications: American Association of Petroleum Geologists, Memoir 57, p. 409–434.

Garber, R.A., Grover, G.A., and Harris, P.M., 1989, Geology of the Capitan shelf margin—subsurface data from the northern Delaware basin, *in* Harris, P.M., and Grover, G.A., eds., Subsurface and Outcrop Examination of the Capitan Shelf Margin, Northern Delaware Basin: SEPM, Core Workshop 13, p. 3–269.

Golonka, J., Ross, M.I., and Scotese, C.R., 1994, Phanerozoic paleogeographic and paleoclimatic modeling maps, *in* Embry, A.F., Beauchamp, B., and Glass, D.J., eds., Pangea: Global Environments and Resources: Canadian Society of Petroleum Geologists, Memoir 17, p. 1–47.

Harland, W.B., Armstrong, R.L., Cox, A.V., Craig, L.E., Smith, A.G., and Smith, D.G., 1989, A Geologic Time Scale: New York, Cambridge University Press, 128 p.

Hayes, P.T., 1964, Geology of the Guadalupe Mountains, New Mexico: U.S. Geological Survey, Professional Paper 446, 69 p.

Hayes, P.T., and Koogle, R.L., 1958, Geology of the Carlsbad Caverns West quadrangle, New Mexico–Texas: U.S. Geological Survey, Geologic Quadrangle Map GQ-112.

Hunt, D., Allsop, T., and Swarbrick, R., 1995, Compaction as a primary control on the architecture and development of depositional sequences: conceptual framework, applications and implications, *in* Howell, J.A., and Aitken, J.F., eds., High Resolution Sequence Stratigraphy: Innovations and Applications: Geological Society of London, Special Publication 104, p. 321–345.

Hurley, N.F., 1989, Facies mosaic of the lower Seven Rivers Formation, McKittrick Canyon, New Mexico, *in* Harris, P.M., and Grover, G.A., eds., Subsurface and Outcrop Examination of the Capitan Shelf Margin, Northern Delaware Basin: SEPM, Core Workshop 13, p. 325–346.

Kendall, C.G.St.C., 1969, An environmental reinterpretation of the Permian evaporite/carbonate shelf sediments of the Guadalupe Mountains: Geological Society of America, Bulletin, v. 80, p. 2503–2526.

Kerans, C., and Fitchen, W.M., 1995, Sequence hierarchy and facies architecture of a carbonate-ramp system: San Andres Formation of Algerita Escarpment and western Guadalupe Mountains, west Texas and New Mexico: The University of Texas at Austin, Bureau of Economic Geology, Report of Investigations no. 235, 86 p.

Kerans, C., and Harris, P.M., 1993, Outer shelf and shelf crest, *in* Bebout, D.G., and Kerans, C., eds., Guide to the Permian Reef Geology Trail, McKittrick Canyon, Guadalupe Mountains National Park, West Texas: The University of Texas at Austin, Bureau of Economic Geology, Guidebook 26, p. 32–43.

Kerans, C., and Tinker, S.W., 1997, Sequence Stratigraphy and Characterization of Carbonate Reservoirs: SEPM, Short Course 40, 130 p.

Kerans, C., Fitchen, W.M., Gardner, M.H., Sonnenfeld, M.D., Tinker, S.W., and Wardlaw, B.R., 1992, Styles of sequence development within uppermost Leonardian through Guadalupian strata of the Guadalupe Mountains, Texas and New Mexico, *in* Mruk, D.H., and Curran, B.C., eds., Permian Basin Exploration and Production Strategies: Applications of Sequence Stratigraphic and Reservoir Characterization Concepts: West Texas Geological Society, Publication 92-91, p. 1–7.

Kerans, C., Lucia, J.F., and Senger, R.K., 1994, Integrated characterization of carbonate ramp reservoirs using Permian San Andres Formation outcrop analogs: American Association of Petroleum Geologists, Bulletin, v. 78, p. 181–216.

King, P.B., 1948, Geology of the southern Guadalupe Mountains, Texas: U.S. Geological Survey, Professional Paper 215, 183 p.

Kutzbach, J.E., and Gallimore, R.G., 1989, Pangaean climates: Megamonsoons of the megacontinent: Journal of Geophysical Research, v. 94, p. 3341–3357.

McKee, E.D., 1945, Cambrian history of the Grand Canyon region—pt. 1, stratigraphy and ecology of the Grand Canyon Cambrian: Carnegie Institution of Washington, Publication 563, 168 p.

Meissner, F.F., 1972, Cyclic sedimentation in Middle Permian strata of the Permian Basin, *in* Elam, J.G., and Chuber, S., eds., Cyclic Sedimentation in the Permian Basin, 2nd Edition: West Texas Geological Society, Publication 72-60, p. 203–232.

Melim, L.A., and Scholle, P.A., 1995, The forereef facies of the Permian Capitan Formation: the role of sediment suppply versus sea-level changes: Journal of Sedimentary Research, v. B65, p. 107–118.

Mitchum, R.M., and Van Wagoner, J.C., 1991, High-frequency sequences and their stacking patterns: sequence-stratigraphic evidence of high-frequency eustatic cycles: Sedimentary Geology, v. 70, p. 131–160.

Mutti, M., and Simo, J.A., 1993, Stratigraphic patterns and cycle-related diagenesis of Upper Yates Formation, Permian, Guadalupe Mountains, *in* Loucks, R.G., and Sarg, J.F., eds., Carbonate Sequence Stratigraphy: Recent Developments and Applications: American Association of Petroleum Geologists, Memoir 57, p. 515–534.

MUTTI, M., BERNOULLI, D., EBERLI, G.P., AND VECSEI, A., 1996, Depositional geometries and facies associations in an Upper Cretaceous prograding carbonate platform margin (Orfento Supersequence, Maiella, Italy): Journal of Sedimentary Research, v. 66, p. 749–765.

NEESE, D.A., AND SCHWARTZ, A.H., 1977, Facies mosaic of the upper Yates and lower Tansill formations, Walnut and Rattlesnake canyons, Guadalupe Mountains, New Mexico, *in* Hileman, M.E., and Mazzullo, S.J., eds., Upper Guadalupian Facies, Permian Reef Complex, Guadalupe Mountains, New Mexico and West Texas: SEPM, Permian Section, Publication 77-16, 1977 Field Conference Guidebook, p. 437–450.

NEWELL, N.D., RIGBY, J.K., FISCHER, A.G., WHITEMAN, A.J., HICKOX, J.E., AND BRADLEY, J.S., 1953, The Permian Reef Complex of the Guadalupe Mountains Region, Texas and New Mexico: San Francisco, Freeman, 236 p.

OSLEGER, D.A., AND TINKER, S.W., in press, Three-dimensional architecture of Upper Permian high-frequency sequences, Yates–Capitan shelf margin, Permian Basin, USA, *in* Harris, P.M., Saller, A.H., and Simo, T., eds., Advances in Carbonate Sequence Stratigraphy—Application to Reservoirs, Outcrops, and Models: SEPM, Special Publication.

POMAR, L., 1993, High-resolution sequence stratigraphy in prograding Miocene carbonates: Application to seismic interpretation: *in* Loucks, R.G., and Sarg, J.F., eds., Carbonate Sequence Stratigraphy: Recent Developments and Applications: American Association of Petroleum Geologists, Memoir 57, p. 389–407.

PRAY, L.C., AND ESTEBAN, M., 1977, Upper Guadalupian facies, Permian reef complex, Guadalupe Mountains, New Mexico and west Texas: SEPM, Permian Section, Publication 77-16, 1977 Field Conference Guidebook, vol. 2, 194 p.

RANKEY, E.C., AND LEHRMANN, D.J., 1996, Anatomy and origin of toplap in a mixed carbonate–clastic system, Seven Rivers Formation (Permian, Guadalupian), Guadalupe Mountains, New Mexico, USA: Sedimentology, v. 43, p. 807–826.

ROSS, C.A., AND ROSS, J.R.P., 1987, Late Paleozoic sea levels and depositional sequences, *in* Ross, C.A., and Haman, D., eds., Timing and Depositional History of Eustatic Sequences, Constraints on Seismic Stratigraphy: Cushman Foundation for Foraminiferal Research, Special Publication 24, p. 137–149.

ROSS, C.A., BAUD, A., AND MENNING, M., 1994, A time scale for Project Pangea, *in* Embry, A.F., Beauchamp, B., and Glass, D.J., eds., Pangea: Global Environments and Resources: Canadian Society of Petroleum Geologists, Memoir 17, p. 81–83.

SALLER, A.H., 1996, Differential compaction and basinward tilting of the prograding Capitan reef complex, Permian, west Texas and southeast New Mexico, USA: Sedimentary Geology, v. 101, p. 21–30.

SARG, J.F., 1981, Petrology of the carbonate–evaporite facies transition of the Seven Rivers Formation (Guadalupian, Permian), southeast New Mexico: Journal of Sedimentary Petrology, v. 51, p. 73–95.

SCOTESE, C.R., 1994, Late Permian paleogeographic map, *in* Klein, G.D., ed., Pangea: Paleoclimate, Tectonics, and Sedimentation during Accretion, Zenith, and Breakup of a Supercontinent: Geological Society of America, Special Paper 288, p. 232–242.

SILVER, B.A., AND TODD, R.G., 1969, Permian cyclic strata, northern Midland and Delaware Basins, west Texas and southeastern New Mexico: American Association of Petroleum Geologists, Bulletin, v. 53, p. 2223–2251.

SMITH, D.B., 1974, Sedimentation of Upper Artesia (Guadalupian) cyclic shelf deposits of northern Guadalupe Mountains, New Mexico: American Association of Petroleum Geologists, Bulletin, v. 58, p. 1699–1730.

SONNENFELD, M.D., AND CROSS, T.A., 1993, Volumetric partitioning and facies differentiation within the Permian upper San Andres Formation of Last Chance Canyon, Guadalupe Mountains, New Mexico, *in* Loucks, R.G., and Sarg, J.F., eds., Carbonate Sequence Stratigraphy: Recent Developments and Applications: American Association of Petroleum Geologists, Memoir 57, p. 475–492.

STAFLEU, J., AND SONNENFELD, M.D., 1994, Seismic models of a shelf-margin depositional sequence: Upper San Andres Formation, Last Chance Canyon, New Mexico: Journal of Sedimentary Research, v. B64, p. 481–499.

TINKER, S.W., 1996, Reservoir-scale sequence stratigraphy: McKittrick Canyon and 3-D subsurface examples, west Texas and New Mexico [unpublished Ph.D. thesis]: The University of Colorado, Boulder, Colorado, 245 p.

VEEVERS, J.J., AND POWELL, C.M., 1987, Late Paleozoic glacial episodes in Gondwanaland reflected in transgressive–regressive depositional sequences in Euramerica: Geological Society of America, Bulletin, v. 98, p. 475–487.

WARD, R.F., KENDALL, C.G.ST.C., AND HARRIS, P.M., 1986, Upper Permian (Guadalupian) facies and their association with hydrocarbons—Permian Basin, west Texas and New Mexico: American Association of Petroleum Geologists, Bulletin, v. 70, p. 239–262.

YE, Q., KERANS, C., FITCHEN, W.M., GARDNER, M.H., SONNENFELD, M.D., AND BOWMAN, S., 1996, Forward stratigraphic modeling of the Permian of the Delaware basin (abstract): American Association of Petroleum Geologists, Annual Convention, San Diego, California, Abstracts with Program, p. A156.

YUREWICZ, D.A., 1977, The origin of the massive facies of the Lower and Middle Capitan Limestone (Permian), Guadalupe Mountains, New Mexico and West Texas, *in* Hileman, M.E., and Mazzullo, S.J., eds., Upper Guadalupian Facies, Permian Reef Complex, Guadalupe Mountains, New Mexico and West Texas: San Diego, California, vol. 1, p. 45–92.

Received 14 March 1997; accepted 9 October 1997.

Shattuck Valley Escarpment

Grayburg Queen Goat-Seep Formations of the Guadalupe Mountains,

Presented by Kim Lankford
and
Jeff Kao

Location of Guadalupe Mountains

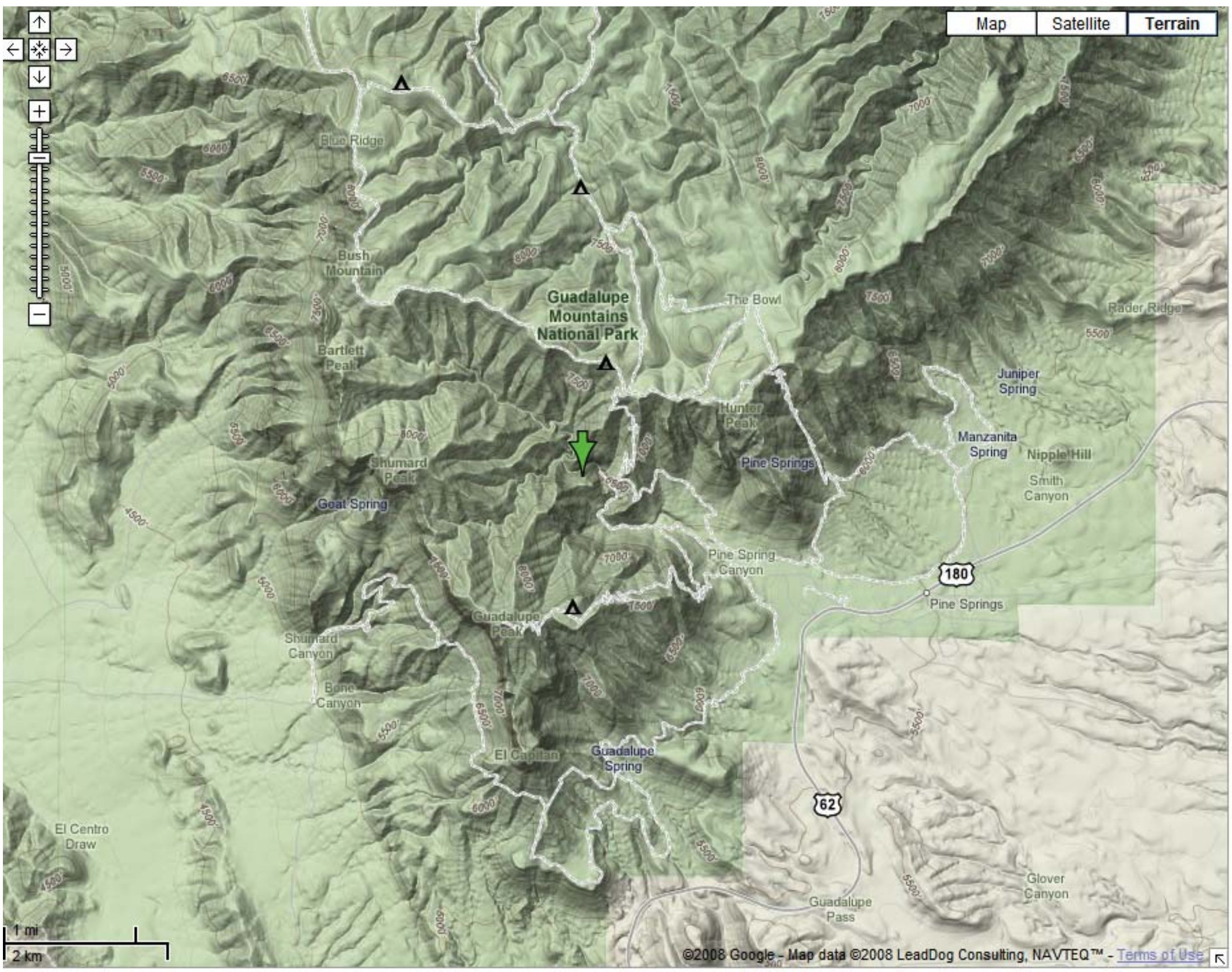

LSAT Image and Locations

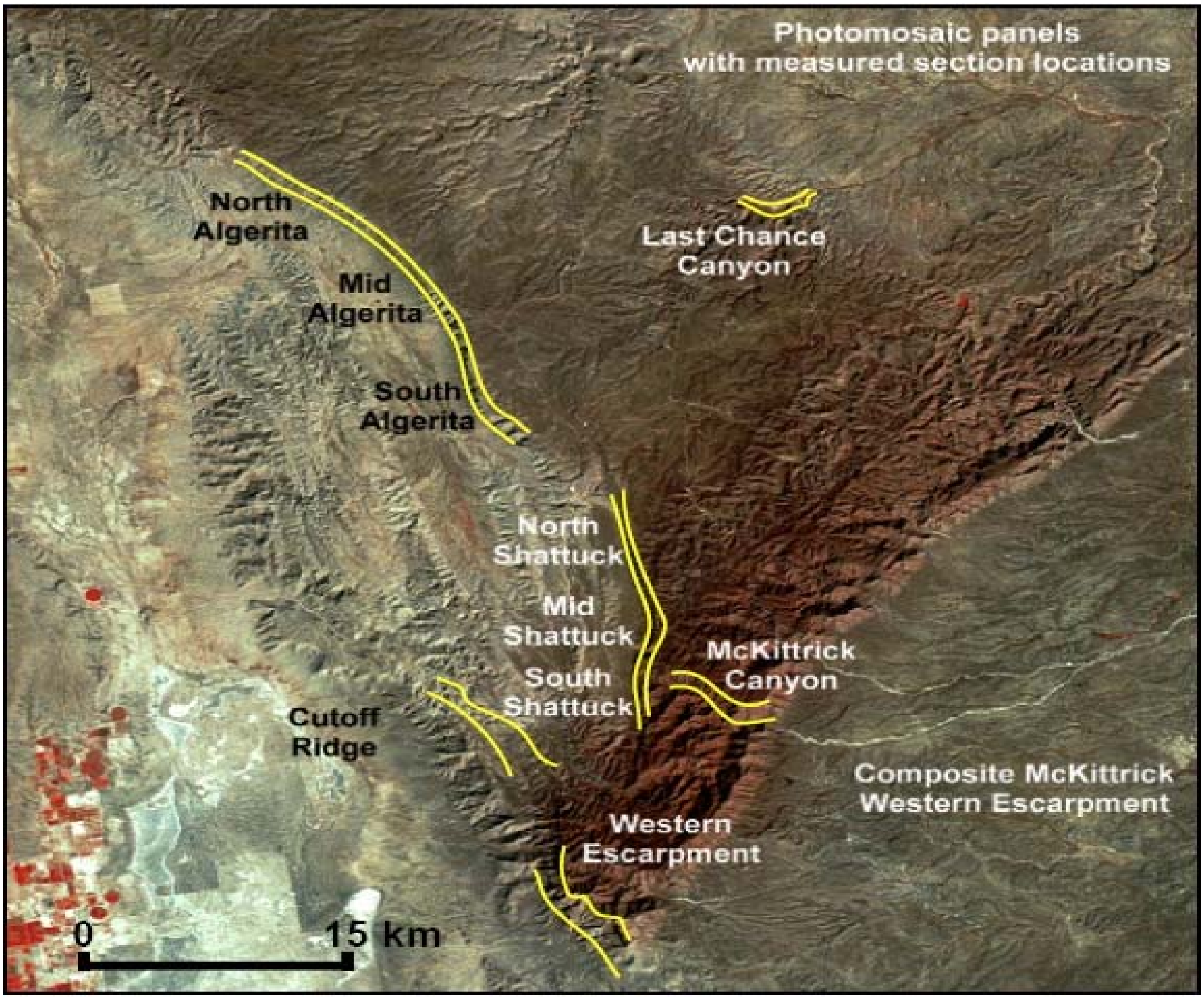

Kerans and Kempter
2002

Aerial View Looking North

Kerans and
Kempter
2002

Stratigraphy

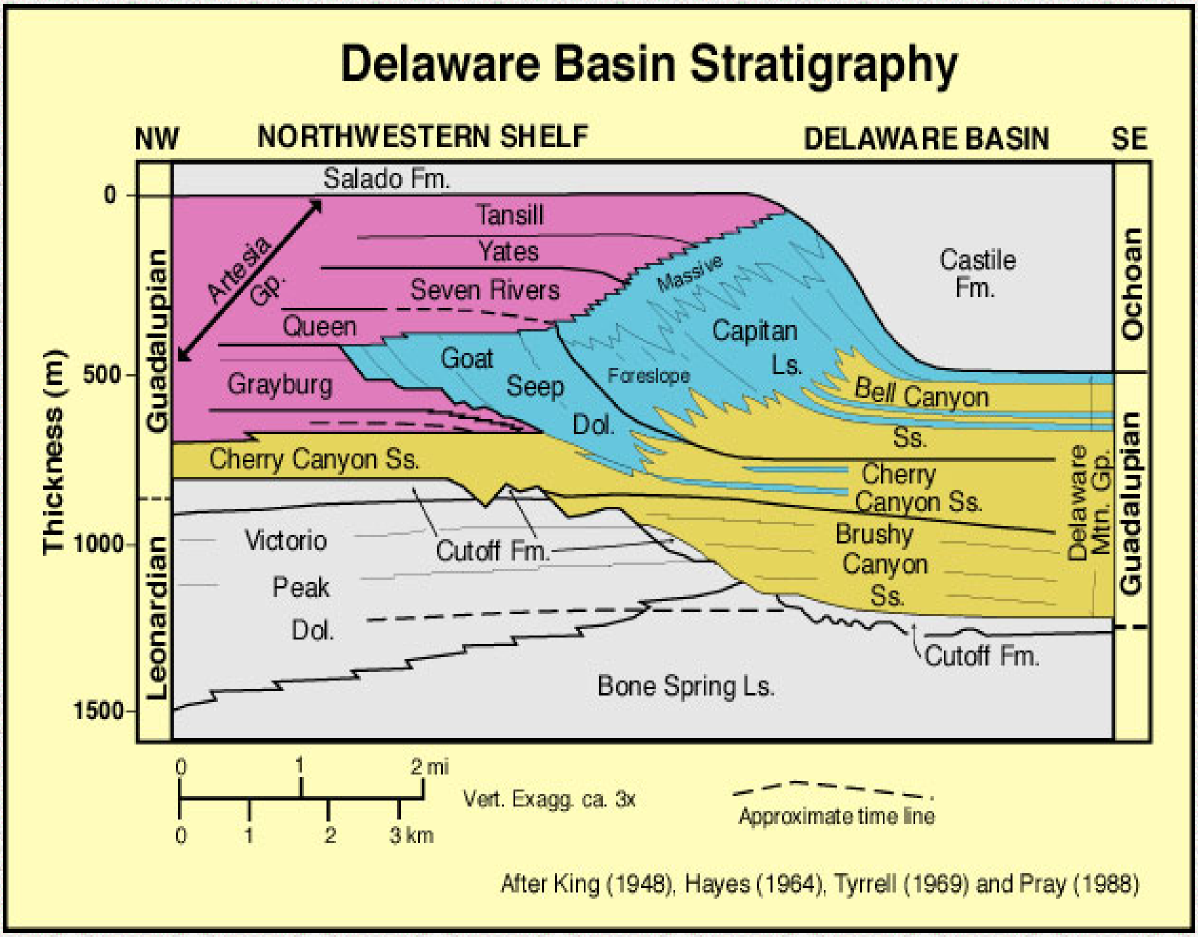

Standard stratigraphic nomenclature of the Permian strata exposed in the Guadalupe Mountains. Modified from many sources including King (1948), Hayes (1964), Tyrrell (1969) and Pray (1988a).

Peter Scholle

Geologic Time Scale of the Guadalupe Mountains

SE NW

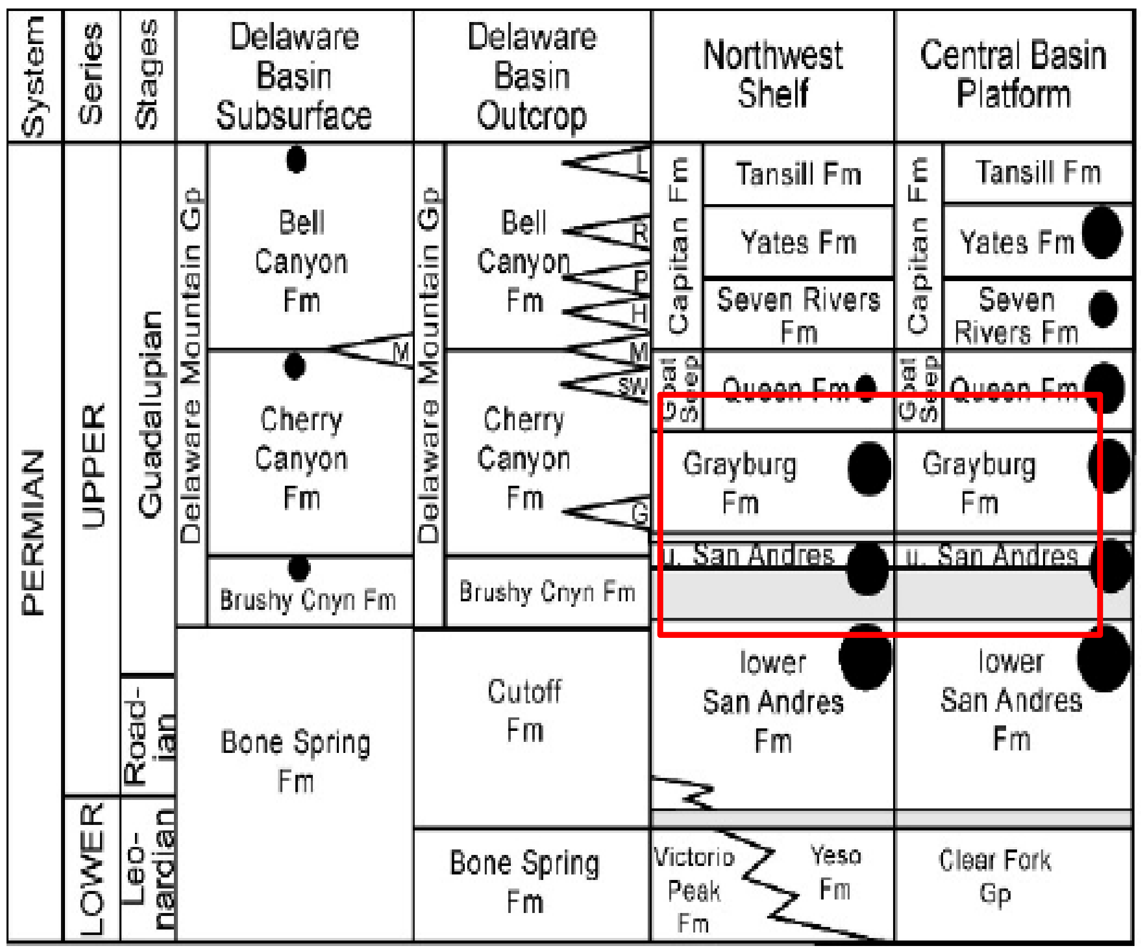

Modified from Galloway et al. (1983);
Ross and Ross (1987)
Kerans and Fitchen (1995)

Regional Separation

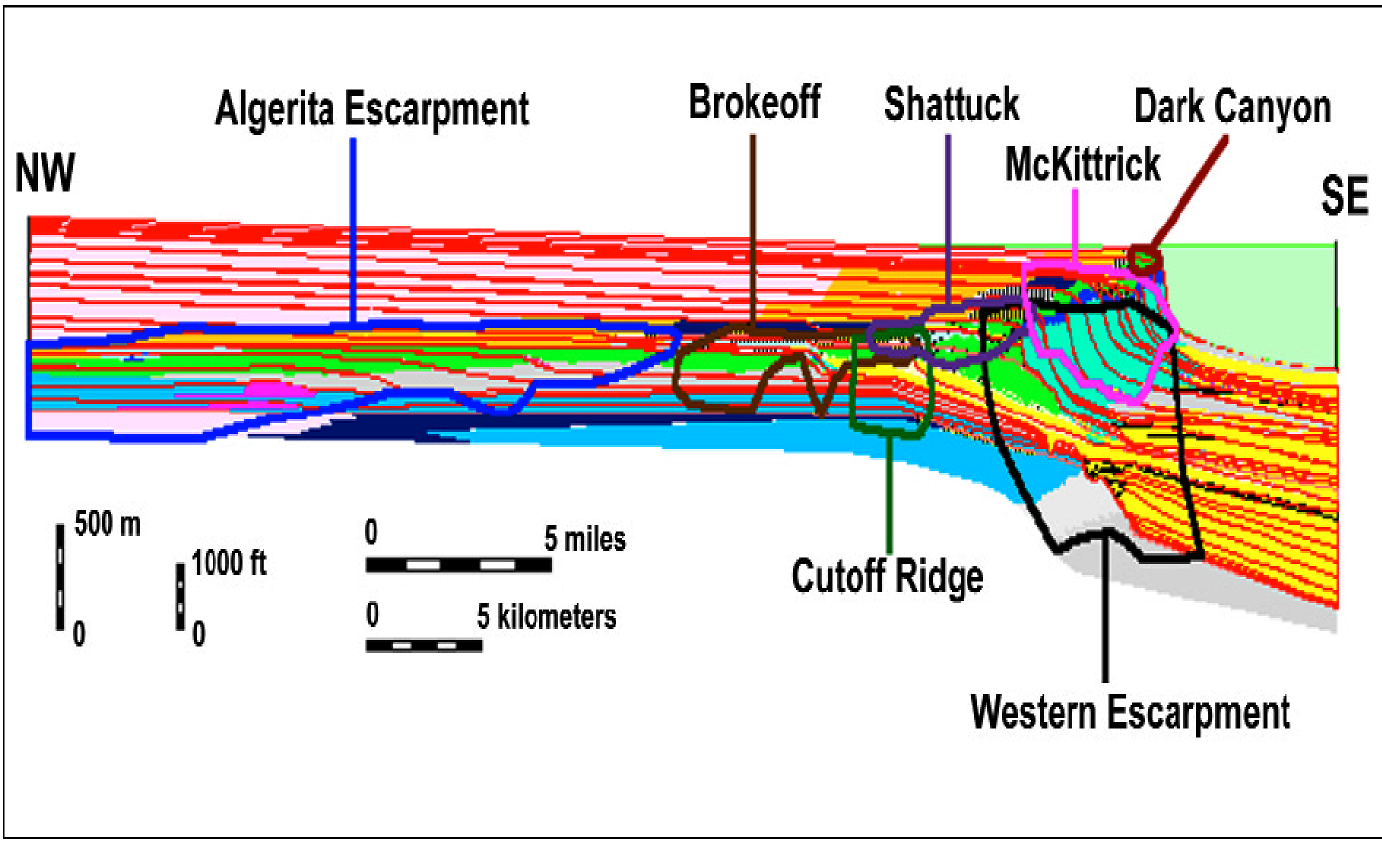

Kerans and Kempter
2002

Correlating CS-11

Composite Sequence Framework of the Guadalupe Mountain Region

Composite Sequence	HFS	Northwest Shelf	Shelf Margin	Foreslope	Delaware Basin	
CS-14	Guad. 27-28	Tansill	Upper - CM	Capitan "bedded"	Bell Canyon	Lamar
	Guad. 25-26	Yates	Middle - CM			McCombs
CS-13	Guad. 21-24					Rader
CS-12	Guad. 17-20	Seven Rivers	Lower - CM			Pinery-Hegler
	Guad. 15-16	Shattuck	Capitan "massive" (CM)		Cherry Canyon	Manzanita
CS-11	Guad.13-14	Queen	Goat Seep			
	Guad. 10-12	Grayburg				South Wells
CS-10	Guad. 8-9	upper San Andres				
	Guad. 5-7				Brushy Canyon	CCT
CS-9	Guad. 1-4	lower-middle San Andres			Cutoff	
	Leon. 7-8					
	Leon. 5-6					

Zoomed Regional Cross-Section

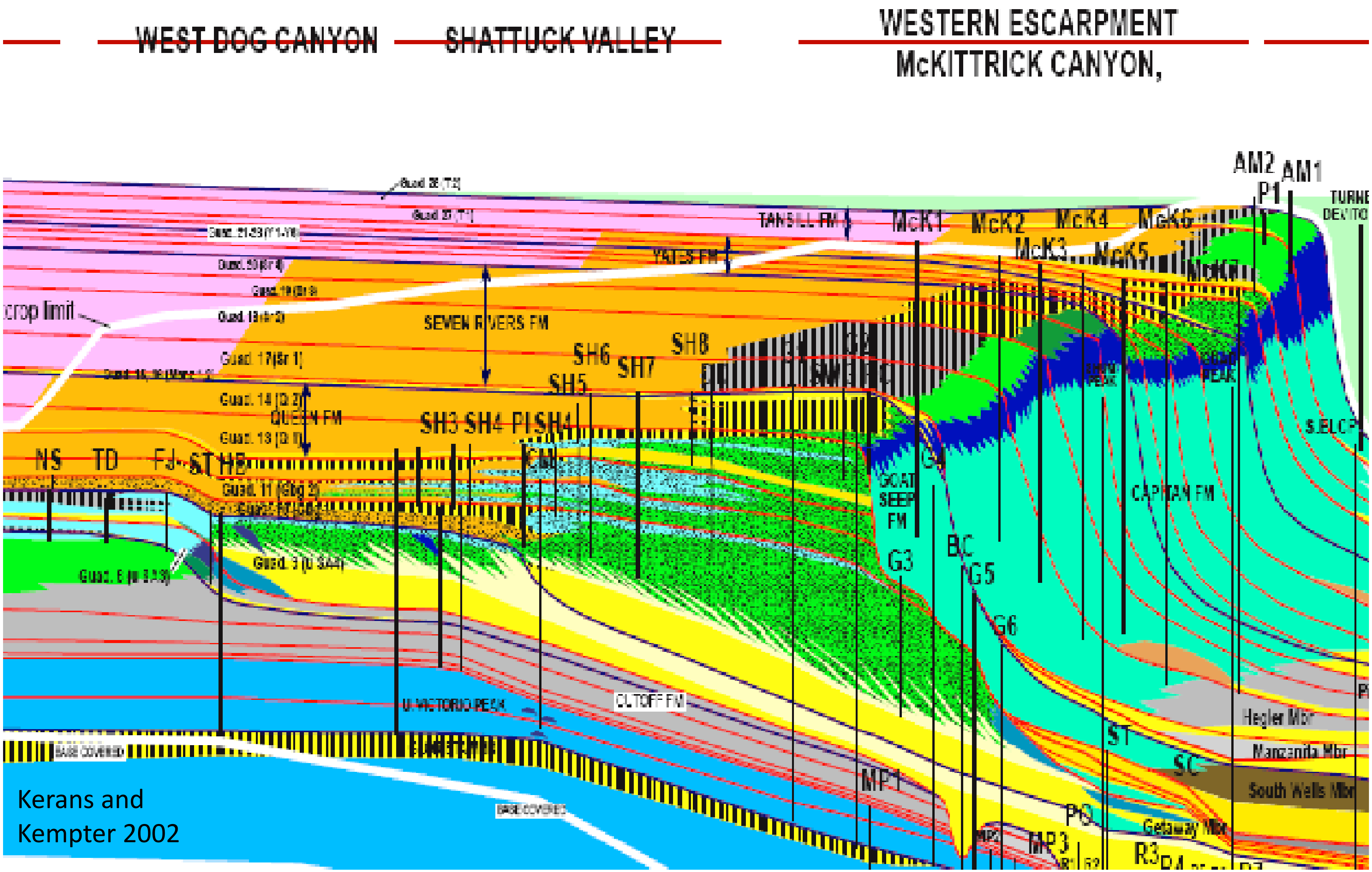

Kerans and Kempter 2002

Overview of Formations

- The Late Permian reflects low amplitude sea level fluctuations, following collapse of the Permo-Carboniferous ice-sheets.
- High frequency sequences (HFS) – stack into lowstand, transgressive, and highstand sequence sets.
  - During lowstand, all but the most seaward portions were covered with siliciclastic eolian ergs
- The Grayburg Formation is made up of 3 HFS
- The Queen Formation is made up of 2 HFS
- Goat Seep is the shelf margin facies that is coeval with the Queen Formation
- Goat Seep Formation is Queen-equivalent shelf margin facies

Example of Eustatic Cycles

The combined effect of climate, subsidence , and sea level changes allow sedimentation of different facies. The vertical stacking of these facies follow the signal of eustic sea level (bottom).

Within individual system tracts there is a tendency for deposition of particular lithologies. Where shale is mainly related with the TST and porous rocks can be either related with HST or LST.

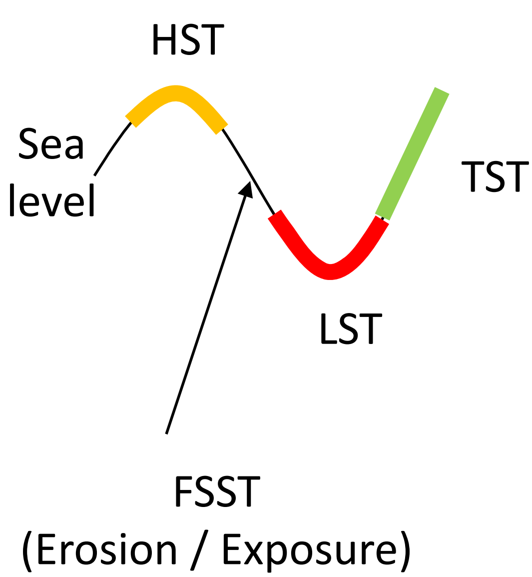

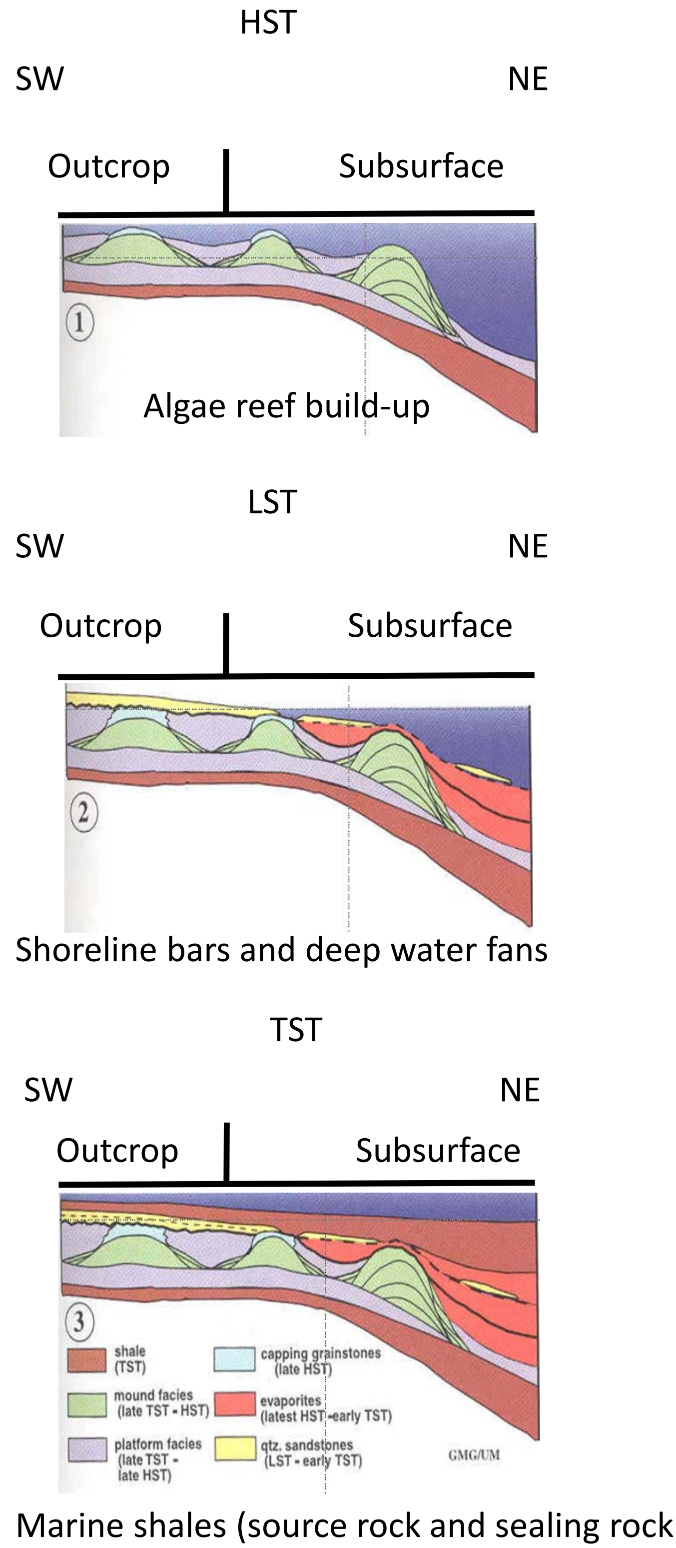

Figure 15: Sequence Stratigraphy of the Paradox Fm. showing the pre-dominant facies within individual system tracts

Depositional Facies

- Grayburg and Queen Formations
- Similar enough that a single set of depositional facies and depositional models is discussed
- 4 HFS deposited over 2 million years
- Changes in basin subsidence rates, sediment supply, comate, eustacy influenced stratigraphic and sedimentologic attributes

Facies for Grayburg and Queen	Description
Massive quartzose siltstone-sandstone	1-30 feet thick Gray, tan/red,mature, well sorted coarse siltstone to fine sandstone Minor bioturbation and haloturbation Define cycle bases
Cross Laminated Siltstone-sandstone	Texturally similar to the massive quartzose Transition zone - sandstone grades upward into carbonate Intervals of cross-laminated sandstone ~< 10 feet thick Increasing peloids and cement toward carbonate
Fusulinid-peloid packstone	Gray massive dolostone intervals with few pellets 1-30 feet thick Dominates more seaward portions Laterally continuous, tapering landward Large vertical burrows
Fusulinid-peloid wackestone	Similar to Fusulinid-peloid packstone Matrix is dense and micritic Less permeable and porous Fusulinids preserved as molds

Facies for Grayburg and Queen cont.	Description
Mollusc-Algal-Crinoid Packstone	.5-2 feet thick Dolomudstone with some pelleted fabric Fine grained, gray and structureless Recessive weathering Rare fusulinid and pelmatozoan debris At or near the base of a cycle
Peloid Packstone	1-3 feet thick, except in most seaward locations Grain-dominated Peloids, bioclasts, ooids or pisoids Structuresless, except for a few cross-bedded intervals
Ooid-Peloid Grainstone	~<20 feet thick in lower half of Grayburg and Queen, but not abundant otherwise Ooids and quartz sand Small to medium trough and planar tabular cross stratification with some hummocky cross stratification
Fenestral/Non-Fenestral-Pisolitic Laminite	Useful for correlation Smooth to crinkly non-fenestral and fenestral cryptalgal laminites Define caps of upward shallowing cycles Weather to resistant ledges

Grayburg-Queen-Goat Seep Formations

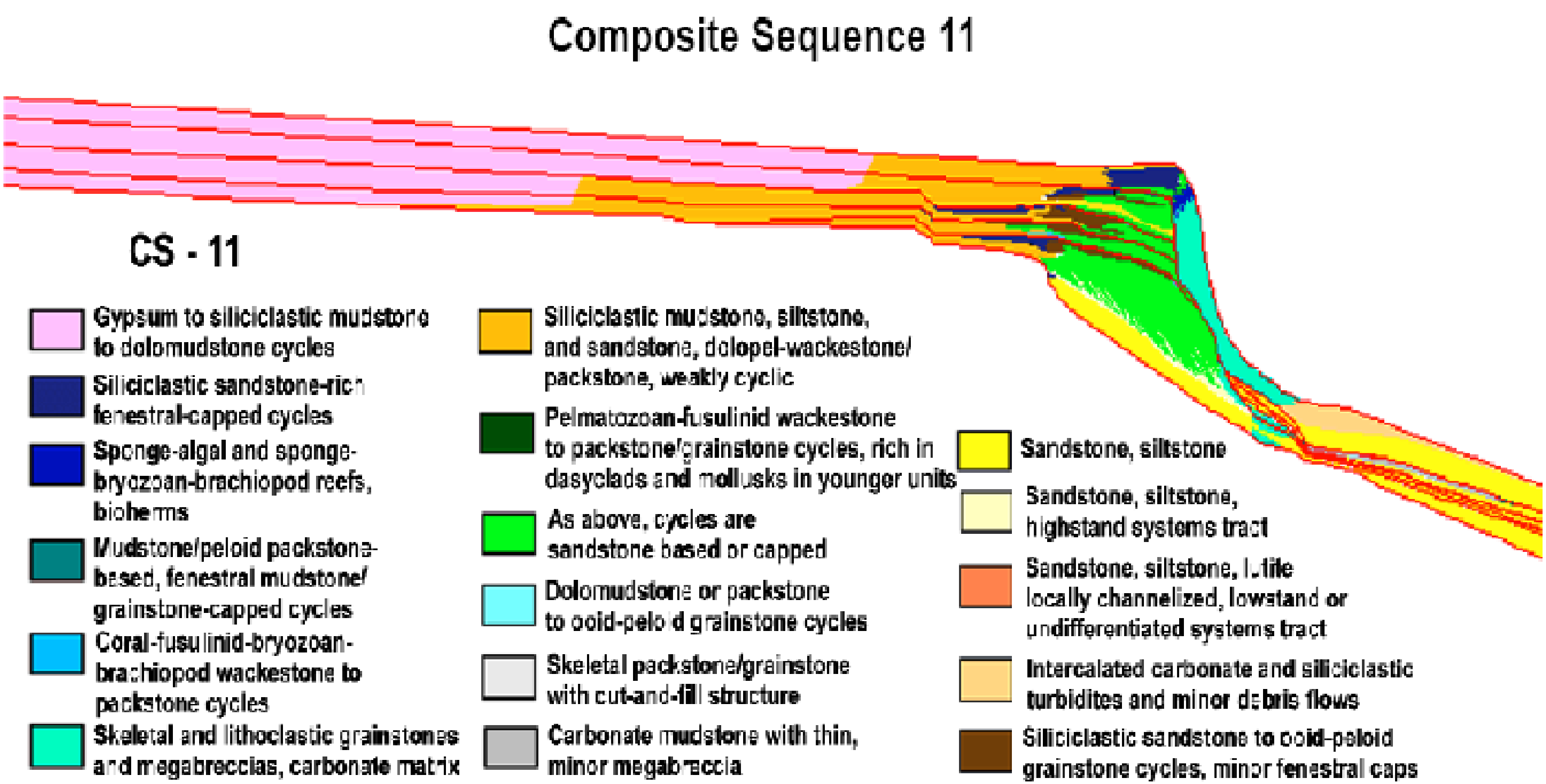

Kerans and Kempter 2002

Lower Grayburg – G10

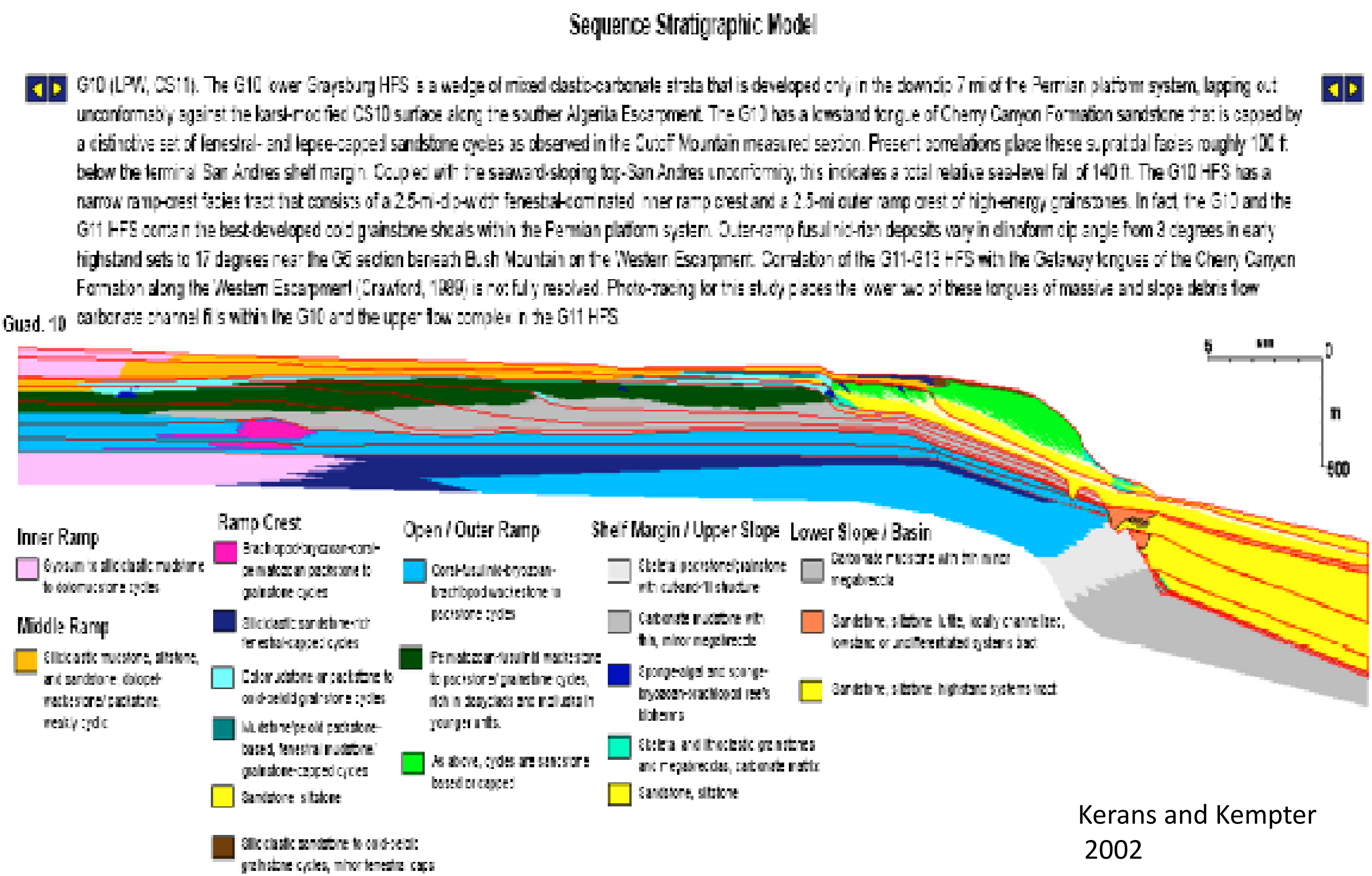

Kerans and Kempter 2002

Grayburg – G10

Shelf-Crest of Mixed Siliciclastic-Carbonate Transitional Ramp/Rimmed Shelf Model, Basal Guad 10 TST (basal Grayburg Fm.), Last Chance Canyon

Tan cross-stratified blocks are of siliciclastic-rich dolopeloid grainstone infilled by light-grey dolopeloid mud-dominated packstone. This sedimentary feature is representative of early lithification of the tan beach facies known as beach rock. This feature is typical of carbonate foreshore facies such as those seen in the onlapping TST cycles of the Guad 10 (basal Grayburg Fm.), Last Chance Canyon. Hammer for scale is 15 in.

Kerans and Kempter 2002

Grayburg – G11

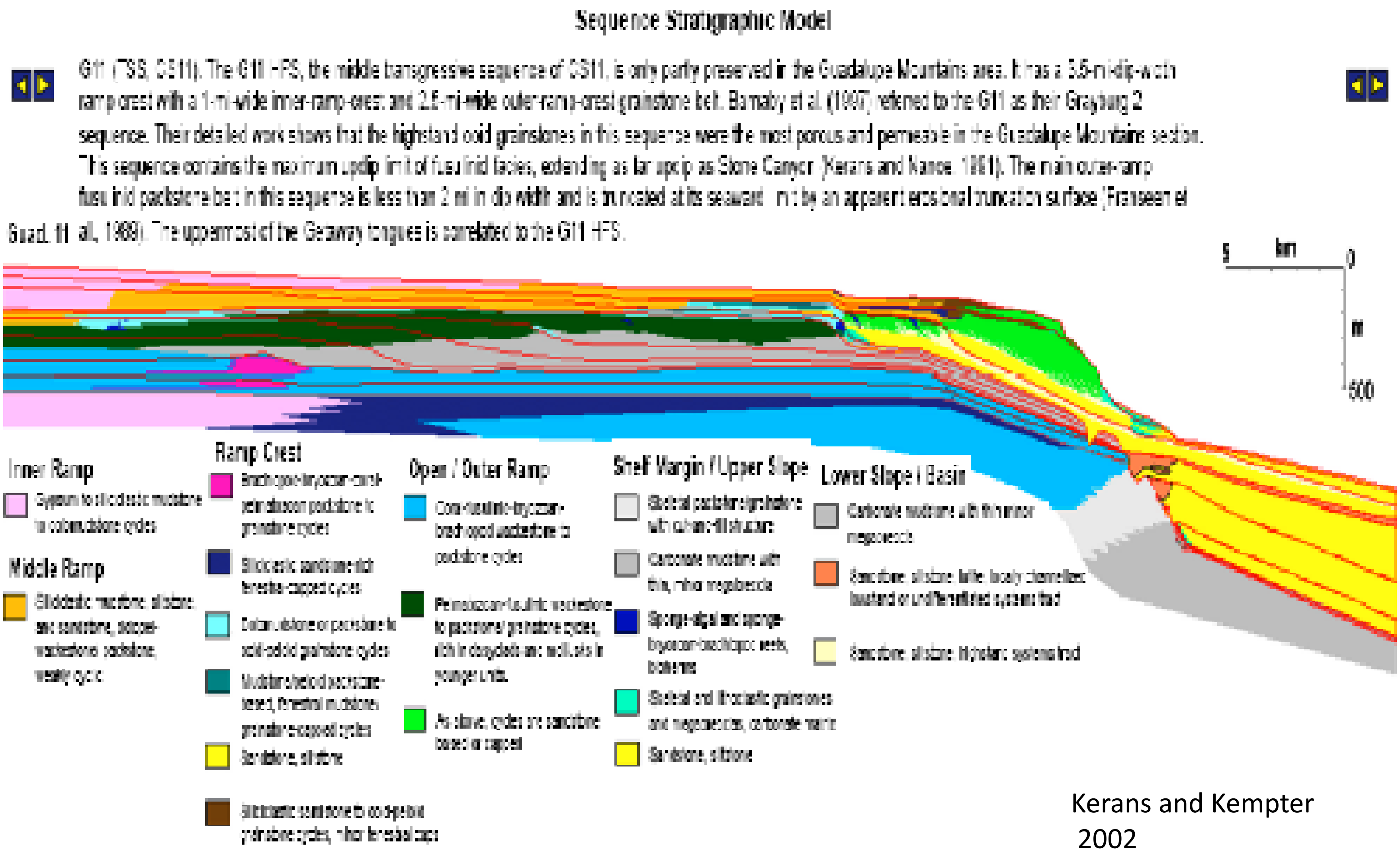

Kerans and Kempter
2002

Grayburg – G12

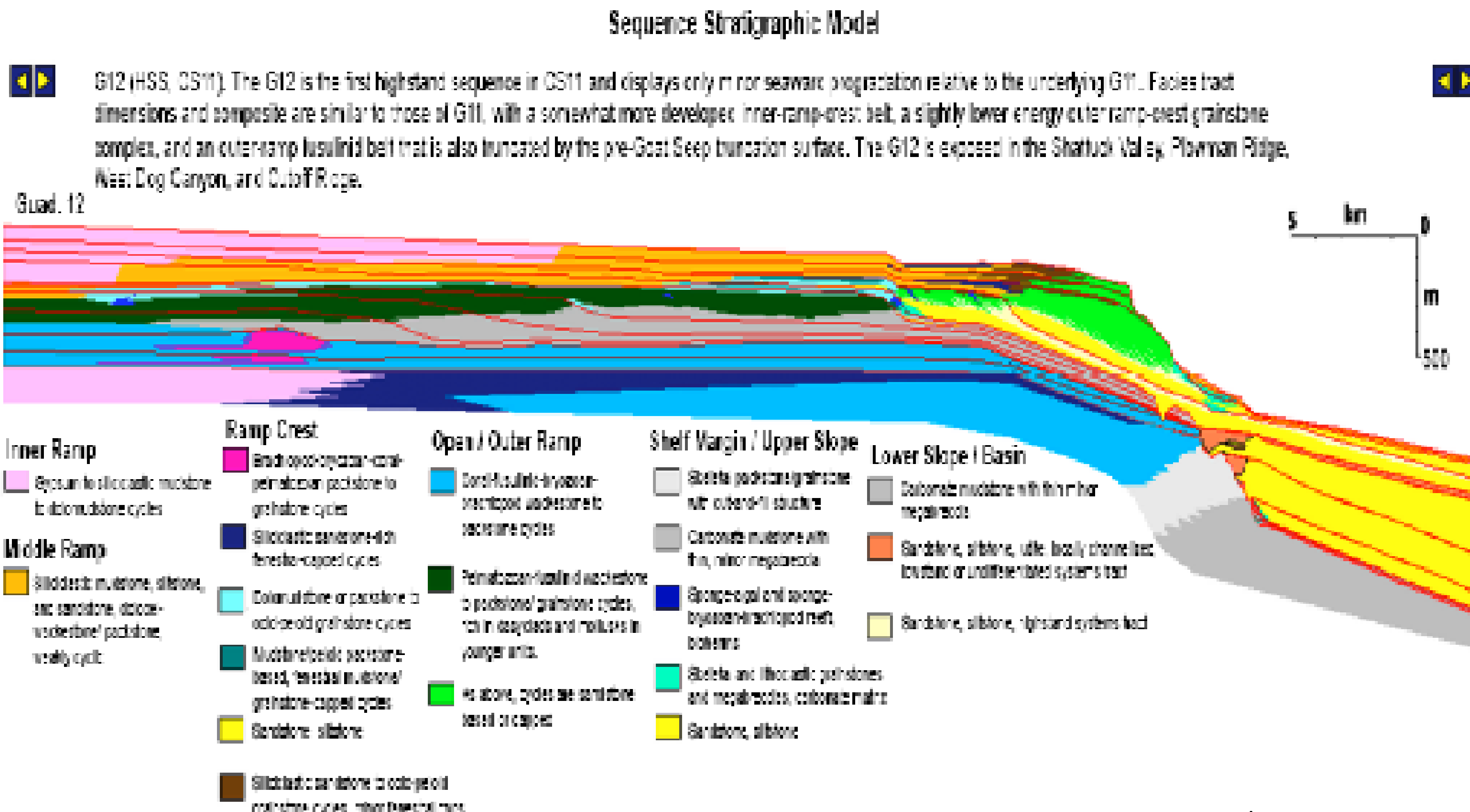

Kerans and Kempter
2002

Queen and Goat Seep Formation – G13

Sequence Stratigraphic Model

G13 (HSS, CS11). The G13 HFS, the lower of two Queen HFS, is the first of the Permian sequences in the Guadalupe Mountains to have preserved middle-shelf facies tract, as seen along the Shattuck Valley Escarpment and on the northern exposures of the Western Escarpment. This depocenter of fine siliciclastics and thin carbonate mudstone intercalations is an analogous belt to that producing in the Seven Rivers and Yates Formations on the west margin of the Central Basin Platform. A 2-mi-dip-width ramp-crest belt is dominated by fenestral-laminite cycles with only one cycle set containing significant ooid grainstone. Outer-shelf facies include both fusulinid packstones similar to those characteristic of all the previous Guadalupian HFS. In addition, pelmatozoan-mollusk-dasyclad packstones with affinities to Capitan-equivalent Seven Rivers and Yates outer-shelf facies tract successions appear. No shelf-margin or slope facies tract strata are preserved for this HFS. Basin-floor sediments include Cherry Canyon sandstones up to and including the Getaway Member.

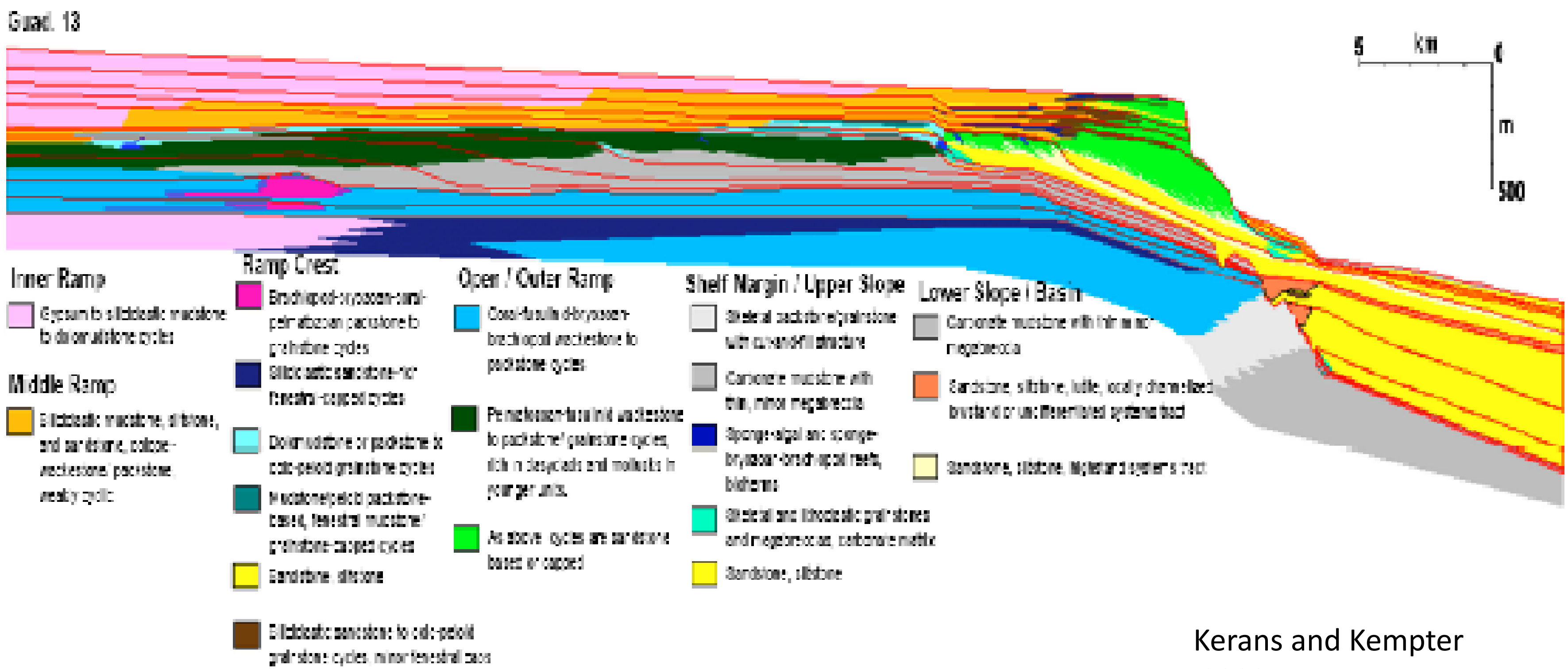

Kerans and Kempter 2002

Queen and Goat Seep Formation – G14

Sequence Stratigraphic Model

G14 (HSS, CS11). The G14 HFS includes the upper half of the Queen Formation, the first preserved shelf-margin reef complex, referred to as the Goat Seep Member, and the Cherry Canyon up to and including the South Wells Member. The main exposures of the G14 are along the middle and southern Shattuck Valley walls, and the Western Escarpment. This HFS is the first true reef-rimmed platform of the Guadalupian succession and has a shelf-crest-to-basin relief of 1,700 ft. This HFS follows the general trend of facies tract compression seen as the sequences evolve from the ramp style of the lower San Andres CS9 through the more steeply dipping upper San Andres and lower Grayburg ramps of the CS10 and CS11. The shelf-crest facies tract for G14 is 1.5 mi and consists of stacked tepee-pisolite facies. This is the first of the true tepee complexes of the Guadalupian section and corresponds to the first appearance of well-developed shallow-water reef-margin facies. The main exposure of the Goat Seep reef is at Bush Mountain on the Western Escarpment. It is also exposed in the South McKittrick Wind Gap section and in the updip portion of North McKittrick Canyon (Crawford, 1989). Most of the volume of the Goat Seep Formation is presumably contained within the slope facies tract (rather than the shelf-margin reef), but extensive dolomitization has obscured detailed facies distribution. Reef faunas are sponges, bryozoans, pelmatozoans, and mollusks.

Guad. 14

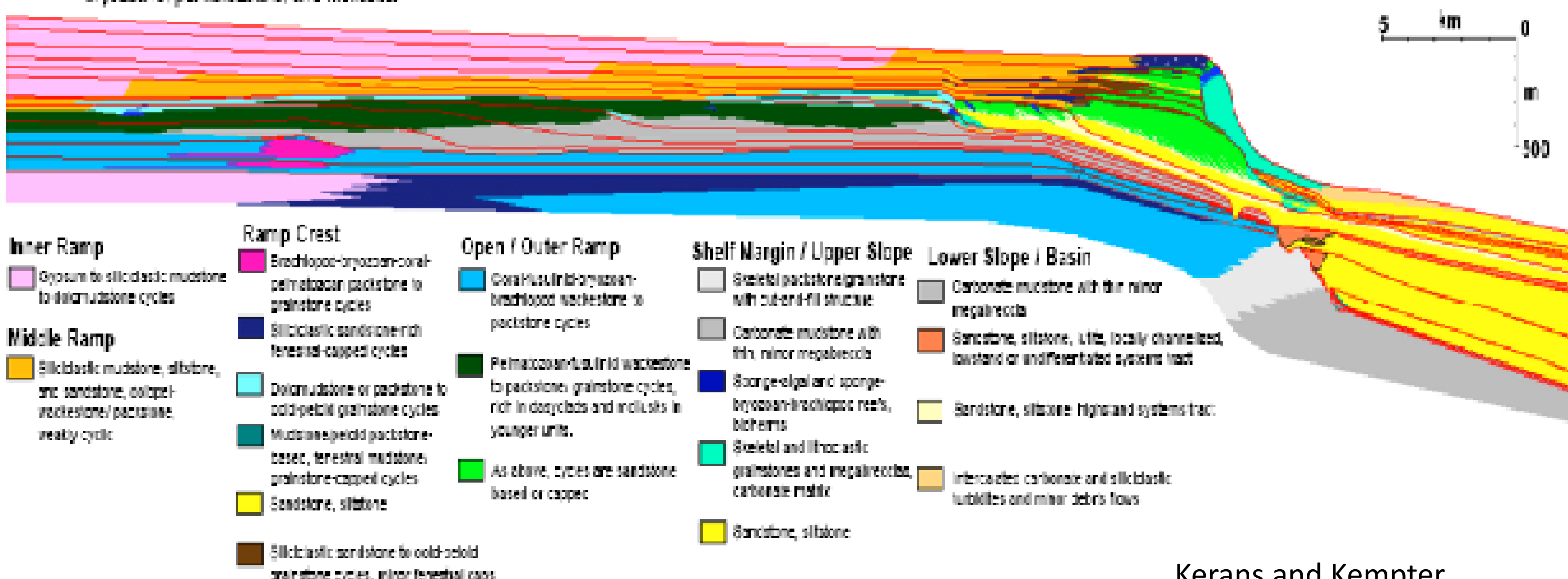

Kerans and Kempter 2002

Toe-of-Slope Breccias of the Mixed Siliciclastic-Carbonate Transitional Ramp to Rimmed Shelf Model, Getaway Member, Guad 12-13 HFS, Shirttail Canyon, Western Escarpment

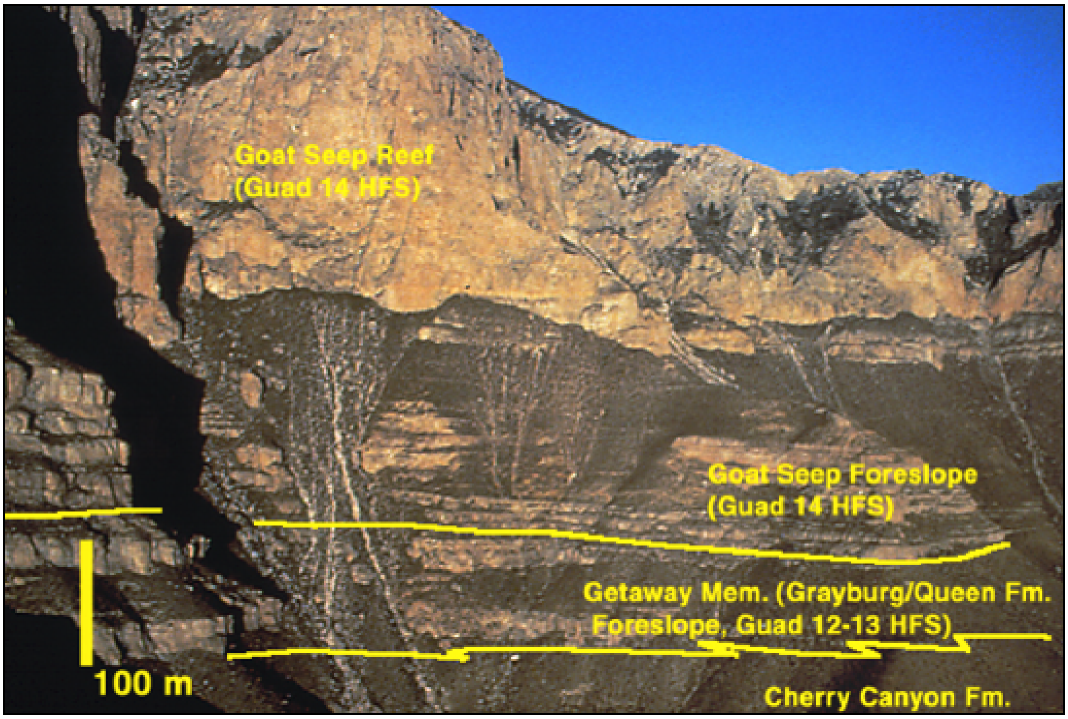

View looking southeast of thick toe-of-slope debris flows in the Getaway Member (Crawford, 1981) Guad 12 or 13HFS (Grayburg?) at Shirttail Canyon. The debris flows under discussion here are in the lower half of the illustration as resistant ledges weathering out relative to the more recessive Cherry Canyon basinal sandstones. The upper massive orange cliff is the Goatseep Reef that makes up the shelf-margin and slope facies tracts of the Guad 14 HFS (upper Queen Fm.). Total section in photo is approximately 1200 ft (Photo courtesy of Pat Lehman).

Kerans and Kempter
2002

References

- Kerans, Charles, 1995, Use of one- and two-dimensional cycle analysis in establishing high-frequency sequence frameworks, in Read, J. F., Kerans, C., and Weber, L. J., organizers, Milankovitch sea level changes, cycles and reservoirs on carbonate platforms in greenhouse and ice-house worlds: SEPM (Society for Sedimentary Geology), Short Course Notes No. 35, p. 1–19.

- Kerans, Charles, and Kempter, Kirt, 2002, Hierarchical stratigraphic analysis of a carbonate platform, Permian of the Guadalupe Mountains: The University of Texas at Austin, Bureau of Economic Geology (American Association of Petroleum Geologists/Datapages Discovery Series No. 5),CD-ROM.

Journal of Sedimentary Research

Journal of Sedimentary Research, 2007, v. 77, 34–58
Research Article
DOI: 10.2110/jsr.2007.007

OUTCROP ANALOG FOR MIXED SILICICLASTIC–CARBONATE RAMP RESERVOIRS—STRATIGRAPHIC HIERARCHY, FACIES ARCHITECTURE, AND GEOLOGIC HETEROGENEITY: GRAYBURG FORMATION, PERMIAN BASIN, U.S.A.

R.J. BARNABY[1] AND W.B. WARD[2]
[1]ConocoPhillips, 14066 Westlake 2 Building, 580 Westlake Park Boulevard, Houston, Texas 77079
[2]Earthworks, LLC and Theoretical and Applied Geology, P.O. Box 178, Newtown, Connecticut 06470, U.S.A.
e-mail: barnabyr@lsu.edu

ABSTRACT: The Grayburg Formation (Late Permian, Guadalupian) is a shallow-marine succession flanking the Delaware and Midland basins of Texas and New Mexico, U.S.A. The Grayburg exemplifies the facies heterogeneity imparted by cyclic interbedding of siliciclastic and carbonate rocks from lithologically diverse, inner-ramp to outer-ramp facies assemblages. High-resolution correlation and mapping of laterally continuous Grayburg strata exposed in the Brokeoff Mountains, New Mexico, allow the stratigraphic architecture, facies distribution, and lateral variability to be characterized in detail. This study provides an outcrop analog for stratigraphically equivalent subsurface reservoirs and comparable carbonate-ramp reservoirs that accumulated during periods of low-amplitude sea-level fluctuations.

Vertical and lateral facies successions in the Grayburg record four hierarchical scales of cyclicity. The entire Grayburg is a composite sequence that initiated with transgression of the San Andres platform and culminated with subaerial exposure, followed by a major basinward shift in deposition. This third-order cycle contains four high-frequency sequences defined by transgressive outer-ramp facies overlain by aggradational ramp-crest to inner-ramp facies capped by an unconformity. Each high-frequency sequence contains several composite cycles, intermediate-scale cyclic successions. The high-frequency (fifth-order) cycles constitute the smallest-scale upward-shoaling facies successions that can be recognized and mapped, comprising the basic correlation entity to delineate lithofacies bodies.

Lateral heterogeneity in the Grayburg reflects both systematic facies transitions and interwell-scale (meters to hundreds of meters) variability due to geologic complexity. Larger-scale systematic facies changes that reflect primary environmental and/or depositional controls (e.g., water depth, platform position, accommodation trends) can be characterized using well and/or seismic data abetted by appropriate depositional models. Interwell heterogeneity due to geologic complexity, however, is difficult to recognize from subsurface datasets. Appropriate outcrop analogs provide information on lateral facies dimensions and heterogeneity architecture that is essential for constructing more realistic three-dimensional reservoir models, rather than oversimplified models based on lithofacies correlations forced between wells by linear interpolation. An understanding of geologic heterogeneity exhibited in outcrop analogs is crucial for geoscientists involved with characterizing and modeling subsurface heterogeneity.

INTRODUCTION

The need to understand, characterize, and model reservoir heterogeneity at all scales has been the impetus for detailed outcrop studies directed towards development of reservoir analogs. In the Permian Basin, outcrop investigations of the San Andres Formation, one of the most productive units (Fig. 1), demonstrate the application of sequence stratigraphic principles for high-resolution correlation and facies mapping (Sonnenfeld 1991; Kerans et al. 1994; Kerans and Fitchen 1995). Such outcrop studies illustrate the hierarchy of different stratal surfaces and the landward and seaward facies shifts that define the sequence stratigraphic framework. These studies also document the utility of stratigraphic analysis for characterization of geologic heterogeneity in subsurface reservoirs.

Reservoirs in the Grayburg Formation display considerable heterogeneity due to cyclic interbedding of diverse assemblages of shallow-water, mixed carbonate, and siliciclastic facies. Because depositional fabrics are well preserved in these dolomitized carbonates and quartz sandstones, porosity and permeability are a function of the original depositional fabric (e.g., Lucia 1995). Consequently, characterization of petrophysical heterogeneity requires detailed stratigraphic analysis, correlation, and facies mapping.

The data and interpretations presented here are based on description, analysis, and mapping of laterally continuous exposures of Grayburg strata on Plowman Ridge and West Dog Canyon in the Brokeoff Mountains (Figs. 2–5). Closely spaced measured sections, photomosaics, and physical tracing of stratal surfaces and facies established detailed chronostratigraphic correlations for high-frequency cycles and component lithofacies for up to 6.5 km along depositional dip. Three-dimensional outcrop views exposed in West Dog Canyon by incised meanders and opposite canyon walls, and correlations with strata on Plowman Ridge, 1.0 km across depositional strike, allow the three-dimensional facies heterogeneity to be characterized in detail.

 1527-1404/07/077-034/$03.00

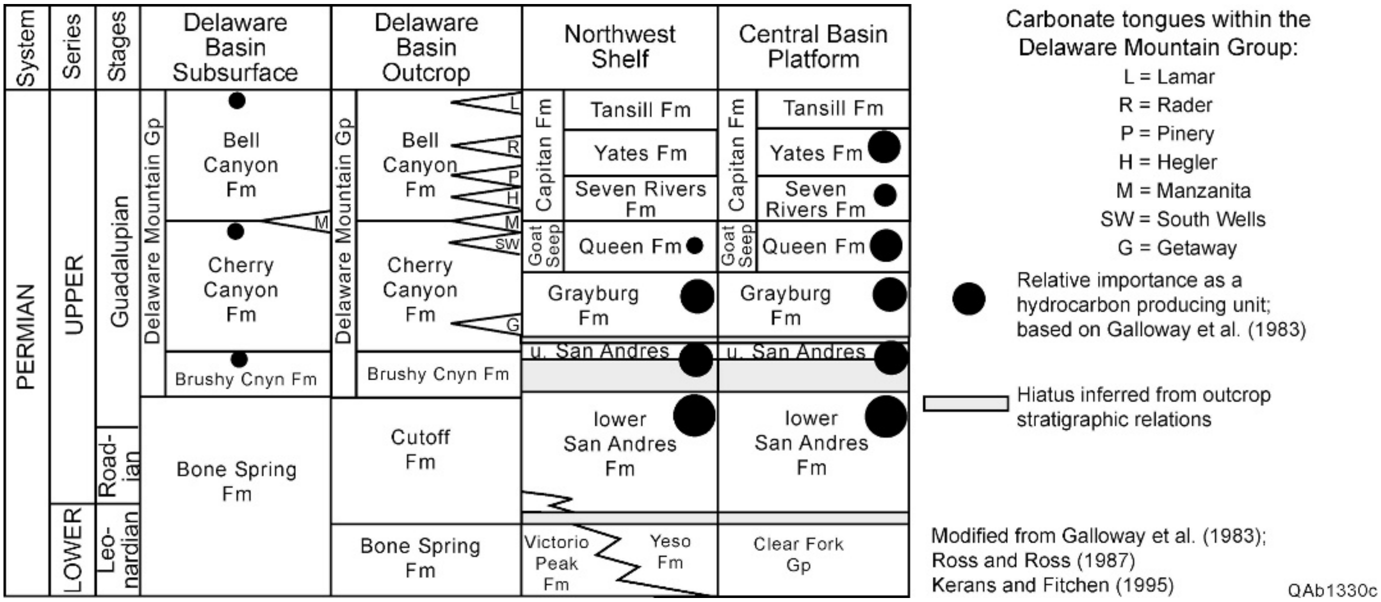

FIG. 1.—Stratigraphic nomenclature of uppermost Leonardian through Guadalupian strata of the Permian Basin showing relative importance as a hydrocarbon-producing unit. The Grayburg Formation has yielded 2.5 billion barrels of oil from West Texas.

A major contribution of this study is delineating lateral facies variability within the context of a reliable, high-resolution chronostratigraphic framework. Lateral heterogeneity reflects both larger-scale systematic facies changes (e.g., due to water depth, platform position, accommodation trends) and interwell-scale (meters to hundreds of meters) heterogeneity arising from geologic complexity. Interwell-scale heterogeneity is difficult to recognize with subsurface data, although simulations based on outcrop-derived petrophysical data demonstrate that such variability strongly influences flow behavior in carbonate reservoirs (Grant et al. 1994; Jennings et al. 2000). Outcrop analogs thus constitute an essential knowledge base for constructing realistic three-dimensional reservoir models from one-dimensional well data and stratigraphic interpretations. Consequently, outcrop analogs such as the Grayburg provide an important tool for reservoir geologists tasked with characterizing and modeling subsurface heterogeneity.

GEOLOGIC SETTING

The Guadalupian (Late Permian) Grayburg Formation is a shallow-marine, mixed carbonate–siliciclastic succession on the periphery of the Delaware and Midland basins (Fig. 2). In the Guadalupe Mountains area, the Grayburg ranges in thickness from 80 meters in the most landward exposure on top of the San Andres platform to more than 365 meters along the Western Escarpment (Fekete et al. 1986; Franseen et

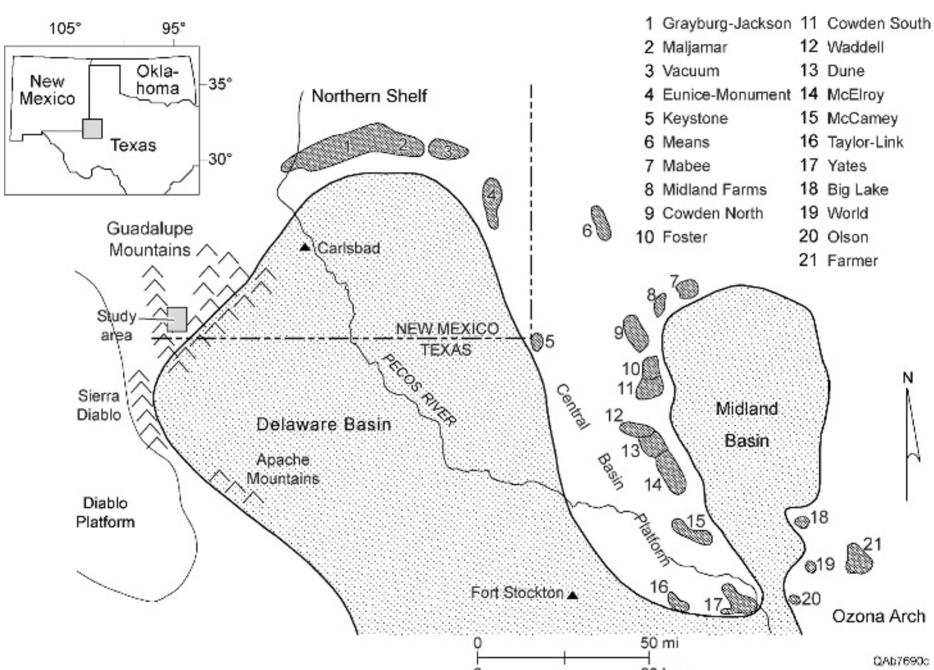

FIG. 2.—Setting of Delaware and Midland basins during Grayburg deposition (modified from Ward et al. 1986). The numbered areas are the 21 major Grayburg fields (more than 10 million barrels production) that occur along the Central Basin Platform, the northern shelf of the Delaware Basin, and the Ozona Arch. The outcrop study area is on the northwestern shelf of the Delaware Basin.

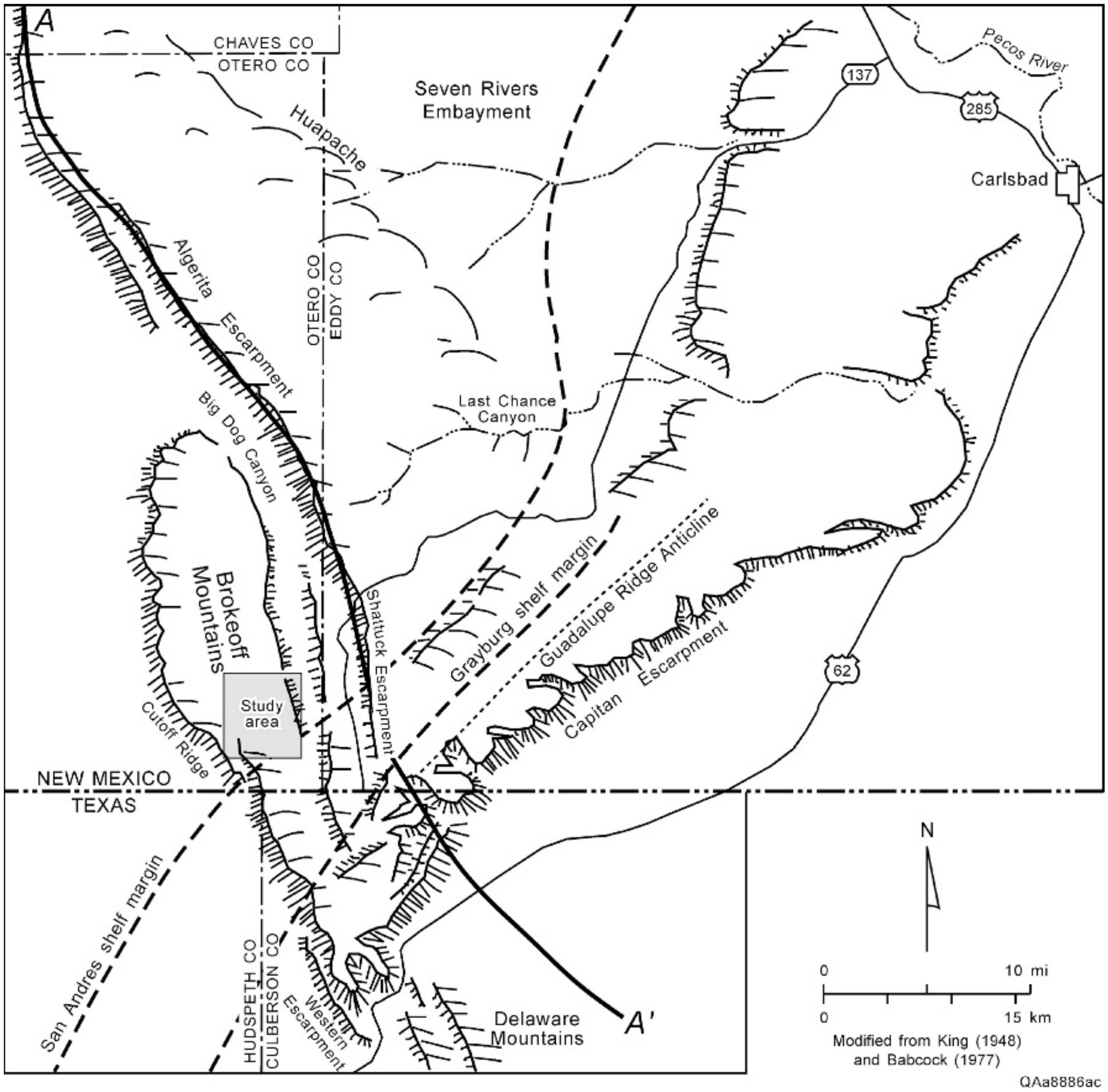

FIG. 3.—Physiographic map of the Guadalupe and Brokeoff mountains region, modified from Fitchen (1993). The outcrop study area (shaded rectangle) is landward of the underlying San Andres margin and is approximately 10 km landward of the Grayburg terminal margin. Line A–A′ delineates general location of the cross section of Kerans et al. (1992) and Kerans et al. (1993) shown in Figure 4.

al. 1989; Kerans and Nance 1991; Kerans et al. 1992; Kerans et al. 1993). This study focused on flat-lying Grayburg strata that accumulated landward of the shelf margin (Figs. 3, 4). This is a depositional setting similar to that of major Grayburg fields (Fig. 2). The Grayburg Formation grades basinward into fine sandstones and siltstones of the Cherry Canyon Formation and passes northward, towards the craton, into evaporites, eolianites, and terrigenous red beds (Silver and Todd 1969; Meissner 1972; Nance 1988).

The Permian is a period of transitional sea-level cyclicity between the high-amplitude (60 to 100 m) glacial-eustatic icehouse fluctuations of the Pennsylvanian (e.g., Crowley and Baum 1991; Soreghan and Giles 1999) and the low-amplitude (less than 10 m) eustatic greenhouse fluctuations of the Triassic (Goldhammer et al. 1990). The Permian Basin is a foreland that developed during the Pennsylvanian–Early Permian collision between Laurentia and Gondwana (Horak 1985; Yang and Dorobek 1992). The Grayburg was deposited during the passive margin phase of tectonic quiescence.

Paleogeographic reconstructions for the Middle to Late Permian place the Permian Basin on the Pangea supercontinent at 0° to 5° N latitude (Scotese and McKerrow 1990; Lottes and Rowley 1990; Coffin et al. 1992), north of the equatorial-aligned tectonic highlands of the Hercynian orogenic belt (Coffin et al. 1992). Despite the equatorial setting, arid conditions in western North America are indicated by widespread Guadalupian-age dolomites, evaporites, eolianites, and terrigenous red beds (Silver and Todd 1969; Meissner 1972). Assembly of the Pangea supercontinent and orogenic uplift disrupted the wet equatorial easterlies bearing moisture from Tethys, creating a rain shadow in central Pangea (Scotese and McKerrow 1990). Paleoclimate modeling (Parrish and Peterson 1988; Parrish 1993, 1995) suggests that a monsoonal atmospheric circulation system developed. During the Northern Hemisphere winter, a high-pressure cell developed over the cold northern landmass, resulting in northeasterly winds (Parrish and Peterson 1988; Parrish 1993, 1995). Measured foresets for Permian eolianites of the Colorado Plateau (Peterson 1988) and Anadarko Basin (Kocurek and Kirkland 1998)

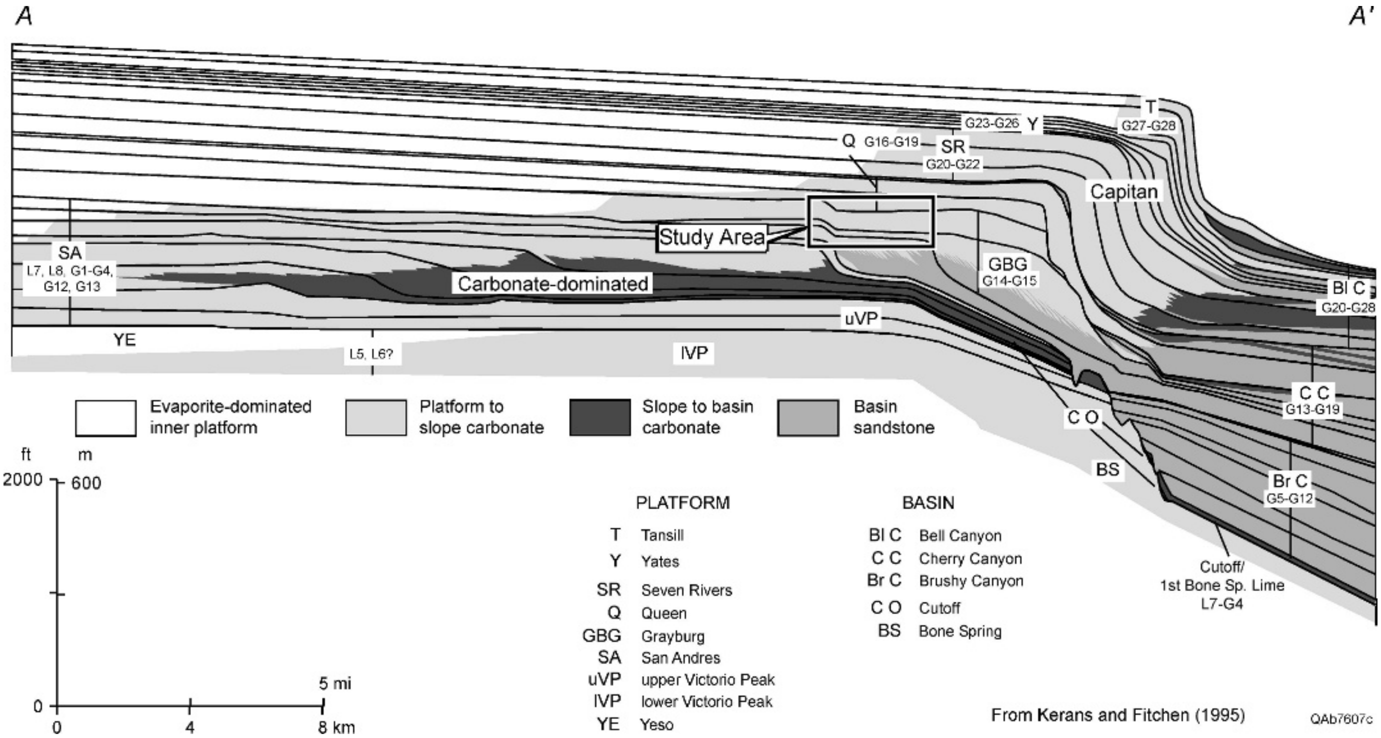

FIG. 4.—Stratigraphic framework of the Leonardian through Guadalupian carbonate platform succession in the Guadalupe and Brokeoff mountains region, compiled by Kerans et. al. (1992) and Kerans et al. (1993), updated by more recent work (Kerans et al. 1994; Kerans and Fitchen 1995). The Grayburg study area is landward of the San Andres and Grayburg platform margins.

coincide with a dominant northeasterly paleowind direction. Karst associated with sequence boundaries in the San Andres Formation (e.g., Kerans and Fitchen 1995) and the Grayburg Formation (this study) attest to episodic development of coastal meteoric aquifer systems during sea-level lowstands.

DEFINITIONS

The high-frequency cycle is the basic stratigraphic unit in this study and refers to the smallest-scale upward-shallowing facies succession that can be correlated across different facies tracts. High-frequency cycles record a single episode of rise and fall in relative sea level (e.g., Grotzinger 1986; Read et al. 1986; Koerschner and Read 1989; Kerans and Tinker 1997) equivalent to the fifth-order cycles of Goldhammer et al. (1990). The high-frequency cycle is analogous to the parasequence (Van Wagoner et al. 1987; Van Wagoner et al. 1990). Grayburg high-frequency cycles range from 0.5 to 10 meters in thickness.

Composite cycles contain several high-frequency cycles arranged into a larger-scale transgressive–regressive succession bound by marine flooding surfaces that may coincide with sequence boundaries. Composite cycles differ from cycle sets (Kerans and Tinker 1997, 1999; Tinker 1998) or parasequence sets (Van Wagoner et al. 1987; Van Wagoner et al. 1990) in that composite cycles define an intermediate-scale transgressive–regressive cycle, whereas cycle sets and parasequence sets display a consistent progradational, retrogradational, or aggradational stacking trend. Grayburg composite cycles are 4 to 12 meters thick.

A high-frequency sequence is a larger-scale cycle composed of genetically related, high-frequency cycles and composite cycles and bounded by unconformities or correlative unconformities (e.g., Mitchum 1977; Mitchum and Van Wagoner 1991). High-frequency sequences contain lowstand and transgressive systems tracts separated by a maximum flooding surface from the highstand systems tract. Composite cycles and high-frequency sequences lie within the range of fourth-order cycles (Goldhammer et al. 1990). Grayburg high-frequency sequences are 30 to 45 meters thick.

The composite sequence (e.g., Mitchum and Van Wagoner 1991) is the lowest order cyclicity considered by this study and is comparable to a depositional sequence (e.g., Mitchum et al. 1977; Vail et al. 1977; Vail 1987; Van Wagoner et al 1988). Composite sequences contain several unconformity-bounded high-frequency sequences arranged into a larger-scale succession with well-defined lowstand, transgressive, and highstand components. A composite sequence is equivalent to a third-order cycle (Goldhammer et al. 1990).

METHODS

The Grayburg Formation data and interpretations presented in this paper are based on more than 4100 meters of vertical section described at Plowman Ridge, West Dog Canyon, and Cork Draw in the Brokeoff Mountains in southeastern Otero County, New Mexico (Fig. 5). Although precursor limestones are replaced by dolomite, well-preserved original rock fabrics can be identified readily in the field. Facies were described from outcrop in conjunction with standard petrographic thin sections of rock samples. We utilize Dunham's (1962) carbonate rock classification system with Lucia's (1995) modification that subdivides packstones into mud-dominated and grain-dominated fabrics.

Initial stratigraphic analysis of the Grayburg Formation was based on exposures from Plowman Ridge, a 6.5-km-long, north-trending ridge that parallels depositional dip (Fig. 5). Vertical sections through the Grayburg were measured and described (e.g., Fig. 6); interpreted high-frequency cycles, cycle sets, and high-frequency sequences were physically correlated by walking out bedding surfaces and by tracing the strata on oblique photographs. The Plowman Ridge stratigraphic cross section (Fig. 7) is based on high-quality exposures with excellent lateral continuity.

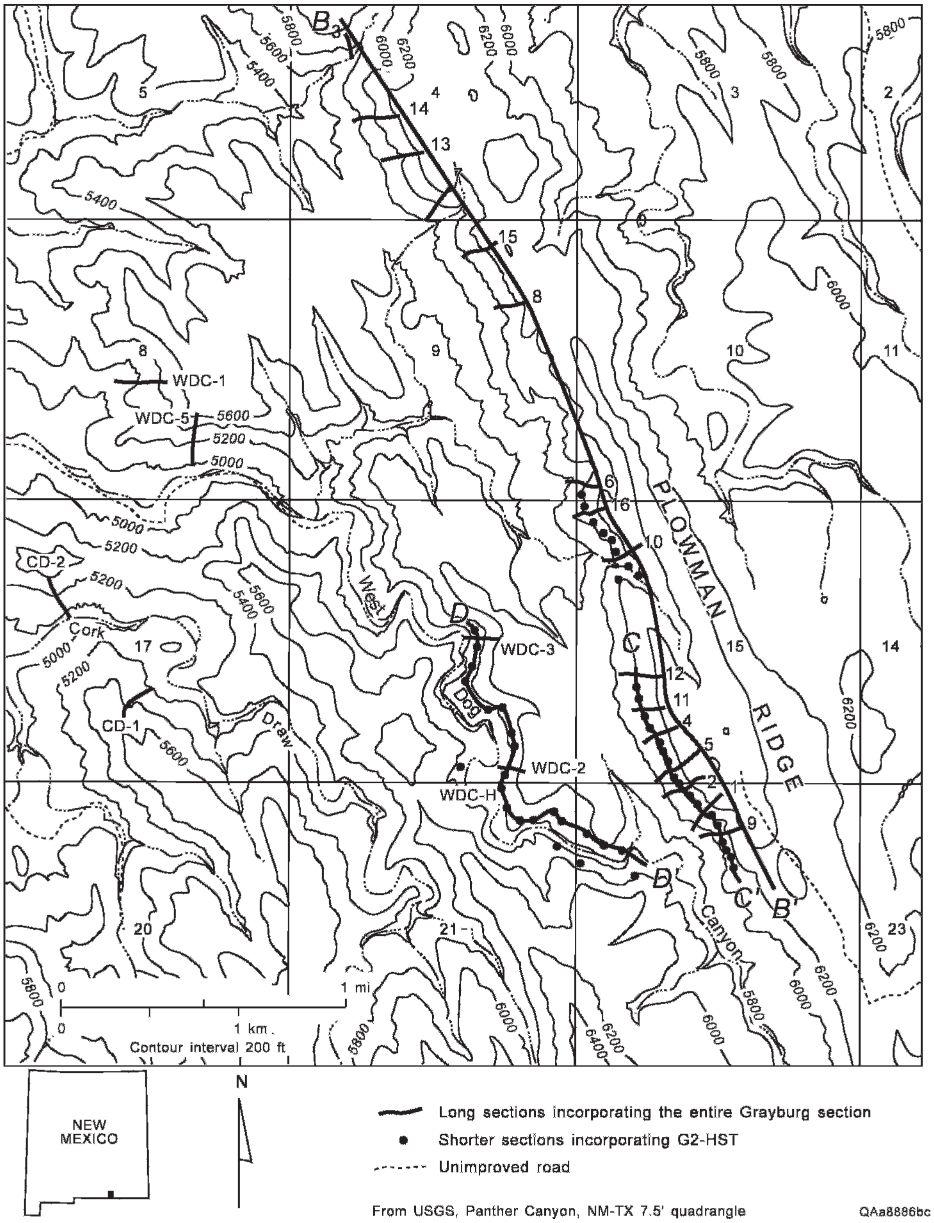

FIG. 5.—Topographic map of study area showing locations of 22 sections (indicated as lines) of the entire Grayburg interval that were described at Plowman Ridge, West Dog Canyon, and Cork Draw. Forty-eight shorter sections of HFS 2 (indicated as dots) were described at Plowman Ridge and West Dog Canyon.

Measured sections of the Grayburg from West Dog Canyon and Cork Draw, 1.0 km and 3 km west of Plowman Ridge across depositional strike, extend the Grayburg stratigraphy throughout the study area.

Detailed stratigraphic analysis and facies mapping within the high-frequency cycle-scale chronostratigraphic framework focused on Grayburg HFS 2 (30 to 35 meters thick) on Plowman Ridge and West Dog Canyon (Figs. 8, 9), two dip-oriented outcrops with laterally continuous exposures. Within these two windows, closely spaced (30 to 125 meters) vertical sections were described and measured. As in mapping formation tops, some cycle tops were mapped in the field before facies were described in detail. In most cases, both high-frequency cycle tops and facies were mapped at the same time. High-frequency cycle tops and lithofacies were physically correlated between adjacent measured sections by walking out high-frequency cycle tops, bedding surfaces, and facies contacts, and by recording the stratal relationships on large-scale (1:100 to 1:200) oblique photographs. Every correlation line and facies contact in the detailed window cross sections was examined and recorded in the field. In areas outside the detailed window along Plowman Ridge, some correlations were made by tracing strata on large-scale oblique photographs; gaps in the outcrop exposure from cover required some correlations to be made between these sections based on stratigraphic interpretations.

PREVIOUS WORK AND SEQUENCE STRATIGRAPHIC FRAMEWORK

Boyd (1958) conducted the first comprehensive geologic mapping of Permian strata in the Brokeoff Mountains. Boyd recognized the platform-to-basin stratigraphic relationships in the upper San Andres Formation and picked the San Andres–Grayburg formational contact using a poorly defined color change. From exposures in Last Chance Canyon, Hayes (1964) subsequently picked the top of the San Andres Formation at an angular unconformity between carbonate clinoforms of the upper San Andres and flat-lying, siliciclastic Grayburg strata. Sarg and Lehmann (1986) interpreted this formational contact as a sequence boundary.

Based on the Last Chance Canyon exposures, Sonnenfeld (1991, 1993) documented 15 meters of stratigraphic relief between the top of the San

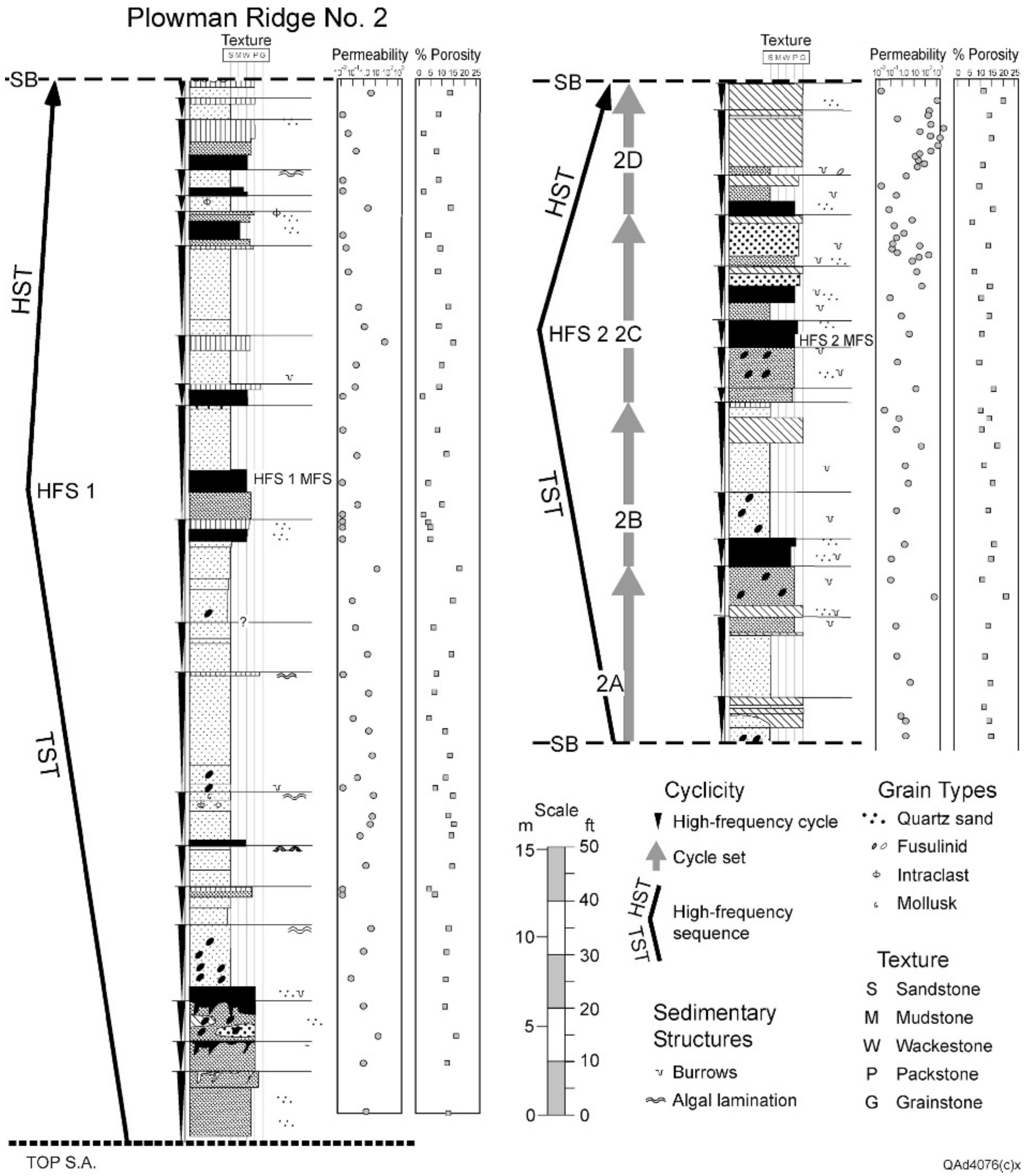

FIG. 6.—Measured section of section PR-2 (with interpretations) of entire Grayburg interval from South Plowman Ridge, location indicated on Figure 5.

Andres sequence boundary and onlapping Grayburg strata, indicating at least 15 meters of sea-level fall following San Andres deposition. On Algerita and Shattuck escarpments, these stratal relationships indicate a sea-level fall of more than 30 meters (Kerans and Nance 1991). A similar magnitude of sea-level fall is documented in the Brokeoff Mountains, where paleokarst dolines extend 30 meters below the San Andres–Grayburg sequence boundary (Fitchen 1993).

Boyd (1958) mapped the Grayburg and Queen formations as an undifferentiated succession. Hayes (1964) placed the top of the Grayburg below a ''locally conspicuous sandstone'' assigned to the Queen Formation. Sarg and Lehmann (1986) interpreted the top of the Grayburg to represent a sequence boundary. Because subaerial exposure features are only locally expressed along this surface, however, this contact is probably inconsistently mapped throughout the area, particularly in areas with poor outcrops (Kerans and Nance 1991). Limited exposure of the uppermost Grayburg on Plowman Ridge and in West Dog Canyon made it difficult for us to unequivocally locate the Grayburg–Queen sequence boundary. Near the top of Plowman Ridge, tepee–pisolite–fenestral and algal-laminated facies (uppermost Grayburg?) with grikes filled with dolomitic quartz siltstone and sandstone are unconformably overlain by recessively

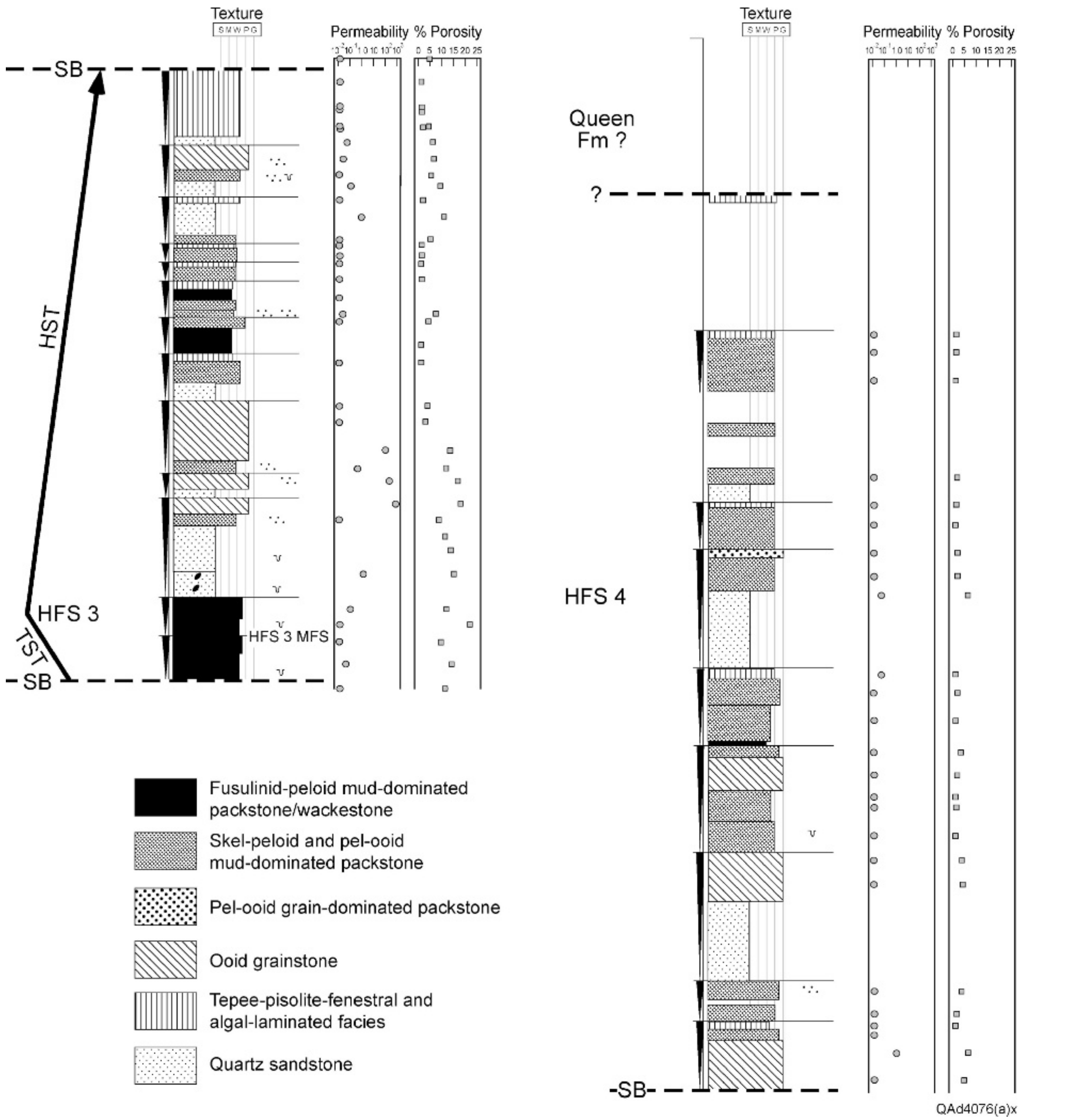

FIG. 6.—Continued.

weathered, yellow-brown to pink, thin-bedded sandstones that we interpret to be the lowermost Queen Formation.

Sarg and Lehmann (1986) interpreted the Grayburg Formation to be a third-order depositional sequence. Kerans and Nance (1991) subdivided this sequence into lowstand/transgressive and highstand systems tracts. Kerans et al. (1992) and Kerans et al. (1993) reinterpreted the Grayburg to be a composite sequence composed of two high-frequency sequences (Guadalupian HFS 14 and 15) and placed the maximum flooding surface of Kerans and Nance (1991) at the transgressive base of Guadalupian HFS 15.

In the study area, the Grayburg Formation thins to 115 meters in the most landward exposures, thickening seaward to 180 meters at the southern terminus of Plowman Ridge. On the Western Escarpment, 10 km basinward of the study area (Fig. 3), the Grayburg Formation attains a thickness of more than 365 meters (Fekete et al. 1986; Franseen et al. 1989). On the Western Escarpment, the lowermost 85 meters of the Grayburg is composed of progradational clinoforms overlain by more than 275 meters of flat-lying strata that record a shift from progradational to aggradational deposition (Fekete et al. 1986; Franseen et al. 1989). Erosional truncation of the Grayburg margin along the Western Escarpment makes it impossible to determine the precise location of the original depositional margin and whether the margin exhibited a ramp or a rimmed shelf morphology (*sensu* Read 1985). Relief on the Grayburg margin is estimated to be at least 200 to 300 meters (Fekete et al. 1986; Franseen et al. 1989).

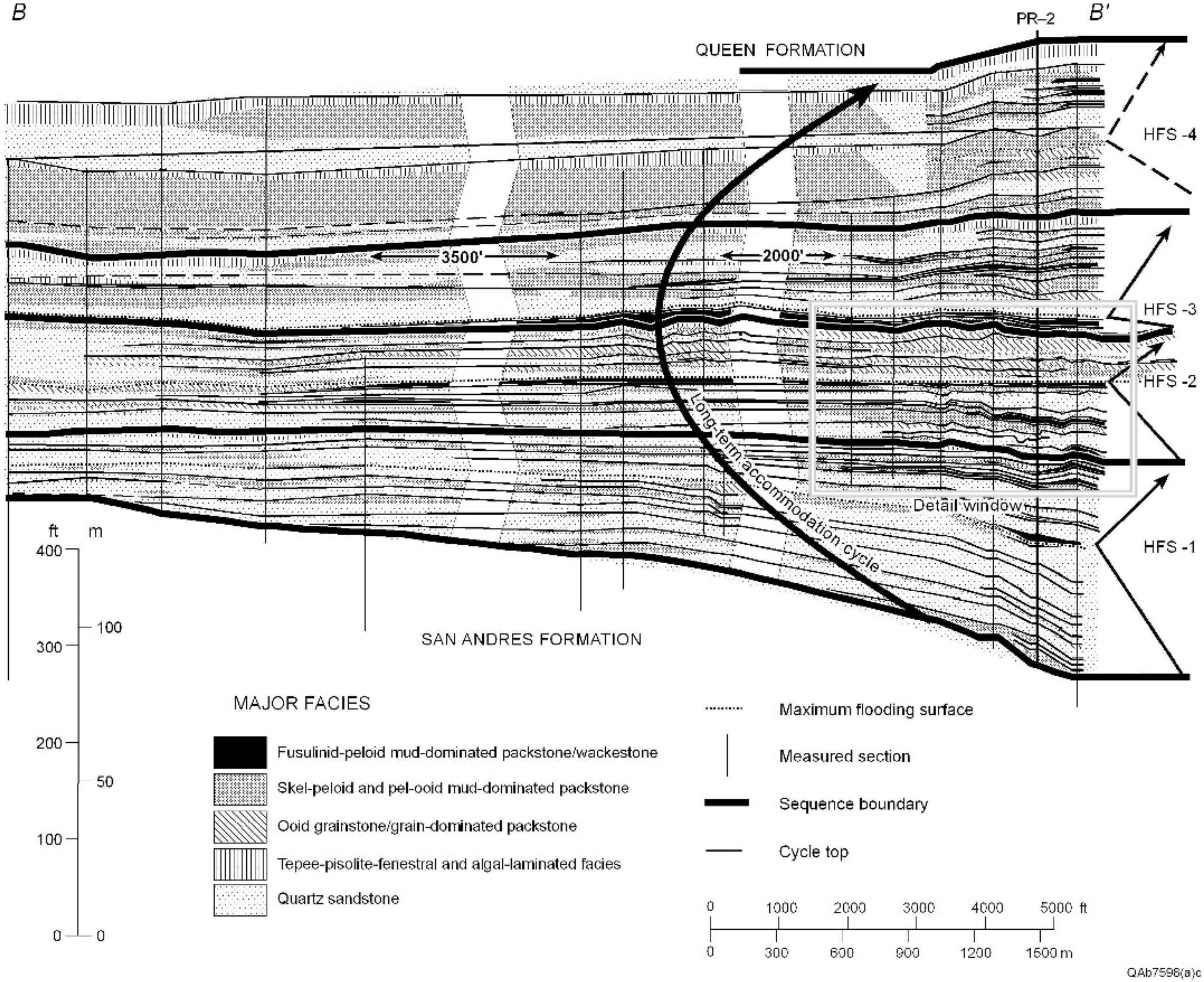

FIG. 7.—Grayburg stratigraphic framework from dip-parallel exposures on Plowman Ridge, location indicated in Figure 5. Vertical black lines delineate measured sections; vertical white bands indicate missing section due to cover. Approximate datum is top HFS-2. Detail window shown in Figure 8.

MAJOR LITHOFACIES

Mixed carbonate and siliciclastic rocks of the Grayburg Formation were grouped into seven major end-member lithofacies: (1) fusulinid–peloid mud-dominated packstone–wackestone; (2) mudstone and skel–peloid wackestone; (3) skel–peloid and pel–ooid mud-dominated packstone; (4) pel–ooid grain-dominated packstone; (5) ooid grainstone; (6) tepee–pisolite–fenestral and algal-laminated facies; and (7) quartz sandstone and quartz sand-rich occurrences of the above carbonate lithofacies. Major lithofacies (Figs. 10, 11, 12) are described in Table 1.

Fusulinid–Peloid Mud-Dominated Packstone–Wackestone

Fusulinid–peloid mud-dominated packstone–wackestone facies (Table 1, Fig. 10A) are relatively uncommon in the platform interior Grayburg strata of the study area (Fig. 4). Fusulinid-rich facies are abundant in locales seaward of the San Andres platform margin; e.g., the Western Escarpment (Fekete et al. 1986; Franseen et al. 1989) and the downdip southern end of Shattuck Escarpment (Kerans and Nance 1991). Similarly, in the subsurface Grayburg of the Central Basin Platform, fusulinid facies dominate outer-ramp strata of the lower Grayburg (e.g., Ruppel and Bebout 2001).

The basinward distribution, along with the abundant carbonate mud, open marine fauna, lack of current-generated sedimentary structures, and intense bioturbation, indicate a low-energy, outer-ramp depositional environment. In the lower San Andres Formation, fusulinid-rich facies are confined to the middle and lower portions of progradational ramp-margin clinoforms; reconstructed depositional profiles from the basinward-dipping stratal surfaces indicate water depths of 10 to 120 meters for this facies (Kerans and Fitchen 1995). This facies is thus interpreted to record maximum transgressive water depths on the shallow-water Grayburg platform. Consequently, fusulinid–peloid mud-dominated packstone–wackestone facies are stratigraphically significant for interpreting longer-term accommodation trends.

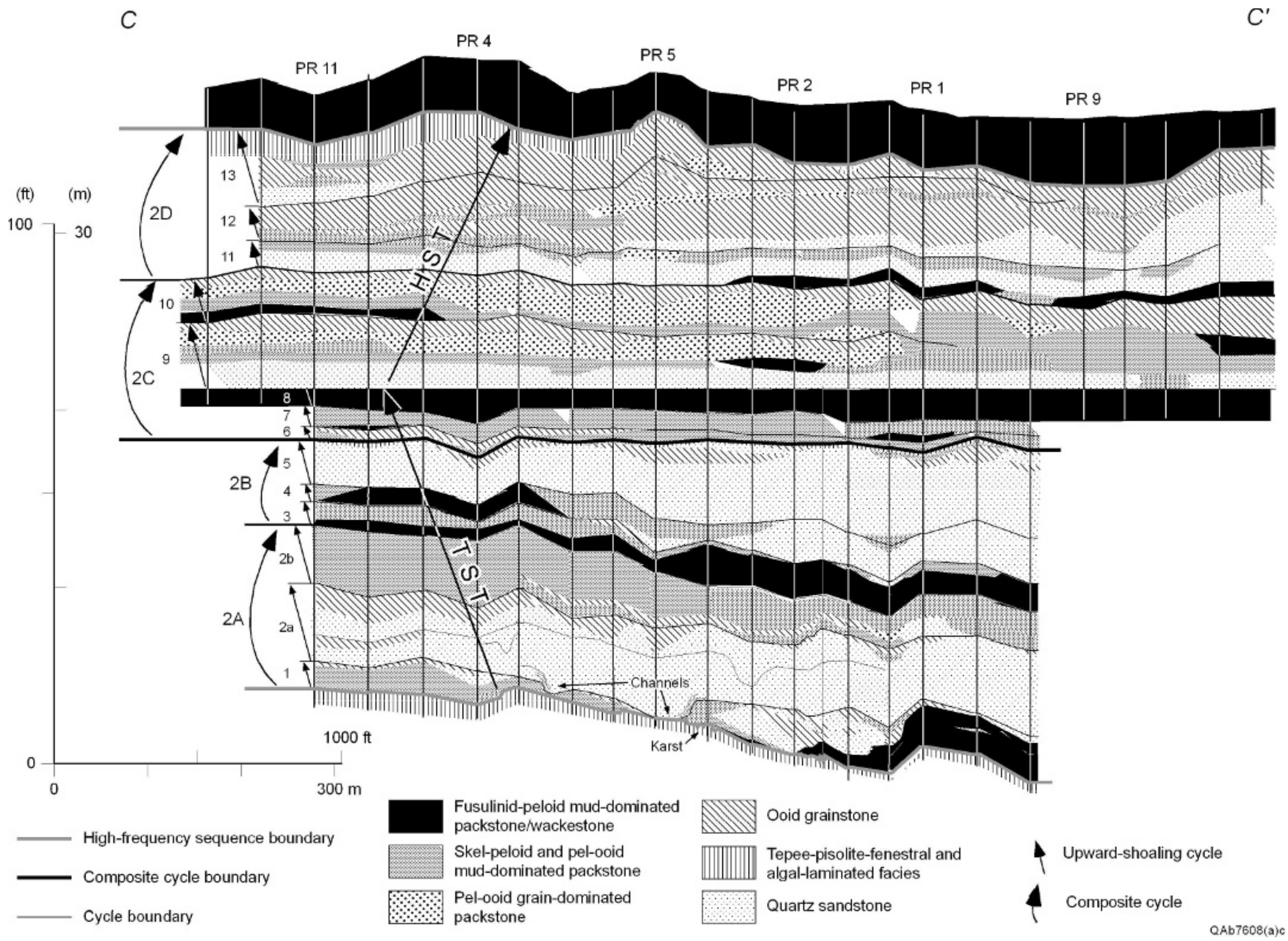

FIG. 8.— Stratigraphic cross section C–C′ of HFS 2 from Plowman Ridge, see Figures 5 and 7 for location. High-frequency sequence 2 is composed of 14 high-frequency cycles organized into 4 composite cycles (2A, 2B, 2C, and 2D). Datum is top of cycle 8, maximum flooding event.

Mudstone and Skel–Peloid Wackestone

Carbonate mudstone and skel–peloid wackestone facies (Table 1) occur locally. True mud-supported fabrics are uncommon in the Grayburg and a relict peloid-supported fabric is usually evident. Mud-supported fabrics record low-energy settings but otherwise provide little direct evidence of depositional environment; consequently, this facies probably records more than one depositional setting. Admixed skeletal material, including crinoids and fusulinids, in outer-platform skel–peloid wackestones suggest proximity to open marine conditions. In platform interior locations, carbonate mudstone is associated with tepee–pisolite–fenestral and algal-laminated facies, implying a restricted shallow subtidal to peritidal environment.

Skel–Peloid and Pel–Ooid Mud-Dominated Packstone

Skel–peloid and pel–ooid mud-dominated packstone (Table 1, Fig. 10B) is the most abundant carbonate facies in the study area (Fig. 7). Carbonate mud and compacted pseudomatrix completely occlude interparticle pore space. Because of bioturbation, compaction, and dolomitization, peloids can be difficult to distinguish from mud matrix.

The interparticle carbonate mud, admixed crinoids and fusulinids, and the extensive biotic reworking indicate a low-energy subtidal environment. This facies records dominantly quiet-water deposition below fair-weather wave base on the middle ramp, and/or a restricted setting protected by seaward ramp-crest shoals.

Pel–Ooid Grain-Dominated Packstone

Pel–ooid grain-dominated packstones (Table 1) are grain-supported rocks that contain minor amounts of carbonate mud; ooids (150 to 400 μm) and peloids (60 to 150 μm) are the dominant grain type (Fig. 10D). Cross-stratification is poorly developed or absent. Carbonate mud partially occludes interparticle pores. Grain-dominated packstone lies stratigraphically above skel–peloid and pel–ooid mud-dominated packstone facies and is overlain by ooid grainstone. Grain-dominated packstone passes basinward into skel–peloid and pel–ooid mud-dominated packstone facies and grades landward into ooid grainstone.

Pel–ooid grain-dominated packstone facies record shoaling into a relatively higher energy environment. Grain-supported fabrics with minor amounts of interparticle mud record a well-winnowed depositional setting, the admixed carbonate mud may have been introduced by bioturbation, which obscured or destroyed primary current stratification.

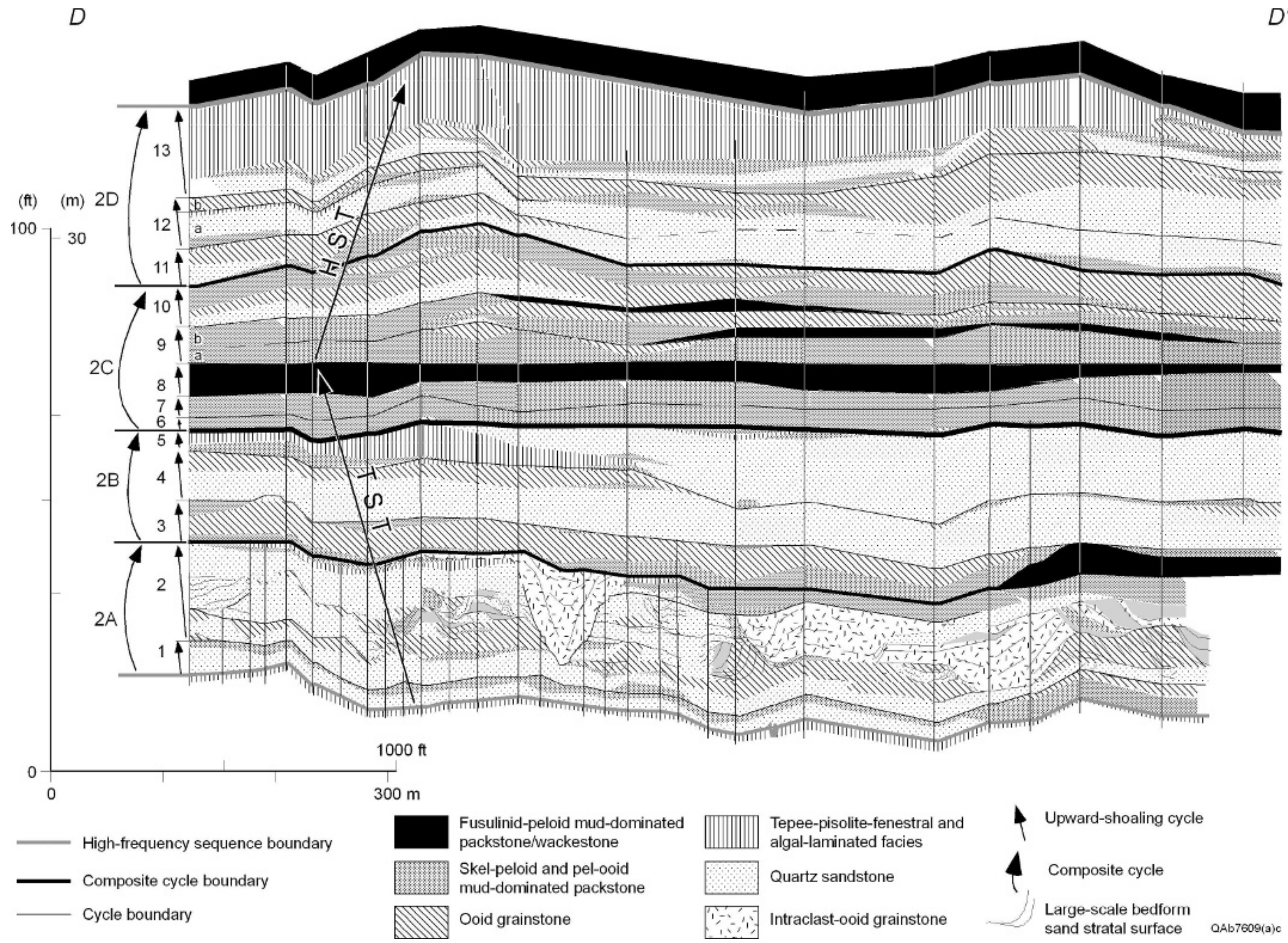

FIG. 9.—Stratigraphic cross section D–D′ of HFS 2 from West Dog Canyon, 1 km across depositional strike from Plowman Ridge; location indicated on Figure 5. Section is generally dip-oriented, however, outcrop exposures along the canyon meanders cause various segments of the cross section to differ in their orientation relative to depositional dip. Datum is top of cycle 8, maximum flooding event.

Ooid Grainstone

Ooid grainstone (Table 1, Figs. 10C, E, B) facies are especially abundant in HFS 2, both in outcrop (Fig. 7) and in the subsurface. Well-sorted ooid grains are 150 to 400 µm in diameter (Fig. 10F). Ooid grainstones are characterized by current stratification features, described in Table 1. The lower contact of ooid grainstones is gradational with underlying pel–ooid grain-dominated packstones, gradational to abrupt with underlying skel–peloid and pel–ooid mud-dominated packstones and quartz sandstones, and abrupt with underlying fusulinid–peloid mud-dominated packstone–wackestone facies. The upper contact of ooid grainstone facies is generally sharp, except where it grades upward into overlying tepee–pisolite–fenestral and algal-laminated facies.

Ooid grainstones form sheet-like bodies or channel-form units. Sheet-like bodies consist of stacked medium to thick beds that are amalgamated into successions up to 4 meters thick. Cross strata predominantly dip basinward whereas contacts between individual stacked beds dip landward. These units are laterally continuous for up to 1 km or more. For example, the grainstone body in Grayburg HFS 2 high-frequency cycle 12 (Fig. 13) is oriented parallel to depositional strike and is laterally continuous for at least 1000 meters across strike and more than 1200 meters along dip. These amalgamated grainstone units locally are interrupted by thin (less than 0.3 meters thick) intervals of bioturbated pel–ooid grain-dominated packstone and skel–peloid and pel–ooid mud-dominated packstone, some of which exhibit lateral continuity of a few hundred meters (Fig. 8) forming potential internal reservoir baffles.

Grainstone channels are up to 4.5 meters thick, with sharp erosional bases that downcut underlying strata (Fig. 11C). The channels are up to several hundred meters wide, oriented parallel to depositional dip (Fig. 14), and extend for at least thousands of meters in a dip direction. Syndepositional relief is at a maximum in these high-energy channels and bars; individual large-scale bedforms have up to 3 to 5 meters of relief from topset to toeset.

Ooid grainstones are interpreted to record high-energy conditions above fair-weather wave base. Ooid grainstones are stratigraphically significant because they are a sensitive indicator of high-energy, shallow-water deposition on the ramp crest and their distribution through successive high-frequency cycles reflects longer-term accommodation trends.

Tepee–Pisolite–Fenestral and Algal-Laminated Facies

Tepee–pisolite–fenestral and algal-laminated facies (Table 1, Figs. 10G, H, 11A), described by Tye (1986) occur throughout the Grayburg. Although they form successions up to 5.5 meters thick, they

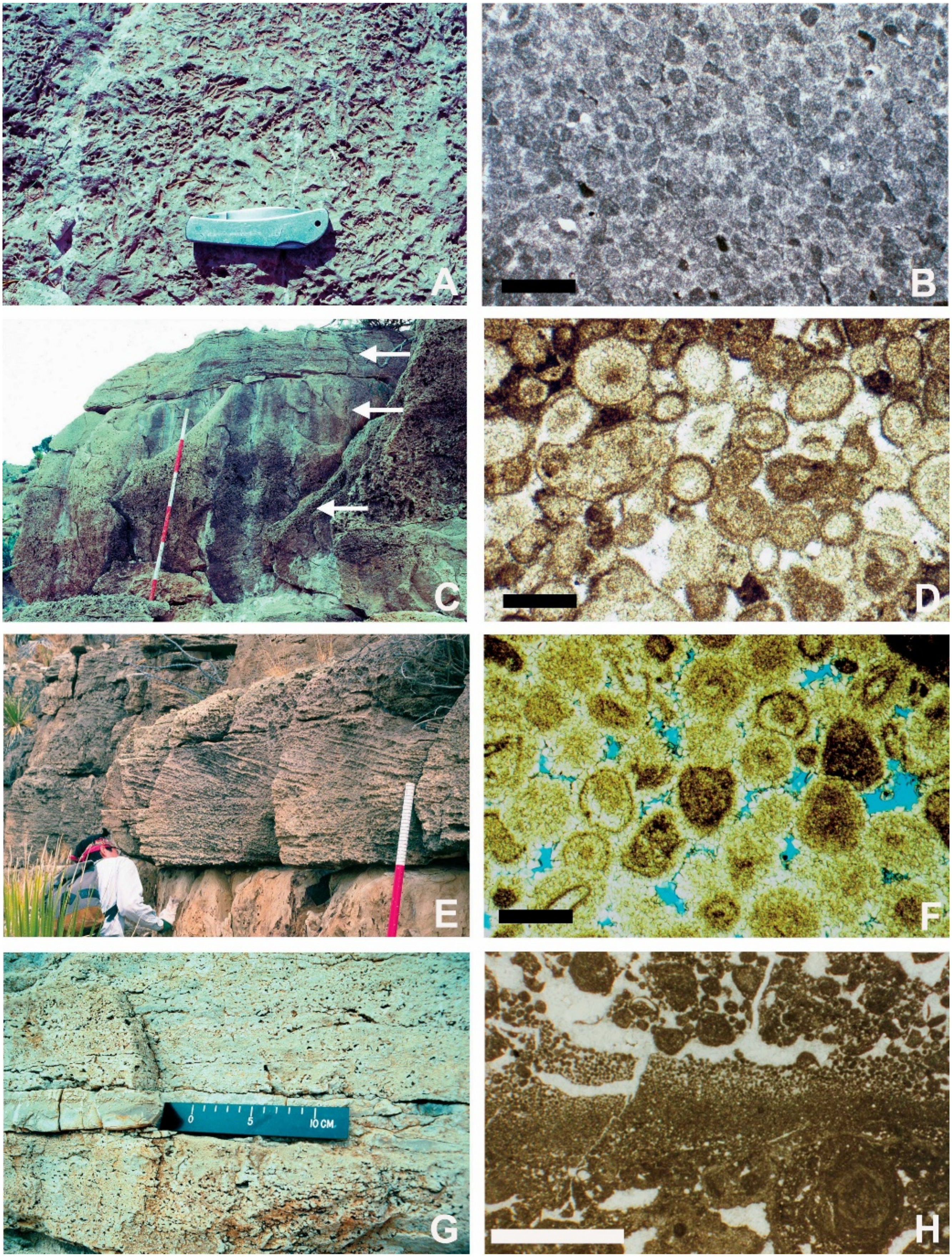
A
B
C
D
E
F
0
5
10 CM.
G
H

commonly exhibit poor lateral continuity (less than several hundred meters). These facies grade landward into skel–peloid and pel–ooid mud-dominated packstone and basinward into pel–ooid grain-dominated packstone and ooid grainstone. Tepee–pisolite–fenestral and algal-laminated facies are locally interbedded with skel–peloid and pel–ooid mud-dominated packstone, pel–ooid grain-dominated packstone, ooid grainstone, and quartz sandstone. The upper bounding surface of the tepee–pisolite–fenestral and algal-laminated facies typically is sharp (Fig. 11A) and displays local erosional truncation and small-scale karst (Fig. 12G). This facies is abruptly overlain by fusulinid–peloid mud-dominated packstone–wackestone, skel–peloid and pel–ooid mud-dominated packstone, pel–ooid grain-dominated packstone, ooid grainstone, or quartz sandstone.

Tepee structures, pisolites, fenestrae, desiccation cracks, and sheet cracks are associated with subaerial exposure in an upper peritidal to supratidal setting (Tye 1986). Botryoidal aragonite cements attest to an evaporative marginal marine environment. Tepee–pisolite–fenestral and algal-laminated structures overprint precursor sediments, including skel–peloid and pel–ooid mud-dominated packstone, pel–ooid grain-dominated packstone, ooid grainstone, and quartzose carbonate. These structures are best developed at the top of these units, grading downwards into more diffuse, poorly defined structures.

Thick accumulations of tepee–pisolite–fenestral and algal-laminated facies on the ramp crest represent grainstone and packstone shoals that formed paleohighs that were subsequently overprinted by marine vadose diagenesis. Interbedded grainstone and packstone beds attest to flanking subtidal facies. Tepee–pisolite–fenestral and algal-laminated facies are stratigraphically significant because they record platform aggradation to intertidal and supratidal environments and thus are an indicator of longer–term accommodation trends. Erosional truncation and small-scale karst at the tops of these units record subaerial exposure. Where these unconformable surfaces are abruptly overlain by transgressive outer-ramp fusulinid–peloid mud-dominated packstone and wackestone facies, this abrupt landward facies tract offset is interpreted to delineate the transgressive portion of the ensuing cycle.

Quartz Sandstone and Mixed Siliciclastic–Carbonate Facies

Siliciclastics in the Grayburg (Table 1) are represented by quartz sandstone, quartzose dolomite, and dolomitic sandstone. Quartz sandstones and mixed siliciclastic–carbonate facies contain coarse quartz silt to very fine- to medium-grained quartz sand, minor feldspar grains, and variable admixtures of dolomitized carbonate material (Fig. 12E, F). Siliciclastic fines (fine silt to clay) are absent. A wide range of sedimentary structures is observed (Table 1), including trough cross-lamination (Fig. 12A), large-scale accretionary foresets (Fig. 12B), burrowing and bioturbation, millimeter-scale wavy to crinkly algal lamination (Fig. 12C), and polygonal desiccation cracks (Fig. 12D).

Siliciclastic–carbonate admixtures range from less than 10 percent to more than 90 percent quartz sand. Quartz sandstones, as designated in this study, contain more than 60 percent quartz sand; the carbonate content and sedimentary structures were used to modify their description. Mixed siliciclastic–carbonate rocks containing less than 30 to 40 percent quartz sand were classified according to their carbonate depositional texture and major carbonate grains.

Quartz sandstone units typically are laterally continuous for several kilometers and form prominent marker beds that can be easily traced and correlated throughout the study area. This lateral continuity is comparable to analogous sandstone units in the Yates and Tansill formations in the Guadalupe Mountains (Borer and Harris 1989; Candelaria 1989). In the subsurface Grayburg (of South Cowden Field), siltstone and sandstone beds can be correlated throughout most of the 15 km^2 field area (Ruppel and Bebout 2001).

The very fine to medium sand size, the good sorting, the well-rounded medium-size quartz sand grains, and the mineralogical maturity implies that the siliciclastic fraction was transported by wind during sea level lowstands (Fischer and Sarnthein 1988). Evidence for subaerial exposure in subjacent facies includes tepee–pisolite–fenestral and algal-laminated fabrics, karst (Fig. 12H), mantling regolith breccias, and quartz sand-filled grikes. Shallow marine reworking of wind-transported quartz sands is indicated by channels, trough cross-lamination (Fig. 12A), bioturbation, and by admixed skeletal grains, ooids, peloids, and carbonate mud (Fig. 12F). Quartz sandstones and mixed siliciclastic–carbonate facies are stratigraphically significant because they record sea-level lowstands and subsequent transgression and are useful to interpret longer-term accommodation trends.

STRATIGRAPHIC HIERARCHY

The three levels of stratigraphic hierarchy (high-frequency cycles, composite cycles, and high-frequency sequences) within the Grayburg composite sequence are defined from a dip-oriented cross section by: (1) transgressive–regressive facies relationships; (2) facies stacking patterns in successive high-frequency cycles; (3) evidence of subaerial exposure (e.g., unconformities or paleokarst) at the tops of cyclic successions; and (4) abrupt vertical facies tract offsets at the transgressive base of each high-frequency sequence. This stratigraphic organization cannot be defined adequately by using vertical facies successions or high-frequency cycle thickness stacking patterns from an individual vertical section alone. Moreover, the significance of many stratal surfaces cannot be determined from a single vertical section, but rather it is the lateral continuity and variable expression (e.g., local paleokarst development) of these stratal surfaces across different facies tracts that define their relative importance. After the stratigraphic relationships and hierarchy are defined for an area, however, they can be readily recognized in additional sections, which can then be correlated into the stratigraphic framework.

High-Frequency Cycles

Grayburg high-frequency cycles are 0.5 to 10 m thick, upward-shoaling facies successions. A thin transgressive lag, composed of reworked

←

FIG. 10.— **A)** Outcrop photograph of fusulinid–peloid mud-dominated packstone with abundant fusulinid molds. Knife is approximately 8 cm long. **B)** Photomicrograph of peloid mud-dominated packstone. Scale bar = 500 µm. Core plug helium porosity = 1.0%, air permeability = 0.01 md. **C)** Outcrop photograph of high-frequency cycle 10 in Grayburg HFS 2. Cycle base is bioturbated ooid–peloid mud-dominated packstone (lower arrow). This grades upward into less intensely bioturbated peloid–ooid grain-dominated packstone (middle arrow). Cycle is capped by cross-stratified ooid grainstone (upper arrow). **D)** Photomicrograph of pel–ooid grain-dominated packstone. Scale bar = 500 µm. Interparticle pore space is largely occluded by carbonate mud and cement. Core-plug helium porosity = 1.9%, air permeability = 0.01 md. **E)** Outcrop photograph of high-frequency cycle 12 in Grayburg HFS 2. Bioturbated dolomitic sandstone at cycle base is abruptly overlain by cross-stratified ooid grainstone, which caps cycle. **F)** Photomicrograph of ooid grainstone. Scale bar = 500 µm. Primary interparticle pore space accounts for high porosity and permeability. Core-plug helium porosity = 12.0%, air permeability = 25.6 md. **G)** Outcrop photograph of laminar fenestral dolomite near top of Grayburg HFS 1. **H)** Photomicrograph of tepee–pisolite–fenestral facies. Scale bar = 2 mm. Matrix consists of pisoids, pelleted (microbial?) mud, and mud with a clotted fabric. Interparticle, fenestral, and early fracture pores are nearly completely occluded by fibrous to inclusion-rich, early marine cement. Core-plug helium porosity = 1.0%, air permeability = 0.01 md.

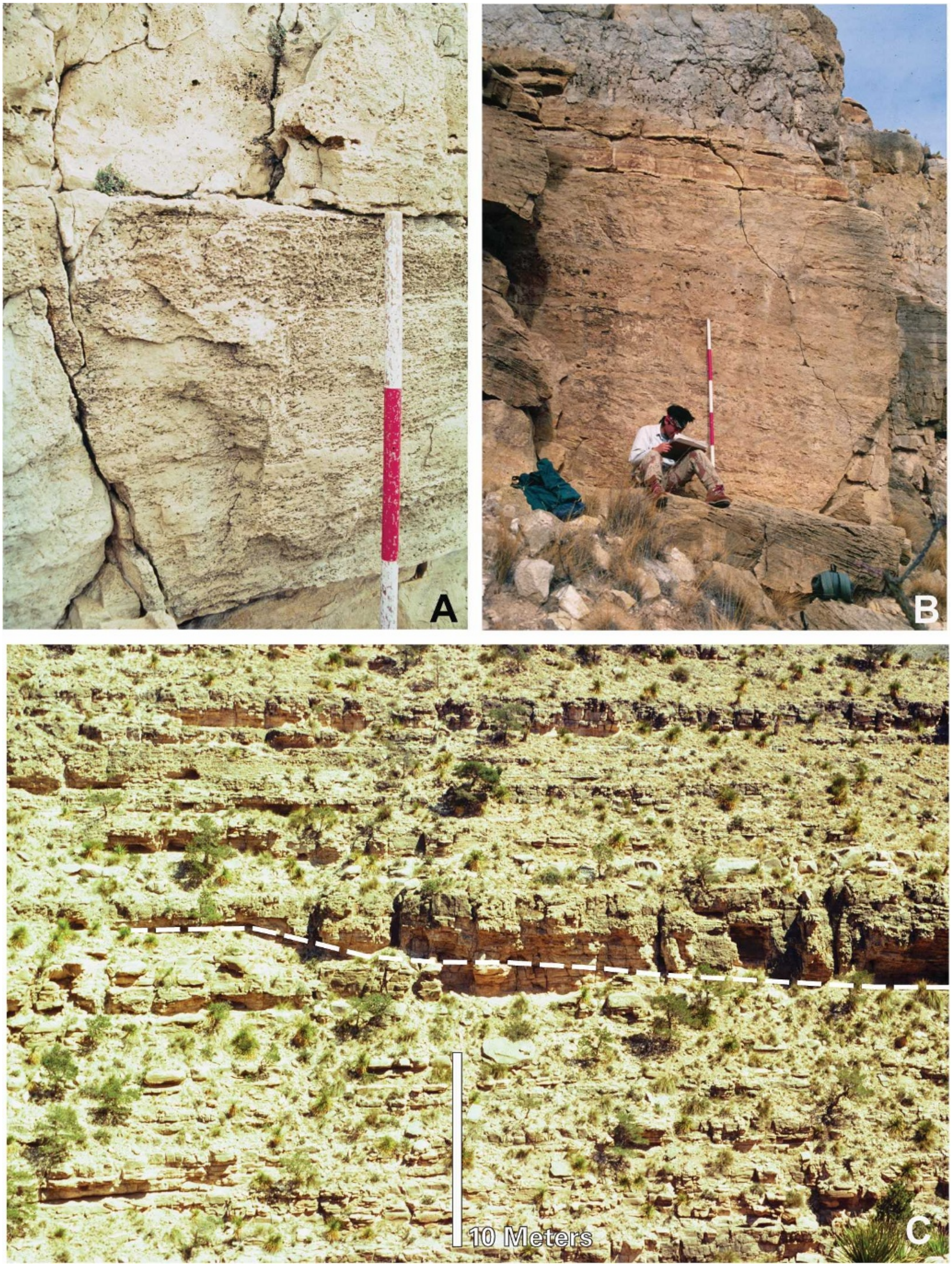
A
B
10 Meters
C

sediment and intraclasts from the underlying cycle, occurs at the base of some high-frequency cycles. Grayburg high-frequency cycles typically are asymmetric, consisting of basal low-energy, carbonate mud-rich, bioturbated facies succeeded by more proximal facies. Some high-frequency cycle tops display *in situ* breccias, sand-filled grikes, paleokarst (Fig. 12G, H), desiccation cracks (Fig. 12D), and erosional truncation. Cycle tops typically are abruptly overlain by low-energy facies at the base of the ensuing cycle.

Grayburg high-frequency cycles exhibit diverse facies, facies proportions, sedimentary structures, and bounding stratal surfaces. Within a single high-frequency cycle, the component lithofacies and facies proportions may vary significantly at different locations along the depositional profile. For example, in high-frequency cycles 4 and 5 (Figs. 8, 9) carbonate-dominated facies at one location pass laterally into equivalent, mixed carbonate–siliciclastic facies, which, in turn, grade laterally into siliciclastic-dominated facies.

In a low-accommodation, shallow-water setting landward of the platform margin, high-frequency cycles typically are asymmetric, with abrupt bases of low-energy, mud-rich, bioturbated facies that reflect maximum flooding followed by successively more proximal facies due to aggradation as sediment infilled accommodation. Fully aggraded high-frequency cycles are capped by peritidal facies. High-frequency cycles are capped by abrupt stratal surfaces that indicate a period of nondeposition, erosion, and/or subaerial exposure prior to transgression by the ensuing cycle.

The preservation potential of high-frequency cycles reflects long-term accommodation, constituent lithology, and the depositional environment of transgressive facies in the overlying cycle. High-frequency cycles deposited during periods of low accommodation are less likely to be preserved due to sediment reworking in an accommodation-limited setting. High-frequency cycles composed of carbonate are more likely to be preserved, because carbonates tend to be indurated by early cementation during subaerial exposure. High-frequency cycles composed of quartz sandstone are less likely to be preserved, because unconsolidated quartz sand is readily reworked by burrowing organisms and currents during the ensuing transgression. For example, anomalously thick successions (up to 10 m) of massive quartz sandstone that display no internal vertical facies successions may reflect amalgamation of several vertically stacked cycles. High-energy tidal channel and shoal facies tracts are more likely to rework underlying sediments of the subjacent high-frequency cycle than overlying low-energy, distal facies.

Representative end-member high-frequency cycle types from a measured section on Plowman Ridge (PR-2) are illustrated in Figure 15.

Sandstone-Dominated High-Frequency Cycles.—The base of these cycles is composed of bioturbated quartz sandstone, with admixed carbonate, including mud, peloids, fusulinids, and other skeletal grains. In one example (Fig. 15A), bioturbated sandstone passes upward into trough cross-stratified sandstone, which is capped by wavy-laminated dolomitic sandstone. Some sandstone-dominated high-frequency cycles are capped by algal stromatolites (Fig. 12C). Erosional truncation, breccias, and desiccation cracks (Fig. 12D) cap some high-frequency cycles.

Bioturbated quartz sandstones with admixed carbonate mud, grains, and skeletal material record reworking of eolian quartz sands (e.g., Fischer and Sarnthein 1988) in a low-energy subtidal setting. Trough cross-stratified sandstones indicate aggradation (or a fall in relative sea level) into a high-energy shallow subtidal environment. Accommodation infilling to a peritidal environment is evidenced by wavy to crinkly laminated sandstones that reflect binding by algal mats and by local fenestrae and pisoids. Desiccation cracks and breccias capping some high-frequency cycles attest to subaerial exposure.

Some sandstone-dominated high-frequency cycles do not exhibit a well-defined, upward-shoaling trend, for example, sandstone units composed entirely of bioturbated massive sandstone. In such cases, the existence of internal cyclicity must be inferred from the depositional model. For example, a thick, laterally continuous bed of quartz sandstone above a carbonate unit implies a fall in relative sea level and eolian transport of quartz sand prior to subtidal reworking during the ensuing transgression.

Mixed Carbonate–Sandstone High-Frequency Cycles.—These cycles typically contain basal quartz sandstones or dolomitic quartz sandstones that grade upward into carbonate-dominated lithologies. In one example (Fig. 15B), the cycle base consists of bioturbated quartz sandstone with fusulinids. This is succeeded by dolomitic sandstone with increasingly abundant admixed carbonate grains that grades upward into a quartzose pel–ooid grain-dominated packstone. The top of this high-frequency cycle is a quartzose cross-stratified ooid grainstone. Another example of a mixed carbonate–sandstone high-frequency cycle (Fig. 10E) shows bioturbated quartz sandstone abruptly overlain by an ooid grainstone. Some mixed carbonate–sandstone high-frequency cycles are capped by algal–pisolitic–fenestral quartzose facies with intraclasts and pisoids. High-frequency cycle tops locally display small-scale karst, grikes, and erosional truncation.

In mixed carbonate–sandstone high-frequency cycles, the carbonate fraction typically becomes increasingly dominant upwards, interpreted to reflect diminishing siliciclastic influx as sea level rose and *in situ* carbonate production increased. High-frequency cycles capped by peritidal facies fully aggraded to intertidal and supratidal depositional environments. Small-scale karst and grikes record subaerial exposure.

Carbonate-Dominated High-Frequency Cycles.—These cycles typically have skel–peloid and pel–ooid mud-dominated packstone facies with intense bioturbation at the base. Skeletal grains are locally abundant. These mud-rich facies pass upward into better sorted, grain-dominated packstone and grainstone. Burrowing decreases upward as current stratification becomes increasingly dominant. An example of this type of high-frequency cycle (Figs. 10C, 15C) shows bioturbated mud-rich facies succeeded by pel–ooid grain-dominated packstone which grades upward into trough and accretionary cross-stratified ooid grainstone. Fully aggraded carbonate-dominated high-frequency cycles are capped by peritidal facies.

Skel–peloid and pel–ooid mud-dominated packstone facies at the cycle base record a low-energy, subtidal setting during flooding. Fusulinids and pelmatozoans attest to an open marine environment. Carbonate mud content decreases upward, and the transition from pel–ooid grain-dominated packstone to overlying grainstones with trough and accretionary cross-stratification reflects increasingly higher energy deposition. Fully aggraded tidal flat-capped high-frequency cycles record supratidal environments; local subaerial exposure is evidenced by small-scale karst and grikes.

←

FIG. 11.—**A)** Outcrop photograph of HFS 2 sequence boundary on Plowman Ridge. Top of staff marks abrupt contact between underlying laminar fenestral facies and overlying transgressive fusulinid–peloid mud-dominated packstone. Staff in 0.3048 meter increments. **B)** Outcrop photograph of HFS 2 sequence boundary 100 meters basinward (south) of photograph shown in part A. At this outer-ramp crest location, a 4.5 meter-thick, cross-stratified ooid grainstone unit (brown, geologist sitting near base) is erosionally truncated and is abruptly overlain by gray bioturbated fusulinid–peloid mud-dominated packstone. **C)** Outcrop photograph of intraclast–ooid grainstone channel. Dashed line indicates erosional base; up to 3 meters of erosional downcutting occurs in underlying quartz sandstones.

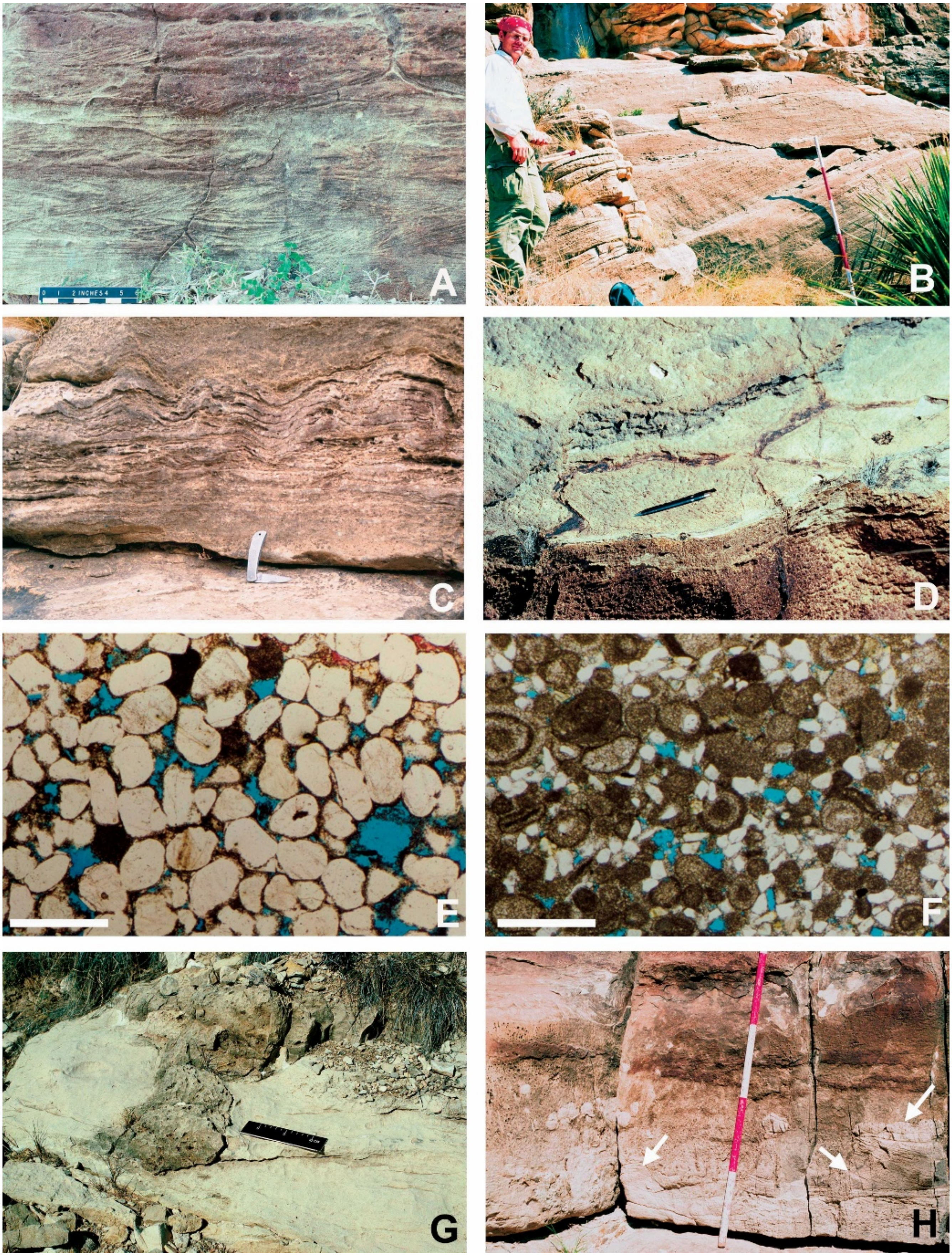
A
B
C
D
E
F
G
H

Composite Cycles

Composite cycles (4 to 12 meters thick) consist of two or more high-frequency cycles arranged into intermediate-scale, transgressive–regressive successions (Figs. 8, 9). At the base of each composite cycle, facies typically consist of fusulinid–peloid or skel–peloid mud-dominated packstone with admixed quartz sand or fossiliferous quartz sandstone. High-frequency cycles in the upper portion of composite cycles contain increasing proportions of more proximal facies, including ooid grainstone and fenestral–pisolite and algal-laminated facies (Figs. 8, 9). Small-scale karst locally caps the composite cycles.

Composite cycles subdivide the high-frequency sequences into intermediate-scale cyclic successions within the longer-term accommodation trend imposed by the high-frequency sequences. Transgressive facies at the base of the composite cycles are succeeded by more proximal ooid grainstone and fenestral–pisolite and algal-laminated facies, interpreted to represent successive infilling of accommodation to shallow subtidal and peritidal environments. Local karst records subaerial exposure following deposition. For many composite cycles, however, the landward facies tract offset at the transgressive base of the overlying composite cycle is the defining aspect of the composite cycle top. This landward facies-tract offset is greater in magnitude than that for high-frequency cycles within the composite cycle.

In the subsurface with widely spaced well control, it can be difficult to identify and correlate individual high-frequency cycles, whereas composite cycles can be more readily recognized. For example, the high-frequency cycle tops within the composite cycle are less well developed than the tops of the composite cycles. In the study area, high-frequency cycles are best developed on the ramp crest. Off the crest, high-frequency cycles may become less well developed so that the composite cycle may be the smallest stratigraphic unit that can be recognized and correlated. Composite cycles also are useful chronostratigraphic units where cycle amalgamation has occurred. Amalgamation is restricted to high-frequency cycles within a composite cycle, and cycle amalgamation does not occur across composite cycle boundaries, retaining the integrity of these chronostratigraphic surfaces.

High-Frequency Sequences

Grayburg high-frequency sequences recognized by this study follow the definition of Mitchum (1977) and Mitchum and Van Wagoner (1991). Because the Grayburg accumulated landward of the shelf margin (Fig. 4), sequences consist of a transgressive systems tract separated by a maximum flooding surface from the highstand systems tract. Except for the lowermost Grayburg, which onlaps the San Andres shelf margin, the high-frequency sequences do not display diagnostic stratal terminations (e.g., onlap, offlap, and toplap) due to limited accommodation in the relatively flat-lying, shallow-water setting (Fig. 7). The Grayburg high-frequency sequences are primarily recognized from facies stacking patterns in successive high-frequency cycles. Each high-frequency sequence contains at its base an unconformity, overlain by a retrogradational succession of high-frequency cycles, succeeded by an aggradational to progradational succession of high-frequency sequences, and capped by an unconformity.

Stratigraphically significant facies for interpreting the accommodation trends of the high-frequency sequences include: (1) fusulinid–peloid mud-dominated packstone–wackestone facies, which record transgression and maximum water depths; (2) ooid grainstones, which indicate aggradation to a shallow-water, high-energy setting; (3) tepee–pisolite–fenestral and algal-laminated facies, which document platform aggradation to intertidal and supratidal environments; and (4) quartz sandstones and mixed siliciclastic–carbonate facies, which represent eolian transport during sea-level lowstands and subsequent subtidal reworking during transgression.

Unconformity-related subaerial exposure is directly indicated by paleokarst and grikes and can be inferred from overlying lowstand-transported quartz sands. An abrupt landward facies-tract offset overlying an unconformity is one of the more diagnostic features of the sequence boundary. For example, at the base of HFS 2 (Fig. 8), transgressive fusulinid–peloid mud-dominated packstone–wackestone facies overlie karsted tidal flat facies of underlying HFS 1, defining the lower sequence boundary.

We interpret four high-frequency sequences (HFS 1–4), each 30 to 45 meters thick, in the Grayburg Formation (Fig. 7). Correlation of our stratigraphic framework with previous studies that subdivide the Grayburg into 2 sequences (Kerans et al. 1992; Kerans et al. 1993) indicates that our Grayburg HFS 1 and 2 are equivalent to their Guadalupian HFS 14 and our Grayburg HFS 3 and 4 are correlative with their Guadalupian HFS 15. Given that the Grayburg composite sequence is approximately 1 Myr in duration (Ross and Ross 1987), the four Grayburg high-frequency sequences may correspond to fourth-order depositional cycles (*sensu* Goldhammer et al. 1990). The four Grayburg sequences are thought to be equivalent to the four sequences interpreted from the subsurface Grayburg, for example, in Maljamar Field on the northern shelf of the Delaware Basin (Modica 1997) and on the Central Basin Platform in South Cowden Field (Ruppel and Bebout 2001), North Cowden Field (Entzminger et al. 2000), and Foster Field (Kerans, personal communication 1995). These regional correlations suggest that the Grayburg high-frequency sequences represent intermediate-scale cyclicity in relative sea level superimposed on the longer-term accommodation trend recorded by the third-order Grayburg composite sequence (Fig. 6).

GRAYBURG STRATIGRAPHIC AND FACIES ARCHITECTURE

Grayburg HFS 1

Description.—The lowermost Grayburg onlaps the San Andres Formation (Fig. 7) and consists of skeletal-rich quartz sandstones and quartzose carbonates that are trough cross-stratified or bioturbated. These subtidal facies cap high-frequency cycles, with local paleokarst and grikes occurring at the cycle tops. At the top of HFS 1, laterally extensive algal-laminated and fenestral–pisolite facies (Figs. 8, 9) are succeeded by an erosional surface with local paleokarst (Fig. 12G). The isopach map for this interval (Fig. 16) displays a basinward increase in thickness.

←

FIG. 12.— **A)** Outcrop photograph of quartz sandstone with small-scale trough cross-stratification. **B)** Outcrop photograph of quartz sandstone with large-scale accretionary foresets interpreted to be relict eolian dune. **C)** Outcrop photograph of wavy to stromatolitic algal laminae in dolomitic sandstone near top of high-frequency cycle. Knife handle is approximately 8 cm long. **D)** Outcrop photograph of polygonal desiccation cracks in dolomitic sandstone filled with siliciclastic silt and carbonate mud near top of high-frequency cycle. **E)** Photomicrograph of well-sorted quartz sandstone. Scale bar = 500 μm. Sediments consist of fine- to medium-grained, rounded to well-rounded, detrital quartz sand and minor peloids. Cements consist of dolomite, quartz overgrowths, and late calcite (stained pink). Porosity includes primary interparticle moldic pores (probably leached feldspar grains). Core-plug helium porosity = 6.1%, air permeability = 1.93 md. **F)** Photomicrograph of quartzose ooid grainstone with very fine- to fine-grained quartz sand. Scale bar = 500 μm. **G)** Outcrop photograph of quartzose fenestral dolomite at top of Grayburg HFS 1 cut by karst dissolution dolines infilled by fusulinid–peloid mud-dominated packstone that delineates onset of transgression for HFS 2. **H)** Outcrop photograph of karsted cross-stratified ooid grainstone at top of Grayburg HFS 1 (white arrows). Up to 0.7 meters of relief exists; this surface is overlain by quartz sandstone at the base of HFS 2.

TABLE 1.—*Summary of lithofacies descriptions.*

Facies	Bedding characteristics	Grain types	Sedimentary structures	Contacts other features
Fusulinid-peloid mud-dominated packstone and wackestone	Massive to bioturbated, recessive weathered beds 0.5–3 m thick	Peloid matrix, fusulinids (10–40%), crinoids, mollusks, quartz silt and very fine to fine grained quartz sand	Bioturbation	Abrupt lower contact, upper contact abrupt to gradational
Mudstone and skel-peloid wackestone	Massive to bioturbated, recessive weathered beds 0.2–1.5 m thick	Mollusks, peloids, crinoids, dasycladaceans, fusulinids (< 10%)	Bioturbation	Abrupt lower contact upper contact gradational
Skel-peloid and pel-ooid mud-dominated packstone	Massive to bioturbated, resistant ledge forming beds 0.3–10 m thick	Peloids, ooids, crinoids, mollusks, fusulinids (< 10%), quartz silt and very fine- to fine-grained quartz sand	Bioturbation, local faint parallel lamination	Lower contact abrupt to gradational upper contact gradational or abrupt
Pel-ooid grain-dominated packstone	Massive to bioturbated, resistant ledge forming beds 0.3–1.5 m thick	Ooids, peloids, crinoids, intraclasts, quartz silt and very fine- to fine-grained quartz sand	Bioturbation, local relict cross-stratification	Gradational upper and lower contacts
Ooid grainstone	Massive resistant cliff-forming units up to 5 m thick	Ooids, peloids, intraclasts, crinoids, fine- to medium-grained quartz sand	Trough cross-stratification, sheet stratification, accretionary bedding, channels	Beds amalgamated, lower contact gradational or abrupt, upper contact abrupt
Tepee-pisolite-fenestral and algal-laminated facies	Resistant cliff-forming units up to 6 m thick	Pisoids, peloids, pelleted sediment, ooids, intraclasts, very fine- to medium-grained quartz sand	Tepees, fenestrae, algal laminations desiccation cracks, aragonite-cemented sheet cracks	Gradational lower contact, abrupt upper contact
Quartz sandstone and mixed siliciclastic-carbonate facies	Recessive, slope-forming units, 0.3–10 m thick	Very fine- to medium-grained quartz sand, minor feldspar, medium sand grains are well rounded, very fine and fine sand grains are angular, ooids, peloids, fusulinids, crinoids, intraclasts, pisoids	Massive and bioturbated, trough- and ripple cross-stratification, accretionary foresets, plane parallel lamination, small-scale channels, fenestrae, mm-scale wavy algal lamination	Beds amalgamated, abrupt lower contact, gradational to abrupt upper contact

Interpretation.—Grayburg onlap onto the San Andres Formation represents a third-order sequence boundary (Sarg and Lehmann 1986). Abundant quartz sand in the lower Grayburg reflects eolian siliciclastic influx during subaerial exposure of the San Andres Formation. High-frequency cycles capped by subtidal facies with subaerial exposure features are interpreted to have been stranded by cyclic falls in relative sea level (e.g., Rankey et al. 1999). The first widespread carbonate-dominated unit is interpreted to represent maximum flooding. Algal-laminated and fenestral–pisolite facies near the top of HFS 1 record aggradation to an upper peritidal to supratidal setting. The erosional surface with local paleokarst at the top of HFS 1 is a sequence boundary that was subsequently transgressed by the base of HFS 2.

The onlapping geometries of lowermost Grayburg strata indicate that the basinward-thickening trend reflects depositional relief on the seaward-dipping top of the San Andres platform. Antecedent topography was infilled by the end of HFS 1, as evidenced by well-developed peritidal to supratidal facies at the top of HFS 1 and by the relatively uniform thickness of overlying HFS 2 (Fig. 17).

Grayburg HFS 2

Detailed stratigraphic analysis focused on Grayburg HFS 2 because this interval contains grain-dominated packstone and grainstone facies of interest in reservoir characterization due to their high porosity and permeability. The stratigraphic succession is similar for the Plowman Ridge and West Dog Canyon locations, although they display differences in facies and high-frequency cycle development (Figs. 8, 9). These disparities reflect the slightly different platform location and depositional variability along strike.

Transgressive Systems Tract: Description.—The base of HFS 2 (Figs. 8, 9) is a fusulinid–peloid mud-dominated packstone–wackestone to fusulinid-bearing dolomitic sandstone. Quartz sand is abundant in the lower TST. Incised channels are common; the largest occurs in West Dog Canyon where algal-laminated and fenestral–pisolite facies are downcut 4.5 meters (Fig. 9). This channel (Fig. 11C) contains ooid–intraclast grainstone with sigmoidal and herringbone cross-stratification and is oriented parallel to depositional dip (Fig. 14).

Fusulinid–peloid mud-dominated packstone–wackestone facies in successive high-frequency cycles display retrogradational relationships and are ultimately succeeded by a widespread unit of this facies (Figs. 8, 9).

Transgressive Systems Tract: Interpretation.—Fusulinid-rich facies at the base of HFS 2 represent an abrupt landward shift in deposition above karsted peritidal facies in HFS 1. Abundant quartz sand reflects high siliciclastic influx during sea-level lowstands; continued transgression eventually restricted siliciclastic influx. The abundant incised channels and well-developed sigmoidal and herringbone cross-stratification document a tidal influence.

The ooid–intraclast grainstone-filled channel (Figs. 11C, 14) is representative of grainstone facies architecture in the transgressive systems tract. These grainstone bodies typically retain their initial depositional morphologies and were not extensively reworked. Development of ooid bars and tidal channels is comparable to that observed in Holocene carbonates in the Joulters Cay area of the Bahamas (Harris et al. 1993). The transgressive systems tracts exhibit the greatest lateral heterogeneity of grainstone bodies, many of which formed dip-elongate channels and bars (Harris et al. 1993). This heterogeneity reflects the tidal setting that dominated during initial transgression, in which ooids were produced and accumulated along dip-oriented tidal channels and bars. Rapid increase in accommodation associated with rising relative sea level

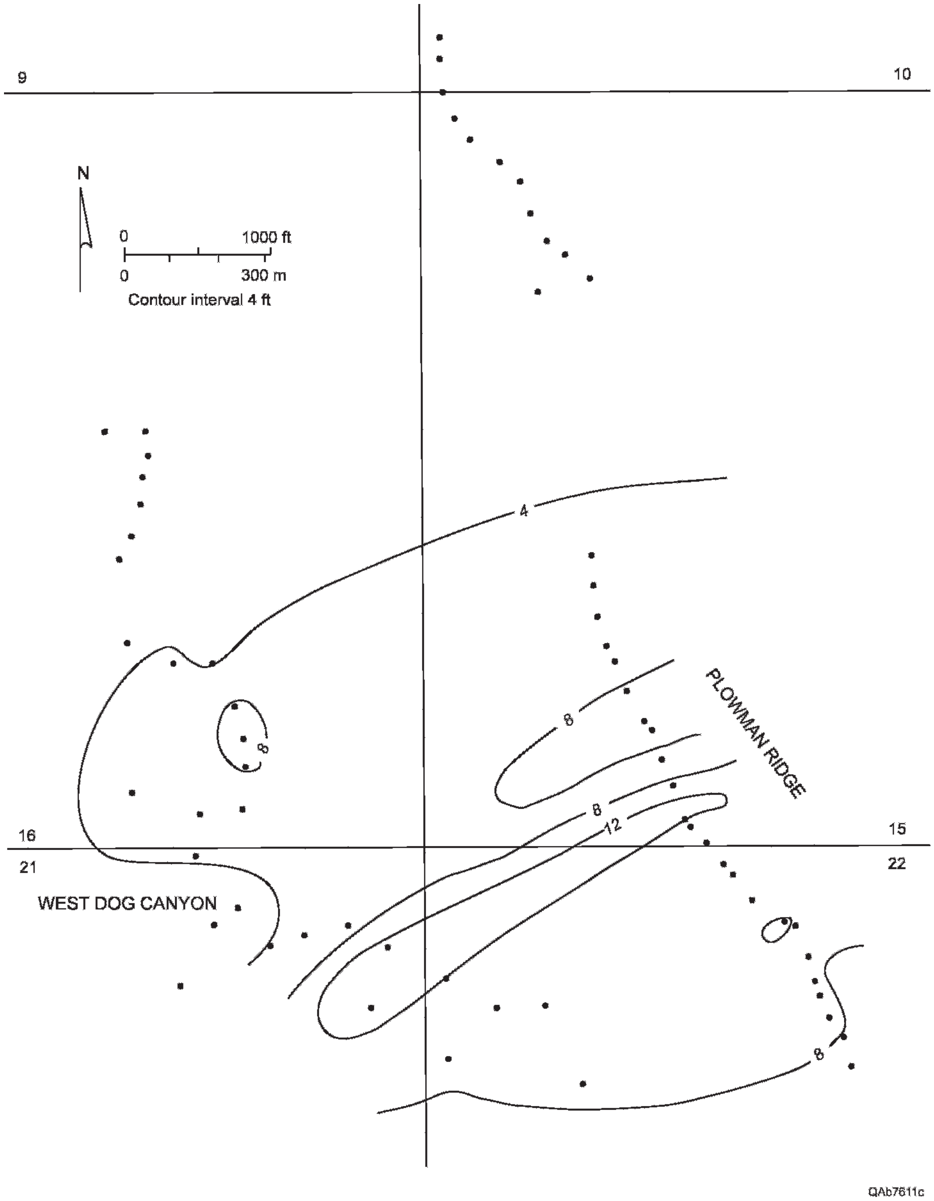

FIG. 13.—Isopach map of ooid grainstone unit in HFS 2 high-frequency cycle 12 (HST) at Plowman Ridge and West Dog Canyon. The measured sections indicated by dots and the continuous outcrop exposures between measured sections were used to generate map. Township and range lines from Figure 5.

resulted in high preservation potential for these dip-elongate grainstone bodies.

Landward-stepping fusulinid–peloid mud-dominated packstone facies in the late TST record continued transgression, which culminated in deposition of a widespread unit of this facies during maximum flooding in HFS 2 (Figs. 8, 9).

Highstand Systems Tract: Description.—High-frequency cycles in the upper portion of HFS 2 are capped by ooid grainstone beds (Figs. 8, 9) up to 4 meters in thickness. The ooid grainstones display dominantly south-dipping accretionary foresets, whereas the contacts between successive stacked beds dip towards the north. The grainstones contain minor amounts of admixed quartz sand.

These grainstone bodies are oriented parallel to depositional strike. For example, the ooid grainstone body in high-frequency cycle 12 attains a maximum thickness of 4.3 meters and forms a strike-elongate shoal (Fig. 13). The shoal has a dip width of more than 1200 meters and extends for at least 1000 meters across strike.

Tepee–pisolite–fenestral and algal-laminated facies near at the top of HFS 2 (Fig. 11A) are capped by an erosional surface with local paleokarst. This surface is overlain by fusulinid–peloid mud-dominated packstone–wackestone facies at the base of HFS 3 (Fig. 11A, B). The isopach map for HFS 2 (Fig. 17) indicates minor (< 3 meters) variation in thickness.

Highstand Systems Tract: Interpretation.—The ooid grainstones record a high-energy, ramp-crest environment and are interpreted to represent aggradation to shallow subtidal conditions. Strike-parallel ooid grainstones that are laterally continuous (hundreds of meters to 1 km) along dip and across strike reflect reworking, coalescence, and amalgamation of ooid grainstone bodies in a limited accommodation highstand setting. South-dipping cross laminae and north-dipping contacts between

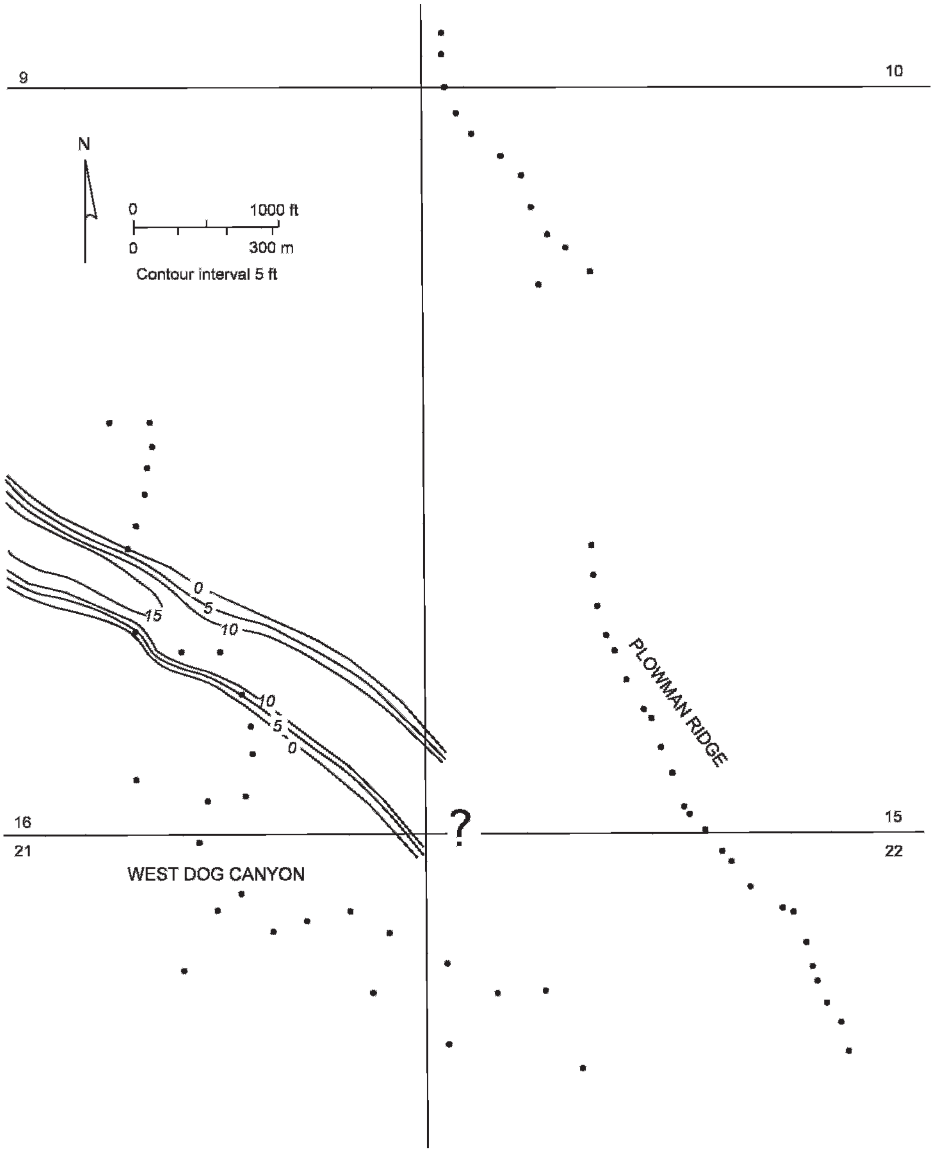

FIG. 14.—Isopach map of ooid–intraclast channel in HFS 2 high-frequency cycle 2 (TST) in West Dog Canyon. The measured sections indicated by dots and the continuous outcrop exposures between measured sections were used to generate map. Township and range lines from Figure 5.

successive stacked beds indicate that the predominant transport direction was to the south and that the shoals within a high-frequency cycle amalgamated by migrating southward and climbing atop the preceding shoal. This is consistent with a northeasterly dominant paleowind direction (Parrish and Peterson 1988; Parrish 1993, 1995) and suggests that ooid formation was on the restricted landward side of the ramp crest where salinities were elevated by evaporation. Highstand ooid grainstones typically contain little or no admixed quartz sand, suggesting that communication with the siliciclastic-dominated inner platform was inhibited by fringing grainstone shoals. This interpretation is consistent with observations of Holocene carbonates in the Bahamas (Harris et al. 1993), where fringing barrier highstand ooid shoals restrict tidal circulation with the platform interior.

Tepee–pisolite–fenestral and algal-laminated wackestone and packstone facies near the top of HFS 2 reflect complete infilling of accommodation. The subaerial exposure surface is interpreted to represent the upper sequence boundary. This surface is transgressed by outer-ramp fusulinid–peloid mud-dominated packstone–wackestone facies at the base of HFS 3.

The isopach map indicates that antecedent relief on the San Andres platform was largely infilled by the end of HFS 1. Changes in thickness in HFS 2 coincide with the thickness trends in the ooid grainstone bodies and thus reflect syndepositional relief due to depositional processes such as sediment production and accumulation on high-energy ramp-crest shoals.

Grayburg HFS 3

Description.—The base of Grayburg HFS 3 is a regionally correlative interval of fusulinid–peloid mud-dominated packstone–wackestone facies (Figs. 6, 7). This is the stratigraphically highest occurrence of this facies in the study area. In more distal locations, such as Shattuck Valley, this facies persists throughout HFS 3 (Kerans and Nance 1991).

The HFS 3 high-frequency cycles consist of cyclically interbedded quartz sandstone and mixed siliciclastic–carbonate facies with skel–peloid and pel–ooid mud-dominated packstone and minor ooid grainstone, some cycles are capped by tepee–pisolite–fenestral and algal-laminated facies. We pick the top of HFS 3 immediately above a unit of tepee–pisolite–fenestral and algal-laminated facies (Figs. 6, 7). This surface is

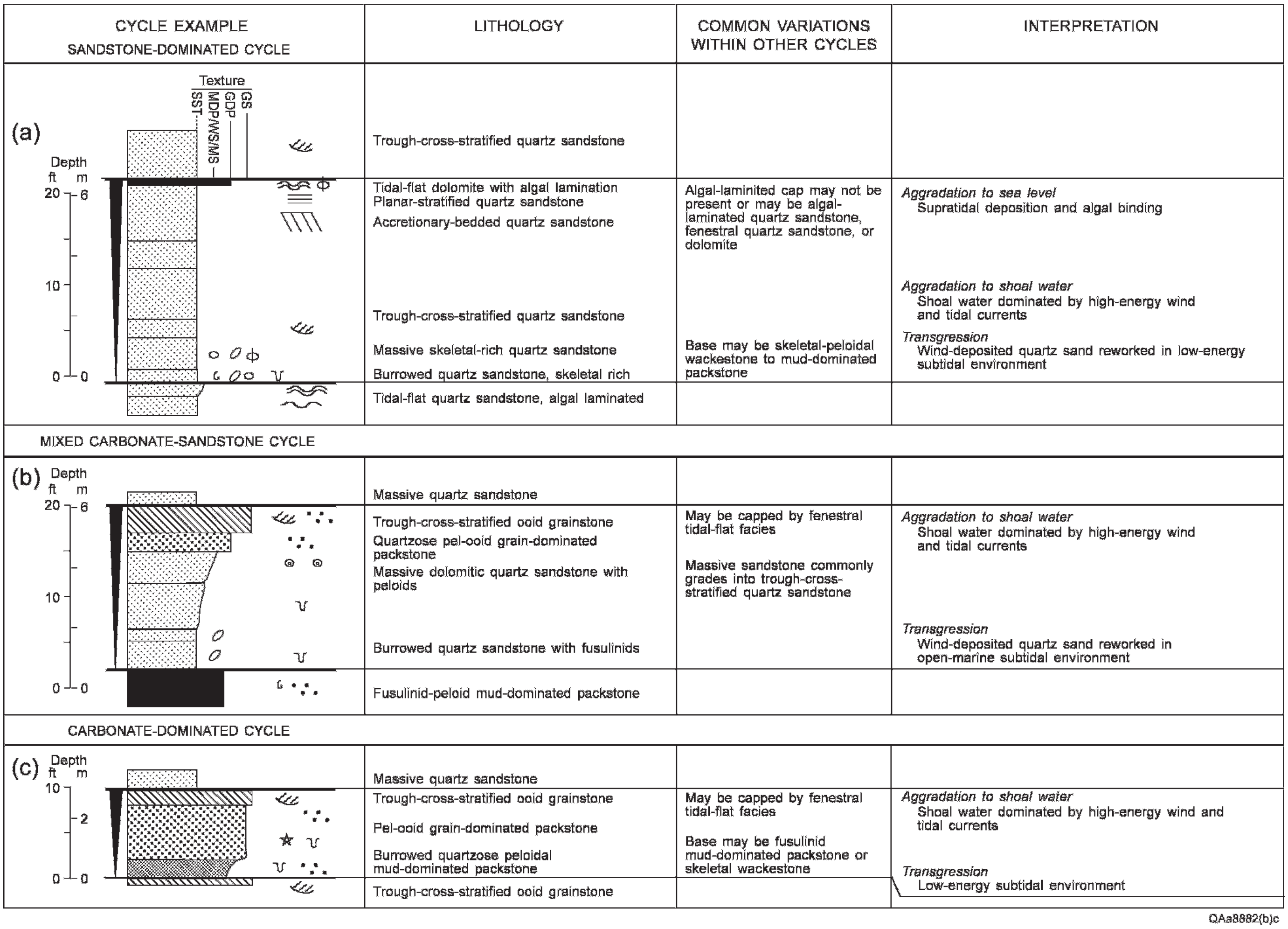

FIG. 15.—Examples of end-member high-frequency cycle types (from measured section PR-2) in Grayburg Formation.

abruptly overlain by skel–peloid and pel–ooid mud-dominated packstone and ooid grainstone at the base of HFS 4.

Interpretation.—The regionally correlative fusulinid–peloid mud-dominated packstone–wackestone unit at the base of HFS 3 records maximum regional flooding in the Grayburg composite sequence (Kerans and Nance 1991; Kerans et al. 1992; Kerans et al. 1993; this study); this event is recognized throughout the Permian Basin in outcrop and subsurface (e.g., Ruppel and Bebout 2001). The paucity of stratigraphically higher fusulinid–peloid mud-dominated packstone–wackestone facies in the study area indicates infilling of long-term accommodation. High-frequency cycles in HFS 3 are aggradational successions of inner-ramp to middle-ramp facies. The upper sequence boundary of HFS 3 is interpreted to be the top of the tepee–pisolite–fenestral and algal-laminated facies. However, due to limited outcrop exposures of this interval, this sequence boundary is poorly constrained. This surface is transgressed by skel–peloid and pel–ooid mud-dominated packstones and ooid grainstones assigned to the base of HFS 4.

Grayburg HFS 4

Description.—There is poor outcrop control for much of HFS 4 in the study area (Fig. 6). The limited exposures are dominated by a suite of relatively restricted, inner-ramp facies, including massive dolomitic quartz sandstone, skel–peloidal and pel–ooid mud-dominated packstone, and tepee–pisolite–fenestral and algal-laminated facies. Fusulinid–peloid mud-dominated packstone–wackestone facies in HFS 4 are rare in Grayburg strata that accumulated landward of the underlying San Andres margin (this study; Ruppel and Bebout 2001). In more distal locations basinward of the San Andres margin, outer-ramp fusulinid–peloid packstone facies persist to the Grayburg–Queen sequence boundary (Fekete et al. 1986; Franseen et al. 1989; Kerans and Nance 1991). On Plowman Ridge, the top of the Grayburg Formation is poorly exposed and is assigned to the top of the uppermost unit of tepee–pisolite–fenestral and algal-laminated facies that is overlain by recessively weathered, yellow-brown to pink, thin-bedded sandstones assigned to the lowermost Queen Formation.

Interpretation.—The suite of restricted, inner-ramp facies and the paucity of fusulinid–peloid mud-dominated packstone–wackestone facies are consistent with an interpretation that this interval consists of dominantly aggradational high-frequency cycles that reflect decreasing long-term accommodation in the Grayburg composite sequence. In more basinward locations, outer ramp fusulinid–peloid packstone facies persist to the Grayburg–Queen sequence boundary, reflecting greater accommodation in more distal outer-ramp locations. Sandstones in the overlying Queen Formation represent a major basinward shift in depositional facies.

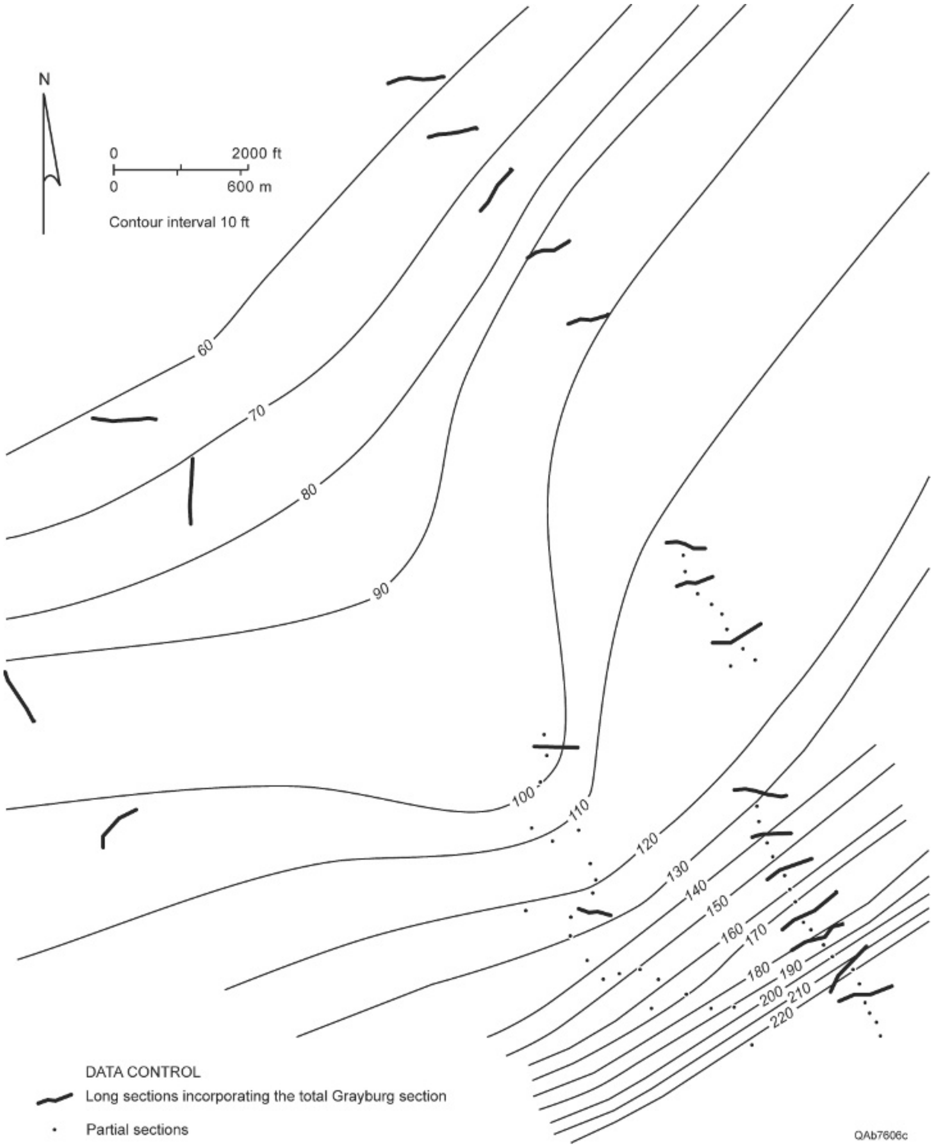

FIG. 16.—Isopach map of HFS 1. In addition to the measured sections indicated by dots, the continuous outcrop exposures between sections were used to generate map.

DISCUSSION

A significant contribution of this study is the detailed facies distribution with respect to the hierarchical stratigraphy of the high-frequency sequences, composite cycles, and high-frequency cycles. Critical facies for interpreting transgressive–progradational aspects of the accommodation trends include: (1) outer-ramp fusulinid–peloid mud-dominated packstone–wackestone facies, which record transgression; (2) ramp-crest ooid grainstones, which represent aggradation and progradation to high-energy subtidal environments; (3) tepee–pisolite–fenestral and algal-laminated facies, which indicate aggradation to sea level; and (4) wind-transported quartz sands, which reflect emergence of the platform during sea-level lowstands. There are no facies, however, that are unique to the transgressive or highstand systems tracts. Instead, the systems tracts and high-frequency sequences are defined by the landward and seaward shifts in facies distribution, facies stacking relationships, and bounding flooding surfaces and unconformities.

For example, in HFS 2, quartz sands are most abundant in the transgressive systems tract (Figs. 8, 9), recording eolian influx of siliciclastics during prolonged sea-level lowstands and subsequent reworking during the ensuing transgression. Quartz sand is least abundant in high-frequency cycles associated with maximum flooding, because widespread transgression restricted siliciclastic influx. Fusulinid–peloid mud-dominated packstone–wackestone facies occur at the base of high-frequency cycles in both the transgressive and highstand systems tracts. This facies displays a retrogradational distribution in the transgressive systems tract, which culminated in deposition of a widespread unit during maximum transgression. Ooid grainstones are present in both transgressive and highstand strata; however, grainstones are best developed in the highstand, where vertically stacked ooid grainstones in successive high-frequency cycles exhibit progradational relationships. Tepee–pisolite–fenestral and algal-laminated facies locally cap composite cycles in both transgressive and highstand systems tracts. In the study area, this facies is best developed where it occurs at the top of the high-frequency sequences. For example, in HFS 2, tepee–pisolite–fenestral and algal-laminated facies cap an overall progradational succession of ooid grainstone-dominated high-frequency cycles, recording successive infilling of accommodation, followed by an unconformity development during sea-level lowstand.

The stratigraphic entities represented by the high-frequency cycle, composite cycle, and high-frequency sequence are three-dimensional bodies. Although the hierarchical stratigraphy may be initially interpreted

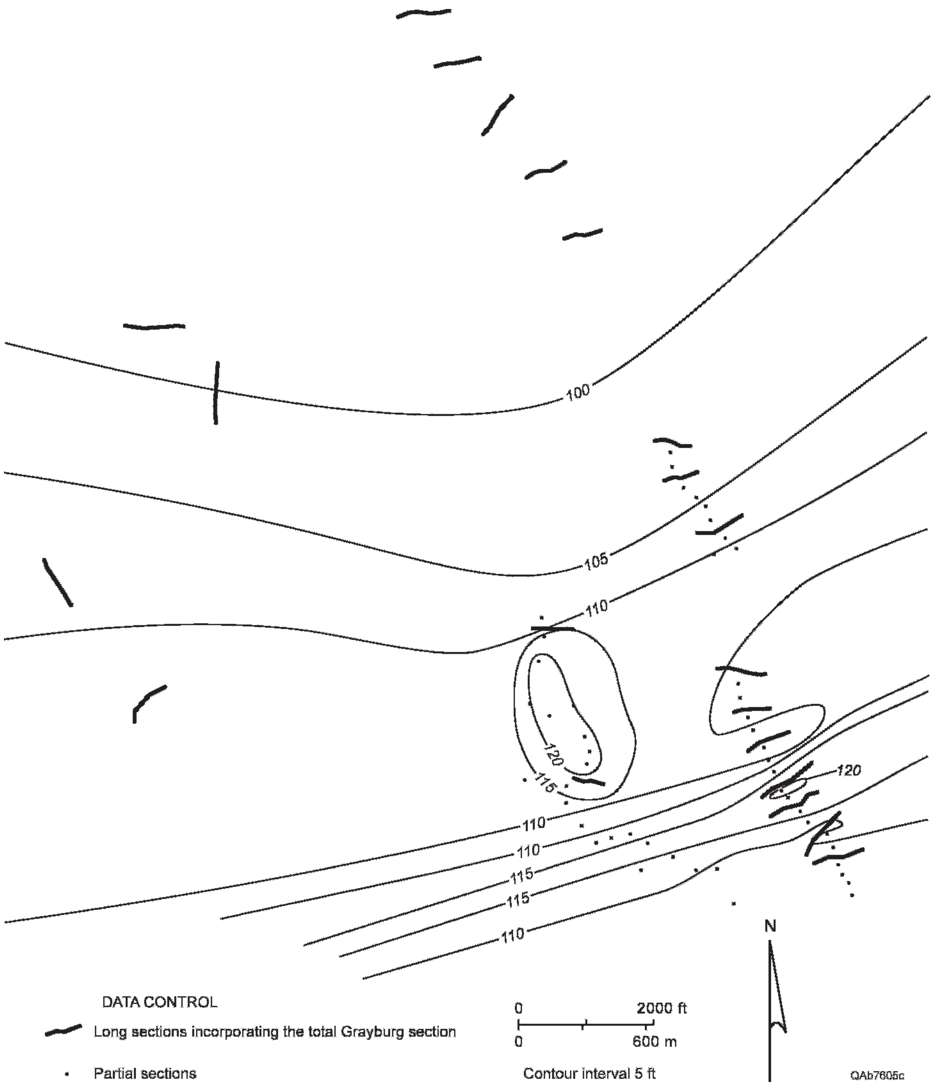

FIG. 17.—Isopach map of HFS 2 displays less pronounced basinward thickening than HFS 1. Local isopach thick in West Dog Canyon represents depositional relief on a ramp-crest ooid shoal that developed at this locale. In addition to the measured sections, the continuous outcrop exposures between sections were used to generate map.

from a vertical section, at minimum, a dip-oriented cross-sectional view is required to fully recognize the hierarchy of stratal surfaces and the landward and seaward facies shifts that define high-frequency cycles and the sequence stratigraphic framework. Evaluation of lateral variation across depositional strike requires information on the shelf orientation and antecedent topography.

The character of the high-frequency cycles and their component facies reflects their platform location. Grayburg strata examined by this study accumulated in shallow-water conditions (0 to 10 meters depth) in a middle-ramp to ramp-crest setting, 10 km landward of the margin. High-frequency cycles are less well developed in the more seaward environments represented by the outer shelf, shelf margin, and foreslope (Fekete et al. 1986; Franseen et al. 1989). Landward of the study area, subaerial exposure was more continuous and the interval is dominated by a suite of restricted inner-shelf facies, including quartz sandstone, dolomitic sandstone, and tepee–pisolite–fenestral and algal-laminated facies.

Antecedent topography profoundly influenced facies distribution within the high-frequency sequences, composite cycles, and high-frequency cycles. For example, the break in slope induced by the underlying San Andres shelf margin influenced facies distribution in the lower Grayburg (HFS 1 and 2). In the lower Grayburg, below the maximum flooding event in HFS 2, outer-ramp fusulinid–peloid mud-dominated packstone–wackestone and mudstone and skel–peloid wackestone facies are generally confined to locations seaward of the San Andres margin. Widespread deposition of a fusulinid–peloid mud-dominated packstone–wackestone unit during maximum flooding in HFS 2 indicates that the antecedent topography in the study area was largely infilled by this time, although more subtle topographic variation continued to influence the location of outer-ramp-crest ooid grainstones and inner-ramp-crest tepee–pisolite–fenestral and algal-laminated facies in the HFS 2 highstand. Smaller-scale variation in antecedent topography caused by depositional processes impacted facies distribution in the high-frequency cycles and composite cycles. For example, in the transgressive systems tract of HFS 2, dip-oriented topographic lows and highs created by channel incision and shoals are maintained in successive high-frequency cycles within a composite cycle. In the highstand systems tract of HFS 2, depositional thicks created by ooid grainstone shoals on the outer ramp crest influence facies distribution in the successive high-frequency cycle.

Detailed characterization of the facies distribution from the Grayburg outcrops demonstrates the application of sequence stratigraphic principles for high-resolution correlation of well-log and core data for characterization of facies heterogeneity in subsurface reservoirs. The high-frequency cycles offer the highest resolution correlation unit to delineate the facies distribution. With widely spaced well data, however, recognition and correlation of individual high-frequency cycles becomes more difficult, whereas the more significant facies tract offsets recorded by the composite cycles and high-frequency sequences are readily identified and confidently correlated. This stratigraphic framework then provides a basis for further interpretation of the smaller-scale accommodation trends and potential correlation of the high-frequency cycles.

Stratigraphic analysis indicates general relationships between stratigraphic setting, depositional environment, and facies geometry and lateral continuity. For example, subtidally reworked lowstand quartz sands form laterally continuous units (more than several kilometers). Transgressive low-energy carbonates display similar lateral continuity. Ooid grainstones that accumulated in a transgressive setting formed dip-elongate tidal channels and bars that are less than a few hundred meters wide and more than one kilometer in length. Conversely, ooid grainstones that accumulated under highstand conditions formed strike-elongate shoals that are laterally continuous along dip and across strike for one kilometer or more.

Prediction of facies distribution and lateral heterogeneity in areas with sparse well data requires knowledge of the general trend of the platform and the relative position within the cyclic hierarchy. Empirical relationships such as those described above between stratigraphic setting, facies orientation, and lateral continuity can be used to improve subsurface correlations and better populate facies in 3-D geocellular models based on limited well data.

SUMMARY

Mixed siliciclastic and carbonate rocks of the Grayburg Formation accumulated on the shallow-water periphery of the Delaware and Midland basins. Facies record depositional environments including outer-ramp, high-energy ramp crest, restricted inner-ramp, and wind-transported lowstand quartz sandstones. Facies successions display vertical and lateral relationships that define four hierarchical scales of sea-level cyclicity.

The entire Grayburg Formation is a composite sequence that records a third-order cycle in eustatic sea level (Ross and Ross 1987). Grayburg deposition began with onlap onto the San Andres platform and culminated with subaerial exposure, followed by a major basinward shift in facies during deposition of the Queen Formation. The Grayburg composite sequence contains four high-frequency sequences. Each high-frequency sequence corresponds to an intermediate-scale cycle in relative sea level and comprises a retrogradational succession of transgressive facies overlain by a progradational to aggradational succession of highstand facies, capped by a sequence boundary. The high-frequency sequences can be subdivided into composite cycles, intermediate-scale transgressive–regressive successions that contain several high-frequency cycles. High-frequency cycles are the smallest-scale, upward-shoaling facies successions that can be traced laterally across different facies tracts and are interpreted to represent fifth-order cycles in relative sea level.

Detailed characterization of the Grayburg outcrops demonstrates the application of sequence stratigraphic principles for high-resolution correlation and facies mapping, documenting the utility of stratigraphic analysis to interpret and correlate well-log and core data for characterization of geologic heterogeneity in subsurface reservoirs. The high-frequency cycles form the basic unit for high-resolution chronostratigraphic correlation and delineation of facies heterogeneity. High-frequency cycles, however, may be difficult to confidently correlate using well data at typical 10 to 40 acre well spacings, whereas the longer-term accommodation trends and greater facies tract offsets recorded by the composite cycles and high-frequency sequences allow more confident chronostratigraphic correlations. These larger-scale correlations then provide the framework for further interpretation of the smaller-scale accommodation trends and potential correlation of the constituent high-frequency cycles.

Because depositional fabrics are well preserved in the dolomitized carbonates and quartz sandstones of the Grayburg, porosity and permeability are a function of the original depositional fabric (Lucia 1995) and high-frequency cycles define the basic flow units.

Lateral heterogeneity reflects both larger-scale systematic facies changes and interwell-scale heterogeneity due to geologic complexity. Systematic facies changes that reflect primary environmental and/or depositional controls (e.g., water depth, platform position, accommodation trends) can be characterized with subsurface data, abetted by depositional models where data are sparse. Interwell heterogeneity due to geologic complexity is more difficult to recognize with subsurface data. Appropriate outcrop analogs provide invaluable information on lateral facies dimensions and heterogeneity styles that can be utilized to construct more realistic three-dimensional reservoir models than over-simplified models based on lithofacies correlations forced between wells by linear interpolation.

ACKNOWLEDGMENTS

This work was completed while the authors were at the Bureau of Economic Geology at The University of Texas at Austin. C. Kerans and F.J. Lucia proposed this study, obtained research support, and contributed to the ideas and interpretations. The manuscript benefited from reviews by Journal of Sedimentary Research Associate Editor E.C. Rankey and Co-Editor K. Milliken, and editorial review by J.B. Southard. Technical reviews by D.L. Cantrell, M.T. Harris, and E.K. Franseen greatly improved the manuscript; C.R. Handford and S.P. Dutton reviewed early versions of the manuscript. J.G. Grubb, M.H. Kwong, K.A. Kempter, and R. Boghici served as research and field assistants. J.W. Jennings, Jr. evaluated petrophysical heterogeneity in the Grayburg; this work is described in Jennings (2000). Funding for this research was provided by the U.S. Department of Energy and by the Industrial Associates of the Reservoir Characterization Research Laboratory.

REFERENCES

Babcock, J.A., 1977, Calcareous algae, organic boundstones, and the genesis of upper Capitan Limestone (Permian Guadalupian) Guadalupe Mountains, West Texas and New Mexico, *in* Hileman, M.E., and Mazzullo, S.J., eds., Upper Guadalupian Facies, Permian Reef Complex, Guadalupe Mountains, New Mexico and West Texas: Permian Basin Section, SEPM, Publication 77-16, p. 3–44.

Borer, J.M., and Harris, P.M., 1989, Depositional facies and cycles in Yates Formation outcrops, Guadalupe Mountains, New Mexico, *in* Harris, P.M., and Grover, G.A., eds., Subsurface and Outcrop Examination of the Capitan Shelf Margin, Northern Delaware Basin: SEPM, Core Workshop 13, p. 305–317.

Boyd, D.W., 1958, Permian Sedimentary Facies, Central Guadalupe Mountains, New Mexico: New Mexico Bureau of Mines and Mineral Resources, Bulletin 49, 100 p.

Candelaria, M.P., 1989, Shallow marine sheet sandstones, Upper Yates Formation, Northwest Shelf, Delaware Basin, New Mexico, *in* Harris, P.M., and Grover, G.A., eds., Subsurface and Outcrop Examination of the Capitan Shelf Margin, Northern Delaware Basin: SEPM, Core Workshop 13, p. 319–324.

Coffin, M., Gahagan, L., Lawver, L., Lee, T.-Y., and Rosencrantz, E., 1992, Atlas of Mesozoic/Cenozoic reconstructions (200 Ma to present day) plates: University of Texas Institute for Geophysics, Technical Report 122, 49 p.

Crowley, T.J., and Baum, S.K., 1991, Estimating Carboniferous sea-level fluctuations from Gondwana ice extent: Geology, v. 19, p. 975–977.

Dunham, R.J., 1962, Classification of carbonate rocks according to depositional texture, *in* Ham, W.E., ed., Classifications of Carbonate Rocks—A Symposium: American Association of Petroleum Geologists, Memoir 1, p. 108–121.

Entzminger, D.J., Ferdinand, K., Lawson, D., Loucks, R., Mescher, P., and Patty, K., 2000, Corrigan–Cowden unit: the next generation, *in* Reid, S.T., ed., Geo-2000: Into the Future: American Association of Petroleum Geologists, Southwest Section, Transactions, West Texas Geological Society, Publication 2000-107, p. 139–159.

Fekete, T.E., Franseen, E.K., and Pray, L.C., 1986, Deposition and erosion of the Grayburg Formation (Guadalupian, Permian) at the shelf-to-basin margin, western escarpment, Guadalupe Mountains, Texas, *in* Moore, G.E., and Wilde, G.L., eds., Lower and Middle Guadalupian Facies, Stratigraphy, and Reservoir Geometries, San Andres–Grayburg Formations, Guadalupe Mountains, New Mexico and Texas: SEPM, Permian Basin Section, Special Publication 25, p. 69–81.

Fischer, A.G., and Sarnthein, M., 1988, Airborne silts and dune-derived sands in the Permian of the Delaware Basin: Journal of Sedimentary Petrology, v. 58, p. 637–643.

Fitchen, W.M., 1993, Sequence stratigraphic framework of the Upper San Andres Formation and equivalent basinal strata in the Brokeoff Mountains, Otero County, New Mexico: New Mexico Geological Society, 44th Field Conference, Guidebook, Carlsbad Region, New Mexico and West Texas, p. 185–193.

Franseen, E.K., Fekete, T.E., and Pray, L.C., 1989, Evolution and destruction of a carbonate bank at the shelf margin: Grayburg Formation (Permian), western escarpment, Guadalupe Mountains, Texas, *in* Crevello, P.D., Wilson, J.L., Sarg, J.F., and Read, J.F., eds., Controls on Carbonate Platform and Basin Development: SEPM, Special Publication 44, p. 289–304.

Galloway, W.E., Ewing, T.E., Garrett, C.M., Tyler, N., and Bebout, D.G., 1983, Atlas of Major Texas Oil Reservoirs: The University of Texas at Austin, Bureau of Economic Geology, 139 p.

Goldhammer, R.K., Dunn, P.A., and Hardie, L.A., 1990, Depositional cycles, composite sea level changes, cycle stacking patterns, and the hierarchy of stratigraphic forcing—examples from platform carbonates of the Alpine Triassic: Geological Society of America, Bulletin, v. 102, p. 535–562.

Grant, C.W., Goggin, D.J., and Harris, P.M., 1994, Outcrop analog for cyclic-shelf reservoirs, San Andres Formation of Permian Basin: stratigraphic framework, permeability distribution, geostatistics, and fluid flow modeling: American Association of Petroleum Geologists, Bulletin, v. 78, p. 23–54.

Grotzinger, J.P., 1986, Cyclicity and paleoenvironmental dynamics, Rocknest platform, northwest Canada: Geological Society of America, Bulletin, v. 97, p. 1208–1231.

Harris, P.M., Kerans, C., and Bebout, D.G., 1993, Ancient outcrop and modern examples of platform carbonate cycles—implications for subsurface correlation and understanding reservoir heterogeneity, *in* Loucks, R.G., and Sarg, J.F., eds., Carbonate Sequence Stratigraphy: American Association of Petroleum Geologists, Memoir 57, p. 475–492.

Hayes, P.T., 1964, Geology of the Guadalupe Mountains, New Mexico: U.S. Geological Survey, Professional Paper 446, 69 p.

Horak, R.L., 1985, Tectonic and hydrocarbon maturation history in the Permian Basin: Oil and Gas Journal, v. 83, p. 124–129.

Jennings, J.W., Jr., 2000, Spatial statistics of permeability data from carbonate outcrops of West Texas and New Mexico: implications for improved reservoir modeling: The University of Texas at Austin, Bureau of Economic Geology, Report of Investigations 258, 50 p.

Jennings, J.W., Jr., Ruppel, S.C., and Ward, W.B., 2000, Geostatistical analysis of permeability data and modeling of fluid-flow effects in carbonate outcrops: Society of Petroleum Engineers, Reservoir Evaluation and Engineering, v. 3, no. 4, p. 292–303.

Kerans, C., and Fitchen, W.M., 1995, Sequence hierarchy and facies architecture of a carbonate-ramp system: San Andres Formation of Algerita Escarpment and Western Guadalupe Mountains, West Texas and New Mexico: The University of Texas at Austin, Bureau of Economic Geology, Report of Investigations 235, 86 p.

Kerans, C., and Nance, H.S., 1991, High-frequency cyclicity and regional depositional patterns of the Grayburg Formation, Guadalupe Mountains, New Mexico, *in* Meader-Roberts, S., Candelaria, M.P., and Moore, G.E., eds., Sequence Stratigraphy, Facies and Reservoir Geometries of the San Andres, Grayburg and Queen Formations, Guadalupe Mountains, New Mexico and Texas: SEPM, Permian Basin Section Publication 32, p. 53–96.

Kerans, C., and Tinker, S.W., 1997, Sequence Stratigraphy and Characterization of Carbonate Reservoirs: SEPM, Short Course Notes 40, 130 p.

Kerans, C., and Tinker, S.W., 1999, Extrinsic stratigraphic controls on development of the Capitan Reef complex, *in* Saller, A.H., Harris, P.M., Kirkland, B.L., and Mazzullo, S.J., eds., Geologic Framework of the Capitan Reef: SEPM, Special Publication 65, p. 15–36.

Kerans, C., Fitchen, W.H., Gardner, M.S., Sonnenfeld, M.D., Tinker, S.W., and Wardlaw, B.R., 1992, Styles of sequence development within uppermost Leonardian through Guadalupian strata of the Guadalupe Mountains, Texas and New Mexico, *in* Mruk, D.H., and Curran, B.C., eds., Permian Basin Exploration and Production Strategies: Applications of Sequence Stratigraphic and Reservoir Characterization Concepts: West Texas Geological Society, Symposium, Publication 91, p. 1–7.

Kerans, C., Fitchen, W.M., Gardner, M.S., and Wardlaw, B.R., 1993, A contribution of evolving stratigraphic framework of Middle Permian strata of the Delaware basin, Texas and New Mexico, *in* Love, D.W., Hawley, J.W., Kues, B.S., Adams, J.W., Austin, G.S., and Barker, J.M., eds., New Mexico Geological Society, 44th Annual Field Conference Guidebook, Carlsbad Region, New Mexico and West Texas, p. 175–184.

Kerans, C., Lucia, F.J., and Senger, R.K., 1994, Integrated characterization of carbonate ramp reservoirs using Permian San Andres Formation outcrop analogs: American Association of Petroleum Geologists, Bulletin, v. 78, p. 181–216.

King, P.B., 1948, Geology of the southern Guadalupe Mountains: U.S. Geological Survey, Professional Paper 215, 183 p.

Kocurek, G., and Kirkland, B.L., 1998, Getting to the source: aeolian influx to the Permian Delaware Basin region: Sedimentary Geology, v. 117, p. 143–149.

Koerschner, W.F., and Read, J.F., 1989, Field and modeling studies of Cambrian carbonate cycles, Virginia Appalachians: Journal of Sedimentary Petrology, v. 59, p. 654–687.

Lottes, A.L., and Rowley, D.B., 1990, Early and Late Permian reconstructions of Pangaea, *in* McKerrow, W.S., and Scotese, C.R., eds., Palaeogeography and Biogeography: Geological Society of London, Memoir 12, p. 383–395.

Lucia, F.J., 1995, Rock-fabric/petrophysical classification of carbonate pore space for reservoir characterization: American Association of Petroleum Geologists, Bulletin, v. 79, p. 1275–1300.

Meissner, F.F., 1972, Cyclic sedimentation in Middle Permian strata of the Permian Basin, West Texas and New Mexico: West Texas Geological Society, Publication 60, p. 118–142.

Mitchum, R.M., 1977, Seismic stratigraphy and global changes of sea level, Part 1: Glossary of terms used in seismic stratigraphy, *in* C.E. Payton, ed., Seismic Stratigraphy—Applications to Hydrocarbon Exploration: American Association of Petroleum Geologists, Memoir 26, p. 205–212.

Mitchum, R.M., and Van Wagoner, J.C., 1991, High frequency sequences and their stacking patterns: sequence stratigraphic correlation evidence of high-frequency eustatic cycles: Sedimentary Geology, v. 70, p. 131–160.

Mitchum, R.M., Vail, P.R., and Thompson, S., III, 1977, Seismic stratigraphy and global changes in sea level, Part 2: The depositional sequence as a basic unit for stratigraphic analysis, *in* Payton, C.E., ed., Seismic Stratigraphy—Applications to Hydrocarbon Exploration: American Association of Petroleum Geologists, Memoir 26, p. 63–81.

Modica, C.J., 1997, Stratigraphic cyclicity and reservoir heterogeneity within upper San Andres and Grayburg strata (Upper Permian–Guadalupian), Maljamar Field, SE New Mexico [M.S. Thesis]: College Station, Texas, Texas A&M University, 103 p.

Nance, H.S., 1988, Interfingering of evaporites and red beds: An example from the Queen/Grayburg Formation, Texas: Sedimentary Geology, v. 56, p. 357–381.

Parrish, J.T., 1993, Climate of the Supercontinent Pangea: The Journal of Geology, v. 101, p. 215–233.

Parrish, J.T., 1995, Geological evidence of Permian climate, *in* Scholle, P.A., Peryt, T.M., and Ulmer-Scholle, D.S., eds., The Permian of Northern Pangea, Volume 1: Paleogeography, Paleoclimates, Stratigraphy: New York, Springer Verlag, p. 53–61.

Parrish, J.T., and Peterson, F., 1988, Wind directions predicted from global circulation models and wind directions determined from eolian sandstones of the western United States—a comparison, *in* Kocurek, G., ed., Late Paleozoic and Mesozoic Eolian Deposits of the Western Interior of the United States: Sedimentary Geology, v. 56, p. 261–282.

Peterson, F., 1988, Pennsylvanian to Jurassic eolian transportation systems in the western United States, *in* Kocurek, G., ed., Late Paleozoic and Mesozoic Eolian Deposits of the Western Interior of the United States: Sedimentary Geology, v. 56, p. 207–260.

Rankey, E.C., Bachtel, S.L., and Kaufman, J., 1999, Controls on stratigraphic architecture of icehouse mixed carbonate–siliciclastic systems; a case study from the Holder Formation (Pennsylvanian, Virgilian), Sacramento Mountains, New Mexico, *in* Harris, P.M., Saller, A.H., and Simo, J.A., eds., Advances in Carbonate Sequence Stratigraphy; Application to Reservoirs, Outcrops, and Models: SEPM, Special Publication 63, p. 127–150.

Read, J.F., 1985, Carbonate platform facies models: American Association of Petroleum Geologists, Bulletin, v. 69, p. 1–21.

Read, J.F., Grotzinger, J.P., Bova, J.A., and Koerschner, W.F., 1986, Models for generation of carbonate cycles: Geology, v. 14, p. 107–110.

Ross, C.A., and Ross, J.R.P., 1987, Late Paleozoic sea levels and depositional sequences, *in* Ross, C.A., and Haman, D., eds., Timing and Depositional History of Eustatic Sequences: Constraints on Seismic Stratigraphy: Cushman Foundation for Foraminiferal Research, Special Publication 24, p. 137–149.

Ruppel, S.C., and Bebout, D.G., 2001, Competing effects of stratal architecture and diagenesis on carbonate reservoir development: Grayburg Formation, South Cowden field, West Texas: The University of Texas at Austin, Bureau of Economic Geology, Report of Investigations 263, 62 p.

Sarg, J.F., and Lehmann, P.J., 1986, Lower–Middle Guadalupian facies and stratigraphy, San Andres–Grayburg formations, Permian Basin, Guadalupe Mountains, New Mexico, *in* Moore, G.E., and Wilde, G.L., eds., Lower and Middle Guadalupian Facies, Stratigraphy, and Reservoir Geometries, San Andres–Grayburg Formations, Guadalupe Mountains, New Mexico and Texas: SEPM, Permian Basin Section, Special Publication 25, p. 1–36.

Scotese, C.R., and McKerrow, W.S., 1990, Revised world maps and introduction, *in* McKerrow, W.S., and Scotese, C.R., eds., Palaeogeography and Biogeography: Geological Society of London, Memoir 12, p. 1–21.

Silver, B.A., and Todd, R.G., 1969, Permian cyclic strata, northern Midland and Delaware basins, West Texas and southeastern New Mexico: American Association of Petroleum Geologists, Bulletin, v. 53, p. 2223–2351.

Sonnenfeld, M.D., 1991, High-frequency cyclicity within shelf-margin and slope strata of the upper San Andres sequence, Last Chance Canyon, *in* Meader-Roberts, S., Candelaria, M.P., and Moore, G.E., eds., Sequence Stratigraphy, Facies and Reservoir Geometries of the San Andres, Grayburg, and Queen Formations, Guadalupe Mountains, New Mexico and Texas: SEPM, Permian Basin Section, Special Publication 32, p. 11–51.

Sonnenfeld, M.D., 1993, Anatomy of offlap: Upper San Andres Formation (Permian, Guadalupian), Last Chance Canyon, Guadalupe Mountains, New Mexico: New Mexico Geological Society, 44th Field Conference, Guidebook, p. 195–203.

Soreghan, G.S., and Giles, K.A., 1999, Amplitudes of Late Pennsylvanian glacioeustasy: Geology, v. 27, p. 255–258.

Tinker, S.W., 1998, Shelf-to-basin facies distributions and sequence stratigraphy of a steep-rimmed carbonate margin: Capitan depositional system, McKittrick Canyon, New Mexico and Texas: Journal of Sedimentary Research, v. 68, p. 1146–1174.

Tye, E.N., 1986, Stratigraphy and formation of tepee structures in the Guadalupian Grayburg Formation, southeast New Mexico, *in* Moore, G.E., and Wilde, G.L., eds., Lower and Middle Guadalupian Facies, Stratigraphy, and Reservoir Geometries, San Andres–Grayburg Formations, Guadalupe Mountains, New Mexico and Texas: SEPM, Permian Basin Section, Special Publication 25, p. 95–105.

Vail, P.R., 1987, Seismic stratigraphy interpretation using sequence stratigraphy, Part 1: Seismic stratigraphy interpretation procedure, *in* Bally, A.W., ed., Atlas of Seismic Stratigraphy, vol. 1: American Association of Petroleum Geologists, Studies in Geology 27, p. 1–10.

Vail, P.R., Mitchum, R.M., and Thompson, S., III, 1977, Seismic stratigraphy and global changes of sea level, Part 4: Global cycles of relative changes of sea level, *in* Payton, C.E., ed., Seismic Stratigraphy—Applications to Hydrocarbon Exploration: American Association of Petroleum Geologists, Memoir 26, p. 83–97.

Van Wagoner, J.C., Mitchum, R.M., Jr., Posamentier, H.W., and Vail, P.R., 1987, Seismic stratigraphy interpretation using sequence stratigraphy, Part 2: Key definitions of sequence stratigraphy, *in* Bally, A.W., ed., Atlas of Seismic Stratigraphy, vol. 1: American Association of Petroleum Geologists, Studies in Geology 27, p. 11–14.

Van Wagoner, J.C., Posamentier, H.W., Mitchum, R.M., Vail, P.R., Sarg, J.F., Loutit, T.S., and Hardenbol, J., 1988, An overview of the fundamentals of sequence stratigraphy and key definitions, *in* Wilgus, C.K., Hastings, B.S., Kendall, C.G.St.C., Posamentier, H.W., Ross, C.A., and Van Wagoner, J.C., eds., Sea-Level Changes: An Integrated Approach: SEPM, Special Publication 42, p. 39–45.

Van Wagoner, J.C., Mitchum, R.M., Campion, K.M., and Rahmanian, V.D., 1990, Siliciclastic Sequence Stratigraphy in Well Logs, Cores, and Outcrops: American Association of Petroleum Geologists, Methods in Exploration Series, 7, 55 p.

Ward, R.F., Kendall, C.G.St.C., and Harris, P.M., 1986, Upper Permian (Guadalupian) facies and their association with hydrocarbons—Permian Basin, West Texas and New Mexico: American Association of Petroleum Geologists, Bulletin, v. 70, p. 239–262.

Yang, K.M., and Dorobek, S.L., 1992, Mechanisms for late Paleozoic synorogenic subsidence of the Midland and Delaware basins, Permian Basin, Texas and New Mexico, *in* Mruk, D.H., and Curran, B.C., eds., Permian Basin Exploration and Production Strategies: Applications of Sequence Stratigraphic and Reservoir Characterization Concepts: West Texas Geological Society, Publication 91, p. 45–60.

Received 16 March 2005; accepted 31 May 2006.

Road to Carlsbad Cavern

Carlsbad Caverns
New Mexico

Base Map

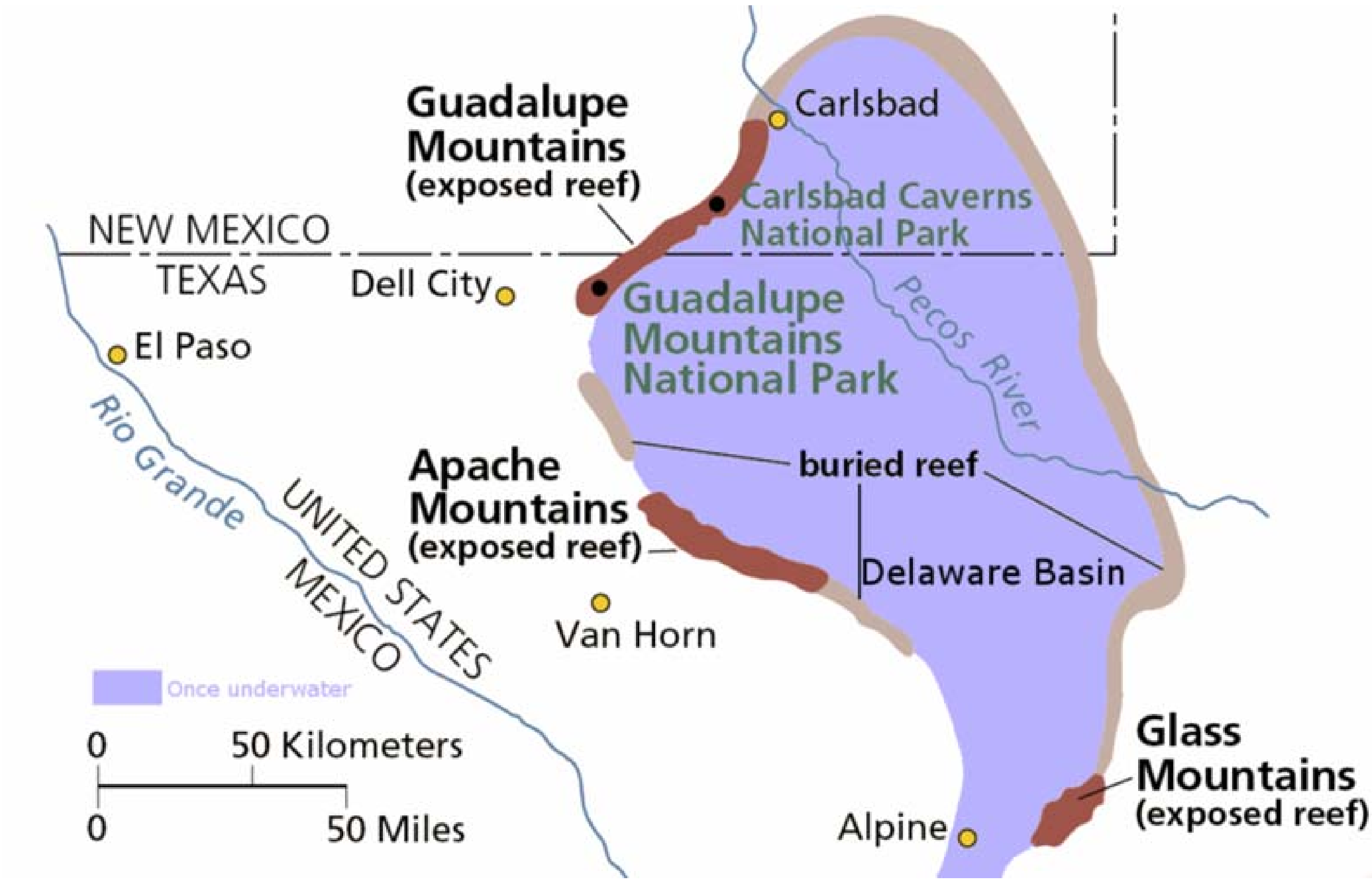

Carlsbad Caverns National Park is located in the Delaware Basin in west Texas and southern New Mexico.

The road to Carlsbad…

Walnut Canyon drive is a seven-mile scenic drive to the park visitor center.

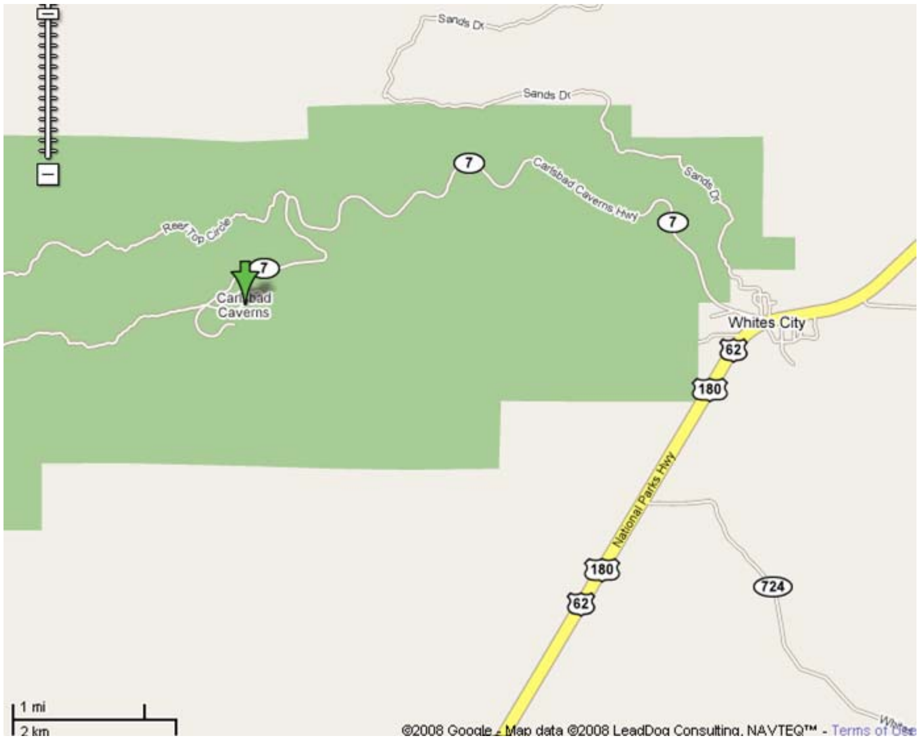

Visitors arrive by way of U.S. Highway 62/180 from either Carlsbad, New Mexico (23 miles to the northeast) or El Paso, Texas (150 miles to the west). A scenic 7-mile (11.3 km) entrance road leads from the park gate at Whites City to the visitor center and cavern entrance.

http://www.nps.gov/cave/planyourvisit/directions.htm

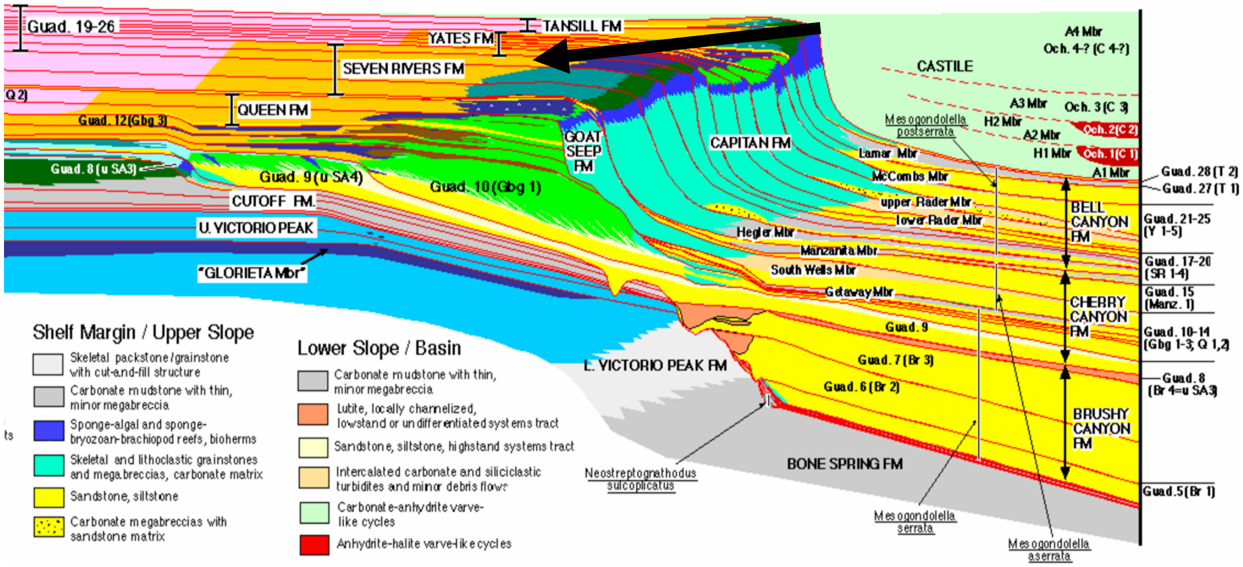

Kerans and Kempter, 2000

The drive into Carlsbad Caverns starts at the Reef (Capitan Formation) and continues up the shelf to the Tansill and Yates Formations.

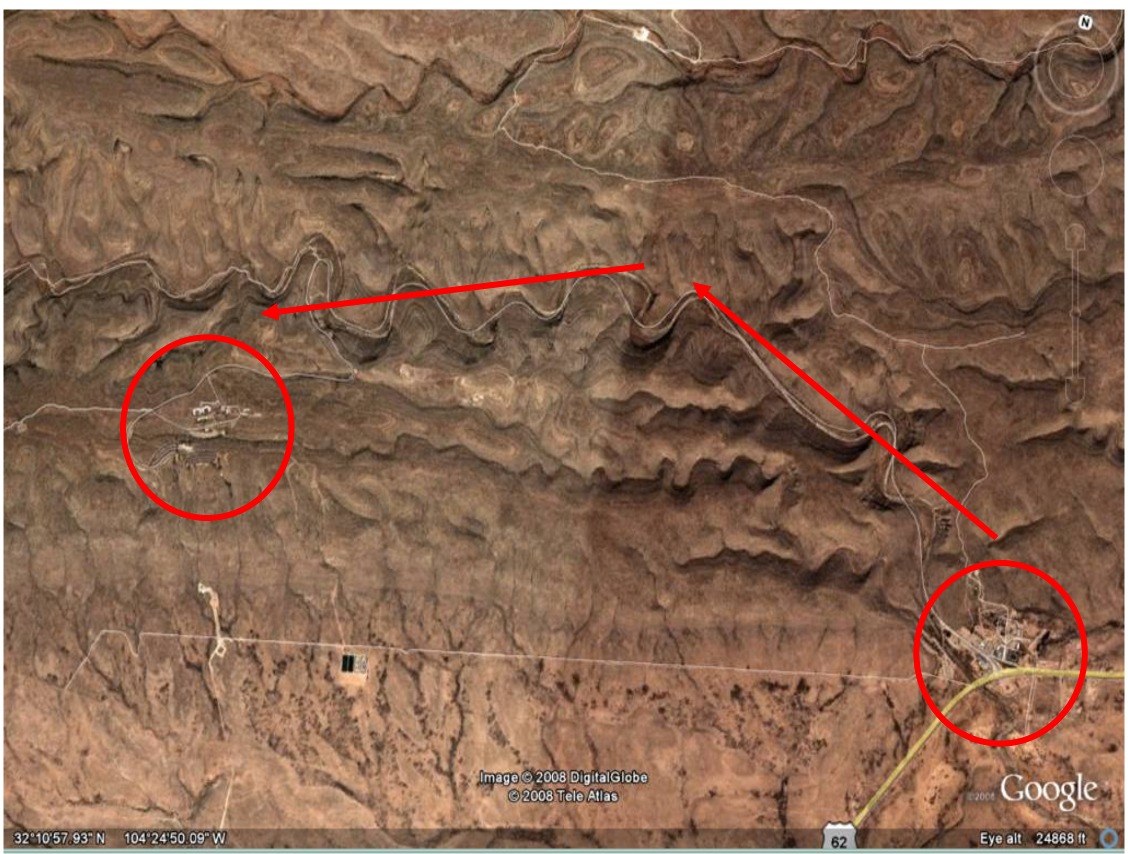

Start from White City

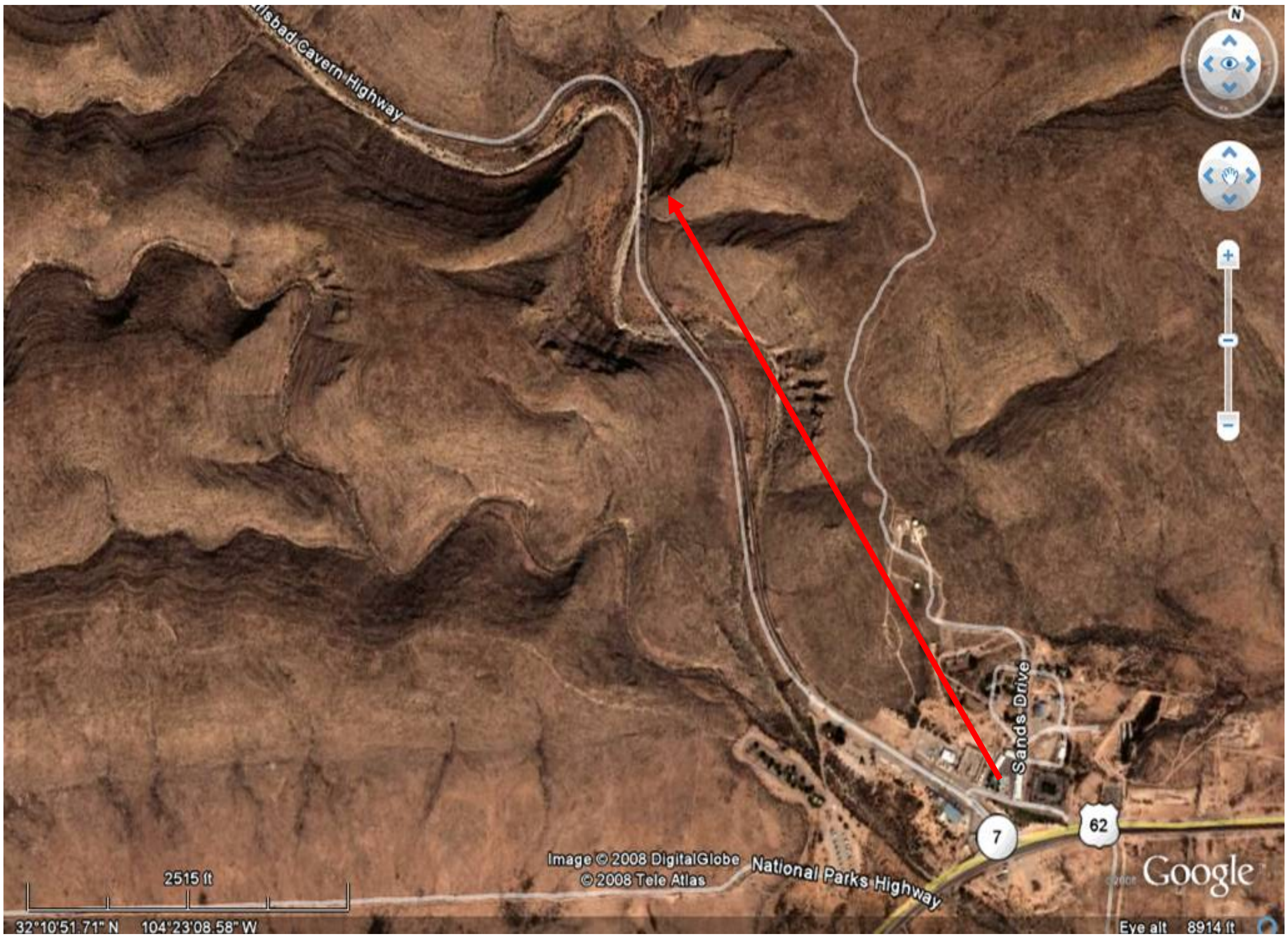

At the entrance to Walnut Canyon, provides excellent exposures of the reef and near-back-reef facies of the upper Capitan Limestone and Tansill and Yates Formations. In this area, the fore-reef facies and part of the reef have been buried beneath the thick Ochoan (and some thin Tertiary-Quaternary) filling of the Delaware basin. The Castile Fm., although completely or partially removed in areas to the southwest, has been preserved in this area because of the northeastward tilting of this region. Thus, only a small exposure of the reef-crest and its transition to the near-back-reef are exposed.

http://geoinfo.nmt.edu/staff/scholle/permstops/pmstop1_3.html

Continuing on 7

Most of the drive to Carlsbad Caverns is through the Yates Formations. In some locations, upper Yates and lower Tansill sediments compose the canyon walls.

Carlsbad Caverns

Before you reach the caverns there is a thin sandstone-siltstone unit which marks the Tansill-Yates contact. The road ascends into Tansill Formation dolomites and to the caverns.

http://geoinfo.nmt.edu/staff/scholle/wc_roadlog.html

Carlsbad Caverns

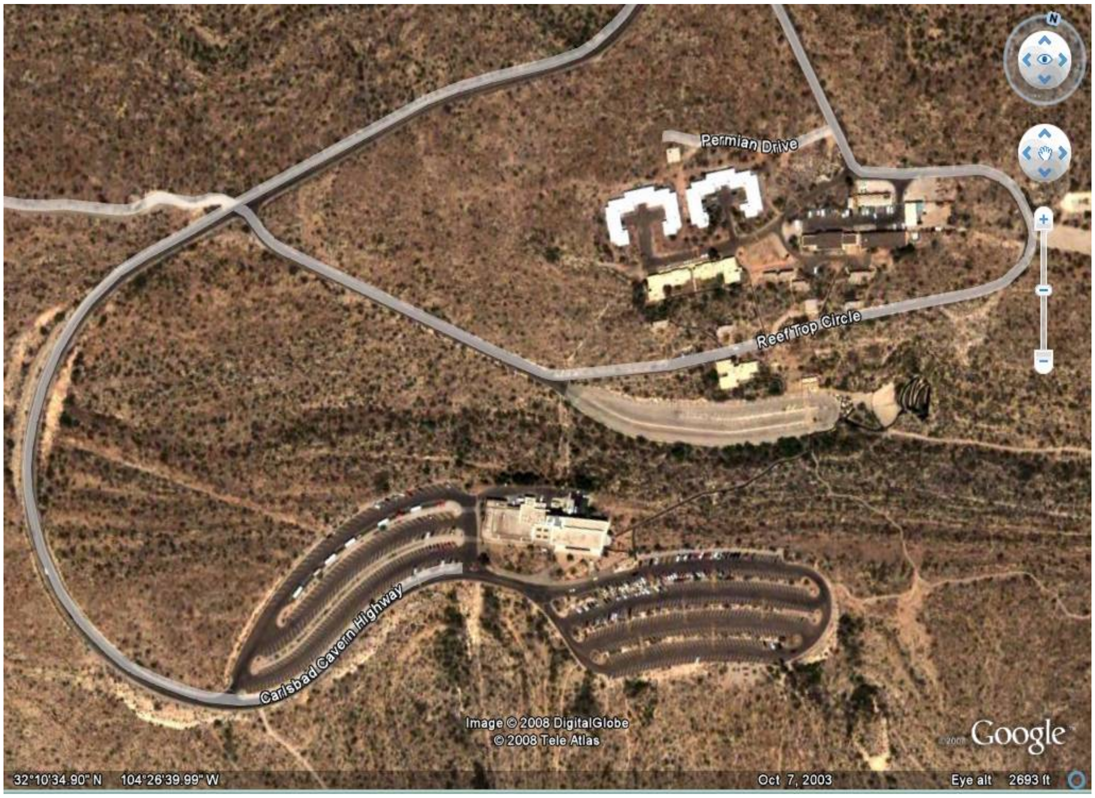

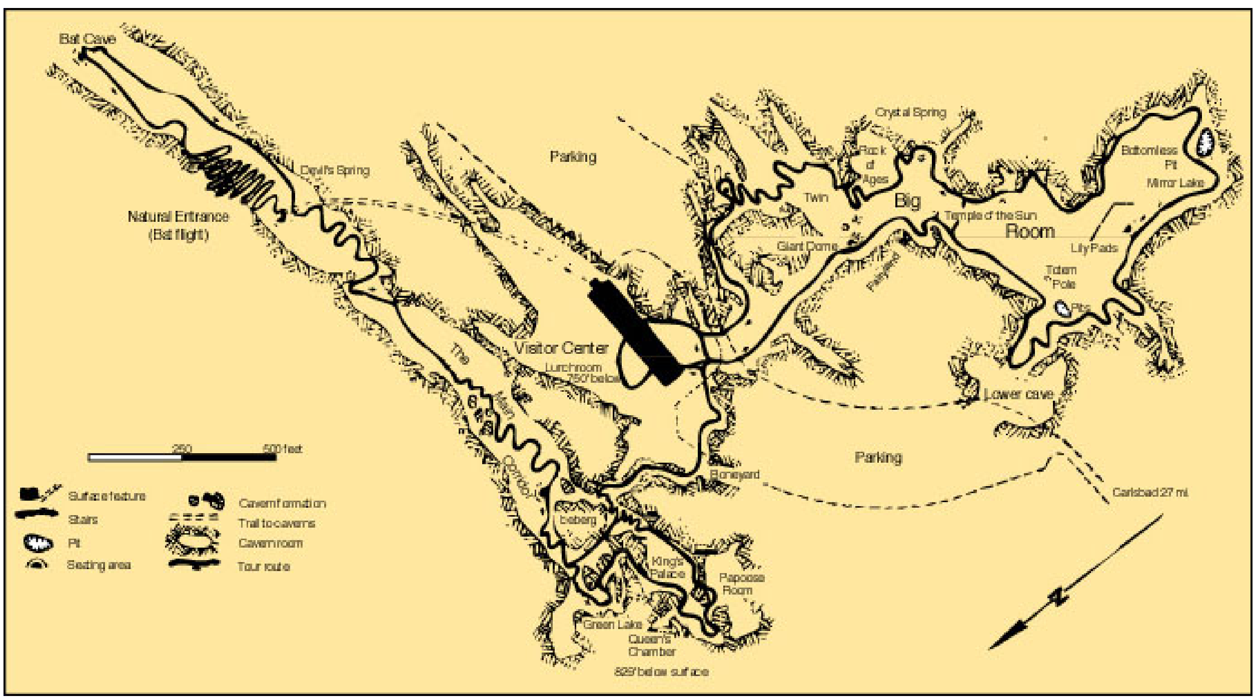

Carlsbad Caverns

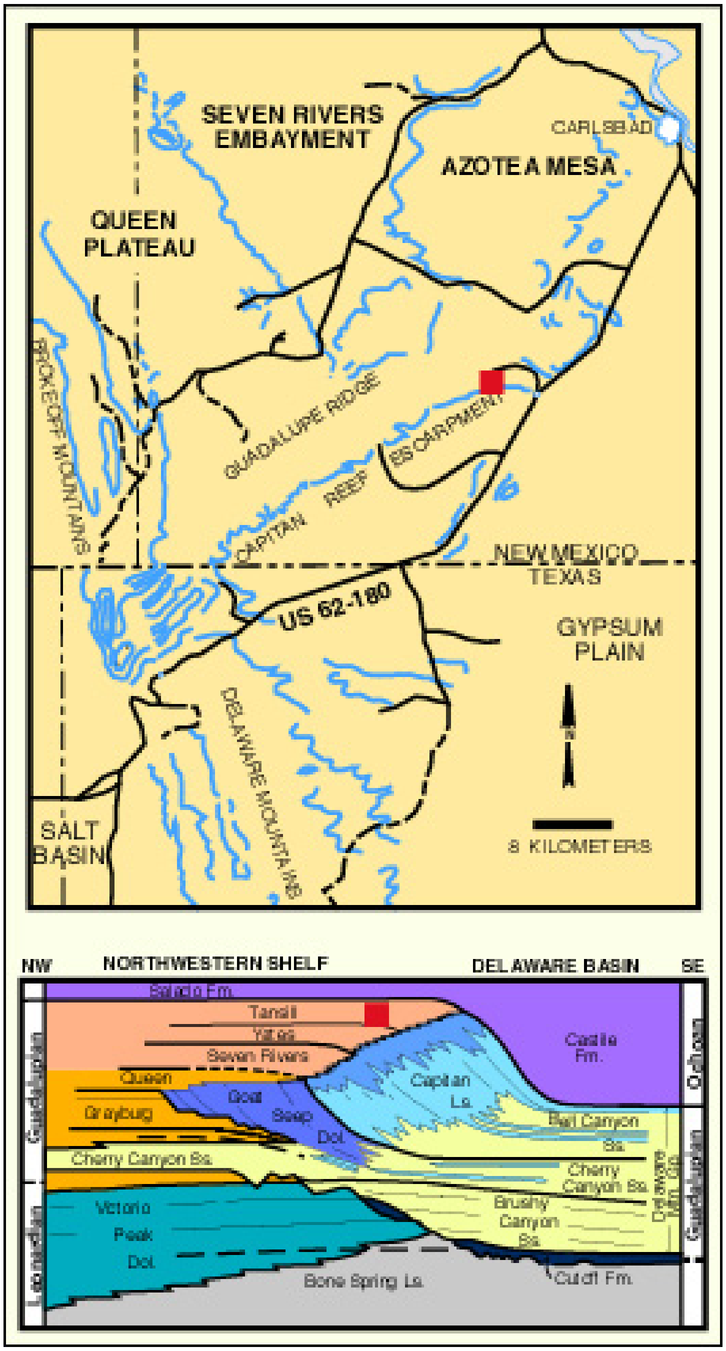

The cave is developed primarily in the fractured reef and forereef Capitan Limestone, but the entrance and all of the upper level are in the back-reef dolomites of the Tansill and Yates Formations.

http://geoinfo.nmt.edu/staff/scholle/permstops/pmstop1_3.html

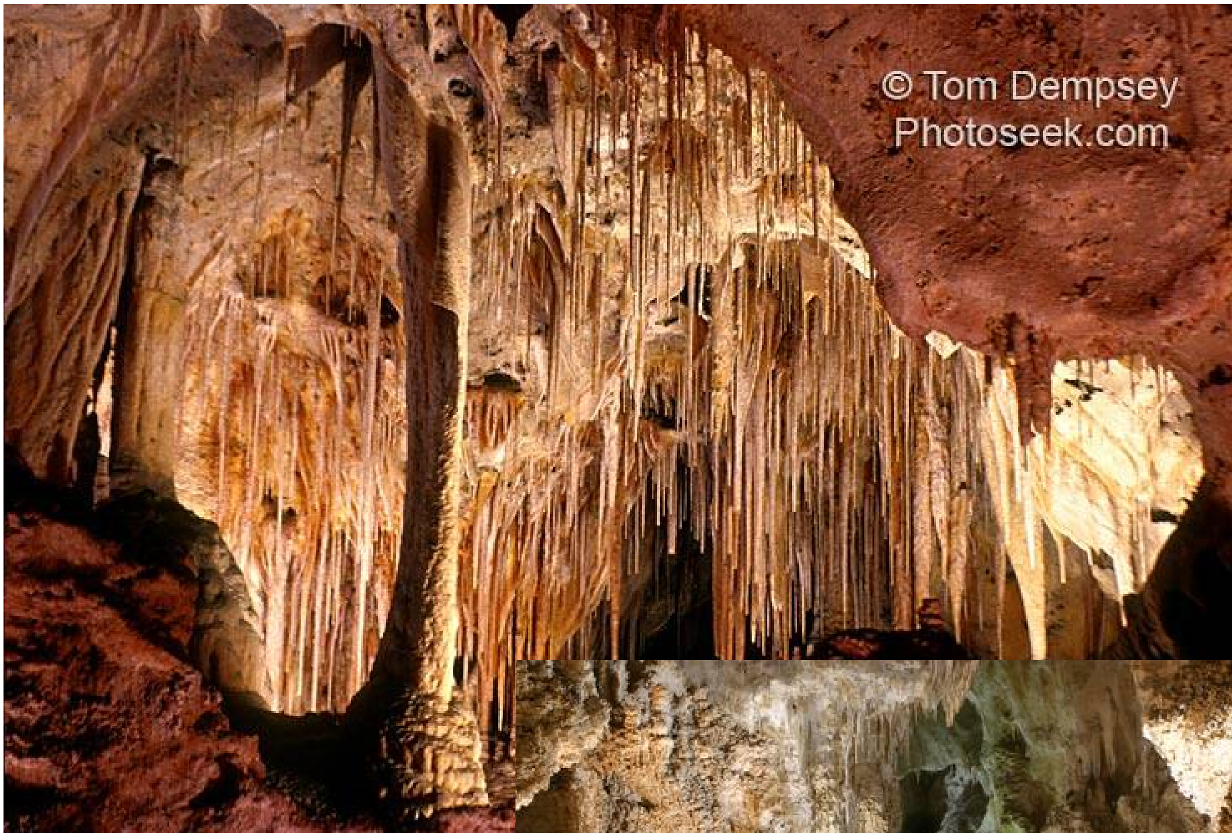

The Natural Entrance route descends more than 750 feet into the earth following steep and narrow trails.

Carlsbad Caverns

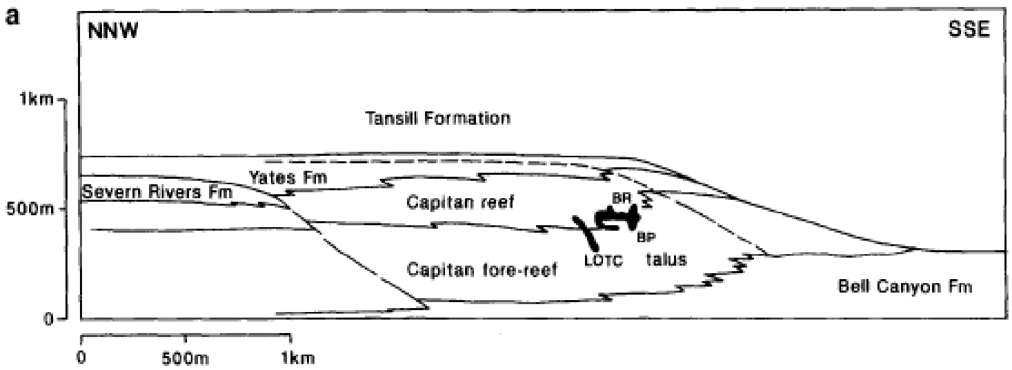

Table 1. Stratigraphic chart of Permian reef (Capitan) and equivalents, Guadlupe Mountains (Carlsbad Caverns are cut predominantly into Yates equivalent reef sediments).

	Shelf	Shelf margin	Basin
Ochoa series	Salado	Salado	Salado Castile
Guadalupe series	Tansill Yates Severn Rivers	**Capitan**	Bell Canyon
	Queen Grayburg	Goat Seep	Cherry Canyon

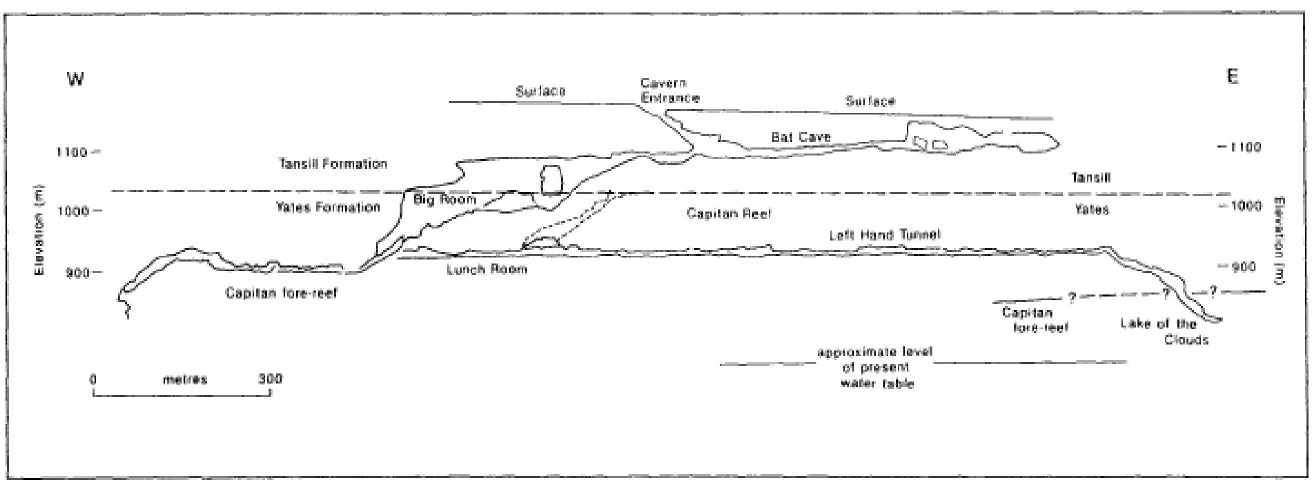

Fig. 2. Strike-perpendicular (a) and strike-parallel (b) cross-sections through the Guadalupe Mountains, showing position of Carlsbad Caverns within the Permian strata. BR, Big Room; BP, Bottomless Pit; LOTC, Lake of the Clouds. Sections compiled and modified from Tyrell (1969), Jagnow (1986, 1987) and Garber *et al.* (1989).

The greater part of Carlsbad Caverns was hollowed into the largely aggradational Yate-equivalent reef facies. Parts of the caverns also extend into the back-reef (Tansill and Yates Formation) and fore-reef talus facies.

Harwood and Kendall, 1999

Tepee Structures in the parking lot

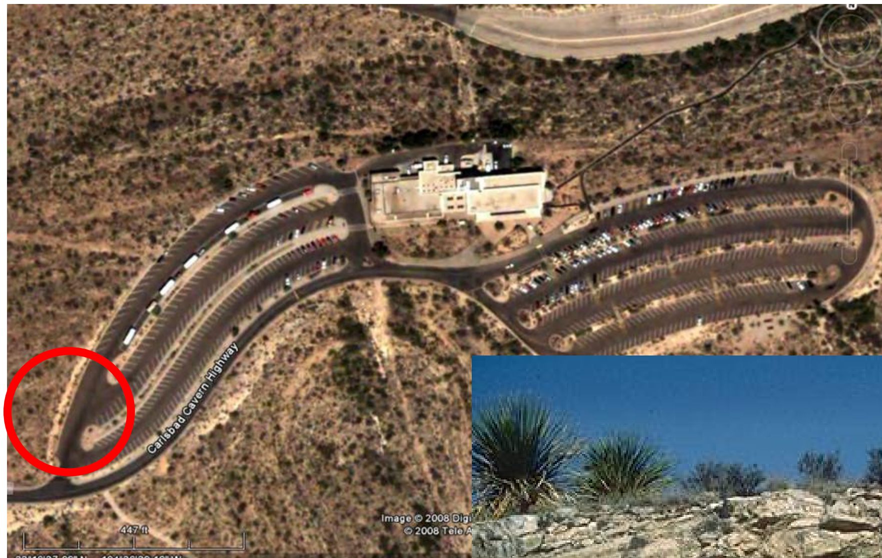

Tepee structure in Tansill Formation.

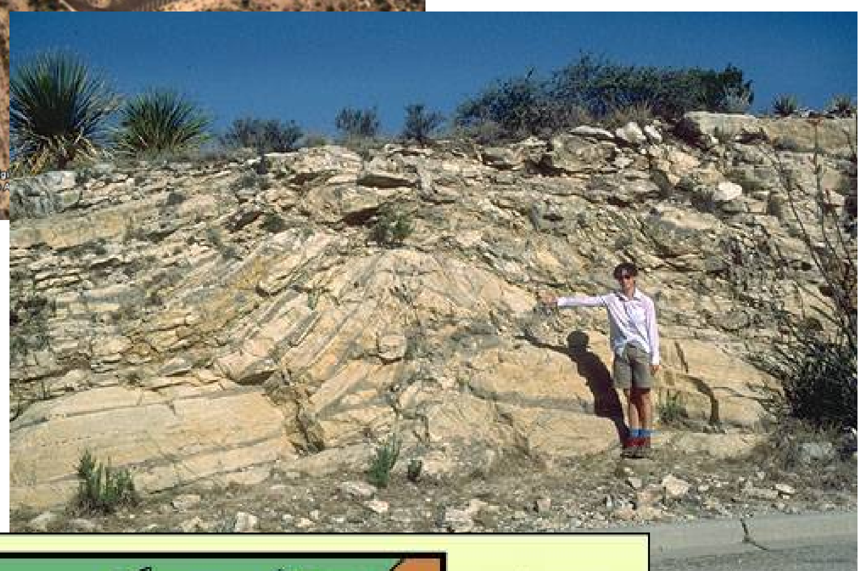

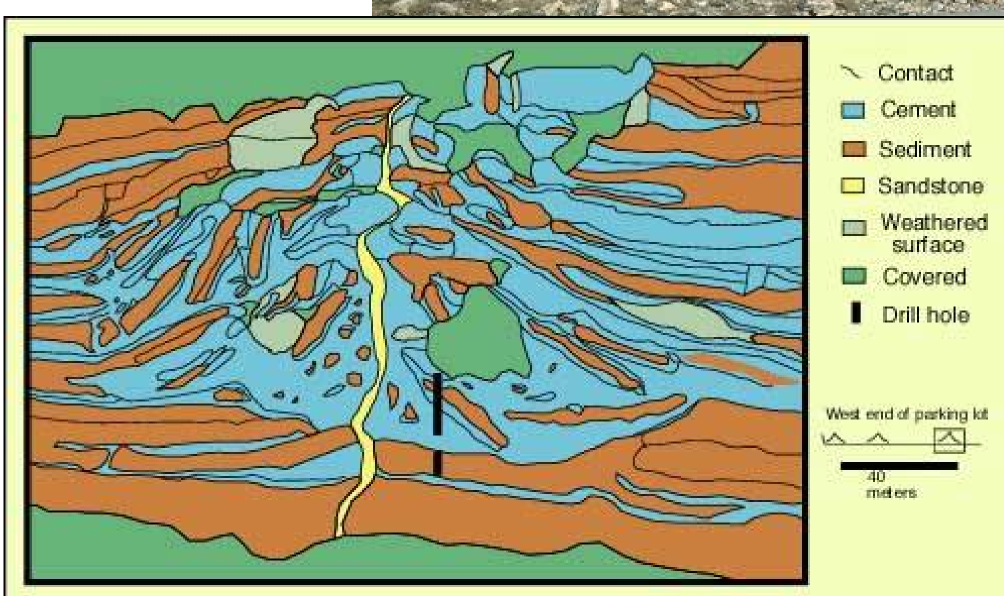

http://geoinfo.nmt.edu/staff/scholle/permstops/pmstop1_3.html

GUADALUPE MOUNTAINS: SEVEN RIVERS-YATES

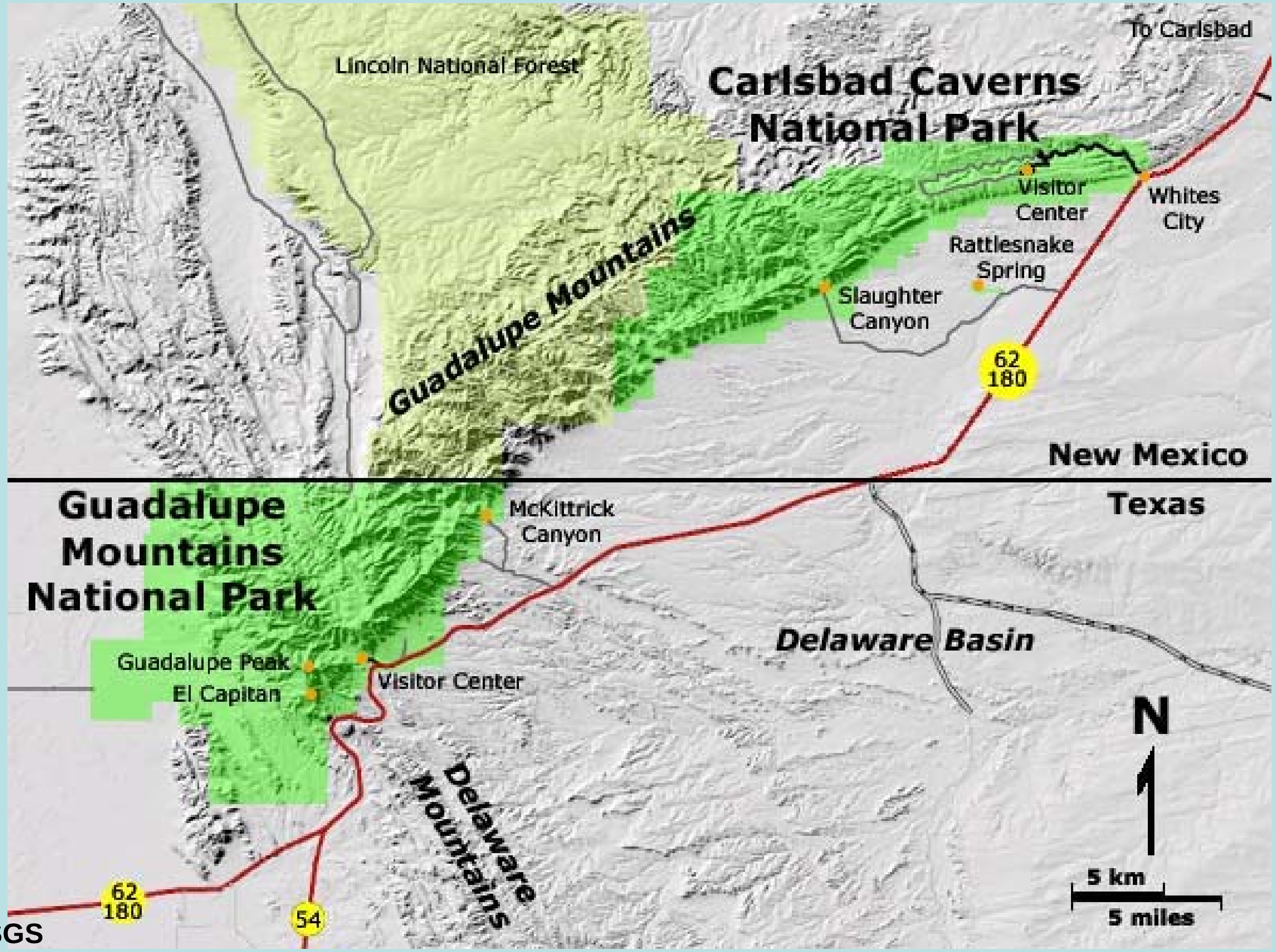

Courtesy of USGS

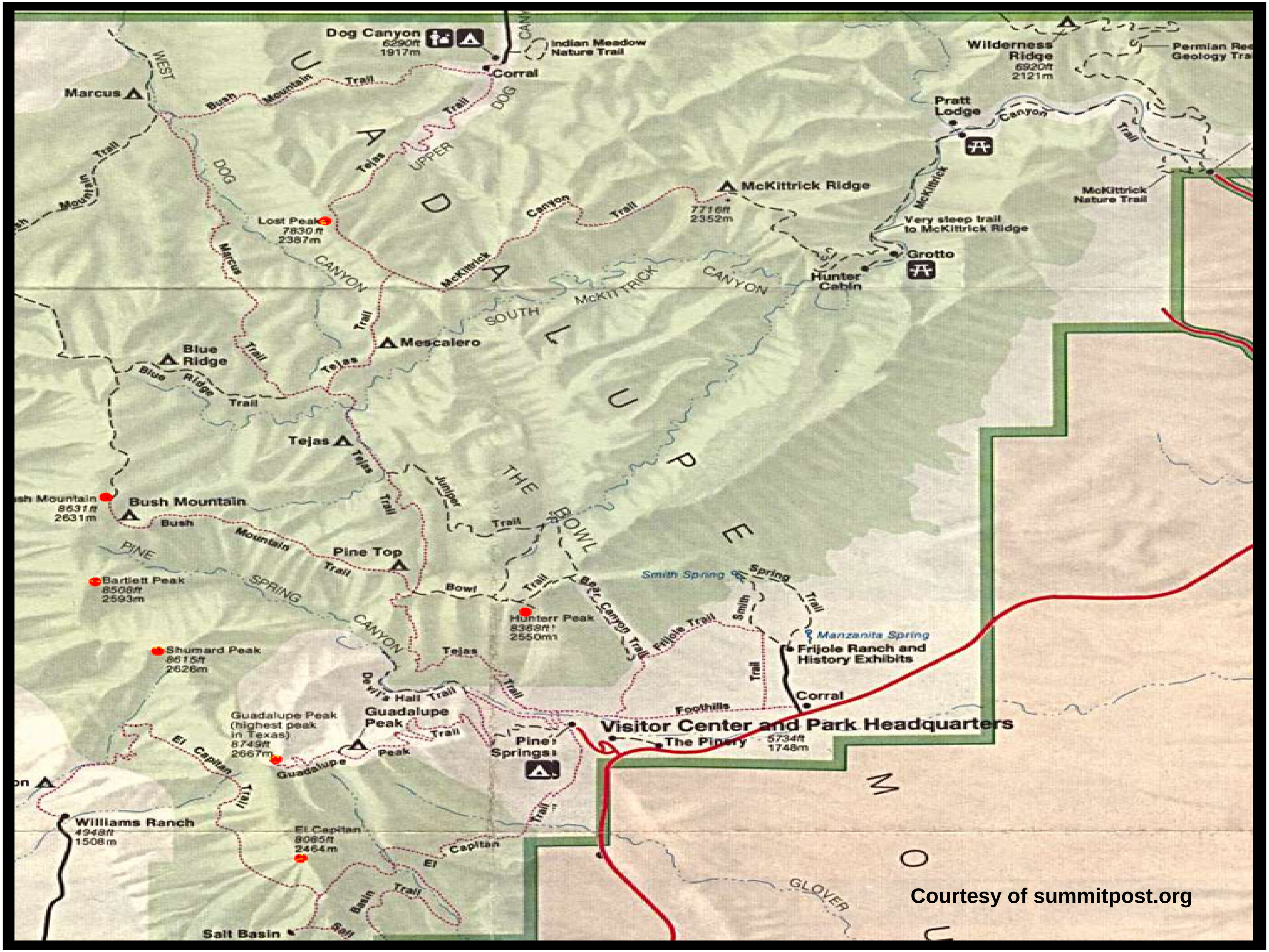

Dog Canyon
6290ft
1917m
Indian Meadow Nature Trail
Corral
Wilderness Ridge
6920ft
2121m
Permian Reef Geology Trail
Marcus
Bush Mountain Trail
Pratt Lodge
McKittrick Ridge
7716ft
2352m
McKittrick Nature Trail
Lost Peak
7830 ft
2387m
Very steep trail to McKittrick Ridge
Grotto
Hunter Cabin
SOUTH McKITTRICK CANYON
Mescalero
Blue Ridge
Blue Ridge Trail
Tejas
Bush Mountain
8631ft
2631m
Bush Mountain
Pine Top
Bartlett Peak
8508ft
2593m
PINE SPRING CANYON
Smith Spring
Spring Trail
Hunterr Peak
8368ft
2550m
Frijole Trail
Manzanita Spring
Frijole Ranch and History Exhibits
Shumard Peak
8615ft
2626m
Devil's Hall Trail
Corral
Foothills Trail
Guadalupe Peak (highest peak in Texas)
8749ft
2667m
Guadalupe Peak
Visitor Center and Park Headquarters
The Pinery
5734ft
1748m
Pine Springs
El Capitan Trail
Williams Ranch
4948ft
1508m
El Capitan
8085ft
2464m
Salt Basin
GLOVER
THE BOWL
GUADALUPE
Courtesy of summitpost.org

Simplified Map of Guadalupian Facies

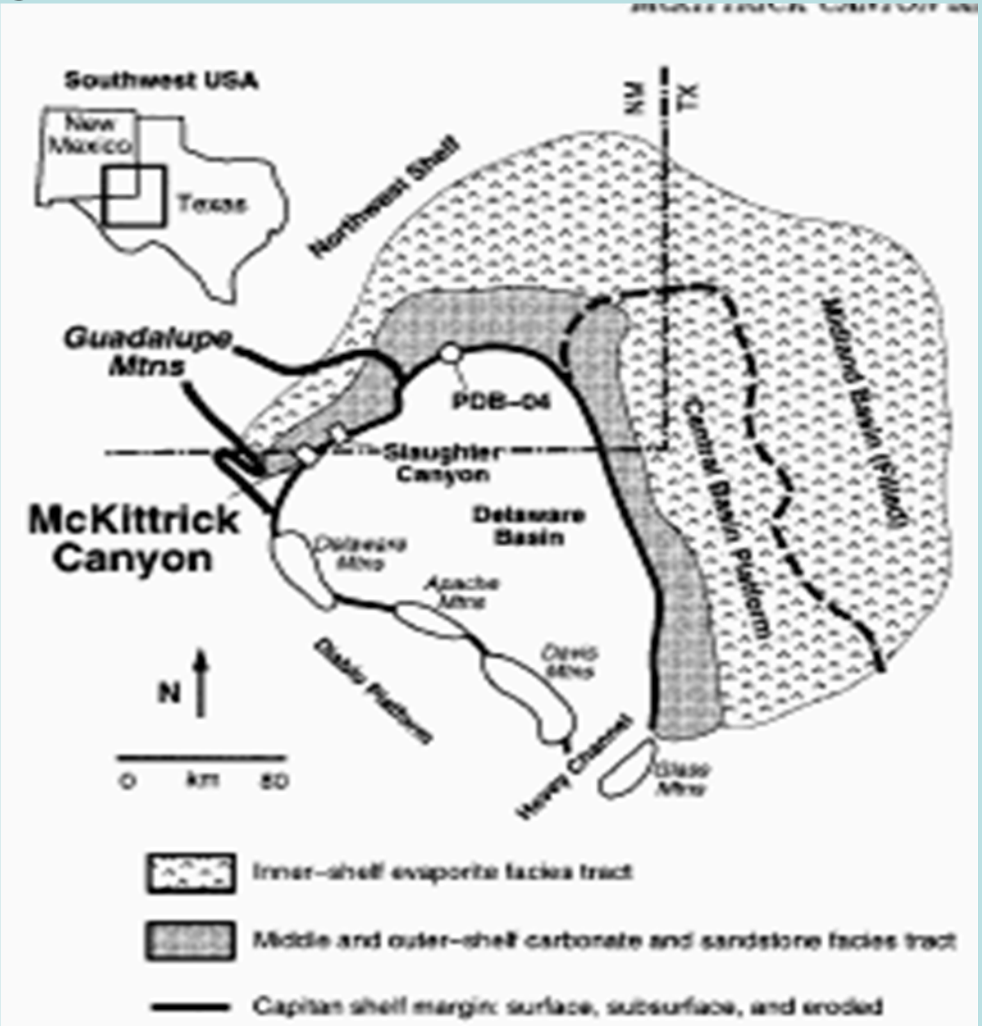

Cross section of Mckittrick Canyon

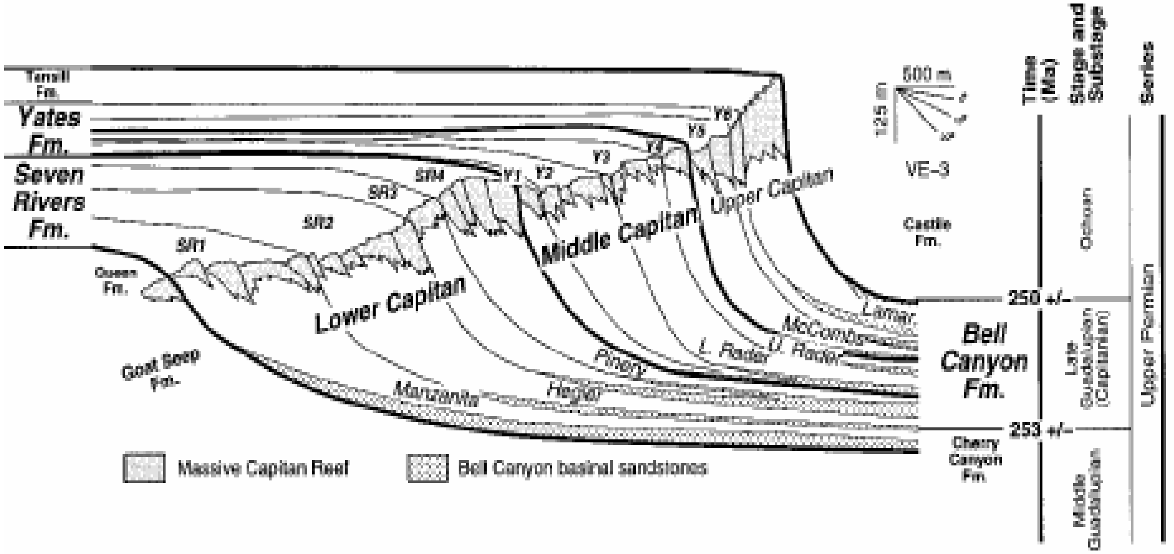

Hierarchy of Cyclicity

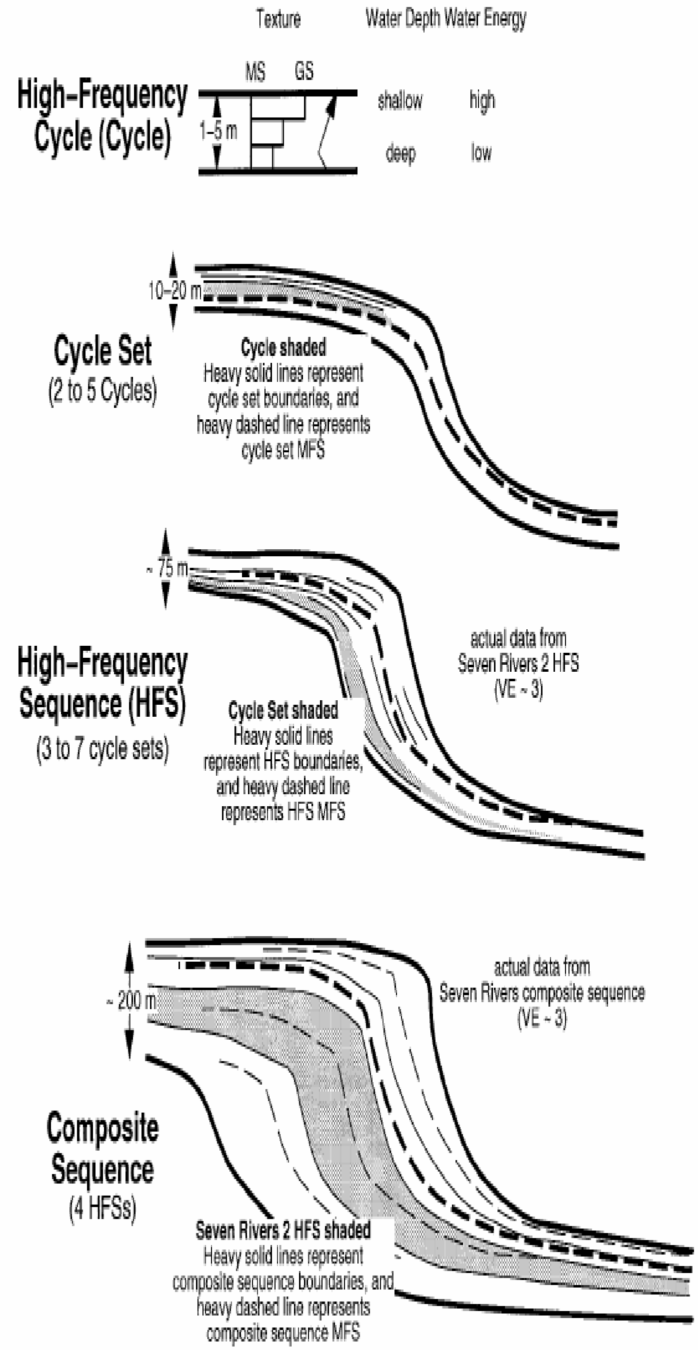

Facies of Seven Rivers and Tansils Formation

Middle Shelf

- Pisoid RS
- Cryptalgal laminite BS
- Ooid coated grainstone GDP/GS
- Peloid, bioclast, intraclast PS/GS
- Peloid, bioclast MS/WS
- Silty Dolomite
- Dolomitic Silt

Outer Shelf/ Shelf Margin

Oncoid RS

Fusilinid GS

Peloid, bioclast, fusilinid GDP/GS

Peloid, bioclast, fusilinid WS/PS

Foram, Mizzia, bioclast PS/GS

Crinoid, Peloid, Foram WS/PS

Peloid bioclast MS/WS

Silty Dolomite

Dolomitic Silt- Vf SS

Sponge, Algal, ALP, cement FS/BS (**reef**)

Slope/Basin

Bioclast, intraclast RS/GS/BR/CG

Bioclast lithoclast RS/PS/WS/CG

Burrowed Peloid MS/WS

Silty Dolomite

Vf-medium sandstone/ dolomitic silt

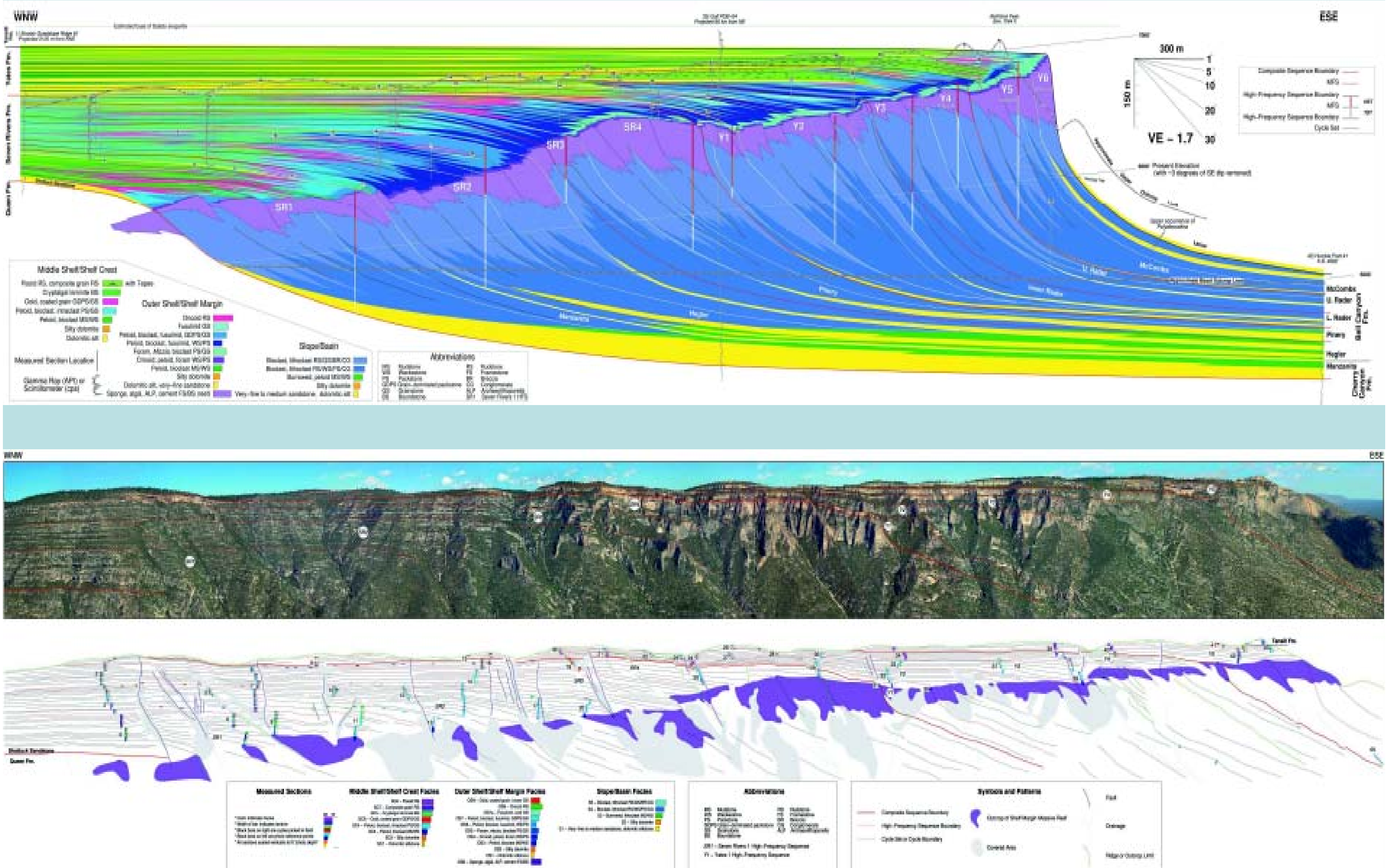

WNW
ESE
300 m
150 m
VE ~ 1.7
SR1
SR2
SR3
SR4
Y1
Y2
Y3
Y4
Y5
Y6
McCombs
U. Rader
L. Rader
Pinery
Hegler
Manzanita
Bell Canyon Fm.
Cherry Canyon Fm.
Middle Shelf/Shelf Crest
Outer Shelf/Shelf Margin
Slope/Basin
Abbreviations
Measured Section Location
Measured Sections
Middle Shelf/Shelf Crest Facies
Outer Shelf/Shelf Margin Facies
Slope/Basin Facies
Symbols and Patterns

System Tracts

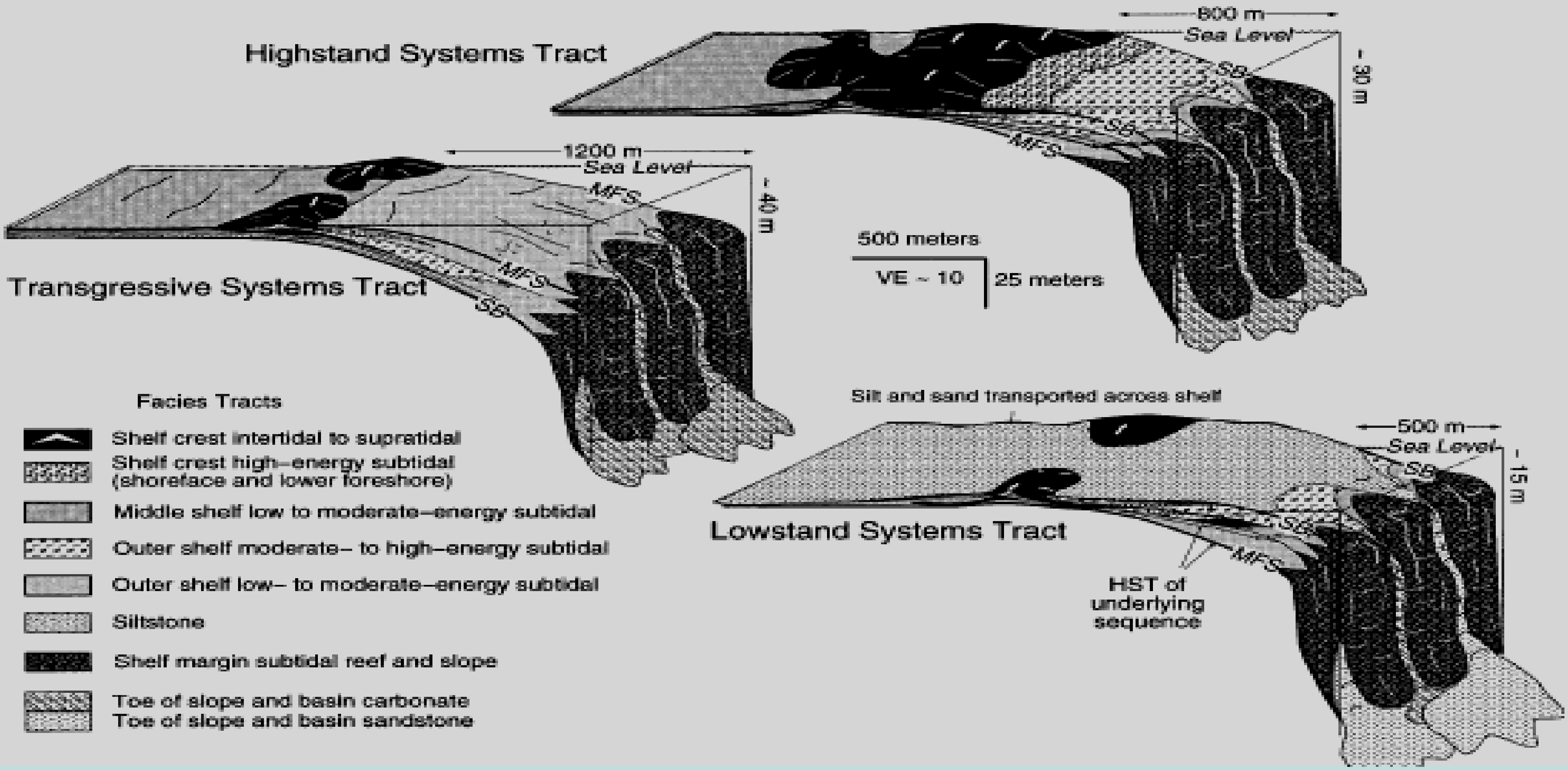

Stacking Patterns

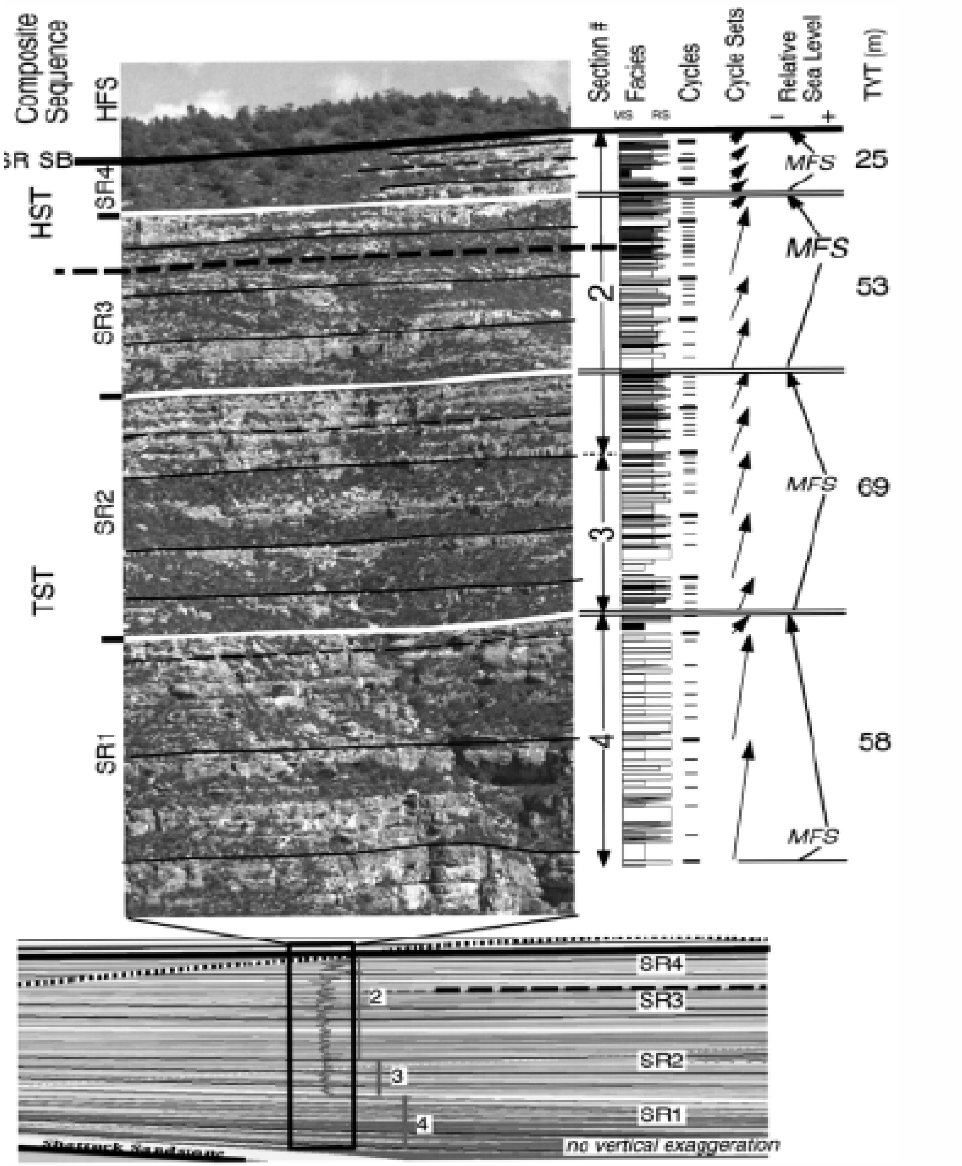

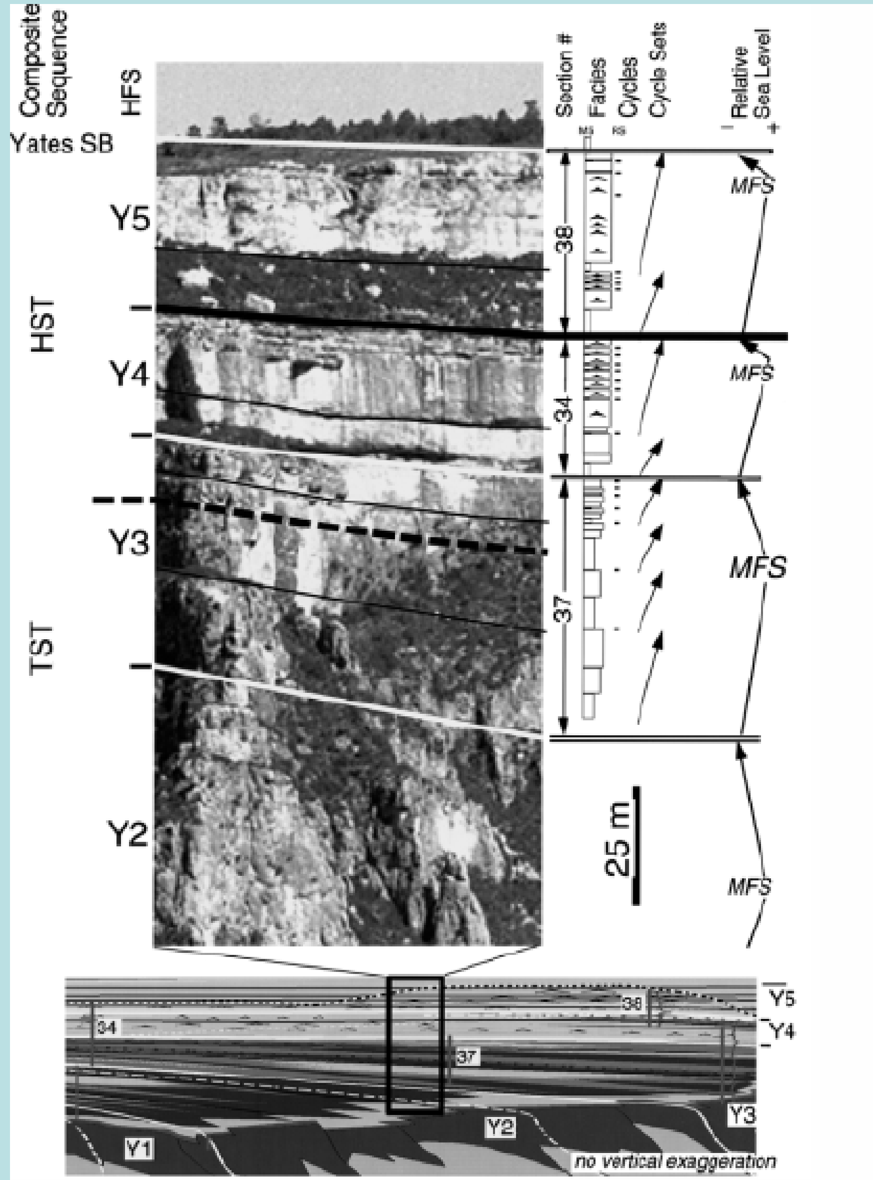

CONCLUSION

- Marginal mound depositional system
- High degree of stratigraphy
- Systematic distribution of facies
- Overall decrease in water depth form Seven Rivers to the Tansil
- Complete sedimentation and accumulation

References

Tinker, 1998. S.W. Tinker , Shelf-to-basin facies distributions and sequence stratigraphy of a steep-rimmed carbonate margin: Capitan depositional system, McKittrick Canyon, New Mexico and Texas. J. Sediment. Res. **68** (1998), pp. 1146–1174

Kerans and Tinker, 1999. C. Kerans and S.W. Tinker , Extrinsic stratigraphic controls on development of the Capitan reef complex. In: A.H. Saller, P.M. Harris, B.L. Kirkland and S.J. Mazzullo, Editors, *Geologic Framework of the Capitan reefSoc. Econ. Paleontol. Mineral., Spec. Publ.* **vol. 65** (1999), pp. 37–49

.

DAY 1 ROAD LOG AND LOCALITY GUIDE: LITHOFACIES, STRATIGRAPHY AND DEPOSITIONAL MODELS OF THE BACK-REEF GUADALUPIAN SECTION (QUEEN, SEVEN RIVERS, YATES AND TANSILL FORMATIONS)

LEADERS: S.J. MAZZULLO AND C.L. HEDRICK

The itinerary of Day 1 field stops will take us from the high-island or shelf crest facies tract to progressively more shelfward facies of the complex, and will then reverse and progress back across the shelf crest to the outer-shelf tract (Figures 1, 2). This series of outcrops will expose for your scrutiny several generalized interpretations regarding the origin of back-shelf siliciclastic and carbonate facies of the Capitan complex. We hope to convince you of what we consider to be two important aspects of facies development in this stratigraphic complex: (1) that most of the widespread, uniformly thick terrigenous sandstones of the back-reef shelf, particularly those of the Seven Rivers and Shattuck member of the Queen Formation, are of eolian origin: that they represent desert sheet sand (erg) and associated facies, locally with relict dunes, and; (2) that island facies in the complex are complex, have varied relations to sea level fluctuations, and that differences in modes of island development through time lead to recognizable diagenetic facies in the back-reef environment.

MILEAGE

Cumulative Interval

0.0 0.0 26.4 **Parking Lot - Stevens Motel.**

1.2 1.2 27.6 **Intersection of U.S. 62 and 285 in the center of Carlsbad (Caverna Hotel). Proceed north on U.S. 285.**

3.6 2.4 30.0 In view ahead to the west are the Ocotillo Hills, a surface expression of one (Tracy Dome) of many domes and anticlinal flexures present on the Carlsbad shelf that are expressed in Tansill and Yates strata of the shelf area west of Carlsbad (see Motts, 1962 and Kelley, 1971). Outcrops of the Ocotillo Hills are largely of thin-bedded evaporitic dolomite and of minor siltstones and sandstones (including the Ocotillo siltstone) of the Tansill Formation.

4.8 1.2 31.2 Living Desert State Park turnoff on left. It is worth a visit if interested in desert plants and animals.

5.0 .2 31.4 **STOP 1. Outcrop on west side of highway.** The section exposed at this locality includes approximately 25 ft of fine-crystalline dolomites, limestones, and interbedded siliciclastics. This section, and that exposed in the steep cut between road level and base of scarp extending to the river, comprise the type section of the Tansill Formation as was described by DeFord and Riggs (1941: AAPG v. 25, p. 1713-1728). They measured the formation here to be 123.5 ft thick, and noted that it thickens markedly as it approaches the Capitan reef. They also formally named the Ocotillo Member as comprising approximately 13.5 ft of siltstone, sandstone and dolomite at this locality. Continuous outcrops of the Tansill and Ocotillo continue on the north side of the road that leads to Living Desert State Park (this road intersects the southern tip of this outcrop).

The Tansill Formation at this locality is situated on the flank of the Tracy Dome, a prominent positive structural feature that is part of a series of such domes in the Carlsbad area. The section exposed in the cliff at and above road level comprises interbedded dolomites, shales, siltstones and sandstones, sandy dolomites, and subordinate limestones. The carbonates include micritic mudstones, evaporite nodule molds, desiccation cracks, algal laminites, fenestral fabrics, and pisolites. These rocks were deposited as a complex of very shallow subtidal and (predominantly) intertidal and supratidal facies.

The siliciclastics occur in two modes in the section: as discrete beds of fine sandstone and/or sandy siltstone and shale, and as "contaminants" in the carbonates, producing what DeFord and Riggs referred to as "marls." The sandstones and finer clastics typically are in sharp contact with underlying and overlying carbonates. Internally, these sands are typified (as elsewhere in the outcrop area) by being devoid of diagnostic sedimentary and biogenic features, and generally are unfossiliferous. Individual units commonly maintain their lithic identity from the base to the top of the bed (e.g., upward coarsening or fining of grain size is not observed) except that many include a thin (several cm) section of gray shales/silty shales at the immediate contact with the overlying carbonate. Of particular significance is the fact that sandstones such as the Ocotillo Member and the Yates Formation sands can be traced on the shelf to cover hundreds of square miles with only minor changes in thickness. Based on the concept proposed by Mazzullo et al. (1984 and 1985), many of these sands are considered

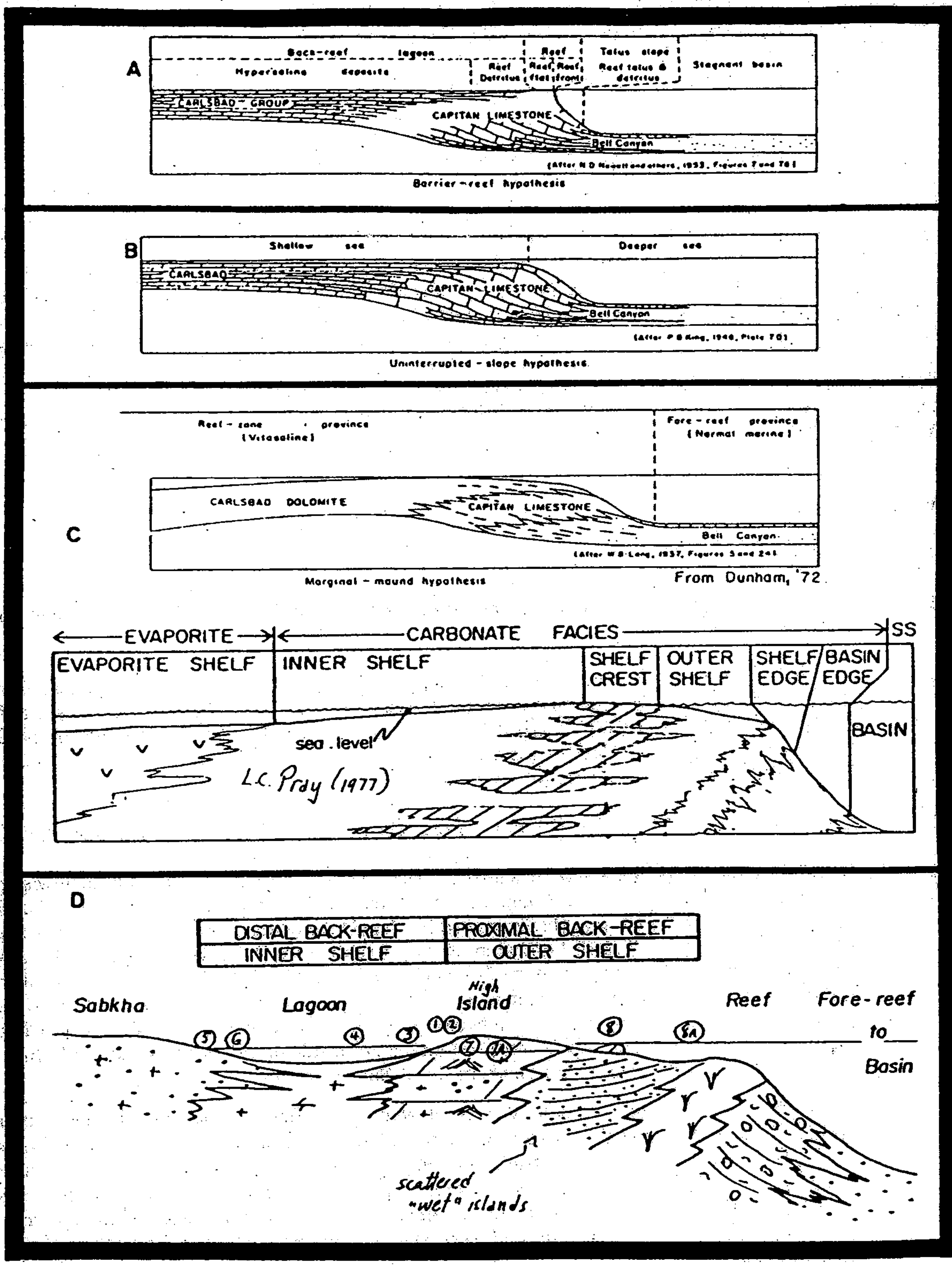

FIGURE 2. Reconstructions of facies relations in Guadalupe Mountains. Pray's (1977) model ("C", lower) invokes an outer shelf of grainstones behind which exists a long-lived high island or shelf crest. Shelfward these facies pass into shallow lagoonal environments with evaporites on the west. Model "D" is the interpretation of S.J. Mazzullo and C.L. Hedrick, which infers the evaporites and associated sandstones to be supratidal sabkah flats; seaward of the high island, the outer shelf facies tract includes scattered "wet" islands. The reef is believed to be somewhat deeper-water buildup. The model is drawn at time of high sea level. Day 1 stops are indicated on model "D."

to represent eolian deposits. We envision a scenario such as exists presently around the western Persian Gulf, where a source of sands from the adjoining desert abuts against a shoreline carbonate sabkha in an arid environment. At times of sea level low, the sand and evaporite flats to the west were left dry, and sands were deflated and transported eastward across the Tansill carbonate supratidal flats (and eventually across the reef and presumably into the Delaware Basin). As in the Persian Gulf, the preserved sedimentary record of such processes does not normally include thick dunes, but more typically leaves behind a blanket sand of near-uniform thickness and widespread occurrence, referred to as an "erg." Internal bedding in such erg sands is represented most commonly by wavy, planar laminae that probably represent, for the most part, adhesion ripples (flattened ripples that slowly migrated across a wet flat). Locally, small-scale cross-stratified sets representing a variety of bedforms may also be present (we will examine several such bedforms at forthcoming Stops 4 and 6). Because such erg sands represent deflation-level surfaces in an arid environment, their top surfaces frequently coincide with groundwater tables which may be fresh to hypersaline. Accordingly, such sands commonly contain relicts of typical desert evaporites (gypsum nodule molds and rosettes, e.g., desert roses). Subsequent sea level transgressions may rework the uppermost surfaces of these sands, although as we will examine at Stop 2, the usual result of such sea level rise is the deposition on top of these sand units, locally, of a thin section of gray lagoonal shales.

9.1 4.1 35.5 Low cuts on both sides of the highway are in the basal Tansill Formation. The lithology here consists largely of evaporitic dolomite showing abundant molds, mostly of anhydrite crystals (crystallotopic fabric). Beds are thin; some are laminated. The dolomite is mostly mudstone. At the west end of the road cut on the south side are several thick beds of gypsum of mosaic texture. Although details are not well exposed, relationships suggest a westward transition in this cut from evaporitic dolomite to gypsum. In outcrops a few feet below the road level on the western edge of the cuts are sandstones of the Yates Formation. With careful search some pieces of this uppermost Yates sandstone may show a few well-rounded medium sand-size quartz grains. These grains, much coarser than normal for Guadalupian sandstones, were considered to be a marker of the "top of the Yates" in the subsurface to the north.

The Seven Rivers Hills form the skyline at a distance of about 10 miles to the northwest. From here we see the gently east-dipping backside of a dolomite cuesta made by stripping off the less resistant, more sandstone-rich strata of the Yates Formation from the underlying Seven Rivers dolomite. The general structure of this area of the shelf is that of gentle east (basinward) dips of the outcropping Tansill, Yates and Seven Rivers Formations.

9.6 .5 36.0 **Intersection with U.S. 285 Truck Route to Carlsbad to the left (south). Continue straight ahead on U.S. 285** passing through Catclaw Draw field, which produces from the Strawn and Morrow at a depth of 11,000 ft. Today's traverse includes Morrow, Strawn, Atoka and Wolfcamp production. Most recent activity has been for the prolific Bone Springs Formation.

11.8 2.2 38.2 **STOP 2. Outcrop on the west side of the road** is in sandstones and dolomites of the Yates Formation. At this locality we will examine various interpreted aspects of the interactive yet noncontemporaneous deposition of carbonates and siliciclastics in the back-reef section.

The massive bedded red sandstones near road level are internally homogeneous to parallel-laminated; diagnostic biogenic or sedimentary structures and fossils are lacking. Note, however, that the contact between the massive sandstones and overlying carbonates typically is occupied by a relatively thin section of gray shales. Also note, where indicated by the trip leader, that these shales are overlain first by a section of laminated dolomite and then by fenestral dolomites. Detailed lithic analyses of these carbonates suggest that the laminated dolomites are subtidal to lower intertidal, mechanically deposited laminites (peloidal fine sands or silts); and the fenestral dolomites represent supratidal deposits. Thus, we interpret the sand—gray shale—carbonate section as follows:

- Exposure of the shallow shelf due to sea level fall, and subsequent deposition of sandstones as erg facies:
- Sea level rise over a flat surface of essentially no relief, and consequent establishment of shallow, nearly anoxic lagoonal environment that receives slow influx of fine siliciclastics until they are replaced by carbonates.
- Deposition in the shallow lagoon of laminated carbonate sands/silts: considering the restricted thickness of this section (less than 1.0 ft.), the inferred depth of the lagoon could not have exceeded 1.0 feet; subsequently,
- Upward-shoaling into peritidal environments represented by fenestral carbonates.

The scenario postulated at Stops 1 and 2 for the deposition of the sands in the back-reef facies of the Tansill and Yates (and units to be observed at subsequent stops) differs from previously proposed models in that we envision these clastics to represent eolian rather than lagoonal facies. Severe problems arise if one considers the subaqueous origin of these sandstones in that a mechanism needs to be invoked that would transfer sands from the west (innermost shelf sabkha facies) into and across the lagoon; obviously if these lagoons are the sites of sand deposition, then sea-level must be high rather than low. In the eolian alternative, sea-level fall results in lowering of groundwater levels on the inner shelf sand/evaporite sabkha, with deflation and sand transport to the east, onto and across emergent flats. Such a model would explain (a) the widespread occurrence of these blanket sands, (b) their fine-grained nature, and (c) the lack of marine depositional/biogenic features and the sharp contacts between these sand units and overlying and underlying carbonates which form *not* when sea level is low. This model also allows for the local reworking of these erg sands as sea level subsequently rises, to be overlain by lagoonal shales and ultimately, shallow subaqueous and peritidal carbonate facies.

12.9 1.1 39.3 Cross Rocky Arroyo, the major drainage from the area of the Seven Rivers embayment to the west. Several levels of alluvial gravels are conspicuous along the arroyo.

13.6 .7 40.0 **Intersection with New Mexico 137 on left. Turn left onto New Mexico 137 and proceed to the southwest.** The road here crosses gravels overlying the Yates Formation. To the west and northeast the gentle east dips are evident on the back-slope of the Seven Rivers Hills cuesta. The Seven Rivers Hills are the type locality of the Seven Rivers (Meinzer, et al., 1926).

The construction office on the right of the highway is the headquarter site for the Brantley Project. The highway is being relocated to accommodate Brantley Dam & Reservoir.

The project was authorized for construction October 20, 1972. The benefits are stated to be for safety of dams (replacing the Lake McMillan Dam) in addition to irrigation, flood control and recreation. The dam will be a 100-foot earthen dam approximately 4 miles long spanning the Pecos River. At initial filling the reservoir will have a surface area of 3100 acres. The final surface area will be 8600 acres extending 10 miles upstream, encompassing Lake McMillan.

As anyone who has worked this area knows, to build this project the government condemned thousands of acres which have excellent oil and gas potential from the Morrow and other horizons.

17.9 4.3 44.3 Entering Rocky Arroyo. Outcrops of dolomite along the lower edge of the arroyo to the south are of the Seven Rivers. The Yates Formation crops out on the crest and east side of the hills south of the arroyo. Note several local gentle anticlinal folds in the strata on the south side of the arroyo (Figure 3).

FIGURE 3. View toward south wall of Rocky Arroyo at mileage 17.9, showing anticlines in Yates Formation.

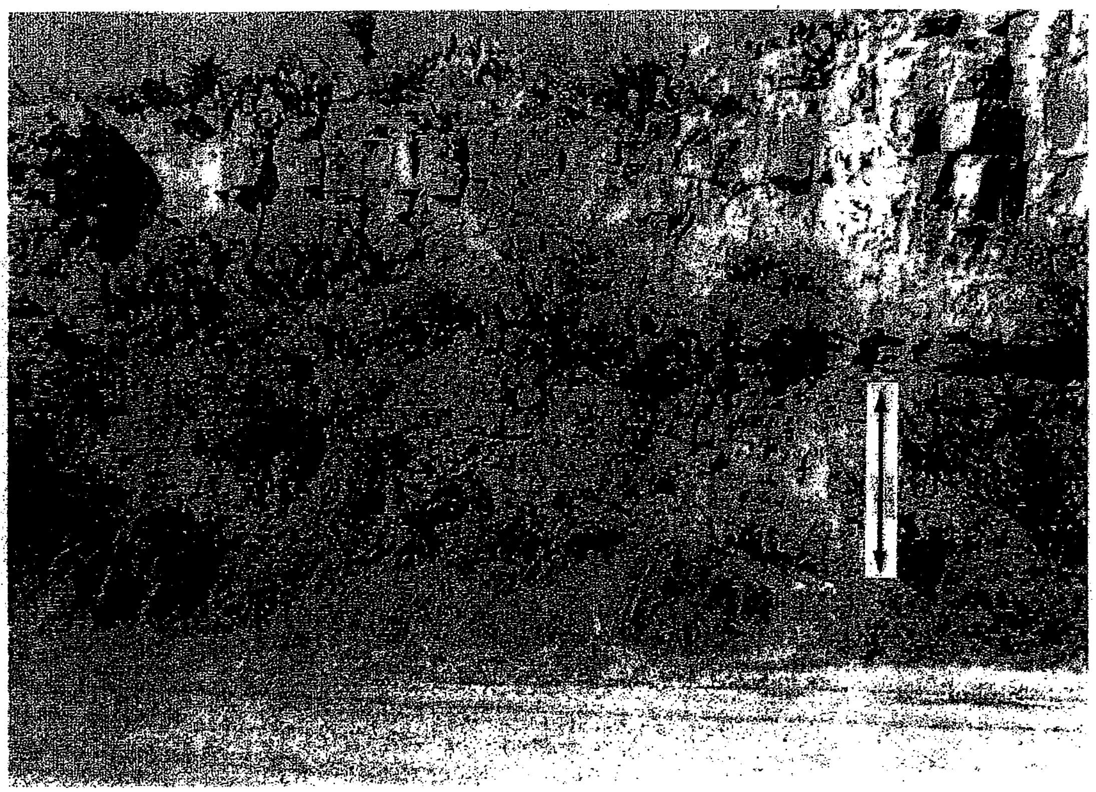

FIGURE 4. Outcrop of lower Seven Rivers Formation, fine-crystalline, peritidal dolomites. Note heavily fractured zone ("f") and less fractured overlying unit ("x").

45.0

18.6 .7 **STOP 3.** These outcrops are located approximately 12 miles shelfward of the Capitan Reef shelf edge. Dolomites of the lower Seven Rivers Formation are exposed in the roadcuts and the arroyo to the southwest. This section consists entirely of stacked, thinning, upward-shoaling cycles of shallow subtidal and intertidal to supratidal facies. In these cycles, the subtidal facies are represented by sparsely fossiliferous dolomite mudstones with ostracodes and calcispheres. These rocks grade rapidly upward to algal-laminated and fenestral dolomites of peritidal origin. This section, 12 miles behind the reef crest, is typical of back-reef facies of the middle shelf complex: interbedded shallow lagoonal and island facies. As we will examine at Stops 4-8 of today's journey, these paleo-environmental units contrast drastically with the inner-shelf siliciclastic/evaporite terrane and the outer shelf, high island (shelf crest) and grainstone belt facies (Figure 2).

Note the heavily fractured dolomites in the lower part of the section ("f" on Figure 4); these rocks in the subsurface would comprise a highly permeable reservoir that is overlain by dense, less fractured dolomites ("x" on Figure 4).

Across the road and in the arroyo are outcrops of Pleistocene travertine that formerly floored the arroyo for at least 2 miles. Dunham states that this travertine formed by progradation of a waterfall, much like modern-day Sitting Bull Falls.

19.2 .6 45.6 New Mexico Highway mileage marker 44.

19.7 .5 46.1 Small cemetery on left. Southeast across the arroyo the high cliff is Seven Rivers dolomite. At the base of the cliffs to the south and rising from the arroyo level toward the west along the arroyo edge are outcrops of the Shattuck Sandstone, an upper unit of the Queen Formation (Figure 5).

20.1 .4 46.5 On left, ranch house and entrance to Rocky Creek recreational areas, a privately owned picnic and swimming area at base of the high cliff. Access to the south bluff area requires permission at ranch house.

The canyon behind the ranch house leads into Walt Canyon. Perry Roehl reported the occurrence of syndepositional and postdepositional hydrocarbons within the pores of the Seven Rivers dolomite (1984 lecture at PBS-SEPM).

20.2 .1 46.6 Crossing of Rocky Arroyo. Travertine outcrops on right. To left, the lower cliffs along the arroyo are the Shattuck Sandstone Member of the upper Queen Formation. Most overlying dolomite is of the basal Seven Rivers Formation.

FIGURE 5. Cliff behind Rocky Creek Recreation Area, exposing the lower Seven Rivers dolomite. The Shattuck crops out at the base of the section, just out of view in this photo.

20.4 .2 46.8 Cattle guard, road to Shafer Ranch house at right. Property to west along both sides of Rocky Arroyo is part of Shafer Ranch. The strata exposed behind the Shafer Ranch house are skeletal-rich pellet packstone.

21.2 .8 47.6 The south-facing hills north of the arroyo consist mostly of Seven Rivers dolomite overlying the Shattuck sandstone which is poorly exposed along the base of the slope.

21.3 .1 47.7 **STOP 4. Enter area of roadcuts on the left** exposing sandstones and dolomites of the upper Queen and lower Seven Rivers Formations. The Shattuck Sandstone Member (upper Queen Formation) crops out in this area as thick, rather massive ledges at the north and south ends of this roadcut. Excellent exposures of this unit occur in the arroyo bottom and cliff to the right, on the north side of the road. At this stop we will first examine the nature of the Shattuck Sandstone in the arroyo on the north side of the road, and then will climb back to road level and examine the upper Queen/lower Seven Rivers sandstones and dolomites in the roadcuts.

In the western part of the arroyo section, the lower part of the Shattuck Sandstone section is anomalously thick as compared to its typical blanket-like, uniformly thick distribution throughout the outcrop area. At this locality, the basal Shattuck occurs as a maximum 12.7 ft of massively bedded, light yellowish-gray sandstones overlain by 0-12.5 ft of thinly bedded, dark gray-weathering flaggy sandstones which in turn are overlain by a section up to road level of massive-bedded, light yellowish-gray, laminated or homogeneous sandstones and siltstones (see Figure 6). The lower massive unit in particular has a dune-shaped geometry when viewed, for example, from the northeast (Figure 6), and this unit clearly represents large-scale foreset beds that dip a maximum of 18-20 degrees to the northeast, the strike of the beds being N60°W. The question we consider here is what environment is represented by these foresets and overlying sandstones? These rocks have been interpreted by several workers as representing a lagoonal deposit, specifically a subaqueous sandwave (dune bedform or megaripple: Sarg, 1977). However, it is our contention and present interpretation that these massive foresets and overlying flaggy sandstones represent the slipface and stoss beds, respectively, of a preserved eolian dune in the lower Shattuck. Evidence of the eolian origin of such sandstones is derived from a conceptual model of sandstone distribution patterns in mixed carbonate siliciclastic environments (Mazzullo et al., 1984, 1985) as well as from the following direct observations: (i) first and foremost, overlying and underlying carbonates are represented by extremely shallow subtidal and intertidal-supratidal facies; as was examined at Stops 1, 2 and 3, water depths of the shelf section behind the Capitan Reef, as inferred from the carbonates present, were mainly at or close to sea level in low-energy environments. According to empirical data presented by various workers, in order for

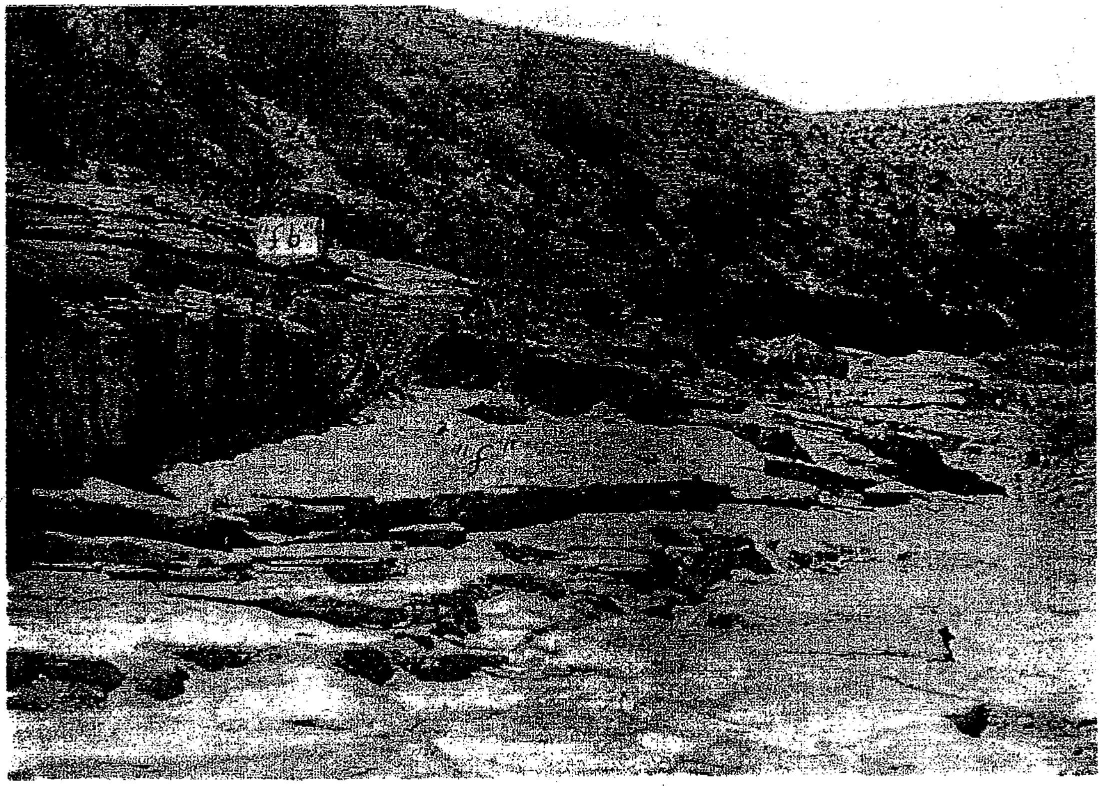

FIGURE 6. View of dune bedform in Shattuck at Stop 4. Note massive foresets ("f") that dip to the northeast overlain by flaggy beds ("fb").

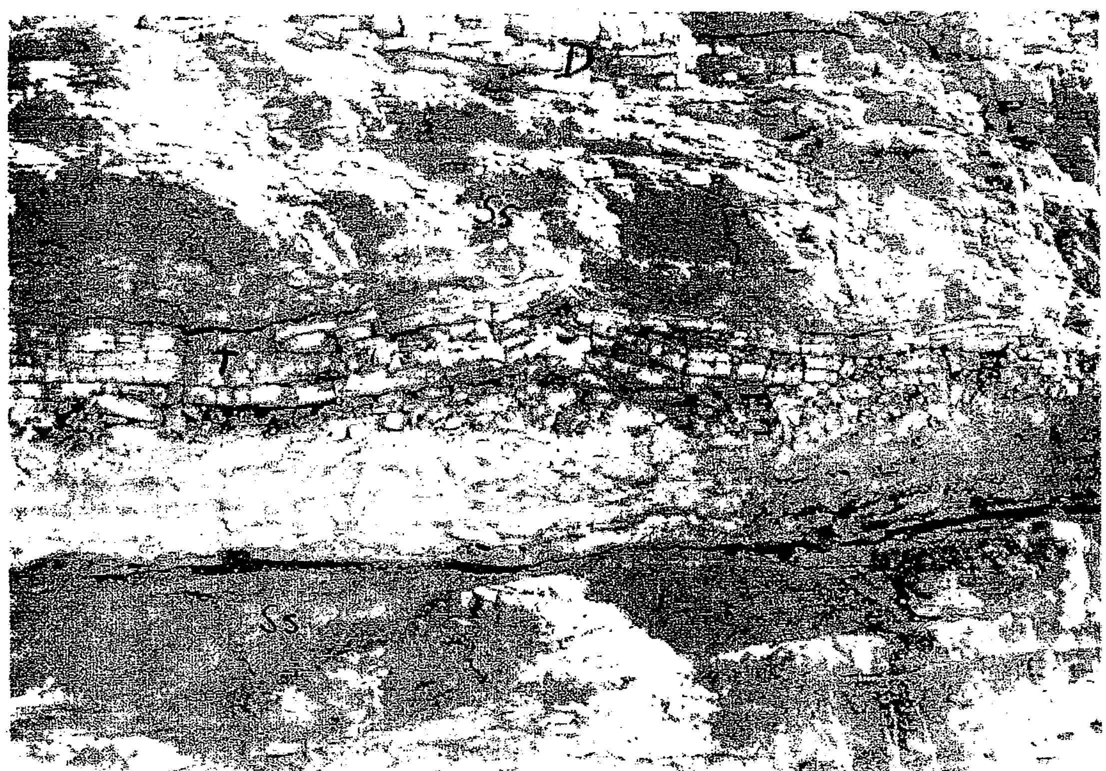

FIGURE 7. View of lower Seven Rivers/upper Queen at Stop 4. Note incipient tepee ("T"), fenesteral dolomites ("D") and interbedded siliciclastics ("Ss").

a bedform such as the 12.5 ft-thick sand section in the lower Shattuck to be developed subaqueously, water depths must be considerably deeper than 12.5 ft deep, with relatively high energy levels, a situation that directly contradicts the rock evidence; (ii) nowhere are marine entities (fossils, etc.) found in these rocks, a situation considered unlikely if marine conditions persisted in this area; (iii) the close physical association of inferred eolian sandstones with (overlying and laterally contiguous) sandstones that contain adhesion ripples and evaporite relicts argues for a close genetic association of many of the sandstones in the Shattuck and associated units in the back-reef section. Interestingly, similar eolian erg (sand sheet) and dunal sandstones are well documented in the Permian Basin as reservoirs in the Queen and Shattuck-equivalent sandstones (Mazzullo et al., 1984).

We are not maintaining, however, that all sandstones of the back-reef shelf section are eolian, for it is obvious that several sandstones exist here that can be interpreted as subaqueous (e.g., Ball et al., 1971). However, many such sandstone units are of only limited extent areally, and conceptually by their distributions and variable thicknesses cannot be assigned an eolian origin in our model. Furthermore, our model does envision two aspects of sand development on the shelf that do not contradict a general eolian setting of many of the sands in this area: (i) that subsequent transgression following erg progradation can locally rework eolian sands by marine processes (although nowhere do we see such processes operating in water deep enough and of such energy levels to produce a 12.5 ft thick sandwave), and (ii) isolated lagoons, ponds or lakes on the erg flat (where the latter two features intersect groundwater tables, for example) may be the local sites of subaqueous sand deposition in an overall eolian setting.

We now return to the roadcut outcrops, where we can examine the upper Queen (Shattuck Sandstone) and overlying basal Seven Rivers dolomite and sandstone-shale units (Figure 7). Recall that at Stop 3, we examined a time-equivalent section of shallow subtidal and intertidal-supratidal dolomites of the lower Seven Rivers, at a locality in the back-reef lagoon where no sandstones were developed. In the roadcuts at the present stop, the low-energy lagoonal facies observed at Stop 3 are replaced by siliciclastics and predominantly supratidal dolomites. Again, we envision that most of the sandstones in this section, particularly those that are blanket units of textureless character (with adhesion ripples and evaporite relicts) and sharp contacts with overlying and underlying supratidal carbonates, are eolian erg deposits. For comparison, take a few moments and visualize the interbedded red sandstones at the western end of this outcrop as the deposits of windblown sand, envisioning a typical windy, spring day in Midland; keeping in mind the beautiful red sand we're all accustomed to as our "soil."

The associated dolomites of the section clearly are supratidal as evidenced by the ubiquitous occurrence of birdseye fabrics, desiccation cracks, algal laminites, and other features indicative of this environment. But beyond this aspect of their formation, these rocks have been so affected by aggressive fluids subsequent to their deposition that features such as collapse breccias, tepee structures, and incipient caliche surfaces run rampant through the section. The association of supratidal deposits and extreme vadose alteration effects are what Roehl (1967) referred to as "diagenetic terrane."

21.6 .3 48.0 Road cut exposing the upper Queen Formation consisting of channel sandstone and interbedded red and green shale. The Queen Formation was named by Crandall (1929) for outcrops in the vicinity of the Queen Post Office about 20 miles south of here. There it consists of 370 feet of dolomite, shaly sandstone, and siltstone. Moran (1954) proposed another type section in the upper end of Dark Canyon.

21.7 .1 48.1 Road cut. Queen Formation.

22.6 .9 49.0 Sharp left turn. Queen Formation exposed in the road cut. Seven Rivers Hills at 2 o'clock.

22.85 .25 49.25 **Junction of County Road 401 and State Road 137. Keep left on State Road 137.** County Road 401 goes into the Indian Basin (Figure 8). Morrow gas is produced at a depth of 9500 feet in the prolific Indian Basin field. The Marathon gas plant can be seen in the distance.

STOP 5. An arm-waving stop to view the north wall of Rocky Arroyo (Figure 9).

The abrupt west-to-east facies change from evaporities and siliciclastics to low-energy carbonates and (inferred eolian) sandstones in the Seven Rivers and upper Queen Formations is readily apparent on the south-facing wall of Azotea Mesa. Note the color change defining this facies change to the left and right of our vantage point; the evaporite realm forms the gentle, reddish slopes, whereas the carbonate realm forms somewhat steeper slopes of a more brownish hue. The prominent ledge capping the mesa is the Azotea Dolomite Member of the Seven Rivers Formation. At the base of the section, the Shattuck Sandstone crops out, and is underlain by massive cryptocrystalline dolomites of the upper Queen Formation. We will examine the sandstones and dolomites of the Queen, and evaporites of the Seven Rivers, at Stop 6.

FIGURE 8. View to the west into Indian Basin; north wall of Rocky Arroyo on right exposes interbedded sandstones and dolomites of the Seven Rivers and upper Queen Formations. Photo at mileage 22.85.

FIGURE 9. North wall of Rocky Arroyo showing transition from siliciclastic/evaporite belt on west (left) to carbonate/siliciclastics to east (right) in the Seven Rivers and upper Queen Formations.

Sarg (1977) believed the entire sequence exposed along the Azotea Mesa was deposited in shallow, subaqueous environments. Ball et al. (1971) considered the section to represent intermixed sabkha and lagoonal facies. Mazzullo et al. (1985) favor a scenario similar to that proposed by Ball et al. (1971), except for advocating a more eolian origin of the sandstones. It is S. J. Mazzullo's opinion that the evaporites and sandstones represent a wide coastal and continental sabkha belt adjoining a lagoon of variable width. The evaporites, much like those in the Seven Rivers Formation exposed due east of Roswell, NM, were deposited both within the sediment (displacive) and subaqueously in shallow ponds or lakes (hollows intersecting groundwater table, or flooded areas on the flats) on the sabkha surface. During times of high sea-level stand, this sabkha belt adjoined a shallow lagoon (back-reef) in which carbonates were deposited as a mosaic of low-energy subtidal facies and coalescent, upward-shoaling islands. During these times, the sands were restricted to the sabkha. We note that even when the carbonate facies had aggraded into broad supratidal flats, no sands were deposited over them in regular, predictable stratigraphic order as postulated by Walther's Law; quite the contrary, the influx of these sands occurred during sporadic events that affected broad areas of the back-reef shelf (emergence!); the sandstones are in sharp contact with the underlying truncated cycles of carbonates. Accordingly, in order to maintain a continual supply of sands that would migrate over this carbonate terrane, sea level must fall so that the sabkha flat is exposed (by groundwater table drop) to deflation. Eolian activity then results in the seaward progradation of sands, leaving behind a widespread erg deposit with scattered, rare preserved dunes. Locally, these sands are reworked by currents in existing lagoonal embayments and by (sporadic, high-intensity) wadi streams on the desert sabkha flat. Subsequent sea level rise again traps the sands on the flats, and inundates this broad sand flat; currents may rework some of these sands, producing the cross-stratification observed by Ball et al. (1971) in proximity to the (Goat Seep) reef.

24.5 1.65 * ? 50.9 50.65 **STOP 6.** The conical hill to the west called the "Tepee" (Figure 10) consists of interbedded gypsum and red siltstones and shales, with minor thin-bedded dolomites, of the Seven Rivers Formation. Toward the south, the escarpment waved upon at Stop 5 exposes the same section of rocks. The Tepee is capped by the massive dolomites of the Seven Rivers, referred to as the Azotea Dolomite Member.

The section exposed in the gully to the south of the Tepee includes interbedded sandstones and dolomites of the Queen and Shattuck. The dolomites are micritic, with evidence of having been exposed in shallow subtidal to supratidal environments. We see a complex of anastomosing facies in the carbonates, suggesting the environment was one of many islands amidst a shallow lagoon. However, note the abrupt contact of the sandstones and dolomites; it's almost as if one froze the carbonate environment in time, shut them off and covered them with sand!

The sandstones are typically like those examined at Stops 1, 2 and 4; they consist of medium- to thick-bedded units with little diagnostic in terms of depositional environment. However, features that are ubiquitous in these sandstones include planar, wavy laminations and adhesion ripples; at a few locations you can observe gypsum nodule casts and desert rosettes. As we proceed down the gully, note the sharp contacts between the sandstones and carbonates: I believe such relations evidence the sporadic events of low sea level stand during which times the sands migrated across the shelf, over truncated cycles of carbonate deposits. For one moment, let us consider that these sandstones are shallow lagoonal deposits; why aren't they fossiliferous, or at least why don't they contain some peloids or tolerant algae? If they are hypersaline deposits, why don't they contain evaporites (desert roses form subaerially!!!). We can continue with this mental exercise, and debate all fine points of sedimentology concerning these sandstones. I merely wish to introduce an attractive alternative to previous models regarding these sandstones in the Guadalupe Mountains.

24.9 .4 Well on the right (Marathon State Gas Com. #1) produces Morrow gas from the Indian Hills Unit.

25.8 .9 Well on the right (Flag-Redfern Oil Company Winston Gas Company #1), a dual completion from the Cisco and Morrow at a total depth of 9730′ in the Indian Basin field.

27.0 1.2 Cut on the right exposes Queen redbeds. Road to the left. **Continue straight.**

27.3 .3 Road and ranch house to the left. **Continue straight.**

27.4 .1 Cattle guard and roads to right and left. **Continue straight.**

28.45 1.05 Cattle guard.

28.75 .3 Road to right. Bandana Point ahead.

31.0 2.25 Road cut. Seven Rivers gypsum.

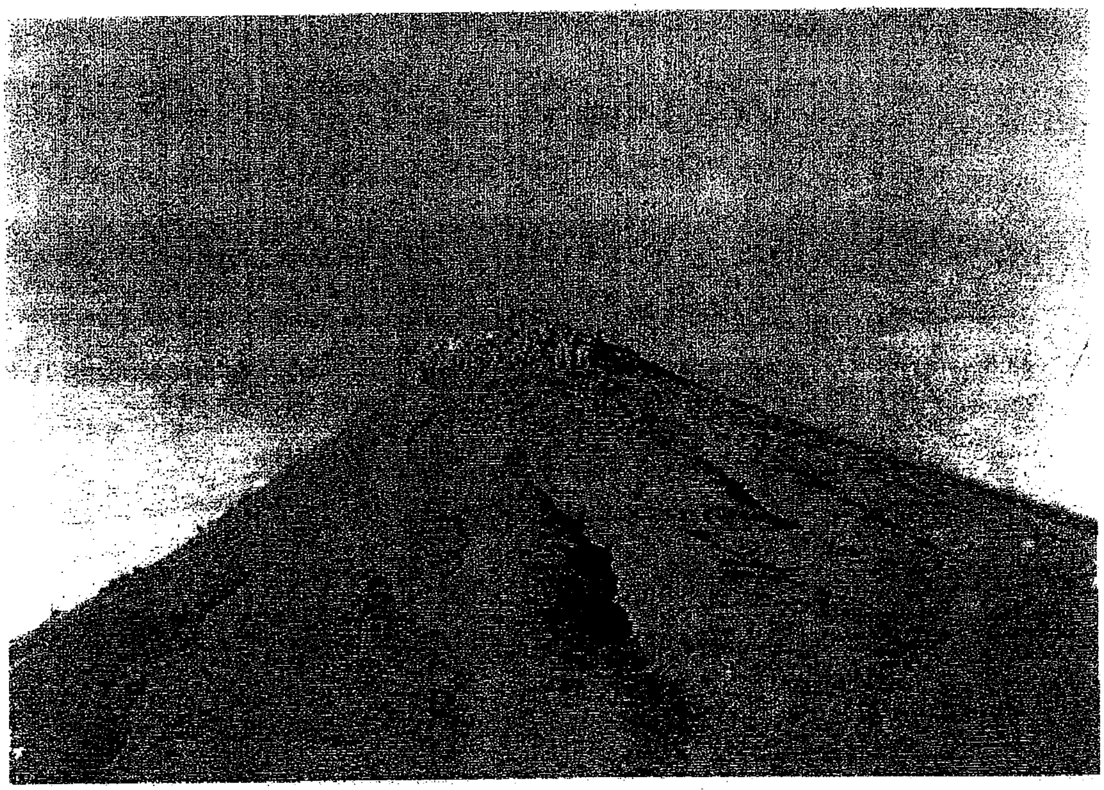

FIGURE 10. The "Tepee," exposing evaporites and siliciclastics of the lower Seven Rivers, capped by the prominent ledge-forming Azotea Dolomite Member.

31.6	.6	Ranch house to left, road to right. Thin-bedded Seven Rivers dolomite in low road cut ahead.
34.2	2.6	**Intersection of State Road 137 with County Road 408. Turn left on County Road 408.** Highway 137 continues to the Queen Plateau, which is the escarpment visible a few miles ahead, then on to El Paso Gap. A side road goes up Last Chance Canyon to Sitting Bull Falls with excellent exposures of the Queen, Grayburg, and San Andres Formations. The escarpment at the edge of the Queen Plateau consists of the Queen and Grayburg Formations downwarped by the Haupache monocline, one of the most prominent structural features of this area with dips of up to 12 degrees and traceable for over 25 miles.
34.35	.15	Cattle guard.
35.3	.95	Seven Rivers dolomite on the right.
36.35	1.05	Ranch house on the left and drainage crossing.
36.45	.1	Cattle crossing.
37.0	.55	Road on the right. **Continue straight.**
37.7	.7	Drainage crossing.
38.15	.45	Road to left to Internorth Incoporated Azotea Mesa Federal #1, which produced a little gas from the Morrow. Production is now listed as Robina Draw Atoka.
40.2	2.05	Cattle guard. Ranch house to the right. The canyon walls consist of Seven Rivers gypsum, red siltstone and medium- to thin-bedded dolomite. The transition from gypsum to dolomite in the Seven Rivers Formation occurs at this point.
40.9	.7	Drainage crossing.
41.6	.7	The cliffs ahead expose the Seven Rivers Formation. It consists of thick- to medium-bedded dolomite, the gypsum having largely disappeared from the section. This is a more open marine shelf deposit. There is some structural deformation displayed in the outcrop.

41.75	.15	Road to the right. **Continue straight.**
42.0	.25	Cattle guard. Well to right. Small folds are exposed across the drainage on the left in medium-bedded Seven Rivers dolomite. We are crossing a low divide and will enter Mosely Canyon.
		Located to the north (left) of the road is the Rock Tank field, producing from the Morrow and Atoka.
43.4	1.4	Drainage crossing. Solution collapse folds are exposed in the canyon wall to the left. The bulk of the Seven Rivers section here is dolomite with occasional thick beds of fossiliferous, open marine carbonate. The environment of deposition includes supratidal, intertidal and open marine shelf. The regional dip is almost flat. The road crosses the Seven Rivers-Yates Formation contact just ahead.
43.8	.4	Drainage crossing. County Road 408B to left. **Continue straight.** Thin- to medium-bedded, light-colored dolomite of the Yates Formation in the creek bank.
44.15	.35	County Road 408A to left. **Continue straight.**
44.65	.5	Lease road to right. **Continue straight.**
45.0	.35	Cattle guard.
45.35	.35	Amoco #1 State "IZ" Com. on left, producing gas from the Morrow at a depth of 10,300′ in the Dark Canyon field.
47.05	1.7	Road to right. Ranch house on left. Cattle guard. **Continue straight.**
47.5	.45	Drainage crossing. Thin- to medium-bedded non-fossiliferous, light-colored dolomite and interbedded shale cropping out in the creek bank. This is the supratidal to intertidal facies of the Yates Formation.
47.7	.2	Ranch road to right. **Continue straight.** There are still some redbeds visible in the canyon walls but they do not extend much closer to the reef than this.
48.4	.7	Anticline exposed to the left in medium-bedded Yates dolomite.
48.6	.2	Drainage crossing. Thick-bedded Yates dolomite exposed. The dip is nearly flat.
48.9	.3	Drainage crossing. A good exposure of Yates medium- to thick-bedded shelf dolomite in the creek bank.
49.35	.45	Drainage crossing.
49.7	.35	Windmill on the left. Road to the right. Drainage crossing just ahead. The Yates exposed in the creek bank is medium-bedded dolomite.
51.1	1.4	Cattle guard. The dip in the canyon wall at 10 o'clock across the canyon is 4° to 5° basinward.
51.6	.5	Drainage crossing. Mosely Canyon drainage joins Dark Canyon drainage.

STOP 7. Outcrops on the right in abandoned quarry, of the contact between the upper Yates and lower Tansill Formations (Figure 11). At this locality, the carbonates of the Yates and Tansill Formations consist entirely of fenestral dolomites with birdseye structures, desiccation cracks, algal laminites, and evaporite molds. We presently may be as close as within 1.0 mile of the shelf edge, so these rocks represent the high island or "shelf crest" facies (of Pray, 1977). We have now progressed in a wide circle, having started in this facies at Stop 1, continued shelfward to low-energy, micritic lagoonal and island facies (Stops 2, 3) and distally to evaporite-siliciclastic sabkha flats (Stops 4, 5, 6), and now have returned to the outer shelf tract (see Figures 1 and 2).

Several important aspects of this outcrop are readily apparent, and specifically relate to the depositional origin of the section in the Guadalupe Mountains. Firstly, note the relations between the upper Yates sand and the underlying and overlying carbonates. Again, it appears as though the carbonate factory was shut down abruptly, and that the sands prograded over the truncated carbonates, leaving behind a deposit of near-uniform thickness and wide areal extent (in our interpretations, an eolian erg sand sea).

Secondly, note the pervasiveness of the depositional facies represented by the carbonates here: entirely intertidal-supratidal. Clearly, we're in an area that persisted as an island through time, much

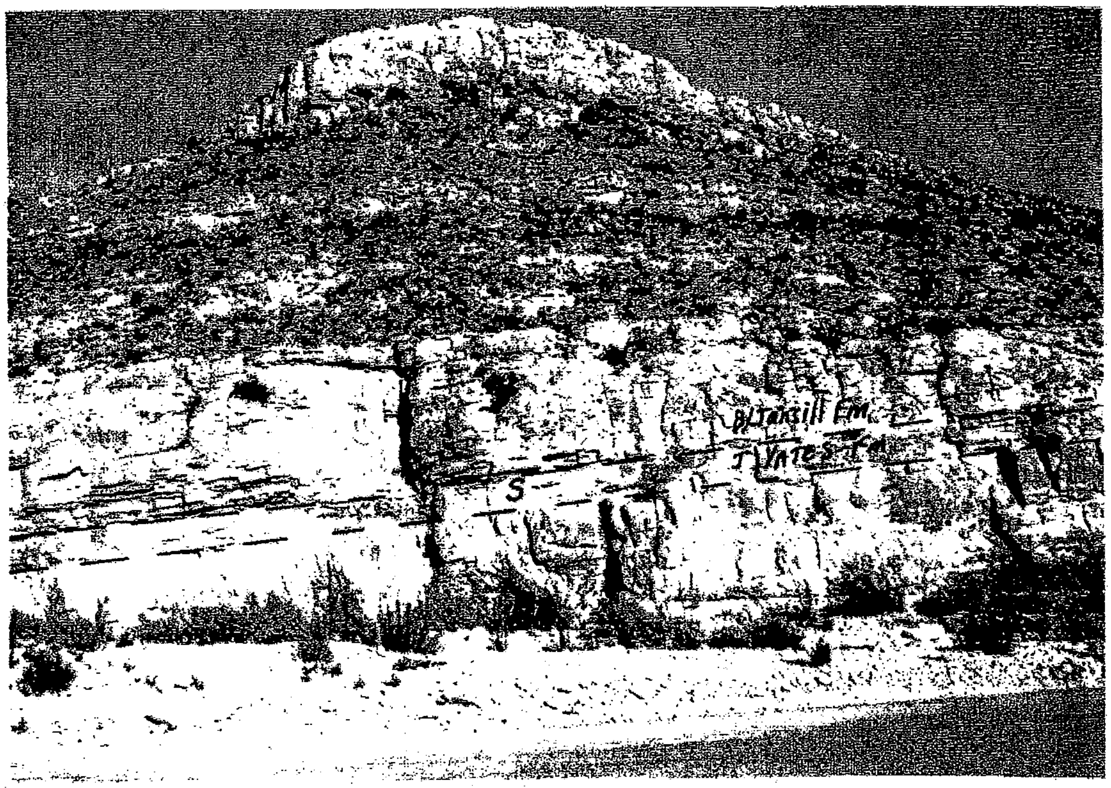

FIGURE 11. Stop 7. Upper Yates and lower Tansill peritidal dolomites of the shelf crest or high island, with prominent eolian upper Yates sand ("S"). The entire section to the top of the hill consists of high island peritidal dolomite facies. Note the abundant tepees in the cliff face.

the same as present-day relations between Ambergris Cay and the outer-shelf carbonate tract in Belize, C.A., and closer to home, Tansill relations with the shelf edge at Cheyenne field in Winkler County, Texas (Ordonez, 1984). Recall that at this locality, we may be approximately 1.0 mile behind the shelf edge; at the next two stops we will move out of this island facies and into the outer shelf sand facies tract behind the reef. One of the most interesting aspects of the section preserved at this locality is the abundance of "tepees." Such features, first described from the Guadalupe Mountains by Adams and Frenzel (1950), have received a tremendous amount of attention from the scientific community, principally because of their curious nature and seeming defiance to being understood. Since Assereto and Kendall's (1977) studies of tepees, it has been inferred by many workers that these tepees are principally upper intertidal-supratidal diagenetic features that are associated with internal sediments, local terra rossa surfaces, incipient caliches and pisolites, fine-crystalline dolomites, and admixed marine cements and local reworked marine fossils. Perhaps the most concise explanation offered to date of tepee formation was that of Warren (1982, 1983), who provided an excellent analog from the supratidal flats of Australia. In his model, the tepees form in partly indurated supratidal carbonates as a result of actual physical displacement by upward-flowing ground waters, generally derived from recharging meteoric sources. In the mixing environment of these supratidal flats, undersaturated fluids (e.g., meteoric and/or dilute mixed meteoric/marine) passing through the partly indurated sediments periodically dissolve and physically erode the crusts and associated less indurated sediments, thus producing features such as caliche and layered internal sediments. The passage through the flat deposits of more marine fluids results in the imprint of marine fabrics on the section, such as the precipitation of aragonite or high-Mg calcite botryoidal cements and pisolites (see Assereto and Kendall, 1977 and Handford et al., 1984 for analogs), and fine-crystalline dolomite formation.

The section examined at this stop offers convincing evidence that the mechanisms responsible for tepee formation were environmentally controlled at the time of deposition; and that a prerequisite for extensive tepee formation must certainly involve the presence of a long-lived supratidal area in which these processes can be active for long periods of time. At the next stop we will examine a similar island setting seaward of the main island/shelf crest facies tract, in which different circumstances of geologic history have effected different resultant carbonate diagenetic fabrics.

One final aspect of this section is the occurrence and interpretation of the formation of the pisolites in the peritidal carbonates. There are as many theories concerning the origin of pisolites as there are sedimentologists. However, as will be discussed in further detail by Lloyd Pray on Day 2 of this trip, the main aspects of pisolite formation center on whether they represent exposure and soil (caliche) formation (the "Dunham" theory), or whether they are inorganic coated particles formed in the marine environment. A concise review of this problem, and interpretations concerning the Capitan pisolites, appear in a recent paper by Esteban and Pray (1983).

According to these workers, many of the pisolites of the Capitan are not caliches in the sense of being modified soil horizons as was propounded by Dunham. Instead, thick beds of nearly pure pisolites are believed to be inorganic particles formed in somewhat hypersaline, shallow peritidal environments of variable energy levels. They demonstrated that many associated features of the rocks that were indicated by Dunham to be evidence of soil-forming processes could also be formed in the peritidal environment. Indeed, the recently discovered Australian analogs certainly support their contention of a mechanical rather than soil-replacement origin for the Capitan pisolites.

We will examine pisolites like those interpreted as marine in Walnut Canyon on Day 2 of this trip. If time permits, we may also be able to view similar pisolites along the arroyo in Dark Canyon, between this and the next stop. At both these localities, the pisolites occur in discrete beds of nearly 100% pisolites, such occurrences being relatively easy to interpret as marine. However, we must bear in mind that there are pisolites and there are pisolites, and that there is more than one environment of pisolite formation. For example, pisolites form in caliche soil horizons, in Holocene supratidal crusts in Australia, and apparently as marine particles (e.g., mega-ooids) in the Permian of west Texas-New Mexico. Accordingly, examine the pisolites in this outcrop, those intimately associated with the fenestral dolomites, and arrive at your own conclusions regarding their origin. But keep in mind, this is only one outcrop out of a spectrum of possible pisolite-forming areas within the reef-shelf complex.

52.15 .55 **OPTIONAL STOP 7-A.** If time permits, we will proceed a short distance toward the mouth of Dark Canyon, across an artifically gravel-covered arroyo (WATCH FOR RATTLESNAKES!!) to a cliff outcrop equivalent stratigraphically to the last outcrop section. At this outcrop, we can walk up-section from the top of the Yates sand to the basal Tansill dolomites. In the basal Tansill, the section consists of similar fenestral dolomites and abundant bedded, coarse pisolite sands. The section here, if not covered by the gravel, includes pisolite grainstones that are cross-stratified and otherwise devoid of evidence of caliche origin. We stress this outcrop because of the still-pervasive thought, among Permian Basin geologists in particular, that the pisolites are soil-caliche features. At this and the outcrops described by Pray on Day 2, we have fairly firm ground on which to stand and argue for a marine origin of these curious little particles.

52.6 .45 **STOP 8.** This outcrop is at a position 0.4 mi shelfward of the basinward reef outcrop in Dark Canyon (Figures 1 and 2), and is considered to be within 0.5 miles of the shelf edge. The quarry section is in the middle to upper lower part of the Tansill Formation, stratigraphically higher than that at the preceding two stops. Exposed here is a section of intermixed dolomites and limestones that record the interplay of shallow (outer) shelf and island sedimentation (Figure 12). Note that the background facies from here to the mouth of the canyon consist predominantly of bedded, outer-shelf biograinstones that pass distally (close to the shelf edge, at optional Stop 8A) to reef facies. Superimposed on this background are a series of upward-shoaling island facies consisting of silty dolomites with evaporites, and fenestral limestones, both developed on porous biograinstones. The accompanying photograph (Figure 12) is a photomosaic that illustrates the essential facies in this quarry outcrop.

There are many significant facets to this outcrop section that cannot be justifiably handled in a road log. However, several important aspects of facies development as indicated by this section are of relevance to our overall picture of Guadalupian sedimentation in this region. Firstly, note on Figure 12 that two separate islands have coalesced in this quarry exposure, overlying "weird" carbonate sands. These "weird" sands are outer-shelf facies, consisting of various forams (e.g., Mizzia), bivalves, fusulinids, crinoids, etc. They are overlain by silty, fine-crystalline dolomites with evaporite molds in the central quarry area (see Figure 12), which pass abruptly into biograinstones to the northeast. These dolomites evidence the initial stages of island development, presumably during a low sea level stand. The "weird" biograinstones beneath this early island section appear to have been affected by a complex of marine and meteoric diagenesis in that marine cements and fresh-water, vadose-phreatic cements, sediments, and dissolution features are observed in the rocks. By this evidence, we conclude that the island formed initially during low sea-level stand, and a fresh-water lens that interfingered with the marine environment was established beneath the dolomites, invading some extent downward into the grainstones. Continued vertical (and lateral) island accretion above sea level occurred during subsequent sea level rise, forming a high island, the section represented by the overlying fenestral limestones (see photomosaic). By evidence of intermixed marine and fresh-water diagenetic fabrics in these limestones, it appears that the grainstones that overlie this high island were deposited not during progradation of updip, contiguous facies, but rather by continued sea level rise (transgression) over these island limestones. Subsequently, another island at a later time abutted against this older island tract, resulting in the stratigraphic complexities recorded at this quarry. As these islands are traced into the canyon along the quarry exposures (westward: shelfward), they pass into the prominent and time-pervasive high-island, shelf crest facies as observed at Stop 7, and are underlain by a patch of reef facies of highly fossiliferous limestones (see Figure 12).

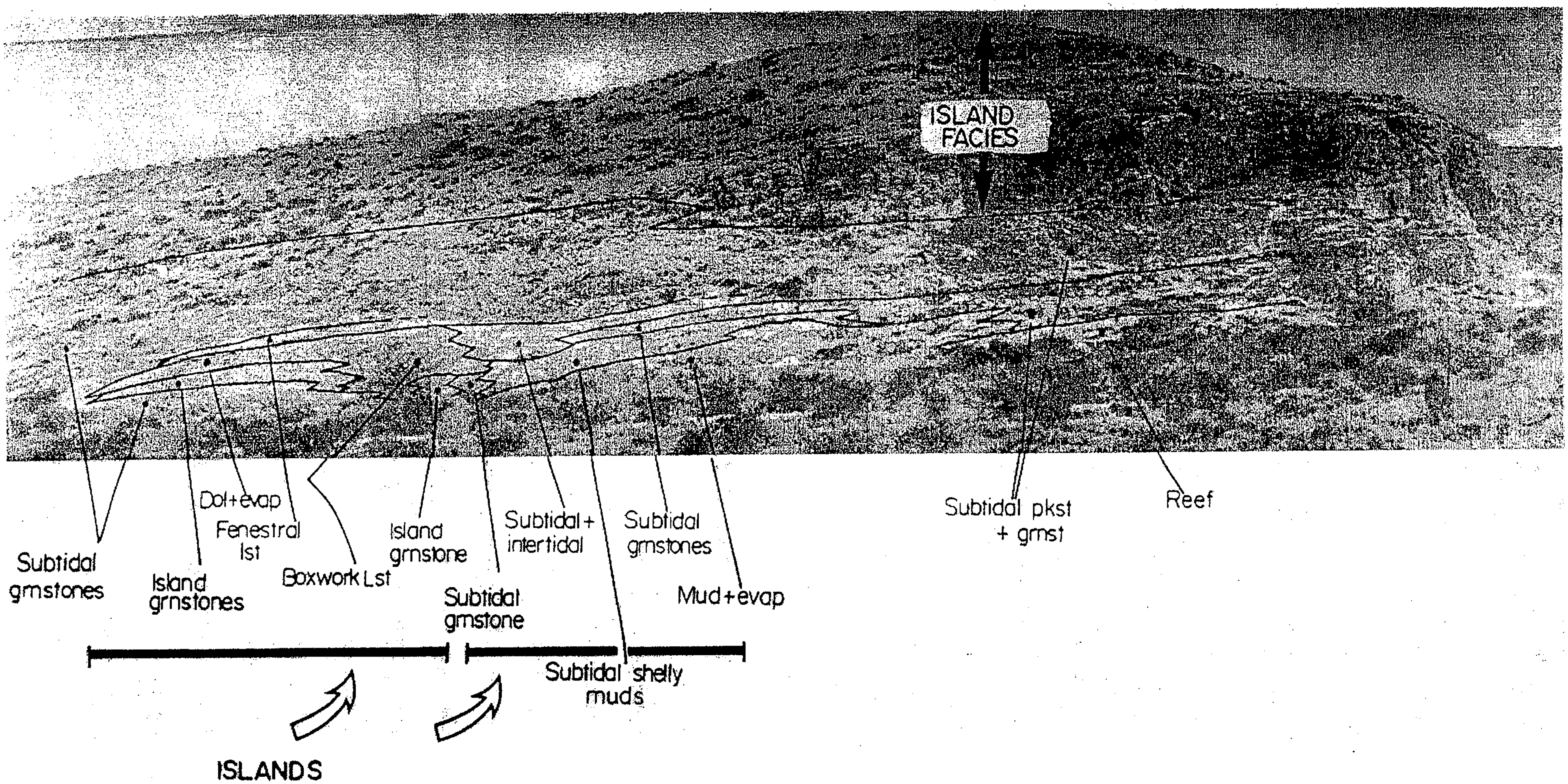

FIGURE 12. Photomosaic of quarry near entrance to Dark Canyon, Stop 8, showing facies relations amd stacked islands within outer-shelf grainstone tract. These facies pass westward in less than one mile to the high island shelf crest dolomites as examined at Stop 7.

Of importance here are the observations that (i) little in the way of pisolites were formed in these islands, and (ii) few tepees are present in the island facies. We believe that such circumstances result from the fact that there are at least two basic types of islands found in carbonate terranes: those that are at or close to sea level ("wet islands"), and those that have accreted vertically and laterally into higher islands. Of the latter, only those that are persistent through time will develop extensive supratidal diagentic features such as pisolites and tepee structures. Those "wet" islands are too allied to groundwater (either marine and/or mixed marine-meteoric) to develop a fluid flow and depositional syst that favor the formation of tepees and pisolites.

53.2 .6 **OPTIONAL STOP 8A.** At the mouth of Dark Canyon is exposed the northernmost outcrop of reef facies of the Capitan complex. The section at this locality has been drilled and cored by Amoco, who found that the reef section here was immediately underlain by back-reef and shelf facies of the Tansill. Therefore, this reef section and that exposed in the quarry at Stop 8 must represent (back-reef) patch reef facies.

The section here and immediately across the canyon has been studied by Toomey and Cys (1977), Babcock (1977), and Mazzullo and Cys (1978). The massive reef limestones are composed principally of massive-bedded, micritic limestones with sponges, corals, crinoids, *Tubiphytes*, and abundant encrusting algae *(Archaeolithoporella)*; brown, fibrous marine cements believed to represent primary marine aragonite are ubiquitous in these rocks (Mazzullo and Cys, 1978, 1983). The reef facies is overlain by and passes laterally shelfward into thin- to medium-bedded biograinstones similar to those examined at the quarry exposures of Stop 8. Further shelfward, or up-section at this locality, the facies pass abruptly into island-type fenestral dolomites with pisolites and evaporite relicts. The sedimentologic and biologic attributes of the section here are essentially identical to those that will be examined in more detail during the stops of Day 2 of this trip.

53.6 .4 Cattle guard.

55.05 1.45 Well on left.

Hills to left are the Cueva Escarpment and to the right are the Frontier Hills.

55.25 .2 Cattle guard.

56.45 1.2 Gravel pit on right.

57.7 1.25 Road on right. **Continue straight.**

57.9 .2 Cattle guard.

58.35 .45 Cattle guard.

58.6 .25 Cattle guard.

58.8 .2 Cattle guard.

59.5 .7 Road to right. **Continue straight.**

60.25 .75 Cattle guard. Skyline view ahead is Quahada Ridge.

60.75 .5 **Junction with Hwy 658. Continue straight on 672.**

60.9 .15 Cattle guard.

61.25 .35 Cattle guard.

61.55 .3 Cattle guard.

62.85 1.3 **Junction with Highway 62-180. Turn left.**

63.0 .15 Civic Center.

65.25 2.25 **Stevens Motel.**

END OF DAY ONE

DAY ONE REFERENCES

Adams, J.E. and Frenzel, H.N., 1950, Capitan barrier reef, Texas and New Mexico: Jour. Geology, v. 58 p. 289-312.

Asserto, R.L.A.M. and Kendall, C.G.St.C., 1977, Nature, origin and classification of peritidal tepee structures and related breccias: Sedimentology, v. 24, p. 153-210.

Babcock, J., 1977, Calcareous algae, organic boundstones, and the genesis of the upper Capitan Limestone (Permian, Guadalupian), Guadalupe Mountains, West Texas & New Mexico, *in* Hileman, M.E., and Mazzullo, S.J. (eds.), Upper Guadalupian Facies, Permian Reef Complex, Guadalupe Mountains, New Mexico and West Texas: Permian Basin Section SEPM Publ. 77-16, p. 3-44.

Ball, S.M., Roberts, J.A., and Pollard, W.D., 1971, Queen Formation (Guadalupian, Permian) outcrops of Eddy County, New Mexico, and their bearing on recently proposed depositional models: AAPG Bull., v. 55, p. 1348-1355.

DeFord, R.K. and Riggs, G.D., 1941, Tansill Formation, West Texas and Southeastern New Mexico: AAPG Bull., v. 25, p. 1713-1728.

Dunham, R.J., 1972, Capitan Reef, New Mexico and Texas: facts and questions to aid interpretation and group discussion: Permian Basin Section SEPM Spec. Publ. 14, p. 182-191.

Esteban, M. and Pray, L.C., 1983, Pisoids and pisolite facies (Permian), Guadalupe Mountains, New Mexico and West Texas, *in* Peryt, T. (ed.), Coated Grains: Springer-Verlag, Berlin, p. 503-537.

Hanford, C.R., Kendall, A. C., Prezbindowski, D.R., Dunham, J.B., and Logan, B.W., 1984, Salina-margin tepees, pisoliths, and aragonite cements, Lake MacLeod, Western Australia: their significance in interpreting ancient analogs: Geology, v. 12, p. 513-576.

Mazzullo, S.J., and Cys, J.M., 1978, Archaeolithoporella-boundstones and marine aragonite cements, Permian Capitan Reef, New Mexico and Texas USA: N. Jahr. f. Palaeontology Mh., v. 10, p. 600-611.

______ and Cys, J.M., 1983, Unusual algal-crystalline carbonate coated grains from the Capitan Reef (Permian, Guadalupian), New Mexico, USA, *in* Peryt, T. (ed.), Coated Grains: Springer-Verlag, Berlin, p. 599-608.

Mazzullo, J.M., Williams, M., and Mazzullo, S.J., 1984, The Queen Formation of Millard Field, Pecos County, Texas: its lithologic characteristics, environment of deposition, and reservoir petrophysics: Trans. SWS-AAPG Publ. 84-78, p. 103-110.

Mazzullo, S.J., Mazzullo, J.M., and Harris, P.M., 1985, The significance of eolian deposition in mixed carbonate-siliciclastic systems, the Permian of the Permian Basin: abst., AAPG Bull., in press.

Ordonez, S.R., 1984, Permian (Guadalupian) shelf deposition and diagenesis; the Tansill Formation of the Cheyenne Field, Winkler County, Texas: Trans. SWS-AAPG, Publ. 84-78, p. 61-80.

Pray, L.C. and Esteban, M.C. (eds.), 1977, Upper Guadalupian Facies, Permian Reef Complex, Guadalupe Mountains, New Mexico and Texas; Vol. 2, Road Logs and Locality Guides: Permian Basin Section SEPM, Publ. 77-16.

Roehl, P.O., 1967, Stony Mountain (Ordovician) and Interlake (Silurian) facies analogs of recent low-energy marine and subaerial carbonates, Bahamas: AAPG Bull., v. 51, p. 1979-2032.

Sarg, J.F., 1977, Locality Guides, Stops VI, VII, & VIII, Rocky Arroyo, *in* Pray, L.C. and Esteban, M.C. (eds.), Upper Guadalupian Facies, Permian Reef Complex, Guadalupe Mountains, New Mexico and Texas; Vol 2, Road Logs and Locality Guides: Permian Basin Section SEPM, Publ. 77-16, p. G165-G176.

Toomey, D.F. and Cys, J.M., 1977, Rock/biotic relationships of the Permian Tansill-Capitan facies exposed on the north side of the entrance to Dark Canyon, Guadalupe Mountains, southeastern New Mexico, *in* Hileman, M.E. and Mazzullo, S.J. (eds.), Upper Guadalupian Facies, Permian Reef Complex, Guadalupe Mountains, New Mexico and West Texas: Permian Basin Section SEPM Publ. 77-16, p. 133-150.

Warren, J.K., 1982, The hydrological significance of Holocene tepees, stromatolites, and boxwork limestones in coastal salinas in South Australia: Jour. Sed. Petrology, v. 52, p. 1171-1201.

______, 1983, Tepees, modern (South Australia) and ancient (Permian-Texas and New Mexico) - A Comparison: Sed. Geology, v. 34, p. 1-19.

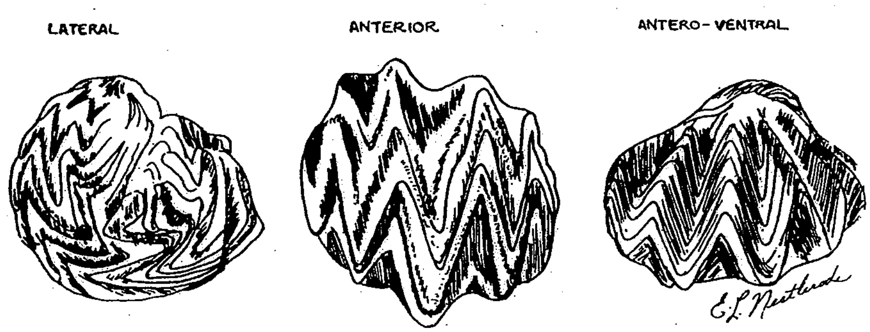

Parenteletes cooperi

Walnut Canyon

THE CAPITAN-MASSIVE AND ITS PROXIMAL CARBONATE, AND MINOR SILICICLASTICS OF THE CAPITAN BACK-REEF, WALNUT CANYON AREA, CARLSBAD CAVERNS NATIONAL PARK, NEW MEXICO

Lloyd C. Pray

Rocks of the Walnut Canyon area of Carlsbad Caverns National Park provide the most accessible and some of the best exposures available of the Capitan-massive facies and its contemporaneous succession of bedded strata for a distance of 1-2 miles shelfward of the Capitan-massive. The Walnut Canyon area we will visit is near the eastern and lower end of the southwest-trending Reef Escarpment. Facies exposed here are considered typical of the younger Guadalupian part of the Capitan Reef Complex along much of its exposed length in the Guadalupe Mountains.

COLLECTING OF SAMPLES OR IN ANY WAY DEFACING THE NATURAL FACE OF THE LANDSCAPE WITHIN CARLSBAD CAVERNS NATIONAL PARK IS STRICTLY PROHIBITED. SEE AND ENJOY, BUT LEAVE LOCALITIES AS YOU FIND THEM.

A generalized geologic map of the area of Walnut Canyon, which extends from the White City area at the intersection of U.S. 62-180 with New Mexico 7 to the entrance to Carlsbad Caverns, is shown in Figure 2-1. Our traverse of facies formed at the shelf edge or shelfward of it 1-2 miles will take most of the half-day allotted. The facies changes in the outermost part of the shelf perpendicular to the trend of the shelf edge are striking as is the facies persistence parallel to the trend of the shelf edge. Dunham (1972, PBS-SEPM), guided in part by interpretations of Lang (1935) but largely by his own careful analysis, envisioned the depositional profile of the shelf to be that of a low marginal mound, the highest part of which (occurring shelfward of the Capitan) restricted or, at times, prevented circulation from the open waters of the Delaware Basin and outermost part of the shelf

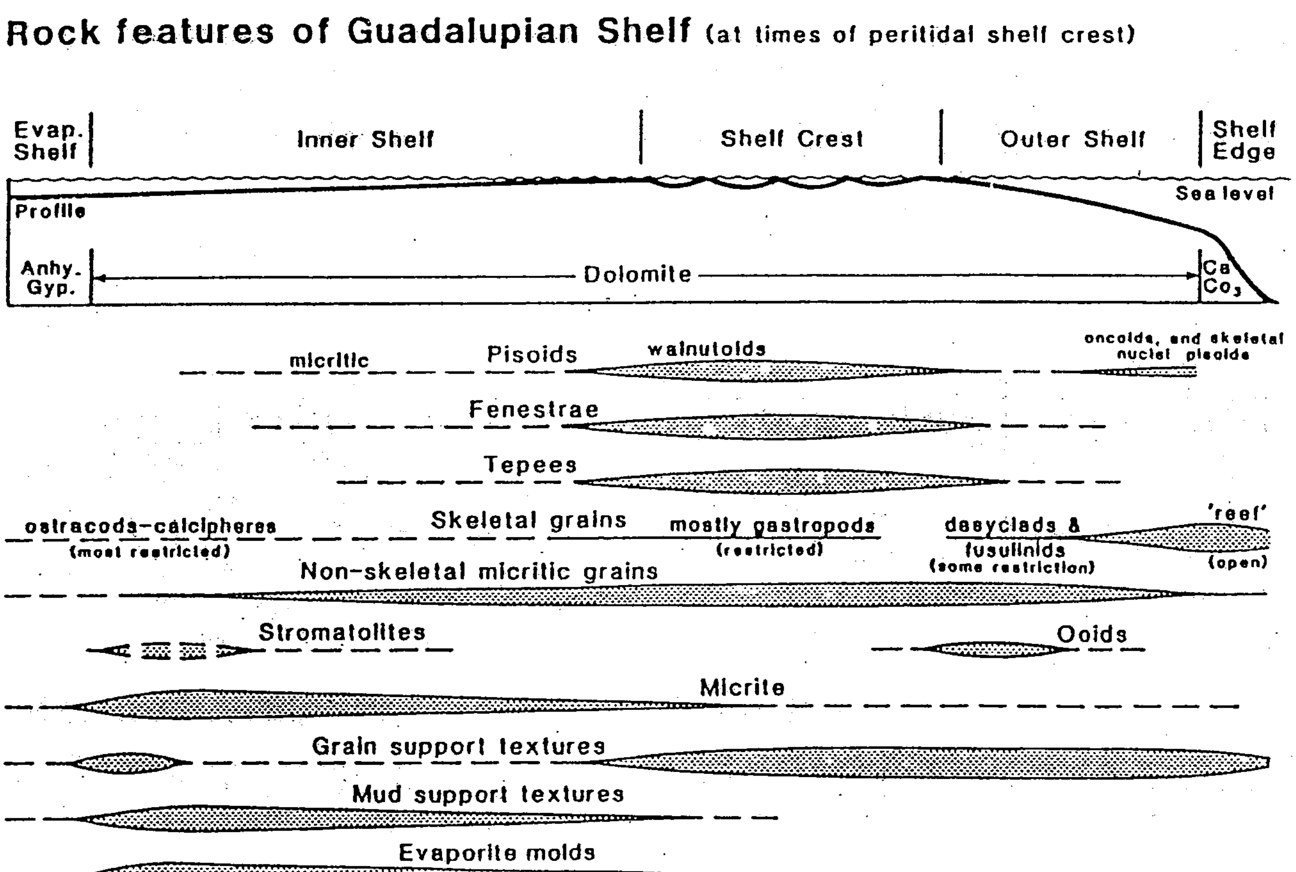

From Esteban and Pray, 1983

FIGURE 2-3. Rock features of the Guadalupian (Capitan age) shelf at times of peritidal carbonate Shelf Crest deposition. Syndepositional carbonate cementation occurred across much of the carbonate depositional area.

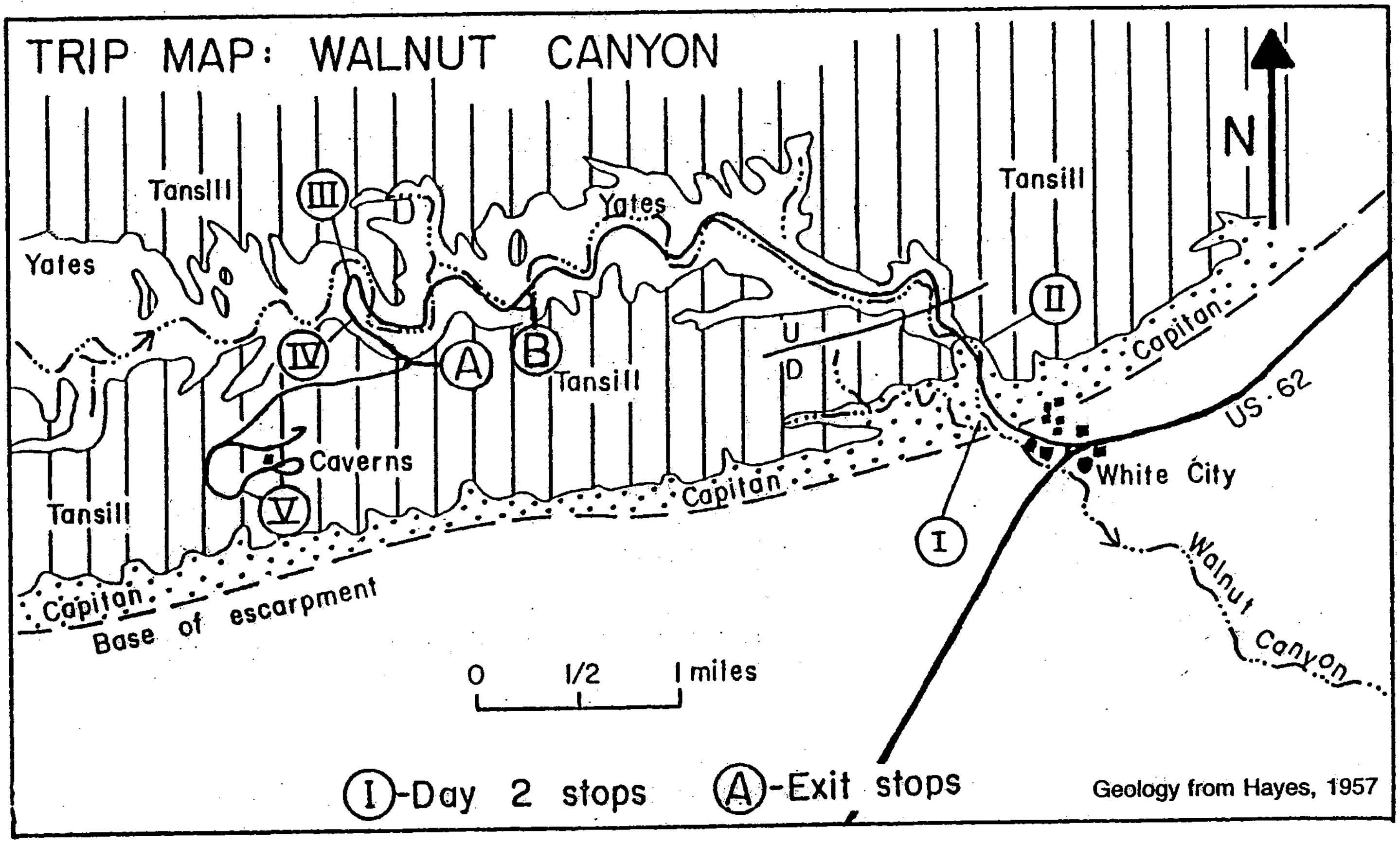

FIGURE 2-1. Geologic map of the Walnut Canyon area showing distribution of the Capitan Limestone and its backreef equivalents of the Tansill and underlying Yates Formations. Major stops are marked I-V, possible short exit stops are marked A and B.

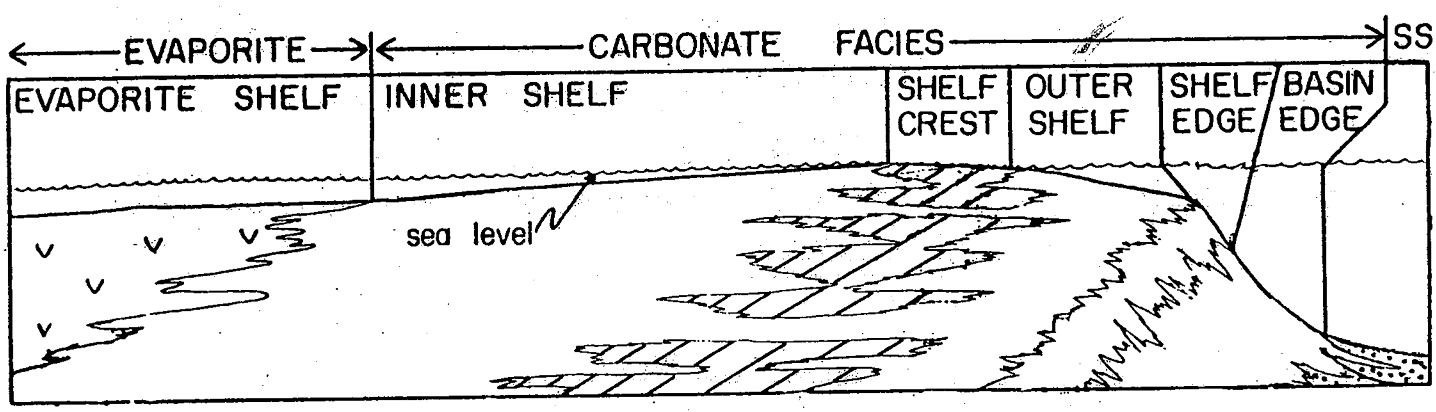

FIGURE 2-2. Diagram showing major subdivisions of the inferred depositional profile (marginal mound hypothesis), the lithologic composition and spatial position of the major facies and of sea level at a time of deposition of peritidal Shelf Crest carbonate facies. Not to scale - width of area 10-20 km.

with a broad inner area (normally a lagoon). He and subsequent investigators have provided much evidence in favor of this marginal mound interpretation. For convenience in referring to both the facies and to the various environments of a marginal mound shelf-top profile, I subdivided the profile (Figure 2-2) into a Shelf Edge, an Outer Shelf (characterized by seaward dips), a Shelf Crest (the paleohigh of the marginal mound), an Inner Shelf (characterized by shelfward dips), and an Evaporitic Shelf, characterized by predominant evaporite rather than carbonate facies. The location of the high on Dunham's marginal mound was placed to coincide with the maximum development of the pisolite facies, which he interpreted as developed by soil processes (a Permian paleocaliche) — hence an area of maximum and most frequent emersion during sea level lows. The mutual association of pisolite, fenestral dolomite and tepees, all compatible under Esteban and Pray's interpretation of peritidal phenomena (the cross-hatched areas on Figure 2-2) is used by us as diagnostic criteria of the Shelf Crest facies (Figure 2-3). Handford and others (Geology, Sept. 1984) recently suggested these facies developed lagoonward of a shelf crest, which they inferred to coincide with some more seaward oolitic and peloidal carbonate sands of this facies succession. Their suggestions, based largely on an inferred analogy of a minor development of pisolites and small tepees discovered at Lake MacLeod of Western Australia, appears unwarranted — at least until more evidence favoring it than has been reported to date can be demonstrated in the facies of the Permian of the Guadalupe Mountains. Major earlier characterizations of the back-reef Capitan shelf have been by Tyrrell (1969), Dunham (1972, PBS-SEPM), Denys Smith (1974, AAPG) and by Neese and Schwartz (1977, v. 1, PBS-SEPM) and in their separate M.S. theses (1978, 1981) at the University of Wisconsin (Madison).

All stops (Figure 2-1) selected for this day's Walnut Canyon field trip are localities described in earlier field guides. See particularly Dunham (1972, PBS-SEPM) who devotes some 35 pages to present Stops 1, 2, 3, 5 and 7, and that of Pray and Esteban, who devote about 100 pages to Stops 1, 2, 3, 4, 5 and 6.

I acknowledge with pleasure here the many contributions of numerous geologists with whom I have been associated in investigations pertinent to this key area of the Guadalupe Mountains, many of whom have been University of Wisconsin (Madison) graduate students with thesis projects on facies we will encounter. Specifically, these have been PhD students Jack Babcock (1974) and Donald Yurewicz (1978), both working on the Capitan Limestone, and M.S. students Magell Candelaria (1983), shelf siliciclastics, and on overall facies studies of the carbonates of the back-reef, Neil Hurley (1978), Douglas Neese (1978), and Mark Rosenblum (1984). The University of Wisconsin geologic field program has received financial support from a number of organizations, particularly from the New Mexico Bureau of Mines and Mineral Resources and from Arco, Conoco, Exxon, Mobil, Shell and the Union Oil Company of California. Most of my work in this region on the Shelf Crest pisolite facies has been in close collaboration with Dr. Mateu Esteban, formerly of the University of Barcelona, Spain and currently with Amoco Production Research, Tulsa. In addition, over the years the personnel of Carlsbad Caverns National Park have been most helpful to the investigations.

* * * *

HYPOTHESES OF SHELF TO BASIN PALEOBATHYMETRY

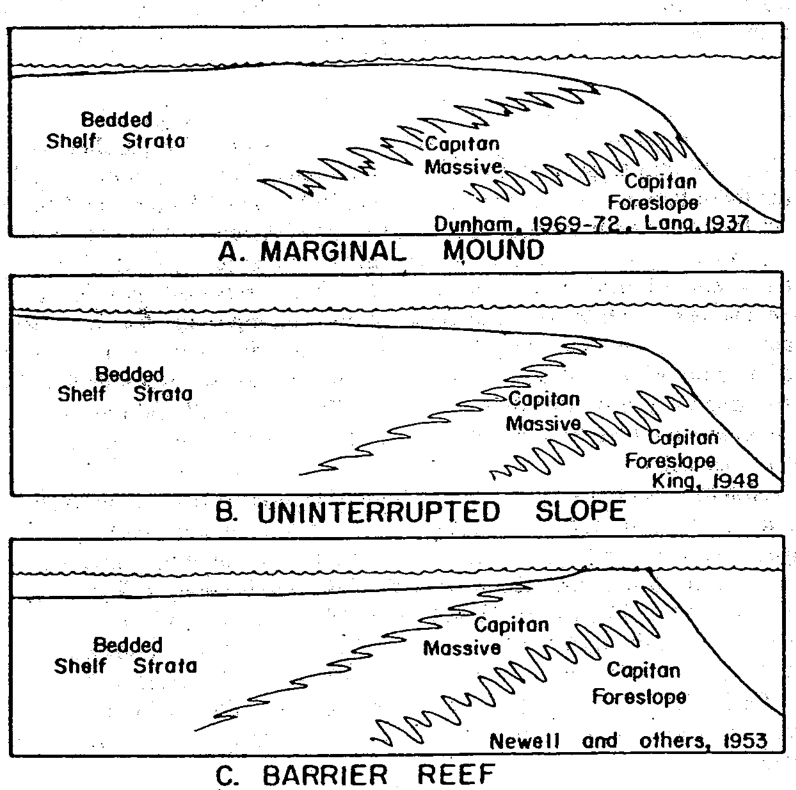

FIGURE 2-4. Schematic diagram of alternative hypotheses compiled by Dunham for the depositional profile of the Capitan-age Guadalupian shelf. The marginal mound hypothesis as advocated by Lang (1935) and Dunham (1972) is strongly favored. Little evidence supports the barrier reef hypothesis.

19.2 0.5 **STOP 1. Parking turnout on right at entrance to Carlsbad Caverns National Park, on New Mexico 7, 0.5 miles west of its intersection with U.S. 62-180.** (A larger parking area is also available west of the road at the boundary sign on the edge of Walnut Canyon. The parking area and the outcrop area to be visited at Stop 1 outside the park is on private land of Mr. James White at White City.)

Capitan-massive, Shelf Edge facies. The outcrops to be observed occur just west of Walnut Canyon, between Walnut and Bat Cave Canyons and south of the east-west line of the park boundary. Figure 2-5A is a map of the area of this stop. Most observations will be in the area of the Figure 2-5B inset of Figure 2-5A, and from there west across the low ridge separating Bat Cave and Walnut Canyons, and thence along the lower slopes north of Bat Cave Canyon to the park boundary. This locality, long a stop on nearly all field trips to the region, affords an excellent opportunity to observe a large mass of the Capitan-massive in an area where it consists almost entirely of a submarine-cemented mass of boundstone that includes some of the major biotic skeletal elements of the Capitan-massive. Detailed observations at this stop are provided by Dunham (1972, PBS-SEPM), Babcock, Pray and Yurewicz (1977, PBS-SEPM, v.2) and Babcock *in* Toomey and Babcock, (1983, CSM). We see here typical skeletal-cement boundstones of the Upper Capitan (Tansill-equivalent) in an area which is inferred to be at or close to the area of the shelf edge where the depositional slope changed from gentle basinward dips observable in the proximal Outer Shelf facies to steeper dips observable in forereef facies underlying the Capitan-massive by 100-200 m (not here exposed). The major objectives of this stop are: 1) to appreciate on the outcrop the massive nature of the part of the Capitan referred to as the Capitan-massive; 2) to observe and appreciate the volumetric importance of submarine cementation in the Capitan-massive in the laminated encrustations that form most of the rock mass (in many places 70-80 percent or more of the rock mass) and its interlamination with a component interpreted by Babcock as a probable calcareous algae; 3) to observe the major types of skeletal fossils associated with the encrusting laminations of the submarine cement and alga [(herein referred to following Babcock (1983, CSM) as *Archeolithoporella* and radial fibrous cement (abbreviated A.-RFC)], and 4) to consider the implications of how much was not observed at this outcrop that is relevant to interpretation of the Capitan-massive in the many years it was visited prior to a decade or so ago.

1) Observe the massive nature of the bulk of the outcrop. Although geopetal fabrics abound in the rocks here, note the apparent absence of bedding planes, of surfaces of erosion or of apparently by-passing of siliciclastics, or of surfaces of emersion. Evidence strongly suggests deposition of the rock of the Capitan-massive at a submerged shelf edge, deep enough to not become emergent during minor fluctuations of sea level. Prevailing seaward depositional slopes of the proximal Outer Shelf facies, supported by some geopetal evidence of primary dips by Hurley (1978, 1980) in his study in North McKittrick Canyon of older Outer Shelf facies (see also Yurewicz *in* 1977, PBS-SEPM), leads to the interpretation that few Permian ships would have gone aground on the Capitan-massive. In essence, it was not a barrier reef (see Figure 2-4) but a submerged shelf edge carbonate buildup.

2) On close inspection, most of the rock mass of the entire area of Stop 1 (Figure 2-5A) consists of tan to brownish calcite in the form of encrusting laminations, each made up of radial or parallel arrays of fibrous to palisade calcite from less than one mm to several mm thick, commonly alternating with irregular thin laminae of lighter-weathering calcite: these laminae may show within them light and dark couplets. The interpretation of this encrusting laminated rock that is currently generally accepted is that of Babcock (1974, PhD; 1977, PBS-SEPM) who considered the radial fibrous to palisade calcite as submarine cement and the lighter intergrown micritic laminae as the probable neomorphosed product of a red calcareous alga, *Archeolithoporella*. The crystals of the radial to palisade calcite are coarse enough to be conspicuous on the outcrop (hand lens may help with much of it); those of the inferred algal laminae are micritic. Some of these micritic layers, as noted in the diagram of Figure 2-5C, may not be of organic origin. Interpretation of these laminated encrustations that form most of the rock of the entire area of the stop is reviewed in Babcock (1983, CSM). Newell and others (1953) and Newell (1955) noted it and interpretations involved both algal processes (stromatolitic) and aragonite cement; Dunham (1972, PBS-SEPM) noted its occurrence in fissures and the main rock mass, referred to it as "recrystallized limestone," noted druse fan structure, and discounted an algal interpretation, partly on the likely absence of light in fissures. But more importantly, he considered it a product of diagenesis, some type of secondary substitution, related to deep vadose diagenesis. It should be noted that his interpretations came at a time when in carbonater's dogma, submarine cements were of no consequence in normal marine environments. Tyrrell (1969 and earlier) had also referred to this calcite of the Capitan as "rayed" and "fibrous recrystallization." But the submarine cement "bandwagon" which started in the mid-1960s was not applied in force here until Babcock's work of the early 1970s. Schmidt and Klement (1971) referred to it as "authigenic early diagenetic calcium carbonate." Several authors in the 1977 PBS-SEPM volumes (Babcock, Yurewicz, Schmidt, and Mazzullo and Cys) discuss this laminated encrusted rock in essentially the terms of the present interpretation, but with somewhat different emphasis on the micritic laminae.

Important to note on the outcrop, and astonishingly evident once one looks for the evidence, is the encrusting habit of A.-RFC coating the conspicuous invertebrate fossils (sponges, phylloid algae, *Tubiphytes*, etc.) and forming much larger nodular masses (Babcock's *A.* nodular boundstone). In many places it can be observed to completely fill large openings in the rock framework, or to nearly fill such, leaving some residual primary

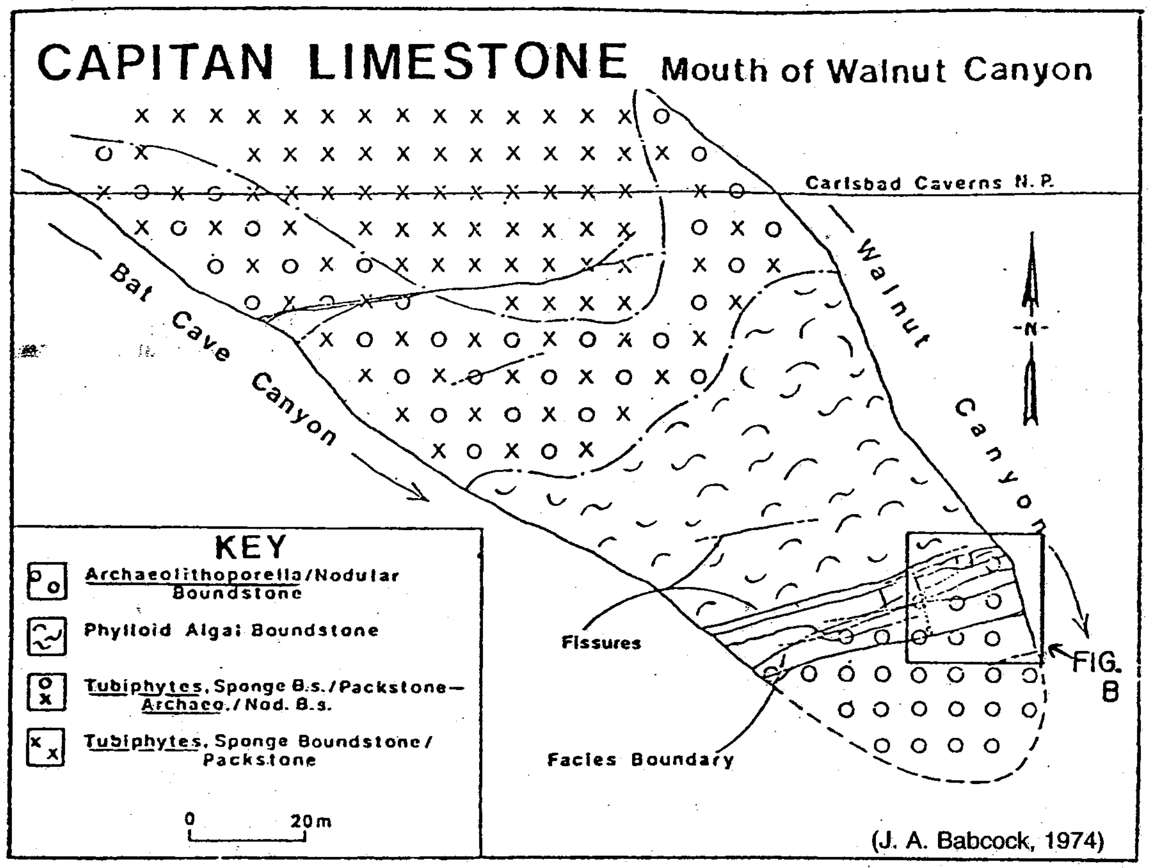

A

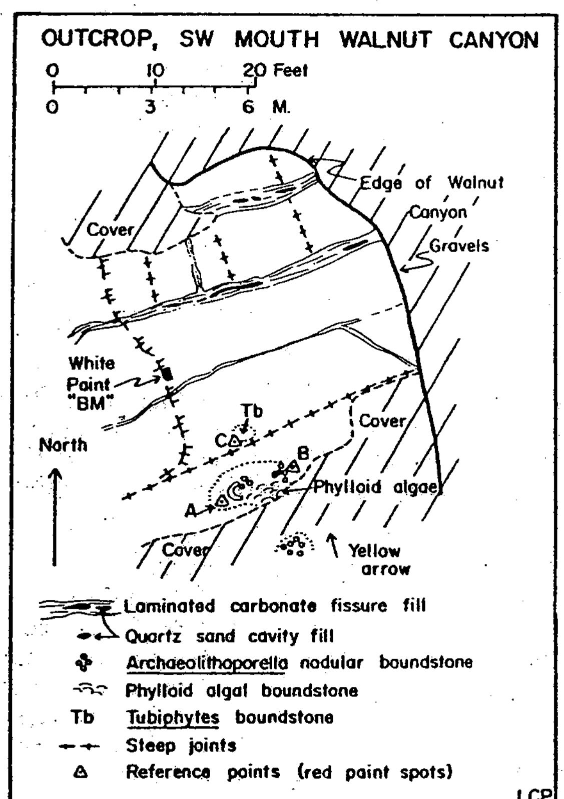

B

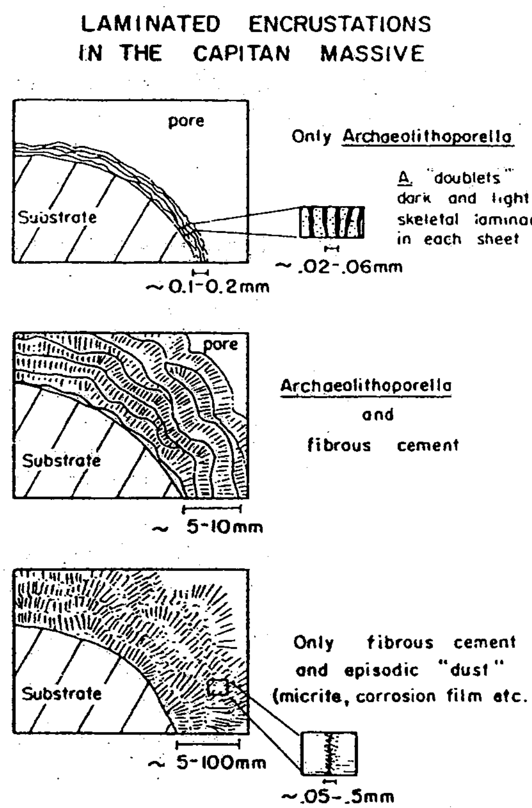

C

FIGURE 2-5. (A) Map of types of boundstone comprising the Capitan-massive at Stop 1, in area between Walnut and Bat Cave Canyons.
(B) Map of area in square of A (above) on southwest side of Walnut Canyon showing fissure fillings and specific observation points (please do not sample or mutilate) for three major types of boundstone.
(C) Schematic diagram of types of the laminated encrustations forming the tan-brown calcite that constitutes most of the volume of the boundstones. The interlaminated *Archeolithoporella* alga and radial fibrous cement predominates.

porosity as a clue of the direction of filling. As evidence of its primary nature pockets of sediment may be detectable on the crusts and in turn covered by later crusts. Locally in the rock coarse radial arrays of darker calcite crystals (Figure 2-6B), interpreted as aragonite botryoids (now known to be forming in modern normal marine submarine environments such as off Belize), occur in pockets filling primary porosity in the cementing rock mass. These also can be found to occur coated by later A.-RFC crusts or by geopetal sediment. As an example of a rigid carbonate buildup formed largely by submarine cement, but closely associated with various skeletal assemblages, the Capitan-massive of Upper Capitan time has no equal. It should be noted that in the Middle and older Capitan, masses of rock composed predominantly of the laminated encrustations seen here are much less common, and cavity linings more commonly seen are thinner isopachous coatings of laminated, more micritic, calcite — perhaps largely *Archeolithoporella*, but perhaps of cement origin.

3) The Capitan-massive here has a rich assemblage of marine fossils, and Babcock has here distinguished three major types of A.-RFC boundstones (see Figure 2-5A and B) for localities. The most abundant invertebrate fossils here are calcareous sponges of a variety of genera and shapes ranging from platy forms half a meter or more across (locality A of Figure 2-5B) to smaller finger-like forms such as predominate in the photograph of Figure 2-6A. Calcareous sponges are a dominant biotic component in Permian and early Mesozoic reefs. Dunham referred to the original rock of the Capitan as a sponge wackestone, and indeed, such is an apt characterization, particularly for much of the Middle and Lower Capitan-massive, but these units may also involve submarine cements.

Particularly conspicuous at Stop 1 outcrops, especially on the low ridge separating Walnut and Bat Cave Canyons west of the diagrammed fissure-rich area, are phylloid algae encased with A.-RFC laminations. Most are about the size of potato chips and many show an orientation roughly paralleling the reef trend. Small light-colored concentrations of sediment on their upper and basinward side, as first noted by Babcock, suggest bottom currents were directed basinward. Inconspicuous in the A.-RFC rock are the small, dense, white, somewhat twig-like masses of *Tubiphytes* that form a third major type of boundstone on these outcrops (Figure 2-5A and B).

4) It is sobering to think of the various differing interpretations that have been made of the Capitan-massive at this outcrop by first-class geologists, and also to realize how much was missed for so long. The primary nature of the A.-RFC, and the presence of phylloid algae was largely unrecognized until the detailed studies of Babcock but a decade ago. What that should be obvious is being missed now? Almost surely something of interpretive importance. And what should have been interpreted long ago was evidence of submarine cementation (the A.-RFC of the fissures that clearly opened in solid rock here near the Capitan basin slope also formed the bulk of the fissured rock!).

We will not have time to make the instructive traverse along the edge of Walnut Canyon into the park area (for details see Babcock, Pray and Yurewicz, 1977, PBS-SEPM). Shelfward, the size and number of fissures diminish, as does the amount of A.-RFC. Sediment increases in abundance, and some patches of dolomitization occur in the more shelfward part of the Capitan-massive.

MILEAGE		
Cumulative	**Interval**	
0.00	0.00	**Park Boundary, Walnut Canyon**, Stop 1 location.
0.15	0.15	Crossing Walnut Canyon. Strata visible to left and right are outermost Outer Shelf carbonate grainstones and packstones of the lower Tansill Formation.
0.2	0.05	**STOP 2. Parking turnout on right side of road.** Walnut Canyon, North Bluff, Outer Shelf Facies. We will walk southeast to intersect the base of Walnut Canyon for initial observations and then proceed up the canyon about 200 m to the vertical cliff area of the meander bend of Walnut Canyon. This locality was Dunham's Stop II-1 and was Stop I, Day 2 of Pray and Esteban, 1977, PBS-SEPM.

Yates and Tansill Formation, Outer Shelf Facies. Where we first intersect the base of Walnut Canyon southeast of the parking area, the strata are largely of limestone, thick-bedded to massive, and with but little dolomitization. Most of the rock is a molluscan-dasycladacean grainsupportstone. Large snails are locally conspicuous. The rock is largely a skeletal grainstone. Finer particles include a wide range of fossils and peloids. Note the basinward dips here and on the cliff west of the highway. These dips are considered to be indicative of the primary seaward dips of the strata here on the outer part of the Outer Shelf. Examination of rocks between here and those of the northern part of Walnut Canyon southwest of the highway crossing indicates a transitional contact of the Outer Shelf strata with a grain-rich, more massive Capitan. **Walk up the canyon floor to the area of vertical cliffs at the meander bend.**

Cliff locality at the meander bend northeast of the parking area: This locality is described in more detail than that given below in Dunham (Stop II-B, Day 1, 1972, PBS-SEPM) and by Pray and Schwartz (1977, PBS-SEPM). Figure 2-7 shows a graphic section of the lower part of the 100 m sequence of cliffs exposed above the floor of the canyon. The dolomite exposed at the base of the section (1-2 meters of which were not exposed when the section was measured in 1977) corresponds to the

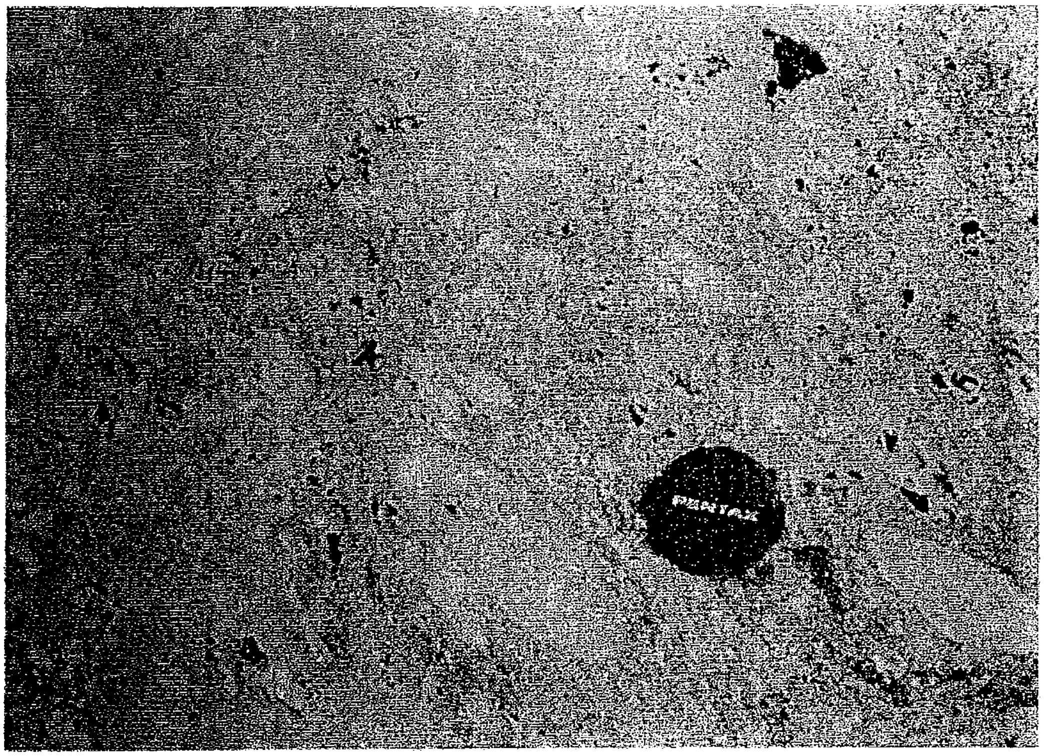

A

B

FIGURE 2-6. Outcrop photographs on south-sloping outcrops of Capitan-massive along Bat Cave **Canyon near National Park** boundary in area of map of Figure 2-5A.
(A) Calcareous sponge-rich laminated encrustation boundstone (radial fibrous cement and ***Archeolithoporella***).
(B) Laminated encrustation boundstone showing several areas of 2-3 cm radial druse fans (dark **near center) of syndepositional** submarine cement.

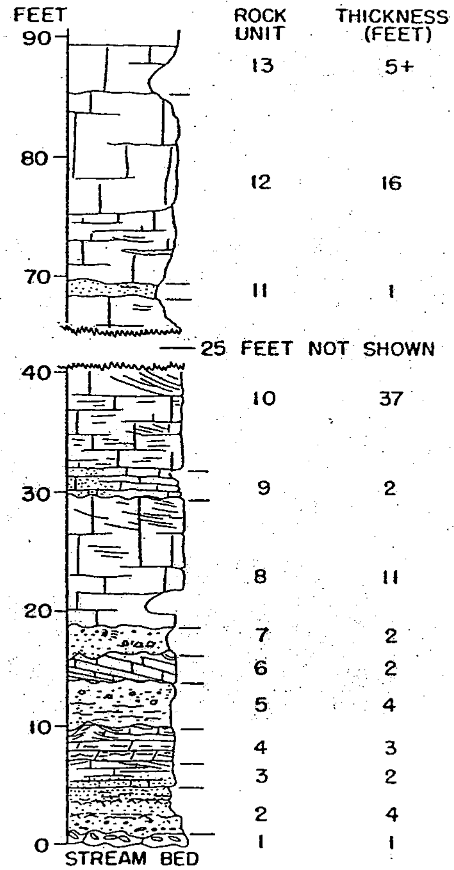

FIGURE 2-7. Stratigraphic section at the elbow of Walnut Canyon (Stop 2) showing major lithologic units, Outer Shelf facies, Yates and Tansill Formations. Recent floods have exposed an additional 1-2 m of the basal dolomite, and strengthened its correlation with the top of the upper Yates informal unit termed the Hairpin Dolomite (see Figure 2-8, Stop 3).

uppermost part of the "Hairpin Dolomite" (Figure 2-8) of the upper Yates Formation. The Yates-Tansill contact is interpreted to be at the top of the thin sandstone unit number 11. The 70-some feet of mixed carbonates and siliciclastics of units 2 through 11 is an appreciably thickened section of the Triplet unit, a thickening caused by addition of carbonates in sufficient quantity to offset the thinning of siliciclastics of the Triplet unit. This is normal with shelf siliciclastics of the Outer Shelf as the Capitan is approched. Features to observe here and brief discussion of such is given below:

1) Sandstone pinchout down dip toward the Capitan. In lower outcrops of the cliff 10-20 feet above the stream level and about 100 feet south of the exposed top of rock unit 1, a relatively thin seam of sandstone pinches out into enveloping carbonate rock. At the pinchout area, the grains are unusually coarse, suggestive of a lag concentrate, a phenomena noted at other basinward pinchouts of Outer Shelf sandstones.

2) Sedimentary structures in the siliciclastics and mixed carbonate-siliciclastic units 2, 5 and 7, but especially well shown in unit 2. Note parallel lamination, and local small scale foresets or ripples, predominantly but not exclusively indicating current flow in a basinward direction. Diagnostic subaqueous sedimentary structures are prevalent in the outermost parts of the commonly structureless sheet sandstones.

3) Fenestral dolomite and small tepees (unit 4), with sheet cracks. Tepees are known in modern areas and ancient rocks to occur in a wide range of environments.

4) Unit 6 shows low-dipping foresets, sloping seaward. This unit consists largely of well-rounded pisolites, with nuclei of marine fossils, in distinction to the non-skeletal nuclei of the predominate pisolites of the back-reef Shelf Crest. This may be the locality of cross-bedded pisolite Kendall (GSA, 1969) referred to in his 1969 Geol. Soc. America article on Guadalupian Facies, as cross-bedding this well developed has not been reported in the Shelf Crest pisolite (see Figure 2-3 for inferred separate facies position of marine versus hypersaline pisolite).

5) Several meters of strata (unit 10) can be seen to have high-angle basin-sloping foresets — viewed best to the right of the vertical cliffs above unit 1. These are oolitic, a facies distinctly uncommon in the Guadalupian back-reef, but one suggested (Handford and others, 1984, Geology) as the possible shelf crest, a suggestion not proven in the Guadalupian work to date.

6) Unit 1 is the uppermost part of the Yates Formation unit termed the Hairpin Dolomite (Figure 2-8). The uppermost Hairpin here is calcitic, and the top surface may represent a fossil weathering surface, whose correlative surface at Stop 3 is interpreted as altered by probable subaerial weathering. Note the conspicuous white intraclasts just above the contact of unit 1, entrained in the basal sandstones of unit 2. Most of the few recognized weathering surfaces (Permian age) of the strata recognized in the Shelf Crest area are not recognized this close to the Capitan, here unlikely to be more than ½ km more basinward. **Return to vehicles and proceed up New Mexico 7.**

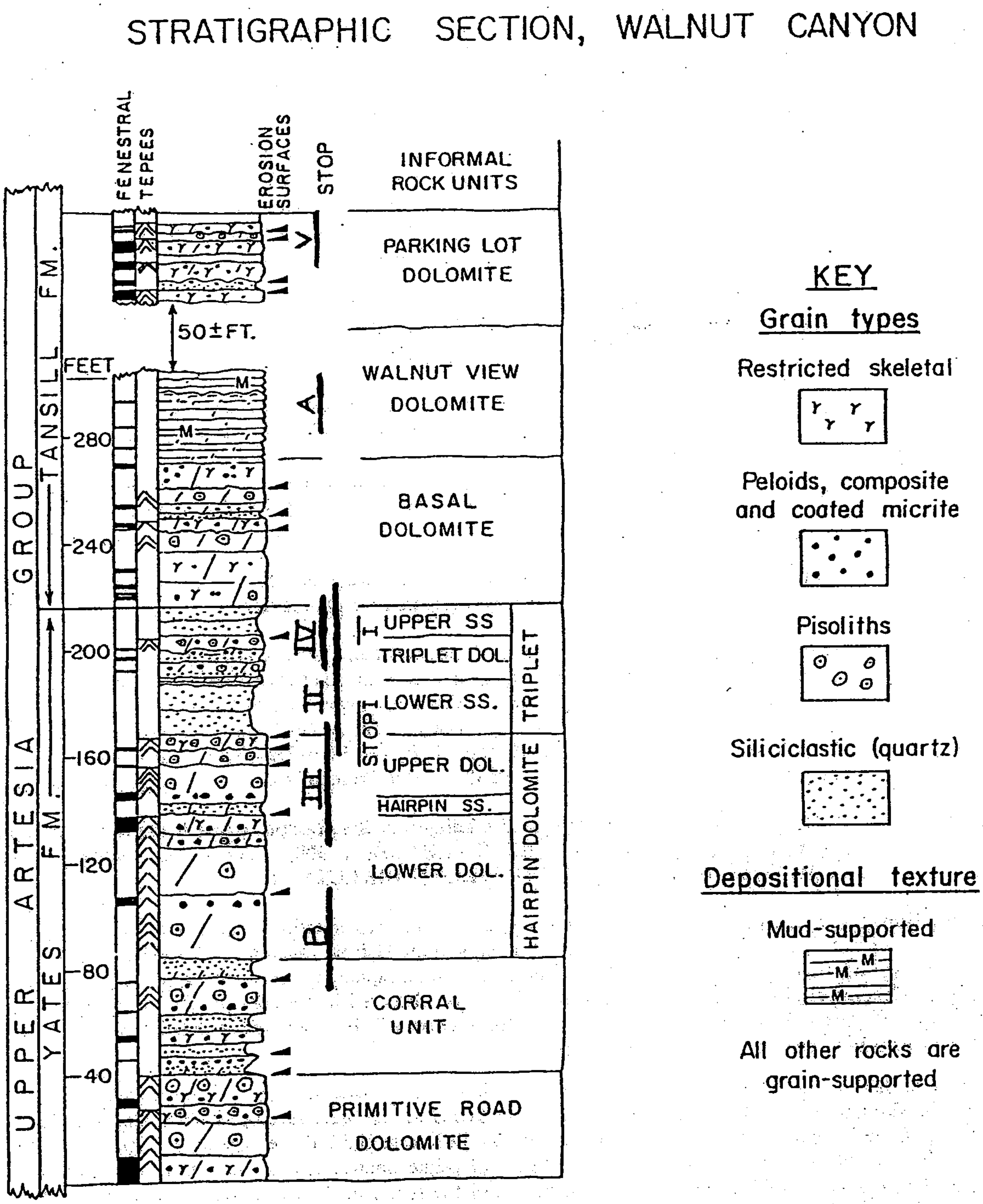

FIGURE 2-8. Generalized stratigraphic section of upper Yates and lower Tansill Formations exposed at Walnut Canyon Stops 3, 4, 5 and Exit Stop A. Strata are of Shelf Crest facies except for the evaporitic, fenestral, mud-rich dolomite of the Walnut View Dolomite representing prograding, Tansill-age, Inner Shelf facies.

0.4	0.2	Cross Walnut Canyon.
0.6	0.2	Road cut exposes faulted section of upper Yates carbonate and sandstone. Displacement is down to the south. Several more high-angle faults along this trend can be seen in the canyon walls to the west.
0.7	0.1	Strata of the upper Yates and lower Tansill are well exposed on the edges of the canyon to the right of the road. (Stop I, Day 2, 1977, PBS-SEPM). This locality, 1-2 km shelfward of the Capitan inner marine, shows well the upper part of the Hairpin Dolomite, the Triplet siliciclastics and carbonates of the uppermost Yates, and the overlying Tansill, upwardly composed predominantly of dolomite. (See the stratigraphic section of Stop 3, Figure 2-8, for above units). The prominent recessive unit a few feet thick in the lower part of the cliff is the Hairpin dolomitic sandstone (see notches and caves along it). The Hairpin "sandstone" unit here is an irregularly laminated dolomitic sandstone

with a few small oscillation ripple marks which grades upward into fossiliferous dolomites. (We will see this unit in a more shelfward position at Stop 2). The base of the Hairpin dolomitic sandstone here truncates (with minor relief) underlying large tepees of the lower part of the Hairpin Dolomite unit. More tepees are evident in the overlying upper part of the Hairpin Dolomite. Ahead and on cliffs on the north side of this locality note the prominent recessive units (grassier and greener than the cliffs). These are made by the two major sandstone units at the base and top of the Triplet (Figure 2-8). These sheet sandstones can be traced along the Shelf Crest with no detected interruptions in their continuity and but gradual changes in thickness (Candelaria, 1982, M.S., Univ. Wis.) and afford no evidence of channelization of sands as a way of moving siliciclastics across the shelf. The strata of this area are transitional between Shelf Crest and Outer Shelf.

0.9	0.2	The lower west-facing cliffs at this meander bed (left) provide excellent exposures of pisolitic and fenestral facies of the Hairpin Dolomite — and of extensive sheet cracks filled largely with calcitic cements, in contrast to dolomitized cements farther shelfward (Stop 3).
1.9	1.0	Curve to left. Some of the siliciclastic unit near road level are unweathered (gray in contrast to normal yellow-brown of most roadcuts and all outcrops). Corral Unit, Yates Formation.
3.4	1.5	Turnout on left for botanical and anthropologic exhibit, and Stop B of exit route; see end of this log. Stream level exposures are of Corral Unit and lower Hairpin Dolomite of the Yates Formation, as are strata along the road for next mile.
4.3	0.9	Small parking turnout on right. At road level are excellent natural exposures of thick pisolitic strata of lower Hairpin Dolomite that are well oriented for photography.
4.4	0.1	Entering the Hairpin Curve section of the Carlsbad Caverns Highway. The stratigraphic sections exposed in roadcuts along the ½ mile of ascending road above on the left provide the best single location for detailed study of the upper Yates and lower Tansill Formations of this area, here about 1-1.5 miles shelfward of the Capitan limestone. These cuts form the site of Stops 3 and 4 and Exit Stop A of this field trip, the site of Stops II, III and IV of Day 2 of the 1977 field trip (Esteban and Pray, PBS-SEPM) and the lower cuts the site of Dunham's Locality II-2 pisolite study area.
4.7	0.3	**STOP 3. Gravel road to right at the hairpin of the Hairpin curve leads to Corral and parking area in 100 m. CAUTION, THIS IS PART OF A ONE-WAY ROAD, AND IN ENTERING, YOU WILL BE GOING IN THE WRONG DIRECTION.**

Upper Yates Formation, Shelf Crest Facies, emphasis on observations and interpretation of Shelf Crest pisolitic strata and their associated facies, in an area of intense development of tepee structures in the Hairpin Dolomite. This locality is 1-2 km shelfward of the inferred inner edge of the Capitan. Figure 2-8 is a generalized stratigraphic section of the upper Yates and lower Tansill Formations along the Caverns Highway in this area. Much of it can be observed in the cliffs of the meander bend north of the Corral parking area. The upper half of the Yates Formation of that section will be examined in detail in the road cuts along the highway. Stop 3 concerns the strata of the Hairpin Dolomite.

A major objective at this stop is to observe the broader relationship of the pisolite facies to the interbedded less- or non-pisolitic dolomites and minor siliciclastics, and the relationship of these facies to the well-developed tepee structures and to several intraformational erosion surfaces at the top of and within the Hairpin Dolomite Unit. These broader stratigraphic relationships are critical to the interpretation of the Shelf Crest pisolite, the facies of prime interest at this stop. A second major objective is to observe in the excellent exposures of the highway cuts the details of the fabric of the rocks, particularly the pisolite-rich rocks, long of major interest in the Capitan back-reef strata, and rocks whose interpretation has provided much controversy. A major impression that should be gained by careful scrutiny of the pisolitic rocks is the variety and probable genetic complexity of these rocks (see Figures 2-9 and 2-10).

The cuts here have long been the location at which pisolitic facies of the Shelf Crest have been most frequently observed and studied. Features of this stop are provided in more detail than that which follows in Esteban and Pray, 1977, PBS-SEPM (27 pages, Stop II, Day 2) and by Dunham (1972, PBS-SEPM, Locality II-2, 11 pages). Interpretations of the pisolite facies of the Shelf Crest have most recently been presented and reviewed in an article by Esteban and Pray in the T. Peryt-edited volume Coated Grains, 1983, Springer-Verlag.

Briefly, the interpretations of the genesis of the Shelf Crest pisolite facies are as follows: early work identified the pisolites as red algae and evidence of an algal reef! For three decades most attention was focused on an algal or non-algal origin for the pisoliths, a subaqueous origin being implied or assumed. Interpretive revolution occurred in 1965 when Dunham, and independently Thomas, interpreted the pisoliths to have formed by secondary processes (weathering — a Permian paleocaliche). See Dunham (1969, Jour. Sed. Pet.) and Thomas (1968, PBS-SEPM, Pub. 68-77) for first published details. Dunham focused principally on the spectacular occurrence of inverse (reverse) graded bedding of some pisolitic strata, pointed out analogous features in known weathering horizons (and also in cave pearls) and made what proved to be persuasive arguments for an in-place vadose origin. The "vadose pisolite" hypothesis was launched and rapidly gained wide acceptance for not only the Shelf Crest pisolite but for rocks with some similar fabrics in other places in the world. Kendall (1969), while accepting the "caliche" interpretation, also

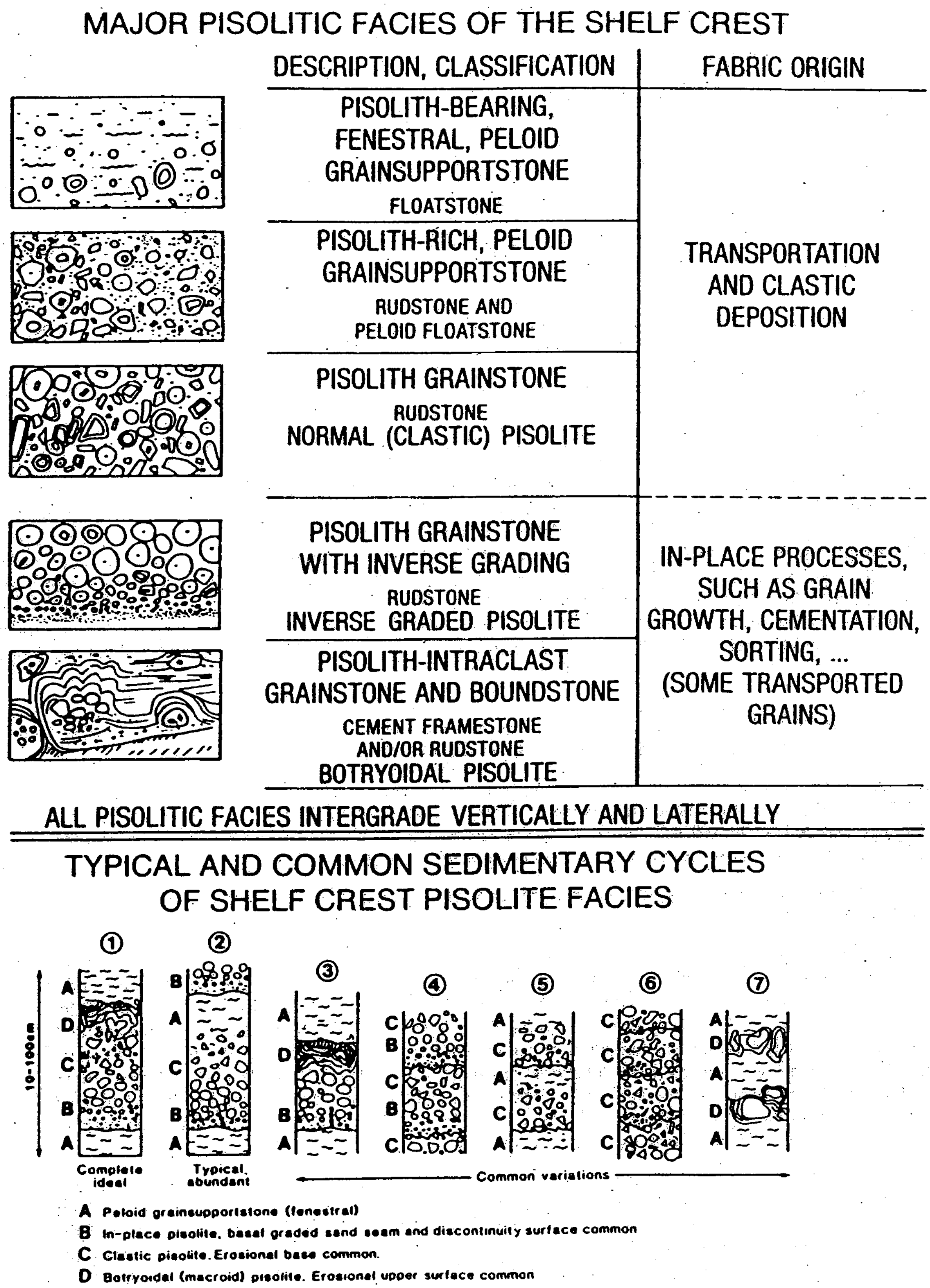

FIGURE 2-9. Diagrams of pisolite facies of the Shelf Crest occurring at Stops 3, 4, 5 and at Exit Stop B. The upper diagram shows the major pisolite facies together with their description, classification (using Dunham's rock classification terms and the Embry-Klovan modification of it) and the major processes involved in the origin of the rock fabric. The lower diagram illustrates typical and common sedimentary cycles involving pisolite-dominated rock in the Shelf Crest facies.

stressed a clastic synsedimentary origin. Starting in 1975, Esteban and Pray rejected the secondary soil or cave origin for the Shelf Crest pisolite and returned to synsedimentary, largely subaqueous origin compatible with processes related to hypersaline water of a peritidal marginal marine environment. They accepted Dunham's in-place origin of the inverse graded pisolite, but stressed the predominant isopachous nature of most pisoliths, even in the inverse graded units, and the interpretation that most vadose fabrics were late stage overprints of earlier isopachous fabrics, and most commonly associated with a distinctive but minor type of pisolite they referred to as "botryoidal." Key elements of their interpretations were based on the broader stratigraphic relationships of the pisolitic strata, as well as the fabric details stressed in most earlier work. These were intergradations with other "normal" sedimentary rocks: position favoring pisolite development in the position of inter-tepee depressions (pools on a partly emergent peritidal flat); pisolite origin prior to erosion and local weathering phenomena associated with a few intraformational erosion surfaces; and the lack of a spatial relationship of pisolite development directly below those erosion surfaces, few in number, that showed evidence of subaerial weathering. Currently, most geologists familiar with the stratigraphic and fabric evidence in this Shelf Crest area accept the interpretation of its formation on a pertidal marginal marine area involving intense precipitation of calcium carbonate from hypersaline water covering or episodically flooding low-relief flats that occurred behind the more deeply (and continuously submerged) Capitan shelf edge.

Pisolite facies of the Guadalupian Shelf Crest have most recently been discussed by Esteban and Pray (1983, Coated Grains, Springer-Verlag). The diagrams of Figures 2-9 and 10 portray some of the key stratigraphic and fabric relationships we observe in Shelf Crest pisolite facies (many of which are observable in the road cut of Stop 3) in close association with predominantly peloidal, fenestral grainsupportstone dolomite and tepee structures with abundant cement-filled sheet cracks. We prefer a subaqueous origin for most pisoliths. Most were probably deposited clastically near their point of origin, some give evidence of in-place growth within a pisolite assemblage by precipitation of outer concentric coatings of cement on free-to-move grains (not linked by cement), thus permitting expansive growth of a pisolite aggregate. Some pisolite aggregates show evidence of early isopachously coated grains growing by late stage non-isopachous accretionary cementation. Some of these late cements are downward-elongated (stalactic or gravity cements) and of vadose origin — probably formed on supratidal parts of tidal flats. Recent geochemical studies of Rosenblum (M.S. 1984, Univ. of Wisconsin) strongly implicates hypersaline marine water for the vadose "overprints." Of the three major types (end-members) of pisolite recognized by Esteban and Pray (Figure 2-10), the botryoidal (which involves generally irregularly shaped, bumpy pisoliths, coated pisolitic intraclasts and irregular seams and coatings of laminated micritic carbonate) most consistently displays gravity fabrics. We believe this type formed in the shoalest, intermittently exposed parts of a peritidal flat — some of their gravity fabrics may be primary splash-zone effects. Most inverse graded pisolite probably formed by in-place growth of free grains receiving successive accretionary coatings of carbonate cement, but some unusual clastic processes (migration of beach cusps — Chafetz and Kocurek, 1980, or sorting mechanisms — David Johnson, 1984, AAPG abstract, etc.) might be involved locally.

At this stop, examination of the Hairpin road cuts will be from north to south. In rough sequence, the following features can be observed (see 1977, PBS-SEPM, for precise locations and more detailed descriptions and illustrations):

1) Lower road cuts, west side, initial 100-200 feet. Note the interbedded pisolite-rich strata with fenestral grainsupportstones and parallel to cross-cutting cement "veins" (filled sheet cracks related to tepee formation). Note in lower cuts where first thick (1 m+) zone of pisolite occurs, that is, shows evidence of sequential pisolite deposition separated by minor erosion surfaces and carbonate sand seams (Figure 2-12A).

2) Initial road cuts, east side. Large tepee structure; another large tepee structure occurs on west side of cuts, axis oblique to highway.

3) East side road cuts 200-300 feet south of entrance to cuts (refer to cross-section of Figure 2-11 showing an upper and a lower tepee complex separated by the thin, carbonate-rich Hairpin "sandstone"). Note the truncation of the lower tepee complex by the erosion surface. It shows no evidence of alteration below it at the base of the Hairpin "sandstone." The surface not only truncates strata of the lower complex, it also truncates cement filled sheet cracks within it. Tepee building, cementation of sedimentary strata, cement filling of tepee-related sheet cracks and intraformational erosion all were repetitive processes in the Shelf Crest depositional area. Note preferential development of pisolite in the inter-tepee depressions and the facies changes on the tepee flank (see in particular the area with the square, upper tepee complex of Figure 2-11). Tepee structures are preferentially developed in fenestral grainsupportstone units relative to pisolith-rich units.

4) Hairpin sandstone. This remarkable persistent ½-1 m-thick unit is composed of very fine sand- to coarse silt-sized siliciclastic grains admixed with carbonate grains and dolomite cement. Its carbonate content increases from about 50% to 75% or more as this unit is traced closer to the edge of the shelf. In this area much of the Hairpin "sandstone" shows the planar to slightly wavy laminations, and fenestral structures. Very locally the sharp eye may see small symmetrical (oscillation) ripple marks a few mm high and about 2 cm wave length — ripple index about 10. Carbonate fossil grains increase in abundance toward the Capitan and upward into the upper Hairpin Dolomite. Candelaria (M.S., 1982, Univ. of Wis.), who has studied in detail the Hairpin and overlying Triplet sandstone outcrops of this region, notes shelfward diminution in sedimentary structures in the Hairpin with only local planar or wavy lamination more than 2.2 km behind the Capitan (see Candelaria article in this volume for details). His interpretation is of very shallow, subaqueous deposition of the Hairpin at a time when a distinct marginal mound was obscure..

5) Fabrics in pisolitic strata of the upper tepee complex (Figure 2-11) on both sides of road south of area of cross-section: these cuts show a variety of the fabrics diagrammed on Figure 2-10, including inverse grading

PISOLITE FABRICS

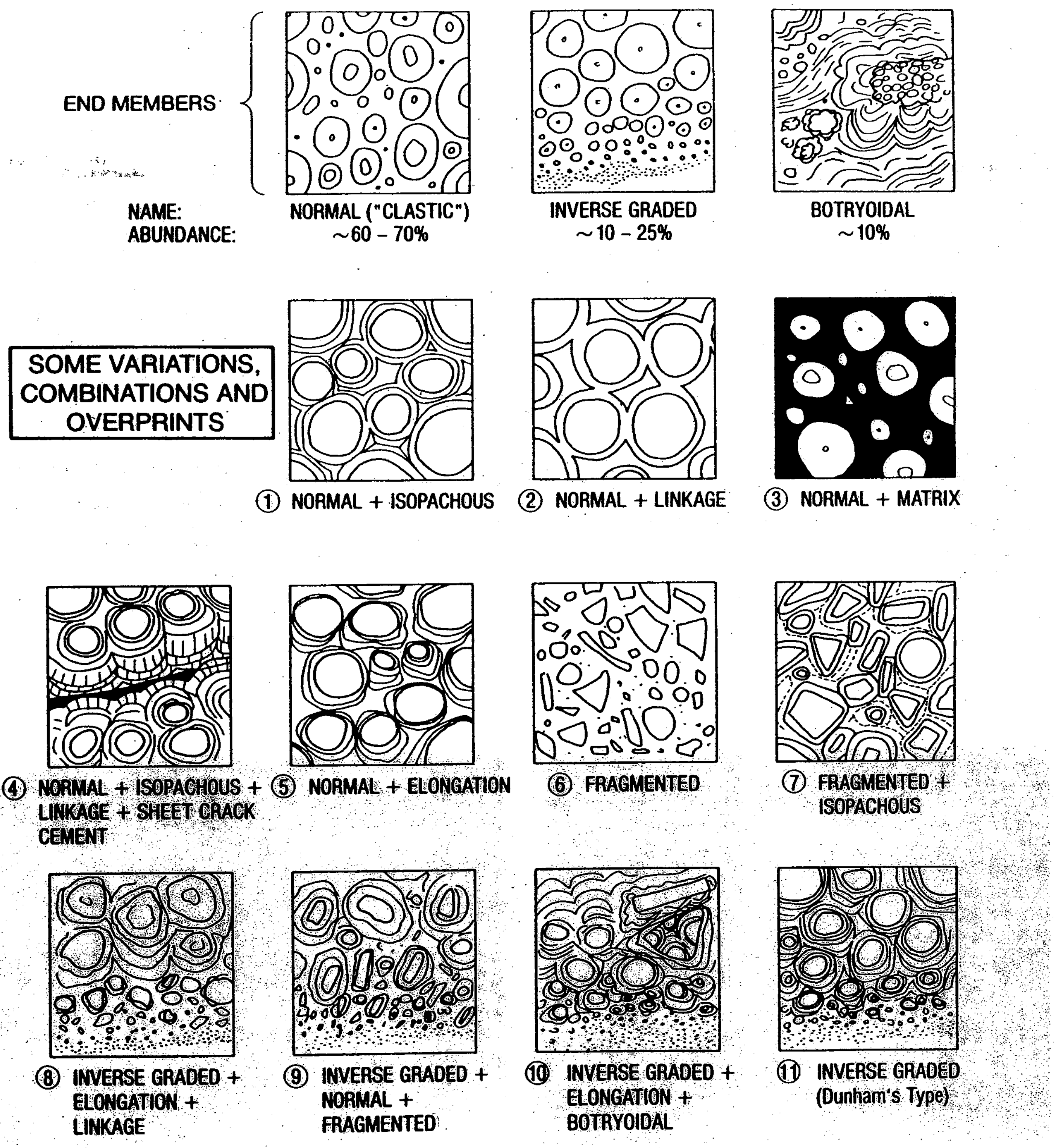

FIGURE 2-10. Upper part of diagram shows the three end members of types of pisolite of the Shelf Crest facies and their estimated relative abundances. The lower 11 boxes show some of the variations encountered in the pisolite-dominated facies of the Shelf Crest.

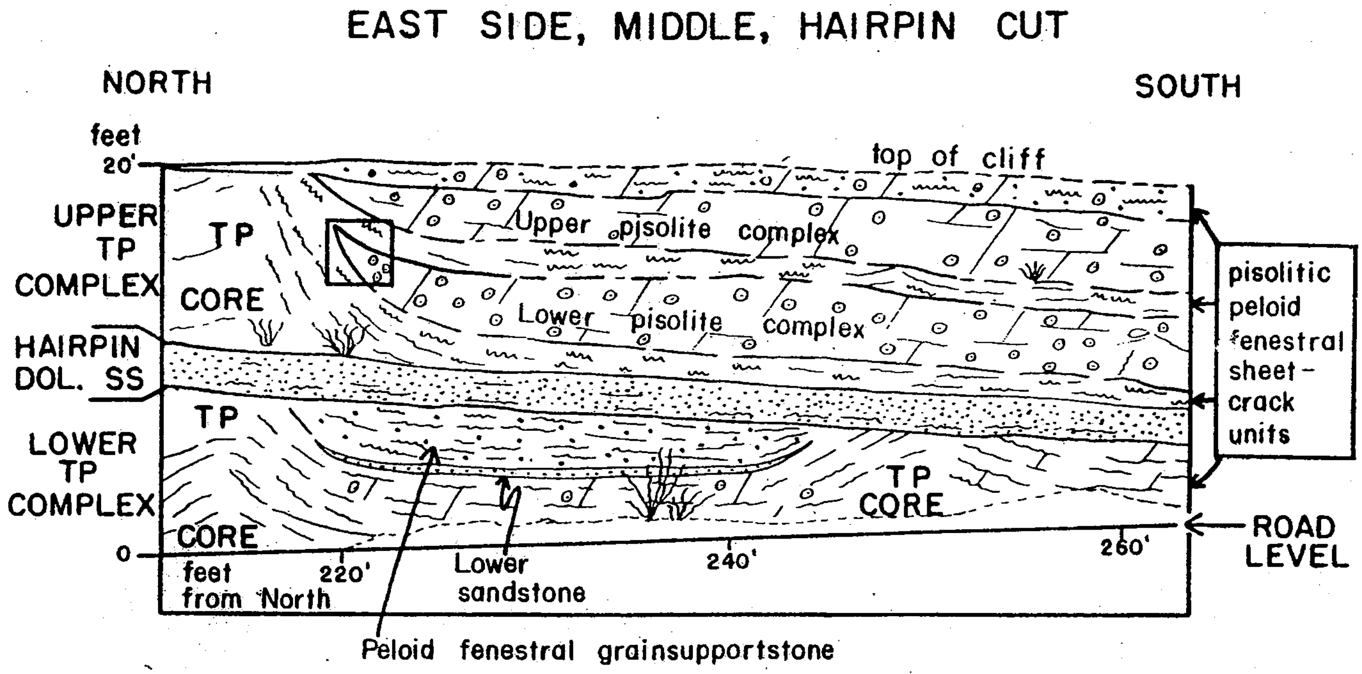

FIGURE 2-11. Diagram of the middle of the east side of the road cuts at Stop 3, Shelf Crest facies. The stratigraphic unit is the uppermost 20 feet of the upper Yates Hairpin Dolomite. Distances along road measured from the start of the road cuts on the west side of highway. Note in particular: 1) the major occurrence of pisolite facies is in the intertepee depression flanking the upper tepee core, 2) the facies changes of the pisolite units in the square marked on the south flank of the upper tepee core, and 3) the truncation of the lower tepee complex (and associated sheet crack cements) by the smooth erosional surface at the base of the Hairpin dolomitic sandstone.

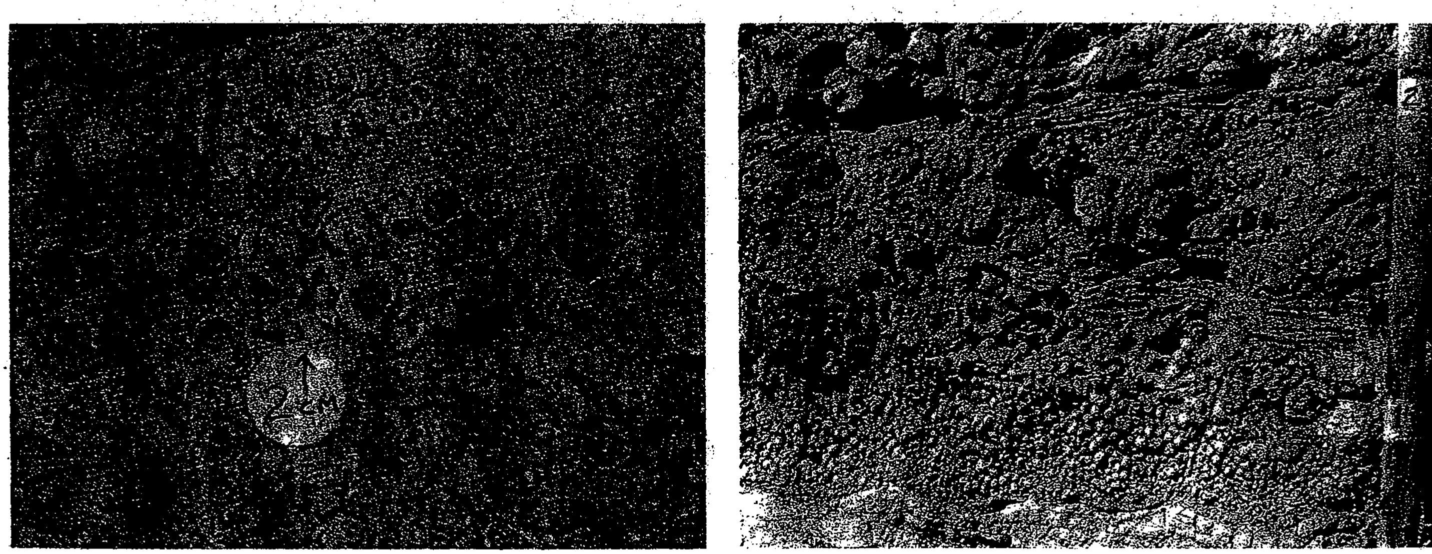

A

B

FIGURE 2-12. Outcrop photographs of two sequences involving pisolite-dominated strata at Stop 3, in the Hairpin Dolomite, Shelf Crest facies. (A) Typical exposure of normal (clastic) pisolite, in which pisoliths predominately show isopachous accretions, and of an overlying carbonate sand-rich unit. Carbonate sand infiltrated into underlying interpisolith porosity; some pisoliths and coatings are truncated as the contact of the two units. Most thick pisolitic units show such erosional and textural depositional discontinuities. (B) Spectacular upward gradation from inverse graded pisolite into botryoidal pisolite. Locality midway along west road cuts, about 1 m below upper surface of Hairpin Dolomite. Pole markings in feet.

with both isopachous and gravity (Dunham) cementation. A superbly exposed sequence of inverse graded pisolite grading upward into nearly a meter of botryoidal pisolite (Figure 2-12B) occurs just below the top of the west road cut, midway along the west side. (Enter from above, or by climbing northward and up along road cut cliffs.) This inverse to botryoidal sequence is part of a late stage of filling of an inter-tepee depression of a tepee complex that shows several stages of growth and filling along the southern road cuts (see diagram in Esteban and Pray, 1977, PBS-SEPM).

6) At the south end of the low continuous cuts west of the road, examine the upper surface of the Hairpin Dolomite, and note micritization, interpreted (Esteban and Pray, 1977, PBS-SEPM) as an alteration product related to the major erosion surface at the top of the Hairpin - the alteration is possibly related to incipient soil processes. **End of Stop 3.** How do you think the pisolite formed? Consider the problem if sampling were permitted (it is **not** here) of selecting a single "typical" sample of pisolite and the tendency (sample or photo) to focus on the unusual fabrics (inverse graded or botryoidal). This partly explains Esteban's and my approach to this stop on this trip — namely providing a diagram of some of the many fabric combinations of Shelf Crest pisolite. **Participants of this field trip will continue walking south across ravine area to the next road cuts — location of Stop 4.**

4.9 0.2 **STOP 4. Parking for this stop is at the exhibit area. Rocks of road cuts to be examined are on both sides of the exhibit area on the western road cuts.**

Triplet Unit, dolomite and sandstones, uppermost Yates Formation, Shelf Crest facies. Facies to be observed are the dolomite of the middle part of the Triplet (including its thin carbonate-rich sandstone in the northernmost cuts near road level) and the upper Triplet Sandstone exposed in road cuts below the level of conspicuous seeps coming out at the Yates-Tansill contact. Major features of interest are the following:

1) **Triplet Dolomite:** The exposed strata are largely a somewhat micritic, fenestral peloidal dolomite with only a few small tepees and pisolitic zones, mostly in the upper portion. Locally (near north end of cuts) several small micritic mounds and oncolites occur; locally, burrowing is evident. The Triplet Dolomite Unit, although in nearly the same position as the underlying Hairpin Dolomite (e.g. Shelf Crest), contrasts markedly with the Hairpin — and with the overlying basal Tansill. Neese and Schwartz (1977, PBS-SEPM, v. 1) stress the appreciable variation in the three major carbonate units (Hairpin, Triplet, basal Tansill) in the marginal mound area. They are not just prograding units of closely similar facies developed at successive times on the carbonate depositional area of the marginal mound. Although the shelfward progression of facies characteristics (Figure 2-3) is generally valid, the widths of the different facies bands and their detailed nature differs significantly (cf. Denys Smith, 1974b, AAPG).

2) **Erosion Surfaces:** Three erosion surfaces are of interest at this stop. The lowest, at the north end of the cuts near road level, underlies a thin carbonate-rich sandstone unit rather similar to the Hairpin carbonate-rich sandstone (Stop 3). As below the Hairpin Sandstone, alteration is not evident below the erosion surface. The middle erosion surface is at the top of the Triplet Dolomite (Figure 2-13A) and below the upper Triplet Sandstone. This erosion surface is underlain by a reddish- to pink-colored, more micritic zone several inches thick. Petrography suggests an incipient alteration or weathering (Permian) zone. The alteration clearly postdates the development of small tepees and pisolitic facies of the upper part of the Triplet Dolomite. The third surface is that at the base of the Tansill Dolomite, here marked by seeps caused by an impermeable clayey zone along the contact at the top of the altered upper sandstone of the Triplet Unit. This alteration zone, affecting the upper half meter or so of the Triplet Sandstone, is the best developed probable soil zone in the area. It was first interpreted as a soil zone (Permian caliche) by Denys Smith (1974b, AAPG). Subsequent detailed study reveals many features supporting his interpretation. Upward from the fresh (but oxidized) sandstone, the siliciclastic content diminishes, carbonate content increases. Some small elongate carbonate nodules (1-3 mm thick) occur, particularly in the uppermost few inches. Thin sections show microspar replacement of quartz grains, a mottled micritic texture, microchanneling and possible cutans. Some nodules could be called caliche pisoliths. This probable soil zone is recognizable shelfward to the limit of Tansill outcrops of this area (4-5 km from the shelf edge) but appears to die out onto the Outer Shelf. Overall, the frequency and tracing of possible subaerial alteration surfaces appears to substantiate Dunham's concept of more frequent emersion of the inferred top of a marginal mound or Shelf Crest.

3) **Upper Triplet Sandstone:** Typical features of the Shelf Crest siliciclastics of the upper Yates Formation are shown at this outcrop. The sandstone unit is a sheet 4 meters thick. Grain size is mostly in the very fine sand size grade, with some coarse silt but little coarser sand sizes. The overall appearance of the unit is massive, and indeed, much of the outcrop shows but little evidence of sedimentary structures. The platy, somewhat undulose structures in the upper part of the cut may relate to obscure textural differences, or may be entirely a product of modern weathering. Locally in the lower 1/3 of the sandstone unit rather obscure parallel laminations and some minor small scale indistinct cross-lamination can be detected. Candelaria (M.S., 1982, Univ. Wis.), who has studied in detail the upper Yates siliciclastics in this region, noted but four occurrences of ripples in the Triplet sandstones. The one occurrence in the upper Triplet is at this stop, where, in the specimen collected, one meter above sandstone base, Candelaria noted obscure, discontinuous symmetrical (oscillation) ripples of 1-3 cm wave length, 1-3 mm amplitude, and a ripple index of about 10.

The general absence of sedimentary structures in the shelf sandstones, and particularly in those of the Yates, such as here in the Shelf Crest area (based on the carbonates) has long been puzzling. Candelaria's detailed study of all known outcrops of cuts exposing the Triplet reveals a differentiation of preserved sedimentary structures from the areas of the Outer Shelf (Stop 2) across the area of the inferred Shelf Crest. He recognized planar and wavy lamination, local cross-lamination and ripple marks (climbing, current, oscillation), and concluded that all observable structures were compatible with a subaqueous origin. The few asymmetric ripples and ripple cross-lamination he observed in the Triplet indicate current direction both in a basinward and shelf direction. Candelaria recognized no sedimentary structures he felt diagnostic of eolian origin. Candelaria's summary of his work is to be part of the symposium portion of this field trip: see also published AAPG Annual Meeting abstract, 1983.

4) **Basal Tansill Dolomite:** The lower 30 feet of the basal Tansill consists largely of grainsupportstones of a variety of dolomite facies. Predominant in the lower, more accessible 12 feet is dolomite composed of sand- to granule-size grains of peloids, composite grains and skeletal material. Some show fenestral fabric, a few are burrowed. Some rather normal marine fossils occur, such as fusulinids. Pisoliths occur locally in the basal 1-2 feet; pisolite and large tepees occur mostly in higher strata exposed along the highway to the southeast.

Reenter vehicles and proceed up highway.

5.2	0.3	Parking for Exit Stop A in area to left of the sharp curve. Road cuts ahead and along remainder of road to Carlsbad Caverns are in Tansill Formation dolomite.
6.2	1.0	Top of Guadalupe Mountain Escarpment. El Capitan may be visible 30 miles ahead to the southwest. The surface inferred from the accordant crests of much of the Guadalupe Mountains is interpreted by King (1948) as an erosional surface which he termed the Summit Peneplain. It is close to the exhumed basal Cretaceous unconformity.
6.3	0.1	Roads to left to former Cavern Headquarters and to right toward Rattlesnake Canyon. This is the one-way road that exits at the Hairpin Curve. **Continue straight ahead.**
6.6	0.3	West end of Visitor Center parking lot at entrance to Carlsbad Caverns. Stop 5 location is in cuts on the west side of this parking lot. **Proceed ahead on main road** (left turn into parking lot is prohibited here) **to west end of Visitors Center Buildings, then turn left (west) into parking lot area and proceed back to Stop 5 location at west end of lot.**

STOP 5. Parking Lot Dolomite, Tansill Formation, Shelf Crest facies. This stop is within 1 km from the Capitan shelf edge. Large well-developed tepees, of historic significance, and their associated pisolitic facies are well exposed in the cut at the western end of the parking lot. It was for these structures, as seen here, that Adams and Frenzel (1950) coined the term "tepees," a term that has subsequently been widely used to apply to antiform, non-tectonic, intraformational structures ranging in height from a few cm to the more common heights of a meter or two. Some are even larger. The focus of this stop is on the tepees, their associated fractures (sheet cracks) and cement fillings, and on the sedimentary fillings of the intertepee depressions.

Tepees and sheet cracks: Tepee structures are now known from a wide range of environments ranging from oceanic deeps, as interpreted for tepees in the Ordovician of Sweden (Lindstrom, 1963) to modern shallow subtidal of the Persian Gulf (Shinn, 1969), to peritidal in many environments from the Persian Gulf to southern Australia, to terrestrial salinas and caliches. The most comprehensive review of tepees is by Assereto and Kendall (1977, Sedimentology). Genetic views of the origin of these "hard-ground buckles" were recently summarized by Kendall and Warren (1985, AAPG, Ann. Mtg. abstract). Tepees are diverse and complex,

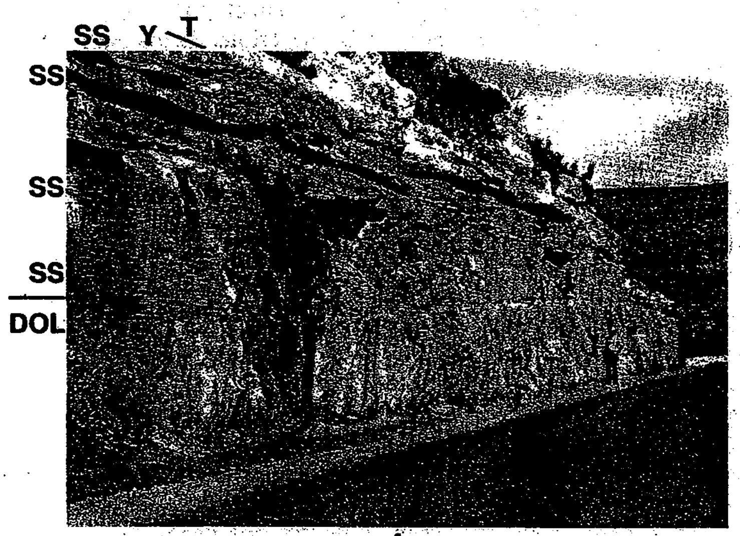

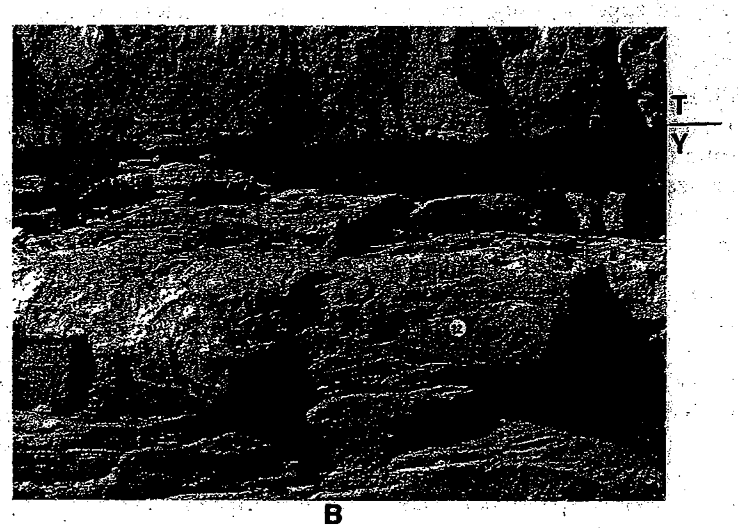

FIGURE 2-13. West road cuts at Stop 4, uppermost Yates and basal Tansill Formations, Shelf Crest facies. (A) In upward succession, Triplet Dolomite and upper Triplet Sandstone of uppermost Yates Formation and of the basal Tansill Dolomite. Basal sandstone directly overlies erosion surface. Sand locally infiltered into truncated small tepee sheet cracks along the micritized erosion surface on the Triplet Dolomite. (B) Contact at seeps of overlying Tansill Dolomite with 1/2 meter-thick weathered zone showing incipient calichification of pre-Tansill age developed on top of the uppermost Yates Triplet Sandstone. Disc is 2 cm in diameter.

and so may be their origin, which is still somewhat enigmatic. Their polygonal patters and associations suggest both shrinkage (dessication-? polygons) and sedimentary expansion (involving repeated cementation and sediment filling of fractures and perhaps of expansion of original sediment layers) are important. Seasonal changes in water table levels have also been invoked — South Australia. Though the mechanisms of formation remain uncertain, there is wide agreement that the tepees of the Guadalupian Shelf Crest are peritidal, marginal marine phenomena. Nearly all are of the type termed "mature" tepees by Assereto and Kendall, including the types seen here and at Stop 3. Some Guadalupian Shelf Crest tepees are of the "embryo" type of Assereto and Kendall in which the uplifted flank beds remain in contact at the tepee crest — a relationship suggested of compressional features as emphasized by Denys Smith (1974a, AAPG). These commonly have preserved sheet crack porosity. Only one occurrence of what we believe would correspond to Assereto and Kendall's "senile" tepee has been recognized in the Shelf Crest upper Yates and lower Tansill strata. This is in the New Mexico 7 Highway cuts of the curve just southwest of the entrance to this parking lot, described together with this locality (Stop 5, Day 2, Esteban and Pray, 1977, PBS-SEPM). The "senile" tepees are largely composed of a chaotic array of brecciated sediment slabs, commonly with large amounts of infiltered sediment and with extensive development of pendant or stalactitic (gravity-sensing) cements interpreted as of vadose origin. Tepee structure and/or traceable sheet cracks may not be recognizable.

Three large tepees and several smaller ones in the larger intertepee depressions are well exposed in the parking lot cut. The northern two are diagrammed in Figure 2-14 from Esteban and Pray, 1977, PBS-SEPM. Details of the tepee core of the northernmost large one are given in Figure 2-15 taken from the recent detailed study of Rosenblum (M.S., 1984, Univ. of Wis.). Most of the host sediment is dolomite; nearly all of the sheet crack cement is calcitic. The intraformational and non-tectonic origin of the tepees is evident from the continuity of the underlying strata exposed along the base of the cut, from the progressively diminution of folding and buckling in the tepee cores, and from the sequences of sedimentary wedges of the intertepee depressions. Sand-filled fissures (Figures 2-14, 15) in the core of the northern tepee and another near the south end of the cut probably represent filtering down of siliciclastics during burial of the intraformational erosion surface (poorly exposed) that forms most of the crest of the cut.

Rosenblum's field and geochemical study (stable isotopes of carbon and oxygen, Sr, Fe and Mg) was undertaken to better understand the cementation history of the sheet cracks. It concentrated on three areas, of which the Figure 2-15 tepee is one, where the cements were largely calcitic, rather than the more pervasively dolomitized cements of areas farther back on the Shelf Crest. The complex history of repeated sedimentation, fracturing, erosion, and cementation is apparent. Different morphologic types of sheet crack cement have been described (Rosenblum recognized eight, named on the diagram, in addition to a late stage coarsely crystalline calcite probably of post-Permian age). Numbers corresponding to the predominant cement of the various sheet crack areas are shown in Figure 2-15. The most abundant cement is that of radial fans, generally formed of fibrous arrays 2-5 cm long, with a radius of curvature of about the same length, that can be observed to grow in any direction and orthogonally and symmetrically from the roof and floor of the sheet cracks. These are interpreted to have been originally aragonitic, formed in a phreatic zone. Palisade cements, with nearly parallel crystals (generally 2-4 cm long, but locally up to 8 cm long) are roof cements whose isopachous growth banding, regardless of angle, indicates phreatic zone development. At the tepee core (Figure 2-15) note the abundance of this cement in the stratigraphically older part of the tepee core, as well as its presence on the underside of some of the displaced sediment slabs tilted to high dips that are midway up the south tepee flank. The various morphologies of sheet crack cements and age relationships indicate changing conditions of cementation or of water during the complex history of tepee development and sheet crack cementation. Rosenblum interprets most sheet crack cement to have formed in a phreatic zone, contrary to Dunham's vadose zone origin. Evidence of any sharp water surface levels within tepees has not been recognized. The stable isotopes of most sheet crack cements analyzed (39) by Rosenblum suggest precipitation from a mixed meteoric-marine water (perhaps mixing of flooding waters of a peritidal flat with that of shallow aquifers carrying meteoric water from far back-shelf areas). Significantly the most marine isotope signatures were from the vadose-interpreted gravity cements associated with sediment-bearing marine fossils of the senile tepee locality just to the southwest, also of Tansill age.

Pisolite facies: The exposures of Stop 5 again demonstrate the preferential development of pisolite in the intertepee depressions (Figure 2-14) and the preferred growth host of tepees to be fenestral grainsupport dolomite. The lower major development of pisolite here is directly above an early erosion surface of the intertepee depression, and here, as in many other places, shows an upward sequence in the pisolite-rich (rudstone) units from inverse graded to the non-inverse graded normal or clastic dolomite. The genetic inference is better development of pisolite in the lower parts of intertepee depressions, with the quieter, deeper water part favoring inverse graded pisolite. Also note that the major development of botryoidal pisolite, as at Stop 3, is high on the tepee flank, a late-stage filling of the intertepee depression. The Tansill strata of the tepee-host fenestral facies and of the successive sedimentary fillings of the intertepee depressions have more skeletal grains, and of less restricted water types, than those of the upper Yates, such as the Hairpin Dolomite. Sedimentary units of the tepee depressions appear to best interpretable as successive shoaling-upward units, deposited on a Shelf Crest repeatedly covered by restricted to hypersaline marine waters. Episodic shelf edge subsidence of a meter or so was probably more significant than minor yo-yoing of sea level.

If time permits, brief stops will be made at Exit Stops A and B enroute to the White City — U.S 62-180 area.

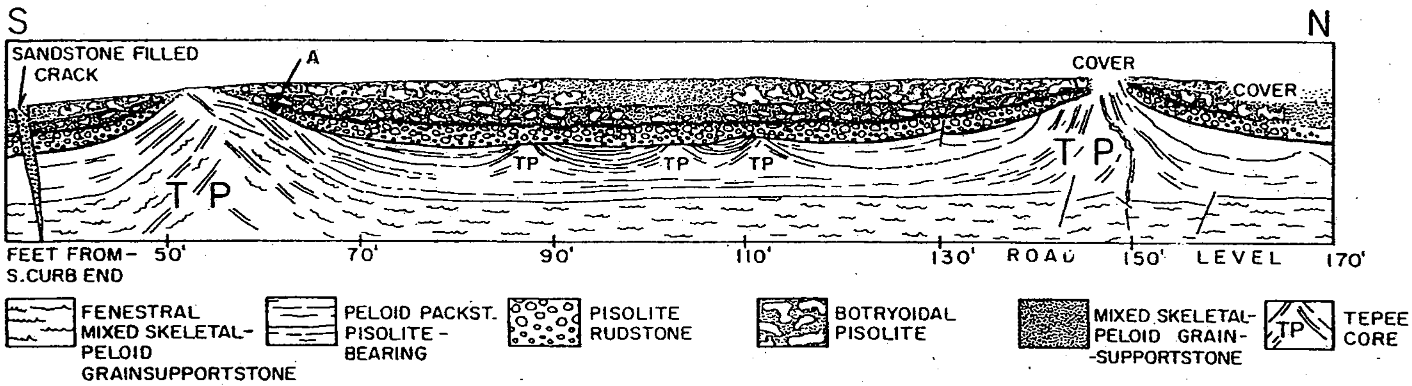

FIGURE 2-14. Western edge of Carlsbad Caverns Visitor Parking Lot, Shelf Crest facies, Tansill Formation, Stop 5. Sketch diagram of tepee area showing relationship of normal (clastic) inverse graded and botryoidal types of pisolite to sedimentary filling of intertepee depression. The initial pisolite rudstone (inverse graded overlain by normal or clastic pisolite) extends across bottom of intertepee depression, truncates smaller tepees and is directly above an erosion surface. Botryoidal pisolite is restricted to a late, partly emergent stage of sedimentary filling of the intertepee depressions and to positions high on flanks.

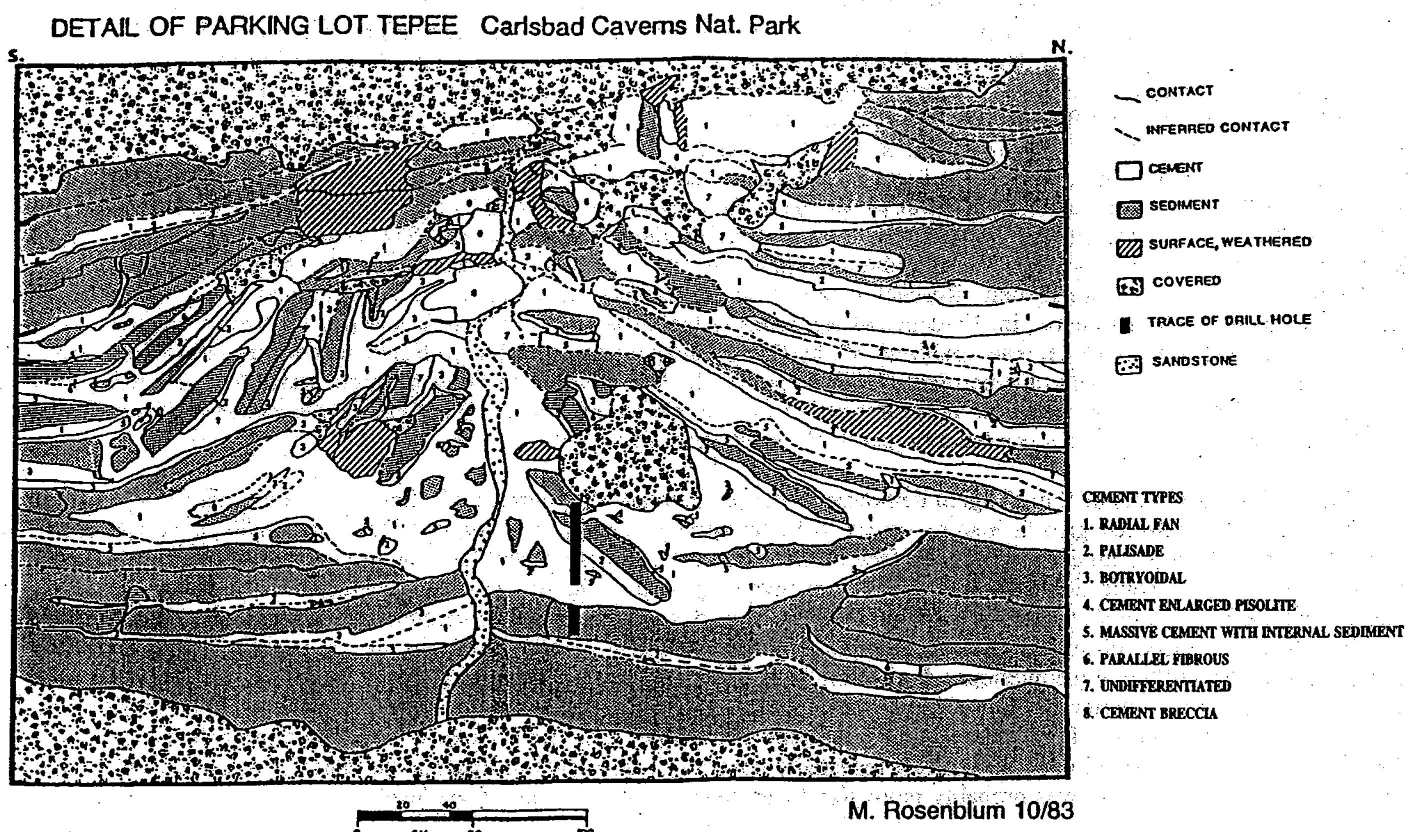

FIGURE 2-15. Stop 5. Field diagram of large tepee structure in Tansill Dolomite showing areas of sediment versus sheet crack cement, with designation of the types of sheet crack carbonate cement. Tepee diagrammed is the northern tepee of Figure 2-14, about 50 m from the south end of the parking lot cut. Dark short lines on edges of diagram show position of discontinuity surfaces formed during tepee growth.